Electrochemical Activation of Catalysis

Promotion, Electrochemical Promotion, and Metal-Support Interactions

Costas G. Vayenas
University of Patras
Patras, Greece

Symeon Bebelis
University of Patras
Patras, Greece

Costas Pliangos
University of Patras
Patras, Greece

Susanne Brosda
University of Patras
Patras, Greece

Demetrios Tsiplakides
University of Patras
Patras, Greece

KLUWER ACADEMIC PUBLISHERS
NEW YORK, BOSTON, DORDRECHT, LONDON, MOSCOW

eBook ISBN: 0-306-47551-0
Print ISBN: 0-306-46719-4

Created in the United States of America

Visit Kluwer Online at: http://kluweronline.com
and Kluwer's eBookstore at: http://ebooks.kluweronline.com

To our parents and children

FOREWORD

I knew nothing of the work of C. G. Vayenas on NEMCA until the early nineties. Then I learned from a paper of his idea (gas interface reactions could be catalyzed electrochemically), which seemed quite marvelous; but I did not understand how it worked.

Consequently, I decided to correspond with Professor Vayenas in Patras, Greece, to reach a better understanding of this concept. I think that my early papers (1946, 1947, and 1957), on the relationship between the work function of metal surfaces and electron transfer reactions thereat to particles in solution, held me in good stead to be receptive to what Vayenas told me. As the electrode potential changes, so of course, does the work function at the interface, and gas metal reactions there involve adsorbed particles which have bonding to the surface. Whether electron transfer is complete in such a case, or whether the effect is on the desorption of radicals, the work function determines the strength of their bonding, and if one varies the work function by varying the electrode potential, one can vary the reaction rate at the interface. I got the idea.

After that, it has been smooth sailing. Dr. Vayenas wrote a seminal article in **Modern Aspects of Electrochemistry, Number 29,** and brought the field into the public eye. It has since grown and its usefulness in chemical catalytic reactions has been demonstrated and verified worldwide.

Electrochemical Activation of Catalysis contains a very full and detailed treatment of the mechanisms of electrochemical promotion. It is likely to remain the standard work on this remarkable new technology; for who other than the present authors will write a book with such a background of authority in the field?

What impressed me particularly was the wealth of high standard theoretical electrochemistry in discussions of the mechanism of NEMCA, for one seldom sees publications showing so much erudition in the theory of electrified surfaces. On the other hand, the book contains a very full treatment, rich in examples, of the practical and experimental side of NEMCA and thus will be attractive to the chemists and chemical engineers who serve in corporate research laboratories. It is likely to lead to advances in industrial

techniques and its long term positive financial value would be difficult to overestimate.

Thus, there is a great deal of substance to this book on the electrochemical promotion of catalysis. But the joy is that it has been set down in a very lucid way so that I seldom had to pause to scan a sentence a second time for meaning.

NEMCA is a triumph, and the latest in a series of advances in electrochemistry which have come about in the last 30 years, all of them situations which are not obviously electrochemical. Examples include corrosion, metabolism, and (part of) photosynthesis.

Greece, thus far, has shown a wealth of electrochemical talent, e.g., in the work of Nikitas in adsorption studies, and the hope is that the excellent contributions of Professor Vayenas and his colleagues will continue to flourish and expand. Given this abundance of expertise and the improvement the new method makes to chemical catalysis, I can only hope that Patras will continue to garner the support that it so richly deserves from the rest of the world.

John O'M. Bockris

PREFACE

Electrochemical promotion, or non-Faradaic Electrochemical Modification of Catalytic Activity (NEMCA) came as a rather unexpected discovery in 1980 when with my student Mike Stoukides at MIT we were trying to influence in situ the rate and selectivity of ethylene epoxidation by fixing the oxygen "activity" on a Ag catalyst film deposited on a ceramic O^{2-} conductor via electrical potential application between the catalyst and a counter electrode.

Since then Electrochemical Promotion of Catalysis has been proven to be a general phenomenon at the interface of Catalysis and Electrochemistry. More than seventeen groups around the world have made important contributions in this area and this number is reasonably expected to grow further as the phenomenon of electrochemical promotion has very recently been found, as analyzed in this book, to be intimately related not only to chemical (classical) promotion and spillover, but also to the "heart" of industrial catalysis, i.e. metal-support interactions of classical supported catalysts.

Sincerest thanks are expressed to Professor J.O.'M. Bockris, the leading electrochemist scientist and educator of the 20th century, for inviting me together with another electrochemist of comparable prominence, Prof. B.E. Conway, to write a Chapter on NEMCA in "Modern Aspects of Electrochemistry", a Chapter which eventually grew into this book. There are also several other individuals which I and my coauthors would like to thank cordially. These include, in alphabetical order, Professor C. Comninellis, Dr. G. Fóti, Professor G. Haller, Dr. K. Howell, Dr. F. Kalhammer and Professor R. Lambert for reading critically parts of the book and suggesting various important improvements.

Looking back to the past, sincerest gratitude is expressed to my parents, grandparents, daughters and other members of my family for their long love and support. Also to my high school teacher Mr. S. Mantzaras and my PhD

Thesis adviser and coadviser at the University of Rochester, Professors H. Saltsburg and W.D. Smith who taught me the hard work and the joy of research. Also to my excellent teachers J. Ferron and M. Feinberg at the University of Rochester and to Gary Haller at Yale and Louis Hegedus, then at W.R. Grace, both lifelong mentors and friends who introduced me into the beauty of catalysis and into the art and hardship of technical writing. Also to Jimmy Wei, Bob Reid and Fred Putnam at MIT who taught me a lot and who, together with all the other ChE colleagues at MIT in the late seventies, created a stimulating intellectual and personal environment.

Sincerest thanks are also expressed to Professor Dr. Lothar Riekert from Mobil and U. Karlsruhe, a true thinker and lifelong mentor and friend and also to my dear colleague Professor Xenophon Verykios at Patras who first introduced me to the mysteries of metal-support interactions.

Many thanks are also expressed to Professors V. Sobyanin and V. Belyaev at Novosibirsk and Dr. Anastasijevic now at Lurgi. Their groups were the first (1990) to report NEMCA outside Patras. The "loneliness" of NEMCA disappeared after a sabbatical year at Yale and our first joint publication in this area with Gary Haller. I am indepted to him and his excellent coworker Dr. Carlos Cavalca.

Cordial thanks are also expressed to Professor Richard Lambert and Professor Christos Comninellis, a prominent surface scientist and a prominent electrochemist whom I first met in 1993 and who both started working enthusiastically with their excellent groups on NEMCA. The impact that the groups of Comninellis and Lambert had in shaping electrochemical promotion in the form we know it today was invaluable. They both brought in numerous significant ideas described in this book.

Many thanks are also expressed to Professor Milan Jaksic who spent years in our lab and played a significant role in our first aqueous and Nafion NEMCA studies. And to Dr. P. Stonehart who from the USA kept sending valuable samples and advice over the years. Also to Professors S. Ladas and S. Kennou for their precious collaboration in the first XPS studies proving O^{2-} backspillover as the origin of NEMCA.

My coworkers and I feel deeply lucky and indebted to have met then Dr. Fritz Kalhammer from EPRI. Not only was EPRI's financial support significant for strengthening our NEMCA work in Patras, but most importantly, Dr. F. Kalhammer, a former student of G.M. Schwab, understood and described NEMCA as deeply, eloquently and concisely as nobody, in my opinion, had ever done before. Fritz's continuing support and friendship is gratefully acknowledged, as is that of Dr. H. Pütter of BASF, another prominent electrochemist whose continuing collaboration is most valuable, as is BASF's, Dupont's and EU's continuing financial support.

Sincere gratitude is also expressed to my PhD students and postdoctoral coworkers, as well as the students of other colleagues mentioned above who

spent longer or shorter periods of time with us in Patras, building a good part of the contents of this book. I am truly indebted to them. They all did a nice job in establishing electrochemical promotion and elucidating various aspects of solid state electrochemistry. In chronological order they are: Mike Stoukides (MIT, now at U. Thessaloniki), Jim Michaels (MIT, now at Merck), Mark Manton (MIT, now at Shell), Roger Farr (MIT), Jim Mulready (MIT), Pablo Debenedetti (MIT, now at Princeton). And then at the U. Patras: Ioannis Yentekakis, my coauthor of this book Symeon Bebelis, Stelios Neophytides. Their three parallel PhD Theses in the late 80's showed that NEMCA is a general phenomenon not limited to any particular catalyst, solid electrolyte or catalytic reaction. Equally grateful I am to those who followed: Panagiotis Tsiakaras (now at the Univ. of Thessaly), Christos Karavassilis, E. Karasali, my coauthor in this book C. Pliangos, Yi Jiang (now at Dalian), A. Kaloyannis, M. Makri (now at U. Patras), C. Yiokari and my youngest coauthor D. Tsiplakides whose PhD Thesis significantly enriched the NEMCA literature, as did the Theses of Carlos Cavalca (Yale) and of Michel Marwood, E. Varkaraki, J. Nicole and S. Wodiunig, all students of Professor Comninellis at EPFL, who spent time in our lab and showed truly extraordinary abilities. Equally indebted I am to my postdoctoral coworkers P. Petrolekas, O. Mari'na, M. Marwood, C. Pliangos, M. Makri and S. Brosda who did a very nice job in advancing various aspects of electrochemical promotion and in guiding our younger PhD students G. Pitselis, C. Raptis, S. Balomenou, A. Giannikos, I. Bafas, A. Frantzis, D. Polydoros, Th. Bathas, A. Katsaounis, I. Constantinou and D. Archonta.

Sincerest thanks and gratitude are also expressed to Ms. Soula Pilisi, our priceless secretary for more than ten years, who typed this book and always worked diligently for our group in happy and in difficult times.

Costas G. Vayenas

NOMENCLATURE

List of acronyms

AES	Auger Electron Spectroscopy
CSTR	Continuous Stirred Tank Reactor
ECP	Effective Core Potential
EELS	Electron Energy Loss Spectroscopy
EP	Electrochemical Promotion
ESCA	Electron Spectroscopy for Chemical Analysis
G/P	Galvanostat/Potentiostat
HF	Hartree-Fock model
HOMO	Highest Occupied Molecular Orbital
HREELS	High-Resolution Electron Energy Loss Spectroscopy
ICP	In-situ Controlled Promotion
IR	Infra Red spectroscopy
LUMO	Lowest Occupied Molecular Orbital
MSI	Metal-Support Interaction
NEMCA	Non-faradaic Electrochemical Modification of Catalytic Activity
OCM	Oxidative Coupling of Methane
PC	Point Charge
PEEM	Photo Electron Emission Spectroscopy
PPR	Potential Programmed Reduction
QMS	Quadrupole Mass-Spectrometer
RPC	Retarding Potential Curve
SCF	Self-Consistent Field
SEP	Solid Electrolyte Potentiometry
SERS	Surface Enhanced Raman Spectroscopy
SOFC	Solid Oxide Fuel Cell

STP	Standard Temperature and Pressure
STM	Scanning Tunneling Microscopy
TOF	Turnover Frequency
TPD	Temperature Programmed Desorption
UHV	Ultra High Vacuum
UPS	Ultra violet Photoelectron Spectroscopy
XPS	X-ray Photoelectron Spectroscopy
YSZ	Yttria-Stabilized Zirconia
abs	absolute
ac, AC	alternating current
cpd	contact potential difference
dc, DC	direct current
lhs	left hand side
o.c.	open circuit condition, I=0
max	maximum value
pzc	point of zero charge
rhs	right hand side
rls	rate limiting step
she	standard hydrogen electrode
soe	standard oxygen electrode
tpb	three phase boundaries

List of Symbols

Symbol	Meaning	Units
a	denotes adsorbed species	
a_O	oxygen activity	Pa
A	electron acceptor adsorbate	
A	solid electrolyte surface area	m^2
A_E	solid electrolyte-catalyst interface area	m^2
A_G	gas exposed catalytically active surface area	m^2
C	capacitance	F
Ca	Carberry number defined in Eq. (5.52)	
C_d	capacitance of the electrode/electrolyte interface	F
C_i	surface concentration of backspillover species	mol/m^2
$C_{i,max}$	maximum surface concentration of backspillover species	mol/m^2
D	electron donor adsorbate	

D	Debye	$1D=3.36\cdot10^{-30}$ C·m
D_A	diffusivity of key reactant A	m^2/s
D_S	surface diffusivity defined in Eq. (5.6)	m^2/s
D_c	catalyst dispersion defined in Eq. (11.1)	
d	thickness of the effective double layer	m
d	average grain size of electrode material	m
d_M	atomic diameter	m
E	energy	kJ/mol
E_A	activation energy	kJ/mol
E_{act}	catalytic activation energy	kJ/mol
E_{ads}	chemisorption bond strength	kJ/mol
E_b	binding energy	kJ/mol
$E_{b,R}$	binding energy of core level electrons	kJ/mol
$E_{b,EL}$	binding energy of core level electrons of species in the electrolyte	kJ/mol
E_C	denotes energy at bottom of the conduction band	eV
E_d	activation energy of desorption	kJ/mol
E_E	electrostatic energy defined in Eq. (7.21)	kJ/mol
E_F	Fermi level ($=\bar{\mu}$)	eV
E_k	kinetic energy	kJ/mol
E_V	denotes energy at top of valence band	eV
$\tilde{E}$	electric field strength	V/m
e	electron charge	$1.6\cdot10^{-19}$ C
F	Faraday constant	96484.6 C
F_M	contact factor defined in Eq. (3.23)	
F_V	flow rate	cm^3 STP/min
f	frequency	Hz
$f(\theta_{O^{\delta-}})$	rate of consumption of $O^{\delta-}$ on the catalyst surface	$mol/m^2\cdot s$
ΔG	change in Gibbs free enthalpy	
$-\Delta H_0$	initial heat of adsorption	
$-\Delta H$	heat of adsorption	kJ/mol
I	current	A
I_0	exchange current	A
i_0	exchange current density defined in Eq. (4.6)	A/m^2
J	dimensionless current defined in Eqs. (11.23) and (11.32)	
k_A	adsorption equilibrium constant of electron acceptor A	

k_{ad}	oxygen adsorption kinetic constant	
k_b	Boltzmann constant	$1.38 \cdot 10^{-23}$ J/K
k_j	adsorption equilibrium constant of species j	
kL	kiloLangmuir	10^{-3} torr·s
L	surface diffusion length	m
L	thickness of the catalyst film	m
ℓ	distance between the centers of the positive and negative charge in the adsorbed dipole	m
ℓ_{tpb}	three phase boundary length	m
$\ell_{tpb,n}$	normalized three phase boundary length defined in Eq. (5.63)	m^{-1}
N_{AV}	Avogadro number	$6.023 \cdot 10^{23}$ atom/mol
N_G	surface area of catalyst in mol	mol
N_M	surface atom density of the catalyst surface	atom/m^2
N_{tpb}	length of three-phase-boundaries in mol	mol
$N_{tpb,n}$	normalized length of three phase boundaries defined in Eq. (5.63)	mol/m^2
$Na^{\delta+}$	backspillover sodium ion	
$[Na^{\delta+}-\delta+]$	overall neutral backspillover sodium species	
n	number of electrons taking part in the overall reaction	
ñ	unit vector normal to the surface	
O(a)	adsorbed oxygen	
O_O	oxygen ion on regular lattice site	
O^{2-}	oxygen ion	
$O^{\delta-}$	backspillover oxygen ion	
$[O^{\delta-}-\delta+]$	overall neutral backspillover oxygen species	
P	total pressure	Pa
$\tilde{P}$	dipole moment, vector	Cm
P_j	dipole moment of the adsorbate in the adsorbed state	Cm
P^o	initial dipole moment of the adsorbate in the adsorbed state	Cm
PI_i	promotion index defined in Eqs (2.19) and (4.34)	
P	partial pressure	Pa

p_A	partial pressure of electron acceptor A	Pa
p_D	partial pressure of electron donor D	Pa
p_R	partial pressure of reactants	Pa
p_j	partial pressure of species j	Pa
pi_i	differential promotion index defined in Eq. (4.35)	
q_j	charge of species j	C
q_j^+	positive partial charge of the adsorbate	C
q_j^-	negative partial charge of the adsorbate	C
R	gas constant	$8.31441\ JK^{-1}mol^{-1}$
R	index for reference electrode	
R	resistance	Ohm
R_p	polarization resistance	Ohm
r	catalytic rate	mol/s
r_e	electrocatalytic rate	mol/s
r_u	unpromoted catalytic rate	mol/s
Δr	change in catalytic rate	mol/s
r_0	catalytic rate under open circuit conditions, I=0	mol/s
r°	preexponential factor	mol/s
r_0°	preexponential factor under open circuit conditions, I=0	mol/s
ΔS	entropy change	$Jmol^{-1}K^{-1}$
S	selectivity	
$S_j(g)$	gas phase species S_j	
$S_j(ad)$	adsorbed species S_j	
S_0	initial sticking coefficient	
T	temperature	K, °C
T_{ads}	adsorption temperature	K
T_P	peak temperature	K
T_θ	temperature of the isokinetic point	K
TOF	turnover frequency	s^{-1}
t	time	s
U_{WC}	cell potential	V
U°_{WC}	cell potential under open circuit conditions	V
U_{WR}	catalyst potential	V
U°_{WR}	catalyst potential under open circuit conditions	V
ΔU_{WR}	change in catalyst potential	V

$V_O^{\bullet\bullet}$	oxygen vacancy in the lattice	
W	index for working electrode	
wt%	weight percent	
X	conversion	
z	distance	m
Z	impedance	Ohm
Z_{Im}	imaginary part of impedance Z	Ohm
Z_{Re}	real part of impedance Z	Ohm

Greek symbols

Symbol	Meaning	Units
α	NEMCA coefficient defined in Eqs. (4.53)	
α_a	anodic transfer coefficient	
α_c	cathodic transfer coefficient	
α_H	enthalpic coefficient defined in Eq. (2.23)	
β	heating rate	K/s
γ	permanent rate enhancement ratio defined in Eq. (4.59)	
δ	spreading length of the tpb zone on the electrode surface defined in Eq. (5.65)	m
$\delta+$	positive image charge, index for partially positive charged species	
$\delta-$	negative image charge, index for partially negative charged species	
ε_0	dielectric constant, electric permeability of vacuum	$8.85 \cdot 10^{-12}$ $C^2/J \cdot m$
η	overpotential ($=U_{WR} - U^o_{WR} = \Delta U_{WR}$)	V
η_{ac}	activation overpotential	V
η_C	overpotential of the counter electrode C	V
η_{conc}	concentration overpotential	V
η_{ohmic}	ohmic overpotential	V
η_P	promotional effectiveness factor defined in Eq. (11.25)	
θ	coverage	
θ_A	coverage of electron acceptor A	
θ_D	coverage of electron donor D	
θ^*_{Na}	linearized Na coverage scale defined in Eq. (4.25)	
θ_O	oxygen coverage	
θ_i	coverage of promoting or poisoning species i	
θ_j	coverage of species j	

θ_v	coverage of vacant sites	
	Faradaic efficiency defined in Eqs (4.19)	
λ_A	partial charge transfer coefficient of electron acceptor A	
λ_D	partial charge transfer coefficient of electron donor D	
λ_j	partial charge transfer coefficient of species j defined in Eq. (6.49)	
μ	chemical potential	kJ/mol
$\mu_{O_2}(g)$	chemical potential of oxygen in the gas phase	kJ/mol
$\mu_j^\circ(a)$	standard chemical potential of adsorbed species j	kJ/mol
$\mu_j^\circ(g)$	standard chemical potential of specie j in the gas phase (θ_j=0.5)	kJ/mol
$\bar{\mu}$	electrochemical potential of electrons	kJ/mol
$\bar{\mu}_R$	electrochemical potential of electrons in the reference electrode	kJ/mol
$\bar{\mu}_W$	electrochemical potential of electrons in the working catalyst-electrode	kJ/mol
$\bar{\mu}_{O^{2-}}(YSZ)$	electrochemical potential of oxygen ions in YSZ	kJ/mol
$\bar{\mu}_{O^{2-}}(M)$	electrochemical potential of oxygen ions on the gas exposed metal electrode surface	kJ/mol
μ_b	Fermi energy	
ν_n	preexponential factor in the Redhead equation	
ξ	dimensionless distance, z/L	
Π	dimensionless potential ($=FU_{WR}/RT$) or work function ($=\Delta\Phi/k_bT$, more generally $=\Delta\Phi\ell\cos\omega/2dk_bT$) or (Eq. 6.37) dipole moment ($=\alpha e n_m P_i/\varepsilon_0 k_b T$)	
ρ	rate enhancement ratio defined in Eq. (4.33)	
ρ_{MSI}	rate enhancement ratio due to metal-support interactions defined in Eq. (11.2)	
σ	conductivity	S/m
σ_0	conductivity preexponential factor	
τ	NEMCA time constant defined in Eq. (4.32)	
τ_{PR}	promoter lifetime	
υ	scan rate in cyclic voltammetry studies	mV/s
Φ	work function	eV
Φ/e	extraction potential	V
Φ_0	work function of a metal surface at the point of zero charge	eV
Φ_P	Thiele modulus defined in Eq. (11.22)	

$\Delta\Phi$	change in work function defined in Eq. (2.21)	eV
φ	Galvani (inner) potential	V
χ	surface potential	V
Ψ	Volta (outer) potential	V

Subscripts

i	index for promoter species, e.g. $O^{\delta-}$, $Na^{\delta+}$
j	index for adsorbed species
A	electron acceptor adsorbate
C	counter electrode
D	electron donor adsorbate
E	denotes electrode/electrolyte interface
G	denotes electrode/gas interface
MSI	metal-support interaction
P	promoter adsorbate
R	reference electrode
W	working electrode
WC	index for potential or resistance between working and counter electrode
WR	index for potential or resistance between working and reference electrode
o	index for open circuit conditions, I=0

Superscripts

o	preexponential factor or initial dipole moment
*	denotes p_j value at rate maximum

Useful Constants

Symbol	Meaning	Value
e	electron charge	1.602×10^{-19} C
F	Faraday's constant	9.649×10^{5} C mol^{-1}
h	Planck's constant	6.626×10^{-34} J s
k	Boltzmann's constant	1.380×10^{-23} J K^{-1}
m_e	mass of electron	9.110×10^{-31} kg
m_p	mass of proton	1.673×10^{-27} kg
N_{AV}	Avogadro's number	6.022×10^{23} mol^{-1}
ε_0	permittivity of free space	8.854×10^{-12} C^{2}N^{-1}m^{-2}
0 K	absolute zero of temperature	-273.15°C
π	Pi	3.14159265358979...

Useful Unit Conversion Factors

Potential	Length	Volume	Mass	Force	Pressure	Energy
1 V	1 m	1 m^3	1 g	1 N	1 Pa	1 J
1 J C^{-1}	100 cm	1000 dm^3	10^{-3} kg	10^5 dynes	1 N m^{-2}	10^7 ergs
	1000 mm	1000 liters			10^{-5} bar	0.239 cal
	10^6 μm				9.872×10^{-6} atm	6.242×10^{18} eV
	10^9 nm				7.502×10^{-3} mmHg	
	10^{10} Å				7.502×10^{-3} torr	
	10^{12} pm					

CONTENTS

Chapter 1
Introduction, Brief History and Basic Concepts

Chapter 2
Promotion in Heterogeneous Catalysis

Chapter 3
Solid Electrolytes, Catalysis and Spillover

Chapter 4
Electrochemical Promotion of Catalytic Reactions

Chapter 5
Origin of NEMCA

Chapter 6
Rules and Modeling of Promotion

Chapter 7
The Absolute Potential

Chapter 8
Electrochemical Promotion with O^{2-} Conductors

Chapter 9
Electrochemical Promotion with Cationic Conductors

Chapter 10
NEMCA with Aqueous Electrolytes and Inorganic Melts

Chapter 11
Electrochemical Promotion and Metal-Support Interactions

Chapter 12
Practical Applications, Summary and Perspectives

Appendix A
Common Questions about Electrochemical Promotion

Appendix B
Materials and Instrumentation for Starting Electrochemical Promotion Experiments

Appendix C
Main Research Groups

CHAPTER 1

INTRODUCTION, BRIEF HISTORY AND BASIC CONCEPTS

1.1 THE PHENOMENON OF ELECTROCHEMICAL PROMOTION

"I have already said, when engaged in reducing common and voltaic electricity to one standard of measurement, and again when introducing my theory of electrochemical decomposition, that the chemical decomposing action of a current is constant for a constant quantity of electricity, not withstanding the greatest variations in its sources, in its intensity, in the size of the electrodes used, in the nature of the conductors (or non-conductors) through which it is passed, or in other circumstances. "

Michael Faraday, Philosophical Transactions of the Royal Society, 1834

With these lines M. Faraday summarized his pioneering work on "electrochemical decomposition" and formulated his famous law which quantified and essentially defined the science and basic terminology (Figure 1.1) of electrochemistry.[1] It was roughly one and a half century later, in the period 1981-1988,[2-5] that it was found that electrochemistry can be used to activate and precisely tune heterogeneous catalytic processes in a way which appears to defy Faraday's law for reactions with negative Gibb's energy change, ΔG.

At that time it was first reported that the catalytic activity and selectivity of conductive catalysts deposited on solid electrolytes can be altered in a very pronounced, reversible and, to some extent, predictable manner by applying electrical currents or potentials (typically up to ± 2 V) between the catalyst and a second electronic conductor (counter electrode) also deposited

1. ἤλεκτρον, and ὁδός, a way.
2. ἄνω, upwards, and ὁδός, a way.
3. κατά, downwards, and ὁδός, a way.
4. ἤλεκτρον, and λύω, solvo. Noun, electrolyte; verb, electrolyze.
5. ἀνιόν, that which goes up. [Neuter participle.]
6. κατιόν, that which goes down.

Figure 1.1. Basic electrochemical terminology as introduced by Faraday in ref. 1. Reprinted with permission from the Royal Society.

on the solid electrolyte. The electrochemically induced catalytic rate increase has been found to be up to 200 times larger than the catalytic rate without current application, i.e. the effect can be quite large. Furthermore the rate increase was found to be typically 10 to 10^5 times larger than the electrochemical rate of supply of ions to the catalyst. According to Faraday's law the latter equals I/nF, where I is the applied current, n is the charge of the ion being supplied to the catalyst via the solid electrolyte and F is Faraday's constant. Consequently the observed rate increase is strongly non-Faradaic, i.e. it exceeds the steady-state rate increase anticipated from Faraday's law by a factor 10 to 10^5 i.e. the Faradaic efficiency, Λ, of the process is 10 to 10^5. Accordingly this effect has been termed non-Faradaic electrochemical modification of catalytic activity (NEMCA effect). The terms electrochemical promotion (EP), electrochemical promotion of catalysis (EPOC) and in situ controlled promotion (ICP) have been also proposed, as synonyms to the NEMCA effect, for the description of the electrochemical activation of heterogeneous catalysis.

Although the term "non-Faradaic" process has been used for many decades to describe transient electrochemical processes where part of the current is "lost" in charging-discharging of metal-electrolyte interfaces, in all these cases the Faradaic efficiency, Λ, is less than 1 (100%). Furthermore such "non-Faradaic" processes disappear at steady state. Electrochemical promotion (NEMCA) must be very clearly distinguished from such transient "non-Faradaic" processes for two reasons:

a. It does not disappear at steady-state.
b. It corresponds to Faradaic efficiencies well in excess of unity.

By 1988[4] it became obvious that the NEMCA effect, this large apparent violation of Faraday's law, is a general phenomenon not limited to a few oxidation reactions on Ag. Of key importance in understanding NEMCA came the observation that NEMCA is accompanied by potential-controlled variation in the catalyst work function.[6] Its importance was soon recognized by leading electrochemists,[7, 8] surface scientists[9] and catalysis researchers.[10] Today the NEMCA effect has been studied already for more than 60 catalytic systems and does not seem to be limited to any specific type of catalytic reaction, metal catalyst or solid electrolyte, particularly in view of

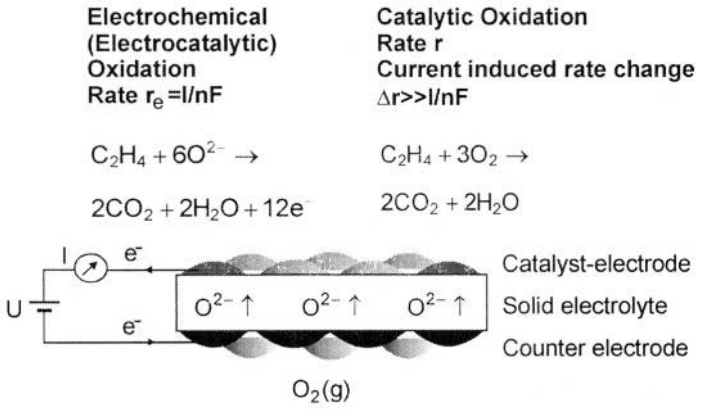

Figure 1.2. Experimental setup used in NEMCA experiments.

recent demonstrations of NEMCA using aqueous electrolyte solutions.[11, 12] Practically all new text books on Electrochemistry[13, 14] or Catalysis[15] contain a section on NEMCA or electrochemical promotion.

There is a wide variety of solid electrolytes and, depending on their composition, these anionic, cationic or mixed conducting materials exhibit substantial ionic conductivity at temperatures between 25 and 1000°C. Within this very broad temperature range, which covers practically all heterogeneous catalytic reactions, solid electrolytes can be used to induce the NEMCA effect and thus activate heterogeneous catalytic reactions. As will become apparent throughout this book they behave, under the influence of the applied potential, as active catalyst supports by becoming reversible in situ promoter donors or poison acceptors for the catalytically active metal surface.

In a typical NEMCA experiment the reactants (e.g. C_2H_4+O_2) are co-fed over a conductive catalyst which also serves, at the same time, as the working electrode in a solid electrolyte cell:

gaseous reactants	catalyst - working electrode	solid electrolyte	counter electrode	auxiliary gas
(e.g.C_2H_4+O_2, H_2+O_2)	(e.g. Pt, Rh, Ag, IrO_2)	(e.g. ZrO_2-Y_2O_3 (YSZ) (O^{2-} conductor), β″-Al_2O_3 (Na^+ conductor))	(e.g. Pt)	(e.g. O_2)

The experimental setup is depicted schematically in Figure 1.2. Upon varying the potential of the catalyst/working electrode the cell current, I, is also varied. The latter is related to the electrocatalytic (net-charge transfer) reaction rate r_e via r_e=I/nF, as well known from Faraday's law. The electrocatalytic reactions taking place at the catalyst/solid electrolyte/gas three-phase-boundaries (tpb), are:

$$O^{2-}(YSZ) \rightarrow O(a) + 2e^- \qquad (1.1)$$

$$C_2H_4 + 6O^{2-}(YSZ) \rightarrow 2CO_2 + 2H_2O + 12e^- \quad (1.2)$$

for the case of YSZ (O^{2-} conductor) and

$$Na^+(\beta''\text{-}Al_2O_3) + e^- \rightarrow Na(a) \quad (1.3)$$

for the case of β''-Al_2O_3 (Na^+ conductor), where O(a) and Na(a) denote atomic oxygen and Na adsorbed on the catalyst surface. That the current, and thus the electrocatalytic rate r_e, changes with changing potential, is well known and well studied in electrochemistry. What was not known until recently, and is somehow surprising at a first glance, is that the *catalytic rate,* r, of the catalytic (no net charge-transfer) reaction:

$$C_2H_4 + 3O_2 \rightarrow 2CO_2 + 2H_2O \quad (1.4)$$

taking place on the metal catalyst/working electrode will also change at the same time and in fact that its change Δr can exceed $\Delta r_e = I/nF$ by several (1 to 5) orders of magnitude. Therefore each ion supplied by the solid electrolyte to the catalyst can cause many (up to 10^5) gaseous molecules to react catalytically. Thus, while in the case of YSZ solid electrolyte one might expect that the extra supply of I/2F O^{2-} ions to the catalyst would cause a

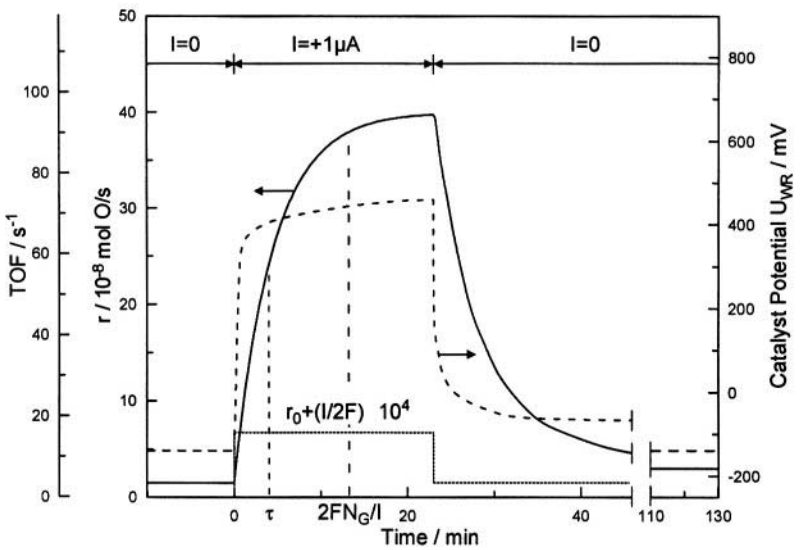

Figure 1.3. Rate and catalyst potential response to step changes in applied current during C_2H_4 oxidation on Pt deposited on YSZ, an O^{2-} conductor. T = 370°C, p_{O_2}=4.6 kPa, $p_{C_2H_4}$=0.36 kPa. The catalytic rate increase, Δr, is 25 times larger than the rate before current application, r_0, and 74000 times larger than the rate I/2F,[16] of O^{2-} supply to the catalyst. N_G is the Pt catalyst surface area, in mol Pt, and TOF is the catalytic turnover frequency (mol O reacting per surface Pt mol per s). Reprinted with permission from Academic Press.

catalytic rate increase, Δr, up to I/2F (if all O^{2-} supplied to the catalyst were reacting with C_2H_4 forming CO_2 and H_2O), one finds that Δr can be several orders of magnitude larger. An example is shown in Figure 1.3.[16]

"The seminal part of this contribution is that there is a non-Faradaic catalysis, that the catalytic reaction of ethylene with oxygen occurs as well and that it depends on the potential difference across the electrode"
J.O.M. Bockris, Electrochimica Acta, 1994[7]

Despite the surprise caused by the first literature reports of such large non-Faradaic rate enhancements, often accompanied by large variations in product selectivity, in retrospect the existence of the NEMCA effect can be easily rationalized by combination of simple electrochemical and catalytic principles.

As shown schematically in Figure 1.4, ions arriving under the influence of the applied current or potential at the three-phase boundaries catalyst/solid electrolyte/gas form there adsorbed species (O(a), Na(a)) which have only three possibilities:

(a) Desorption to the gas phase
(b) Reaction with a coadsorbed species
(c) Migration over the entire gas-exposed catalyst electrode surface (spillover) followed by possible desorption or reaction with coadsorbed species

It is clear that in case (a) the rate, r, of the catalytic reaction (e.g. CO oxidation) will not be affected while in case (b) the rate increase, Δr, will at most equal I/nF (e.g. direct reaction of O^{2-} with CO). In case (c), however, the new species introduced electrochemically onto the catalyst surface will interact with coadsorbed reactants and will change the catalytic properties of the catalyst surface in an a priori unpredictable manner, which is nevertheless not subject to Faraday's law. Thus in cases (a) and (b) there will be no NEMCA but in case (c) it is entirely logical to anticipate it. Even in case (b) one may anticipate NEMCA, if the product remains on the surface and has some catalytic or promotional properties.

The electrochemist reader will realize that cases (a) and (b) usually correspond to small overpotential, i.e. small change in catalyst-electrode potential with changing current. It is thus not accidental that NEMCA appears only under conditions of significant (a few hundred mV) catalyst-electrode overpotential ΔU_{WR}. This, in solid state electrochemistry, usually implies moderate (below 600°C) temperature. Under such conditions experiment has shown that the work function of the gas exposed, i.e. catalytically active, electrode surface changes significantly and up to $e\Delta U_{WR}$ with changing potential, manifesting the migration of ionic species from the solid electrolyte onto the catalyst surface.

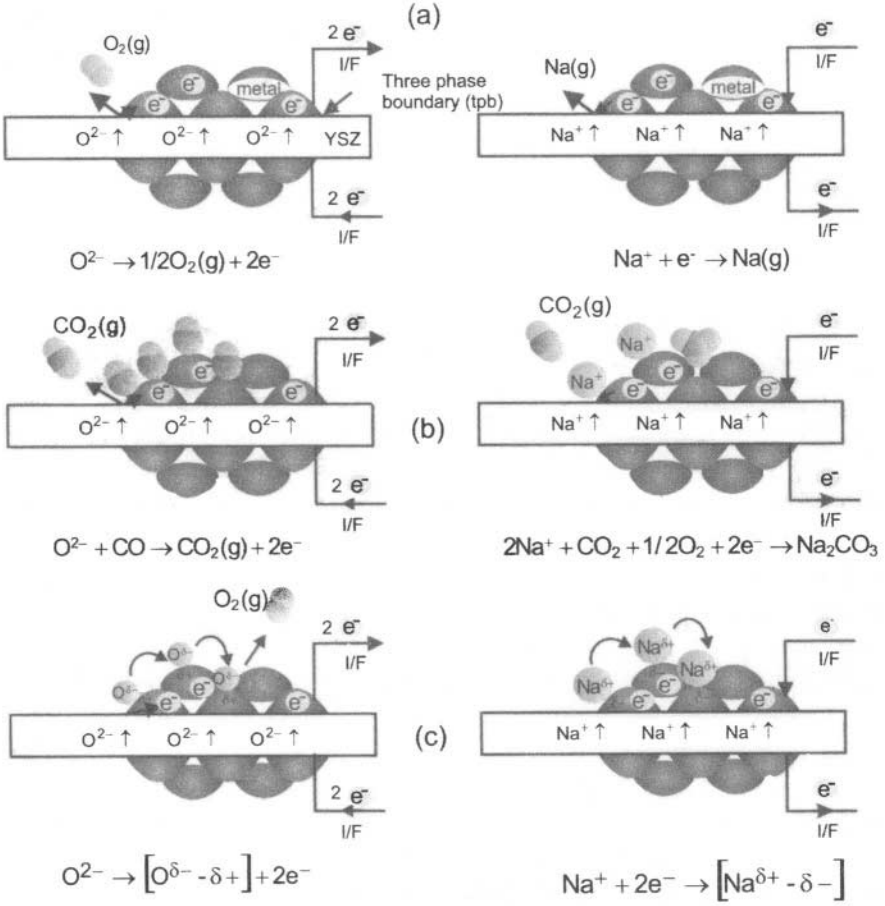

Figure 1.4. Possible pathways of O(a) and Na(a) adsorbed species created at the three-phase boundaries via application of electric current: (a) Desorption; (b) Reaction; (c) Backspillover.

Thus, as will be shown in this book, the effect of electrochemical promotion (EP), or NEMCA, or *in situ* controlled promotion (ICP), is due to an electrochemically induced and controlled migration (backspillover) of ions from the solid electrolyte onto the gas-exposed, that is, catalytically active, surface of metal electrodes. It is these ions which, accompanied by their compensating (screening) charge in the metal, form an effective electrochemical double layer on the gas-exposed catalyst surface (Fig. 1.5), change its work function and affect the catalytic phenomena taking place there in a very pronounced, reversible, and controlled manner.

Electrochemical promotion (NEMCA) bears several similarities with electrolysis in the sense that potential application controls the rate of a process. This is shown in Fig. 1.6, prepared by N. Anastasijevic, a member of the team which made the first NEMCA observations with aqueous

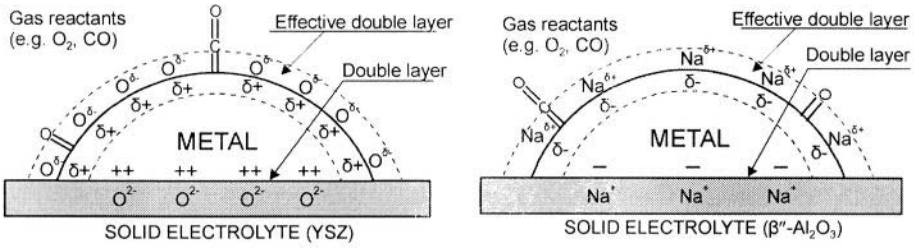

Figure 1.5. Schematic representation of a metal electrode deposited on a O^{2-}-conducting (left) and on a Na^+-conducting (right) solid electrolyte, showing the location of the metal-electrolyte double layer and of the effective double layer created at the metal/gas interface due to potential-controlled ion migration (backspillover).

solutions.[11] But while in electrolysis or fuel cell operation potential controls an electrocatalytic (net charge transfer) process the rate of which obeys Faraday's law, in the case of NEMCA, potential also controls the rate of a catalytic (no net charge transfer) process the rate of which is not subject to Faraday's law. Which law(s) govern the dependence of this catalytic rate enhancement on potential? How can we utilize this new phenomenon? These are the main subjects of the present book.

Wagner was first to propose the use of solid electrolytes to measure *in situ* the thermodynamic activity of oxygen on metal catalysts.[17] This led to the technique of solid electrolyte potentiometry.[18] Huggins, Mason and Gür were the first to use solid electrolyte cells to carry out electrocatalytic reactions such as NO decomposition.[19, 20] The use of solid electrolyte cells for "chemical cogeneration", that is, for the simultaneous production of electrical power and industrial chemicals, was first demonstrated in 1980.[21] The first "non-Faradaic" enhancement in heterogeneous catalysis was reported in 1981 for the case of ethylene epoxidation on Ag electrodes,[2, 3] but it was only

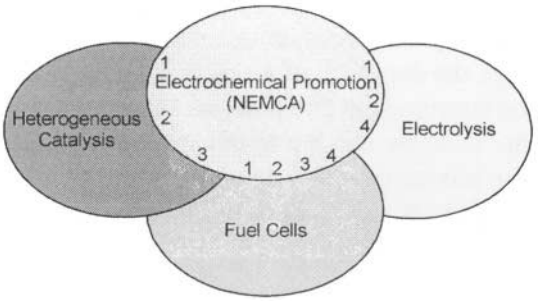

Figure 1.6. Common features of Heterogeneous Catalysis, Fuel Cell operation, Electrolysis and Electrochemical Promotion: 1. Solid state catalyst, 2. Adsorption, 3. $\Delta G < 0$, 4. Yield control via DC current or voltage application (Adapted from N. A. Anastasijevic).

in 1988 that it was realized that electrochemical promotion is a general phenomenon.[4-6] In addition to the group which first reported the electrochemical promotion effect,[2-6] the groups of Sobyanin,[22, 23] Comninellis,[24] Lambert,[25, 26] Haller,[27, 28] Anastasijevic,[29] Stoukides,[30] Smotkin,[31] Imbihl,[32] Pacchioni,[33] Bjerrum,[34] Lee,[35] Metcalfe,[36] Janek[37] and Barbier[38] have also made significant contributions in this area.

The importance of NEMCA in electrochemistry, surface science and heterogeneous catalysis has been discussed by Bockris,[7] Wieckowski,[8] Pritchard[9] and Haber[10] respectively. Electrochemical promotion, or NEMCA, has found its position in recent years as a separate section in practically all new general or graduate level textbooks on electrochemistry[13, 14] and catalysis.[15]

Detailed and shorter[39-45] reviews of the electrochemical promotion literature prior to 1996 have been published, mainly addressed either to the catalytic or to the electrochemical community. Earlier applications of solid electrolytes in catalysis, including solid electrolyte potentiometry and electrocatalysis have been reviewed previously. The present book is the first on the electrochemical activation of catalytic reactions and is addressed both to the electrochemical and catalytic communities. We stress both the electrochemical and catalytic aspects of electrochemical promotion and hope that the text will be found useful and easy to follow by all readers, including those not frequently using electrochemical, catalytic and surface science methodology and terminology.

1.2 BASIC CONCEPTS AND TERMINOLOGY

The reader must have already identified some of the basic concepts which play a key role in understanding the electrochemical activation of heterogeneous catalysis: catalysis, electrocatalysis, promotion, electrochemical promotion, spillover, backspillover. It is therefore quite important to define these terms unambiguously so that their meaning is clearly determined throughout this book.

Catalysis: By definition, a catalyst is a substance (in this book a solid) which can accelerate the approach of a reactive gas mixture to equilibrium, without itself being consumed in this process.

Throughout the book we use the terms catalysis, catalyst and catalytic reaction referring to processes which do *not* involve any *net* charge transfer, such as e.g. the oxidation of CO on Pt or the ammonia synthesis on Fe:

$$CO(g) + 1/2\ O_2(g) \xrightarrow{Pt} CO_2(g) \tag{1.5}$$

$$N_2(g) + 3H_2(g) \xrightarrow{Fe} 2NH_3(g) \tag{1.6}$$

Most industrial catalysts are supported, i.e. distributed in fine form (1-10 nm) on the surface of a porous, high surface area and usually inert support (e.g. SiO_2, γ-Al_2O_3, TiO_2).[15] In this book, however, we will deal quite often with catalysts in the form of a porous film deposited on a solid electrolyte.

Electrocatalysis: Again by definition, an electrocatalyst is a solid, in fact an electrode, which can accelerate a process involving a *net charge transfer,* such as e.g. the anodic oxidation of H_2 or the cathodic reduction of O_2 in solid electrolyte cells utilizing YSZ:

$$H_2(g) + O^{2-}(YSZ) \xrightarrow{Pt} H_2O(g) + 2e^- \tag{1.7}$$

$$1/2O_2(g) + 2e^- \xrightarrow{Pt} O^{2-}(YSZ) \tag{1.8}$$

Most of the electrocatalysts we will discuss in this book are in the form of porous metal films deposited on solid electrolytes. The *same* film will be also used as a *catalyst* by cofeeding reactants (e.g. C_2H_4 plus O_2) over it. This idea of using the *same conductive film as a catalyst and simultaneously as an electrocatalyst* led to the discovery of the phenomenon of electrochemical promotion.

Promotion: We use the term *promotion,* or classical promotion, to denote the action of one or more substances, the promoter or promoters, which when added in relatively small quantities to a catalyst, improves the activity, selectivity or useful lifetime of the catalyst. In general a promoter may either augment a desired reaction or suppress an undesired one. For example, K or K_2O is a promoter of Fe for the synthesis of ammonia. A promoter is not, in general, consumed during a catalytic reaction. If it does get consumed, however, as is often the case in electrochemical promotion utilizing O^{2-} conducting solid electrolytes, then we will refer to this substance as a *sacrificial promoter.*

The opposite of a promoter is a poison, i.e. a substance which hinders the performance of a catalyst.

When a promoter is added continuously to the reactive gaseous mixture, as e.g. in the case of a few ppm $C_2H_2Cl_2$ addition to C_2H_4 and O_2 during C_2H_4 epoxidation on Ag catalysts, this promoter ($C_2H_2Cl_2$) is also sometimes referred to as a moderator.

Promoters are usually added to a catalyst during catalyst preparation (classical or chemical promotion). Thus if they get somehow lost (evaporation) or deactivated during prolonged catalyst operation, this leads to significant catalyst deterioration. Their concentration cannot be controlled in situ, i.e. during catalyst operation. As we will see in this book one of the most important advantages of electrochemical promotion is that it permits direct in situ control of the amount of the promoter on the catalyst surface.

The concept of a promoter can also be extended to the case of substances which enhance the performance of an electrocatalyst by accelerating the rate of an electrocatalytic reaction. This can be quite important for the performance, e.g., of low temperature (polymer electrolyte membrane, PEM) fuel cells where poisoning of the anodic Pt electrocatalyst (reaction 1.7) by trace amounts of strongly adsorbed CO poses a serious problem. Such a promoter which when added to the Pt electrocatalyst would accelerate the desired reaction (1.5 or 1.7) could be termed an electrocatalytic promoter, or electropromoter, but this concept will not be dealt with in the present book, where the term promoter will always be used for substances which enhance the performance of a *catalyst.*

Electrochemical promotion or *NEMCA* is the main concept discussed in this book whereby application of a small current ($1\text{-}10^4$ $\mu A/cm^2$) or potential (±2 V) to a catalyst, also serving as an electrode (electrocatalyst) in a solid electrolyte cell, enhances its *catalytic performance.* The phenomenology, origin and potential practical applications of electrochemical promotion, as well as its similarities and differences with classical promotion and metal-support interactions, is the main subject of this book.

Spillover-backspillover: These terms originate from the catalysis and surface science literature[15] and denote migration of one or more species between a catalyst and a support. Traditionally the term spillover refers to a migration *from* the dispersed catalyst (e.g. Pt) *to* the support (e.g. TiO_2), while the term *backspillover* denotes migration (e.g. of H or O atoms) *from* the support *to* the metal catalyst. Spillover-backspillover phenomena have been invoked, not always correctly, to explain various phenomena in heterogeneous catalysis. It is only recently that spillover and backspillover have been documented and studied, using in situ surface spectroscopic techniques. They play an important role in several aspects of heterogeneous catalysis. They certainly play a key role in electrochemical promotion, as documented by several surface spectroscopic techniques including XPS, UPS and STM which have shown clearly an electrochemically controlled reversible migration of species (e.g. O^{2-}, Na^+) between solid electrolytes and metals deposited on them. In accordance to the classical catalytic-surface science literature, we use the term *backspillover* to denote migration *from* the support (solid electrolyte) *to* the metal (catalyst) and the term spillover to denote migration in the opposite direction, i.e. from the metal electrode surface to the solid electrolyte.

1.3 STRUCTURE OF THIS BOOK

Due to the interdisciplinary nature of electrochemical promotion, which involves elementary but important concepts from at least five different fields (catalysis, surface science, electrochemistry, solid state ionics, chemical reaction engineering) we have structured the book in such a way to make it possible for readers from all the above fields to follow the entire book.

Thus Chapter 2 discusses the phenomenology and basic concepts of classical promotion, a subject quite familiar to catalysis and surface science researchers and graduate students, at a level which should be comfortable to electrochemists, solid state ionics and chemical reaction engineering researchers.

Chapter 3 discusses solid electrolytes and some of their early applications in fuel cells and catalysis. This material is quite familiar to the solid state ionics community but may be helpful to surface scientists, aqueous electrochemists and chemical reaction engineers.

The reader already familiar with some aspects of electrochemical promotion may want to jump directly to Chapters 4 and 5 which are the heart of this book. Chapter 4 epitomizes the phenomenology of NEMCA, Chapter 5 discusses its origin on the basis of a plethora of surface science and electrochemical techniques including ab initio quantum mechanical calculations. In Chapter 6 rigorous rules and a rigorous model are introduced for the first time both for electrochemical and for classical promotion. The kinetic model, which provides an excellent qualitative fit to the promotional rules and to the electrochemical and classical promotion data, is based on a simple concept: Electrochemical and classical promotion is catalysis in presence of a controllable double layer.

Chapter 7 introduces the concept of absolute electrode potential in solid state electrochemistry. This concept has some important implications not only in solid state electrochemistry but also, potentially, in heterogeneous catalysis of supported catalysts.

Chapters 8 to 10 discuss the detailed phenomenology of electrochemical promotion for the more than 60 catalytic reactions studied so far.

Chapter 11 analyzes the recently discovered mechanistic equivalence of electrochemical promotion and metal-support interactions on ionic and mixed conducting supports containing ZrO_2, CeO_2 or TiO_2. The analysis focuses on the functional identity and operational differences of promotion, electrochemical promotion and metal support interactions.

Chapter 12 discusses recent advances aiming at practical applications of electrochemical promotion and summarizes in perspective the main findings and future challenges.

In Appendix A the reader may want to test his understanding of the book: Thirty-three important questions regarding electrochemical promotion (collected during the last ten years in more than 100 presentations by the authors in conferences and seminars) are posed and answered.

Appendix B answers the basic question: What materials and instruments are needed to start electrochemical promotion experiments?

Appendix C provides a short profile of the main research groups working already in this area.

REFERENCES

1. M. Faraday, Experimental Researches in Electricity. Seventh Series.§ 11. On Electrochemical Decomposition, *Philosophical Transactions of the Royal Society,* 77-122 (1834).
2. M. Stoukides, and C.G. Vayenas, The effect of Electrochemical Oxygen Pumping on the Rate and Selectivity of Ethylene Oxidation on Polycrystalline Silver, *J. Catal.* **70**, 137-146(1981).
3. M. Stoukides, and C.G. Vayenas, The effect of electrochemical oxygen pumping on the Rate and Selectivity of Propylene Oxidation on Silver in a Solid Electrolyte Cell, *J. Electrochem. Soc.* **131**(4), 839-845 (1984).
4. C.G. Vayenas, S. Bebelis, and S. Neophytides, Non-Faradaic Electrochemical Modification of Catalytic Activity, *J. Phys. Chem.* **92**, 5083-5085 (1988).
5. I.V. Yentekakis, and C.G. Vayenas, The Effect of Electrochemical O^{2-} Pumping on the Steady State and Oscillatory Behavior of CO oxidation on Polycrystalline Pt, *J. Catal.* **111**, 170-188(1988).
6. C.G. Vayenas, S. Bebelis, and S. Ladas, Dependence of Catalytic Rates on Catalyst Work Function, *Nature* **343**, 625-627 (1990).
7. J.O' M. Bockris, and Z.S. Minevski, Electrocatalysis: Past, present and future, *Electrochim. Acta* **39**(11/12), 1471-1479 (1994).
8. G.-Q. Lu, and A. Wieckowski, Heterogeneous Electrocatalysis: A Core field of Interfacial Science, *Current opinion in Colloid and Interface Science* **5**, 95 (2000).
9. J. Pritchard, Electrochemical Promotion, *Nature* **343**, 592 (1990).
10. B. Grzybowska-Swierkosz, and J. Haber, *Annual Reports on the Progress of Chemistry,* The Royal Society of Chemistry, Cambridge (1994), p. 395.
11. H. Baltruschat, N.A. Anastasijevic, M. Beltowska-Brzezinska, G. Hambitzer, and J. Heitbaum, Electrochemical detection of organic gases: The development of a formaldehyde sensor, *Ber. Buns. Phys. Chem.* **94**, 996-1000 (1990).
12. S. Neophytides, D. Tsiplakides, P. Stonehart, M.M. Jaksic, and C.G. Vayenas, Non-Faradaic Electrochemical enhancement of H_2 oxidation in alkaline solutions, *J. Phys. Chem.* **100**, 14803-14814 (1996).
13. J.O' M. Bockris, A.K.M. Reddy, and M. Gamboa-Aldeco, *Modern Electrochemistry,* Kluwer Academic/Plenum Publishers (2000).
14. C.H. Hamann, A. Hamnett, and W. Vielstich, *Electrochemistry,* Wiley-VCH, Weinheim (1998).
15. G. Ertl, H. Knötzinger, and J. Weitcamp, eds., *Handbook of Catalysis,* VCH Publishers, Weinheim (1997).
16. S. Bebelis, and C.G. Vayenas, Non-Faradaic Electrochemical Modification of Catalytic Activity: 1. The case of Ethylene Oxidation on Pt, *J. Catal.* **118**, 125-146 (1989).
17. C. Wagner, Adsorbed Atomic Species as Intermediates in Heterogeneous Catalysis, in *Adv. Catal.,* (1970), pp. 323-381.
18. C.G. Vayenas, and H.M. Saltsburg, Chemistry at Catalyst Surfaces: The Oxidation of SO_2 on noble metals, *J. Catal.* **57**, 296-314 (1979).
19. S. Pancharatnam, R.A. Huggins, and D.M. Mason, Catalytic Decomposition of Nitric Oxide on Zirconia by Electrolytic Removal of Oxygen, *J. Electrochem. Soc.* **122**(7), 869-875(1975).
20. T.M. Gür, and R.A. Huggins, Decomposition of Nitric Oxide on Zirconia in a Solid-state electrochemical cell, *J. Electrochem. Soc.* **126**(6), 1067-1075 (1979).
21. C.G. Vayenas, and R.D. Fair, Cogeneration of Electric Energy and Nitric Oxide, Science **208**, 593-595 (1980).

22. T.I. Politova, V.A. Sobyanin, and V.D. Belyaev, Ethylene hydrogenation in electrochemical cell with solid proton-conducting electrolyte, *Reaction Kinetics and Catalysis Letters* **41**(2), 321-326 (1990).
23. O.A. Mar'ina, and V.A. Sobyanin, The effect of electrochemical oxygen pumping on the rate of CO oxidation on Au electrode-catalyst, *Catal. Lett.* **13**, 61-70 (1992).
24. E. Varkaraki, J. Nicole, E. Plattner, C. Comninellis, and C.G. Vayenas, Electrochemical Promotion of IrO_2 catalyst for the gas phase combustion of ethylene, *J. Appl. Electrochem.* **25**, 978-981 (1995).
25. I. Harkness, and R.M. Lambert, Electrochemical Promotion of the NO + Ethylene Reaction over Platinum, *J. Catal.* **152**, 211-214 (1995).
26. I.R. Harkness, C. Hardacre, R.M. Lambert, I.V. Yentekakis, and C.G. Vayenas, Ethylene oxidation over Platinum: In situ electrochemical promotion using β''-Al_2O_3 and studies with a Pt(l 1 l)/Na model catalyst, *J. Catal.* **160**, 19-26 (1996).
27. C. Cavalca, G. Larsen, C.G. Vayenas, and G. Haller, Electrochemical Modification of CH_3OH oxidation selectivity and activity on a Pt single-pellet catalytic reactor, *J. Phys. Chem.* **97**, 6115-6119(1993).
28. C.A. Cavalca, and G.L. Haller, Solid Electrolytes as Active Catalyst Supports: Electrochemical Modification of Benzene Hydrogenation Activity on $Pt/\beta''(Na)Al_2O_3$, *J. Catal.* **177**, 389-395(1998).
29. N.A. Anastasijevic, E. Hillrichs, K. Lohrberg, and G. Ungar, US Patent **5**,637,206 (1997).
30. P.H. Chiang, D. Eng, and M. Stoukides, Solid electrolyte aided direct coupling of methane, *J. Catal.* **139**, 683-687 (1993).
31. L. Ploense, M. Salazar, B. Gurau, and E.S. Smotkin, Proton Spillover Promoted Isomerization of n-Butylenes on Pt-black Cathodes/Nafion 117, *JACS* **119**, 11550-11551(1997).
32. J. Poppe, S. Voelkening, A. Schaak, E. Schuetz, J. Janek, and R. Imbihl, Electrochemical promotion of catalytic CO oxidation on Pt/YSZ catalysts under low pressure conditions, *Phys. Chem. Chem. Phys.* **1**, 5241-5249 (1999).
33. G. Pacchioni, J.R. Lomas, and F. Illas, Electric field effects in heterogeneous catalysis, *Molecular Catalysis A: Chemical* **119**, 263-273 (1997).
34. I.M. Petrushina, V.A. Bandur, F. Cappeln, and N.J. Bjerrum, Electrochemical Promotion of Sulfur Dioxide Catalytic Oxidation, *J. Electrochem. Soc.* **147(8)**, 3010-3013(2000).
35. J.K. Hong, I.-H. Oh, S.-A. Hong, and W.Y. Lee, Electrochemical Oxidation of Methanol over a Silver Electrode Deposited on Yttria-Stabilized Zirconia Electrolyte, *J. Catal.* **163**, 95-105 (1996).
36. D.A. Emery, P.H. Middleton, and I.S. Metcalfe, The effect of electrochemical current pumping on the work function of solid electrolyte supported catalysts, *Surf. Sci.* **405**, 308-315(1998).
37. J. Janek, M. Rohnke, B. Luerssen, and R. Imbihl, Promotion of catalytic reactions by electrochemical polarization, *Phys. Chem. Chem. Phys.* **2**, 1935-1941 (2000).
38. E. Lamy-Pitara, S.E. Mouahid, and J. Barbier, Effect of anions on catalytic and electrocatalytic hydrogenations and on the electrocatalytic oxidation and evolution of hydrogen on platinum, *Electrochim. Acta* **45**, 4299-4308 (2000).
39. C.G. Vayenas, S. Bebelis, I.V. Yentekakis, and H.-G. Lintz, Non-Faradaic Electrochemical Modification of Catalytic Activity: A Status Report (Review Paper), *Catalysis Today* **11**(3), 303-442 (1992).

40. C.G. Vayenas, I.V. Yentekakis, S.I. Bebelis, and S.G. Neophytides, In situ Controlled Promotion of Catalyst Surfaces via Solid Electrolytes: The NEMCA effect, *Ber. Buns. Phys. Chem.* **99**(11), 1393-1401 (1995).
41. C.G. Vayenas, M.M. Jaksic, S. Bebelis, and S.G. Neophytides, The Electrochemical Activation of Catalysis, in *Modern Aspects of Electrochemistry,* J.O.M. Bockris, B.E. Conway, and R.E. White, eds., Kluwer Academic/Plenum Publishers, New York (1996), pp. 57-202.
42. C.G. Vayenas, and S. Neophytides, Electrochemical Activation of Catalysis: In situ controlled promotion of catalyst surfaces, in *Catalysis-Special periodical Report,* Royal Society of Chemistry, Cambridge (1996), pp. 199-253.
43. C.G. Vayenas, S. Bebelis, I.V. Yentekakis, and S. Neophytides, Electrocatalysis and Electrochemical Reactors, in *CRC Handbook on Solid State Ionics,* P.J. Gellings, and H.J.M. Bouwmeester, eds., *CRC* Press, Inc., Boca Raton (1997), pp. 445-480.
44. C.G. Vayenas, R.M. Lambert, S. Ladas, S. Bebelis, S. Neophytides, M.S. Tikhov, N.C. Filkin, M. Makri, D. Tsiplakides, C. Cavalca, and K. Besocke, Direct STM, XPS and TPD observation of spillover phenomena over mm distances on metal catalyst films interfaced with solid electrolytes, *Stud. Surf. Sci. Catal.* **112**, 39-47 (1997).
45. C.G. Vayenas, and I.V. Yentekakis, Electrochemical Modification of Catalytic Activity, in *Handbook of Catalysis,* G. Ertl, H. Knötzinger, and J. Weitcamp, eds., VCH Publishers, Weinheim (1997), pp. 1310-1338.

CHAPTER 2

PROMOTION IN HETEROGENEOUS CATALYSIS

2.1 INTRODUCTION

Promoters play a key role in heterogeneous catalysis.[1] Their use is of paramount importance in the design of successful commercial catalysts.[2,3] Broadly speaking they can be divided into *structural promoters* and *electronic promoters.* In the former case they enhance and stabilize the dispersion of the active phase on the catalyst support. In the latter case they enhance the catalytic properties of the active phase itself. This stems from their ability to modify the chemisorptive properties of the catalyst surface and to significantly affect the chemisorptive bond strength of reactants and intermediates. At the molecular level this is the result of direct ("through the vacuum") and indirect ("through the metal") interactions.[1,4] The term "through the vacuum" denotes direct electrostatic, Stark type, attractive or repulsive, interactions between the adsorbed reactants and the local electric field created by the coadsorbed promoter. The term "through the metal interactions" refers to changes in the binding state of adsorbed reactants due to promoter-induced redistribution of electrons near the Fermi level of the metal.

A classical example of promotion is the use of alkalis (K) on Fe for the ammonia synthesis reaction. Coadsorbed potassium (in the form of K_2O) significantly enhances the dissociative adsorption of N_2 on the Fe surface, which is the crucial and rate limiting step for the ammonia synthesis[5] (Fig. 2.1).

There is a very rich literature and a comprehensive book[6] on the role of promoters in heterogeneous catalysis. The vast majority of studies refers to the adsorption of promoters and to the effect of promoters on the chemisorptive state of coadsorbed species on well characterized single crystal surfaces. A

nice example[7] is shown in Fig. 2.2 for the case of coadsorption of CO and K on Pt(100). Increasing K dosing on the Pt(100) surface causes CO to desorb at higher temperatures, i.e., it strengthens the Pt-carbon monoxide chemisorptive bond. At higher K coverages a new chemisorption state appears corresponding to dissociatively chemisorbed CO. The Pt- carbon bond has been strengthened to the point that the CO bond has been broken.

In recent years both rigorous and semi-rigorous quantum mechanical calculations have been used to enhance our understanding of chemisorption and promotion on metal clusters and single crystal surfaces.[8-13]

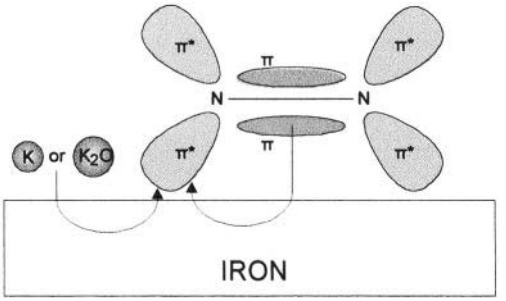

Figure 2.1. Spatial distribution of the main orbitals of N_2 involved in molecular chemisorption on iron promoted by potassium (K or K_2O). Arrows indicate the direction of transfer of electron density.[5]

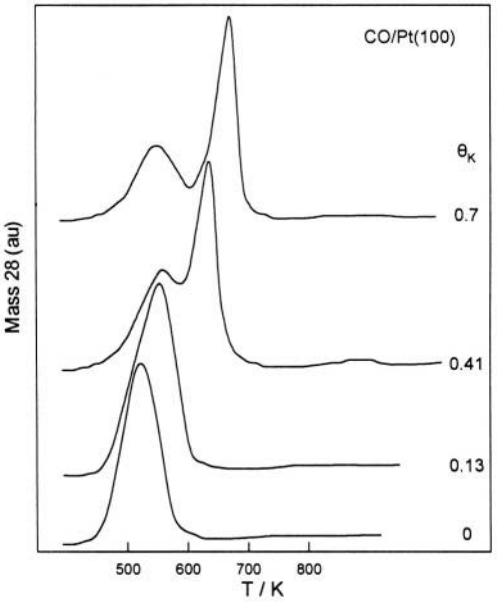

Figure 2.2. Thermal desorption spectra of carbon monoxide, measured mass spectrometically at mass 28 (atomic units, a.u.), on a platinum (100) surface upon which potassium has been pre-adsorbed to a surface coverage of θ_K.[7] Reprinted with permission from Elsevier Science.

Significant progress has and is being made but it will certainly take many years before such rigorous theoretical approaches can be used to compute promoted reaction rates or to select actual promoters for practical applications. There is little experimental or theoretical information regarding polycrystalline surfaces and about the effect of promoters on catalytic rates. Part of this is due to the experimental difficulty of dosing catalyst surfaces with promoters under realistic atmospheric or high pressure catalyst operating conditions. One of the most attractive features of electrochemical promotion is that it allows for controlled and reversible in situ introduction of promoters on catalyst surfaces under catalytic operating conditions, and thus allows for a detailed study of their kinetic effects on catalyst performance. Numerous cases will be presented in this book.

2.1.1 Catalysis, Chemical and Electrochemical Promotion: An Example

The strength and interrelation of catalysis, classical promotion and electrochemical promotion is illustrated in Fig. 2.3. The reaction under consideration[14] is the reduction of NO by CO in presence of O_2. This is a complex reaction system but of great technological importance for the development of efficient catalytic converters able to treat the exhaust gases of lean burn and Diesel engines.

The main reactions are:

$$2CO+2NO \rightarrow N_2+2CO_2 \tag{2.1}$$

$$CO+2NO \rightarrow N_2O+CO_2 \tag{2.2}$$

$$CO+1/2O_2 \rightarrow CO_2 \tag{2.3}$$

The desired product is N_2 (vs N_2O) and a good catalyst must not only catalyze NO reduction at as low a temperature as possible (preferably below 200°C) but must also exhibit good selectivity to N_2. The latter, S_{N_2}, is defined as:

$$S_{N_2} = r_{N_2} / (r_{N_2} + r_{N_2O}) \tag{2.4}$$

Without a catalyst there is no N_2 and CO_2 production below 600°C.[14] When using a polycrystalline Rh film of mass m_{Rh}=2 mg and surface area $N_{Rh}=10^{-7}$ mol one obtains the curve labeled "catalysis" in Fig. 2.3. It is worth pointing out that Rh is the best known noble metal catalyst for NO reduction due to its ability to chemisorb NO, to a large extent dissociatively. This Rh film is deposited on YSZ (Y_2O_3-stabilized-ZrO_2), an O^{2-} conductor, but the

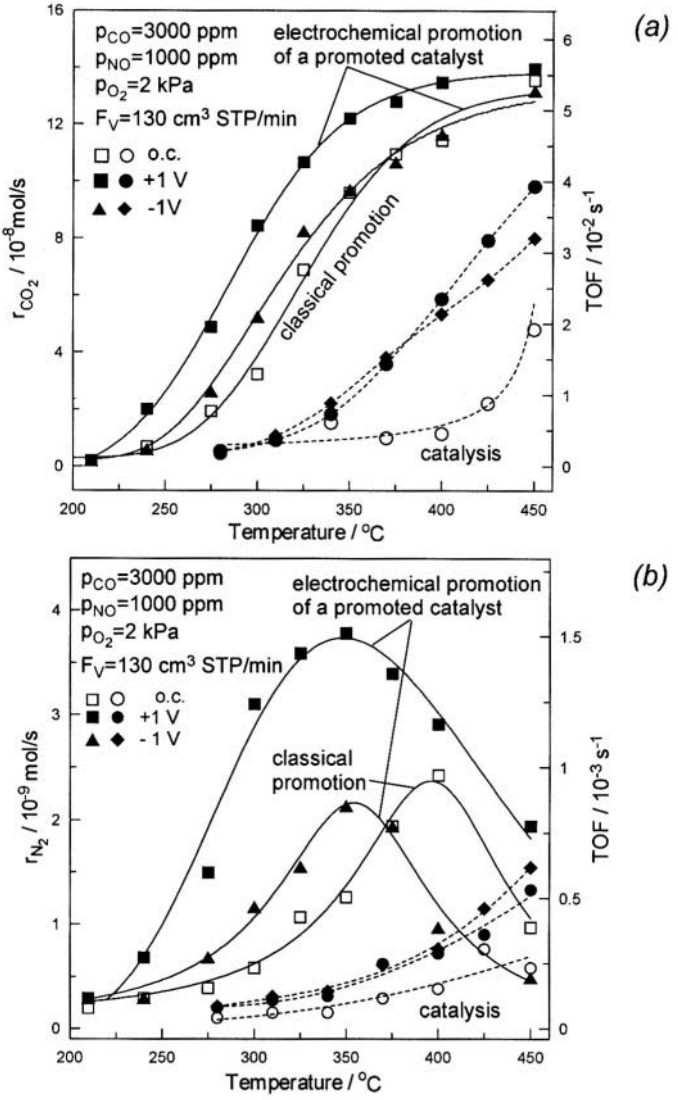

Figure 2.3. Catalysis (○), classical promotion (□), electrochemical promotion (●,◆) and electrochemical promotion of a classically promoted (sodium doped) (■,▲) Rh catalyst deposited on YSZ during NO reduction by CO in presence of gaseous O_2.[14] The Figure shows the temperature dependence of the catalytic rates and turnover frequencies of CO_2 (a) and N_2 (b) formation under open-circuit (o.c.) conditions and upon application (via a potentiostat) of catalyst potential values, U_{WR}, of +1 and −1V.[14] Reprinted with permission from Elsevier Science.

rate vs T curves in Fig. 2.3 labeled "catalysis" (open circles) have been obtained under open-circuit (o.c.) conditions, i.e. without any current or potential application. They thus reflect, to a large extent, the inherent catalytic properties of Rh for NO reduction, without the aid of promotion or electrochemical promotion.

Electrochemical promotion of the unpromoted Rh/YSZ film, via application of 1 or -1 V, leads to significant rate enhancement (tenfold increase in r_{CO_2}, four fold increase in r_{N_2} (filled circles and diamonds in Fig. 2.3). This is a catalytic system which as we will see in Chapters 4 and 8 exhibits "inverted volcano" behaviour, i.e. the catalytic rate is enhanced both with positive and with negative potential.

Then the same Rh film has been classically promoted by depositing on its surface 1 μl of a 10^{-2} N NaOH solution followed by drying and thorough H_2O evaporation in a classical "dry impregnation" process. The resulting promoted Rh film exhibits now a dramatic enhancement in its catalytic performance, as shown by the curves labeled "classical promotion" in Figure 2.3 (open squares). Its "light-off" temperature has been decreased by 150°C and the N_2 selectivity, S_{N_2}, has been enhanced. Therefore sodium (or NaOH) is an excellent promoter of Rh for this catalytic system. Actually the idea to use Na as a classical promoter of Rh for this reaction came directly from an electrochemical promotion investigation of the same reaction on Rh films deposited on β''-Al_2O_3, a Na^+ conductor. That study,[15] as previous ones using Pt films,[16] had shown that sodium, electrochemically supplied, in the form of Na^+, to noble metal catalysts (Pt, Pd, Rh) enhances dramatically the catalytic properties of the noble metal catalyst-electrode. The main reason is that Na further enhances NO dissociation.[15-17]

Can one further enhance the performance of this "classically" promoted Rh catalyst by using electrochemical promotion? The promoted Rh catalyst, is, after all, already deposited on YSZ and one can directly examine what additional effect may have the application of an external voltage U_{WR} (±1 V) and the concomitant supply (+1 V) or removal (-1 V) of O^{2-} to or from the promoted Rh surface. The result is shown in Fig. 2.3 with the curves labeled "electrochemical promotion of a promoted catalyst". It is clear that positive potentials, i.e. supply of O^{2-} to the catalyst surface, further enhances its performance. The light-off temperature is further decreased and the selectivity is further enhanced. Why? This we will see in subsequent chapters when we examine the effect of catalyst potential U_{WR} on the chemisorptive bond strength of various adsorbates, such as NO, N, CO and O. But the fact is that positive potentials (+1V) can further significantly enhance the performance of an already promoted catalyst. So one can electrochemically promote an already classically promoted catalyst.

Why do negative potentials (U_{WR}=-1 V) fail to further enhance to any significant extent catalyst performance of the promoted catalyst whereas the unpromoted Rh catalyst is electrochemically promoted with both positive and negative potentials? (Fig. 2.3). The answer will become apparent in subsequent chapters: In a broad sense negative potential application is equivalent to alkali supply on the catalyst surface. They both lead to a substantial decrease (up to 2-3 eV) in the catalyst work function, Φ, aquantity which as we will see, plays an important role in the description of promotion

and electrochemical promotion. Consequently a metal catalyst, already promoted with an alkali, and thus having already a low work function Φ, can only be marginally affected by negative potential application.

2.2 CHEMISORPTION AND CATALYTIC KINETICS

Catalysis and also promotion are intimately related to the phenomenon of chemisorption. For a catalytic reaction:

$$A + B \rightarrow \text{products} \tag{2.5}$$

to take place on a catalyst surface it is necessary that at least one of the reactants, and usually both, can chemisorb on the catalyst surface.

$$A(g) + M \leftrightarrows A\text{-}M \tag{2.6}$$

where M is a site on the catalyst surface.

The chemisorptive bond A-M is a chemical bond, thus chemisorption is reactant- and catalyst-specific. The enthalpy, ΔH, of chemisorption is typically of the order of -1 to -5 eV/atom (-23 to -115 kcal/mol, 1eV/molecule=23.06 kcal/mol).

Langmuir was first to model chemisorption and to relate the surface coverage, θ_A, of an adsorbate A with the gaseous activity or partial pressure, p_A, and temperature:

$$\theta_A/(1-\theta_A) = k_A(T)\cdot p_A \tag{2.7}$$

where $k_A(T)$ is the adsorption coefficient or adsorption equilibrium constant of A on a specific substrate. Due to the exothermicity of chemisorption ($\Delta H < 0$), k_A is a decreasing function of temperature:

$$k_A = \exp(\Delta S_A^0 / R) \exp(-\Delta H_A^0 / RT) \tag{2.8}$$

where ΔS_A^0 (practically always > 0) and the ΔH_A^0 are the standard entropy and enthalpy of chemisorption of A on a specific substrate. For the Langmuir isotherm (Eq. 2.7) the standard state of the adsorbed state corresponds to θ_A=0.5.

The assumptions made to derive the Langmuir isotherm (Eq. 2.7) are well known: Energetic equivalence of all adsorption sites, and no lateral (attractive or repulsive) interactions between the adsorbate molecules on the surface. This is equivalent to a constant, coverage independent, heat ($-\Delta H$) of adsorption.

For dissociative chemisorption, e.g.:

$$O_2 + 2M \leftrightarrows 2\ O\text{-}M \tag{2.9a}$$

or:

$$H_2 + 2M \leftrightarrows 2\ H\text{-}M \tag{2.9b}$$

the Langmuir isotherm becomes:

$$\theta_A^2 /(1-\theta_A)^2 = k_A(T)p_A \tag{2.10}$$

where again $k_A(T)$ and thus ΔH_A are coverage-independent.

For associative (not dissociative) coadsorption of A and B on a catalyst surface the Langmuir isotherm takes the form:

$$\theta_A = k_A p_A /(1+k_A p_A+k_B p_B) \tag{2.11}$$

$$\theta_B = k_B p_B /(1+k_A p_A+k_B p_B) \tag{2.12}$$

and this leads to the well known Langmuir-Hinshelwood-Hougen-Watson (LHHW) kinetics for catalytic processes.[18] For example when the rate limiting step of a catalytic reaction is the surface reaction between coadsorbed A and B:

$$r = k_R\theta_A\theta_B \tag{2.13}$$

one combines equations (2.11) to (2.13) to obtain:

$$r=k_R k_A k_B p_A p_B/(1+k_A p_A+k_B p_B)^2 \tag{2.14}$$

The LHHW kinetics represent a large oversimplification but, nevertheless, constitute a first step in quantifying catalytic kinetics.

There are several reasons for deviations from the LHHW kinetics: Surface heterogeneity, surface reconstruction, adsorbate island formation and, most important, lateral coadsorbate interactions.[18, 19] All these factors lead to significant deviations from the fundamental assumption of the Langmuir isotherm, i.e. constancy of ΔH_A (and ΔH_B) with varying coverage.

Calorimetric chemisorption studies have clearly shown that even on single crystal surfaces $-\Delta H_A$ varies with θ_A. Usually $(-\Delta H_A)$ decreases with θ_A and this implies repulsive lateral interactions between the coadsorbed A molecules. In the simplest case of a linear variation:

$$(-\Delta H_A) = (-\Delta H_{A,O})-\alpha\theta_A \tag{2.15}$$

one can derive, as an approximation, the Temkin isotherm:

$$\theta_A = k_A \ln(C_A p_A) \tag{2.16}$$

where k_A and C_A are constants.

This type of isotherm is more realistic for describing chemisorption at intermediate θ_A values but quickly leads to mathematically cumbersome or intractable expressions with many unknown parameters when one considers coadsorption of two gases. One needs to know how $-\Delta H_A$ is affected both by θ_A and by the coverages of all other adsorbates. Thus for all practical purposes the LHHW kinetics represent even today the only viable approach for formulating mathematically tractable, albeit usually highly inaccurate, rate expressions for catalytic kinetics. In Chapter 6 we will see a new, "medium field" type, approach which generalizes the LHHW kinetics by accounting also for lateral interactions.

2.3 CATALYTIC KINETICS AND PROMOTERS

Despite the already discussed oversimplifications built into the Langmuir isotherm and in the resulting LHHW kinetics, it is useful and instructive at this point to examine how a promoter can affect the catalytic kinetics described by the LHHW expressions (2.11) to (2.14).

A promoter is, first of all, just another adsorbate on the catalyst surface. In a Langmuirian context it blocks sites. Thus if its coverage on the catalyst surface is θ_p, the simplest LHHW rate expression (2.14) becomes:

$$r = (1-\theta_p)k_R k_A k_B p_A p_B/(1+k_A p_A+k_B p_B)^2 \qquad (2.17)$$

Such an expression is sometimes found to provide an adequate description of catalyst poisoning, i.e. the reverse of promotion. But for a promoter, i.e. a coadsorbate which enhances r, it is clear that at least one of the following two events must happen:

(a) The promoter increases the intrinsic rate constant k_R.

(b) The promoter affects k_A and k_B.

Although an increase in k_R, perhaps accompanied by the creation of new catalytic reactions sites, might at first glance appear to be the most probable and common reason of the promoting action (mechanism (a)) the experimental promotional kinetics (both from the classical and the electrochemical promotion literature) presented in this book show that mechanism (b) is at least as important as mechanism (a). Thus upon adding promoters on catalyst surfaces the catalytic kinetics usually change dramatically and the kinetic order of the reaction with respect to the reactants partial pressures, $(\partial r/\partial p_A)_{p_B}$ and $(\partial r/\partial p_B)_{p_A}$, change drastically between positive, zero and negative values. This cannot be accounted by changes in k_R and implies drastic effects of the promoter on the reactant adsorption equilibrium constants k_A and k_B.

It therefore becomes important first to examine the chemisorption of promoters on clean catalyst surfaces and then to examine how the presence of promoters affects the chemisorptive bond of catalytic reactants.

2.4 INTERACTIONS OF ADSORBATES ACTING AS PROMOTERS OR POISONS WITH CATALYST SURFACES

2.4.1 Definitions

As already discussed in Chapter 1, a promoter is a substance which when added to a catalyst, usually on its surface, enhances its catalytic performance, i.e. it increases the rate, r, of a catalytic reaction or the selectivity to a desired product.

Thus denoting by θ_p the coverage of the promoter on the catalyst surface and by p_j the partial pressures of reactants, j, of the catalytic reaction we can formulate mathematically the above definition as:

$$\left.\frac{\partial r}{\partial \theta_p}\right)_{p_j} > 0 \Leftrightarrow \text{p is a promoter} \qquad \left.\frac{\partial r}{\partial \theta_p}\right)_{p_j} < 0 \Leftrightarrow \text{p is a poison} \quad (2.18)$$

The promotional propensity of a promoter, p, can be quantified by defining[20] a promotional index, PI_p, from:

$$PI_p = (\Delta r/r_0)/\Delta\theta_p \quad (2.19)$$

where r_0 is the unpromoted catalytic rate.

Thus the promotional index PI_p is positive for promoters and negative for poisons. In the latter case the definition of PI_p coincides with that of the "toxicity" defined by Lamy-Pitara, Bencharif and Barbier several years ago.[21] In the case of pure site-blocking it is PI_p=-1. Values of $PI_{O^{2-}}$ up to 150 and of $PI_{Na^{\delta+}}$ up to 6000 have been measured as we will see in Chapter 4.

Another useful parameter for quantifying the promotional action is the promotional rate enhancement ratio, ρ_p, which can be defined from:

$$\rho_p = r/r_0 \quad (2.20)$$

Promotional rate enhancement ratio, ρ_p, values of the order 10-100 are rather common as one can see already from Figure 2.3.

2.4.2 Electropositive (Electron Donor) and Electronegative (Electron Acceptor) Promoters

Adsorbates acting as promoters usually interact strongly with the catalyst surface. The chemisorptive bond of promoters is usually rather strong and this affects both the chemical (electronic) state of the surface and quite often

also its geometry (surface reconstruction). In all cases significant changes are observed in the work function, Φ, of the catalyst surface.

The work function, Φ, of a solid surface, in eV/atom, is the minimum energy which an electron must have in order to escape from the Fermi level, E_F, of that solid through that surface when the surface is electrically neutral. More precisely Φ is defined as the energy to bring an electron from the Fermi level, E_F, at a distance of a few μm outside the surface under consideration so that image charge forces are negligible. Clean metal surfaces have work function, Φ_0, values ranging from 2 eV for alkalis to 5.5 eV for noble transition metals such as Pt. For the same solid, Φ_0 can also vary, up to 1eV, from one crystallographic plane to another.

Depending on the change a promoter induces on the work function, Φ, of a catalyst surface, a major distinction can be made between electropositive (electron donor) and electronegative (electron acceptor) adsorbates.

Electropositive adsorbates cause a decrease in the work function, Φ, of surfaces while electronegative adsorbates increase Φ. The variation in Φ with the coverage, θ_j, of an adsorbate is described by the Helmholtz equation:

$$\Delta\Phi = \frac{eN_M}{\varepsilon_o} P_j \Delta\theta_j \tag{2.21}$$

where $e=1.6\cdot10^{-19}$ C, $\varepsilon_o=8.85\cdot10^{-12}$ $C^2/J\cdot m$, N_M is the surface atom density ($atom/m^2$) of the surface under consideration and P_j ($C\cdot m$) is the dipole moment of adsorbate j in the adsorbed state. Typically P_j is of the order of 10^{-29} $C\cdot m$ or 3D (Debye). The Debye unit, D, equals $3.36\cdot10^{-30}$ $C\cdot m$. The dipole moments of adsorbates, P_j, are taken by convention positive in this book when the adsorbate dipole vector, $\tilde{P}_j$, is pointing to the vacuum (electronegative adsorbates, e.g. $O^{\delta-}$) and negative when $\tilde{P}_j$ is pointing to the surface (electropositive adsorbates, e.g. $Na^{\delta+}$).

2.4.3 Electropositive Promoters: Alkali Metals

Alkalis are the most important electropositive promoters of metal and metal oxide catalysts. They are used in many important industrial catalysts but are also quite suitable for fundamental studies since they can be easily introduced under vacuum conditions on well-characterized model metal surfaces.

Alkali metals are strongly electropositive elements with low (2-3 eV) work function and low ionization potential. Upon adsorption on other metal surfaces they cause a severe (up to 3 eV) lowering of the metal work function, as already established by Langmuir in the early 1920's.

The adsorption of alkali metals on single crystal surfaces can result in the formation of ordered structures (commensurate or incommensurate super-

structures) with or without surface reconstruction of the substrate. The actual form of these structures depends mainly on the adsorption temperature, the geometric and electronic structure of the surface and the alkali coverage, which controls the antagonistic action of adatom-adatom (Madelung type) and adatom-surface interactions. Alkali metal multilayers can also be built on catalyst surfaces when the surface temperature is lower than the sublimation temperature of the alkali metal.

The adsorption of alkali metals on both transition and free-electron metals is accompanied by distinctive changes in the work function of the metal. These changes reflect the interaction of the adsorbed alkali atoms with the substrate surface and with the other adatoms within the adsorbate overlayer. A very typical example is shown in Figure 2.4, which depicts the effect of alkali coverage on the change $\Delta\Phi$ in the work function of Ru(0001) and $Ru(10\bar{1}0)$ single crystals.[22] For low alkali metal coverages a strong initial decrease of the ruthenium work function (by almost 4 eV) is observed, followed by a work function minimum at an alkali coverage, θ_{alk}, of the order of 0.25 and by an increase to a work function value corresponding, at $\theta_{alk} \approx 1$, to near bulk alkali metal work function. This behavior is general for all *transition metal surfaces* and independent of temperature for adsorption temperatures below the onset of desorption of the first alkali layer.[6]

Using the Helmholtz equation (2.21) and the initial $\Delta\Phi$ vs θ_{alk} slopes of Fig. 2.4 one computes alkali initial dipole moments P_i as high as 15 D.

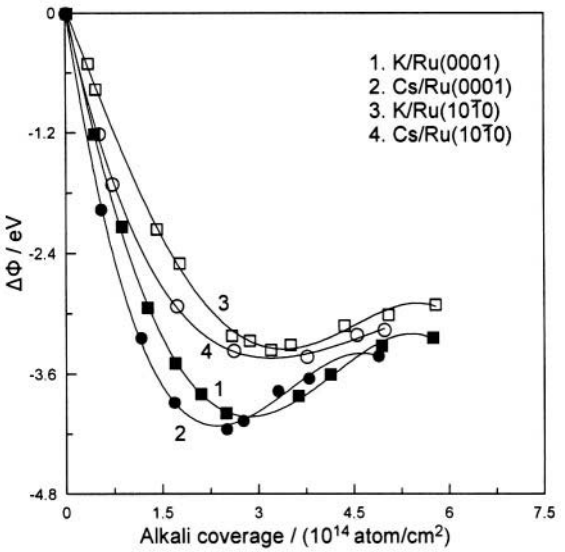

Figure 2.4. Work function changes, $\Delta\Phi$, as a function of K and Cs coverages for Ru(0001) (1 and 2) and for Ru$(10\bar{1}0)$ (3 and 4).[22] Reprinted with permission from Springer-Verlag GmbH & Co.

On the contrary, for electron-free metals (e.g. Al) the $\Delta\Phi$ vs θ_{alk} plots are temperature dependent[23] (Fig. 2.5). For sufficiently low adsorption temperatures (e.g. 100 K) the $\Delta\Phi$ vs θ_{alk} plots are similar to those obtained on transition metal surfaces. But for higher adsorption temperatures (e.g. 350 K, Fig. 2.5) the characteristic minimum disappears and a second straight line segment appears, due to two-dimensional condensation of the alkali adspecies.[6,23] The initial dipole moments are quite high (Fig. 2.5) but generally smaller than the ones on transition metal surfaces. For example the initial dipole moment of Na on Al(111) is 1.6 D vs 5.3 D for Na on Pt(111).[6,24,25]

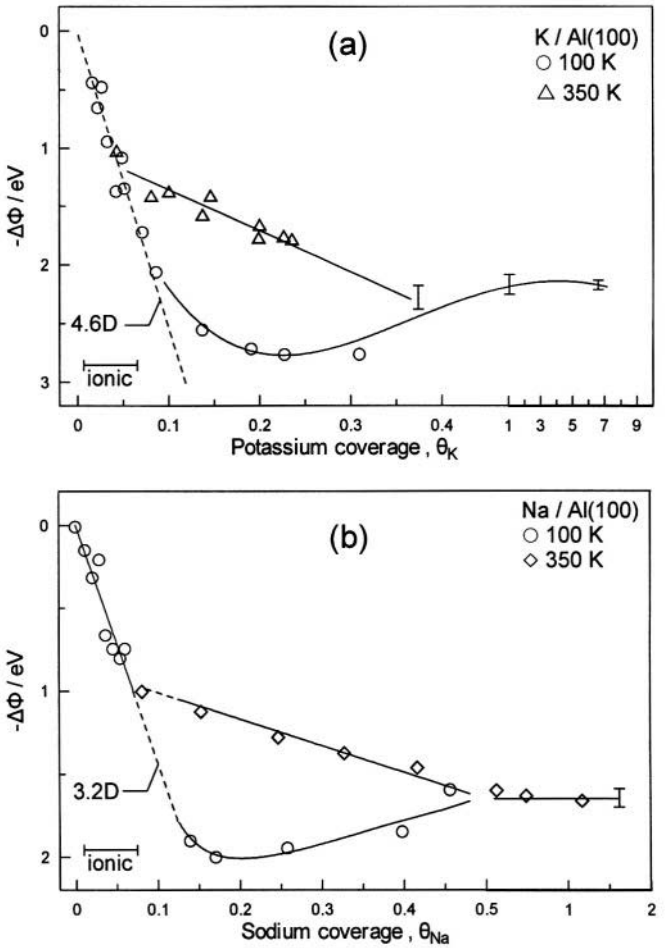

Figure 2.5. Potassium (a) and sodium (b) induced work function changes for adsorption at 100 K (open circles) and after annealing to 350 K or upon alkali adsorption at 350 K (open triangles) on Al single crystals.[23] Reprinted with permission from the American Vacuum Society.

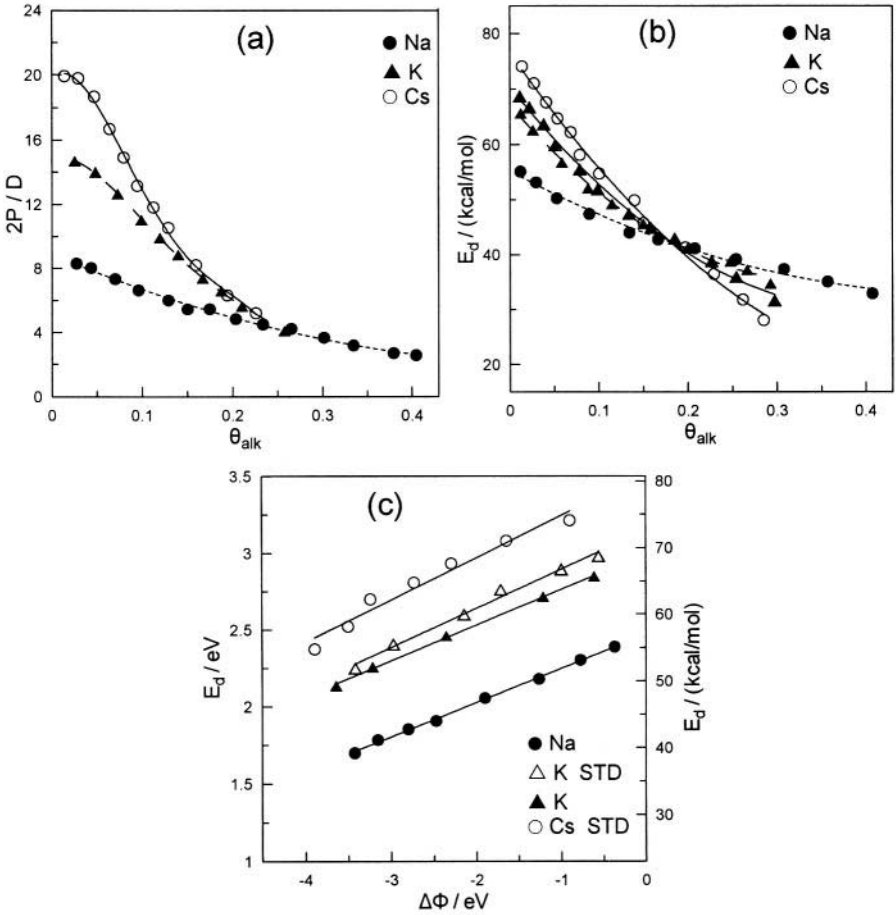

Figure 2.6. Effect of alkali coverage on (a) the alkali adatom dipole moment and alkali desorption energy (b) for Na, K and Cs adsorbed on Ru (0001) and corresponding effect of work function change $\Delta\Phi$ on the alkali desorption energy (c).[26] Reprinted with permission from Elsevier Science.

On the basis of the dipole moment, P_{alk}, values computed from the Helmholtz equation (2.21) and the alkali ion radius one can estimate the effective positive charge, q, on the alkali adatom, provided its coordination on the surface is known. Such calculations give q values between 0.4 and 0.9 e (e.g. 0.86e for K on Pt(111) at low coverages) which indicate that even at very low coverages the alkali adatoms are not fully ionized.[6] This is confirmed by rigorous quantum mechanical calculations.[27,28]

The strength of the metal-alkali chemisorptive bond is also decreased significantly with increasing alkali coverage. The activation energy for alkali desorption, E_d, can be obtained from the standard Redhead-Madix-Falconer analysis[29] of temperature programmed desorption (TPD) spectra obtained at different heating rates β:

$$\ln(\beta/T_p^2)=\ln(R\nu\theta_0^{n-1}/E_d)-E_d/RT_p \quad (2.22)$$

where T_p is the peak adsorption temperature, ν is the preexponential factor for desorption, n is the desorption order and θ_0 is the initial coverage. Thus upon plotting $\ln(\beta/T_p^2)$ vs $1/T_p$ one can easily obtain E_d, which practically also equals minus the enthalpy ΔH of alkali adsorption. As shown in Figure 2.6 b increasing θ causes a significant decrease in E_d. This is due primarily to the repulsive lateral interactions between the alkali adatoms. Upon plotting the E_d data vs work function Φ (Fig. 2.6c) a linear variation is observed with a positive slope. As we shall see below and throughout this book this type of behaviour is quite common and reflects strong lateral repulsive interactions between the adsorbed atoms.

The strong lateral repulsive interactions between the adatoms favours uniform distribution of alkali promoters on catalyst surfaces and formation of ordered structures. Such an ordered structure is shown in Figure 2.7 for the case of Na adsorption on a Pt single crystal surface consisting mostly of Pt(111) terraces covered by an O(2x2) overlayer at room temperature in ambient air.[30] The spheres covering the terraces correspond to Na adatoms at a coverage near 0.01 which have been introduced electrochemically to the Pt surface by interfacing the Pt single crystal with β''-Al_2O_3, a Na^+ conductor.[30,31] Only the Na adatoms are to be seen in this STM (Scanning tunneling microscopy) image, not the underlying Pt(111)-(2×2)-O adlattice which we shall see in more detail in Chapter 5. The Na adatoms form an ordered Pt(1 1 1)-(12×12)-Na adlayer where each Na adatoms is at a distance of 33.6 Å from its nearest neighbors. It is noteworthy that the Na adlayer appears dense although it corresponds to a coverage of less than 0.01 (1/144). This implies that each Na adatom affects the electron distribution in several neighboring Pt atoms, as well as in the underlying (2×2)-O adlattice. Thus the effect of alkali adsorption can be a long-range effect, extending over more than 12 neighboring substrate atoms, as also manifest by IR spectroscopy,[32] photoemission spectroscopy of noble gases (Xe)[33] and by electrochemical promotion, kinetic data.[20,34] There are also several theoretical studies supporting this view.[35]

On corrugated surface planes, thus also on real catalysts, non-uniform distribution of the alkali species can also be observed, accompanied by formation of islands of ordered structure domains. This has been confirmed by work function and LEED data[6] but also by STM[30,31] as shown in figure 2.8. This image has been obtained on a Pt(111)-(2×2)-O adlattice surface partly covered by the ordered Pt(111)-(12×l2)-Na adlayer under transient conditions of electrochemical Na removal from the Pt surface. Three different surface domains are clearly visible, one corresponding to the Pt(1 1 1)-(12×12)-Na adlayer, another to the cleaned Pt(111)-(2×2)-O surface and a third region corresponding to a higher coverage Pt(111) $(\sqrt{3}\times\sqrt{3})$-Na overlayer.

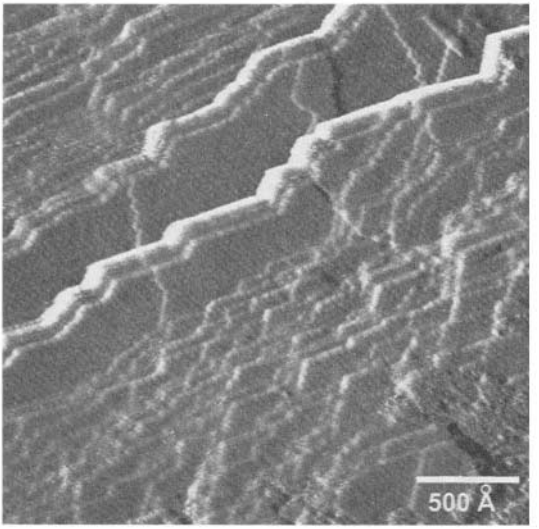

Figure 2.7. STM image (unfiltered) of a Pt single crystal surface consisting mainly of Pt(111) terraces and covered by a Pt(111)-(12×12)-Na adlattice formed via electrochemical Na^+ supply (from a β''-Al_2O_3 Na^+ conductor interfaced with the Pt single crystal)[30,36] on a Pt(111)-(2×2)-O adlattice. Each sphere on the image corresponds to a Na atom.[30,36] Reproduced from ref. 36 by permission of The Electrochemical Society.

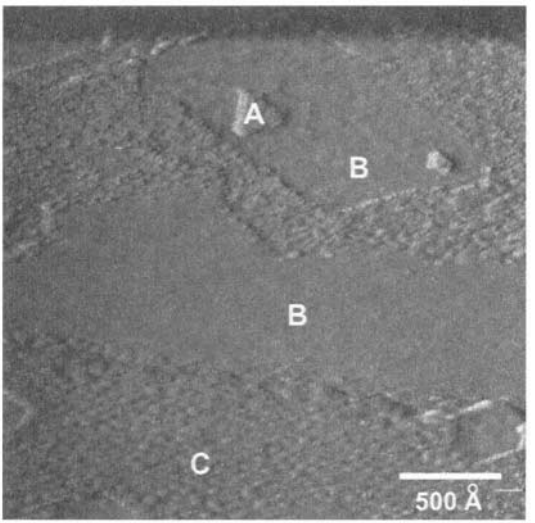

Figure 2.8. STM image (unfiltered) of a Pt(111) surface of a Pt single crystal interfaced with β''-Al_2O_3, a Na^+ conductor showing different domains of Na coverage.[30] The Pt(111)-(2×2)-O surface was initially covered by the Pt(111)-(2×2)-Na adlattice (domain A) and was intentionally only partly electrochemically cleaned (via positive U_{WR}=1V potential application and Na^+ removal into the β''-Al_2O_3 lattice)[30] leading to the formation of "clean" domains (domain B) and of higher Na coverage domains (domain C) corresponding to a ($\sqrt{3} \times \sqrt{3}$)-Na adlattice.

Regardless of the exact extent (shorter or longer range) of the interaction of each alkali adatom on a metal surface, there is one important feature of Fig 2.6 which has not attracted attention in the past. This feature is depicted in Fig. 2.6c, obtained by crossploting the data in ref. 26 which shows that the activation energy of desorption, E_d, of the alkali atoms decreases *linearly* with decreasing work function Φ. For non-activated adsorption this implies a *linear* decrease in the heat of chemisorption of the alkali atoms $|\Delta H_{ad}|$ ($=E_d$) with decreasing Φ:

$$\Delta|\Delta H_{ad}| = \alpha_H \Delta\Phi \tag{2.23}$$

where the parameter α_H has in this case a value near 0.25 (Fig. 2.6c). As will become apparent in this book, equation (2.23) is of broad significance as it approximates, in most cases with reasonable accuracy, the observed variation in heats of adsorption of adsorbates (promoters but also catalytic reactants and products) with varying catalyst surface work function. Several examples will be seen in this Chapter but mostly in Chapters 4 and 5 where it will also be seen (Chapter 4) that equation (2.23) can be derived by simply taking into account the electrostatic (through the vacuum) interactions in the adsorbed layer and that this linear behaviour is in good agreement with rigorous quantum mechanical calculations using metal clusters (Chapter 5).

The parameter α_H *is positive for electropositive (electron donor) adsorbates and negative for electronegative (electron acceptor) adsorbates.* Even when deviations from linearity exist, the main feature of Eq. (2.23) remain valid and form the basis for understanding the main kinetic features of classical and electrochemical promotion:

Increasing catalyst surface work function causes an increase in the heat of adsorption (thus chemisorptive bond strength) of electropositive (electron donor) adsorbates and a decrease in the heat of adsorption (thus chemisorptive bond strength) of electronegative (electron acceptor) adsorbates.

2.4.4 Electronegative Promoters

Electronegative promoters are less commonly used in industrial practice than electropositive ones. There are several reasons for this. One main reason is their strong adsorption on metal surfaces which often results in extensive site-blocking.[6] The bond strengths of S, C, N and O on transition metal surfaces are in general higher than 250 kJ/mol and often higher than 550 kJ/mol for C. In general the adsorbed electronegative additives on metal surfaces are more stable than the corresponding bulk compounds. A second reason, which will become apparent in Chapter 5 in conjunction with the promotional kinetics, is related to the predominantly electron donor

character of many, most, industrial feedstocks. Most studies of the bonding and structure of electronegative additives on catalyst surfaces deal with P, C, S and other chalcogens as they are the most common industrial catalyst poisons.

There are, however, numerous cases where electronegative additives can act as promoters for catalytic reactions. Typical examples are the use of Cl to enhance the selectivity of Ag epoxidation catalysts and the plethora of electrochemical promotion studies utilizing O^{2-} as the promoting ion, surveyed in Chapters 4 and 8 of this book. The use of O, $O^{\delta-}$ or O^{2-} as a promoter on metal catalyst surfaces is a new development which surfaced after the discovery of electrochemical promotion where a solid O^{2-} conductor interfaced with the metal catalyst acts as a constant source of promoting $O^{\delta-}$ ions under the influence of an applied voltage. Without such a constant supply of O^{2-} onto the catalyst surface, the promoting $O^{\delta-}$ species would soon be consumed via desorption or side reactions. This is why promotion with O^{2-} was not possible in classical promotion, i.e. before the discovery of electrochemical promotion.

Electronegative adatoms cause significant changes in the metal surface electronic structure, manifest as changes in the surface work function. In general electronegative additives increase the work function of the metal substrate. Typical examples are shown in Figures 2.9 and 2.10 for the adsorption of Cl and coadsorption of Cl and O on the work function of

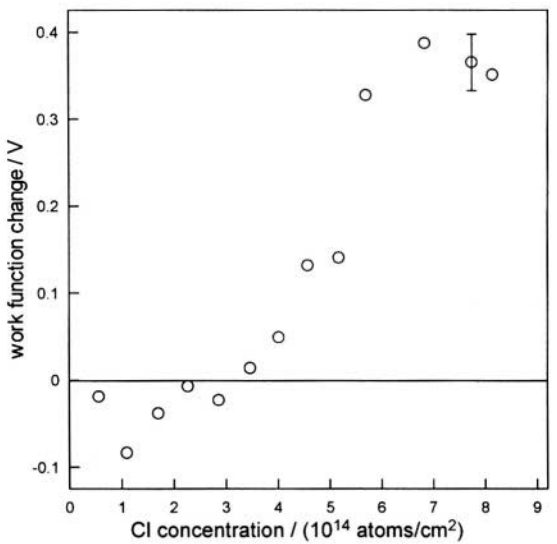

Figure 2.9. Change of the work function ($\Delta\Phi$) with increasing chlorine concentration on an initially clean Pt(111) surface at room temperature.[37] Reprinted with permission from Elsevier Science.

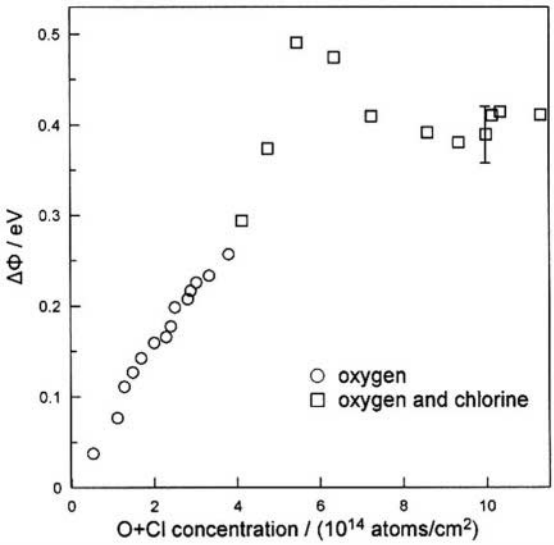

Figure 2.10. Increase in work function (ΔΦ) with increasing oxygen concentration up to 3.8×10^{14} O atoms cm^{-2} (circles) at room temperature. The squares show the change in work function (ΔΦ) with increasing total (oxygen plus chlorine) concentration, when chlorine is dosed on the saturated oxygen adlayer at room temperature.[37] Reprinted with permission from Elsevier Science.

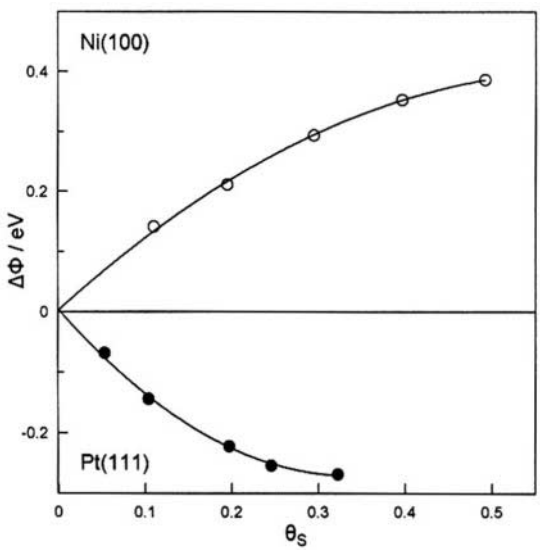

Figure 2.11. Work function changes induced by S adsorption on Ni(100) and Pt(111) surface.[6,38] Reprinted from ref. 6 with permission from Elsevier Science.

Pt(111).[37] The increase in metal work function induced by electronegative adsorbates (Cl, O, S, P, C) on metal surfaces is at most up to 1 eV and in

most cases below 0.5 eV, i.e. significantly smaller in magnitude than the work function decrease caused by electropositive adsorbates (e.g. alkalis where $\Delta\Phi$ reaches -3 V as already discussed). Thus the dipole moments of electronegative adatoms are smaller, typically up to 2D. There are some exceptions where the adsorption of an electronegative modifier induces a negative work function change. This is shown on Figure 2.11 for the cases of S adsorption on Ni(100) and Pt(111), where work function increase and decrease upon sulfur adsorption is observed, respectively. Positive work function change has also been observed for sulfur adsorption on Ni(111), Mo(100) and Ru(0001), but in the vast majority of cases negative work function changes are observed e.g. sulfur adsorption on Pt(100) and Pd (111), as well as for other electronegative additives, e.g. Cl on W(110) and W(211), N on W(100), I on W(100) etc.[6]

Since all electronegative additives are expected to behave as electron acceptors, the observed positive work function changes have been explained by taking into account not only the work function change due to the presence of the adatom layer on the surface and the corresponding electrostatic contribution with an electron coming out from the metal, but also the work function change due to the interaction of the adspecies with the hybridized surface d-p orbitals, that is the work function change due to internal polarization. The adsorbate induced internal polarization work function change $(\Delta\Phi)_{int}$ is always small and in general insignificant compared to the work function change $(\Delta\Phi)_{ext}$ corresponding to the electrostatic dipole moment (the dipole moment due to charge transfer between the surface atoms and the modifier adatoms). However, when the formation of the adsorption bond involves a small charge transfer in the direction perpendicular to the surface the contribution of $(\Delta\Phi)_{int}$ may prevail, resulting in negative work function change upon electronegative modifier adsorption. Alternatively such anomalous work function changes may reflect surface reconstruction and/or adsorption on sites slightly below the top metal atomic layer.

2.4.4.1 Structure of the Adsorbed Adatom Layer and Adatom Induced Surface Reconstruction

As supported by the results of many single crystal studies using a variety of surface science techniques,[39] electronegative additives show, in most cases, a strong tendency towards formation of ordered structures on metal surfaces, at submonolayer coverages, accompanied in certain cases by reconstruction of the substrate. On low Miller index surfaces of transition metal single crystals sulfur forms p(2×2) islands for coverages far below 0.25. As the coverage increases, these islands grow forming either larger domains or domain boundaries. At sulfur coverages higher than ~0.25, the c(2×2) and $(\sqrt{3}\times\sqrt{3})R30^{o}$ overstructures appear. The appearance of these structures is

usually associated with a complete deactivation of the catalyst surface. The same ordered structures are formed in the case of other chalcogens (e.g Se and Te) and halogen atoms (e.g. Cl and I). For other electronegative additives with a smaller size, such as C, N and O, the same ordered structure p(2×2) is observed up to coverages of ~0.25. In the case of these electronegative additives substrate surface reconstruction can be induced at higher coverages.

Regarding the type of the adsorption sites, the general trend is that the adsorption of electronegative additives takes place at the highest coordination adsorption sites, e.g. on three-fold adsorption sites for (111) planes or four-fold adsorption sites for (100) or (110) planes.[6] Deviations from this general trend are encountered usually for systems where reconstruction of the substrate or formation of bulk compounds takes place. The number of the metal substrate atoms coordinated to the electronegative adatoms, depends on the crystallographic plane and the type of the adsorption site. The coordination state of the electronegative adatom affects its chemisorptive bond strength and the corresponding bond length. The latter tends to increase for higher adatom coordination numbers and in most cases is shorter than the bond length in the corresponding bulk compound, indicating a stronger adatom-metal surface bonding compared to the bulk compound.

The presence of electronegative adatoms on metal catalyst surfaces (e.g. transition metal surfaces) may affect not only the electronic structure of surface atoms close to them but also result, in many cases, in reconstruction of the substrate surface. This adsorbate induced surface reconstruction is favored at high coverages of the electronegative adatoms (in general, higher than ~0.25) and on more open crystallographic planes, although strongly bonded adatoms can induce reconstruction even of closed-packed surfaces and at low coverages, as in the case of oxygen adsorption on Ru(001).[40] Besides S and O, nitrogen and carbon atoms usually induce surface reconstruction when adsorbed on transition metal surfaces. The tendency for reconstruction is strongly dependent not only on the specific electronegative adatom and metal surface, but also on surface orientation, temperature and the presence of surface defects, such as steps, kinks etc, on which the electronegative atoms are preferentially adsorbed. Adsorbate induced surface reconstruction can result in the appearance of new active adsorption sites and plays an important role in the interpretation of the catalytic properties of metal surfaces, especially with respect to surface sensitive reactions. Besides surface reconstruction and depending on the substrate and the electronegative modifier two- or three dimensional compounds (such as oxides, sulfides or carbides) may also be formed at high adatom coverages and high temperatures. In this case the catalytic properties of the substrate will be closer to the ones of the formed compound.[6]

2.5 ADSORPTION ON SURFACES MODIFIED BY ELECTROPOSITIVE OR ELECTRONEGATIVE PROMOTERS

The key of the promotional action is the effect of electropositive and electronegative promoters on the chemisorptive bond of the reactants, intermediates and, sometimes, products of catalytic reactions. Despite the polymorphic and frequently complex nature of this effect, there are two simple rules always obeyed which can guide us in the phenomenological survey which follows in this chapter.

Rule 1: Electropositive (electron donor) promoters enhance the chemisorption of electron acceptor adsorbates and weaken the chemisorption of electron donor adsorbates.

Rule 2: Electronegative (electron acceptor) promoters enhance the chemisorption of electron donor adsorbates and weaken the chemisorption of electron acceptor adsorbates.

The rules are simple as long as we also keep site-blocking effects in mind and as long as we can identify the electron acceptor or electron donor character of the various adsorbates.

2.5.1 Adsorption of Gases on Surfaces Modified by Alkali Promoters

The interactions of various molecules and atoms with alkali-modified surfaces are complex and depend on the type and coverage of alkali as well as on the substrate. The presence of alkalis may influence the adsorption rate and the maximum uptake of the surface, the stability of the adsorbed species, the strength of intramolecular bonds, the strength of the bonds formed between the adsorbed species and the substrate and the propensity for dissociative adsorption. Furthermore compound-like surface species may be formed between the adsorbed species and the alkalis, above a certain alkali coverage. This critical alkali coverage corresponds to the right side of the minimum observed in the work function vs alkali coverage plots (Fig. 2.4), where the alkali overlayer becomes metal-like and the interaction (coupling) with the surface becomes rather weak.

Most studies of the effect of alkalis on the adsorption of gases on catalyst surfaces refer to CO, NO, CO_2, O_2, H_2 and N_2, due to the importance of these adsorbates for numerous industrial catalytic processes (e.g. N_2 adsorption in NH_3 synthesis, NO reduction by CO). Thus emphasis will be given on the interaction of these molecules with alkali-modified surfaces, especially transition metal surfaces, aiming to the identification of common characteristics and general trends.

2.5.1.1 CO Adsorption

Carbon monoxide is chemisorbed molecularly on some *transition metals* but dissociatively on others. An approximate borderline can be drawn through

Table 2.1. Dissociative (D) and molecular (M) chemisorption of CO on metal surfaces.

IIIB	IVB	VB	VIB	VIIB	VIII	VIII	VIII	IB
Sc	Ti D	V	Cr	Mn	Fe D	Co	Ni M	Cu
Y	Zr	Nb	Mo D	Tc	Ru M	Rh	Pd M	Ag
La	Hf	Ta	W D,M	Re	Os	Ir M	Pt M	Au

the periodic table from cobalt in the first transition series, through rhenium in the third. As shown in Table 2.1, metals to the right of this borderline (such as Pt and Pd) tend to chemisorb CO molecularly under ordinary catalytic reaction conditions, while those to the left (such as Fe and Mo) tend to chemisorb CO dissociatively.

As shown in Figure 2.12, alkalis, such as K, have little effect on the total saturation coverage of CO on transition metal surfaces, such as the Pt(111) surface.[41,42] They also have a small effect on the initial sticking coefficient[41,42] (Figure 2.13) except at high K coverage (θ_K=0.44) where the rate of CO adsorption decreases significantly. The CO coverage vs CO exposure dependence at high (θ_K=0.44) alkali coverages indicates nucleation-controlled CO adsorption kinetics suggesting that CO adsorption sites are created by the interaction between CO and the dense alkali overlayer.

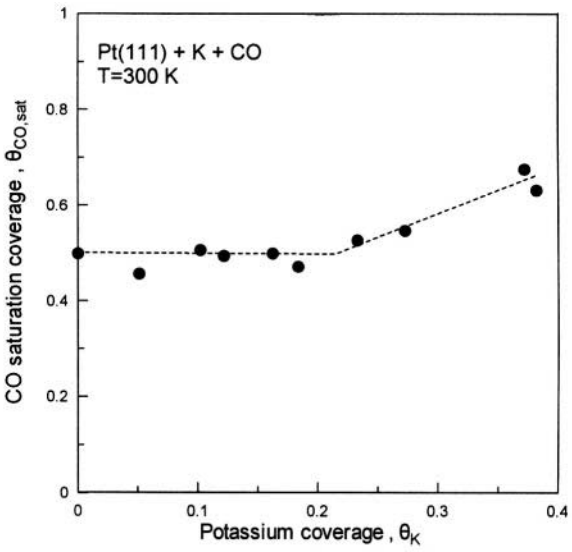

Figure 2.12. Effect of K coverage on the total saturation coverage of CO on Pt(111).[42] Reprinted with permission from Elsevier Science.

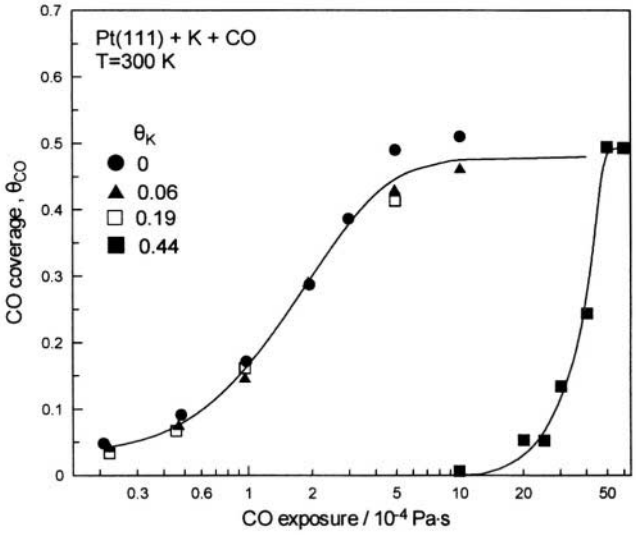

Figure 2.13. CO uptake curves for clean and K covered Pt(111) at 300 K.[41,42] Reprinted with permission from Elsevier Science.

Although the saturation coverage and sticking coefficient of CO are usually rather insensitive to alkali coverage, the latter has a pronounced effect on the chemisorptive binding strength of CO as already shown in Figure 2.2: Increasing alkali coverage causes a pronounced increase in the bonding strength of CO which leads to enhanced CO dissociation even on metals which normally chemisorb CO molecularly.

2.5.1.1.1 Alkali Effect on the CO Molecular Chemisorption.

The molecular chemisorption of CO *on transition metals* can be considered to involve components of charge transfer in opposite directions. Fig. 2.14 shows the spatial distribution of key orbitals involved in this chemisorption[5] and their energy in comparison with vacuum and with the Fermi level of Pt(111).[11] According to the well accepted Blyholder model, the molecular chemisorption of CO on metal surfaces involves (i) transfer of electron density from the 5σ bonding orbital highest occupied molecular orbital (HOMO) towards empty levels in the metal bands and (ii) transfer of electron density in the reverse direction (backdonation) from the populated levels in the vicinity of the Fermi level of the metal into the empty $2\pi^*$ antibonding orbital of CO. Since the 5σ HOMO is essentially nonbonding, due to its spatial distribution, and the $2\pi^*$ lowest occupied molecular orbital (LUMO) is strongly antibonding, the transfer of electron density that accompanies CO chemisorption weakens the binding between the carbon and oxygen atoms in the CO molecule but strengthens the carbon - metal bond by increasing the shared electron density. The weakening of the carbon-oxygen bond in the CO molecule due to chemisorption is manifest by a shift to lower

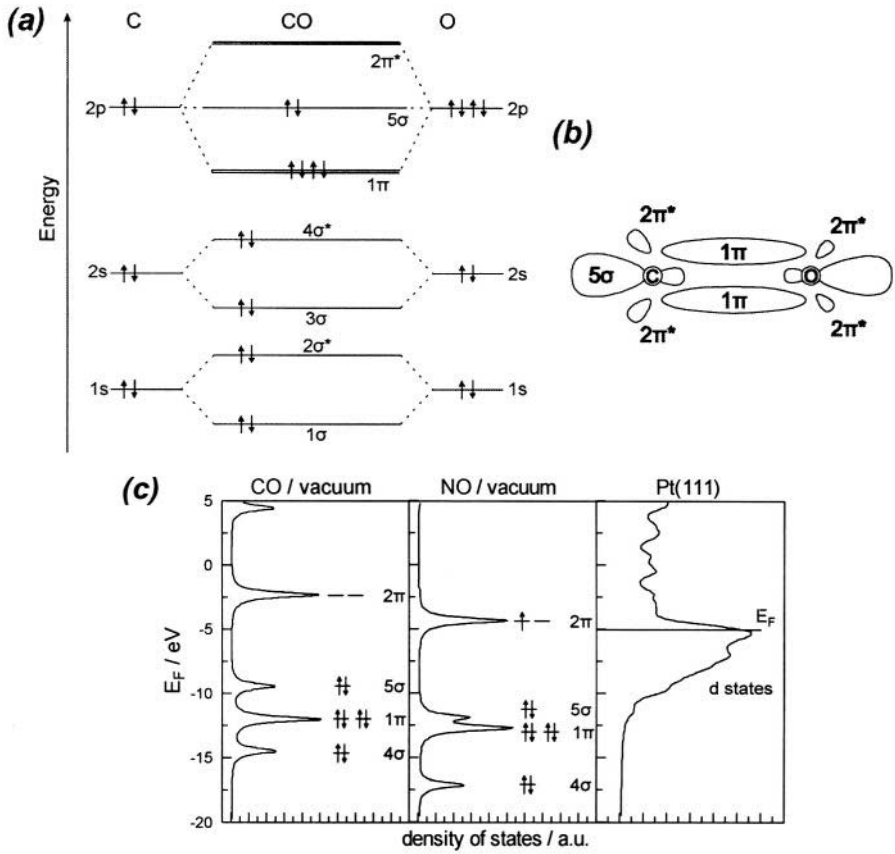

Figure 2.14. The molecular orbitals of gas phase carbon monoxide. (a) Energy diagram indicating how the molecular orbitals arise from the combination of atomic orbitals of carbon (C) and oxygen (O). Conventional arrows are used to indicate the spin orientations of electrons in the occupied orbitals. Asterisks denote antibonding molecular orbitals. (b) Spatial distributions of key orbitals involved in the chemisorption of carbon monoxide. Barring indicates empty orbitals.[5] (c) Electronic configurations of CO and NO in vacuum as compared to the density of states of a Pt(111) cluster.[11] Reprinted from ref. 11 with permission from Elsevier Science.

values (red shift) of the wave number corresponding to the stretching frequency of this bond, e.g from 2143 cm^{-1} in the gas phase molecule to 2100 cm^{-1} for CO adsorbed on platinum.

The molecular chemisorption of CO on various alkali-modified metal surfaces has been studied extensively in the literature. It is well established that alkali modification of the metal surface enhances both the strength of molecular chemisorption and the tendency towards dissociative chemisorption. This effect can be attributed to the strongly electropositive character of the alkali, which results in donation of electron density from the alkali to the metal and then to the adsorbed CO, via increased backdonation into the

antibonding π^* orbitals of the adsorbed molecule. The effect is pronounced for transition metal surfaces, where the backdonation of the metal d-electronic density to the $2\pi^*$ antibonding orbitals of adsorbed CO is strong.

For alkali modified noble and sp-metals (e.g. Cu, Al, Ag and Au), where the CO adsorption bond is rather weak, due to negligible backdonation of electronic density from the metal, the presence of an alkali metal has a weaker effect on CO adsorption. A promotional effect in CO adsorption (increase in the initial sticking coefficient and strengthening of the chemisorptive CO bond) has been observed for K- or Cs-modified Cu surfaces as well as for the CO-K(or Na)/Al(100) system.[6,43] In the latter system dissociative adsorption of CO is induced in the presence of alkali species.[43]

The alkali-induced strengthening of the metal-CO bond is clearly manifest by the alkali-induced changes in the peak temperatures of the CO temperature programmed desorption (TPD) spectra. In general various additives (Na, K, Cs) have the same effect on the CO TPD spectra, with the exception that the amount of CO molecules affected by one alkali adatom seems to increase moving from Na to Cs in the periodic system. Figure 2.2 shows TPD spectra of CO, initially adsorbed at room temperature, on potassium modified Pt(100) surfaces. The peak desorbed from the unpromoted platinum surface corresponds to CO which has been chemisorbed molecularly. This kind of peak is conventionally termed "α-peak". Within the lower range of potassium coverage (θ_K) values, the α-peak shifts to higher temperatures, i.e. from 520 K for θ_K=0 to 550 K for θ_K=0.13. This indicates a significant strengthening in the platinum-GO bond as the potassium coverage increases. This increase is also manifest from HREELS[41] and IR[44] spectra of adsorbed CO on alkali modified transition metal surfaces, where the wavenumber corresponding to the carbon-oxygen stretching frequency in the adsorbed CO decreases dramatically with increasing alkali coverage, shifting to values lower than 1400 cm^{-1} at high alkali coverages.

For coverages higher than the one corresponding roughly to the minimum of work function vs alkali coverage plot (Fig. 2.4), a sharp peak to the right of the α-peak appears. This new desorption state reflects the formation of compound-like surface complexes of the type CO-K-Pt. Interestingly this desorption peak appears in the range 640 to 680 K for most of the transition metals studied, while coincident alkali metal and CO desorption is observed. The similarity in the TPD peaks corresponding to this CO desorption state and to the alkali metal as well as their unusually small half widths are indicative of a decomposition of an alkali metal-CO- metal surface complex. Spectroscopic data corroborate this conclusion, as the carbon-oxygen bond stretching frequency in the adsorbed CO molecule becomes independent of CO coverage for near monolayer alkali coverage, where it reaches its lowest value, i.e. ~1400 cm^{-1}.

From TPD data obtained at low CO coverages, it is possible to estimate the initial heats of adsorption,[45,46] ΔH^0_{CO}, of CO on alkali modified surfaces. Figure 2.15a shows the dependence of ΔH^0_{CO} on alkali coverage, for CO adsorption on alkali modified Ru(10$\bar{1}$0) It is clear that up to moderate alkali coverages the

initial heat of adsorption of CO increases linearly with increasing alkali coverage, while at higher coverages it reaches a plateau. This shows the strengthening of the molecularly adsorbed CO-transition metal bond with increasing alkali metal coverage, in agreement with EELS and IR spectroscopic data.[41]

Upon replotting the data of Fig. 2.15a in terms of the work function change, $\Delta\Phi$, induced by the presence of the alkali (Na) promoter one obtains Fig. 2.15b which shows a *linear* decrease in $\left|\Delta H^0_{CO}\right|$ with increasing Φ and conforms nicely to Eq. (2.23)

$$\Delta\left|\Delta H^0_{CO}\right| = \alpha_H \Delta\Phi \tag{2.24}$$

with an α_H value of –0.2. This shows that CO behaves overall as an electron acceptor, since its heat of adsorption decreases with increasing work function Φ.

The last point is confirmed by measuring the work function changes upon CO chemisorption on clean and alkali-promoted metal surfaces. Figures 2.16 and 2.17 show the work function changes induced by CO adsorption on a K/Pt(111) and on a Na/Ru(10$\bar{1}$0) surface respectively, for various alkali coverages.[42,45]

The main features, which are common for all studies reported in literature, irrespective of the behavior of the work function on CO coverage for the clean surface, are: (i) For alkali coverages lower than the ones corresponding to the minima in the work function vs alkali coverage plots, an increase of the surface work function with increasing CO coverage is observed, proportional to the initial alkali coverage, (ii) For higher alkali coverages, a relatively weaker increase in the surface work function with increasing CO coverage is observed , as well as a more complex behavior, corresponding to an initial slight decrease of the work function for very low CO coverages.

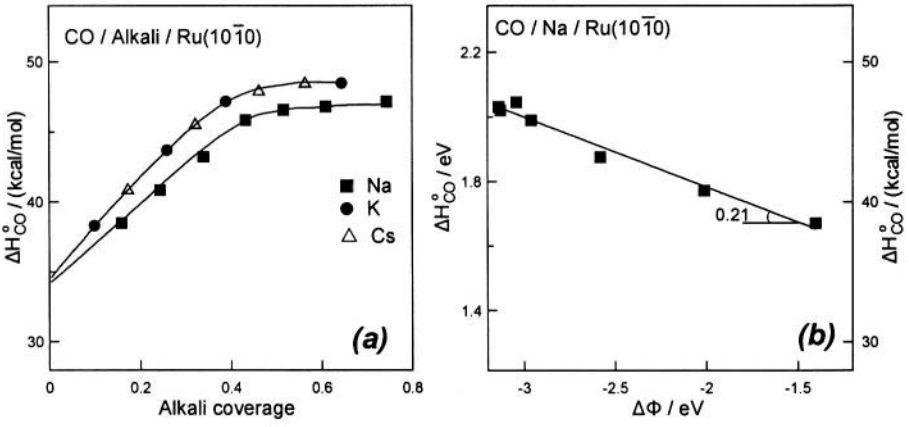

Figure 2.15. Dependence of the initial heats of CO adsorption. ΔH^0_{CO} , on the alkali coverage, as estimated from the CO TPD spectra at very low CO coverages assuming invariable frequency factor[45,46] (a) and on the corresponding work function change $\Delta\Phi$[45,46] (b). Reprinted with permission from Elsevier Science.

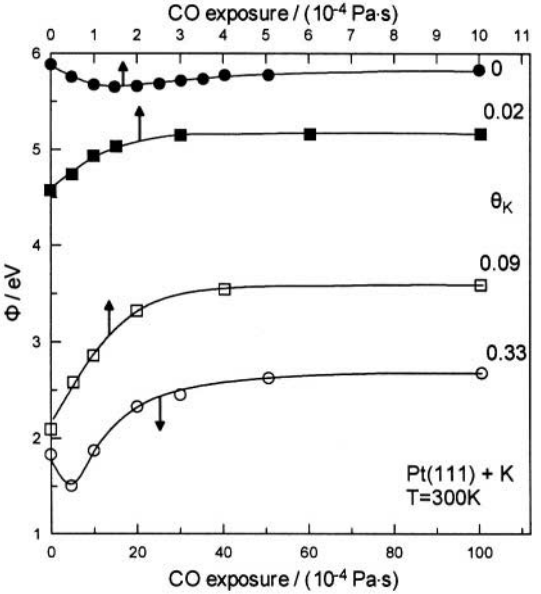

Figure 2.16. Work function changes versus CO exposure for clean and K-covered Pt(111) at 300 K measured from the onset of the electron emission of He I UPS spectra.[42] Reprinted with permission from Elsevier Science.

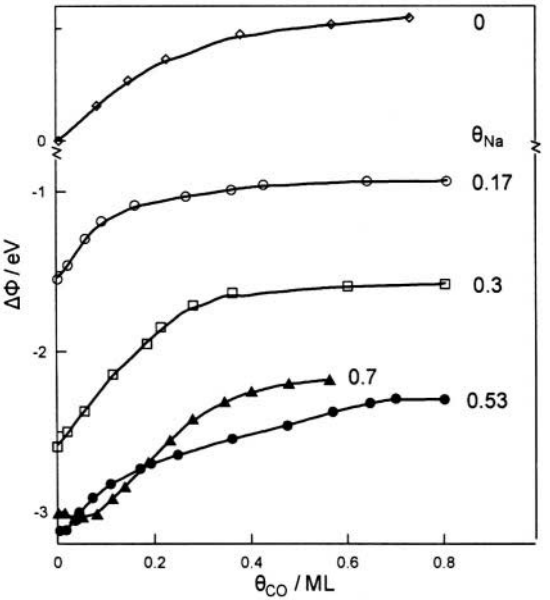

Figure 2.17. Work function changes versus θ_{CO} for clean and Na covered Ru($10\bar{1}0$) at 300 K.[45] Reprinted with permission from Elsevier Science.

The similar behavior observed for all CO-alkali-transition metal systems indicates the same type of alkali-CO interactions, irrespective of the nature of the transition metal. Interestingly these work function data confirm that *adsorbed CO on alkali modified transition metal surfaces shows overall the behavior of an electron acceptor molecule.*

Besides the effect of the presence of alkali on CO adsorption, there is also a stabilizing effect of adsorbed CO on the adsorption state of alkali. Within the high alkali coverage range the number of CO molecules adsorbed on promoted surface sites becomes practically equal to the number of alkali metal species and their properties are not dependent on the CO coverage. In this region CO adsorption causes also stabilization of the adsorbed alkali, as indicated by the observed high temperature shift of the onset of alkali desorption.

2.5.1.1.2 Alkali Effect on the Dissociative CO Chemisorption.

The dissociation propensity of chemisorbed CO on metal surfaces depends largely on the substrate, reflecting not only the differences in the strength of the metal-CO bond but also the differences in the energy of the precursor state (molecularly adsorbed CO) and the final dissociation products (carbon and oxygen). The promoting action of alkali metals for the dissociative adsorption of CO is thus expected to involve both stabilization of the molecularly adsorbed CO and a decrease in the activation energy for dissociation of the molecularly adsorbed state. As the alkali-induced weakening of the carbon-oxygen bond in the adsorbed CO does not vary appreciably on different transition metal surfaces, the main differences concerning the promotion of CO dissociation can be related with the stability of the dissociation products on different substrates.

The alkali promotion of CO dissociation is substrate-specific, in the sense that it has been observed only for a restricted number of substrates where CO does not dissociate on the clean surface, specifically on Na, K, Cs/Ni(100),[38,47,48] Na/Rh[49] and K, Na/Al(100).[43] This implies that the reactivity of the clean metal surface for CO dissociation plays a dominant role. The alkali induced increase in the heat of CO adsorption (not higher than 60 kJ/mol)[50] and the decrease in the activation energy for dissociation of the molecular state (on the order of 30 kJ/mol)[51] are usually not sufficient to induce dissociative adsorption of CO on surfaces which strongly favor molecular adsorption (e. g. Pd or Pt).

2.5.1.2 CO_2 Adsorption

Alkali promoters are often used for altering the catalytic activity and selectivity in Fischer-Tropsch synthesis and the water-gas shift reaction, where CO_2 adsorption plays a significant role. Numerous studies have investigated the effect of alkalis on CO_2 adsorption and dissociation on Cu, Fe, Rh, Pd, Al and Ag[6,52] As expected, CO_2 always behaves as an electron acceptor.

The adsorption of CO_2 on metal surfaces is rather weak, with the exception of Fe, and no molecular or dissociative adsorption takes place at room temperature on clean metal surfaces. At low temperatures, lower than 180 to 300 K, a chemisorbed $CO_2^{\delta-}$ species has been observed by UPS[6] on Fe(111) and Ni(110) surfaces, which acts as a precursor for further dissociation to CO and adsorbed atomic oxygen. A further step of CO dissociation takes place on Fe(111) above 300 to 390 K.

The presence of alkali species on metal surfaces causes a significant enhancement of both the sticking coefficient of CO_2, which reaches a value of unity at moderate alkali coverages, and the adsorptive capacity of the surface. Furthermore, it results in creation of new sites where CO_2 is more strongly bound, i.e it enhances the stability of the chemisorbed $CO_2^{\delta-}$ species and increases their propensity for dissociation. For example, on K-covered Pd(100), the CO_2 TPD β-peak shifts gradually from 185 to 556 K as the K-coverage, θ_K, changes from 0.05 to 0.4. Furthermore, no CO_2 dissociation is observed for θ_K lower than 0.2, while for θ_K higher than ~0.3 a new CO_2 TPD peak is observed at 672 K, associated with a preceding CO_2 dissociation on the metal surface.[52,53] A similar effect of alkali-induced stabilization of molecularly adsorbed CO_2 has beed reported for the K-covered Rh(111) surface.

At high alkali coverages and elevated temperatures formation of new intermediates and compound-like species has been observed as a result of reaction of the CO_2 with the alkali overlayer. For example, on K-covered Ag, HREELS and Raman spectra taken upon CO_2 adsorption at 50K show strong evidence for the formation of binary surface compounds.[54] While at low alkali coverages $CO_2^{\delta-}$ species are the ones most likely stabilized on the alkali modified sites, at high alkali coverages, when the alkali overlayer becomes metal-like, oxalate ($C_2O_4^-$) and carbonate (CO_3^{2-})-like surface compounds are formed . The formation of these compounds, which exhibit a thermal stability similar to the one of the corresponding bulk compounds decomposing with simultaneous evolution of CO_2 and alkali metal, results also to stabilization of the adsorbed alkali state.

2.5.1.3 NO Adsorption

The effect of alkali addition on the adsorption of NO on metal surfaces is of great importance due to the need of development of efficient catalysts for NO reduction in stationary and automotive exhaust systems. Similar to CO, NO always behaves as an electron acceptor in presence of alkalis.

2.5.1.3.1 Alkali Effect on the Molecular NO Chemisorption

The presence of alkali promoters on the substrate surface can affect both the rate of chemisorption, (e.g. on K/Rh(100))[55] and the adsorptive capacity

of the surface. The latter is shown on Fig. 2.18 where NO uptake curves are compared for clean and K-modified Rh(100). Similar enhancement of the adsorptive capacity of the surface has been observed for Na or Rb modified Ag(110)[56-58], while for K/Pt(111) the same effect is observed only above 300 K, where the saturation coverage on the alkali-free surface is low(~0.23).[6] In general, the effect of alkali promotion on the adsorptive capacity of the substrate depends both on the specific substrate and temperature.

As in the case of CO adsorption, alkali addition results in strengthening of the metal-NO bond, with concomitant weakening of the N-O intramolecular bond. For example, this is exemplified in the case of NO adsorption on Pt(111) at 120 K by the shift of the N1s and O1s core level binding energies in XPS spectra to lower values upon addition of K on the substrate surface.[59] The strengthening of the metal-NO bond, which is due to increased backdonation of electron density from the metal surface to the NO $2\pi^*$ antibonding molecular orbitals, is also reflected in the work function change upon chemisorption of NO on clean and alkali-promoted surfaces. In the latter case a significant increase in the substrate work function is observed with increasing NO coverage, indicating that molecularly adsorbed NO on alkali promoted metal surfaces exhibits electron acceptor behavior. This is clearly seen in Fig. 2.19 which presents the effect of NO adsorption on the work function of clean and K-covered Pt(111).[59] From these data a rather large initial dipole moment equal to 3.2D can be estimated via Eq. (2.21) for NO adsorbed on K promoted sites of Pt(111).

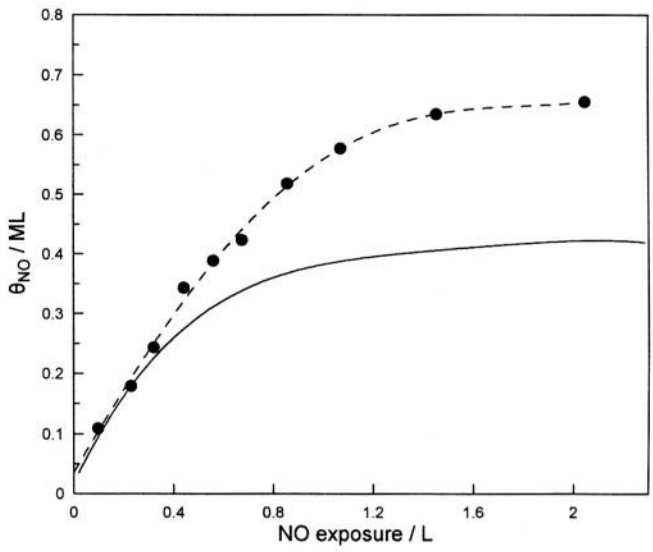

Figure 2.18. NO uptake curves for clean (solid line) and 0.18 ML K-covered (dashed line) Rh(100).[55] Reprinted with permission from the American Institute of Physics.

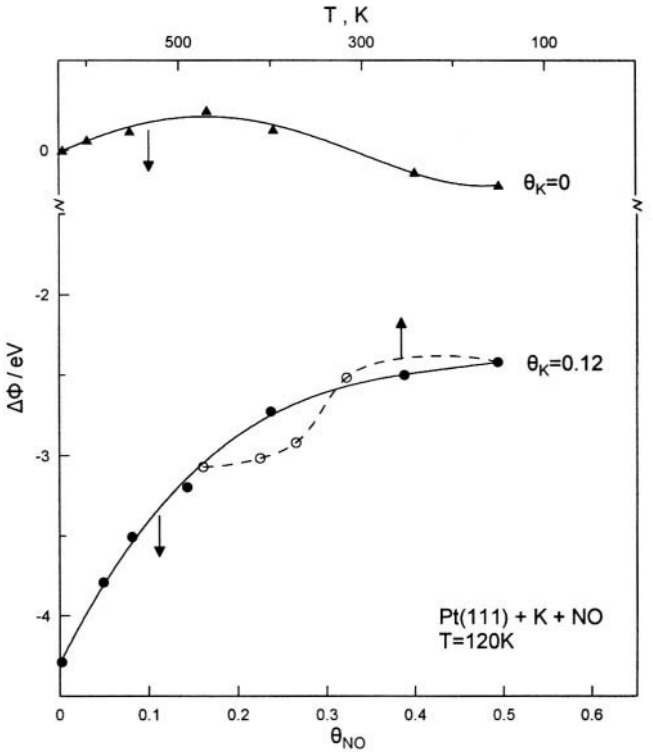

Figure 2.19. NO induced work function changes, $\Delta\Phi$, vs θ_{NO} for clean and K-covered Pt(111) at 120 K. The dashed line indicates the work function changes after heating the NO saturated K-covered Pt(111) to various temperatures up to 500 K.[59] Reprinted with permission from Elsevier Science.

It is worth noting in Fig. 2.19 how the presence of a strong electropositive adsorbate (K^+) on the catalyst surface causes NO to behave as an electronegative adsorbate. Thus while on the clean surface NO behaves at high coverages as an electron donor it always behaves as an electron acceptor on the K^+ promoted surface.

2.5.1.3.2 Alkali Effect on the Dissociative NO Chemisorption

Similar to the case of CO, the dissociation propensity of NO depends largely on the substrate, following the same general trends. Alkali introduction on metal substrates promotes the dissociative adsorption of NO, both by weakening the N-O intramolecular bond and by stabilizing the molecular state which acts as a precursor for dissociation.

Alkali promoted NO dissociation is clearly illustrated in the case of NO adsorption on K/Pt(111), as NO is not adsorbed dissociatively on the alkali-clean surface. The dissociative adsorption of NO on K/Pt(111) takes place at temperatures higher than 300 K and the number of dissociated NO molecules

is proportional to the potassium coverage. NO dissociation is accompanied both by an abrupt decrease of the platinum surface work function at 320 to 360 K (Fig. 2.19, dashed line) and the appearance of an O-related peak at ~5 eV in the UPS spectra.[59] The produced atomic oxygen is more stable on the substrate surface compared to adsorbed nitrogen and manifests its presence by the observed plateau in the work function as the temperature approaches 500 K. This plateau value is ~1.2 eV higher than the one corresponding to zero NO coverage (oxygen free surface).

The dissociation propensity of NO is also strongly enhanced on substrates where NO dissociation takes place to some extent even on the alkali-clean surface, e.g. in the case of K/ Rh(100) or K/Rh(111).[6,55]

The undissociated NO molecules and the dissociation products can participate in secondary reactions in the mixed alkali-NO overlayers and result both in products which immediately desorb (e.g. N_2) or further decompose (e.g. N_2O), and in alkali stabilized compound-like products (nitrite-like salts). As in the case of CO or CO_2 adsorption, the formation of such surface compounds is favoured at elevated temperatures and at alkali coverages higher than those corresponding to the work function minimum.

2.5.1.4 Oxygen Adsorption

The effect of alkali presence on the adsorption of oxygen on metal surfaces has been extensively studied in the literature, as alkali promoters are used in catalytic reactions of technological interest where oxygen participates either directly as a reactant (e.g. ethylene epoxidation on silver) or as an intermediate (e.g. NO+CO reaction in automotive exhaust catalytic converters). A large number of model studies has addressed the oxygen interaction with alkali modified single crystal surfaces of Ag, Cu, Pt, Pd, Ni, Ru, Fe, Mo, W and Au.[6]

Molecular adsorption of oxygen is practically restricted to low temperatures (lower than room temperature), consequently the adsorption of oxygen on metal surfaces under real catalytic conditions is dissociative. The temperature above which dissociation of the molecular state takes place depends on the specific substrate. Depending on the substrate and the conditions (temperature, oxygen partial pressure) bulk (e.g. on Pd), sub-surface (e.g. on Ag) or surface (e.g. on Pt) oxide can also be formed. The formation of such oxide phases has been observed under UHV conditions in the case of Ni, Fe, W and Mo single crystals, i.e. on the most reactive metal surfaces where the sticking coefficient of oxygen is near unity. Lower sticking coefficient values correspond to the less reactive metals (such as Au, Ag, Pt), e.g. ~10^{-3} for Ag.

The maximum oxygen uptake as well as the heat of adsorption also vary significantly with varying substrate. The adsorption of oxygen is accompanied

by transfer of electron density from the metal surface, thus the strength of the chemisorption bond of atomic oxygen decreases with progression along each transition series of the periodic table, following the corresponding increase of the work function of the metal. Oxygen always behaves as a strong electron acceptor.

The alkali modification of a metal surface results in an increase of both the dissociative adsorption rate (initial sticking coefficient) and of the adsorptive capacity of the surface. This is shown in Figs 2.20 and 2.21 which present the dependence of oxygen coverage on oxygen exposure for alkali promoted Ru(001) at 300 K. This is a reactive surface for O_2 dissociative chemisorption with an initial sticking coefficient of 0.35. Both the saturation oxygen coverage and the initial sticking coefficient increase with increasing alkali coverage, reaching a value of unity at alkali coverages higher than ~0.3. The latter is near the coverage corresponding to the work function minimum.

Similar behaviour is also observed for metals such as Au, Ag and Pt where the initial sticking coefficient is low. In the case of alkali-modified substrates where the high reactivity of the clean surface for oxygen results both in rapid decrease of the sticking coefficient above a certain oxygen coverage and in oxide formation (e.g. Ni), the alkali effect is twofold: First, it suppresses the self-poisoning effect of the adsorbed oxygen, maintaining a sticking coefficient value of ~1 over higher oxygen coverages. Second it enhances the oxidation rate because it allows for the rapid build-up of the critical oxygen coverage needed for formation of the first surface oxide nuclei.

The interpretation of the beneficial effect of alkali modification on oxygen adsorption has to include both stabilization of the adsorbed oxygen atoms on alkali modified sites, due to direct alkali-oxygen interactions, but also

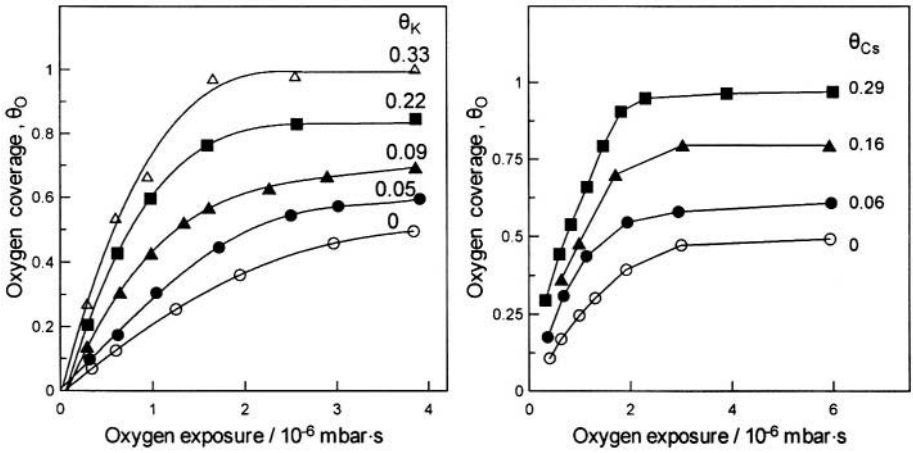

Figure 2.20. Oxygen uptake curves for K (left)[61] and Cs (right)[60] dosed Ru(001) at T=300 K.[60,61] Reprinted with permission from Elsevier Science.

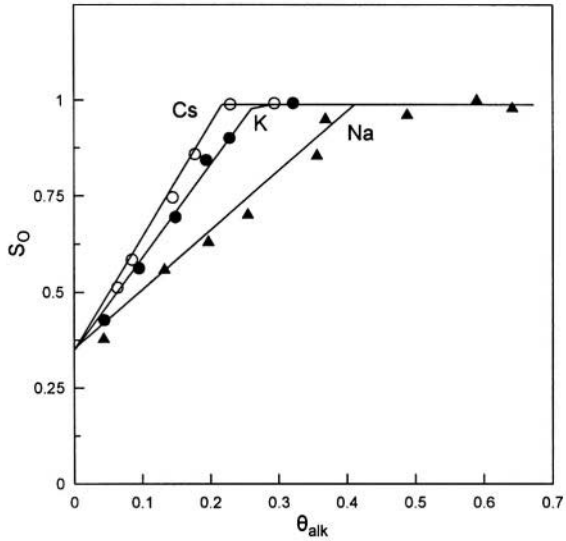

Figure 2.21. Initial sticking coefficient of oxygen, S_0, on alkali modified Ru(001) as a function of alkali coverage.[61] Reprinted with permission from Elsevier Science.

stabilization of the molecular precursor and lowering of the activation barrier for dissociation, due to enhancement of the backdonation of electron density into the $1\pi^*$ antibonding orbitals of oxygen molecule.[6] The preferred adsorption state of oxygen on the alkali modified surfaces and the dependence of the variation of the surface work function with increasing oxygen coverage on preadsorbed alkali coverage is largely determined by the competition between the metal surface atoms and the alkali adspecies for bonding with the adsorbed oxygen. Above some critical oxygen and alkali coverages, depending on the metal substrate, the formation of stable alkali-oxygen surface complexes can be observed as the interactions between the adsorbed oxygen and alkali species become dominant.

2.5.1.5 Hydrogen Adsorption

The effect of alkali additives on H_2 chemisorption has been studied in detail since hydrogen is a main reactant in many catalytic reactions of industrial importance (Fischer-Tropsch synthesis, ammonia synthesis etc). On most of the transition metals hydrogen is dissociatively adsorbed with initial sticking coefficient on the order of 0.5 to 1, it is strongly bonded to the metal surface and occupies the sites with the highest coordination. The strength of the hydrogen chemisorptive bond increases with increasing d-electron density of the substrate,

A general conclusion regarding H_2 adsorption on alkali modified metal surfaces is that alkali addition results in a pronounced decrease of the dissociation adsorption rate of hydrogen as well as of the saturation coverage.

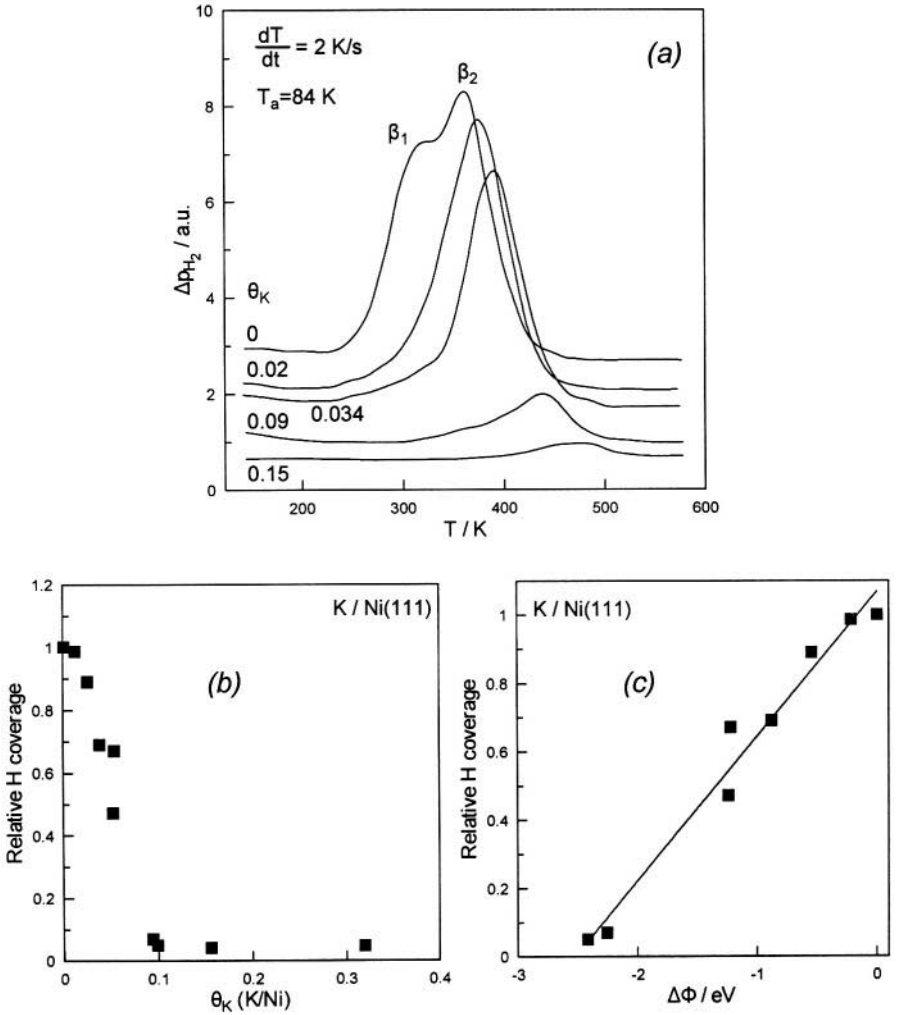

Figure 2.22. (a) H_2 TPD spectra from K-covered Ni(111) for various K coverages. (b) Effect of K coverage on saturation hydrogen coverage (c) effect of corresponding work function value[63] on the saturation hydrogen coverage.[63] Reprinted with permission from the American Institute of Physics.

On K modified Ni(100) and Ni(111)[62,63] and Pt(111)[64] the dissociative adsorption of hydrogen is almost completely inhibited for potassium coverages above 0.1. This would imply that H behaves as an electron donor. On the other hand the peaks of the hydrogen TPD spectra shift to higher temperatures with increasing alkali coverage, as shown in Fig. 2.22a for K/Ni(111), which would imply an electron acceptor behaviour for the chemisorbed H. Furthermore, as deduced from analysis of the TPD spectra, both the pre-exponential factor and the activation energy for desorption

increase with increasing alkali coverage which indicate electron donor and electron acceptor behaviour respectively. As shown in Fig. 2.22b the relative H uptake decreases linearly with increasing K coverage and with decreasing work function Φ (Fig. 2.18c), again consistent with electron donor behaviour. It may thus be concluded that in presence of alkalis, H adsorption is significantly hindered but exhibits amphoteric, i.e. both electron acceptor and electron donor characteristics with site blocking playing an important role.

2.5.1.6 Nitrogen Adsorption

The effect of alkali additives on N_2 chemisorption has important implications for ammonia synthesis on iron, where alkali promoters (in the form of K or K_2O) are used in order to increase the activity of the iron catalyst.

The chemisorption of nitrogen on transition metal surfaces shows similarities to the chemisorption of CO, as the two molecules are isoelectronic and have a similar structure. Two molecular N_2 adsorption states can be observed (termed γ-N_2 and α-N_2, respectively), depending on the substrate and the presence of modifier adatoms. The γ-N_2 state corresponds to a weakly bonded molecular state (the corresponding adsorption binding energy on transition metals ranges from 20 to 40 kJ/mol) with the molecular axis perpendicular to the surface plane. The bonding of the γ-N_2 state to the metal surface takes place mainly via transfer of 5σ-electron density from the adsorbed molecule to the metal, i.e. molecular N_2 adsorbed in this state shows electron donor behavior. The α-N_2 state has been detected only on Fe(111)[65-67] and corresponds to a 'side-on' bonded state where both nitrogen atoms interact with the metal. In this case the key orbitals of the nitrogen molecule participating in bonding with the substrate surface are the 1π (bonding) and $1\pi^*$ (antibonding) orbitals. Contrary to the γ-N_2 state, the α-N_2 state exhibits electron acceptor behavior due to the much stronger backdonation into the $1\pi^*$ antibonding orbitals.

This backdonation of electron density from the metal surface also results in an unusually low N-N streching frequency in the α-N_2 state compared to the one in the γ-N_2 state, i.e. 1415 cm^{-1} and 2100 cm^{-1}, respectively, for Fe(111)[68]. Thus the propensity for dissociation of the α-N_2 state is comparatively higher and this state is considered as a precursor for dissociation. Because of the weak adsorption of the γ-state both the corresponding adsorption rate and saturation coverage for molecular nitrogen are strongly dependent on the adsorption temperature. At room temperature on most transition metals the initial sticking coefficient does not exceed 10^{-3}.

The adsorption in the α-N_2 state proceeds mainly via previous adsorption in the γ-N_2 state. Direct adsorption in the α-N_2 state corresponds to a rather low sticking coefficient ($\sim 10^{-3}$) but is the only adsorption route at higher

temperatures where the coverage of the α-N_2 state becomes negligible. At temperatures higher than the desorption temperature of the molecularly adsorbed nitrogen, the only stable surface species is adsorbed nitrogen atoms resulting from dissociative adsorption of N_2 via the precursor γ-N_2 state. Contrary to the weakly bonded molecularly adsorbed nitrogen, the adsorbed nitrogen atoms are strongly bonded to the metal substrate surface.

The presence of alkali additives on transition metal surfaces inhibits the molecular adsorption of N_2 in the electron donor γ-N_2 state, due to the repulsive barrier introduced by the alkali adspecies. On K/Ru(001)[69] and K/Ni(111),[70] where no other molecular state except the γ-N_2 state is detected, molecular adsorption of nitrogen is completely suppressed at potassium coverages higher than 0.1. The same inhibiting effect of K preadsorption on the γ-N_2 coverage is observed on Fe(111),[68,71] where, as revealed by vibrational and TPD data,[71] at K coverages above 0.16 the initial γ-N_2 state is completely removed with the concomitant appearance of a more strongly bonded donor state, termed promoted γ*-N_2 state. This promoted state, which can be converted to the α-N_2 state, corresponds to stabilization of the initial γ-N_2 state via short-range attractive interactions with the alkali adspecies, allowed by the close proximity of the nitrogen and alkali adspecies at high alkali coverages.

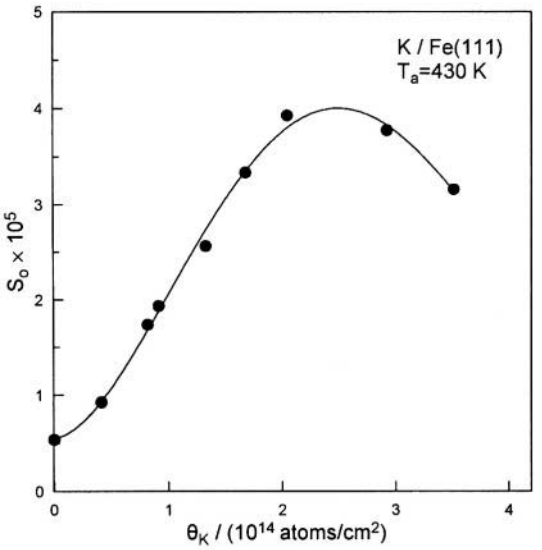

Figure 2.23. Changes in the initial sticking coefficient for N_2 dissociative adsorption on K-covered Fe(111) as a function of K coverage. T_a=430 K.[72] Reprinted with permission from Elsevier Science.

Contrary to the γ-N_2 state, on the same Fe(111) surface the presence of alkali adatoms enhances the adsorption rate, stability and saturation coverage of the π-bonded α-N_2 state, which exhibits electron acceptor behavior. This behavior is explained by the donation of electron density initially from the strongly electropositive alkali species to the metal which enhances the backdonation of electron density from the metal into the π^*orbitals of the chemisorbed nitrogen molecules (Fig. 2.1). Since the α-N_2 state acts as a precursor for nitrogen dissociative adsorption, the presence of alkali adspecies also increases the rate of dissociative adsorption at higher temperatures of catalytic interest. This is shown in Fig. 2.23 which depicts the promoting effect of K on the initial sticking coefficient for N_2 dissociative adsorption on K/Fe(111) at 430 K. Interestingly the presence of alkali does not affect significantly the saturation coverage of N on the K-promoted Fe(111) surface. At this temperature (430 K) or higher temperatures of catalytic interest the maximum alkali coverage cannot exceed ~0.2, i.e. it is always lower than the coverage corresponding to the minimum in the surface work function vs alkali curve.

2.5.1.7 Adsorption of Organic Compounds

Hydrocarbons as well as oxygenated compounds, such as alcohols, are reactants or products in a large number of metal catalyzed reactions of great industrial importance (e.g. Fischer-Tropsch synthesis). The mode and strength of adsorption of organic compounds on catalytic surfaces plays a dominant role, concerning not only the activity but, more important, the selectivity to specific products. In this respect the effect of additives, acting as poisons or promoters, is crucial in determining the desired direction of a reaction where organic species participate. Here we examine the effect of alkali additives on the adsorption of C_2H_4 and CH_3OH.

2.5.1.7.1 Adsorption of Ethylene

Unsaturated organic molecules, such as ethylene, can be chemisorbed on transition metal surfaces in two ways, namely in π-coordination or di-σ coordination. As shown in Fig. 2.24, the π type of bonding of ethylene involves donation of electron density from the doubly occupied π orbital (which is σ-symmetric with respect to the normal to the surface) to the metal ds-hybrid orbitals. Electron density is also backdonated from the p_x and d_{xz} metal orbitals into the lowest unoccupied molecular orbital (LUMO) of the ethylene molecule, which is the empty asymmetric π^* orbital. The corresponding overall interaction is relatively weak, thus the sp^2 hybridization of the carbon atoms involved in the ethylene double bond is retained.

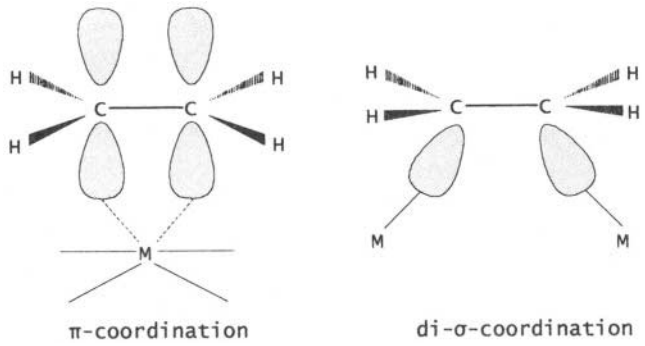

Figure 2.24. π- and σ- coordination of ethylene on metal surfaces.[73] Reprinted with permission from Elsevier Science.

The di-σ type of bonding corresponds to coordination of an ethylene molecule with two surface metal atoms, forming two σ-bonds via two electrons originally participating in the ethylene double bond. This bonding is accompanied by rehybridization of the carbon atoms to produce four tetrahedrally directed bonds corresponding to sp^3 hybridization. It also involves significant backdonation from the ds-hybrid metal orbitals to the antibonding π* orbitals of the adsorbed ethylene. Rehybridization accompanying the di-σ type of bonding allows for overcoming of the repulsive interaction between the π orbitals of ethylene and the d_{z^2} metal atomic orbital, when the latter becomes nearly completely occupied, as, for example, in the case of Pd or Pt.[73]

The relative amount of the di-σ and π-bonded ethylene is different for different transition metals and crystallographic planes. The di-σ bonded ethylene is more strongly bonded on the metal surface compared to the π-bonded ethylene and is the most favorable configuration at low ethylene coverages. At temperatures above ~300 K it is dehydrogenated in stages forming as a final product a graphitic layer of carbon. For instance, on a Pt(111) face, where the molecular adsorption state of ethylene at T>100 K corresponds solely to di-σ bonded species, the adsorbed intermediates and their corresponding formation temperatures, as determined by TPD, are the following:

$$C_2H_4(ads) \xrightarrow{250\ K} C\text{-}CH_3(ads) \xrightarrow{440\ K} CH_x(ads) \xrightarrow{>600\ K} C(ads)$$

The temperature regimes for the stability of intermediates is different for various transition metals. For example on Fe(111) the adsorbed ethylene decomposes partially at 200 K, while the conversion to surface carbon is complete at 370 K. Similarly, on nickel faces molecular chemisorption of ethylene is restricted to temperatures below ambient. At temperatures between approximately 290 K and 450 K ethylene chemisorption on nickel

faces is dissociative, resulting in chemisorbed hydrogen atoms and chemisorbed ethylidyne species ($C\text{-}CH_3(ads)$), which can be further dehydrogenated at higher temperatures.

The effect of the presence of alkali promoters on ethylene adsorption on single crystal metal surfaces has been studied in the case of Pt (111).[74-77] The same effect has been also studied for C_6H_6 and C_4H_8 on K-covered Pt(111).[78,79] As ethylene and other unsaturated hydrocarbon molecules show net π- or σ-donor behavior it is expected that alkalis will inhibit their adsorption on metal surfaces. The requirement of two free neighboring Pt atoms for adsorption of ethylene in the di-σ state is also expected to allow for geometric (steric) hindrance of ethylene adsorption at high alkali coverages.

This is indeed shown in Fig. 2.25 which depicts the effect of K coverage on the TPD spectra of C_2H_4, H_2 and C_2H_6 following C_2H_4 adsorption at T_a=100 K.

Increasing K coverage suppresses remarkably the adsorption of C_2H_4 at its strongly bonded state (α_2) and forces it to adsorb in the very weakly bonded α_1 state. As expected increasing K coverage also remarkably suppresses the adsorption of H and C_2H_6. Thus C_2H_4, H_2 and C_2H_6 all behave as electron donors.

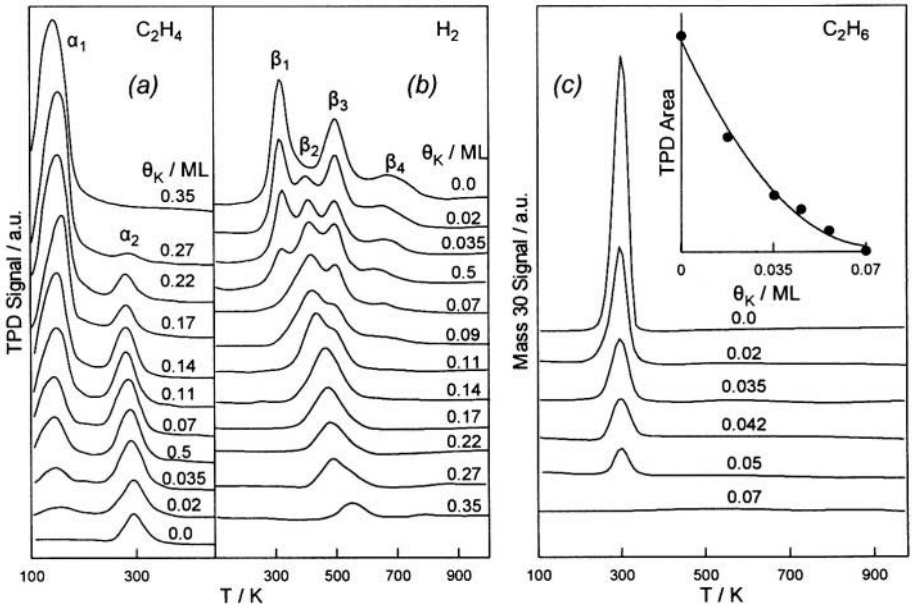

Figure 2.25. C_2H_4 (a), H_2 (b) and C_2H_6 (c) TPD spectra recorded after ethylene adsorption on clean and K-covered Pt(111). T_a = 100 K. θ_K values are relative to the saturation K coverage in the first layer taken as unity. Inset: effect of θ_K on C_2H_6 TPD area. The real coverage in monolayers (K adatoms per surface atom) is 3.03 times smaller.[74] Reprinted with permission from Elsevier Science.

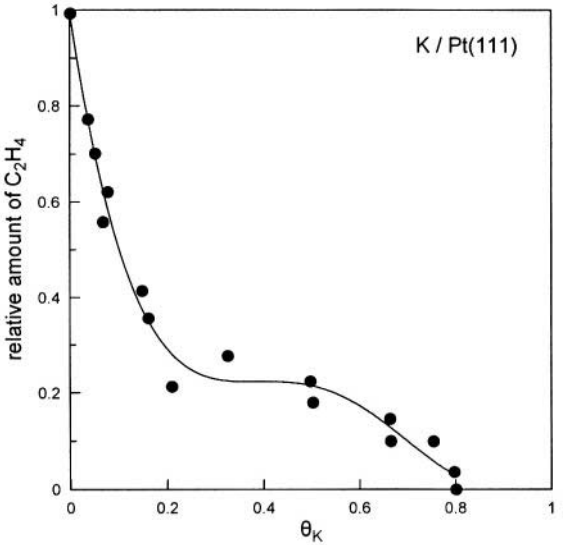

Figure 2.26. Effect of increasing K coverage on the amount of decomposed C_2H_4. θ_K(sat)=0.33 ML.[76] Reprinted with permission from the American Chemical Society.

In addition, as shown in Fig. 2.26, the increase in K coverage causes a dramatic decrease in the amount of decomposed ethylene, which is accompanied by a decrease in the total amount of desorbed hydrogen (Fig. 2.25).

2.5.1.7.2 Adsorption of Methanol

Methanol is adsorbed dissociatively on most transition metal surfaces, in some cases even at temperatures as low as ~100 K, in the form of adsorbed methoxy (CH_3O) and atomic hydrogen species. Molecularly adsorbed methanol or adsorbed methoxy species can appear either with an electron donor configuration (η_1(O) bonding), favoured on surfaces with high work function or an electron acceptor configuration (η_2(C,O) bonding), favoured on surfaces with low work function and thus also on surfaces exposed to aqueous electrolyte media, as also discussed in Chapter 6. The η_1(O) bonding state corresponds to overlapping of the non-bonding oxygen lone pair orbital with a ds hybrid orbital of the metal surface, with negligible backdonation to the π^*-CO antibonding orbital. On the other hand, the η_2(C,O) bonding state corresponds to donation of electron density from the π-CO bonding orbital to a ds hybrid orbital of the metal surface and to strong backdonation of electron density from the metal (ds orbitals) to the π^*-CO orbital, resulting in the weakening of the C-O intramolecular bond and to increasing of the bond strength with the metal surface. With increasing temperature the adsorbed methoxy radical can be decomposed to CO and H_2 or dehydrogenated forming formaldehyde, which can also be further

dehydrogenated to CO on H_2. The reaction channel followed in each case depends on the stability of the methoxy radical and the desorption of formaldehyde on the specific transition metal surface, while it is greatly influenced by the presence of additives on the metal surface.

The interaction of methanol with alkali modified metal surfaces has been studied both on metals which exhibit a high reactivity for decomposition of methanol, e.g. on K/Ru(001)[80,81] or K/Rh(111),[82] and on metals inactive for methanol decomposition, such as on Na/Cu(111).[83,84] In the former case the effect of alkali is coverage-dependent. At low alkali coverages, the presence of alkali adatoms inhibit the methoxy species formation, by inhibiting the breaking of the O-H bond in the methanol molecule[80,81] and stabilize the adsorbed methanol molecular state. By increasing temperature the adsorbed methanol is decomposed and desorbed in the form of CO and H_2, which, due to the presence of alkali, are more strongly bound on the metal surface and desorb at higher temperatures than on the clean surface. The observed effect has been attributed both to steric interactions and to through-the-metal interactions of the alkali adatoms with methanol.

At high alkali coverages (near monolayer coverage), when the adsorbed alkali overlayer shows a metal-like character, alkali-methoxy species are formed. As shown by TPD experiments in the system K/Ru(001) these alkali-methoxy species are more stable than the methoxy species on clean Ru(001) and adsorbed methanol on 0.1K/Ru(001). On metal surfaces inactive for methanol decomposition, e.g. Cu(111), these alkali-methoxy species are formed even at low alkali coverages, due to the weaker interaction of the alkali atoms with the metal surface. The formation of these species stabilizes the methoxy species on the metal surface and enhances the activity of the metal surface for methanol decomposition.

2.5.2 Adsorption of Gases on Surfaces Modified by Electronegative Adatoms

2.5.2.1 CO Adsorption

As already mentioned (section 2.5.1.1.) CO exhibits electron acceptor behavior when adsorbed on transition metal surfaces, due to the increased electron backdonation into the antibonding π^* orbitals of the adsorbed molecule. Thus it is not surprising that the presence of electronegative additives on transition metal surfaces results both in weakening of the CO-metal surface bond and to reduction of the total capacity of the surface for CO adsorption. Furthermore, it reduces the CO adsorption rate and its dissociation propensity. The effect of the electronegative modifier depends not only on its electronegativity and coverage but also on the specific substrate, being different for different substrate crystallographic planes. This is related both to the mode of adsorbed CO (e.g. bridge or on top) and the

configuration of the modifier adsorption sites. The chemical state of the electronegative modifier also plays a certain role in the extent of poisoning of CO adsorption. This is well demonstrated in the case of oxygen (chemisorbed oxygen or subsurface or surface oxide) and carbon (graphitic or carbidic carbon) modifiers, where subsurface oxygen or carbidic carbon have a weaker effect on both the adsorptive capacity of the surface and the dissociation propensity of CO.

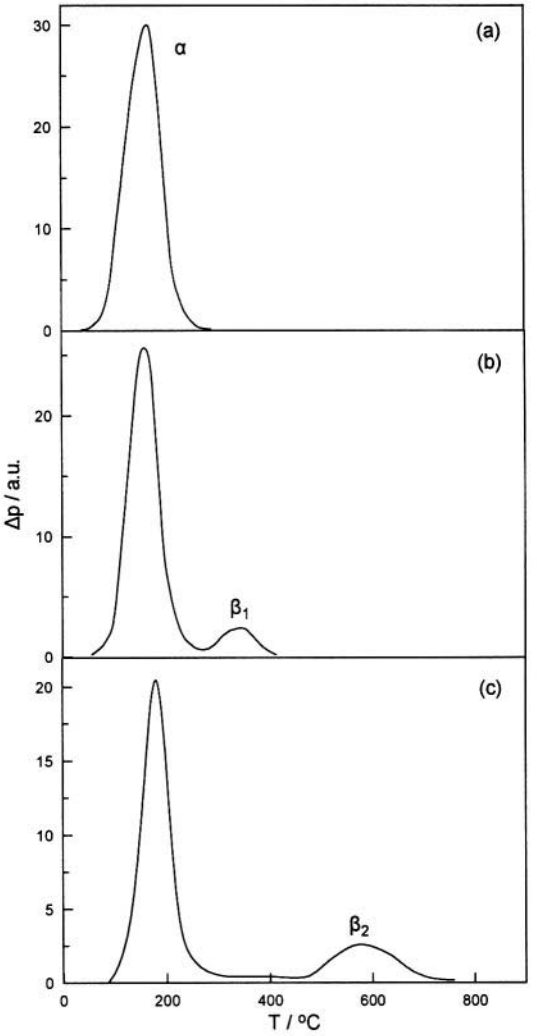

Figure 2.27. Temperature programmed desorption (TPD) spectra of carbon monoxide (measured by Δp) as a function of temperature from nickel surfaces: (a) Ni(111), (b) Ni(111) when the initially dosed surface has been subjected to an electron beam (150 μA for 10 minutes over an area of 1 mm^2) and (c) a cleaved nickel surface.[85] Reprinted with permission from Elsevier Science.

The effect of the presence of electronegative additives on the adsorption of CO and other gases (such as NO, H_2 and hydrocarbons) has been studied mainly using temperature programmed desorption (TPD), as the desorption temperature of the electronegative additives is much higher than the desorption temperature of the adsorbed gases. CO TPD spectra on clean metal surfaces exhibit in general three distinct peaks (Fig. 2.27). The lower temperature peak, termed conventionally the **α-peak,** corresponds to molecularly chemisorbed CO. At higher temperatures a second peak, termed the **β_1-peak,** appears due to the association of chemisorbed carbon and oxygen atoms originating from CO dissociative adsorption. Dissociation of CO on surface defects (e.g. steps) gives rise to a second **β-peak,** termed the **β_2-peak,** at even higher temperatures. The coadsorption of electronegative modifiers changes both the location of the TPD peaks and the shape of the TPD spectra of CO.

The main general features observed in CO TPD spectra with increasing electronegative modifier coverage are: (i) in the case of dissociative CO adsorption (eg. on Ni(100)) a significant decrease of the **β_2-peak,** a less pronounced depopulation of the lower desorption peaks and the appearance of new low temperature peaks, associated with desorption from modifier-induced weakly-bound states. This is shown for example in Fig. 2.28 for the CO TPD spectra, starting from saturation CO coverage, and using Cl or S coadsorbates on a Ni(100) surface.

Similar is the effect of S coadsorption on the CO TPD spectra on Pt(111) as shown in Figure 2.29. Sulfur coadsorption weakens significantly the chemisorptive bond of CO.

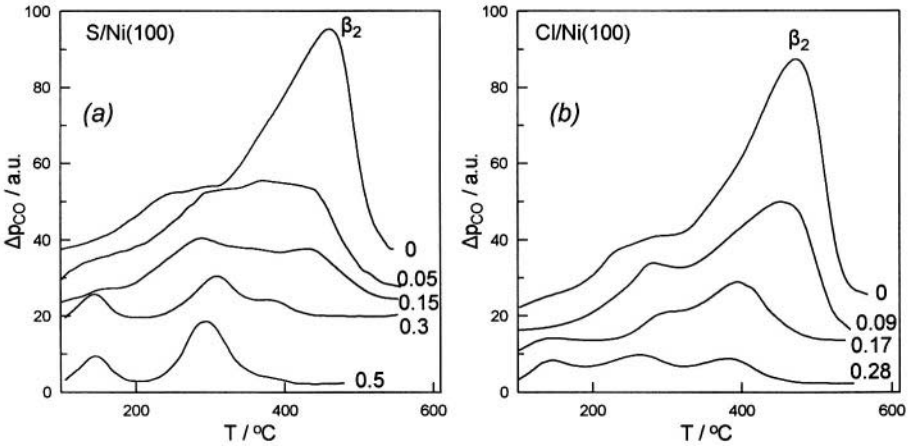

Figure 2.28. Effect of different amounts of (a) S and (b) Cl on the CO TPD spectra from Ni(100) for saturation CO coverages at 100 K.[86] Reprinted with permission from Elsevier Science.

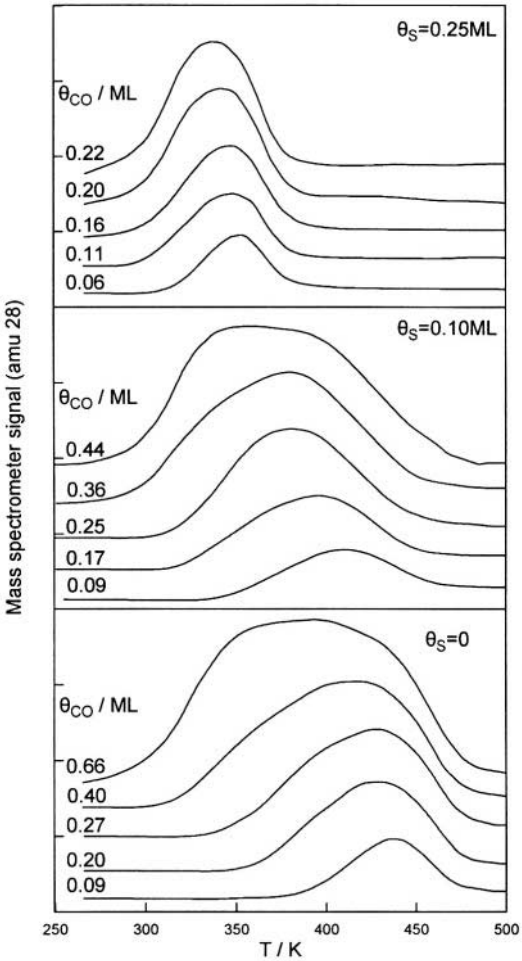

Figure 2.29. CO TPD spectra for clean and sulfided Pt(111) at adsorption temperature T_α=90 K.[87] Reprinted with permission from the American Institute of Physics.

The effect induced by different electronegative additives is more pronounced in the case where the additive adatoms occupy the most coordinated sites forming ordered structures (e.g Cl addition on Ni(100)). In this case (Fig. 2.28) one modifier adatom affects 3-4 CO adsorption sites and complete disappearance of the CO β_2-peak is observed above modifier coverages of ~0.25 or less. The lack of ordering and the tendency of the modifier to form amorphous islands (e.g. P on Ni(100)) diminishes the effect. Thus in the case of P on Ni(100) the disappearance of the CO β_2-peak is observed at P coverages exceeding 0.6.

The effect of electronegative modifiers on the activation energy of CO desorption, E_d, and on the corresponding pre-exponential factor, ν_d, can be quantified by analysis of the TPD spectra at very low CO coverages. The

general conclusion is that E_d and, thus, the strength of the CO-metal bond are always reduced by the addition of electronegative modifiers. For example, a S coverage of ~0.25 on the Pt(111) surface decreases E_d at low CO coverages by 48 kJ/mol compared to the clean Pt(111) surface.

Interestingly, the decrease in E_d is accompanied by a decrease in the pre-exponential factor.[6] The value of the latter, being determined by the entropy of the adsorption state, is affected by the change in the CO chemisorptive bond strength and the presence of neighbouring coadsorbed species which exert strong repulsive forces to the adsorbed CO atoms and also induce changes in the surface potential energy contour.[6]

Besides reduction in the total adsorptive capacity of the surface with respect to CO molecular adsorption, the presence of electronegative modifiers on metal surfaces affects also the CO adsorption kinetics, i.e the sticking coefficient of CO and its dependence on adsorption temperature and CO coverage. As shown in Fig. 2.30, the initial sticking coefficient S_0 of the most strongly bonded adsorbed CO state (β_2-peak) on Ni(100) decreases at 300K almost linearly with increasing electronegative modifier coverage. The effect is more pronounced in the case of Cl (Fig. 2.28) and can be explained in the frame of the precursor state model for non-activated adsorption by a decrease of the lifetime of the precursor, due at least partly to its reduced migration mobility in the presence of the modifier adatoms.[6]

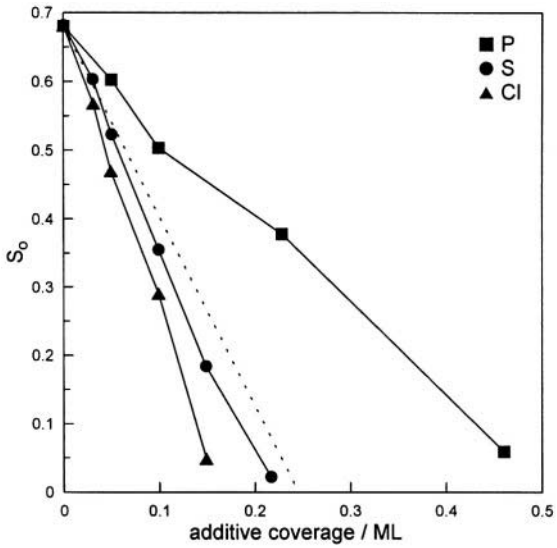

Figure 2.30. Initial sticking coefficient. S_0, of the β_2-CO state on Ni(100) as a function of the additive coverage. The dashed line represents the theoretical dependence according to the relationship $S_0^X = S_0^O (1-\theta_X)$.[6,86] Reprinted with permission from Elsevier Science.

One exception to this general behavior is the system p(2×2) 0.25 O/Pt(111), where, due to the high tendency of coadsorbed CO and O for CO_2 formation on Pt(111), the value of S_0 for CO adsorption is the same to the one for the clean surface, although on other substrates oxygen behaves as a typical electronegative modifier of CO adsorption.

The presence of electronegative modifiers also affects the electronic properties of coadsorbed CO and thus the degree of coupling of its molecular orbitals with the metal surface. This is manifest by photoelectron spectroscopy (core and valence electron energies) and work function data concerning the study of CO chemisorption on clean and modified metal surfaces. Fig. 2.31 shows the effect of CO chemisorption on the work function of clean and oxygen-modified Ni(111) surfaces. The increase in the surface work function observed on the clean metal surface with increasing CO coverage is a general feature for all transition metal surfaces (with the exception of Pt) and manifests that adsorbed CO on these surfaces shows electron acceptor behavior. For oxygen coverages equal to 0.25 or higher, the adsorbed CO starts behaving as an electron-donor and the surface work function decreases with increasing CO coverage.

This is an important observation and is frequently encountered in electrochemical promotion experiments:

In presence of a strong electron acceptor (e.g. O) a weaker electron acceptor (e.g. CO) behaves as an electron donor.

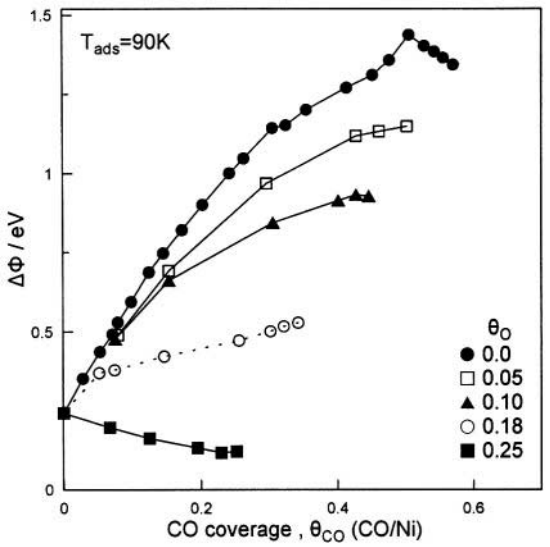

Figure 2.31. CO induced work function changes during adsorption on Ni(111) modified with increasing amounts of oxygen.[88] Reprinted with permission from Elsevier Science.

It is worth remembering the complementary rule already demonstrated in Figure 2.19 regarding NO adsorption on Pt(111) at high NO coverages where, on a clean surface NO behaves as a weak electron donor but shifts to a strong electron acceptor in presence of K:

In presence of a strong electron donor (e.g. Na, K) a weaker electron donor (e.g. NO) behaves as an electron acceptor.

These two "amphoteric" rules play an important role both in classical and in electrochemical promotion as further discussed at the end of this Chapter and in the mathematical modeling of Chapter 6.

As expected, the CO dissociation propensity is reduced in the presence of electronegative modifiers. This is manifest, for example, by the gradual elimination of the β-peak in CO TPD spectra upon coadsorption of electronegative modifier (Figs. 2.28, 2.29 and 2.30).

2.5.2.2 NO Adsorption

The adsorption of NO in presence of electronegative modifiers exhibits similarities with the adsorption of CO, as the electron structure of the two molecules is similar, with the only significant difference the existence of an additional unpaired electron in the $2\pi^*$ molecular orbital of NO. This difference is responsible for the higher dissociative propensity of NO on clean metal surfaces compared to the one of CO. Although both molecules behave in general as electron acceptors, the different reactivity of NO and CO towards certain electronegative modifiers, such as adsorbed oxygen atoms, results in certain cases in characteristic differences concerning the effect of the modifier. For example, oxygen poisons NO adsorption on Pt(111) while it exhibits no poisoning action for CO adsorption, due to the high affinity for CO +O reaction.

2.5.2.2.1 Electronegative Modifiers Effect on the Molecular NO Chemisorption

The effect of electronegative modifiers on the NO molecular adsorption is better illustrated in the case of Pt(111), Pd(111) and Pd(100) systems, where no NO dissociation occurs. The differences observed in the effect of various electronegative modifiers (e.g. between S and O) can be justified in view of the differences both in their effective radius and in their electronegativity, as both short range (steric) and long range electronic (through the metal or direct electrostatic) interactions contribute to the poisoning effect of the modifier. Concerning the effect of coadsorbed oxygen, both the NO saturation coverage of the surface and the initial heat of adsorption are reduced by the presence of oxygen, although the sticking coefficient is not significantly affected at oxygen coverages up to 0.25. Although oxygen has a higher electronegativity, the poisoning effect is much more pronounced in the case of sulfur or Se, where a decrease in the NO initial

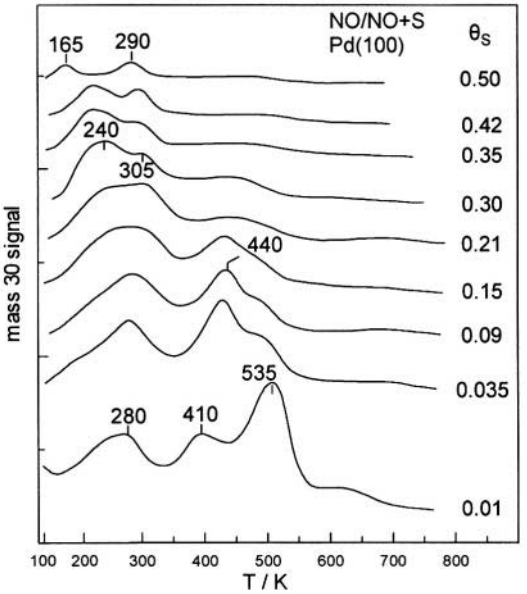

Figure 2.32. NO TPD spectra for saturated NO coverages from sulphur predosed Pd(100). $T_\alpha = 80$ K.[89] Reprinted with permission from Elsevier Science.

sticking coefficient is also exhibited. Similar effects on the adsorptive capacity of the metal surface for NO adsorption and on the NO chemisorptive bond strength have been reported for coadsorption of electronegative modifiers on other transition metal surfaces, e.g. S/Pt(100),[90] S/Ni(100),[91] O/Ni(111),[92] O/Rh(111)[93] and S/Pd.[94]

Fig. 2.32[89] shows the effect of sulfur coverage on NO TPD spectra from Pd(100), for NO adsorption at saturated coverage at 80K. It is clear that by increasing sulfur coverage the most strongly bonded state of NO is removed first at low sulfur coverages (it dissapears at sulfur coverages above ~0.1), while at moderate and high sulfur coverages new weakly bonded NO adsorption states appear. The appearance of such states has also been reported in the case of oxygen-covered Pt(111) surfaces, at high oxygen coverages and has been explained by a transition from bridge-bonded NO to "on-top" bonding.[6]

The same behavior, i.e. modifier-induced changes in the electronic structure of the NO molecule adsorbed on the affected sites, has been observed in other systems, such as O-precovered Rh(111),[93] where at oxygen coverages higher than 0.8 a return to the bridged configuration takes place and on O-precovered Ni(111).[92] In the latter case parallel work function measurements have shown a change in the sign of the dipole moment corresponding to the adsorbed NO, i.e. increase in the work function of the clean surface and decrease in the work function of the oxygen precovered surface with increasing NO coverage. This work function behavior is in

agreement with the two "amphoteric" electron acceptor-electron donor rules discussed in the previous section.

2.5.2.2.2 Electronegative Modifiers Effect on the Dissociative NO Adsorption

On most of the transition metal surfaces, with the exception of Pt(111), Pd(111) and Pd(100), and at temperatures higher than 200 K NO dissociation takes place to a significant extent, competing with molecular NO desorption. The introduction of an electronegative modifier on the metal surface always results in inhibition of the dissociative adsorption and, to a lesser extent, in lowering of the capacity of the surface for molecular adsorption. A typical example is the adsorption of NO on Ni(100) in the presence of coadsorbed sulfur,[91] where NO dissociation is completely inhibited for sulfur coverages of 0.25, corresponding to the formation of a p(2×2) S ordered structure. The poisoning action of sulfur for NO dissociation is higher compared to other electronegative modifiers with higher electronegativity (e.g. O), which can be attributed to the larger size of its adatoms (steric effects).

The same trends regarding the effect of sulfur have been reported for NO adsorption on Pt(100)[90] and Rh(100).[6] In the case of Pt(100) dissociative adsorption is completely inhibited upon formation of a p(2×2) overlayer at a sulfur coverage equal to 0.25, while the binding strength of molecularly adsorbed NO is lowered by more than 50 kJ/mol, as calculated by analysis of NO TPD data. Due to this complete inhibition of dissociative adsorption, the CO+NO reaction is completely deactivated, although it proceeds easily on sulfur free Pt(100). In the case of Rh(100) a sulfur coverage of only 0.08 suffices to completely inhibit NO dissociation at 300 K.

Besides sulfur, which exhibits the strongest poisoning action, other electronegative adatoms, such as O and N, also act as inhibitors of NO dissociative adsorption. For example, in the case of oxygen precovered Rh(111) the complete inhibition of NO dissociation takes place at oxygen coverages higher than ~0.8. In addition, the presence of oxygen destabilizes the molecularly adsorbed NO and the adsorbed nitrogen from the dissociation of NO, resulting in desorption of both NO and N_2 at lower temperatures compared to the oxygen free surface.

This observation is directly related to the observed dramatic electrochemical promotion of NO reduction by CO and C_3H_6 in presence of O_2 on Rh/YSZ upon electrochemical O^{2-} supply to the Rh catalyst surface (Fig. 2.3 and Chapters 4 and 8).

2.5.2.3 Oxygen Adsorption

As already mentioned in section 2.5.1.4, oxygen is dissociatively adsorbed on most metals even below room temperature. Thus under conditions of technological interest (e.g. in the NH_3 oxidation reaction) the

adsorbed oxygen atoms are the only catalytically important oxygen species. The high dissociation propensity of oxygen is due to the strong backdonation of electron density from the metal surface to the $1\pi^*$ antibonding orbitals of the O_2 molecule, which weakens the O-O intramolecular bond. The backdonation contribution to the bonding of oxygen on metal surfaces, which is responsible for the electron acceptor character of the adsorbed oxygen, is higher than in the case of molecules like CO, NO and N_2, the bonding of which also exhibits a donation and a backdonation contribution.

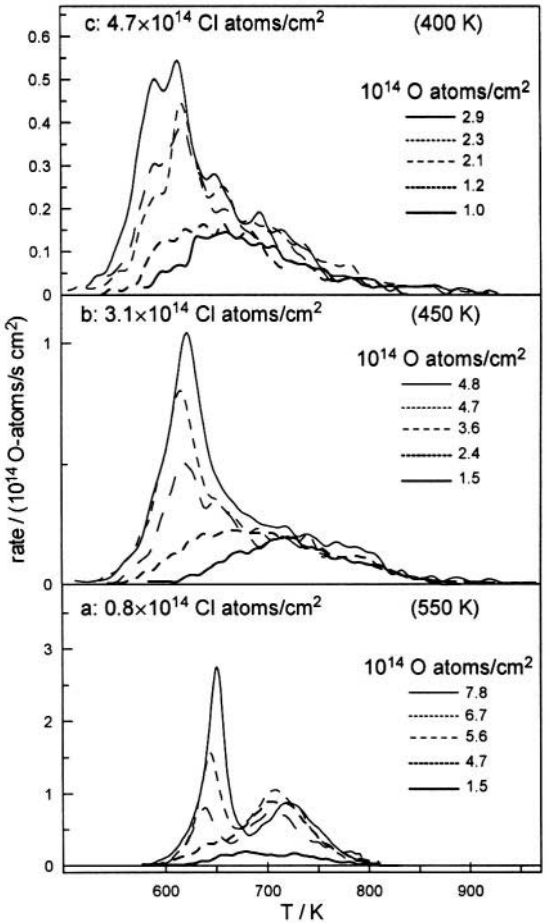

Figure 2.33. Thermal desorption spectra of oxygen from mixed oxygen-chlorine adlayers on Pt(100).[95] The initial chlorine and oxygen concentrations as well as the dosing temperatures are indicated in the figure. Heating rate: 20 K s^{-1}. [95] Reprinted with permission from Elsevier Science.

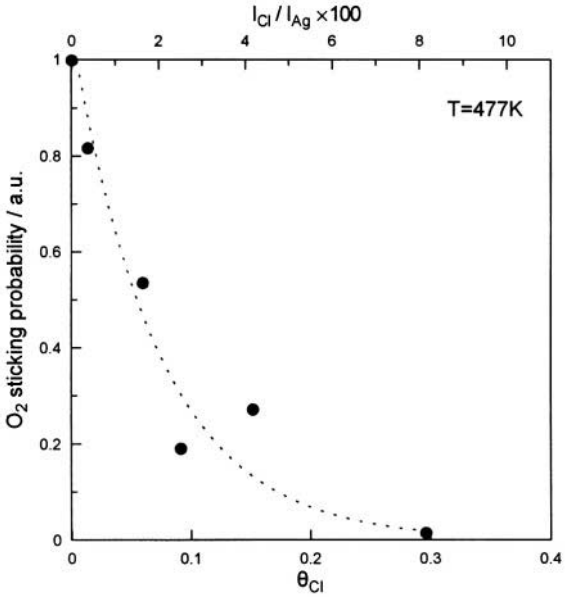

Figure 2.34. The effect of Cl coverage on the rate of oxygen dissociative adsorption on Ag(110).[96] Reprinted with permission from Elsevier Science.

The presence of electronegative additives is expected to destabilize adsorbed molecular states which involve a significant backdonation contribution and thus exhibit electron acceptor behavior. The dissociative adsorption of oxygen (as well as of CO, NO and N_2) proceeds via such a molecular precursor state. Thus it is expected to be inhibited by the presence of electronegative additives due to the resulting mediation of the backdonation to the precursor state. Besides the electronic effect, the presence of electronegative additives may result to blocking of surface sites and reduction of the number of available sites for oxygen atoms adsorption.

Typical examples are shown in Figure 2.33 for the adsorption of O on chlorine-modified Pt(100).[95] Increasing preadsorbed Cl coverage causes a pronounced weakening in the Pt=O bond as manifest by the significant decrease in the peak adsorption temperature.

Figure 2.34 shows the effect of Cl coverage on the sticking probability for the dissociative adsorption of oxygen on Ag(110). Addition of Cl hinders the rate of dissociative adsorption of oxygen, suppressing it almost completely for Cl coverage higher than ~0.25. An almost linear decrease of the saturation oxygen coverage with increasing Cl coverage is also observed and the saturation coverage vanishes for Cl coverages higher than 0.5.

Despite the poisoning action of Cl for oxygen dissociative adsorption on Ag, it is used as moderator in the ethylene epoxidation reaction in order to attain high selectivity to ethylene oxide. The presence of Cl adatoms in this

case favor the adsorption of oxygen in the weakly bonded conformation of atomic oxygen which is responsible for the epoxidation reaction.[97,98]

2.5.2.4 Hydrogen Adsorption

The effect of electronegative additives on H_2 chemisorption is of importance, as hydrogen is a main reactant in many catalytic reactions of industrial importance (Fischer-Tropsch synthesis, ammonia synthesis etc). All relevant studies have shown that this effect appears mainly as a pronounced reduction of the hydrogen dissociative adsorption rate and a decrease in the hydrogen saturation coverage. This is shown, for example, in Figs. 2.35 and 2.36 for Ni(100).[86] It is clear from Fig. 2.35 that the introduction of electronegative

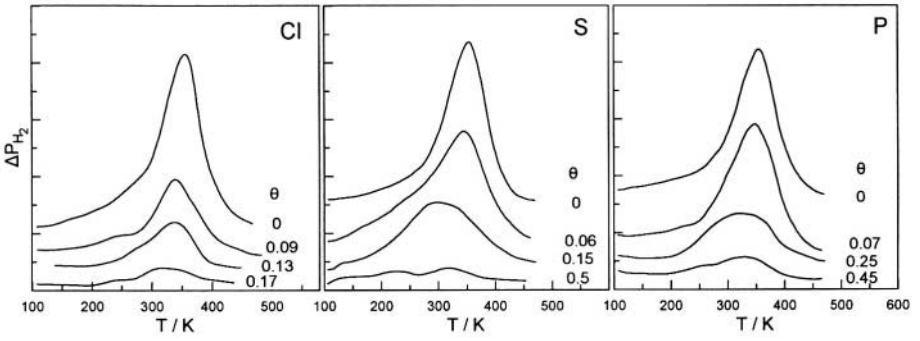

Figure 2.35. Effect of varying chlorine, sulphur and phosphorus precoverages on the H_2 TPD spectra from Ni(100). H_2 exposure 10 L; T_α = 100 K.[86] Reprinted with permission from Elsevier Science.

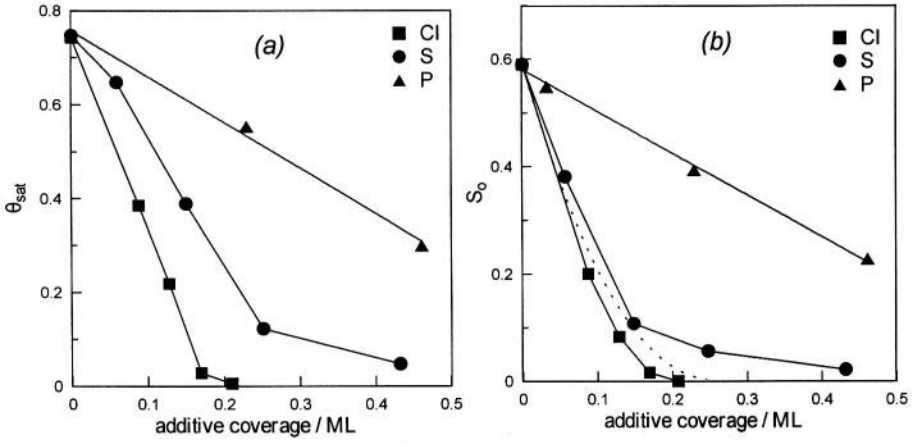

Figure 2.36. (a) Dependence of the hydrogen saturation coverage, θ, at 100 K on the additive coverage. (b) The initial sticking for dissociative hydrogen adsorption, S_0, as a function of the additive coverage. The dashed line represents the theoretical dependence according to the relationship $S_0 = S_0(\text{clean})\,(1-4\theta_X)^2$.[86] Reprinted with permission from Elsevier Science.

adatoms on the Ni(100) surface results in a pronounced reduction of the hydrogen uptake with a parallel small lowering of the peak temperature (opposite to the case of alkali coadsorption) and broadening of the TPD peaks. As can be concluded by analysis of the TPD spectra,[6,86] these changes correspond to a pronounced decrease of both the pre-exponential factor and the activation energy for desorption, opposite to the case of alkali coadsorption, as well as a small weakening of the metal-hydrogen bond (by 10 to 30 kJ/mol). The same general behaviour has been observed for other transition metal surfaces, such as Fe(100), Pd(100) and Pd(111).[6]

Thus, it may again be concluded, as in the case of alkali coadsorption with H, that chemisorbed H exhibits amphoteric, i.e. both electron donor and electron acceptor characteristics.

2.5.2.5 Adsorption of Organic Compounds

The adsorption of organic compounds, such as hydrocarbons and alcohols, is an important step for a large number of industrially important catalytic reactions. It is thus important to examine the effect of electronegative additives, acting as poisons or promoters, on the adsorption of organic compounds on metal surfaces. As in the case of alkali additives, we will focus on the adsorption of C_2H_4 and CH_3OH, as the adsorption of these organic compounds has been extensively studied and the observed effects, are to a large extent common for all similar compounds.

2.5.2.5.1 Adsorption of Ethylene

The coadsorption of oxygen as well as of other electronegative additives on metal surfaces favors in general the π-bonded molecular state of ethylene, as the latter exhibits, compared to the di-σ bonded state, a more pronounced electron donor character and a negligible backdonation of electron density from the metal surface.

On metal surfaces where no secondary reactions take place under UHV between oxygen and hydrocarbon radicals originating from ethylene (due to the high strength of the metal-oxygen bond), e.g. on Ru and Fe,[99,100] the presence of oxygen adatoms reduces the total amount of adorbed ethylene. It also reduces the fraction of adsorbed ethylene molecules which decompose at high temperatures, as it causes stabilization of the adsorbed intermediates originating from ethylene decomposition. For example, on Ru(001) the saturation coverage of the metal surface reduces from 0.3 on the clean surface to 0.1 on Ru(001) covered with a p(2×l) 0.5 O overlayer.[99] In addition the dissociation of ethylene is fully suppressed.

On the contrary, on oxygen-modified metal surfaces where secondary reactions between the adsorbed oxygen and ethylene decomposition products can easily occur, the effect of oxygen on the adsorptive capacity of the

surface and the dissociation propensity of ethylene is negligible at low and moderate oxygen coverages. Typical examples are Pt, Pd and Ir surfaces,[101-105] which are known to be active for CO and hydrogen oxidation reactions. On these metal surfaces the effect of oxygen coadsorption is mainly restricted to stabilization of the π-state of adsorbed ethylene.

Most of the studies concerning the effect of electronegative additives on ethylene adsorption deal with the effect of coadsorbed oxygen and chlorine on different Ag crystallographic planes. This is due to the industrial importance of ethylene epoxidation. As already mentioned (section 2.5.1.7.1), HREELS and IR studies[106,107] have shown that, contrary to the case of other metals, even at fairly high temperatures the adsorption of ethylene on clean Ag (as well as the molecular adsorption of higher olefins) corresponds to a π-bonded (not rehybridized) state with the C-C bond parallel to the surface and with transfer of electron density from the double bond to the surface. The addition of an electron-acceptor species, such as oxygen, increases the amount of adsorbed ethylene, as the π-state exhibits a pronounced electron donor character. The increase in the amount of molecularly adsorbed ethylene and its stabilization on the silver surface is also observed in the presence of other electronegative additives, such as chlorine, which is used as moderator in the selective oxidation of ethylene on silver in order to increase the selectivity to ethylene oxide. This is shown on Fig. 2.37 for the case of ethylene and Cl coadsorption on Ag(111)),[96] where increasing Cl coverage up

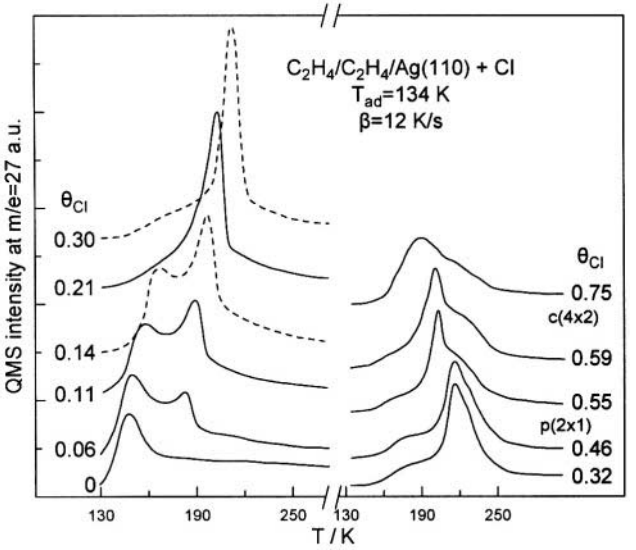

Figure 2.37. C_2H_4 TPD spectra from Ag(110) surfaces with various Cl coverages. Exposure: 10^{-6} mbars, T_α = 134 K.[96] Reprinted with permission from Elsevier Science.

to 0.5 causes an increase in the ethylene TPD peak and a shift of the peak to a higher desorption temperature. The opposite effect is observed at high chlorine coverages, due to the increased occupation by Cl of sites available for ethylene adsorption. For the same reason chlorine also hinders the adsorption of atomic oxygen when it is used as moderator in the ethylene epoxidation reaction. However its introduction has a beneficial effect on selectivity to ethylene oxide as it favors the adsorption of atomic oxygen in its more loosely bound conformation which is responsible for ethylene epoxidation.

The effect of electronegative additives on the adsorption of ethylene on transition metal surfaces is similar to the effect of S or C adatoms on the adsorption of other unsaturated hydrocarbons.[6] For example the addition of C or S atoms on Mo(100) inhibits the complete decomposition (dehydrogenation) of butadiene and butene, which are almost completely decomposed on the clean surface.[108] Steric hindrance plays the main role in certain cases, i.e the addition of the electronegative adatoms results in blocking of the sites available for hydrocarbon adsorption. The same effect has been observed for saturated hydrocarbons.[108,109] Overall, however, and at least for low coverages where geometric hindrance plays a limited role, electronegative promoters stabilize the adsorption of ethylene and other unsaturated and saturated hydrocarbons on metal surfaces.

2.5.2.5.2 Adsorption of Methanol.

The influence of the presence of sulfur adatoms on the adsorption and decomposition of methanol and other alcohols on metal surfaces is in general twofold. It involves reduction of the adsorption rate and the adsorptive capacity of the surface as well as significant modification of the decomposition reaction path. For example, on Ni(100) methanol is adsorbed dissociatively at temperatures as low as ~100K and decomposes to CO and hydrogen at temperatures higher than 300 K. As shown in Fig. 2.38 pre-adsorption of sulfur on Ni(100) inhibits the complete decomposition of adsorbed methanol and favors the production of HCHO in a narrow range of sulfur coverage (between 0.2 and 0.5).

The inhibition of the complete dissociation of the methoxy species in the presence of sulfur can be attributed to the preferable adsorption of the methoxy species in the weakly bonded η_1(C) configuration, as the latter exhibits an electron acceptor character, which favors the molecular desorption of methanol from the metal surface (in general η_n (or η^n) denotes a ligand bonding with n-atoms to the surface). On the other hand, the observed volcano-type behavior in the dependence of HCHO production on sulfur coverage has been attributed to the competition between the sulfur induced increase in the activation energy for complete dehydrogenation of the methoxy species (stabilization of the methoxy species) and the blocking

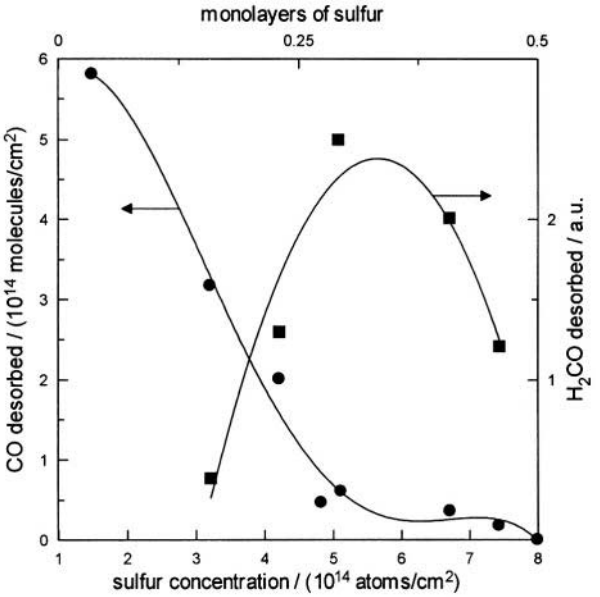

Figure 2.38. Effect of preadsorbed S on the amount of H_2CO and CO formed as a result of CH_3OH interaction with Ni(100).[110] Reprinted with permission from the American Vacuum Society.

by the adsorbed sulfur of the surface sites necessary for dissociative adsorption of methanol to form the methoxy species.[110] This explanation agrees with the complete suppression of HCHO formation at sulfur coverages above 0.4 (Fig. 2.38), where no dissociation of adsorbed methanol is observed.

Carbidic carbon affects the adsorption capacity of metal surfaces for methanol in the same way as sulfur, although the poisoning effect of carbon is less pronounced. Concerning the effect of oxygen coadsorption on methanol adsorption, it has to be taken into account that in this case oxygen acts both as a reactant and as a poison. Similar to the effect of sulfur and carbon coadsorption, the presence of oxygen favors the formation of formaldehyde, inhibiting the complete decomposition of the adsorbed methanol. For example, on Fe(100)[111] formation of HCHO is maximized at oxygen coverages between 0.2 and 0.25, while at oxygen coverages above 0.4 methanol decomposition is completely inhibited and only molecular desorption of methanol is observed in the TPD spectra. Methoxy formation is promoted at low oxygen coverages due to the oxygen assisted abstraction of hydrogen from the methanol molecule, but it is inhibited at high oxygen coverages due to blocking of the methoxy species adsorption sites.

2.6 CATALYTIC ACTIVITY ON SURFACES MODIFIED BY PROMOTERS OR POISONS

In section 2.5 we have examined the effect of promoters and poisons on the chemisorption of some key reactants on catalyst surfaces.We saw that despite the individual geometric and electronic complexities of each system there are some simple rules, presented at the beginning of section 2.5 which are always obeyed. These rules enable us to make some predictions on the effect of electropositive or electronegative promoters on the coverage of catalytic reactants during a catalytic reaction.

Thus referring to the very simple promotional LHHW rate expression (2.17) we can already write it as:

$$r = (1-\theta_p)k_R \cdot k_D(\theta_p) \cdot k_A(\theta_p) \cdot p_D \cdot p_A / [1+k_D(\theta_p) \cdot p_D + k_A(\theta_p) \cdot p_A]^2 \quad (2.25)$$

where the subscripts "D" and "A" from now on and throughout this book refer to an electron donor and an electron acceptor reactant, respectively. By writing $k_D(\theta_p)$ and $k_A(\theta_p)$ we emphasize that the adsorption equilibrium constants k_D and k_A are functions of the coverage, θ_p, of the promoter, p, and in fact, according to the rules of section 2.5 that:

$$\frac{\partial k_D}{\partial \theta_p} < 0 \qquad \frac{\partial k_A}{\partial \theta_p} > 0 \quad (2.26)$$

when $\frac{\partial \Phi}{\partial \theta_p} < 0$, i.e. when p is electropositive and

$$\frac{\partial k_D}{\partial \theta_p} > 0 \qquad \frac{\partial k_A}{\partial \theta_p} < 0 \quad (2.27)$$

when $\frac{\partial \Phi}{\partial \theta_p} > 0$, i.e. when p is electronegative.

Rules 2.26 and 2.27 can be rewritten as:

$$\frac{\partial k_D}{\partial \Phi} > 0 \qquad \frac{\partial k_A}{\partial \Phi} < 0 \quad (2.28)$$

and thus equation (2.25) can also be expressed as:

$$r = (1-\theta_p)k_R \cdot k_D(\Phi) \cdot k_A(\Phi) \cdot p_D \cdot p_A / [1+k_D(\Phi) \cdot p_D + k_A(\Phi) \cdot p_A]^2 \quad (2.29)$$

It should be emphasized that Φ is the actual, promoter modified, work function of the catalyst surface and not that of a clean metal surface for which we reserve the symbol Φ_0. It should also be clarified that the kinetic constant k_R is also expected to vary with Φ. Since, however, we have no rules on how it varies with Φ we will attempt here to rationalize some classical promotional kinetics treating it as a constant. What is amazing is that this procedure works, which indicates that the promoter action effect on k_D and k_A, together with the $1-\theta_p$ term, is dominant.

Needless to remind that Equation (2.29) is a very approximate expression which can be expected to provide only a qualitative description and not a quantitative fit to actual promotional kinetic data.

Most of the published promotional kinetic studies have been performed on well defined (single crystal) surfaces. In many cases atmospheric or higher pressure reactors have been combined with a separate UHV analysis chamber for promoter dosing on the catalyst surface and for application of surface sensitive spectroscopic techniques (XPS, UPS, SIMS, STM etc.) for catalyst characterization. This attempts to bridge the pressure gap between UHV and real operating conditions.

In the following we will concentrate on three important cases, i.e. CO oxidation on alkali doped Pt, ethylene epoxidation on promoted Ag and synthesis gas conversion on transition metals. We will attempt to rationalize the observed kinetic behaviour on the basis of the above simple rules.

2.6.1 CO Oxidation on Li-doped Pt(111) Surfaces

The oxidation of CO on Pt is one of the best studied catalytic systems. It proceeds via the reaction of chemisorbed CO and O. Despite its complexities, which include island formation, surface reconstruction and self-sustained oscillations, the reaction is a textbook example of a Langmuir-Hinshelwood mechanism the kinetics of which can be described qualitatively by a LHHW rate expression. This is shown in Figure 2.39 for the unpromoted Pt(111) surface.[112] For low p_{CO}/p_{O_2} ratios the rate is first order in CO and negative order in O_2, for high p_{CO}/p_{O_2} ratios the rate becomes negative order in CO and positive order in O_2. Thus for low p_{CO}/p_{O_2} ratios the Pt(l 11) surface is covered predominantly by O, at high p_{CO}/p_{O_2} ratios the Pt surface is predominantly covered by CO.

What predictions can we make about the effect of an electropositive additive, such as Li, on the basis of the rules of Section 2.5 or, equivalently, from equations (2.28) and (2.29)?

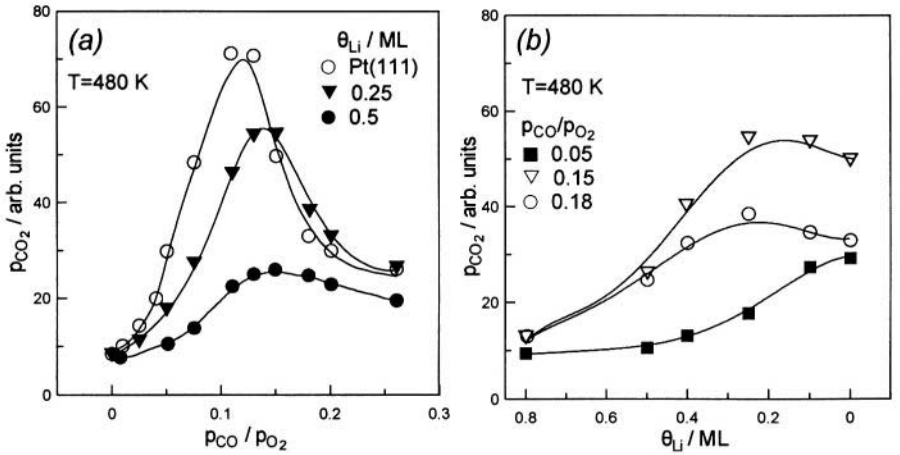

Figure 2.39. (a) Effect of p_{CO}/p_{O_2} on the rate of CO oxidation (measured as p_{CO_2}) on Pt(111) covered with various Li coverages θ_{Li}[112] (b) Effect of Li coverage on the rate of CO oxidation at various fixed p_{CO}/p_{O_2} values.[112] Reprinted with permission from Elsevier Science.

It is clear that as we introduce Li on the Pt(111) surface, the work function Φ will *decrease* (Eq. 2.21) and thus (Eq. 2.28) k_D will *decrease* and k_A will *increase.*

It is also clear that in the present case oxygen is the electron acceptor (A) while CO is the electron donor (D). It has been already discussed that CO is an amphoteric adsorbent, i.e., its chemisorptive bond involves both electron donation and backdonation and that, in most cases, its electron acceptor character dominates. However, in presence of the coadsorbed strong electron acceptor O (see section 2.5.2.1) it always behaves as an electron donor.

Consequently upon adding Li on the Pt surface $k_{CO}(=k_D)$ *decreases* and k_O $(=k_A)$ *increases.* Thus from Eq. (2.29) one expects a *decrease* (poisoning) in the rate under CO *lean conditions* and an *increase* (promotion) in the rate under CO *rich conditions.* This is exactly what Figure 2.39 shows for moderate Li coverages. Note that when the Li coverage, θ_p, becomes too high (>0.4) then the $(1-\theta_p)$ term in Eq. (2.29) dominates and Li poisons the rate under both CO lean and CO rich conditions.

Thus the promoting and poisoning role of Li, or any other alkali, can be *predicted* in a qualitative way from the simple rules of section 2.5 or, equivalently, from equations (2.28) and (2.29).

2.6.2 Ethylene Epoxidation

The epoxidation of ethylene on Ag is a reaction of great industrial importance which has been studied extensively for many decades. From a

promotional viewpoint this is an extremely interesting and complex system, as the goal here is not so much to increase the rate but rather to enhance the selectivity to ethylene oxide vs CO_2. Thus the promotional rules of section 2.5 have to be adjusted for selectivity maximization by recognizing that the selectivity to ethylene oxide depends crucially on the state of chemisorbed ethylene and oxygen which can be significantly affected by promoters.

Ethylene is currently converted to ethylene oxide with a selectivity of more than 80% under commercial conditions. Typical operating conditions are temperatures in the range 470 to 600 K with total pressures of 1 to 3 Mpa. In order to attain high selectivity to ethylene oxide (>80%), alkali promoters (e.g Rb or Cs) are added to the silver catalyst and ppm levels of chlorinated hydrocarbons (moderators) are added to the gas phase. Recently the addition of Re to the metal and of ppm levels of NO_x to the gas phase has been found to further enhance the selectivity to ethylene oxide.

Understanding the mechanism of ethylene epoxidation has been the focus of a large number of studies using supported and single crystal surfaces. A summary of the work in this area can be found in a comprehensive review.[97] There is a general agreement that atomic oxygen is the active oxygen species both for ethylene epoxidation and deep oxidation,[97,98,113-115] while molecularly adsorbed oxygen is rather inactive and behaves as a "spectator" species.[113,114] Subsurface oxygen plays also an important role, as it is necessary for obtaining high selectivity to ethylene oxide, although it does not directly participate in catalytic events.[98,113,114] As ethylene oxide formation involves insertion of atomic oxygen into the ethylene molecule carbon-carbon bond, epoxidation requires that ethylene is molecularly adsorbed on the silver catalyst at the reaction temperature, which is the case since silver (d^{10}) has no open (unfilled) d-shell (section 2.5.1.7.1). As mentioned in section 2.5.2.5.1, the weak **π-type** ethylene adsorption on clean silver is enhanced in the presence of preadsorbed oxygen, which acts as electron acceptor and creates positively charged adsorption sites necessary for ethylene adsorption.

It is generally agreed in the literature that the selectivity to ethylene oxide is governed by the binding state of atomic oxygen,[97,98,115,116] which can exist on the catalyst surface in two extreme conformations (Fig. 2.40) rather than two intrinsically distinct forms.[98,114] Weakly bound, electrophilic adsorbed oxygen (**α-oxygen** or electrophilic oxygen) reacts preferentially with the **π-electrons** of adsorbed ethylene thus producing epoxide. On the other hand, strongly bound, bridging oxygen atoms coordinated to Ag ions of low charge (**β-oxygen** or ionic oxygen) attack preferentially the hydrogen atoms of adsorbed ethylene with concomitant C-H bond rupture and CO_2 formation.[98,114] This mechanism explains the role of subsurface oxygen, the presence of which causes a weakening in the bond strength of adsorbed atomic oxygen via withdrawal of electrons from the silver sites, thus favoring the formation of the electrophilic oxygen atoms which produce ethylene oxide. The ability of

silver to adsorb ethylene molecularly (in the π-state) at fairly high temperatures and also to adsorb oxygen in a weakly bound electrophilic atomic state is most likely the reason that Ag is rather unique for the epoxidation of ethylene.

The role of alkali promoters and electronegative moderators in ethylene epoxidation is related to their effect on the coverage and binding strength of adsorbed atomic oxygen and of ethylene,[97,98,113-117] according to the basic ideas described in the previous sections. The effect of chlorine moderator can be understood as follows: Chlorine atoms replace strongly adsorbed oxygen atoms, as they compete with them for the same sites.[117] Chlorine can also adsorb into the subsurface layer[67,118,119] weakening the bond strength of co-adsorbed oxygen by withdrawal of electrons from the silver atoms and by creation of sites for the adsorption of weakly bound electrophilic oxygen, which interacts with the double bond of ethylene molecule producing ethylene oxide.[97] Regarding ethylene adsorption, the presence of chlorine atoms stabilize the molecularly adsorbed π-state, similar to the effect of oxygen co-adsorption. However, the induced increase in the strength of the chemisorptive bond of ethylene may render it at high chlorine coverages more susceptible to preferential complete oxidation

The presence of alkali promoters has been reported to destabilize the molecular adsorption state of ethylene (electron donor) and to increase both the adsorption rate and the saturation coverage of adsorbed oxygen but also the bond strength of adsorbed oxygen.[120] As a result, in the absence of chlorine moderator alkali adsorption does not increase the selectivity to ethylene oxide or does so only slightly. On the other hand, the alkali induced increase in selectivity in the presence of chlorine has been attributed[121] to stabilization of the adsorbed chlorine and maintainance of a high chlorine coverage. In effect, alkali stabilizes the silver-oxychloride surface complex, which is formed by attachement of oxygen and chlorine to the same silver

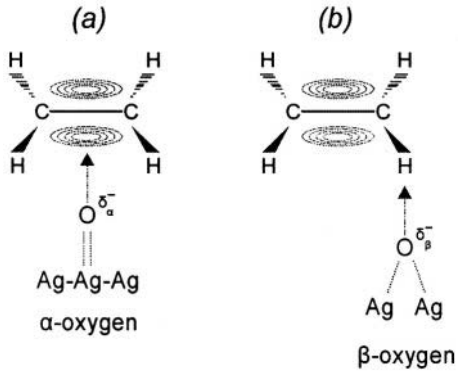

Figure 2.40. Schematic of the two extreme conformations of adsorbed atomic oxygen on Ag: covalently bonded electrophilic oxygen (α-) and ionically bonded oxygen (β-).[98] Reprinted with permission from Academic Press.

atom and which is actually the ethylene epoxidation agent. The inhibition of the isomerization of ethylene oxide to acetaldehyde,[122] which is considered as the rate determining step in the further conversion of ethylene oxide to complete oxidation products,[98] may also contribute to the alkali induced selectivity increase.

In summary one can view the ethylene epoxidation system as one where selectivity maximization requires the coexistence of the following two adsorption reactant states:

(a) π-bonded electron donor ethylene (D)
(b) weakly bonded electrophilic oxygen (A)

According to the first rule of section 2.5 both desired states are stabilized by:

(i) coadsorbed Cl
(ii) coadsorbed ionically bonded O
(iii) subsurface oxygen

In this sense subsurface oxygen is also acting as a promoter. The role of the alkali promoter is then to stabilize Cl and anionically bonded O (or nitrate ions) on the catalyst surface, so they can exert their promotional action. Thus alkalis in this system, which requires electronegative promoters according to the rules of section 2.5, are not really promoters but rather promoter stabilizers. This is proven by their inability to promote selectivity in absence of Cl.

The commonly held view of the uniqueness of Ag for ethylene epoxidation may soon change in view both of the propene epoxidation work of Haruta and coworkers on Au/TiO_2 catalysts upon cofeeding H_2 [123] and also in view of the recent demonstration by Lambert and coworkers[124-126] that Cu(111) and Cu(110) surfaces are both extremely efficient in the epoxidation of styrene and butadiene to the corresponding epoxides. In fact Cu was found to be more selective than Ag under UHV conditions with selectivities approaching 100%.[124-126] The epoxidation mechanism appears to be rather similar with that on Ag as both systems involve O-assisted alkene adsorption and it remains to be seen if appropriately promoted Cu[124-126] can maintain its spectacular selectivity under process conditions.

2.6.3 Synthesis Gas Conversion Reactions

Synthesis gas $(CO+H_2)$ can be converted into a wide range of products, which range from methane (methanation reaction), through longer chain alkanes and alkenes (Fischer-Tropsch synthesis), to methanol or higher oxygenates (alcohols and aldehydes). The distribution of products depends upon the nature of the catalyst and the reaction conditions employed. Typical catalysts used are Ni/Al_2O_3 for methanation, Fe/SiO_2 for transformation to higher alkanes and alkenes, Cu/ZnO (or Pd/La_2O_3) for methanol synthesis

and Rh/SiO_2 for transformation to higher oxygenates. It is obvious that in the CO hydrogenation catalytic system selectivity is the most interesting aspect. In this respect, the role of promoters (including alkali promoters) is critical, especially for methanol or higher oxygenates synthesis.

The hydrogenation of CO is very appropriate for single crystal studies as it is structurally insensitive. Furthermore, the activation energies and turnover frequencies measured using single crystal surfaces agree well with the values measured for supported catalysts, which facilitates the extrapolation of the results of single-crystal studies to real catalysts. In order to understand the role of alkali promoters in this reaction it is important to refer to the main steps of its mechanism, which are: (i) The adsorption of CO (dissociative or associative), (ii) the dissociative adsorption of hydrogen, (iii) the surface reaction of adsorbed hydrogen atoms with CO or the CO dissociation products to form a wide range of adsorbed reaction intermediates and water and (iv) the formation and desorption of the final products.

The mode of chemisorption of CO is a key-factor concerning selectivity to various products. Hydrocarbons can only be produced if the carbon-oxygen bond is broken, whereas this bond must stay intact for the formation of oxygenates. It is obvious that catalysts favoring the production of hydrocarbons must chemisorb carbon monoxide dissociatively (e.g. Fe) while those favoring the formation of oxygenates must be able to chemisorb carbon monoxide molecularly (e.g. Rh).

It is also clear that in the former case electropositive promoters (alkalis) should enhance the rate of hydrocarbon formation while in the latter case a beneficial effect is to be expected only if CO is weakly adsorbed and to the extent that the alkali does not induce CO dissociation.

To confirm these predictions we examine here in some detail only the case of hydrocarbon production where alkali promoters play an important role in industrial practice.

There is a general agreement in literature[127] that two carbon types are present on the catalyst surface during CO hydrogenation under conditions and catalysts favoring the dissociative adsorption of CO: (i) a reactive carbonacious species, which is commonly termed 'carbidic carbon' and (ii) a graphitic inactive phase which is formed after carbidic carbon has reached a certain coverage and is responsible for the deactivation of the catalyst surface. Carbidic carbon can be hydrogenated before or after the formation of carbon-carbon bonds, resulting either in methane or in higher hydrocarbon formation. The latter case is favored with increasing surface coverage of carbonaceous species. The steady state reservoir of carbidic species on the catalyst surface is controlled by the surface concentration of the competitively adsorbed hydrogen atoms, thus it is expected that besides CO adsorption, the role of alkali promoters should also involve their effect on hydrogen chemisorption.

2.6.3.1 Effect of Alkali Promoters

It is obvious that one can use the basic ideas concerning the effect of alkali promoters on hydrogen and CO chemisorption (section 2.5.1) to explain their effect on the catalytic activity and selectivity of the CO hydrogenation reaction. For typical methanation catalysts, such as Ni, where the selectivity to CH_4 can be as high as 95% or higher (at 500 to 550 K), the modification of the catalyst by alkali metals increases the rate of heavier hydrocarbon production and decreases the rate of methane formation.[128] Promotion in this way makes the alkali promoted nickel surface to behave like an unpromoted iron surface for this catalytic action. The same behavior has been observed in model studies of the methanation reaction on Ni single crystals.[129]

According to the results of such model studies of the methanation reaction on Ni(100) concerning the effect of added K,[129] the rate of methane formation decreases almost linearly with potassium coverage, θ_K, up to θ_K ~0.15, whilst the rate of heavier hydrocarbon production increases. These rate changes are accompanied by an increase of the steady state coverage of carbon (typically 30%), compared to the K-free surface, which manifests directly the enhancement of the dissociative adsorption of CO on the K-promoted nickel surface. The observed shift of the selectivity from methane to hydrocarbons with longer chains and a lower hydrogen content shows clearly that the alkali promoter ihnibits the hydrogen dissociation rate and thus stabilizes on the catalyst surface the carbidic species (mainly in the form of hydrogenated CH_x species), also in view of the fact that the strength

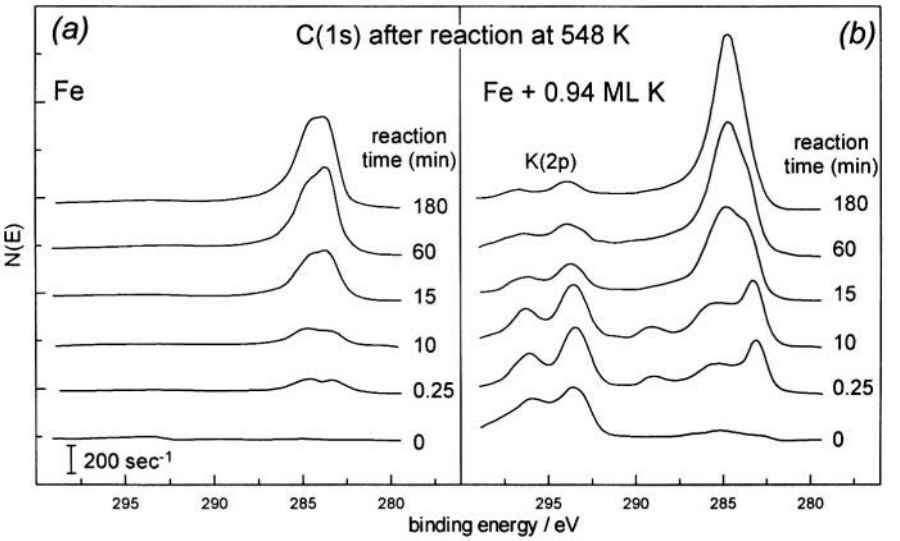

Figure 2.41. X-ray photoemission spectra of Fe foil after CO hydrogenation at 548 K in CO/H_2=1:20 at 1 bar total pressure and varying reaction times. (a) C 1s spectra from K-free Fe. (b) K 2p and C 1s spectra from K-covered Fe, θ_K~0.3.[128] Reprinted with permission of the American Chemical Society.

of the carbon-metal bond increases, promoting the preferential formation of C-C bonds rather than C-H bonds.

The effect of alkali promoters is basically the same for typical catalysts used in Fischer-Tropsch synthesis, such as iron. On an unpromoted Fe surface in contact with synthesis gas under reaction conditions, coverage by carbidic carbon is extensive. Alkali promotion (e.g. by potassium, which in the present reaction acts most effectively compared to the other alkalis) would be expected to enhance the dissociative adsorption rate of CO and inhibit the H_2 dissociation rate, thus leading to even higher carbidic carbon coverage and to the suppression of the hydrogen coverage. This is clearly shown on Fig. 2.41 which compares C1s XPS spectra for a clean and a K-covered Fe foil surface after different reaction times at 548K and 1bar total pressure. Both the carbidic carbon peak at 283.6eV and the graphitic carbon peak at 285.8 eV are increased in the case of the K-promoted Fe surface compared to the unpromoted one.

It is obvious that the higher ratio of carbon to hydrogen on the alkali promoted iron surface will enhance the formation of C-C bonds, thus the formation of longer chain hydrocarbons, and the formation of unsaturated products, as the availability of the chemisorbed hydrogen atoms is reduced and the reactive desorption by hydrogenation is suppressed. This is exactly the behavior observed in alkali promoted iron catalysts, either supported or unsupported ones. When the surface concentration of alkali promoters is too high, formation of waxes[130] or even a decrease in the total reaction rate is observed, due to the alkali induced increase of the coverage of the unreactive graphitic carbon (Fig. 2.41). Thus there is always an optimum concentration of promoters, different for different Fischer-Tropsch catalysts. In commercial iron catalysts some nitrogen is also introduced on the alkali promoted surface, as it has been found to enhance the promoting action of alkalis.[5]

Summarizing, the main promoting action of alkali additives in the CO hydrogenation reaction is the induced change of the selectivity of the promoted catalysts towards the formation of higher hydrocarbons and unsaturated products. A decrease in the overall reaction activity can be observed in certain cases, such as for Fe catalysts, above a certain alkali concentration. The promoting action is due (i) to the enhancement of the CO dissociation propensity, which increases the coverage of the carbon species (ii) the inhibition of the hydrogen dissociation, which decreases the coverage of adsorbed hydrogen atoms (iii) the suppression of the hydrogenation reactions, due to the preferential formation of C-H bonds under the conditions of high carbon to hydrogen ratio on the catalyst surface and (iv) the destabilization of the adsorbed state of the unsaturated hydrocarbons, as the alkali presence results in decrease of their adsorption energy.

2.6.3.2 Effect of Electronegative Additives

As in the case of alkali promoters, the basic ideas concerning the effect of electronegative additives on hydrogen and CO chemisorption (section 2.5.2) can be used to to explain their effect on the catalytic activity and selectivity of the CO hydrogenation reaction. The electronegative additive most thoroughly studied is sulfur, which in a variety of chemically combined forms is a commonly encountered impurity in the CO hydrogenation rections. Most studies focus on nickel catalysts, either supported or single crystals. The poisoning action of sulfur and other electronegative adatoms may reflect both geometrical and electronic effects and depends also on the specific substrate and the difference in the electronegativities of the adatom and the substrate.

The influence of electronegative additives on the CO hydrogenation reaction corresponds mainly to a reduction in the overall catalyst activity.[131] This is shown for example in Fig. 2.42 which compares the steady-state methanation activities of Ni, Co, Fe and Ru catalysts relative to their fresh, unpoisoned activities as a function of gas phase H_2S concentration. The distribution of the reaction products is also affected, leading to an increase in the relative amount of higher unsaturated hydrocarbons at the expense of methane formation.[6] Model kinetic studies of the effect of sulfur on the methanation reaction on Ni(100)[132,135] and Ru(001)[133,134] at near atmospheric pressure attribute this behavior to the inhibition effect of sulfur to the dissociative adsorption rate of hydrogen but also to the drastic decrease in the

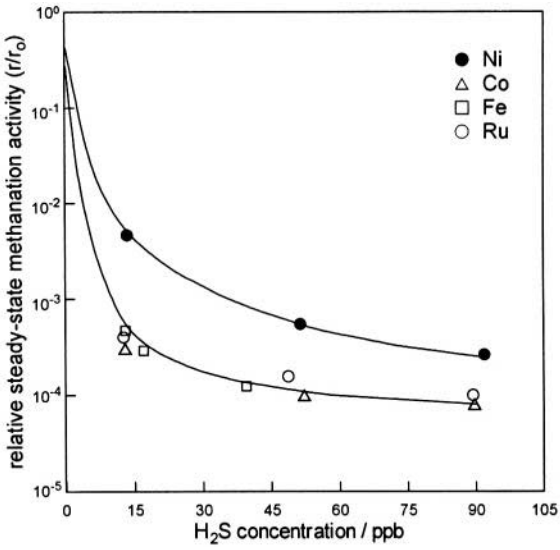

Figure 2.42. Relative steady-state methanation activity profiles for Ni (●), Co (△), Fe (□), and Ru (○) as a function of gas-phase H_2S concentration. Reaction conditions: 100 kPa, 400°C, 1% CO/99%H_2 for Co, Fe, and Ru, 4% CO/96% H_2 for Ni.[131] Reprinted with permission from Academic Press.

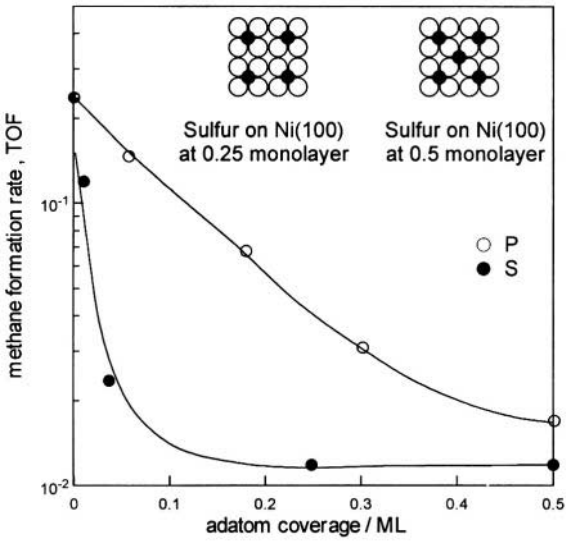

Figure 2.43. Methanation rate, r_{CH4} as a function of S or P coverage on a Ni(100) catalyst at 120 Torr. p_{H2}/p_{CO}=4 and reaction temperature 600 K.[132,136] Reprinted with permission from Elsevier Science.

mobility (surface diffusion coefficient) of the hydrogen adatoms.[132,133] The latter decrease justifies the observed more severe decrease in the methanation rate compared to the decrease in the coverages of the reactants[86,133] and results in a reduced H/C ratio on the modified surface, although the coverage of the adsorbed CO is also reduced due to the presence of the electronegative adatoms. Consequently, the fraction of heavier and unsaturated hydrocarbons is increased. At high sulfur coverages the carbidic carbon formation step (CO dissociation) is also severely inhibited, as confirmed by the absence of surface carbon after the reaction. This is also corroborated by the observed change in the methanation reaction order on S/Ni(100) with respect to CO, from zero to first order for sulfur coverages higher than ~0.1.[135]

Figure 2.43 shows the effect of S and P on the rate of methane production[132] on Ni(100) at 600 K.The observed smaller poisoning effect in the case of P is in agreement with the less pronounced effect of P on the adsorption of the reactants (Section 2.3).

2.7 SUMMARIZING COMMENTS AND RULES

Despite the individual complexities of the systems surveyed here, several simple rules must have emerged in the reader's mind. Aside from the omnipresent site-blocking geometric effects, chemical or classical promotion can be understood, at least qualitatively, in terms of two simple and complementary rules, already outlined is section 2.5:

Rule 1: Electropositive adsorbates strengthen the chemisorptive bond of electron acceptor (electronegative) adsorbates and weaken the chemisorptive bond of electron donor (electropositive) adsorbates.

Rule 2: Electronegative adsorbates weaken the chemisorptive bond of electron acceptor (electronegative) adsorbates and strengthen the chemisorptive bond of electron donor (electronegative) adsorbates.

These rules must be supplemented by the following two "amphoteric" rules already discussed in section 2.3.2.1, which supplement the definition of electron acceptor and electron donor adsorbates.

Rule 3: In presence of a strong electron donor (electropositive) adsorbate (e.g. K, Na) a weaker electron donor (e.g. NO on Pt(111)) behaves as an electron acceptor.

Rule 4: In a presence of a strong electron acceptor (electronegative) adsorbate (e.g. O) a weaker electron acceptor (e.g. CO on Ni(111)) behaves as an electron donor.

The reader can check through the figures of this chapter to confirm that there are no exceptions to these simple rules. There are two molecular mechanisms which lead to these rules:

Direct electrostatic ("through the vacuum") dipole attraction or repulsion which, in the case of attraction, may lead even to surface compound formation.

Indirect ("through the metal") interaction due to the redistribution of electrons in the metal. In this case an electropositive promoter decreases the work function of the surface and this in turn weakens the chemisorptive bond of electropositive (electron donor) adsorbates and strengthens the chemisorptive bond of electronegative (electron acceptor) adsorbates.

The extent of the contribution of each of these two mechanisms varies from one system to the other as recent quantum mechanical calculations have shown.[8,13] In either case, however, linear variations are often obtained in the change in heat of adsorption vs the change in the work function, with slopes on the order of ±1, in good agreement with experiment as shown in Chapter 5.

On the basis of the above simple rules one can formulate the following two promotional rules:

Rule 5: If a catalyst surface is predominantly covered by an electronegative (electron acceptor) adsorbate then an electronegative promoter is to be recommended.

Rule 6: If a catalyst surface is predominantly covered by an electropositive (electron donor) adsorbate then an electropositive promoter is to be recommended.

As will be shown in Chapter 6, but also Chapters 8 to 10, these simple rules are in excellent agreement with experiment.

REFERENCES

1. G. Ertl, H. Knötzinger, and J. Weitcamp, eds., Handbook of Catalysis, VCH Publishers, Weinheim (1997).
2. L.L. Hegedus, R. Aris, A.T. Bell, M. Boudart, N.Y. Chen, B.C. Gates, W.O. Haag, G.A. Somorjai, and J. Wei, *Catalyst design: Progress and Perspectives,* John Wiley & sons, New York (1987).
3. R.J. Farrauto, and C.H. Bartholomew, *Fundamentals of industrial catalytic processes,* Chapman & Hall, London (1997).
4. V. Ponec, Review: Forty years in CATALYSIS: what have we learned?, *Journal of Molecular Catalysis A: Chemical* **133**, 221-239 (1998).
5. I.M. Campbell, *Catalysis at Surfaces,* Chapman and Hall (1988).
6. M. Kiskinova, Poisoning and Promotion in Catalysis based on Surface Science Concepts and Experiments, in *Stud. Surf. Sci. Catal.* **70**, Elsevier, Amsterdam (1992).
7. J.C. Bertolini, P. Delichere, and J. Massardier, The influence of potassium and the role of coadsorbed oxygen on the chemisorptive properties of Pt(100), *Surf. Sci.* **160**, 531-541 (1985).
8. B. Hammer, and J.K., Norskov, Theoretical surface science and catalysis - calculations and concepts, *Adv. Catal.* **45**, 71 (2000).
9. M.T.M. Koper, and R.A.van Santen, Interaction of H, O and OH with metal surfaces, *J. Electroanal. Chem.* **472**, 126-136 (1999).
10. M.T.M. Koper, and R.A.van Santen, Interaction of halogens with Hg, Ag and Pt surfaces: a density functional study, *Surf. Sci.* **422**, 118-131 (1999).
11. M.T.M. Koper, and R.A.van Santen, Electric field effects on CO and NO adsorption at the Pt(111) surface, *J. Electroanal Chem.* **476**, 64-70 (1999).
12. G. Pacchioni, F. Illas, S. Neophytides, and C.G. Vayenas, Quantum-Chemical Study of Electrochemical Promotion in Catalysis, *J. Phys. Chem.* **100**, 16653-16661 (1996).
13. G. Pacchioni, J.R. Lomas, and F. Illas, Electric field effects in heterogeneous catalysis, *Molecular Catalysis A: Chemical* **119**, 263-273 (1997).
14. C. Pliangos, C. Raptis, T. Badas, D. Tsiplakides, and C.G. Vayenas, Electrochemical Promotion of a Classically Promoted Rh catalyst for the Reduction of NO, *Electrochim. Ada* **46**, 331-339 (2000).
15. C. Pliangos, C. Raptis, T. Badas, and C.G. Vayenas, Electrochemical promotion of NO reduction by C_3H_6 on Rh/YSZ catalyst-electrodes, *Solid State Ionics* **136/137**, 767-773 (2000).
16. A. Palermo, R.M. Lambert, I.R. Harkness, I.V. Yentekakis, O. Mar'ina, and C.G. Vayenas, Electrochemical promotion by Na of the Platinum catalyzed reaction between CO and NO, *J. Catal.* **161**, 471-479 (1996).
17. R.M. Lambert, F. Williams, A. Palermo, and M.S. Tikhov, Modelling alkali promotion in heterogeneous catalysis: in situ electrochemical control of catalytic reactions, *Topics in Catalysis* **13**, 91-98 (2000).
18. M. Boudart, and G. Djega-Mariadassou, *Kinetics of Heterogeneous Catalytic Reactions,* Princeton Univ. Press, Princeton, NJ (1984).
19. M.T.M. Koper, A.P.J. Jansen, and J.J. Lukkien, Lattice-gas modeling of electrochemical Langmuir-Hinshelwood surface reactions, *Electrochim. Acta* **45**, 645-651 (1999).
20. C.G. Vayenas, S. Bebelis, I.V. Yentekakis, and H.-G. Lintz, Non-Faradaic Electrochemical Modification of Catalytic Activity: A Status Report (Review Paper), *Catalysis Today* **11**(3), 303-442 (1992).
21. E. Lamy-Pitara, L. Bencharif, and J. Barbier, Effect of sulphur on the properties of platinum catalysts as characterized by cyclic voltammetry, *Appl. Catal.* **18**, 117-131 (1985).

22. S. Surnev, and M. Kiskinova, Formation of Patchy Surface Overlayers: Alkali Adsorption and Alkali Cabon Monoxide and oxygen coadsorption on Ru(001) and Ru(10 $\bar{1}$ 0), *Appl. Phys.* **46**, 323-329 (1988).
23. J. Paul, Alkali overlayers on aluminum, alumina, and aluminum carbide, *Journal Vacuum Science Technology A* **5**(4), 664-670 (1987).
24. J. Hölzl, and F.K.Schulte, Work Function of Metals, in *Solid Surface Physics,* Springer-Verlag, Berlin (1979), pp. 1-150.
25. W. Schröder, and J. Hölzl, Electronic structure of adsorbed sodium on Pt(III), *Solid State Communications* **24**, 777-780 (1977).
26. G. Rangelov, and L. Surnev, Alkali Metal Adsorption on Ru(001), *Surf. Sci.* **185**, 457-468 (1987).
27. P.J. Feibelman, and D.R. Hamann, Modification of transition metal electronic structure by P, S, Cl, and Li adatoms, *Surf. Sci.* **149**, 48-66 (1985).
28. J.K. Nørskov, *Physics and Chemistry of Alkali Metal Adsorption,* Material Science Monographs, H.P. Bonzel, A.M. Bradshaw, and G. Ertl, eds., Elsevier (1989).
29. J.L. Falconer, and R.J. Madix, Flash desorption activation energies: DCOOH decomposition and CO desorption from Ni(110), *Surf. Sci.* **48**, 393-405 (1975).
30. A. Frantzis, and C.G. Vayenas, *Surf. Sci.,* submitted (2001).
31. M. Makri, C.G. Vayenas, S. Bebelis, K.H. Besocke, and C. Cavalca, Atomic resolution STM imaging of Electrochemically Controlled Reversible Promoter Dosing of Catalysts, *Surf. Sci.* **369**, 351-359 (1996).
32. K.J. Uram, L. Ng, and J.R.Yates Jr., Electrostatic effects between adsorbed species-The K-CO interaction on Ni(111) as studied by infrared reflection - absorption spectroscopy, *Surf. Sci.* **177**, 253-277 (1986).
33. K. Wandelt, Studies Surface Science and Catalysis, P. Wissman, ed. Elsevier, Amsterdam (1987), p. 280.
34. C.G. Vayenas, M.M. Jaksic, S. Bebelis, and S.G. Neophytides, The Electrochemical Activation of Catalysis, in *Modern Aspects of Electrochemistry,* J.O.M. Bockris, B.E. Conway, and R.E. White, eds., Kluwer Academic/Plenum Publishers, New York (1996), pp. 57-202.
35. N.D. Lang, and A.R. Williams, Theory of local-work-function determination by photoemission from rate-gas adsorbates, *Physics Review B* **25**(4), 2940-2942 (1982).
36. D. Tsiplakides, and C.G. Vayenas, Electrode work function and absolute potential scale in solid state electrochemistry, *J. Electrochem. Soc.* **148**(5), E189-E202 (2001).
37. M. Hohenegger, E. Bechtold, and R. Schennach, Coadsorption of oxygen and chlorine on Pt(111), *Surf. Sci.* **412/413**, 184-191 (1998).
38. M. Kiskinova, *Habilitation Thesis,* (1989).
39. H. Ohtani, C.-T. Kao, M.A.V. Hove, and G. Somorjai, A tabulation and classification of the structures of clean solid surfaces and of adsorbed atomic and molecular monolayes as determined from low energy electron diffraction patterns, *Progress in Surface Science* **23**(2,3), 155-316 (1986) and reference therein.
40. M. Lindroos, H. Pfnur, G. Held, and D. Menzel, Adsorbate induced reconstruction by strong chemisorption: Ru(001) p(2x2)-O, *Surf. Sci.* **222**, 451 (1989).
41. G. Pirug, and H.P. Bonzel, Short range interaction of a K and CO coadsorbed on Pt(111), *Surf. Sci.* **199**, 371-390 (1988).
42. M. Kiskinova, G. Pirug, and H.P. Bonzel, Coadsorption of potassium and CO on Pt(111), *Surf. Sci.* **133**, 321-343 (1983).
43. J. Paul, and F.M. Hoffmann, Alkali promoted CO bond weakening on aluminum: A comparison with transition metal surfaces, *J. Chem. Phys.* **86**(9), 5188-5195 (1987).
44. R.A. DePaola, J. Hrbek, and F.M. Hoffmann, Potassium promoted C-O bond weakening on Ru(001). I. Through-metal interaction at low potassium precoverage, *J. Chem. Phys.* **82**(5), 2484-2498 (1985).

45. M. Kiskinova, Interactions of CO and sodium coadsorbed on Ru(10$\bar{1}$0), *Surf. Sci.* **182**, 150-160(1987).
46. M. Kiskinova, and M. Tikhov, Adsorption of CO on Ru(10$\bar{1}$0) doped with different amounts of K and Cs, *Surf. Sci.* **194**, 379-396 (1988).
47. M. Kiskinova, CO adsorption on alkali-metal covered Ni(100), *Surf. Sci.* **111**, 584-594 (1981).
48. H.S. Luftman, Y.M. Sun, and J. White, Coadsorption of CO an K on Ni(100). I TDS studies, *Appl. Surf. Sci.* **19**, 59-72 (1984).
49. H. Höchst, and E. Colavita, The interaction of CO, NO, and O_2 with sodium-promoted Rh(100) surfaces, *Journal of Vacuum Science and Technology* **A4**(3), 1442-1445 (1986).
50. J. Rodriguez, W. Clendening, and C.T. Campbell, Adsorption of CO and CO_2 on clean and cesium-covered Cu(110), *J. Phys. Chem.* **93**, 5238-5248 (1989).
51. S.D. Cameron, and D.J. Dwyer, Charge transfer effects on CO bond cleavage: CO and potassium on Fe(100), *Surf. Sci.* **198**, 315-330 (1988).
52. F. Solymosi, and A. Berko, Adsorption of CO_2 on clean and potassium-covered Pd(100) surfaces, *J. Catal.* **101**, 458-472 (1986).
53. A. Berko, and F. Solymosi, Effects of potassium on the chemisorption of CO_2 and CO on the Pd(100) surface, *Surf. Sci.* **171**, L498-L502 (1986).
54. K.J. Maynard, and M. Moskovits, A surface enhanced Raman study of carbon dioxide coadsorption with oxygen and alkali metals on silver surfaces, *J. Chem. Phys.* **90**(11), 6668-6679 (1989).
55. L.J. Whitman, and W. Ho, The kinetics and mechanisms of alkali metal-promoted dissociation: A time resolved study of NO adsorption and reaction on potassium-precovered Rh(100), *J. Chem. Phys.* **89**(12), 7621-7645 (1988).
56. R.A. Marbrow, and R.M. Lambert, Chemisorption and surface reactivity of nitric oxide on clean and sodium-dosed Ag(110), *Surf. Sci.* **61**, 317-328 (1976).
57. P.J. Goddard, J. West, and R.M. Lambert, Adsorption, coadsorption and reactivity of sodium and nitric oxide on Ag(111), *Surf. Sci.* **71**, 447-461 (1978).
58. P.J. Goddard, and R.M. Lambert, Surface crystallography of rubidium on Ag(111) and the chemical reactivity of nitric oxide on rubidium-dosed silver, *Surf. Sci.* **79**, 93-108 (1979).
59. M. Kiskinova, G. Pirug and H.P. Bonzel, Interaction of NO with potassium promoted Pt(111), *Surf. Sci.* **140**, 1-17 (1984).
60. M. Kiskinova, G. Rangelov, and L. Surnev, Coadsorption of oxygen and cesium on Ru(001), *Surf. Sci.* **172**, 57-70 (1986).
61. L. Surnev, G. Rangelov, and M. Kiskinova, Interaction of oxygen with an alkali modified Ru(001) Surface, *Surf. Sci.* **179**, 283-296 (1987).
62. Y.M. Sun, H.S. Luftman, and J.M. White, Potassium and coadsorbed potassium and deuterium on Ni(100), *Surf. Sci.* **139**, 379-395 (1984).
63. A.-M. Lanzillotto, M.J. Dresser, M.D. Alvey, and J.T.Yates Jr., Alkali sensitization of H^+ electron stimulated desorption from H adsorbed on Ni(111), *J. Chem. Phys.* **89**(1), 570-576 (1988).
64. H.-L. Zhou, and J.M. White, Stabilization by potassium of adsorbed hydrogen on Pt(111), *Surf. Sci.* **185**, 450-456 (1987).
65. P.J. Goddard, and R.M. Lambert, Basic studies of the oxygen surface chemistry of silver: Oxygen, dioxygen, oxide and superoxide on rubidium-dosed Ag(111), *Surf. Sci.* **107**, 519-532 (1981).
66. C.A. Papageorgopoulos, Studies of separate adsorption and coadsorption of Cs and O_2 on Cu(100), *Physical Review B* **25**(6), 3740-3749 (1982).
67. M. Ayyoob, and M.S. Hegde, An XPS study of the adsorption of oxygen on silver and platinum surfaces covered with potassium or cesium, *Surf. Sci.* **133**, 516-532 (1983).

68. L.J. Whitman, C.E. Bartosch, and W. Ho, A new mechanism for K promotion of surface reactions: N_2 on K-precovered Fe(111), *J. Chem. Phys.* **85**(6), 3688-3698 (1986).
69. R.A. De Paola, F.M. Hoffmann, D. Heskett, and E.W. Plummer, Adsorption of molecular nitrogen on clean and modified Ru(001) surfaces: The role of σ bonding, *Physical Review B* **35**(9), 4236-4249 (1987).
70. E. Umbach, Electronic structure and interactions in well-defined coadsorbed layers, *Appl. Phys.* **47**, 25-36 (1988).
71. L.J. Whitman, C.E. Bartosch, W. Ho, G. Strasser, and M. Grunze, Alkali-metal promotion of a dissociation precursor: N_2 on Fe(111), *Physical Review Letters* **56**(18), 1984-1987 (1986).
72. G. Ertl, S.B. Lee, and M. Weiss, Adsorption of nitrogen on potassium promoted Fe(111) and (100) surfaces, *Surf. Sci.* **114**, 527-545 (1982).
73. J.A. Moulijn, P.W.N.M.van Leeuwen, and R.A.van Santen, eds., CATALYSIS. An integrated Approach to Homogeneous, Heterogeneous and Industrial Catalysis, in *Stud. Surf. Sci. Catal.***79**, (1993), pp. 1-460.
74. X.-L. Zhou, X.-Y. Zhu, and J.M. White, A TPD, SIMS and $\Delta\Phi$ study of the infuence of coadsorbed potassium on the adsorption and decomposition of ethylene on Pt(111), *Surf. Sci.* **193**, 387-416 (1988).
75. R.G. Windham, M.E. Bartram, and B.E. Koel, Coadsorption of ethylene and potassium on Pt(111). 1. Formation of a π-bonded state of ethylene, *J. Phys. Chem.* **92**, 2862-2870 (1988).
76. R.G. Windham, and B.E. Koel, Coadsorption of Ethylene and Potassium on Pt(111). 2. Influence of Potassium on the Decomposition of Ethylene, *J. Phys. Chem.* **94**, 1489-1496 (1990).
77. A. Cassuto, M. Touffaire, M.B. Hugenschmidt, P. Dolle, and J. Jupille, Ethylene π-species on bare and K-, Cs- and O- precovered Pt(111): a TDS and UPS study, *Vaccum* **41**, 161-162 (1990).
78. E.L. Garfunkel, M.H. Farias, and G.A. Somorjai, The modification of benzene and carbon monoxide adsorption on Pt(111) by the Coadsorption of potassium or sulfur, *JACS* **107**, 349 (1985).
79. E.L. Garfunkel, J.J. Maj, J.C. Frost, M.H. Farias, and G.A. Somorjai, Interaction of potassium with π-electron orbital containing molecules on Pt(111), *J. Phys. Chem.* **87**, 3629-3635 (1983).
80. J. Hrbek, R.A. De Paola, and P.M. Hoffmann, The interaction of methanol with modified Ru(001) surfaces: The effects of oxygen and potassium, *Surf. Sci.* **166**, 361-376(1986).
81. R.A. De Paola, J. Hrbek, and F.M. Hoffmann, The formation of potassium methoxide on Ru(001), *Surf. Sci. Lett.* **169**, L348-L354 (1986).
82. A. Berko, T.I. Tarnoczi, and F. Solymosi, Interaction of CH_3OH with K-dosed Rh(111) surfaces at 300 K, *Surf. Sci.* **189/190**, 238-244 (1987).
83. J. Paul, UPS spectra of H_2O, CH_3OH and C_5H_9OH adsorbed onto Cu(111)/Na and Na(cp), *Surf. Sci.* **160**, 599-617 (1985).
84. J. Paul, L. Wallden, and A. Rosen, The reactivity of adsorbed Na atoms probed by coadsorbed CH_3OH, *Surf. Sci.* **146**, 43-60 (1984).
85. W. Erley, and H. Wagner, Thermal decomposition of CO on a stepped Ni surface, *Surf. Sci.* **74**, 333-341 (1978).
86. M. Kiskinova, and D.W. Goodman, Modification of chemisorption properties by electronegative adatoms: H_2 and CO on chlorined, sulfided, and phosphided Ni(100), *Surf. Sci.* **108**, 64-76 (1981).
87. M. Kiskinova, A. Szabo, and J.T.Yates Jr., CO adsorption on Pt(111) modified with sulfur, *J. Chem. Phys.* **89**(12), 7599-7608 (1988).
88. Z. Xu, L. Surnev, K.J. Uram, and J.T.Yates Jr., Interactions between chemisorbed CO and oxygen on Ni(111), *Surf. Sci.* **292**, 235-247 (1993).

89. S.W. Jorgensen, N.D.S. Canning, and R.J. Madix, A HREELS, TPD study of nitric oxide adsorption, desorption and reaction on clean and sulfur covered palladium (100), *Surf. Sci.* **179**, 322-350 (1987).
90. T.E. Fischer, and S.R. Kelemen, Model experiments on the poisoning of Pt catalysts by sulfur, *J. Catal.* **53**, 24-34 (1978).
91. E.L. Hardegree, and J.M. White, Adsorption of NO on S/Ni(100), *Surf. Sci.* **175**, 78 (1986).
92. F. Bozso, J. Arias, C.P. Hanrahan, J.T.Yates Jr., R.M. Martin, and H. Metiu, Study of adsorption and decomposition of NO on clean and oxygen-covered Ni(111) by metastable quenching spectroscopy, *Surf. Sci.* **141**, 591-603 (1984).
93. T.W. Root, G. Fischer, and L.D. Schmidt, Electron energy loss characterization of NO on Rh(111). I. NO coordination and dissociation, *J. Chem. Phys.* **85**(8), 4679-4686 (1986).
94. Y. Matsumoto, T. Onishi, and K. Tamaru, Effects of Sulphur on a Palladium Surface on the Adsorption of Carbon Monoxide and the Adsorption and decomposition of nitric oxide, *J.C.S. Faraday I* **76**, 1116-1121 (1980).
95. R. Schennach, and E. Bechtold, Adsorption of oxygen on chlorine-modified Pt(100) surfaces, *Surf. Sci.* **369**, 277-288 (1996).
96. C.T. Campbell, and M.T. Paffett, The role of chlorine promoters in catalytic ethylene epoxidation over the Ag(110) surface, *Applications of Surface Science* **19**, 28-42 (1984).
97. R.A.van Santen, and H.P.C.E. Kuipers, The mechanism of ethylene epoxidation, *Adv. Catal.* **35**, 265-321 (1987).
98. C. Karavasilis, S. Bebelis, and C.G. Vayenas, Non-Faradaic Electrochemical Modification of Catalytic Activity: 10. Ethylene epoxidation on Ag deposited on stabilized ZrO_2 in presence of chlorine moderators, *J. Catal.* **160**, 190-204 (1996).
99. M.M. Hills, J.E. Parmeter, and W.H. Weinberg, Chemisorption and reaction of ethylene on chemically modified Ru(001) surfaces, *JACS* **109**(14), 4224-4232 (1987).
100. U. Seip, M.-C. Tsai, J. Kuppers, and G. Ertl, Interaction of acetylene and ethylene with an Fe(111) surface, *Surf. Sci.* **147**, 65-88 (1984).
101. E.M. Stuve, and R.J. Madix, Oxidation of ethylene on Pd(100); Bonding of ethylene and scavenging of dehydrogenation fragments by surface oxygen, *Surf. Sci.* **160**, 293-304 (1985).
102. E.M. Stuve, and R.J. Madix, Bonding and dehydrogenation of ethylene on palladium metal. Vibrational spectra and temperature-programmed reaction studies on Pd(100), *J. Phys. Chem.* **89**, 105-112 (1985).
103. D. Ehrlich, S. Wohlrab, J. Wambach, H. Kuhlenbeck, and H.-J. Freund, Reaction of CO_2 on Pd(111) activated via promotor action of alkali coadsorption, *Vacuum* **41**(1-3), 157-160 (1990).
104. P. Berlowitz, C. Megiris, J.B. Butt, and H.H. Kung, Temperature-Programmed Desorption Study of Ethylene on a Clean, a H-Covered, and an O-Covered Pt(111) Surface, *Langmuir* **1**, 206-212 (1985).
105. H. Steininger, H. Ibach, and S. Lehwald, Surface reactions of ethylene and oxygen on Pt(111), *Surf. Sci.* **117**, 685-698 (1982).
106. M.V. Badani, and M.A. Vannice, Effects of cesium and chlorine on oxygen adsorption on promoted $Ag/\alpha\text{-}Al_2O_3$ catalysts, *Appl. Catal. A* **204**, 129-142 (2000).
107. E.M. Stuve, R.J. Madix, and C.R. Brundle, The adsorption and reaction of ethylene on clean and oxygen covered Pd(100), *Surf. Sci.* **152/153**, 532-542 (1985).
108. D.G. Kelly, M. Salmeron, and G.A. Somorjai, The adsorption and reactions of hydrocarbons on molybdenum single crystal surfaces; when clean and in presence of coadsorbed sulfur or carbon, *Surf. Sci.* **175**, 465 (1986).
109. J.B. Benziger, E.I. Ko, and R.J. Madix, Reactions of formaldehyde on W(100) and W(100) -(5x1)C, *J. Catal.* **64**, 132-142 (1980).

110. R.J. Madix, S.B. Lee, and M. Thornburg, The effects of adsorpbed sulfur on the adsorption and reaction of CO and methanol on Ni(100), *Journal Vacuum Science Technology A* **1**(2), 1254-1260 (1983).
111. J.-P. Lu, M. Alberts, S.L. Bernasek, and D.S. Dwyer, Decomposition of methanol on oxygen-modified Fe(100) surfaces. I. The effect of high temperature oxygen modification, *Surf. Sci.* **218**, 1 (1989).
112. I.N. Yakovkin, V.I. Chernyi, and A.G. Naumovetz, Oxidation of CO on Li-precovered Pt, *Surf. Sci.* **442**, 81-89 (1999).
113. S.A. Tan, R.B. Grant, and R.M. Lambert, The silver-catalysed decomposition of N_2O and the catalytic oxidation of ethylene by N_2O over Ag(111) and $Ag/\beta''\text{-}Al_2O_3$, *J. Catal.* **104**, 156-163 (1987).
114. S.A. Tan, R.B. Grant, and R.M. Lambert, Secondary Chemistry in the selective oxidation of ethylene: Effect of Cl and Cs promoters on the adsorption, isomerization and combustion of ethylene oxide on Ag(111), *J. Catal.* **106**, 54-64 (1987).
115. V.I. Bukhtiyarov, A.I. Boronin, and V.I. Savchenko, Stages in the Modification of a Silver Surface for Catalysis of the Partial Oxidation of Ethylene I. Action of Oxygen, *J. Catal.* **150**(2), 262-267 (1994).
116. K.A. Jorgensen, and R. Hoffmann, Oxygen transfer to ethylene catalyzed by the Ag(110) surface: Possible adsorption sites for molecular and atomic oxygen and a model for the oxygen-transfer step, *J. Phys. Chem.* **94**, 3046-3054 (1990).
117. C. Karavasilis, S. Bebelis, and C.G. Vayenas, In Situ Controlled Promotion of Catalyst Surfaces via NEMCA: The Effect of Na on the Ag-Catalyzed Ethylene Epoxidation in the Presence of Chlorine Moderators, *J. Catal.* **160**, 205-213 (1996).
118. M. Bowker, and K.C. Waugh, The adsorption of chlorine and chloridation of Ag(111), *Surf. Sci.* **134**, 639-664 (1983).
119. M. Bowker, and K.C. Waugh, Chlorine adsorption and chloridation of Ag(110), *Surf. Sci.* **155**, 1-14 (1985).
120. M. Kitson, and R.M. Lambert, Basic studies of the oxygen chemistry of silver: Oxygen, dioxygen and superoxide on potassium-dosed Ag(100), *Surf. Sci.* **109**, 60-74 (1981).
121. R.A.van Santen, Chemical basis of metal catalyst promotion, *Surf. Sci.* **251/252**, 6-11 (1991).
122. R.B. Grant, and R.M. Lambert, Ethylene oxide isomerization on Single-crystal Ag(111) in Atomically clean and Cs-moderated conditions, *J. Catal.* **93**, 92-99 (1985).
123. B.S. Uphade, M. Okumura, S. Tsubota, and M. Haruta, Effect of physical mixing of CsCl with Au/Ti-MCM-41 on the gas-phase epoxidation of propene using H_2 and O_2: Drastic depression of H_2 consumption, *Appl. Catal. A* **190**, 43-50 (2000).
124. J.J. Cowell, A.K. Santra, R. Lindsay, A. Baraldi, A. Goldoni, and R.M. Lambert, Heterogeneous alkene epoxidation without the use of silver: The bonding and reactivity of styrene on Cu(110), *Surf. Sci.* **437**, 1-8 (1999).
125. J.J. Cowell, A.K. Santra, and R.M. Lambert, Ultra-selective epoxidation of butadiene on Cu(111) and the effects of Cs promotion, *JACS* **122**, 2381-2382 (2000).
126. A.K. Santra, J.J. Cowell, and R.M. Lambert, Ultra-selective epoxidation of styrene on pure Cu(111) and the effects of Cs promotion, *Catal. Lett.* **67**(2-4), 87-92 (2000).
127. D.W. Goodman, R.D. Kelley, T.E. Madey, and J.M. White, Measurement of carbide buildup and removal kinetics on Ni(100), *J. Catal.* **64**, 479-481 (1980).
128. D.A. Wesner, F.P. Coenen and H.P. Bonzel, Influence of potassium on carbon monoxide hydrogenation over iron: A surface analytical study, *Langmuir* **1**, 478-487 (1985).
129. G.A. Mills, and F.W. Steffgen, Catalytic Methanation, *Catal. Rev.* **8**, 159-210 (1973).
130. V. Ponec, and G.C. Bond, Catalysis by metals and alloys, in *Stud. Surf. Sci. Catal.* **95**, Elsevier Science B.V., Amsterdam (1995), pp. 679-716.
131. C.H. Bartholomew, P.K. Agrawal and J.R. Katzer, Sulfur poisoning of metals, *Adv. Catal.* **31**, 135-242 (1981).

132. M.P. Kiskinova, Electronegative additives and poisoning in catalysis, *Surf. Sci. Rep.* **8**, 359-402 (1988).
133. J.L. Brand, A.A. Deckert, and S.M. George, Surface diffusion of hydrogen on sulfur-covered Ru(001) surfaces studied using laser-induced thermal desorption, *Surf. Sci.* **194**, 457-474 (1988).
134. C.H.F. Peden, and D.W. Goodman. *Catalysts Characterisation Science in ACS Symposium Series 288,* 185 (1985) Washington DC.
135. D.W. Goodman, and M. Kiskinova, Chemisorption and reactivity studies of H_2 and CO on sulfided Ni(100), *Surf. Sci.* **105**, L265-L270 (1981).
136. D.W. Goodman, Chemical modification of chemisorptive and catalytic properties of Nickel, *Appl. Surf. Sci.* **19**, 1-13 (1984).

CHAPTER 3

SOLID ELECTROLYTES, CATALYSIS AND SPILLOVER

"In fact, the key to understand electrochemical promotion is to understand the mechanism by which the effect of polarization at the catalyst/electrolyte interface propagates to the catalyst/gas interface "

G. Foti, S. Wodiunig and Ch. Comninellis, Current topics of Electrochemistry, 2000

3.1 SOLID ELECTROLYTES

Michael Faraday was first to observe in 1834 that solid PbF_2, when heated at 500°C, becomes an electrical conductor. It took almost a century to explain this observation and establish that PbF_2 is a F^- ion conductor. In the meantime, other solid electrolytes such as AgI, a Ag^+ conductor, had been discovered by Tubandt and Strock and it soon became apparent that ions can diffuse as rapidly in some solids as in aqueous salt solutions. The atomistic interpretation of ionic conduction in solids was largely established by the pioneering work of Joffé, Frenkel, Wagner and Schottky in the twenties and early thirties.[1] These works established that ion conduction can take place either by hopping of ions through a series of interstitial sites (Frenkel disorder) or by hopping of vacancies among lattice positions (Schottky disorder).

Today, the term solid electrolyte or fast ionic conductor or, sometimes, superionic conductor is used to describe solid materials whose conductivity is wholly due to ionic displacement. Mixed conductors exhibit both ionic and electronic conductivity. Solid electrolytes range from hard, refractory materials, such as 8 mol% Y_2O_3-stabilized ZrO_2(YSZ) or sodium β''-Al_2O_3 ($NaAl_{11}O_{17}$), to soft proton-exchange polymeric membranes such as Du Pont's Nafion and include compounds that are stoichiometric (AgI), non-stoichiometric (sodium β''-Al_2O_3) or doped (YSZ). The preparation, properties, and some applications of solid electrolytes have been discussed in a number of books[2-5] and reviews.[6,7] The main commercial application of solid electrolytes is in gas sensors.[8,9] Another emerging application is in solid oxide fuel cells.[4,5,10,11]

The classification of solid electrolytes is usually based on the ion mainly responsible for the conductivity. There exist:

(i) Oxygen ion conductors: They are solid solutions of divalent and trivalent metal oxides (e.g. Y_2O_3, Yb_2O_3, CaO) in quadrivalent metal oxides (e.g. ZrO_2, ThO_2, CeO_2). Calcia- or Yttria-stabilized Zirconia (YSZ), containing 5-15 mol% CaO or 6-10 mol% Y_2O_3 in ZrO_2, is widely used in oxygen sensors, normally in the temperature range 400° to 1200°C.

(ii) H^+ and Li^+ conductors: Several polymeric solid electrolytes belong here. Of particular importance are the Proton Exchange Membranes (PEM), such as Nafion 117, which is a copolymer of polytetrafluoroethylene and polysulfonylfluoride containing pendant sulfonic acid groups, which exhibit substantial conductivity at room temperature. High cationic conductivity is also exhibited by several alkali salt solutions in polyethyleneoxide. Proton conduction is also exhibited by $CsHSO_4$,[12] by H-substituted β''-Al_2O_3,[3] and by $SrCeO_3$[13] and $C_{0.9}In_{0.1}ZrO_{3-\alpha}$[14,15] based compounds.

(iii) Na^+ conductors: These are β- and β''-aluminas which are non-stoichiometric compounds corresponding to $Na_{1+x}Al_{11}O_{17+x/2}$ ($0.15 \leq x \leq 0.3$) and $Na_{1+x}M_xAl_{11-x}O_{17}$, respectively, where M is a divalent metal (e.g. Mg^{2+}, Ni^{2+}, Zn^{2+}). They exhibit high conductivity in the range 150-300°C.

(iv) K^+, Cs^+, Rb^+, Tl^+ conductors: They are substituted β- and β''-Al_2O_3 and are conductive in the range 200- 400°C.

(v) Ag^+ conductors, e.g. α-AgI, $RbAg_4I_5$, and Ag_2HgI_4, which are conductive in the range 150-350°C.

(vi) Cu^+ conductors, e.g. Cu_2Se and KCu_4I_5 are conductive in the range 250-400°C.

(vii) F^- conductors, e.g. PbF_2 and CaF_2, which are conductive above 500 and 600°C, respectively.

Detailed information about the conductivity of solid electrolytes can be found elsewhere.[2,3,6-8,10,11] As shown in Fig. 3.1, the temperature dependence of the ionic conductivity σ can, in general, be described by the semiempirical equation:

$$\sigma = (\sigma_o / T) \exp(-E_A / k_b T) \tag{3.1}$$

where σ_o is a function of the ionic charge, the concentration of the mobile ions and the frequency with which these ions attempt to move to a neighboring site (attempt frequency); E_A is the activation energy for defect motion and k_b is the Boltzmann constant. The activation energy E_A is usually on the order of 0.5-2 eV. The minimum ionic conductivity value of a solid electrolyte for practical fuel cell applications[4,5,10,11] is 0.1-1 $\Omega^{-1}cm^{-1}$. This places very stringent restrictions on the choice of material and operating temperature. For catalytic (promotional) and sensor applications, however, much lower conductivity values ($\sim 10^{-4}$ $\Omega^{-1}cm^{-1}$) are usually sufficient. This

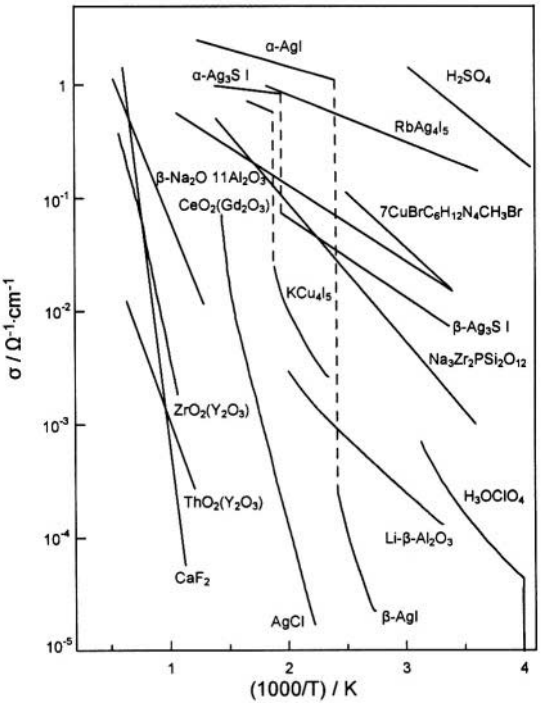

Figure 3.1. Temperature dependence of the ionic conductivity of some solid electrolytes. The conductivity of concentrated H_2SO_4 (37 wt%) is included for comparison.[16] Reprinted with permission from WILEY-VCH.

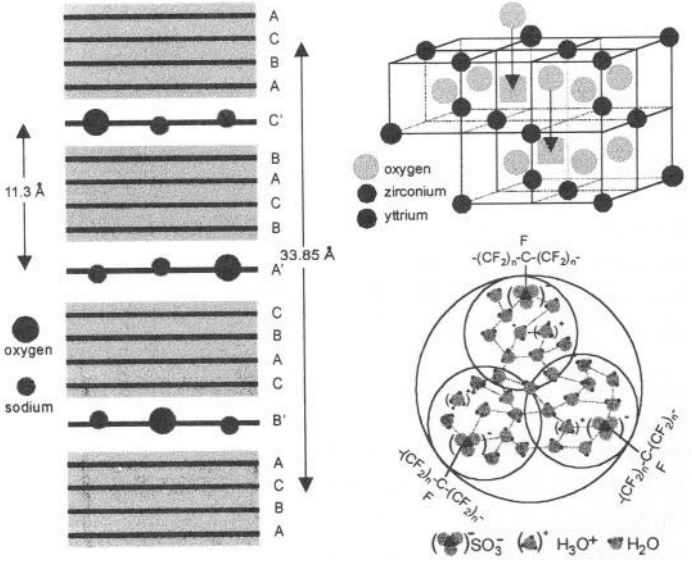

Figure 3.2. Unit cells of β″-Al_2O_3, Y_2O_3-stabilized-ZrO_2 (YSZ) and Nafion.[17,20]

permits the use of a large variety of solid electrolytes over a very wide temperature range. Electrochemical promotion (EP) studies[18,19] have so far utilized:

(i) Yttria-stabilized-zirconia (YSZ), an O^{2-} conductor, at temperatures 280 and 650°C.
(ii) β''-Al_2O_3, and $Na_3Zr_2Si_2PO_{12}$ (NASICON) which are Na^+ conductors at temperatures between 180° to 400°C.
(iii) $CsHSO_4$, $CaZr_{0.9}In_{0.1}O_{3-\alpha}$ and Nafion, which are proton conductors at temperatures 150 and 25°C, respectively.
(iv) CaF_2, a F^- conductor, at temperatures between 550 and 700°C.
(v) Aqueous alkaline or acidic solutions at temperatures 25 and 60°C.
(vi) Mixed ionic-electronic conductors such as TiO_2 and CeO_2.
(vii) Molten salts, such as V_2O_5-$K_2S_2O_7$.

A complete classification of electrochemical promotion (EP) studies on the basis of the type of solid electrolyte used is given in Table 4.1 of Chapter 4 together with the corresponding references. These studies are further discussed in detail in Chapters 8 to 10.

3.2 SOLID ELECTROLYTE POTENTIOMETRY (SEP)

When a solid electrolyte component is interfaced with two electronically conducting (e.g. metal) films (electrodes) a solid electrolyte galvanic cell is formed (Fig. 3.3). Cells of this type with YSZ solid electrolyte are used as oxygen sensors.[8] The potential difference U^o_{WR} that develops spontaneously between the two electrodes (W and R designate working and reference electrode, respectively) is given by:

$$U^o_{WR} = (RT/4F)\ln(p_{O_2,W}/p_{O_2,R}) \tag{3.2}$$

where F is Faraday's constant (96487 C/mol) and $p_{O_2,W}$ and $p_{O_2,R}$ are the oxygen partial pressures over the two electrodes. The superscript "o" designates hereafter open-circuit conditions, i.e., there is no current (I=0) flowing between the two electrodes. The Nernst equation (3.2) is valid provided there is equilibrium between gaseous oxygen and oxygen, O(tpb), adsorbed at the solid electrolyte-metal-gas three-phase-boundaries (tpb). It is also necessary that the net-charge-transfer (electrocatalytic) reaction at the tpb is:

$$O(a)+2e^- \leftrightarrow O^{2-}(YSZ) \tag{3.3}$$

i.e., that there is no interference from other gases, e.g. H_2, CO, which may react with O^{2-} (YSZ) at the tpb establishing mixed potentials.[20]

Wagner first proposed the use of such galvanic cells in heterogeneous catalysis, to measure in situ the thermodynamic activity of oxygen O(a) adsorbed on metal electrodes during catalytic reactions.[21] This led to the technique of solid electrolyte potentiometry (SEP).[22-26]

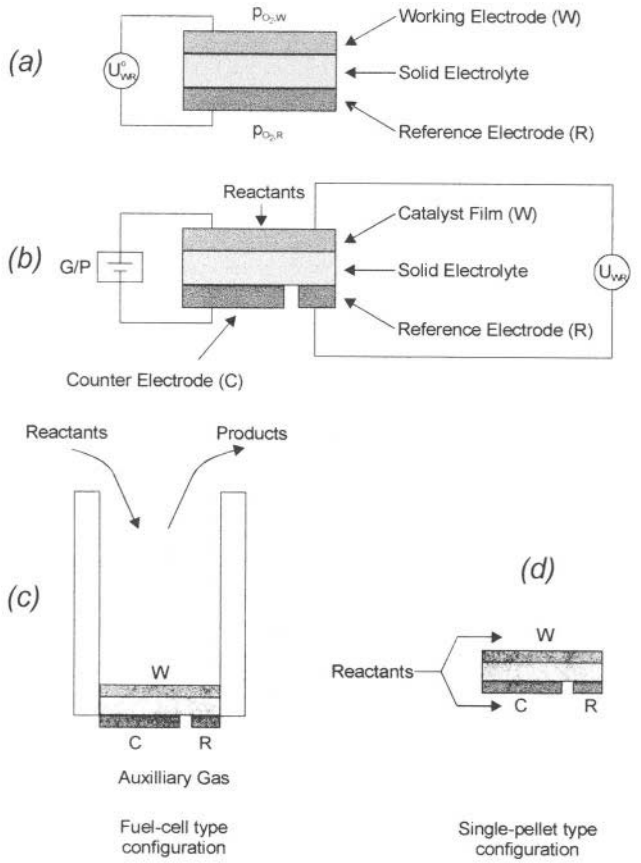

Figure 3.3. Electrode configuration for SEP (a) and for electrochemical promotion (or NEMCA) studies (b). The latter can be carried out using the fuel-cell type configuration (c) or the single chamber type configuration (d).

In this technique the working electrode W (e.g. Pt) is exposed to the reactive gas mixture (e.g. C_2H_4 plus O_2) and also serves as the catalyst for a catalytic reaction, e.g.:

$$C_2H_4+3O_2 \rightarrow 2CO_2+2H_2O \tag{3.4}$$

The measured potential difference U^o_{WR} is related to the oxygen activity, α_O, on the catalyst surface via:[22-27]

$$U^o_{WR} = (RT/4F)\ln(\alpha_O^2 / p_{O2,R}) \tag{3.5}$$

which is again derived on the basis of the equilibrium (3.3). The SEP technique, used in conjunction with kinetic studies, is a useful tool for

mechanistic investigations, particularly suitable for the study of oscillatory reactions.[23,27] The limitations of Eq. (3.5) together with detailed reviews of the SEP literature can be found elsewhere.[19,23-26] Today it is well established both theoretically[19,28] and experimentally[19,29,30] that SEP with metal catalyst electrodes is a work-function ($e\Phi$) measuring technique:

$$eU^{o}_{WR} = \Phi_W - \Phi_R \tag{3.6}$$

where Φ_W and Φ_R are the actual, adsorption and spillover modified, work functions Φ of the gas-exposed surfaces of the working (W) and reference (R) electrodes. Equation (3.6) is more general than equation (3.5) as it does not depend on the nature of the solid electrolyte and does not require the establishment of any specific charge-transfer equilibrium (e.g. Eq. (3.3)) at the tpb.[19] It also holds under closed-circuit conditions. It shows that solid electrolyte galvanic cells are work function probes and work function controllers for their gas-exposed, i.e. catalytically active, electrode surfaces. This important point is analyzed in detail in Chapters 4, 5 and 6, in relation to the effect of electrochemical promotion.

In addition to solid electrolyte potentiometry, the techniques of cyclic voltammetry[31,32] and linear potential sweep[32] have been also used recently in solid electrolyte cells to investigate catalytic phenomena occuring on the gas-exposed electrode surfaces. The latter technique, in particular is known in catalysis under the term Potential-programmed reduction (PPR).[32] With appropriate choice of the sweep rate and other operating parameters both techniques can provide valuable kinetic[31] and thermodynamic[32] information about catalytically active chemisorbed species and also about the NEMCA effect[31,32] as analyzed in detail in Chapter 5.

3.3 ELECTROCATALYTIC OPERATION OF SOLID ELECTROLYTE CELLS

Solid electrolyte fuel cells have been investigated intensively during the last four decades.[10,33-37] Their operating principle is shown schematically in Fig. 3.4. The positive electrode (cathode) acts as an electrocatalyst to promote the electrocatalytic reduction of O_2 (g) to O^{2-}:

$$1/2O_2(g) + 2e^- \rightarrow O^{2-} \tag{3.7}$$

Although several metals, such as Pt and Ag, can also act as electrocatalysts for reaction (3.7) the most efficient electrocatalysts known so far are perovskites such as $La_{1-x}Sr_xMnO_3$. These materials are mixed conductors, i.e., they exhibit both anionic (O^{2-}) and electronic conductivity. This, in principle, can extend the electrocatalytically active zone to include not only the three-phase-boundaries but also the entire gas-exposed electrode surface.

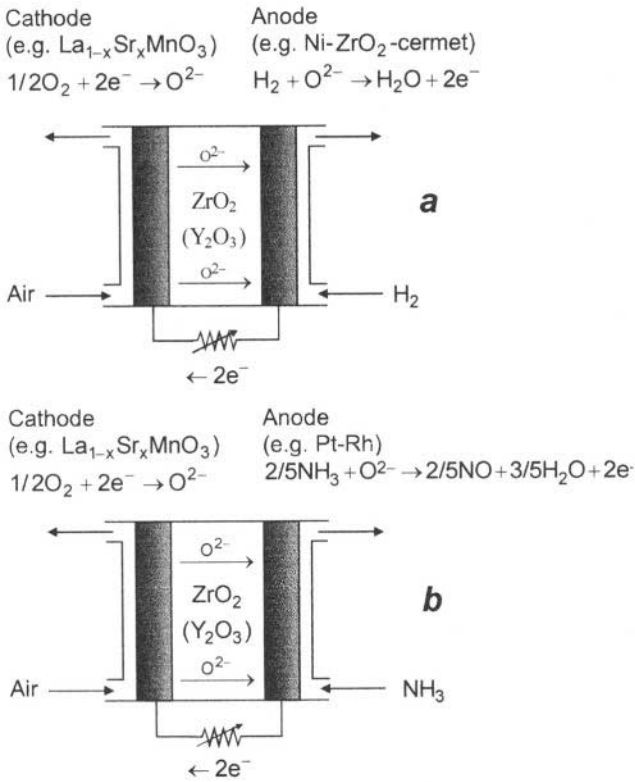

Figure 3.4. Operating principle of a solid oxide fuel cell (a) and of a chemical cogenerator (b).[41] Reprinted with permission from the American Chemical Society.

The negative electrode (anode) acts as an electrocatalyst for the reaction of O^{2-} with the fuel, e.g. H_2:

$$H_2 + O^{2-} \rightarrow H_2O + 2e^- \tag{3.8}$$

A Ni-stabilized ZrO_2 cermet is used as the anodic electrocatalyst in state-of-the-art solid oxide fuel cells. Nickel is a good electrocatalyst for reaction (3.8) and the Ni-stabilized ZrO_2 cermet is used to create a large metal-gas-solid electrolyte three-phase-boundary length, since it is exactly at these three phase boundaries (tpb) where electrocatalytic reactions usually take place in solid electrolyte cells. Thus the use of Ni in a Ni-ZrO_2 cermet to carry out electrocatalytic reactions is analogous to the use of Ni, or other transition metals, in a highly dispersed form on SiO_2, Al_2O_3 or TiO_2 supports to carry out catalytic reactions. Throughout this book the term electrocatalytic reaction is used to denote reactions such as (3.7) and (3.8) involving a net charge transfer.

Fuel cells such as the one shown on Fig. 3.4a convert H_2 to H_2O and produce electrical power with no intermediate combustion cycle. Thus their thermodynamic efficiency compares favorably with thermal power generation which is limited by Carnot-type constraints. One important advantage of solid electrolyte fuel cells is that, due to their high operating temperature (typically 700° to 1100°C), they offer the possibility of "internal reforming" which permits the use of fuels such as methane without a separate external reformer.[33-36]

One can only admire the insight of the first researchers who used Ni as the active electrode material in the Ni/YSZ cermet anodes: In addition to being a good electrocatalyst for the charge transfer reaction (3.8), Ni is also an excellent catalyst for the steam or CO_2-reforming of methane:

$$CH_4+H_2O \leftrightarrow CO+3H_2 \tag{3.9}$$

$$CH_4+CO_2 \leftrightarrow 2CO+2H_2 \tag{3.10}$$

as well as for the water-gas-shift reaction:

$$CO + H_2O \leftrightarrow CO_2 + H_2 \tag{3.11}$$

Reactions (3.9) to (3.11) proceed rapidly to equilibrium in most anodic solid oxide fuel cell (SOFC) environments and thus H_2 (Eq. 3.8) rather than CH_4 is oxidized electrochemically resulting in low polarization losses. Upon doubling the stoichiometric coefficients of equation (3.8), summing equations (3.8) to (3.11) and dividing the resulting coefficients by two one obtains:

$$CH_4 + O^{2-} \rightarrow CO + 2H_2 + 2e^- \tag{3.12}$$

Thus indeed CH_4 oxidation in a SOFC with a Ni/YSZ anode results into "partial oxidation" and the production of synthesis gas, instead of generation of CO_2 and H_2O as originally believed. The latter happens only at near-complete CH_4 conversion. However the partial oxidation overall reaction (3.12) is not the result of a "partial oxidation" electrocatalyst but rather the result of the catalytic reactions (3.9) to (3.11) coupled with the electrocatalytic reaction (3.8). From a thermodynamic viewpoint the partial oxidation reaction (3.12) is at least as attractive as complete oxidation to CO_2 and H_2O.

In recent years it was shown that solid electrolyte fuel cells with appropriate electrocatalytic anodes can be used for chemical cogeneration i.e. for the simultaneous production of electrical power and useful chemicals.

This mode of operation, first demonstrated for the case of NH_3 conversion to NO[38-40] combines the concepts of a fuel cell and of a chemical reactor (Fig. 3.4b). The economics of chemical cogeneration have been discussed and modelled.[41,42] Several other exothermic reactions have been investigated more recently, including the oxidation of H_2S to SO_2,[43] of CH_3OH to H_2CO[44] and of methane to ethylene.[45] In the latter case it was found that ethylene yields up to 85% can be obtained in a gas-recycle solid electrolyte cell reactor-separator using a Ag-Sm_2O_3 anode and a molecular sieve adsorbent.[45] It is possible that if solid electrolyte fuel cells operating on H_2 or natural gas become commercially available, then they can be also used, with appropriate anodic electrocatalysts, by several chemical industries.

Table 3.1 lists some of the anodic reactions which have been studied so far in small cogenerative solid oxide fuel cells. A more detailed recent review has been written by Stoukides.[46] One simple and interesting rule which has emerged from these studies is that the selection of the anodic electrocatalyst for a selective *electrocatalytic* oxidation can be based on the heterogeneous catalytic literature for the corresponding selective *catalytic* oxidation. Thus the selectivity of Pt and Pt-Rh alloy electrocatalysts for the anodic NH_3 oxidation to NO turns out to be comparable (>95%) with the

Table 3.1. **Electrocatalytic reactions investigated in doped ZrO_2 solid electrolyte fuel cells for chemical cogeneration**

Reaction	Electrocatalyst	Reference(s)
$2NH_3+5O^{2-} \rightarrow 2NO+3H_2O+10e^-$	Pt, Pt-Rh	38-40
$CH_4+NH_3+3O^{2-} \rightarrow HCN+3H_2O+6e^-$	Pt, Pt-Rh	47
$CH_3OH+O^{2-} \rightarrow H_2CO+H_2O+2e^-$	Ag	44
$C_6H_5\text{-}CH_2CH_3 + O^{2-} \rightarrow C_6H_5\text{-}CH{=}CH_2 + H_2O + 2e^-$	Pt, Fe_2O_3	48,49
$H_2S + 3O^{2-} \rightarrow SO_2+H_2O+6e^-$	Pt	43
$C_3H_6+O^{2-} \rightarrow C_3$ dimers$+2e^-$	Bi_2O_3-La_2O_3	50
$2CH_4+2O^{2-} \rightarrow C_2H_4+2H_2O + 4e^-$	Ag,Ag-Sm_2O_3	45

selectivity of Pt and Pt-Rh alloy catalysts for the corresponding commercial catalytic oxidation.[38-40] The same applies for Ag which turns out to be equally selective as an electrocatalyst for the anodic partial oxidation of methanol to formaldehyde[44]:

$$CH_3OH+O^{2-} \rightarrow H_2CO + H_2O + 2e^- \tag{3.13}$$

as it is a catalyst for the corresponding catalytic reaction:

$$CH_3OH+ 1/2O_2 \rightarrow H_2CO + H_2O \tag{3.14}$$

Aside from chemical cogeneration studies, where the electrocatalytic anodic and cathodic reactions are driven by the voltage spontaneously

generated by the solid electrolyte cell, several other electrocatalytic reactions have been investigated in solid electrolyte cells.[51] These reactions are listed in Table 3.2. Earlier studies by Kleitz and coworkers had focused mainly on the investigation of electrocatalysts for H_2O electrolysis. Huggins, Gür and coworkers were first to show that other electrocatalytic reactions, such as NO decomposition[52,53] and CO hydrogenation can be carried out in zirconia cells. Later the groups of Otsuka[54] and Stoukides,[55-57] among others, have concentrated on the study of the oxidative coupling of CH_4 utilizing a variety of metal and metal oxide electrodes. Interesting electrocatalytic partial oxidation work has been produced for years by the group of Hayakawa and Takehira.[58]

Table 3.2. **Electrocatalytic reactions investigated in doped ZrO_2 solid electrolyte fuel cells with external potential application**

Reaction	Electrocatalyst	Reference(s)
$H_2O + 2e^- \rightarrow H_2 + O^{2-}$	Ni	51,59
$2NO + 4e^- \rightarrow N_2 + 2O^{2-}$	Pt, Au	52,53
$CO + 2H_2 + 2e^- \rightarrow CH_4 + O^{2-}$	Pt, Ni	60,61
$C_3H_6 + O^{2-} \rightarrow C_3H_6O + 2e^-$	Au	58
$CH_4 + yO^{2-} \rightarrow C_2H_6, C_2H_4, CO, CO_2, H_2O + 2ye^-$	Ag,Ag-MgO, Ag-Bi_2O_3 Ag-Sm_2O_3	54-57

With the exception of H_2O electrolysis[51,59] it is likely that, for all other electrocatalytic reactions listed on Table 3.2, catalytic phenomena taking place on the gas-exposed electrode surface or also on the solid electrolyte surface, had a certain role in the observed kinetic behaviour. However, this role cannot be quantified, since the measured increase in reaction rate was, similarly to the case of the reactions listed on Table 3.1, limited by Faraday's law, i.e.:

$$\Delta r \approx I/2F \tag{3.15}$$

where I is the cell current and Δr (expressed in mol O) is the measured change in global reaction rate. As already mentioned, the fact that no non-Faradaic, i.e., no NEMCA behaviour was observed during these interesting early studies can be safely attributed to the high operating temperature and concomitant low polarizability of the metal-solid electrolyte interface. This dictated that electrocatalysis at the three-phase-boundaries, rather than catalysis on the gas-exposed electrode surface, dominated the global kinetic picture. The limits between *electrocatalysis* $|\Delta r| \leq |I/2F|$ and *electrochemical promotion* $|\Delta r| \gg |I/2F|$ will become apparent in Chapters 4 and 5 of this book.

3.4 SPILLOVER-BACKSPILLOVER PHENOMENA

3.4.1 Phenomenology

The effect of spillover plays an important role in heterogeneous catalysis and was extensively studied during recent years. It was first noticed in the 1950s by Kuriacose.[62] Work in this area has been reviewed by Teichner[63] and by Conner et al.[64]

The spillover effect can be described as the mobility of sorbed species from one phase on which they easily adsorb (donor) to another phase where they do not directly adsorb (acceptor). In this way a seemingly inert material can acquire catalytic activity. In some cases, the acceptor can remain active even after separation from the donor. Also, quite often, as shown by Delmon and coworkers,[65-67] simple mechanical mixing of the donor and acceptor phases is sufficient for spillover to occur and influence catalytic kinetics leading to a Remote Control mechanism, a term first introduced by Delmon.[65] Spillover may lead, not only to an improvement of catalytic activity and selectivity but also to an increase in lifetime and regenerability of catalysts.

The effect of spillover was observed for different species such as H,[68] O,[69] N,[70] NO[64] or CO.[69] Most of the research has been carried out with hydrogen spillover.

Bond et al.[69] reported one of the first examples of spillover of nonhydrogen species. They observed a spillover of O and CO from Pd onto SnO_2 during the oxidation of CO. On pure SnO_2 the rate-limiting step is the oxidation of CO by SnO_2. Adding Pd to the SnO_2 leads to a change in the rate-limiting step towards reoxidation of the SnO_2 due to spillover of O and CO. The rate of CO oxidation was greatly increased by adding Pd to SnO_2.

The simplest example of oxygen spillover is found in the adsorption of oxygen on carbon. The spillover oxygen migrates from the basal carbon (donor) to carbon atoms exposed at steps between layers of the graphite surface, where it reacts with the edge carbons (acceptor).[71] In this case the donor and acceptor phase consist of the same material with different surface properties.

Examples of reverse spillover (or backspillover) are the dehydrogenation of isopentane and cyclohexane on active carbon. Deposition of a transition metal on the active carbon accelerates the recombination of H to H_2 due to a reverse spillover or backspillover effect.[72]

3.4.2 Mechanisms: Donor and Acceptor Phases

In cases of spillover in heterogeneous catalysis the usual kinetic models can no longer be applied in a direct way. The creation of new surface sites or

modification of the surface concentrations leads to new terms in the rate equations. A general reaction scheme of oxygen spillover formation, transfer, activation, and deactivation was proposed by Delmon, Block and coworkers.[66] A schematic representation of reactions (3.16) to (3.20) is given in Fig. 3.5.

$O_2 + 2\,D \rightarrow 2\,O{\cdot}D$ production of spillover species O on donor D (3.16)

$2\,O{\cdot}D \rightarrow O_2 + 2\,D$ recombination of O_2 (3.17)

$A + O{\cdot}D \leftrightarrow D + O{\cdot}A$ transfer of O between donor D and acceptor A (3.18)

$O{\cdot}A + B \rightarrow C$ formation of active site C (3.19)

$E + C \rightarrow E'$ deactivation of C by reaction with E (3.20)

Equations (3.16) and (3.17) describe the dissociative adsorption and recombination of oxygen on a donor D. The transfer between the donor D and acceptor A is described by eq. (3.18). The spillover oxygen (O) is a mobile species which is present on the acceptor surface without being associated with a particular surface site. The mobile spillover species can interact with a particular surface site B forming an active site C (eq. 3.19). Eq. (3.20) represents the deactivation of the active site C by interaction with a reactant E.

Delmon and coworkers[73] presented the following mathematical model for the dehydration of formamides on the donor/acceptor system α-Sb_2O_4/MoO_3. The net rate of spillover oxygen formation on α-Sb_2O_4 (donor) is described by the dynamic balance between dissociation of molecular oxygen from the gas phase and recombination of spillover oxygen (e.g. eqs. (3.16) and (3.17)):

$$r_F = [k_d \cdot p_{O2} \cdot (1 - \theta_{SO\cdot D})^2 - k_{-d} \cdot \theta_{SO\cdot D}{}^2] \cdot S_D \qquad (3.21)$$

where r_F is the net rate of formation of spillover oxygen expressed in $mol{\cdot}s^{-1}$ per gram of the mixture of α-Sb_2O_4 and MoO_3, $\theta_{SO\cdot D}$ is the surface fraction occupied with spillover oxygen on the donor, k_d and k_{-d} are the rate constants for the formation and recombination of spillover oxygen respectively, and S_D is the surface area developed by the donor phase per gram of the mixture of α-Sb_2O_4 and MoO_3. The rate of migration of the spillover oxygen from the donor phase onto the acceptor phase (r_M) depends on the fraction of surface sites occupied by spillover oxygen on the two phases

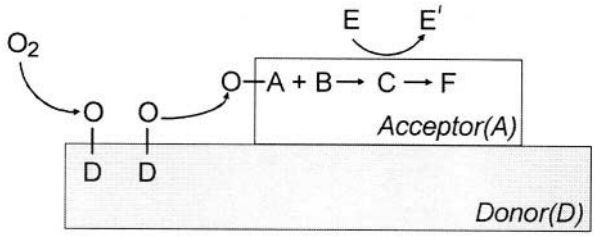

Figure 3.5. Schematic representation of the spillover mechanism described in reactions (3.16) to (3.20).

$$r_M = k_M F_M(\theta_{SO\cdot D}-\theta_{SO\cdot A}) \tag{3.22}$$

with the rate constant k_M and the contact factor F_M. The contact factor F_M accounts for the contact quality Q_M between the two phases, which depends on the mixing procedure of the donor and acceptor phases and the surface areas developed by the donor (S_D) and acceptor (S_A) phases per gram of the mixture of α-Sb_2O_4 and MoO_3:

$$F_M=Q_M S_D S_A \tag{3.23}$$

The rate of creation of active sites (r_C) on the acceptor is proportional to the fraction of the acceptor covered with spillover oxygen ($\theta_{SO\cdot A}$) and to the fraction of inactive MoO_3 surface sites ($1-\alpha$)

$$r_C= k_C a(1-\alpha)\theta_{SO\cdot A} S_A \tag{3.24}$$

where k_C is the rate constant of creation of active sites, a is the maximal density of active sites on the acceptor, α is the fraction of active sites on the acceptor surface, and S_A is the surface area developed by the acceptor phase per gram of the mixture of α-Sb_2O_4 and MoO_3. The rate of destruction of the active surface sites on the acceptor (r_D) is linked to the catalytic process. The destruction of the active surface site is seen as a side reaction occurring with a rate proportional to the turnover rate. The turnover rate depends on the partial pressure of the reactant (p_R), in this case on the partial pressure of formamide. The rate of destruction is described by

$$r_D = k_D a \alpha p_R S_A \tag{3.25}$$

where k_D is the rate constant of destruction of the active surface sites on the acceptor phase. At steady state the rates of spillover oxygen formation (r_F), migration (r_M) and creation of active sites (r_C) are equal:

$$r_F = r_M = r_C \tag{3.26}$$

and so are the rates of creation (r_C) and destruction (r_D) of active sites:

$$r_C = r_D \tag{3.27}$$

The mathematical model was found to describe well the observed activity increase for numerous mechanical mixtures of α-Sb_2O_4/MoO_3 at different oxygen partial pressures and temperatures.[73]

It is now well established that spillover-backspillover phenomena play an important role in numerous catalytic systems. It is worth reminding that the effect of strong-metal-support interactions (SMSI), which was discovered by Tauster[74] and attracted the intense interest of the catalytic community for the least a decade[75] was eventually shown to be due to backspillover of ionic species from the TiO_2 support onto the supported metal surfaces.

For reasons which will become apparent in Chapters 4,8 and 11 of this book it is very likely that the increasing commercial importance of ZrO_2 and CeO_2 supports for conventional supported metal catalyst is due to the ability of these supports to continuously provide backspillover anionic oxygen on the surface of the supported metal catalyst.

Also the similarity between the "remote control" spillover mechanism of Fig. 3.5 and the mechanism of electrochemical promotion (NEMCA) already outlined in Figure 1. 4c and thoroughly proven in Chapter 5, should be noted. In electrochemical promotion the solid electrolyte is the "donor" phase and the conductive catalyst is the "acceptor" phase, using Delmon's terminology.

A difference between the two systems is that in NEMCA experiments the spillover-backspillover rate can be accurately measured and controlled by simply measuring the imposed current or potential. Another difference is that in electrochemical promotion experiments backspillover provides a promoting species, not an active site, to the catalyst surface. This latter difference can however be accommodated by a broader definition of the "active site".

3.4.3 Thermodynamics and Kinetics of Spillover-Backspillover Between a Solid Electrolyte and a Metal Catalyst-Electrode

Based on the preceding discussion on spillover-backspillover and in anticipation of Chapter 4 it is worth to briefly examine the thermodynamic driving force for ion (e.g. O^{2-}) backspillover between a solid electrolyte (e.g. YSZ) and the gas-exposed surface of a metal (e.g. Pt) electrode.

We start from equation (3.7) which under open-circuit conditions is at equilibrium at the three-phase-boundaries (tpb) metal (M)-gas-YSZ:

$$1/2O_2(g) + 2e^-(M) \leftrightarrows O^{2-}(YSZ) \tag{3.7}$$

The equilibrium condition is:

$$1/2\mu_{O_2}(g)+2\bar{\mu}_e(M)=\bar{\mu}_{O^{2-}}(YSZ) \tag{3.28}$$

where $\mu_{O_2}(g)$ is the chemical potential of O_2 in the gas phase (assumed constant) $\bar{\mu}_e(M)$ is the electrochemical potential (or Fermi level) of electrons in the metal (which is also constant over the entire metal electrode) and $\bar{\mu}_{O^{2-}}(YSZ)$ is the electrochemical potential of O^{2-} in the YSZ.

We then note that the equilibrium condition for reaction (3.7) now taking place not only at the tpb (three phase boundaries), but over the entire gas exposed Pt electrode surface is very similar to Eq. (3.28), i.e.

$$1/2\mu_{O_2}(g)+2\bar{\mu}_e(M)=\bar{\mu}_{O^{2-}}(M) \tag{3.29}$$

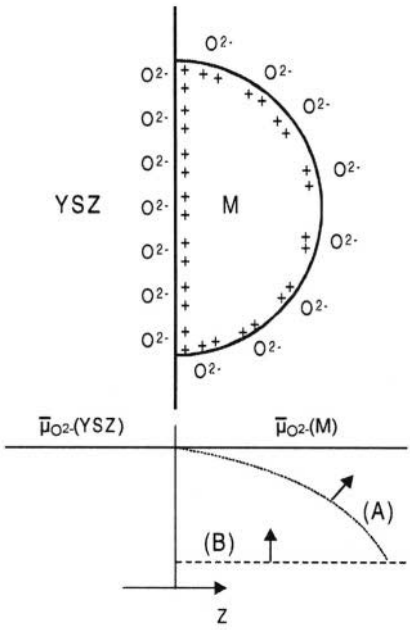

Figure 3.6. Spatial variation of the electrochemical potential, $\bar{\mu}_{O^{2-}}$, of O^{2-} in YSZ and on a metal electrode surface under conditions of spillover (broken lines A and B) and when equilibrium has been established. In case (A) surface diffusion on the metal surface is rate limiting while in case (B) the backspillover process is controlled by the rate, I/nF, of generation of the backspillover species at the three-phase-boundaries. This is the case most frequently encountered in electrochemical promotion (NEMCA) experiments as shown in Chapter 4.

where now $\bar{\mu}_{O^{2-}}(M)$ is the electrochemical potential of O^{2-} on the gas exposed metal electrode surface. Thus at equilibrium, i.e. when spillover-backspillover is not kinetically frozen, one has:

$$\bar{\mu}_{O^{2-}}(M) = \bar{\mu}_{O^{2-}}(YSZ) \tag{3.30}$$

Thus the driving force for O^{2-} backspillover from YSZ to the gas exposed, i.e. catalytically active, electrode surface exists and equals $\bar{\mu}_{O^{2-}}(YSZ) - \bar{\mu}_{O^{2-}}(M)$. It vanishes only when O^{2-} backspillover has taken place and established the "effective" double layer shown in Fig. 3.6.

The kinetics of ion backspillover on the other hand will depend on two factors: On the rate, I/nF, of their formation at the tpb and on their surface diffusivity, D_s, on the metal surface. As will be shown in Chapters 4 and 5 the rate of electrochemically controlled ion backspillover is normally limited by I/nF, i.e. the slow step is their transfer at the tpb. Surface diffusion is usually fast. Thus, as shown in Chapter 5, for the case of Pt electrodes where reliable surface O diffusivity data exist, obtained by Gomer and Lewis several years ago,[76] D_s is at least $4 \cdot 10^{-11}$ cm^2/s at 400°C and thus an O^{2-} ion can move at least 1 μm per s on a Pt(111) or Pt(110) surface. Therefore ion backspillover from solid electrolytes onto electrode surface is not only thermodynamically feasible, but can also be quite fast on the electrode surface. But does it really take place? This we will see in the next Chapter.

REFERENCES

1. C. Wagner, and W. Shottky, Theorie der geordneten Mischphasen, Z. *Phys. Chem. (Leipzig)* **B11**, 163-210 (1930).
2. H. Rickert, in *Electrochemistry of Solids,* Springer-Verlag, Berlin (1982).
3. G.C. Farrington, B. Dunn, and J.C. Thomas, The multivalent β″-Aluminas in High Conductivity Solid Ionic Conductors, E.T. Takahashi, ed. World Sci. Publ., Singapore (1989) pp. 327-365.
4. P.J. Gellings, and H.J.M. Bouwmeester, eds., The CRC Handbook of Solid State Electrochemistry, CRC Press, Boca Raton (1997).
5. H.L. Tuller, J. Schoonman, and I. Riess, eds., Oxygen ion and mixed conductors and their technological applications, in *NATO ASI Series, E: Applied Sciences,* Kluwer Academic Publishers, Dordecht (2000).
6. E.C. Subbarao, and H.S. Maiti, Solid electrolytes with oxygen ion conduction, *Solid State Ionics* **11**, 317-338 (1984).
7. J. Maier, *Solids - defects and function: Principles in the Physical Chemistry of solid state chemistry,* B.G. Teubner Verlag (2000).
8. W. Göpel, New Materials and transducers for chemical sensors, *Sensors and Actuators B* **18-19**, 1-21 (1994).
9. A. Mandelis, and C. Christofides, Solid State Gas Sensor Devices, in *Chemical Analysis,* John Wiley & Sons, New York (1993).
10. F. Grosz in Proc. *2nd Intl. Symp. on Solid Oxide Fuel Cells,* (1991) Athens, Greece: CEC Publ., Luxembourg, pp. 7-24.

11. B.C.H. Steele. Dense Ceramic ion conducting membranes in Oxygen ion and mixed conductors and their technological applications, (1997) Erice, Italy: Kluwer.
12. T.I. Politova, V.A. Sobyanin, and V.D. Belyaev, Ethylene hydrogenation in electrochemical cell with solid proton-conducting electrolyte, *Reaction Kinetics and Catalysis Letters* **41**(2), 321-326 (1990).
13. H. Iwahara, H. Uchida, K. Ono, and K. Ogaki, Proton Conduction in Sintered Oxides based on $BaCeO_3$, *J. Electrochem. Soc.* **135**(2), 529-533 (1981).
14. A. Buekenhoudt, W. Engelen, J. Vangruderbeek, J. Luyten, and D.D. Schutter, Humidity Effects on Calcium Zirconate Ceramics in Electrochemical Hydrogen Cells, *Ionics* **1**, 384-386 (1995).
15. N. Kurita, N. Fukatsu, K. Ito, and T. Ohashi, Protonic Conduction Domain of Indium-Doped Calcium Zirconate, *J. Electrochem. Soc.* **142**(5), 1552-1559 (1995).
16. H. Rickert, Solid Ionic Conductors: Principles and Applications, *Angew. Chem. Int. Ed. Engl.* **17**,37-46(1978).
17. K. Kordesch, and G. Simader, *Fuel cells and their application,* VCH (1996).
18. C.G. Vayenas, S. Bebelis, and S. Ladas, Dependence of Catalytic Rates on Catalyst Work Function, *Nature* **343**, 625-627 (1990).
19. C.G. Vayenas, M.M. Jaksic, S. Bebelis, and S.G. Neophytides, The Electrochemical Activation of Catalysis, in *Modern Aspects of Electrochemistry,* J.O.M. Bockris, B.E. Conway, and R.E. White, eds., Kluwer Academic/Plenum Publishers, New York (1996), pp. 57-202.
20. C.G. Vayenas, S. Bebelis, I.V. Yentekakis, and H.-G. Lintz, Non-Faradaic Electrochemical Modification of Catalytic Activity: A Status Report (Review Paper), *Catalysis Today* **11**(3), 303-442 (1992).
21. C. Wagner, Adsorbed Atomic Species as Intermediates in Heterogeneous Catalysis, in *Adv. Catal.* **21**, (1970), pp. 323-381.
22. C.G. Vayenas, and H.M. Saltsburg, Chemistry at Catalyst Surfaces: The Oxidation of SO_2 on noble metals, *J. Catal.* **57**, 296-314 (1979).
23. C.G. Vayenas, Catalytic and Electrocatalytic Reactions in Solid Oxide Fuel Cells, *Solid State Ionics* **28-30**, 1521-1539 (1988).
24. M. Stoukides, Applications of Solid Electrolytes in Heterogeneous Catalysis, *Industrial & Engineering Chemistry Research* **27**, 1745-1750 (1988).
25. P.J. Gellings, H.S.A. Koopmans, and A.J, Burgraaf, Electrocatalytic Phenomena in Gas Phase Reactions in Solid Electrolyte Electrochemical Cells, *Appl. Catal.* **39**, 1-24 (1988).
26. H.-G. Lintz, and C.G. Vayenas, Feste Ionenleiter in der Heterogene Katalyse, *Angewande Chemie* **101**(6), 725-732 (1989).
27. C.G. Vayenas, C.Georgakis, J. Michaels, and J. Tormo, The role of PtOx in the isothermal rate and oxygen activity oscillations of the Ethylene Oxidation on Pt, *J. Catal.* **67**, 348-361 (1981).
28. C.G. Vayenas, On the work function of the gas exposed electrode surfaces in solid state electrochemistry, *J. Electroanal. Chem.* **486**, 85-90 (2000).
29. C.G. Vayenas, and D. Tsiplakides, On the work function of the gas-exposed electrode surfaces in solid state electrolyte cells, *Surf. Sci.* **467**, 23-34 (2000).
30. D. Tsiplakides, and C.G. Vayenas, Electrode work function and absolute potential scale in solid state electrochemistry, *J. Electrochem. Soc.* **148**(5), E189-E202 (2001).
31. C.G. Vayenas, A. loannides, and S. Bebelis, Solid Electrolyte Cyclic Voltammetry for in situ Investigation of Catalyst Surfaces, *J. Catal.* **129**, 67-87 (1991).

32. Y. Jiang, I.V. Yentekakis, and C.G. Vayenas, Potential-programmed reduction: A new technique for investigating chemisorption on catalysts supported on solid electrolytes, *J. Catal.* **148**, 240-251 (1994).
33. B.C.H. Steele, ed., in *Electrode Processes in Solid State Ionics,* Reidel Publ. Co., Dordrecht (1976).
34. J.N. Michaels, C.G. Vayenas, and L.L. Hegedus, A Novel Cross-Flow Design for Solid State Electrochemical Reactors, *J. Electrochem. Soc.* **133**, 522-525 (1986).
35. O. Yamamoto, Solid oxide fuel cells: fundamental aspects and prospects, *Electrochim. Acta* **45**, 2423-2435 (2000).
36. S.C. Singhal, Advances in solid oxide fuel cell technology, *Solid State Ionics* **135**, 305-313 (2000).
37. F.R. Kalhammer, Polymer Electrolytes and the Electric Vehicle, *Solid State Ionics* **135**, 315-323 (2000).
38. C.G. Vayenas, and R.D. Farr, Cogeneration of Electric Energy and Nitric Oxide, *Science* **208**, 593-595 (1980).
39. R.D. Farr, and C.G. Vayenas, Ammonia High Temperature Solid Electrolyte Fuel Cell, *J. Electrochem. Soc.* **127**, 1478-1483 (1980).
40. C. Sigal, and C.G. Vayenas, Ammonia Oxidation to Nitric Oxide in a Solid Electrolyte Fuel Cell, *Solid State Ionics* **5**, 567-570 (1981).
41. C.G. Vayenas, S. Bebelis, and C. Kyriazis, Solid Electrolytes and Catalysis. Part 1: Chemical Cogeneration, *Chemtech* **21**, 422-428 (1991).
42. C.G. Vayenas, S. Bebelis, and C. Kyriazis, Solid Electrolytes and Catalysis. Part 2: Non-Faradaic Catalysis, *Chemtech* **21**, 500-505 (1991).
43. I.V. Yentekakis, and C.G. Vayenas, Chemical Cogeneration in Solid Oxide Fuel Cells: The Oxidation of H_2S to SO_2, *J. Electrochem. Soc.* **136**, 996-1002 (1989).
44. S. Neophytides, and C.G. Vayenas, Chemical Cogeneration in Solid Electrolyte Cells: The Oxidation of CH_3OH to H_2CO, *J. Electrochem. Soc.* **137**(3), 839-845 (1990).
45. Y. Jiang, I.V. Yentekakis, and C.G. Vayenas, Methane to Ethylene with 85% Yield in a Gas-Recycle Electrocatalytic Reactor-separator, *Science* **264**, 1583-1586 (1994).
46. M. Stoukides, Solid-Electrolyte Membrane reactors: Current experience and future outlook, *Catalysis Reviews - Science and Engineering* **42**(1 &2), 1 -70 (2000).
47. N. Kiratzis, and M. Stoukides, The synthesis of Hydrogen Cyanide in a Solid Electrolyte Fuel Cell, *J. Electrochem. Soc.* **134**(8), 1925-1929 (1987).
48. J.N. Michaels, and C.G. Vayenas, Kinetics of Vapor-Phase Electrochemical Oxidative Dehydrogenation of Ethylbenzene, *J. Catal.* **85**, 477-488 (1984).
49. J.N. Michaels, and C.G. Vayenas, Styrene Production from Ethylbenzene on Platinun in a zirconia Electrochemical Reactor, *J. Electrochem. Soc.* **131**, 2544-2550 (1984).
50. R. DiCosimo, J.D. Burrington, and R.K. Grasselli, Oxidative dehydrodimerization of propylene over a Bi_2O_3-La_2O_3 oxide ion-conductive catalyst, *J. Catal.* **102**, 234-239 (1986).
51. E.J.L. Schouler, M. Kleitz, E. Forest, E. Fernandez, and P. Fabry, *Solid State Ionics* **5**, 551 (1981).
52. S. Pancharatnam, R.A. Huggins, and D.M. Mason, Catalytic Decomposition of Nitric Oxide on Zirconia by Electrolytic Removal of Oxygen, *J. Electrochem. Soc.* **122**(7), 869-875(1975).
53. T.M. Gür, and R.A. Huggins, Decomposition of Nitric Oxide on Zirconia in a Solid-state electrochemical cell, *J. Electrochem. Soc.* **126**(6), 1067-1075 (1979).
54. K. Otsuka, K. Suga, and I. Yamanaka, *Catal. Lett.* **1**, 423 (1988).
55. D. Eng, and M. Stoukides, Catalytic and Electrocatalytic Methane Oxidation with Solid Oxide Membranes, *Catalysis Reviews - Science and Engineering* **33**, 375-412 (1991).

56. D. Eng, and M. Stoukides, Catalytic and electrochemical oxidation of methane on platinum, *J. Catal.* **130**, 306-309 (1991).
57. P.M. Chiang, D. Eng, and M. Stoukides, Electrocatalytic methane dimerization with a Yb-doped $SrCeO_3$ solid electrolyte, *J. Electrochem. Soc.* **138**(6), L11-L12 (1991).
58. T. Hayakawa, T. Tsunoda, H. Orita, T. Kameyama, H. Takahashi, K. Takehira, and K. Fukuda, *Journal Chemical Soc. Jpn. Chemical Commun.,* 961 (1986).
59. W. Doenitz, and E. Erdle, High-temperature electrolysis of water vapor - Status of development and perspectives for application, *International Journal Hydrogen Energy* **10**, 291-295(1985).
60. T.M. Gür, and R.A. Huggins, Methane Synthesis on Nickel by a Solid-State Ionic Method, *Science* **219**, 967-969 (1983).
61. T.M. Gür, and R.A. Huggins, Methane synthesis over transition metal electrodes in a solid state ionic cells, *J. Catal.* **102**, 443-446 (1986).
62. J. Kuriacose, *Industrial Journal of Chemistry* **5**, 646 (1957).
63. S.J. Teichner. New Aspects of Spillover Effect in Catalysis for Development of Highly Active Catalysts in *Third International Conference on Spillover,* 27 (1993) Amsterdam: Elsevier.
64. W.C. Conner, G.M. Pajonk, and S.J. Teichner, Spillover of Sorbed Species, *Adv. Catal.* **34**, 1-79 (1986).
65. B. Delmon, and H. Matralis, The remote control mechanism, general phenomena, possible consequences concerning unsteady state processes, unsteady state processes in catalysis, Y.S. Matros, ed. USF, Utrecht, The Netherlands (1991), p. 25.
66. T. Rebitzki, B. Delmon, and J.H. Block, Isothermal instability due to remote control: A model for selective catalytic oxidation, *AIChE Journal* **41**, 1543-1549 (1995).
67. B. Delmon, and G.F. Froment, Remote Control of Catalytic Sites by Spillover Species: A Chemical Reaction Engineering Approach, *Catal. Rev.-Sci. Eng* **38**(1), 69-100 (1996).
68. T. Inui, and T. Takeguchi, Effective conversion of carbon dioxide and hydrogen to hydrocarbons, *Catalysis Today* **10**, 95-106(1991).
69. G.C. Bond, in *Proc. 6th Int. Congr. Catalysis,* p. 356 (1977).
70. Z. Knor, and J. Sotola, Supported Bimetallic Catalysts, *Coll. Czech. Chemical Comm.* **53**, 2399-2411 (1988).
71. R.T. Yang, and C. Wong, *J. Chem. Phys.* **75**, 4471 (1981).
72. K. Fujimoto, and S. Toyoshi, *Proc. 7th Int. Congr. Catalysis,* p. 235 (1981).
73. F.M. Faus, B. Zhou, H. Matralis, and B. Delmon, Catalytic cooperation between MoO_3 and Sb_2O_4 in N-ethyl formamide dehydration. III. Comparison of a mathematical model based on the remote control mechanism with experimental results, *J. Catal.* **132**, 200-209 (1991).
74. S.J. Tauster, S.C. Fung, and R.L. Garten, Strong metal-support interactions. Group 8 noble metals supported on TiO_2, *JACS* **100**, 170-175 (1978).
75. G.L. Haller, and D.E. Resasco, Metal-Support Interaction: Group VIII Metals and Reducible Oxides, *Advances in Catalysis* **36**, 173-235 (1989).
76. R. Lewis, and R. Gomer, Adsorption of Oxygen on Platinum, *Surf. Sci.* **12**, 157-176 (1968).

CHAPTER 4

ELECTROCHEMICAL PROMOTION OF CATALYTIC REACTIONS

"One of the most remarkable advances in electrochemistry since 1950 is described ..... It is the effect of electrical potential changes on catalyst surfaces. The subject-though only a few years old-is fully described in a remarkable chapter"

J.O'M. Bockris, B.E. Conway, R.E. White, Editors "Modern aspects of electrochemistry", 1996

4.1 EXPERIMENTAL SETUP

4.1.1 The Reactor and the Gas Analysis System

A typical experimental setup for NEMCA studies is shown in Figs. 4.1 and 4.2. Two types of catalytic-electrocatalytic reactors can be used:

In the fuel cell type reactor (Fig. 4.1a) the catalyst-working (W) electrode is exposed to the catalytic reactants (e.g. $C_2H_4+O_2$) and products (e.g. CO_2+H_2O) but the counter (C) and reference (R) electrodes are in a separate compartment and are exposed to a reference gas, e.g. air.

In the single-chamber type reactor (Fig. 4.1b) all three electrodes (catalyst-working (W), counter (C) and reference (R)), electrode are all in the same chamber and are all exposed to the reactants and products.[1-3] In this case the counter and reference electrodes must be made from a catalytically inert (e.g. Au) material for otherwise the catalytic rate on them will obscure the measured (via gas-chromatography or mass-spectrometry, Fig. 4.2) rate on the catalyst-working electrode.

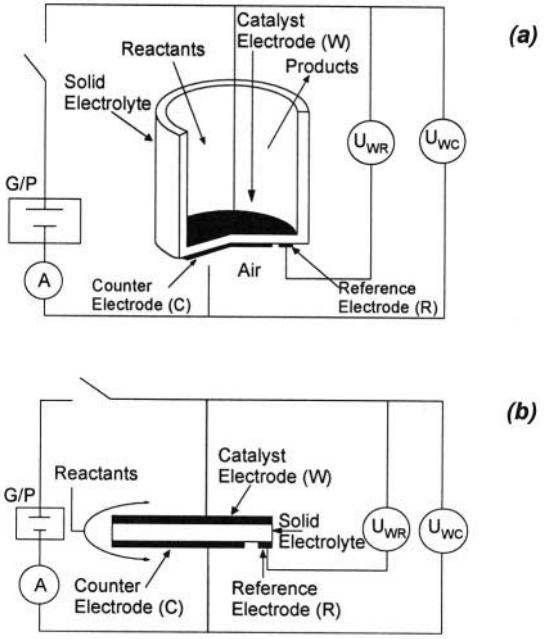

Figure 4.1. Electrode configuration for NEMCA studies using (a) the fuel cell type reactor and (b) the single-chamber type reactor.

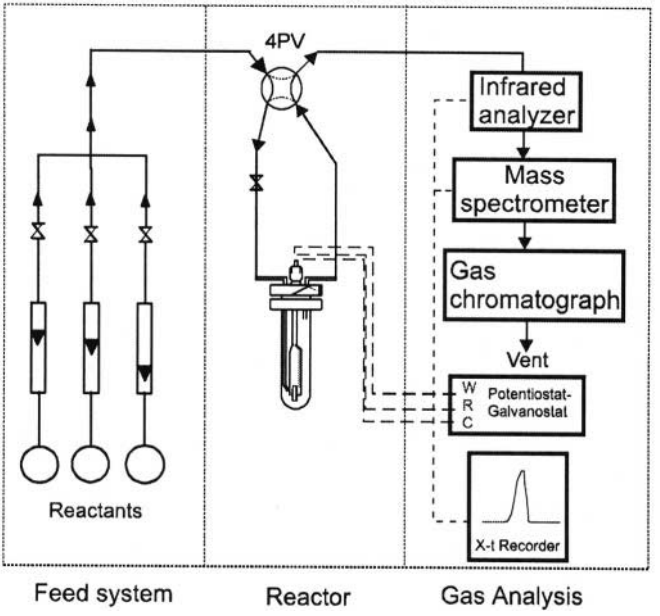

Figure 4.2. Typical gas-flow experimental setup used in electrochemical promotion studies (4 PV): Four-port valve.

In both designs the catalyst-working electrode acts simultaneous as a catalyst for the catalytic reaction (e.g. C_2H_4 oxidation by gaseous O_2) and as an electrode for the electrochemical charge transfer reaction:

$$O^{2-} \leftrightarrow O(a) + 2e^- \tag{4.1}$$

taking place at the three-phase boundaries (tpb) metal-gas-solid electrolyte.

Both reactor designs of Figure 4.1 give similar results. The single-chamber design offers ease of scale-up but has the disadvantage of a quasi-reference electrode which can easily cause inaccuracies of 0.1 V in measuring the thermodynamic catalyst potential (see section 4.1.3). The fuel cell type design has an accurate reference electrode but suffers from all the scale-up difficulties of fuel cells.

4.1.2 The Catalyst Film

4.1.2.1 General Features

The catalyst film, typically 1-10 μm thick is connected to a wire which acts as electron collector or supplier. The film must have enough porosity so that its gas-exposed, i.e. catalytically active, surface area A_G can give a measurable catalytic reaction rate in the desired operating temperature range. Typically A_G must be 30 to 3000 times larger than the electrolyte surface area A_E on which the catalyst film is supported. Scanning electron micrographs of Pt and Ag catalyst films used in some NEMCA studies are shown on Figs. 4.3, 4.5 and 4.6. Both the top view of the films and cross-sections of the catalyst film-solid electrolyte interface are shown. Figure 4.4 shows a scanning tunneling micrograph (STM) of the surface of a Pt catalyst film.

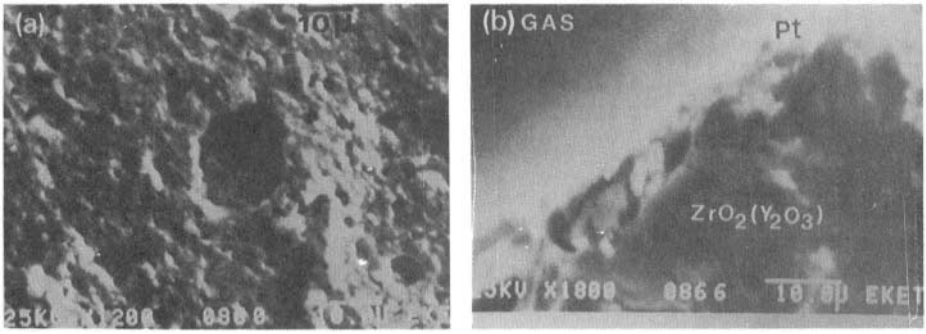

Figure 4.3. Scanning electron micrographs of the top side of a porous Pt catalyst film (a) and of a section perpendicular to the Pt catalyst-yttria-stabilized zirconia (YSZ) interface (b).[4] Reprinted with permission from Academic Press.

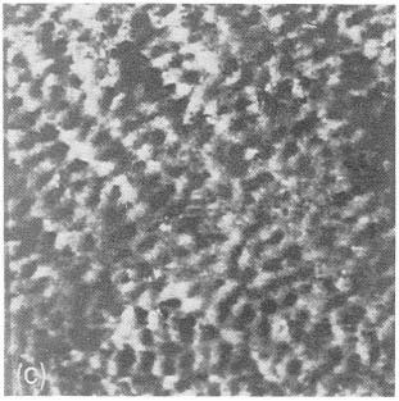

Figure 4.4. Scanning tunneling micrograph of the surface of a Pt catalyst used in NEMCA studies: Scan size 62 Å; V_{bias}=0.5 V, I_{tunnel}=15 nA.[1] Reprinted with permission from Elsevier Science.

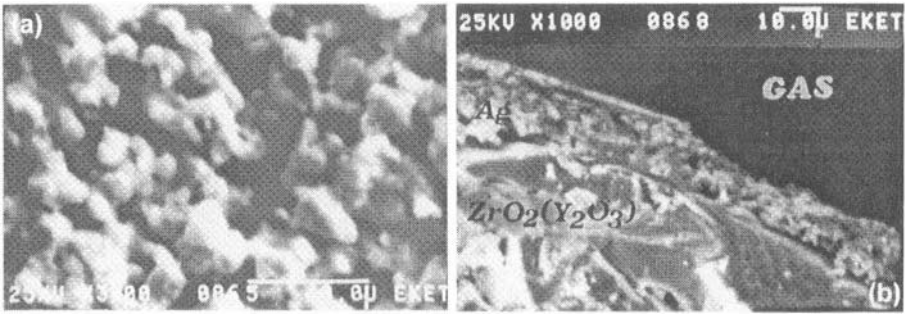

Figure 4.5. Scanning electron micrographs of a porous Ag catalyst film (a) and of a section perpendicular to the Ag catalyst-yttria-stabilized zirconia interface (b).[1] Reprinted with permission from Elsevier Science.

As discussed below, the porosity and surface area of the catalyst film is controllable to a large extent by the sintering temperature during catalyst preparation. This, however, affects not only the catalytically active surface area A_G but also the length, ℓ, of the three-phase-boundaries between the solid electrolyte, the catalyst film and the gas phase (Fig. 4.7).

Electrocatalytic reactions, such as the transformation of O^{2-} from the zirconia lattice to oxygen adsorbed *on the film* at or near the three-phase-boundaries, which we denote by O(a), have been found to take place primarily at these three phase boundaries.[5-8] This electrocatalytic reaction will be denoted by :

$$O^{2-} \rightarrow O(a)+2e^- \tag{4.1a}$$

or, in Kröger-Vink notation,[9]

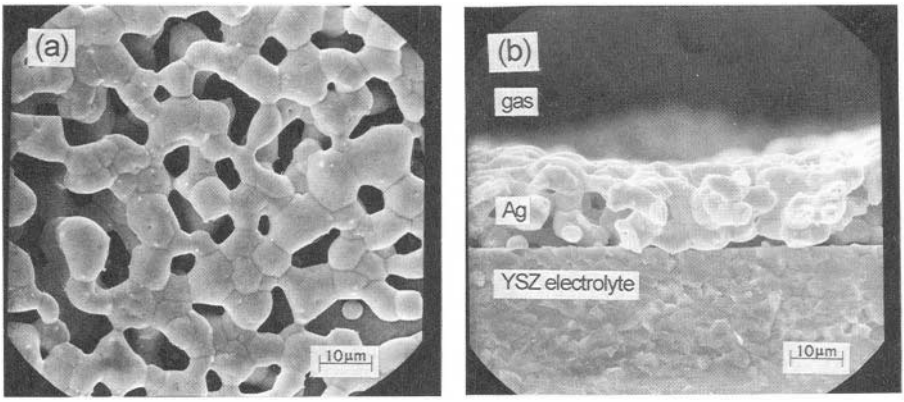

Figure 4.6.Scanning electron micrographs of a Ag catalyst-electrode deposited on YSZ and used for NEMCA studies[10] (a) Top view (b) Cross section of the Ag/YSZ interface. Reprinted with permission from Academic Press.

$$O_O \rightarrow O(a) + V_O^{\bullet\bullet} + 2e^- \qquad (4.1b)$$

where, O_O denotes an oxygen anion O^{2-} in the yttria-stabilized-zirconia (YSZ) lattice and $V_O^{\bullet\bullet}$ stands for an O^{2-} vacancy in the lattice with a double positive charge. There is some experimental evidence that reaction (4.1) can also take place, to some extent, at the two phase boundaries between the zirconia and the metal, followed by diffusion of oxygen through the metal or through the two phase boundaries to the three phase boundaries.[7] However, this scheme becomes important apparently only with metals having a high oxygen solubility, such as Ag,[11,12] or when metal foils are used instead of porous metal films or with very dense non-porous metal films acting as blocking electrodes. There is also some evidence that under reducing gas phase conditions and large applied negative (cathodic) currents, so that the applied potential is near the potential required for the decomposition of zirconia (~2.4 V at 800 K), then the electrocatalytic reaction can also take place directly at the zirconia-gas interface.[13] The above conditions are usually referred to as "zirconia blackening" conditions, as the electrolyte surface indeed turns black. Such operation has not been employed, at least intentionally, in the NEMCA studies reviewed here. Also the porosity of the catalyst films employed was usually high enough so that the *electrocatalytic* reaction (4.1) can be safely assumed to occur at the three-phase-boundaries only, with the exception of Ag electrodes, which act as oxygen "sponges"[11,12] and where the reaction in Eq. (4.1) takes place at the Ag/YSZ interface as well.[11,12] Methods for estimating the three-phase boundary length by the use of solid electrolyte cyclic voltammetry[8] or AC Impedance spectroscopy[14] will be discussed in Chapter 5.

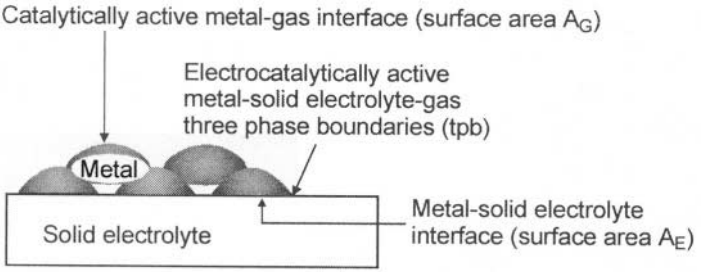

Figure 4.7. Schematic representation of the location of electrocatalytically and catalytically active sites in a section perpendicular to the catalyst film-solid electrolyte interface.

In order to complete our discussion about the location where the electrocatalytic reaction (4.1) takes place (tpb) it is useful to note the following regarding the ultimate fate of the metal-adsorbed species O(a) generated at the tpb via reaction (4.1). As already noted in Chapter 1 (Fig. 1.4) this species (which as we will see in Chapter 5 is very ionic and resembles O^{2-} with a compensating +2 charge in the metal) may desorb as O_2, may react with a combustible molecule (e.g. CO or C_2H_4) or may migrate (backspillover) on the entire metal/gas interface acting as a strong electronegative promoter and causing NEMCA. In absence of an oxidizable species O(a) will at steady state eventually desorb as O_2 so that the net electrochemical (anodic) reaction will be:

$$O^{2-} \rightarrow 1/2O_2(g) + 2e^- \qquad (4.2)$$

This electrochemical reaction contains the elementary step (4.1) and under conditions of backspillover can be considered to take place over the entire metal/gas interface including the tpb.[1,15-18] This is usual referred to as extension of the electrochemical reaction zone over the entire metal/gas interface. But even under these conditions it must be noted that the elementary charge transfer step 4.1 is taking place at the three-phase-boundaries (tpb).

4.1.2.2 Catalyst Preparation

Metal catalyst films used in NEMCA studies[1,4,11,12,19] are usually prepared by using commercial unfluxed metal pastes although there have been also several recent reports using evaporated metal films. When using a metal paste, *thin* coatings of the paste are applied on the solid electrolyte surface, followed by drying and calcining. The calcination temperature program depends on the metal to be deposited and on paste composition and plays a key role in obtaining a well-adhered film, which is, of course, essential for NEMCA studies. Thus for Pt catalyst preparation a proven procedure[1,4,19] is to use a *thin* coating of Engelhard A1121 Pt paste, using a fine brush,

followed by drying and then calcining in air first for 2h at 400°C and then for 20 min at 820°C. When using a Demetron Pt paste, final calcination temperatures of at least 100°C higher were found necessary to produce sufficiently polarizable Pt-zirconia interfaces. For Ag catalyst film preparation one may use thin coatings of Ag solution in butyl acetate[11,12] followed by drying at 80°C and calcining at 650°C. In general it appears preferable to use a slow heating rate (e.g. 2°C/min) during calcination and to always maintain a high flowrate of air (e.g. 0.2 l/min) through the furnace. Increasing calcination temperatures even by only 20-30°C for a given metal paste leads to increased sintering and loss both in catalyst surface area and in metal-gas-zirconia three-phase-boundaries length. The latter has a beneficial effect for increasing the polarizability of the metal-solid electrolyte interface and thus observing strongly non-Faradaic catalytic rate changes. The decrease in catalyst surface area may, however, be undesirable in many cases, if the intrinsic catalytic rate is very small. In general, the optimal calcination temperature for each catalyst and paste has to be found by trial and error. Some details are given in Appendix B.

A proven procedure for enhancing the adherance of metal or metal oxide films on flat YSZ surfaces is to first roughen the YSZ surface by adding a slurry containing fine (1-2 μm) YSZ powder, followed by drying and calcining at 1450-1500°C. Catalyst deposition on such a roughened surface may, of course, lead to a long three-phase-boundary line length and to a concomitant decreased polarizability of the zirconia-solid electrolyte interface, but this is definitely preferable than a not well-adhered film.

The deposition of thin conductive oxide films on flat zirconia components has also received considerable attention both for fuel cell applications[20] and also for SEP[21] and NEMCA studies.[22,23] The interested reader is referred to the original references for experimental details.

A final, obvious but important, caution about catalyst film preparation: Its thickness and surface area A_G must be low enough, so that the catalytic reaction under study is not subject to external or internal mass transfer limitations within the desired operating temperature range. Direct impingement of the reactant stream on the catalyst surface[1,19] is advisable in order to diminish the external mass transfer resistance.

4.1.3 Counter and Reference Electrodes

As shown on Fig. 4.1, the counter and reference electrodes are deposited on the opposite side of the gas-impervious solid electrolyte component, which is typically 500 μm to 2 mm thick. The electrolyte thickness is not crucial, but it is preferable to keep it low, so that the ohmic drop in it is small during operation, preferably below 100-600 mV.

Both the counter and the reference electrodes are essential for fundamental NEMCA studies. They need not be of the same material with the catalyst. The counter electrode-solid electrolyte interface does not have to be polarizable. In fact, it is advantageous when it is not, because then most of the applied potential difference ends up as overpotential at the catalyst and not at the counter electrode.

The reference electrode-solid electrolyte interface must also be non-polarizable, so that rapid equilibration is established for the electrocatalytic charge-transfer reaction. Thus it is generally advisable to sinter the counter and reference electrodes at a temperature which is lower than that used for the catalyst film. Porous Pt and Ag films exposed to ambient air have been employed in most previous NEMCA studies.[1,19]

4.1.4 Quasireference Electrodes

When using the so called "single-chamber design[1-3] (Fig. 4.1(b)) the reference and counter electrodes are exposed to the reacting gas mixture itself. Consequently it is advantageous to use a reference electrode whose potential is weakly dependent on gaseous composition. Au electrodes have been shown to act as satisfactory quasi-reference electrodes since their potential has been found to vary little (0.1 V) with changing gaseous composition[24,25] at fixed p_{O_2}. This has also been recently confirmed by measuring the work function of Au reference electrodes deposited on solid electrolytes.[17]

4.2 Catalyst-Electrode Film Characterization

Since electrochemical promotion (NEMCA) studies involve the use of porous metal films which act simultaneously both as a *normal catalyst* and as a *working electrode,* it is important to characterize these catalyst-electrodes both from a catalytic and from an electrocatalytic viewpoint. In the former case one would like to know the gas-exposed catalyst surface area A_G (in m^2 or in metal mols, for which we use the symbol N_G throughout this book) and the value, r_0, of the catalytic rate, r, under open-circuit conditions.

In the latter case one would like to know the length ℓ_{tpb} of the metal-solid electrolyte-gas three-phase-boundaries (tpb) (in m or in metal mols, for which we use the symbol N_{tpb} throughout this book) and the value of the exchange current I_0, where $(I_0/2F)$ expresses the value of the (equal and opposite under open-circuit conditions) forward and reverse rates of the charge-transfer reaction 4.1.

When one starts NEMCA experiments only r_0 is important to measure and this is very easy. However the subsequent measurement of N_G and I_0 is quite important for a better understanding the system and this we will discuss here. The measurement of ℓ_{tpb} and N_{tpb} is discussed in Chapter 5.

4.2.1 Catalytic Characterization: Measurement of the Metal/Gas Interface Area A_G

As already noted SEM, but also STM, provide useful information on the morphology of metal films deposited on solid electrolytes. As with every catalyst used in fundamental studies, one would like to know as much as possible about the cleanliness of the catalyst surface. This can be examined using ex-situ surface spectroscopic techniques such as X-ray photoelectron spectroscopy (XPS), ultraviolet photoelectron spectroscopy (UPS) and Auger electron spectroscopy (AES). Such studies have shown that the surface of metal catalyst-electrodes prepared from Engelhard metal pastes contain no detectable metal impurities and are overall surprisingly clean, even from C, as long as they have been calcined under oxidizing conditions.[26-28] This may be due to the large amounts of oxygen emitted from YSZ upon heating in vacuum above 600°C.[29-31]

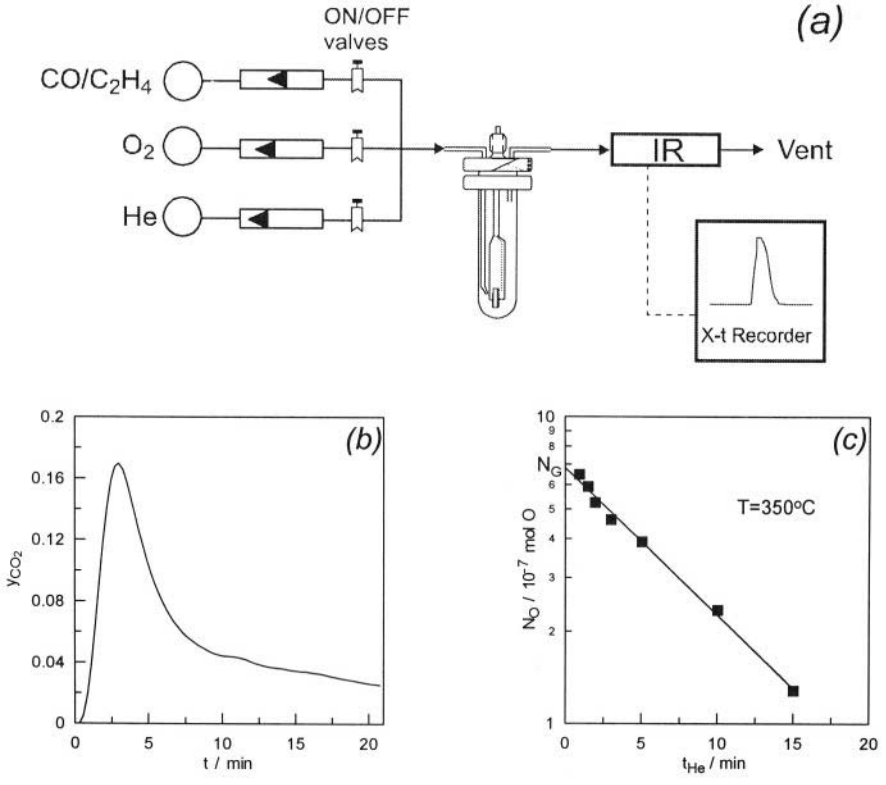

Figure 4.8. (a) Experimental apparatus for measuring the catalyst-electrode metal/gas interface area A_G. (b) typical y_{CO_2} peak obtained upon reacting the preadsorbed O with C_2H_4 or CO; its area gives N_O. (c) Plot of N_O vs the O_2 desorption time, t_{He}, to obtain N_G.

On the other hand metal films deposited on β''-Al_2O_3, a Na^+ conductor, are usually found after calcination to contain on their surface large amounts of sodium, which can nevertheless be easily pumped backed into the β''-Al_2O_3 lattice via electrical current application.[32,33]

In principle any standard catalytic metal surface area measuring technique, such as H_2 or CO chemisorption can be used to measure the metal/gas interface area A_G or N_G. This is because solid electrolytes such as YSZ chemisorb practically no H_2 or CO at any temperature.

Most reported A_G and N_G measurements have been carried out using the isothermal titration technique.[1,19,26,27,34,35] The basic apparatus is shown in Figure 4.8. In this technique the catalyst-electrode is initially exposed to a flowing stream of O_2 for a time denoted t_{O_2} sufficiently long (e.g. 10-15 min) to reach equilibrium coverage of atomic oxygen on the surface. The operating temperature T, which is kept constant throughout the entire experiment, is chosen so that the following two conditions are met:

a. The equilibrium oxygen coverage is near saturation.
b. The reaction of chemisorbed O with a combustible gas, such as CO or C_2H_4, is fast.

For Pt catalyst-electrodes a good operating temperature is 350-380°C[34,35] while lower temperatures (300-330°C) are suitable for Ag.[26,27]

After the oxygen equilibrium period, t_{O_2}, the catalyst-electrode is immediately exposed to a flowing stream of ultrapure (99.999%) He. During this time period, denoted t_{He}, molecular O_2 desorption is taking place. One must choose t_{He} to be at least 8 times longer than the residence time (V/F_v) of the catalytic reactor (V is the reactor volume and F_v is the volumetric flowrate) to ensure that all gaseous O_2 is removed from the reactor.

Subsequently the catalyst-electrode is immediately exposed to a flowing stream of C_2H_4 (or CO) in He and an infrared CO_2 analyzer is used to monitor the mole fraction, y_{CO_2}, of CO_2 formed by the reaction of C_2H_4 (or CO) with adsorbed oxygen. By integrating the peak area one determines the amount N_O (mol O) of O adsorbed on the surface after the desorption time t_{He}.

The above procedure is then repeated by varying the O_2 desorption time, t_{He}, and measuring the corresponding N_O value.

Subsequently one plots $\ln N_O$ vs t_{He} and extrapolates to $t_{He}=0$. This plot provides the O_2 desorption kinetics at the chosen temperature T. The intersect with the N_O axis gives the desired catalyst surface area N_G (Fig. 4.8) from which A_G can also be computed. More precisely N_G is the maximum reactive oxygen uptake of the catalyst-electrode but this value is sufficient for catalyst-electrode characterization.

Alternative variations of the isothermal titration technique utilize CO adsorption followed by reaction with gaseous O_2. Experiment has shown that similar N_G values are obtained.[1,19]

4.2.2 Electrochemical Characterization: Measurement of the Catalyst-Solid Electrolyte Exchange Current I_0

Although NEMCA is a catalytic effect taking place over the entire catalyst gas-exposed surface, it is important for its description to also discuss the electrocatalytic reactions taking place at the catalyst-solid electrolyte-gas three phase boundaries (tpb). This means that the catalyst-electrode must also be characterized from an electrochemical viewpoint. When using YSZ as the solid electrolyte the electrochemical reaction taking place at the tpb is:

$$O^{2-} \leftrightarrow O(a)+2e^- \tag{4.1}$$

In the presence of oxidizable reactants over the catalyst surface, other electrocatalytic reactions may also take place in parallel with reaction (4.1) at the tpb. Thus in presence of high CO concentrations, direct reaction of CO with O^{2-} can also take place:

$$CO(a)+O^{2-} \leftrightarrow CO_2(g)+2e^- \tag{4.3a}$$

The extent to which such reactions take place in parallel with the dominant reaction (4.1) is, in general, difficult to quantify as the overall reaction (4.3a) may consist of the elementary step (4.1) followed by reaction between adsorbed CO and adsorbed oxygen on the metal surface:

$$CO(a)+O(a) \leftrightarrow CO_2(g) \tag{4.3b}$$

When other types of solid electrolyte are used, such as the Na^+ conducting β''-Al_2O_3, then the dominant electrocatalytic reaction at the tpb is:

$$Na^+ + e^- \leftrightarrow Na(a) \tag{4.4}$$

where Na(a) stands for Na adsorbed on the catalyst surface. However, in the presence of H_2O, other parallel reactions can also take place[36] such as:

$$H_2O+e^- \leftrightarrow OH^- + H(a) \tag{4.5}$$

Again the extent to which such parallel reactions contribute to the measured current is not very easy to quantify. However, fortunately, such a quantification is not necessary for the description of NEMCA. What is needed is only a measure of the overall electrocatalytic activity of the metal-solid electrolyte interface or, equivalently, of the tpb, and this can be obtained by determining the value of a single electrochemical parameter, the exchange current I_0, which is related to the exchange current density i_0 via:

$$i_0 = I_0/A_E \tag{4.6}$$

Strictly speaking I_0 is a measure of the electrocatalytic activity of the tpb for a given electrocatalytic reaction. It expresses the rates of the forward (anodic) and reverse (cathodic) electrocatalytic reaction under consideration, e.g. reaction (4.1), when there is no *net* current crossing the metal-solid electrolyte or, equivalently, the tpb. In this case the rates of the forward and the reverse reactions are obviously equal. It has been recently shown that, in most cases, as one would intuitively expect, I_0 is proportional to the length, ℓ_{tpb}, of the tpb.[8]

The measurement of I_0, or i_0, is based on the classical Butler-Volmer[37-41] equation:

$$I=I_0[\exp(\alpha_\alpha F\eta_{ac,j}/RT)-\exp(-\alpha_c F\eta_{ac,j}/RT)] \tag{4.7}$$

where α_α and α_c are the anodic and cathodic transfer coefficients and $\eta_{ac,j}$ is the *activation overpotential* of the electrode j under consideration. Before discussing the use of the Butler-Volmer equation (4.7) to extract the values of I_0 and of α_a and α_c, it is important to first discuss some issues regarding the activation overpotential.

When a current I flows in an electrochemical cell, such as the one shown in Fig. 4.1, between the catalyst, or working electrode (W) and the counter electrode (C), then the potential difference U_{WC} deviates from its open-circuit value U^o_{WC}. The electrochemical cell overpotential η_{WC} is then defined from:

$$\eta_{WC} = U_{WC} - U^o_{WC} \tag{4.8}$$

The cell overpotential η_{WC} is the sum of three terms:

$$\eta_{WC}=\eta_W+\eta_C+\eta_{ohmic,WC} \tag{4.9}$$

where η_W, η_C are the overpotentials of the catalyst (W) and counter (C) electrodes, respectively, and $\eta_{ohmic,WC}$ is the ohmic overpotential due to the resistance of the electrolyte between the working and counter electrodes.

The latter equals IR_{WC} where R_{WC} is the ohmic resistance between the working and counter electrode. Experimentally it is rather easy to measure the $\eta_{ohmic,WC}$ term using the current interruption technique as shown in Figure 4.9. Upon current interruption the ohmic overpotential $\eta_{ohmic,WC}$ vanishes within less than 1 μs and the remaining part of the overpotential which vanishes much slower is $\eta_W+\eta_C$ (Eq. 4.9).

It is worth emphasizing that although overpotentials are usually associated with electrode-electrolyte interfaces, in reality they refer to, and are measured as, deviations of the potential (φ or $\bar{\mu}_e$ as we will discuss in Chapter 5) of the electrodes only. Thus the concept of overpotential must be associated with *an electrode* and not with an electrode-electrolyte interface, although the nature of this interface will, in general, dictate the magnitude of the measured overpotential.

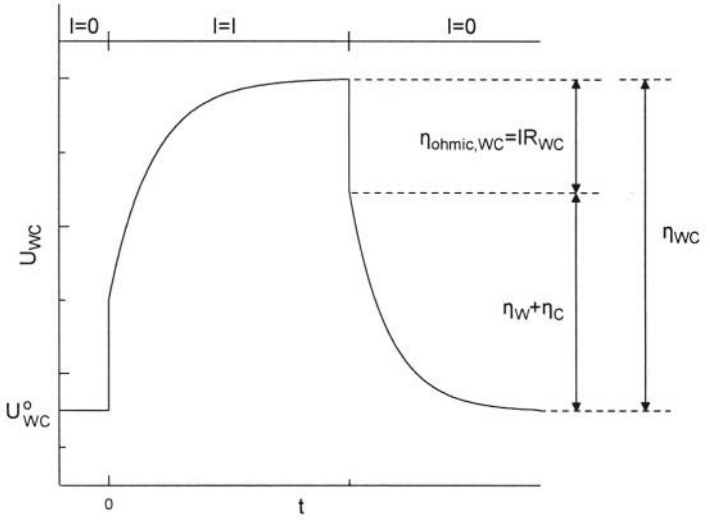

Figure 4.9. Use of the current interruption technique to measure the ohmic overpotential, $\eta_{ohmic,WC}$, between the working (W) and counter (C) electrode.

When studying the catalyst-electrode in electrochemical promotion (NEMCA) studies, or more generally when studying a working electrode in electrochemistry one would like to separate the η_W and η_C terms in order to know η_W for any fixed value of I. How can this be done? Simply via the use of a reference electrode (Fig. 4.10). For the non-electrochemist it is worth reminding that a galvanostat always fixes the current between the working (W) and counter (C) electrode at a desired value. A potentiostat always fixes the current between the working and counter electrode so that the potential between the working (W) and reference (R) electrode is at a fixed desired value U_{WR}. In either case the current, I, is flowing between the working and counter electrodes. In principle no current at all passes through the reference electrode. In practice a usually very small current is passing through the reference electrode and an appropriate correction has to be made as discussed below.

We start by rewriting equations (4.8) and (4.9) but now considering the working (W) and reference (R) electrodes:

$$\eta_{WR} = U_{WR} - U^{o}_{WR} \tag{4.10}$$

where η_{WR} is the working-reference overpotential and U^{o}_{WR} is the open-circuit (I=0) value of the potential difference U_{WR}. Again η_{WR} consists of three terms:

$$\eta_{WR} = \eta_W + \eta_R + \eta_{ohmic,WR} \tag{4.11}$$

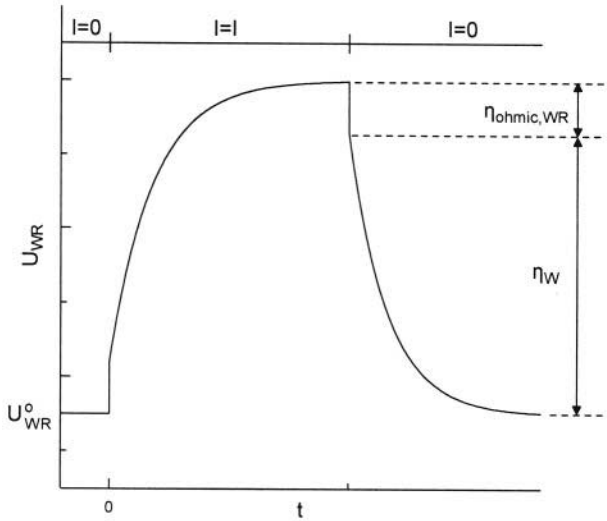

Figure 4.10. Use of the current interruption technique to measure the uncompensated ohmic drop, $\eta_{ohmic,WR}$, between the working (W) and reference (R) electrode.

Ideally no current flows through the reference electrode, therefore it should be $\eta_R=0$ and $\eta_{ohmic,WR}=0$. In practice the first assumption is usually good for reasonably non-polarizable reference electrodes, since the parasitic uncompensated current flowing via the reference electrode is usually very small.[19] The ohmic drop, however, between the working and reference electrodes, i.e., $\eta_{ohmic,WR}$, may in general be not negligible and must be determined using the current interruption technique in conjunction with a recording oscilloscope.[1,5,19] The ohmic component decays to zero within less than 1 μs and the remaining part of η_{WR} is η_W (Fig. 4.10). As in aqueous electrochemistry, the reference electrode must be placed as near to the catalyst as possible to minimize $\eta_{ohmic,WR}$.

The overpotential η of an electrode, e.g. (W), can be considered to be the sum of three terms, i.e.:

$$\eta_W = \eta_{ac,W} + \eta_{conc,W} + \eta_{ohmic,W} \tag{4.12}$$

The activation overpotential $\eta_{ac,W}$ is due to slow charge transfer reactions at the electrode-electrolyte interface and is related to current via the Butler-Volmer equation (4.7). A slow chemical reaction (e.g. adsorption, desorption, spillover) preceding or following the charge-transfer step can also contribute to the development of activation overpotential.

The concentration overpotential $\eta_{conc,W}$ is due to slow mass transfer of reactants and/or products involved in the charge-transfer reaction. There

exist simple equations for computing its magnitude in terms of mass transfer coefficients or, more frequently, in terms of the limiting current I_L, which is the maximum current obtained when the charge-transfer reaction is completely mass-transfer controlled.[40,42] Contrary to aqueous electrochemistry, where concentration overpotential is frequently important due to low reactant and/or product diffusivities in the aqueous phase, in solid electrolyte cells mass transfer in the gas phase is fast and, consequently, gaseous concentration overpotential is usually negligible, particularly in NEMCA applications where the currents involved are usually very small.

The ohmic overpotential $\eta_{ohmic,W}$ is also negligible, provided the catalyst-electrode is sufficiently conductive.

Thus, to a good approximation the η_W determined via current interruption (Fig. 4.10) can be considered to be an activation overpotential.

The usual procedure for extracting the exchange current I_0 is then to measure η_W $(=\Delta U_{WR})$ as a function of I and to plot lnI vs η_W (Tafel plot). Such plots are shown on Figs. 4.11 and 4.12 for Pt and Ag catalyst electrodes. Throughout the rest of this book we omit the subscript "W" from η_W and simply write η,

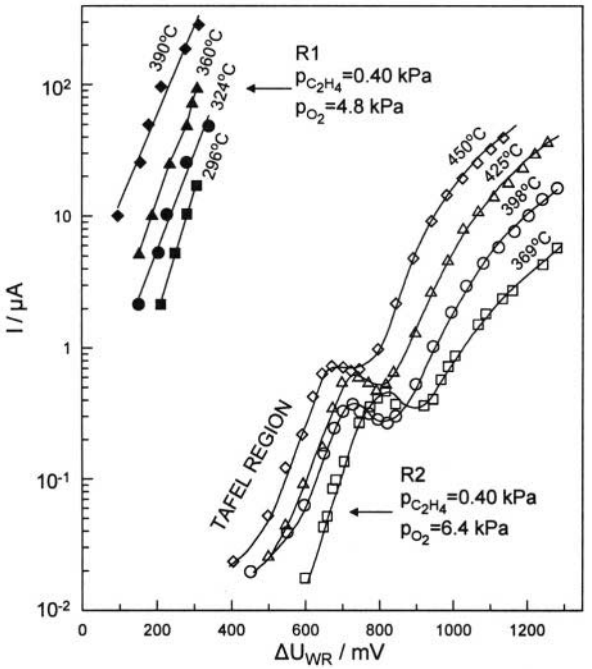

Figure 4.11. Typical Tafel plots for Pt catalyst-YSZ interfaces during C_2H_4 oxidation on Pt; the large difference in I_0 values between the two Pt films (labeled R1 and R2) is due to the higher calcination temperature of Pt film R2 vs Pt film R1.[4] Reprinted with permission from Academic Press.

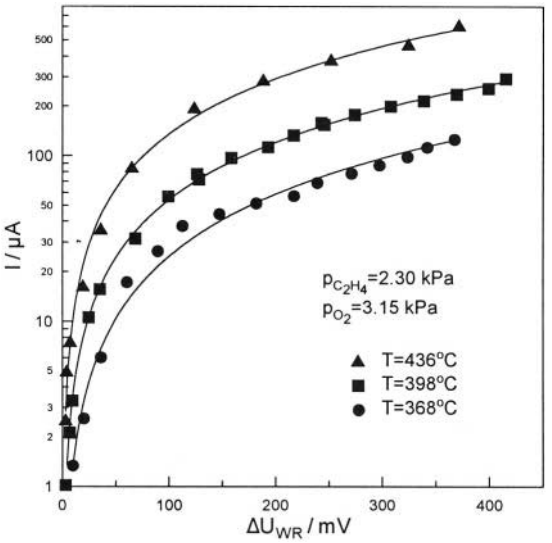

Figure 4.12. Effect of temperature on the Tafel plots and corresponding I_0 values of a Ag catalyst-YSZ interface during C_2H_4 oxidation on Ag.[12] Reprinted with permission from Academic Press.

since the only overpotential of interest is that of the catalyst film. When $|\eta|>100$ mV then the Butler-Volmer equation (4.7) reduces to its "high field approximation" form, i.e.:

$$\ln(I/I_0)=\alpha_a F\eta/RT \tag{4.13}$$

for anodic ($I>0$, $\eta>0$) operation and to:

$$\ln(-I/I_0)=-\alpha_c F\eta/RT \tag{4.14}$$

for cathodic ($I<0$, $\eta<0$) operation. Thus by extrapolating the linear part of the $\ln|I|$ vs η plot to $\eta=0$ one obtains I_0. The slopes of the linear parts of the plot give the transfer coefficients α_a and α_c. One can then plot I vs η and use the "low field" approximation of the Butler-Volmer equation which is valid for $|\eta|< 10$ mV, i.e.,

$$I/I_0=(\alpha_a+\alpha_c)F\eta/RT \tag{4.15}$$

in order to check the accuracy of the extracted I_0, α_a and α_c values.

It is worth noting that I_0 is, in general, strongly dependent both on temperature and on gaseous composition. It increases with temperature with an activation energy which is typically 35-45 kcal/mol for Pt and 20-25 kcal/mole for Ag films deposited on stabilized zirconia.[1,5-7,43]

The I_0 dependence on gaseous composition is usually complex. Thus Manton[43] has shown that I_0 goes through a maximum with increasing p_{O_2} at any fixed temperature for $Pt|ZrO_2(Y_2O_3)$ catalyst films. These results can be described adequately on the basis of Langmuir-type adsorption of oxygen at the tpb, i.e.:

$$\theta_O = K_O p_{O_2}^{1/2} / (1 + K_O p_{O_2}^{1/2}) \tag{4.16}$$

where θ_O is the oxygen coverage. It can be shown[5-7] that:

$$I_0 \sim [\theta_O(1-\theta_O)]^{1/2} \tag{4.17}$$

or, equivalently:

$$I_0 \sim K_O p_{O_2}^{1/4} / (1+K_O p_{O_2})^{1/2} \tag{4.18}$$

which explains nicely the observed maxima and the fact that I_0 is proportional to $p_{O_2}^{1/4}$ for low p_{O_2} and to $p_{O_2}^{-1/4}$ for high p_{O_2}.[5-7,19,43] According to this successful model, the I_0 maxima correspond to θ_O=1/2. It has been found, however, that for low T and high p_{O_2} the situation becomes more complicated due to the formation of surface Pt oxide PtO_2.[43-47]

When other gases are present in the gas phase in addition to O_2, then I_0 can be affected in two different ways: First because θ_O may be affected due to a catalytic reaction and/or due to competitive chemisorption. Second because these gases may react with O^{2-} at the tpb. In general it is difficult to determine experimentally which one of these two factors is more important.

The exchange current I_0 is an important parameter for the quantitative description of NEMCA. As subsequently analyzed in this chapter it has been found both theoretically and experimentally[1,4,19] that the order of magnitude of the absolute value $|\Lambda|$ of the NEMCA enhancement factor Λ defined from:

$$\Lambda = \Delta r/(I/2F) \tag{4.19}$$

where Δr is the NEMCA-induced change in catalytic rate and I is the applied current, can be usually estimated for any catalytic reaction from:

$$|\Lambda| \approx 2Fr_0/I_0 \tag{4.20}$$

where r_0 is the regular, i.e., open-circuit catalytic rate. When using equation (4.20) to estimate the order of magnitude of the enhancement factor Λ expected for a given catalytic reaction, one must use the I_0 value measured in the presence of the reacting gas mixture. The fact that I_0 increases

exponentially with temperature in conjunction with the fact that Λ is inversely proportional to I_0 explains why NEMCA is limited usually to temperatures below 600°C.

4.3 A NEMCA EXPERIMENT: GALVANOSTATIC AND POTENTIOSTATIC TRANSIENTS

4.3.1 Electrochemical Promotion Using O^{2-} Conductors

A typical electrochemical promotion (EP), or in situ controlled promotion (ICP) or NEMCA experiment utilizing YSZ, an O^{2-} conductor, as the promoter donor is shown in Fig. 4.13. The reaction under study is the oxidation of C_2H_4 on Pt:

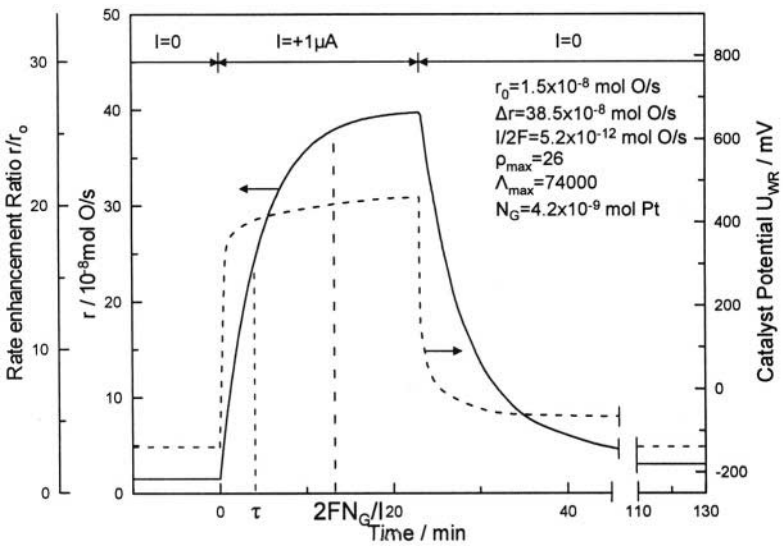

$$C_2H_4+3O_2 \rightarrow 2CO_2+2H_2O \tag{4.21}$$

The Pt film, with a surface area corresponding to $N_G=4.2\cdot10^{-9}$ mol Pt, measured via surface titration of oxygen with C_2H_4,[1,4] is exposed to p_{O_2} = 4.6 kPa, $p_{C_2H_4}$ = 0.36 kPa at 370°C in a continuous flow gradientless (CSTR) reactor of volume 30 cm^3. The rate of CO_2 formation is monitored via an infrared analyzer.[1,4]

Figure 4.13. NEMCA: Rate and catalyst potential response to step changes in applied current during C_2H_4 oxidation on Pt; T=370°C, p_{O_2}=4.6 kPa, $p_{C_2H_4}$=0.36 kPa. The experimental (τ) and computed ($2FN_G/I$) rate relaxation time constants are indicated on the figure. See text for discussion. $r_0=1.5\cdot10^{-8}$ mol O/s, $\Delta r=38.5\cdot10^{-8}$ mol O/s, $I/2F=5.2\cdot10^{-12}$ mol O/s, ρ_{max}=26, Λ_{max}=74000, $N_G=4.2\cdot10^{-9}$ mol Pt.[4] Reprinted with permission from Academic Press.

Figure 4.13 depicts a typical galvanostatic transient experiment. Initially (t<0) the circuit is open ($I=0, U^{o}_{WR}=-150$ mV) and the unpromoted catalytic rate, r_0, is $1.5\cdot10^{-8}$ mol O/s. The corresponding turnover frequency, TOF,[48] based on the reactive oxygen uptake of $4.2\cdot10^{-9}$ mol O, i.e. oxygen atoms reacting per surface site per s, is $3.57\ s^{-1}$.

At t=0 the galvanostat is used to apply a constant current $I=1\ \mu A$ between the catalyst and the counter electrode (Fig. 4.1). Consequently O^{2-} is supplied to the catalyst at a rate $I/2F=5.2\cdot10^{-12}$ mol O/s. The catalytic rate, r, increases gradually to a steady-state value of $4\cdot10^{-7}$ mol O/s, which is 26 times larger than r_0. The new TOF is $95.2\ s^{-1}$. The increase in catalytic rate $\Delta r=r-r_0=3.85\cdot10^{-7}$ mol O/s is 74,000 times larger than the rate, I/2F, of supply of O^{2-} to the Pt catalyst. Thus each O^{2-} supplied to the catalyst, creating a backspillover $O^{\delta-}$ species, causes at steady-state 74,000 additional chemisorbed oxygen atoms to react with C_2H_4 and form CO_2 and H_2O. This is why this phenomenon was termed Non-Faradaic Electrochemical Modification of Catalytic Activity (NEMCA)[1,4,19] The apparent Faradaic efficiency, Λ, of the process defined as:

$$\Lambda = \Delta r/(I/2F) \tag{4.19}$$

equals 74,000 for the experiment of Figure 4.13. If all the electrochemically supplied O^{2-} were reacting with C_2H_4 and the catalytic rate were unaffected then one would have $\Lambda=1$ and the rate increase in Figure 4.13 would be 74,000 times smaller, i.e. hardly measurable.

How can one explain such a huge Faradaic efficiency, Λ, value? As we shall see there is one and only one viable explanation confirmed now by every surface science and electrochemical technique, which has been used to investigate this phenomenon. We will see this explanation immediately and then, in much more detail in Chapter 5, but first let us make a few more observations in Figure 4.13. It is worth noting that, at steady-state, the catalyst potential U_{WR}, has increased by 0.62 V. Second let us note that upon current interruption (Fig. 4.13), r and U_{WR} return to their initial unpromoted values. This is due to the gradual consumption of $O^{\delta-}$ by C_2H_4.

Then let us examine the rate relaxation time constant τ, defined as the time required for the rate increase Δr to reach 63% of its steady state value. It is comparable, and this is a general observation, with the parameter $2FN_G/I$, (Fig. 4.13). This is the time required to form a monolayer of oxygen on a surface with N_G sites when oxygen is supplied in the form of O^{2-}. This observation provided the first evidence that NEMCA is due to an electrochemically controlled migration of ionic species from the solid electrolyte onto the catalyst surface,[1,4,49] as proven in detail in Chapter 5 (section 5.2), where the same transient is viewed through the use of surface sensitive techniques.

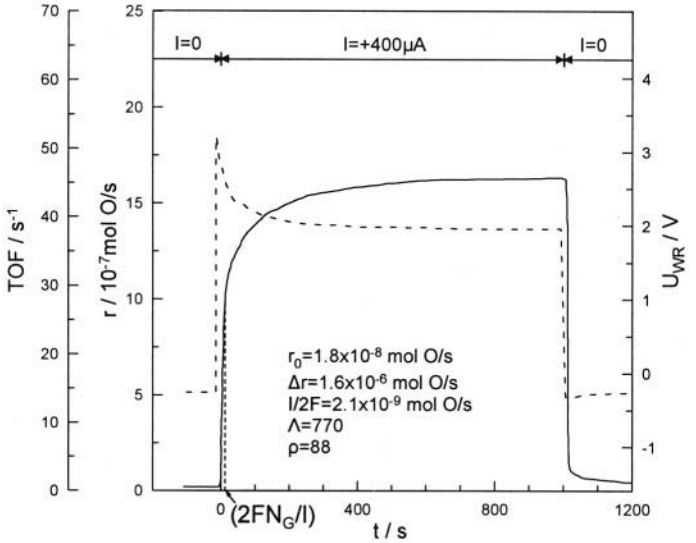

Figure 4.14. NEMCA: Rate and catalyst potential response to step changes in applied current during C_2H_4 oxidation on Rh; T=350°C, p_{O_2}=2.6 kPa, $p_{C_2H_4}$=5.9 kPa, $r_0=1.8\cdot10^{-8}$ mol O/s, $\Delta r=1.6\cdot10^{-6}$ mol O/s, $I/2F=2.1\cdot10^{-9}$ mol O/s, ρ=88, Λ=770.[50] Reprinted with permission from Academic Press.

So the explanation for Figure 4.13 and for all NEMCA studies utilizing O^{2-} conductors, such as YSZ, is simply the following: Promoting anionic species $O^{\delta-}$ (accompanied by their compensating charge δ+ in the metal) are generated in an electrochemical step at the tpb:

$$O^{2-}(YSZ) \rightarrow [O^{\delta-} - \delta+] + 2e^- \qquad (4.22)$$

at a rate I/2F. The promoting backspillover species $[O^{\delta-}-\delta+]$ (most likely O^{2-}-2+) migrates all over the catalyst surface. At steady-state it is consumed by reaction with C_2H_4 at the same rate it is produced, i.e. I/2F. Normally chemisorbed atomic oxygen O(a), coming from the gas phase, is now consumed at a rate $r_0+\Delta r\approx\Delta r$ which is Λ times larger than I/2F. This simple model can explain Fig. 4.13 and implies that Λ, as defined by equation (4.19), also expresses the ratio of the reactivities (for C_2H_4 oxidation) of chemisorbed O(a) *at the electrochemically promoted state* and of the electrochemically generated promoting $O^{\delta-}$ species.

How can we confirm this sacrificial promoter model? By simply looking at the r vs t transient behaviour of Figure 4.13 or of any galvanostatic NEMCA experiment upon current interruption (I=0).

The TOF of O(a) at the promoted state of Fig. 4.13 is 95.2 s^{-1} as already noted. Thus if the sacrificial promoter model is correct the TOF of the promoting $O^{\delta-}$ species is Λ (=74,000) times smaller, i.e. equals, $1.3\cdot10^{-3}$ s^{-1}.

Thus the average lifetime, τ, of $O^{\delta-}$ on the catalyst surface (τ=TOF^{-1}) equals 770 s or 13 min. This then should be the time needed for the rate, r, to decay to its unpromoted value upon current interruption. This is in excellent agreement with experiment (Fig. 4.13) and nicely confirms the sacrificial promoter concept of NEMCA: The promoter ($O^{\delta-}$) is "sacrificed" by eventually reacting with the oxidizable species (C_2H_4). But before being "sacrificed", i.e. consumed, it has caused on the average the reaction of Λ extra oxygen atoms with the oxidizable species.

This is the essence of NEMCA. The reader can check the validity of the sacrificial promoter concept in all NEMCA galvanostatic transients of this book.

Figure 4.14 shows a similar galvanostatic transient obtained during C_2H_4 oxidation on Rh deposited on YSZ.[50] Upon application of a positive current I=400 μA with a concomitant rate of O^{2-} supply to the catalyst $I/2F=2.1\cdot10^{-9}$ mol O/s the catalytic rate increases from its open-circuit value $r_0=1.8\cdot10^{-8}$ mol O/s to a new value $r=1.62\cdot10^{-6}$ mol O/s which is 88 times larger than the initial unpromoted rate value. The rate increase Δr is 770 times larger than the rate of supply of O^{2-} ions to the Rh catalyst surface.

Both C_2H_4 oxidation on Pt/YSZ (Fig. 4.13) and C_2H_4 oxidation on Rh/YSZ (Fig. 4.14) are *electrophobic* reactions, i.e. the rate r is an increasing function of catalyst potential U_{WR}. They are therefore enhanced with positive currents (I>0) which leads to an increase in U_{WR}. As we will see soon this is one of the four main types of experimentally observed r vs U_{WR} behavior.

4.3.2 Electrochemical Promotion Using Na^+ Conductors

4.3.2.1 CO Oxidation on Pt/β″-Al_2O_3

A typical electrochemical promotion experiment utilizing β″-Al_2O_3, a Na^+ conductor, as the promoter donor is shown in Fig. 4.15. The reaction under study is the oxidation of CO on Pt.[51]

The Pt film with a surface area corresponding to $N_G=6.3\cdot10^{-7}$ mol Pt, as measured via surface titration of O with CO, is exposed to p_{CO} = 2 kPa, p_{O_2} = 2 kPa at 350°C in a gradientless continuous flow reactor. The Pt surface has been cleaned from Na via previous (t<-1min) application of a positive potential (U_{WR}=0.4 V, Fig. 4.15). The steady-state unpromoted rate of CO oxidation is $r_0=3.5\cdot10^{-7}$ mol O/s. At t=-1 min the galvanostat is disconnected (I=0) and U_{WR} relaxes to ~0 V, i.e. to the value imposed by the gaseous composition and corresponding surface coverages of O and CO. There is a small (~30%) corresponding increase in r. Then at t=0 the galvanostat is used to impose a constant current I=-20 μA with a concomitant supply $-I/F = 2.07\cdot10^{-10}$ mol Na/s of Na^+ to the catalyst surface:

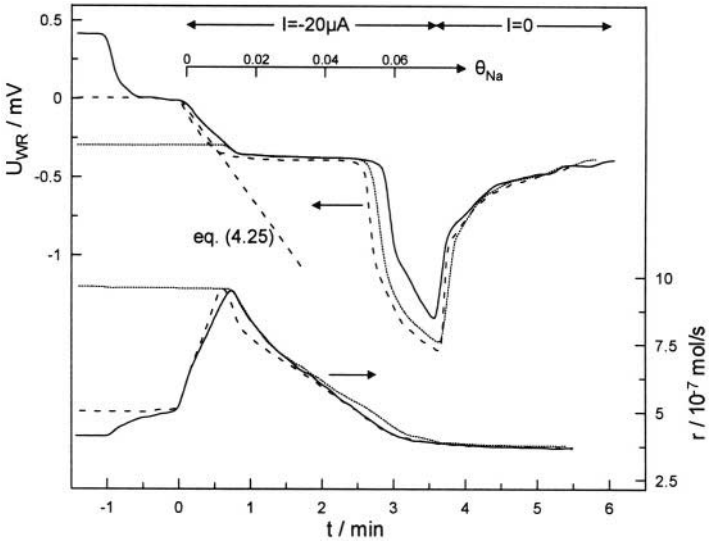

Figure 4.15. Rate and catalyst potential response to application of negative currents (a,b), for the case of "volcano-type" behaviour, see text for discussion. Conditions: p_{CO}=2 kPa, p_{O_2}=2 kPa, T=350°C. Catalyst C1.[51] Reprinted with permission from Academic Press.

$$Na^+(\beta''\text{-}Al_2O_3)+e^- \rightarrow Na(Pt) \tag{4.23}$$

The corresponding Na coverage on the Pt surface, θ_{Na}, can be computed from Faraday's law, i.e.:

$$\theta_{Na} = \frac{-It}{FN_G} \tag{4.24}$$

where N_G is the Pt surface area (N_G=6.3·10^{-7} mol Pt) and t is the time of current application.

As shown in Fig. 4.15, increasing θ_{Na} up to 0.02 causes a linear decrease in U_{WR} and a concomitant 230% *increase* in catalytic rate. The rate increase $\Delta r \approx 5.5 \cdot 10^{-7}$ mol O/s is 2600 times larger than –I/F. Upon further increasing θ_{Na} in the interval $0.02<\theta_{Na}<0.06$, U_{WR} remains practically constant while r decreases sharply and reaches values below the initial unpromoted value r_0. When θ_{Na} exceeds 0.06, U_{WR} starts decreasing sharply while r decreases more slowly. The system cannot reach steady state since θ_{Na} is constantly increasing with time due to the applied constant current.

Setting I=0 gradually restores U_{WR} to –0.3 V while r remains practically unaffected. Restoration of the initial r value requires potentiostatic setting of U_{WR} at 0.4 V, and thus removal of Na(Pt) from the Pt catalyst surface.

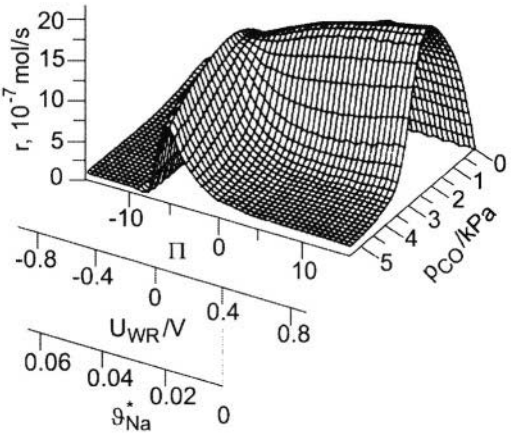

Figure 4.16. Effect of catalyst potential, dimensionless catalyst potential $\Pi(=FU_{WR}/RT)$, corresponding linearized[51] Na coverage θ^*_{Na} and p_{CO} on the rate of CO oxidation on Pt/β″-Al_2O_3. T=350°C, p_{O_2}=6 kPa.[51] Reprinted with permission from Academic Press.

The complex transient r vs t, or equivalently r vs θ_{Na} or r vs U_{WR} behaviour of Fig. 4.15 parallels the *steady-state* r vs U_{WR} behaviour shown in Fig. 4.16, where for each point U_{WR} has been imposed potentiostatically, until the current I has vanished and the corresponding rate value, r, has been measured. This shows that the catalyst surface readjusts fairly fast to the galvanostatically imposed transient θ_{Na} values (Fig. 4.15). The dashed and dotted line transients on the same figure were obtained with the same gaseous composition but with initial U_{WR} values of 0 and –0.3 V respectively. It is noteworthy that the three transients are practically identical which shows the reversibility of the system.

There is an important point to be made regarding U_{WR} vs t transients such as the ones shown in Fig. 4.15 when using Na^+ conductors as the promoter donor. As will be discussed in the next section (4.4) there is in solid state electrochemistry an one-to-one correspondence between potential of the working electrode (U_{WR}) and work function (Φ) of the gas exposed (catalytically active) surface of the working electrode ($e\Delta U_{WR}=\Delta\Phi$, eq. 4.30). Consequently the U_{WR} vs t transients are also $\Delta\Phi$ vs t transients.

On the other hand, as already discussed in Chapter 2, Eq. (2.21), $\Delta\Phi$ is directly related to the coverage, θ_{Na}, of the backspillover $Na^{\delta+}$ species and to its dipole moment P_{Na} via the Helmholz equation (2.21). Thus one can directly derive the equations:

$$\frac{\Delta U_{WR}}{\Delta t} = \frac{N_M P_{Na}}{\varepsilon_0} \cdot \frac{\Delta\theta_{Na}}{\Delta t} \qquad \theta^*_{Na} = -\varepsilon_0 \Delta U_{WR} / P_{Na} \cdot N_M \quad (4.25)$$

where N_M is the surface atom density (atom/m^2) of the surface under consideration, ε_0=8.85·10^{-12} C^2/J·m and θ^*_{Na} is a linearized[51] Na coverage scale computed on the assumption that the Na dipole moment, P_{Na}, can be treated as a constant.[51]

This equation would enable one to *predict* the U_{WR} vs t behaviour in galvanostatic transients such as those of Fig. 4.15 if the value of the Na dipole moment on Pt were exactly known. The surface science literature (Chapter 2) suggests P^0_{Na} =5.2 D for the initial dipole moment of Na on Pt(111). This value has been used, in conjunction with Eq. (4.25) to draw the lines labeled "Eq. (4.25)"] in Fig. 4.15 and in subsequent figures throughout this book. As shown in Fig. 4.15 there is very good qualitative agreement between Eq. (4.25) and the initial U_{WR} vs t transient. This supports the approach and underlines the similarities between electrochemical and classical promotion.

Experiment[51] has shown that the linearized θ^*_{Na} scale provides a reasonably good approximation (within 50%) of the actual θ_{Na} scale, computed from Eq. 4.24, when using an average P_{Na} of 1.2·10^{-29} C·m, or 3.6 D, for polycrystalline Pt catalysts.[51] An actual comparison of θ_{Na} and θ^*_{Na} will be seen subsequently in Figure 4.31.[51] The usefulness of the θ^*_{Na} scale is that it enables one to estimate the Na coverage only on the basis of ΔU_{WR} or $\Delta\Phi$ data, without having to carry out galvanostatic experiments of the type shown in Figure 4.15 in conjunction with Eq. 4.24.

As will be seen in Chapter 5, STM has shown that the subsequent leveling of the U_{WR} vs t transient of Fig. 4.15 is due to the formation of an ordered (12x12) Na structure (adlattice) on the Pt surface.[33]

As evidenced both by the galvanostatic transient of Fig. 4.15 and by the steady-state results of Fig. 4.16, the oxidation of CO on Pt/ β''-Al_2O_3 under CO rich conditions exhibits *volcano-type* behaviour, i.e. the rate passes through a maximum upon varying U_{WR} or, equivalently, upon varying the coverage of the promoting Na species on the catalyst surface. This volcano type r vs U_{WR} behaviour is one of the four main types of experimentally observed r vs U_{WR} dependence in electrochemical promotion studies and its physical origin is discussed in Chapter 6.

4.3.2.2 NO Reduction by H_2 on Pt/ β''-Al_2O_3

Figure 4.17 shows another galvanostatic transient obtained on Pt/β''-Al_2O_3 at 375°C. The reaction under study is the reduction of NO by H_2, a reaction of significant technological interest[52]:

$$2NO + 2H_2 \rightarrow N_2 + 2H_2O \tag{4.26}$$

which is accompanied by the undesirable side reaction:

$$2NO + H_2 \rightarrow N_2O + H_2O \tag{4.27}$$

The same experimental procedure used in Fig. 4.15 is followed here. The Pt surface is initially (t < - 1 min) cleaned from Na via application of a positive potential (U_{WR}=0.2 V) using the reverse of reaction (4.23). The potentiostat is then disconnected (I=0, t=-1min) and U_{WR} relaxes to ~0 V, i.e. to the value imposed by the gaseous composition and corresponding surface coverages of NO and H. Similar to the steady-state results depicted in Fig. 4.18 this decrease in catalyst potential from 0.2 to 0 V causes a six-fold enhancement in the rate, r_{N_2}, of N_2 production and a 50% increase in the rate of N_2O production. Then at t=0 the galvanostat is used to impose a constant current I=-20 μA; Na^+ is now pumped to the Pt catalyst surface at a

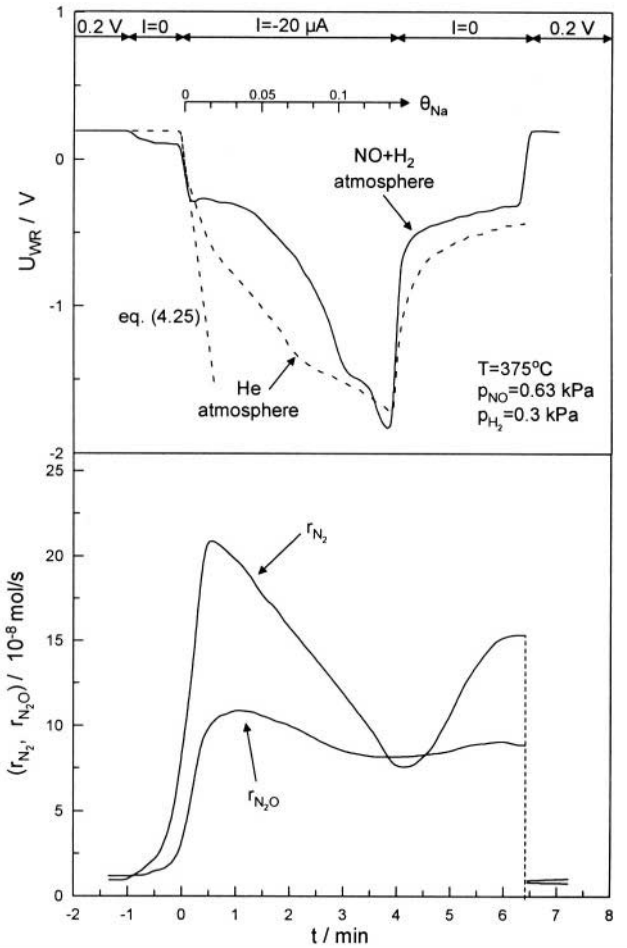

Figure 4.17. NO reduction by H_2 on Pt/β″-Al_2O_3.[52] Transient effect of applied constant negative current (Na supply to the catalyst) on catalyst potential (a) under reaction conditions (solid line) and in a He atmosphere (dashed line) and on the rates of formation of N_2 and N_2O (b). Potentiostatic restoration of the initial rates; see text for discussion. Reprinted with permission from Academic Press.

rate $-I/F=2.07\cdot10^{-10}$ mol Na/s (eq. (4.23)). The corresponding Na coverage, θ_{Na}, starts increasing according to eq. (4.24, $N_G=3.8\cdot10^{-7}$ mol Pt) causing a pronounced decrease in the catalyst potential U_{WR} and a pronounced *increase* in the rates of N_2 and N_2O production (electrophilic behaviour) which go through a maximum at U_{WR}=-0.2 V. At this point r_{N_2} has increased by a factor of 20. This rate increase is 10^3 times larger than the rate –I/F of Na supply to the catalyst. The selectivity to N_2, S_{N_2}, has also increased substantially. The latter is defined from:

$$S_{N_2} = r_{N_2} /(r_{N_2} + r_{N_2O}) \tag{4.28}$$

Upon current interruption at t=4 min, U_{WR} relaxes to –0.3 V causing r_{N_2} and r_{N_2O} to return to their corresponding values at this potential during the previous galvanostatic transient. Potentiostatic imposition of the initial U_{WR} value (=0.2 V) restores both rates to their initial, unpromoted, values showing the reversibilty of the system. Again the transient behaviour of Fig. 4.17 can be better understood on the basis of the steady-state behaviour shown in Figure 4.18. Both r_{N_2} and r_{N_2O} exhibit predominantly *electrophilic* behaviour, i.e. they increase with decreasing U_{WR} ($\partial r/\partial U_{WR}<0$) but they do go through a small maximum so that their overall behaviour can be described as *volcano-type.*

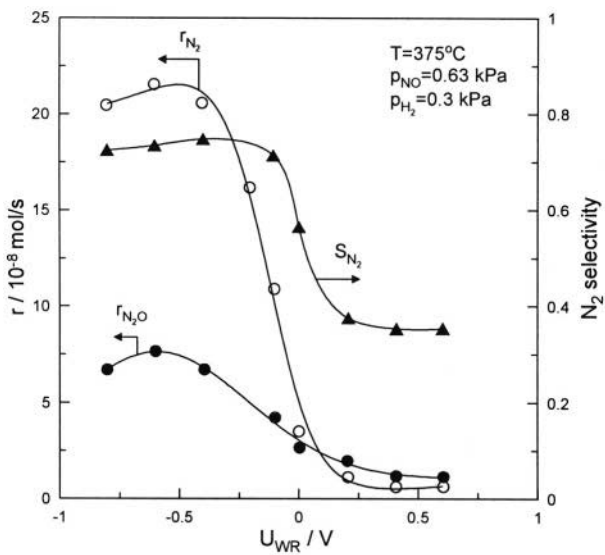

Figure 4.18. NO reduction by H_2 on Pt/β″-Al_2O_3. Effect of catalyst potential on the rates of formation of N_2 and N_2O and on the selectivity to N_2.[52] Reprinted with permission from Academic Press.

It is important to observe that the electrochemically promoted Pt surface (U_{WR}<0 V) gives S_{N_2} selectivity values above 70% vs 35% on the unpromoted surface (U_{WR}>0 V). The Pt surface is thus made as selective as a Rh surface would be under similar conditions. The ability of electrochemical promotion to alter the product selectivity of catalyst surfaces is one of its most attractive features for practical applications.

4.3.3 General Features and Comparisons

It is instructive at this point to make some comparisons between the galvanostatic transients obtained with O^{2-} conductors (Figs. 4.13 and 4.14) and those obtained with Na^+ conductors (Figs. 4.15 and 4.17) and also to explain some of the salient and distinguishing features of the latter including the dotted straight lines marked "eq. (4.25)" on Figs. 4.15 and 4.17.

The common feature of galvanostatic electrochemical promotion experiments is that, both in the case of O^{2-} and Na^+-conductors, one obtains pronounced changes in catalytic rate which are orders of magnitude larger than the rate of supply of ions onto the catalyst surface.

The main difference is that in the case of O^{2-} conductors galvanostatic operation leads to a steady state (Figs. 4.13 and 4.14) while in the case of Na^+ conductors galvanostatic operation *does not* lead to a steady state, as the Na coverage on the catalyst surface is continuously increasing (Fig. 4.15 and 4.17).

This is easy to understand: In the former case the backspillover species (O^{2-}) is also a reactant in the catalytic reaction. Thus as its coverage on the catalyst surface increases during a galvanostatic transient its rate of consumption with C_2H_4 also increases and at steady state its rate of consumption equals its rate of creation, I/2F. This means that the backspillover O^{2-} species reacts with the fuel (e.g. C_2H_4) at a rate which is Λ times slower than the rate of reaction of more weakly bonded chemisorbed oxygen formed via gaseous chemisorption.

In the latter case, however, Na is not involved as a reactant in the catalytic reaction, thus cannot be removed from the surface and consequently its coverage, θ_{Na}, can only increase in time as long as the current, I, remains constant. Thus no steady-state can be achieved (Figs. 4.15 and 4.17).

Conclusion: when using ionic conductors where the conducting, i.e. backspillover ion participates in the catalytic reaction under study (e.g. O^{2-} ions in the case of catalytic oxidations) then both galvanostatic and potentiostatic operation lead to a steady-state and allow one to obtain steady-state r vs U_{WR} plots.

When using, however, ionic conductors where the conducting, i.e. backspillover, species does not participate to the catalytic reaction and does not desorb from the surface at an appreciate rate, then only potentiostatic operation allows one to obtain steady-state r vs U_{WR} plots such as the ones shown in Figures 4.16 and 4.18.

In the latter case, however, galvanostatic transients such as the ones shown in Figures 4.15 and 4.17 should not be considered useless, as they

provide important information about the properties of the backspillover species as analyzed in the next section 4.5. The reader may, for example, be intrigued by the peculiar U_{WR} vs time behaviour obtained during such galvanostatic transients (Figs. 4.15 to 4.17) including the near constant U_{WR} values with increasing θ_{Na} over relatively wide θ_{Na} ranges. As will be shown in Chapter 5, scanning tunneling microscopy (STM) has shown that these near constant U_{WR} regions correspond to the formation of ordered chemisorbed adlattices on the catalyst surface by the backspillover Na ions.

4.4 CATALYST WORK FUNCTION VARIATION WITH POTENTIAL IN SOLID ELECTROLYTE CELLS

As discussed already in Chapter 2 the work function, Φ, of a solid surface is one of the most important parameters dictating its chemisorptive and catalytic properties. The work function, Φ (eV/atom) of a surface is the minimum energy which an electron must have to escape from the surface when the surface is electrically neutral. More precisely Φ is defined as the energy to bring an electron from the Fermi level, E_F, of the solid at a distance of a few μm outside of the surface under consideration so that image charge interactions are negligible.

The work function, Φ_0, of a clean metal surface is as low as 2 eV/atom for alkali metals and as high as 5.5 eV/atom for transition metals such as Pt (Fig. 4.19).[53]

It is important to notice that the work function, Φ, of a given solid surface changes significantly with chemisorption. Thus oxygen chemisorption on transition metal surfaces causes up to 1 eV *increase* in Φ while alkali chemisorption on transition metal surfaces causes up to 3 eV *decrease* in Φ. In general *electronegative, i.e. electron acceptor adsorbates* cause an *increase in Φ* while *electropositive, i.e. electron donor adsorbates cause a decrease in Φ. Note* that in the former case the dipole vector $\tilde{P}$ formed by the adsorbate and the surface points to the vacuum while in the latter case $\tilde{P}$ points to the surface (Fig. 4.20).

The work function, Φ, of a metal surface can be measured relatively easily and when using the Kelvin probe technique, in situ, i.e., during catalyst operation.[54,55] Three techniques are the most commonly used[54-58]:

1. The Kelvin probe technique where a flat Au element of known work function (~5 eV) is brought at a distance of ~0.5 mm from the metal sample and is vibrated via a piezocrystal element while monitoring via an oscilloscope the ac current generated in the circuit due to the oscillating capacitance of the vibrating capacitor.[54-56] The applied voltage U_a is adjusted until the ac current vanishes. At this point the electrostatic potentials (Volta potentials, Chapter 5) outside the metal sample and the Au element become equal and the work function Φ of the sample is given by:

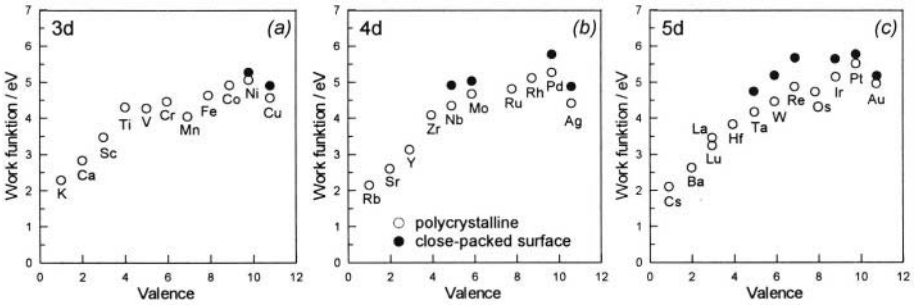

Figure 4.19. Experimental work function values, Φ_0, for the 3d, 4d and 5d series including the alkali, alkaline-earth, and noble metals for polycrystalline surfaces (open circles) and for single crystal surfaces (filled circles).[53] Reprinted with permission from the American Physical Society.

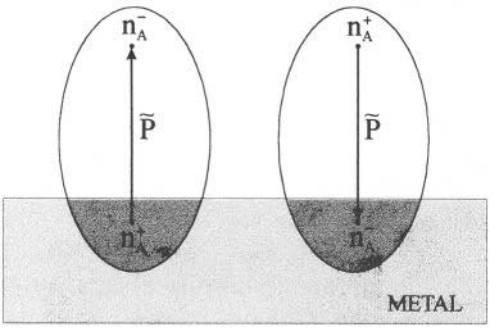

Figure 4.20. Schematic of an electron acceptor (left) and an electron donor (right) adsorbate on a metal surface. The former increases the metal work function, Φ, the latter decreases it.

$$\Phi = \Phi_{Au} + eU_a \tag{4.29}$$

2. The UPS technique (ultra violet photoelectron spectroscopy), by measuring the cutoff energy of secondary electrons.[56,57]

3. The PEEM technique (photoelectron emission microscopy),[58] which additionally allows for spatial resolution of about 1 mm^2.

All three techniques are quite straightforward to use. The Kelvin probe technique has the advantage that it does not require vacuum conditions, thus a catalyst can be studied under atmospheric or higher pressure.

One of the most important, but not too surprising experimental observations after the discovery of electrochemical promotion is that the work function, Φ, of the gas exposed catalyst-electrode surfaces changes significantly (up to 2 eV) during galvanostatic transients such as the ones shown in Figures 4.13, 4.14, 4.15 and 4.17 as well as at steady-state and in fact that, over wide experimental conditions, it is (Fig. 4.21)[54]:

$$\Delta\Phi = e\Delta U_{WR} \tag{4.30}$$

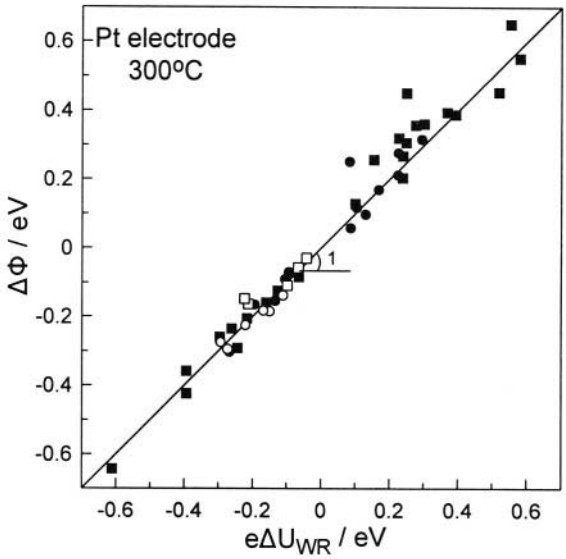

Figure 4.21. Effect of catalyst-electrode potential U_{WR} on the work function of the gas exposed catalyst-electrode surface. Open symbols: open circuit operation varying gas composition. Closed symbols: closed circuit operation C_2H_4, O_2, He and NH_3, O_2, He mixtures.[54,55] Reprinted from ref. 55 with permission from Elsevier Science.

where ΔU_{WR} is the change in (ohmic-drop-free) catalyst-electrode potential induced either by changing the gaseous composition or by imposing a new U_{WR} value via a potentiostat.

The implications of Equation (4.30) for solid state electrochemistry and electrochemical promotion in particular can hardly be overemphasized: It shows that solid electrolyte cells are both *work function probes* and *work function* controllers for their gas-exposed electrode surfaces.

It also allows for the first time to perform catalytic experiments under conditions of independently controllable catalyst work function.

Another implication is that, for all practical purposes, one can use interchangeably eU_{WR} and Φ in all figures related to electrochemical promotion, such as the Figs. 4.13 to 4.17.

4.5 DEFINITIONS, PHENOMENOLOGY AND KEY ASPECTS OF ELECTROCHEMICAL PROMOTION

4.5.1 NEMCA Time Constant τ

The NEMCA time constant, τ, is defined[1,4] as the time required for the rate increase Δr to reach 63% of its steady-state value during a galvanostatic transient, such as the one shown in Fig. 4.13 and 4.14. Such rate transients can usually be approximated reasonably well by:

$$\Delta r = \Delta r_{max}[1-\exp(-t/\tau)] \quad (4.31)$$

A general observation in NEMCA studies with O^{2-} conductors is that the magnitude of τ can be predicted by:

$$\tau \approx 2FN_G/I \quad (4.32)$$

where N_G (mol) is the reactive oxygen uptake of the metal catalyst[1,19] which expresses, approximately, the surface mols of metal. The parameter $2FN_G/I$ expresses the time required to form a monolayer of $O^{\delta-}$ on the metal surface. Equation (4.32) is nicely rationalized on the basis of recent XPS investigations of Pt films during electrochemical promotion studies[28-31] which showed that the maximum coverages of $O^{\delta-}$ and normally chemisorbed, i.e. reactive, atomic oxygen are comparable.

4.5.2 Enhancement Factor or Faradaic Efficiency Λ:

As already noted, the enhancement factor or faradaic efficiency, Λ, is defined from:

$$\Lambda = \Delta r/(I/2F) \quad (4.19)$$

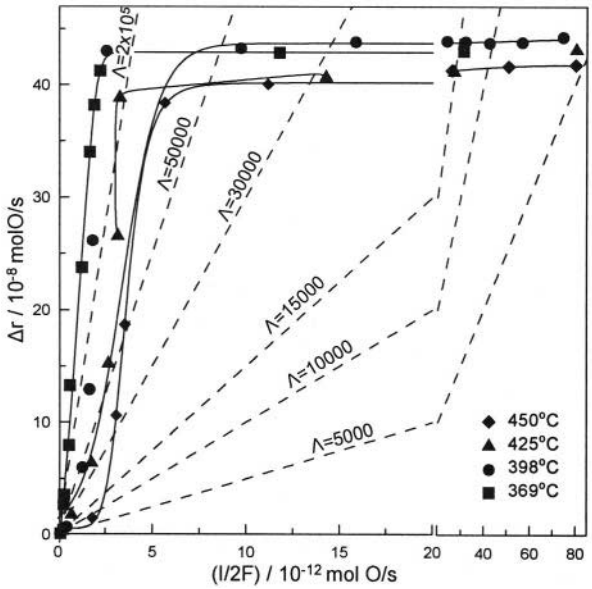

Figure 4.22. Effect of the rate of O^{2-} supply to the catalyst electrode on the increase in the rate of C_2H_4 oxidation on Pt deposited on YSZ.[1,4] Dashed lines are constant faradaic efficiency, Λ, lines. Reprinted from ref. 4 with permission from Academic Press.

where Δr is the promotion-induced change in catalytic rate expressed in mol O per s. More generally, Λ is computed by expressing Δr in g-equivalent and dividing by I/F.

In the experiments of Figs. 4.13 and 4.14, the Λ value at steady-state are 74,000 and 770 respectively. A reaction is said to exhibit the NEMCA effect when $|\Lambda|>1$.

Figure 4.22 shows the steady-state effect of current, or equivalently rate, I/2F, of O^{2-} supply to the catalyst on the rate increase Δr during C_2H_4 oxidation on Pt/YSZ. According to the definition of Λ (Eq. 4.19), straight lines passing from the (0,0) point are constant faradaic efficiency Λ lines.

As shown on the figure, small I/2F values lead to Λ values up to $3\cdot10^5$. This implies that each O^{2-} supplied to the catalyst causes up to $3\cdot10^5$ coadsorbed O atoms to react and form CO_2 and H_2O.

An important step in the elucidation of the origin of NEMCA was the observation[1,19] that the magnitude of $|\Lambda|$ for any reaction can be estimated from:

$$|\Lambda| \approx 2Fr_0/I_0 \tag{4.20}$$

where r_0 is the unpromoted catalytic rate and I_0 is the exchange current of the catalyst-solid electrolyte interface. As previously noted, this parameter can be measured easily by fitting η vs I data to the classical Butler-Volmer equation:

$$I/I_0=\exp(\alpha_\alpha F\eta/RT)- \exp(-\alpha_c F\eta/RT) \tag{4.7}$$

where α_α and α_c, usually on the order of unity, are the anodic and cathodic transfer coefficients.

As analyzed in section 4.6, equation (4.20) can be derived theoretically and is in good qualitative agreement with experiment over five orders of magnitude (Fig. 4.23). This important relationship shows that:

i) Highly polarizable, i.e. low I_0, metal-solid electrolyte interfaces are required to obtain large $|\Lambda|$ values. The magnitude of I_0 is proportional to the tpb length[8,19] and can be controlled during the catalyst film preparation by appropriate choice of the sintering temperature which in turn determines the metal grain size and thus the tpb length.[1]

ii) The measurement of Λ is important for determining if a reaction exhibits the NEMCA effect but its magnitude is not a fundamental characteristic of a catalytic reaction, since for the same reaction different $|\Lambda|$ values can be obtained by varying I_0 during catalyst preparation. Thus the magnitude of $|\Lambda|$ depends both on catalytic (r_0) and on electrocatalytic (I_0) kinetics.

For $\Lambda\gg1$, the Faradaic efficiency Λ has, as already noted, an interesting physical meaning[50]: For oxidation reactions it expresses the ratio of the reaction rates of normally chemisorbed atomic oxygen on the promoted

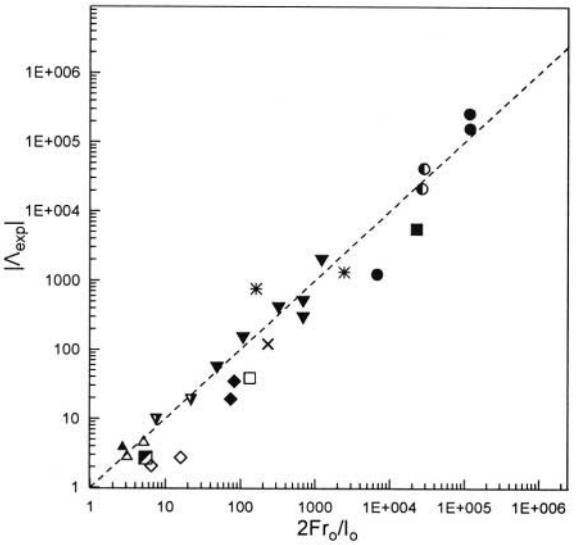

Figure 4.23. Comparison of predicted and measured enhancement factor Λ values for some of the early studies of catalytic reactions found to exhibit the NEMCA effect.[1,19] Reprinted with permission from Elsevier Science.[1]

surface and of backspillover oxide ions with the oxidizable species, e.g. C_2H_4. As already discussed and as further proven in Chapter 5 the backspillover $O^{\delta-}$ ions are significantly less reactive than normally chemisorbed oxygen.

The maximum Λ values measured so far in NEMCA studies utilizing YSZ is 3×10^5, [1,4] as shown in Table 4.1 which lists all catalytic reactions studied so far under electrochemical promotion conditions.

When the promoting, ion does not react at all with any of the reactants (e.g. Na^+) then, in principle, "infinite" Λ values are expected. In practice Λ is always measurable due to a very slow consumption of Na^+ to form surface oxides and carbonates.[32,36,51] Nevertheless in all cases the most important parameter from a catalytic viewpoint is the promotion index[19], PI_i, defined in Chapter 2 (eq. 2.19) and also shown in Table 4.1.

Table 4.1 lists all published electrochemical promotion studies of 58 catalytic reactions on the basis of the type of electrolyte used. Each of these reactions is discussed in Chapters 8 to 10 which follow the same reaction classification scheme.

The table also gives the catalyst material, the operating temperature range, the maximum (for Λ>1) or minimum (for Λ<-1) measured Λ value and the maximum (for ρ>1) or minimum for (ρ<1) rate enhancement, ρ, value. It also provides the maximum measured promotion index, PI_i, value. An asterisk in the ρ column indicates that electrochemical promotion causes also a change in product selectivity.

Table 4.1. Electrochemical promotion studies classification based on the type of solid electrolyte

1. EP studies utilizing YSZ. Promoting ion: O^{2-}

Reactants		Products	Catalyst	T (°C)	$\Lambda_{max}(>0)$ or $\Lambda_{min}(<0)$	$\rho_{max}(>1)$ or $\rho_{min}(<1)$	$PI_{O^{2-}}$	Ref.
Electron Donor (D)	Electron Acceptor (A)							
C_2H_4	O_2	CO_2	Pt	260-450	3×10^5	55	55	4,59,60
C_2H_6	O_2	CO_2	Pt	270-500	300	20	20	24
					-100	7	-	
CH_4	O_2	CO_2	Pt	600-750	5	70	70	19,61
CO	O_2	CO_2	Pt	300-550	2×10^3	3	2	62
					-500	6	-	
CO	O_2	CO_2	Pt	468-558	1000	5	5	19,63,64
CH_3OH	O_2	H_2CO,CO_2	Pt	300-500	1×10^4	4,15*	3	19,65
C_3H_6	O_2	CO_2	Pt	350-480	-3×10^3	6	-	25
CH_3OH		$H_2CO,CO,$ CH_4	Pt	400-500	-10	3*	-	65,66
C_2H_4	NO	$CO,CO_2,N_2,$ N_2O	Pt	380-500	-50	7	-	67
C_2H_4	O_2	CO_2	Rh	250-400	5×10^4	90	90	50,68,69
H_2	CO_2	CH_4, CO	Rh	300-450	200	3*	2	19
C_3H_6	NO, O_2	N_2,N_2O,CO_2	Rh	250-450	1×10^3	150*	15	70
CO	NO, O_2	N_2,N_2O,CO_2	Rh	250-450	20	20*	20	71
C_2H_4	O_2	CO_2	Pd	290-360	10^4	2	-	14,72
CO	O_2	CO_2	Pd	400-550	1×10^3	2	1	19,66
H_2	CO	$C_xH_y,C_xH_yO_z$	Pd	300-370	10	3*	2	19
H_2S		S_x, H_2	Pt	600-750	-	11	10	19,73
CH_4	O_2	CO_2	Pd	380-440	2×10^3	90	90	14,74
H_2	CO_2	CO	Pd	500-590	-50	10	-	19,66
CO	NO	CO_2,N_2,N_2O	Pd	320-480	-700	3	-	75,76
CO	N_2O	CO_2,N_2	Pd	440	-20	2	-	75
C_2H_4	O_2	C_2H_4O,CO_2	Ag	320-470	300	30*	30	11,12,49 ,77
C_3H_6	O_2	C_3H_6O,CO_2	Ag	320-420	300	2*	1	19,78
CH_4	O_2	$CO_2,C_2H_4,$ C_2H_6	Ag	650-850	5	30*	30	19,79
CO	O_2	CO_2	Ag	350-450	20	15	15	19,80
CH_3OH		H_2CO, CO, CH_4	Ag	550-750	-25	6*	-	19,81
CH_3OH	O_2	H_2CO, CO_2	Ag	500	-95	2	-	10
CH_4	O_2	$C_2H_4,C_2H_6,$ CO_2	Ag	700-750	-1.2	8*	-	82,83
CO	O_2	CO_2	Ag-Pd	450-500	30	5	4	84
CH_4	H_2O	CO, CO_2	Ni	600-900	12	2*	-	19,85
CO	O_2	CO_2	Au	450-600	-60	3	-	82,83
CH_4	O_2	CO_2	Au	700-750	-3	3*	-	82,83,86
C_2H_4	O_2	CO_2	IrO_2	350-400	200	6	5	87,88
C_2H_4	O_2	CO_2	RuO_2	240-500	4×10^3	115	115	23

2. EP studies utilizing F^- conductors

Reactants									
Electron Donor (D)	Electron Acceptor (A)	Products	Catalyst	Solid Electrolyte	T (°C)	$\Lambda_{max}(>0)$ or $\Lambda_{min}(<0)$	$\rho_{max}(>1)$ or $\rho_{min}(<1)$	PI_{F^-}	Ref.
CO	O_2	CO_2	Pt	CaF_2	500-700	200	2.5	1.5	19,89

3. EP studies utilizing mixed conductors

Reactants									
Electron Donor (D)	Electron Acceptor (A)	Products	Catalyst	Solid Electrolyte	T (°C)	$\Lambda_{max}(>0)$ or $\Lambda_{min}(<0)$	$\rho_{max}(>1)$ or $\rho_{min}(<1)$	$PI_{O^{2-}}$	Ref.
C_2H_4	O_2	CO_2	Pt	TiO_2 (TiO_x^+, O^{2-})	450-600	5×10^3	20	20	90
C_2H_4	O_2	CO_2	Pt	CeO_2 (CeO_x^+, O^{2-})	500	-10^5	3	-	91
C_2H_4	O_2	CO_2	Pt	YZTi10#	400-475	-250	2	-	92
C_3H_6	O_2	CO_2	Pt	YZTi10#	400-500	1000 -1000	2.4	-	92

4. EP studies utilizing Na^+ conductors

Reactants									
Electron Donor (D)	Electron Acceptor (A)	Products	Catalyst	Solid Electrolyte	T (°C)	$\Lambda_{max}(>0)$ or $\Lambda_{min}(<0)$	$\rho_{max}(>1)$ or $\rho_{min}(<1)$	PI_{Na^+}	Ref.
C_2H_4	O_2	CO_2	Pt	β''-Al_2O_3	180-300	5×10^4	0.25	-30	19,36
CO	O_2	CO_2	Pt	β''-Al_2O_3	300-450	1×10^5 -1×10^5	0.3 8	-30 250	19,51
H_2	C_6H_6	C_6H_{12}	Pt	β''-Al_2O_3	100-150	-	~0	-10	93,94
H_2	C_2H_2	C_2H_4, C_2H_6	Pt	β''-Al_2O_3	100-300	-	-*	-	95
C_2H_4	NO	CO_2,N_2, N_2O	Pt	β''-Al_2O_3	280-400	-	∞	500	32
CO	NO	CO_2,N_2, N_2O	Pt	β''-Al_2O_3	320-400	-	13*	200	96-98
C_3H_6	NO	CO_2,N_2, N_2O	Pt	β''-Al_2O_3	375	-	10	-	97-99
H_2	NO	N_2,N_2O	Pt	β''-Al_2O_3	360-400	-	30	6000	52
H_2	C_2H_2, C_2H_4	C_2H_4, C_2H_6	Pd	β''-Al_2O_3	70-100	-	0.13	-	100
C_2H_4	O_2	C_2H_4O, CO_2	Ag	β''-Al_2O_3	240-280	-	-	40	101
CO	O_2	CO_2	Ag	β''-Al_2O_3	360-420	-	2	-	19
C_2H_4	O_2	CO_2	Pt	$Na_3Zr_2Si_2PO_{12}$	430	-	10	300	102

5. EP studies utilizing K^+ conductors

Reactants									
Electron Donor (D)	Electron Acceptor (A)	Products	Catalyst	Solid Electrolyte	T (°C)	$\Lambda_{max}(>0)$ or $\Lambda_{min}(<0)$	$\rho_{max}(>1)$ or $\rho_{min}(<1)$	PI_{K^+}	Ref.
NH_3		N_2, H_2	Fe	$K_2YZr(PO_4)_3$	500-700	-	4.5	-	103

6. EP studies utilizing H^+ conductors

Reactants									
Electron Donor (D)	Electron Acceptor (A)	Products	Catalyst	Solid Electrolyte	T (°C)	$\Lambda_{max}(>0)$ or $\Lambda_{min}(<0)$	$\rho_{max}(>1)$ or $\rho_{min}(<1)$	PI_{H^+}	Ref.
C_2H_4	O_2	CO_2	Pt	$CaZr_{0.9}In_{0.1}O_{3-a}$	385-470	-3×10^4	5	-	104
H_2	N_2	NH_3	Fe	$CaZr_{0.9}In_{0.1}O_{3-a}$	440	6	∞	6	105
NH_3		N_2, H_2	Fe	$CaZr_{0.9}In_{0.1}O_{3-a}$	530-600	150	3.6	-	103
CH_4		C_2H_6, C_2H_4	Ag	$SrCe_{0.95}Yb_{0.05}O_3$	750	-	8*	10	19, 106
H_2	C_2H_4	C_2H_6	Ni	$CsHSO_4$	150-170	300	2	12	19, 107
H_2	O_2	H_2O	Pt	Nafion	25	20	6	5	108
1-C_4H_8		C_4H_{10}, 2-C_4H_8 (cis,trans)	Pd	Nafion	70	-28	40*	-	109

7. EP studies utilizing aqueous alkaline solutions

Reactants									
Electron Donor (D)	Electron Acceptor (A)	Products	Catalyst	Solid Electrolyte	T (°C)	$\Lambda_{max}(>0)$ or $\Lambda_{min}(<0)_x$	$\rho_{max}(>1)$ or $\rho_{min}(<1)$	PI_{OH^-}	Ref.
H_2	O_2	H_2O	Pt	H_2O - 0.1N KOH	25-50	20	6	20	19,110, 111

8. EP studies utilizing molten salts

Reactants								
Electron Donor (D)	Electron Acceptor (A)	Products	Catalyst	Solid Electrolyte	T (°C)	$\Lambda_{max}(>0)$ or $\Lambda_{min}(<0)_x$	$\rho_{max}(>1)$ or $\rho_{min}(<1)$	Ref.
SO_2	O_2	SO_3	Pt	V_2O_5-K_2SO_4	350-450	-100	6	112

*: Change in product selectivity observed.
#: 4.5 mol% Y_2O_3 - 10 mol% TiO_2 - 85.5 mol% ZrO_2

4.5.3 Rate Enhancement Ratio ρ

The rate enhancement ratio, ρ, is defined as the ratio of the promoted, r, and unpromoted, r_0, catalytic rate:

$$\rho = r/r_0 \tag{4.33}$$

In the galvanostatic transient experiment of Fig. 4.13 the steady-state ρ value is 26. The maximum ρ value measured with C_2H_4 oxidation on Pt/YSZ is 60[1,4] (Fig. 4.24) vs 100 for the same reaction on Rh/YSZ (Fig. 4.14).[50] Even higher ρ values have been obtained by Lambert and coworkers[32] for the NO reduction by C_2H_4 on Pt/β″-Al_2O_3 and by Yiokari et al[105] for the synthesis of ammonia on Fe/$CaIn_{0.1}Zr_{0.9}O_{3-\alpha}$. The catalytic rate was practically nil on the unpromoted surfaces and quite significant on the Na-promoted Pt surface[32] or H^+-promoted Fe surface.[105] At the opposite extreme Cavalca and Haller[93] have obtained ρ values approaching zero for the hydrogenation of benzene to cyclohexane on Pt/β″-Al_2O_3. They showed that Na coverages of less than 0.1 suffice to completely poison the rate of hydrogenation.[93]

Figure 4.25 shows the effect of catalyst potential and work function Φ on the measured ρ values for the formation of CO_2 and N_2 during NO reduction by C_3H_6 on Rh/YSZ[70,71] in presence of gaseous O_2. This is a catalytic system of great practical significance. Figure 4.25 shows ρ_{CO_2} values up to 70 and ρ_{N_2} values up to 16. Interestingly both reactions are enhanced electrochemically both with positive and with negative $\Delta\Phi$ and ΔU_{WR}. This type of r vs Φ behaviour is called *inverted volcano* behaviour.

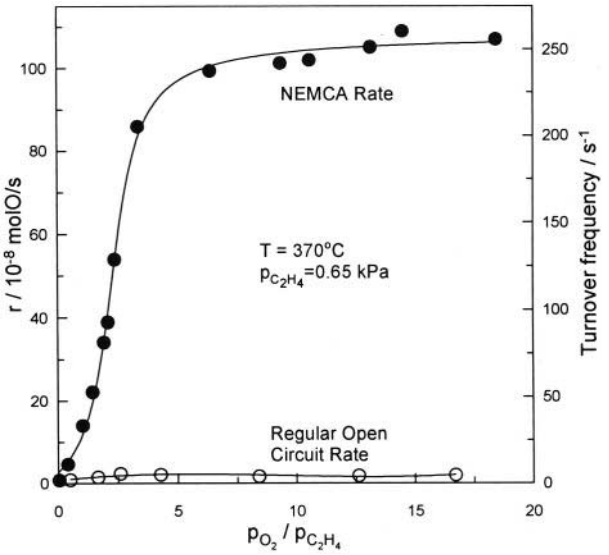

Figure 4.24. Effect of gaseous composition on the regular (open-circuit) catalytic rate of C_2H_4 oxidation on Pt/YSZ and on the NEMCA-induced catalytic rate on the same Pt catalyst film maintained at U_{WR}=1V. T=370°C, $p_{C_2H_4}$ =0.65 kPa.[4] Reprinted with permission from Academic Press.

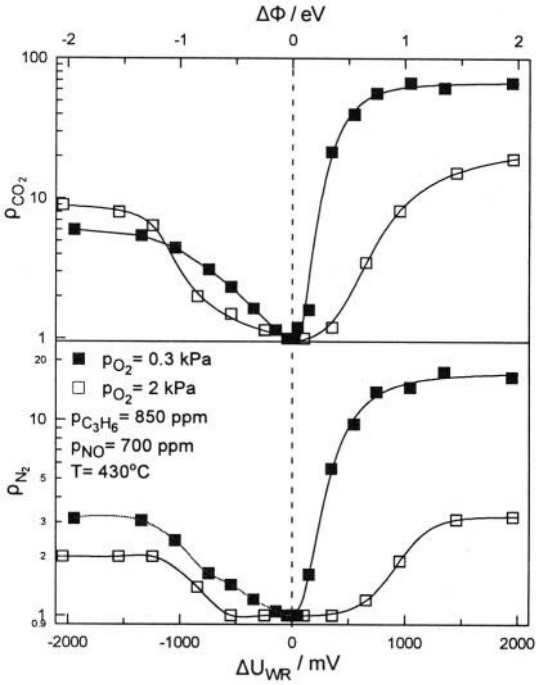

Figure 4.25. Dependence of ρ_{CO_2} and ρ_{N_2} on the catalyst potential and on the oxygen concentration during NO reduction by C_3H_6 in presence of O_2 on Rh/YSZ.[70] Reprinted with permission from Elsevier Science.

4.5.4 Promotion Index PI_i

From a catalytic viewpoint this is the most important phenomenological parameter for quantifying the promoting or poisoning effect of a given coadsorbed species i (e.g. O^{2-}, F^-, Na^+, H^+) on the rate of a catalytic reaction.

Similarly to the case of classical promotion (eq. 2.19), it is defined from:

$$PI_i = \frac{\Delta r/r_0}{\Delta\theta_i} \tag{4.34}$$

where r_0 is the unpromoted catalytic reaction rate and θ_i is the coverage of the promoting or poisoning species. Thus for a coadsorbed species i which just blocks surface sites it is PI_i=-1. When PI_i>0 the species i is a promoter for the reaction. When PI_i<-1 it is a poison for the reaction. Promoter index PI_{Na} values up to 250 and down to -30 have been measured during CO oxidationon Pt/β″-Al_2O_3[51] at different gaseous compositions and θ_{Na} values, implying strong electronic interactions. Similar or even higher PI_{Na} values

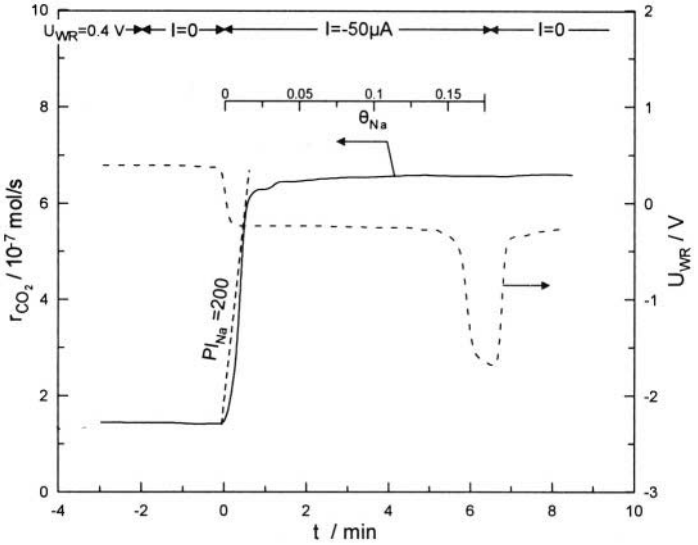

Figure 4.26. Transient response of the rate of CO_2 formation and of the catalyst potential during NO reduction by CO on Pt/β″-Al_2O_3[96] upon imposition of fixed current (galvanostatic operation) showing the corresponding (Eq. 4.24) Na coverage on the Pt surface and the maximum measured (Eq. 4.34) promotion index PI_{Na} value. T=348°C, inlet composition: $p^o_{NO} = p^o_{CO} = 0.75$ kPa. Reprinted with permission from Academic Press.

have been measured on transition metals during the reduction of NO by H_2,[52] CO[96] or light hydrocarbons.[32] Two examples are shown in Figs. 4.26 and 4.27 for the reduction of NO on Pt/β″-Al_2O_3 by CO[96] and H_2[52] respectively. Figure 4.26 shows a galvanostatic transient (I=-50 μA) which, as previously noted, allows one to directly examine the effect of θ_{Na} on r and U_{WR}. As shown on Fig. 4.26, PI_{Na} values exceeding 200 are obtained at low θ_{Na} values.

Figure 4.27 presents steady-state potentiostatic r vs θ_{Na} results during NO reduction by H_2 on Pt/β″-Al_2O_3,[52] PI_{Na} values well in excess of 4000 are obtained for θ_{Na} values below 0.002. This is due to the tremendous propensity of Na to induce NO dissociation on transition metal surfaces. Since PI_i is often found to be strongly dependent on θ_i (Figs. 4.26 and 4.27), it is also useful to define a differential promotion index pi_i from:

$$pi_i = \frac{dr/r_0}{d\theta_i} \tag{4.35}$$

which is proportional to the slope of the r vs θ_{Na} curves of Figs. 4.26 and 4.27.

It follows then that:

$$PI_i = \int_0^{\theta_i} pi_i d\theta_i' \tag{4.36}$$

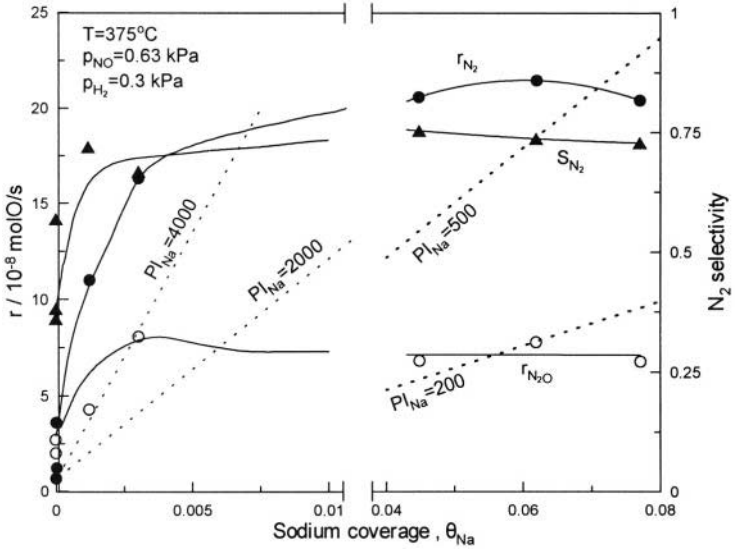

Figure 4.27. Steady state effect of the Na coverage on the rates of formation of N_2 and N_2O and on the selectivity to N_2 during NO reduction by H_2 on Pt/β″-Al_2O_3.[52] Straight lines correspond to fixed PI_{Na} values. Reprinted with permission from Academic Press.

The measurement of PI_i and pi_i is quite straightforward when the promoting species (e.g. Na^+) does not react appreciably with any of the reactants or products. In this case, as already noted, the coverage θ_{Na} of sodium on the metal surface can be easily measured coulometrically via:

$$\theta_{Na} = -\int_0^t \frac{I dt'}{F N_G} \tag{4.37}$$

where N_G is the catalyst surface area (mol metal) and t is the time of current application. When I is constant then equation (4.37) simplifies to:

$$\theta_{Na} = -It/FN_G \tag{4.24}$$

When the promoting species is also partially consumed by one of the reactants, as e.g. in the case of C_2H_4 oxidation when using YSZ as the solid electrolyte catalyst support (in which case C_2H_4 reacts with the promoting species $O^{\delta-}$ at a rate Λ times smaller than with normally chemisorbed oxygen), then the measurement of PI_i is more complicated due to the difficulties in measuring the surface coverage of $O^{\delta-}$. In such cases a conservative estimate of PI_i can be obtained from $PI_i=(\Delta r/r_0)_{max}$, i.e., by assuming[4,19] that the maximum rate enhancement is obtained for $\Delta\theta_O{}^{\delta-}=1$. With this assumption it can be shown easily that:

$$PI_i = \rho_{max} - 1 \tag{4.38}$$

Consequently the maximum $PI_{O^{\delta-}}$ values measured so far are on the order of 60 and 100, respectively, for the oxidation of C_2H_4 on Pt[4,59] and on Rh.[50]

4.5.5 Electrophobic and Electrophilic Reactions

Depending on the rate behaviour upon variation of the catalyst potential U_{WR} and, equivalently work function Φ, a catalytic reaction can exhibit two types of behaviour, electrophobic or electrophilic. These terms, introduced since the early days of electrochemical promotion, are synonymous to the terms electron donor and electron acceptor reaction introduced by Wolkenstein[113] in the fifties. Electrochemical promotion permits direct determination of the electrophobicity or electrophilicity of a catalytic reaction by just varying U_{WR} and thus Φ.

A catalytic reaction is termed electrophobic[1,19,54] when its rate increases with increasing catalyst work function Φ:

$$\partial r/\partial \Phi > 0 \tag{4.39}$$

There are several equivalent definitions:

$$\partial r/\partial U_{WR} > 0 \tag{4.40}$$

$$\Lambda > 0 \text{ (oxidations)} \tag{4.41}$$

$$\Lambda < 0 \text{ (hydrogenations)} \tag{4.42}$$

$$PI_{O^{2-}} > 0;\ PI_{Na^+} < 0 \tag{4.43}$$

A typical example of an electrophobic reaction is the oxidation of C_2H_4 on Pt[4,59] (Fig. 4.13), Rh[50] and Ag[11,12,49,77] under fuel-lean conditions.[59]

A catalytic reaction is termed electrophilic[1,19,54] when its rate increases with decreasing catalyst work function Φ:

$$\partial r/\partial \Phi < 0 \tag{4.44}$$

or, equivalently:

$$\partial r/\partial U_{WR} < 0 \tag{4.45}$$

$$\Lambda < 0 \text{ (oxidations)} \tag{4.46}$$

$$\Lambda > 0 \text{ (hydrogenations)} \tag{4.47}$$

$$PI_{O^{2-}} < 0;\ PI_{Na^{+}} > 0 \tag{4.48}$$

Typical examples of electrophilic reactions are the reduction of NO by ethylene on Pt[32] and the CO oxidation on Pt under fuel-rich conditions.[51,62]

Many reactions exhibit both electrophobic and electrophilic behaviour over different U_{WR} and Φ ranges leading to volcano-type[51] (Fig. 4.16) or inverted-volcano-type (Fig. 4.25) behaviour.[70]

As analyzed in Chapter 6 the electrophobicity or electrophilicity of a catalytic reaction depends strongly on the electron donor or electron acceptor characteristics of the adsorbates and on their binding strength. It can also depend on the polarity of the metal-adsorbate or intra-adsorbate bond broken in the rate limiting step (rls). Thus all catalytic oxidations on metals under fuel lean conditions are found to be electrophobic reactions[59] (Table 4.1). In these cases the surface is predominantly covered by chemisorbed O and cleavage of the metal-chemisorbed oxygen bond is involved in the rls. As discussed in Chapter 6 increasing catalyst potential U_{WR} and work function Φ weakens metal-electron acceptor bonds[1,19] thus leading to a rate increase with increasing Φ, i.e. to electrophobic behaviour as experimentally observed. In the case of electrophilic reactions, such as NO reduction or CO hydrogenation, decreasing Φ is known to strengthen the metal-adsorbate bond and thus to weaken the intra-adsorbate N=O or C=O bonds, the cleavage of which is usually rate limiting. Consequently decreasing U_{WR} enhances the catalytic rate, leading to electrophilic behaviour as experimentally observed. A qualitative but rigorous model is presented in Chapter 6.

4.5.6 Dependence of Catalytic Rates and Activation Energies on Catalyst Potential U_{WR} and Work Function Φ

4.5.6.1 Catalytic Rate Dependence on U_{WR} and Φ

A general observation which has emerged from electrochemical promotion studies is that over wide ranges of catalyst work function Φ (0.2 - 1.0 eV) catalytic rates depend exponentially on catalyst work function Φ:

$$\ln(r/r_0)=\alpha(\Phi-\Phi^{*})/k_bT \tag{4.49}$$

where α and Φ^{*} are catalyst and reaction - specific constants. The "NEMCA coefficient" α, positive for *electrophobic* reactions and negative for *electrophilic* ones, typically takes values between -1 and 1.[1,19]

Typical examples of electrophobic reactions are shown on Fig. 4.28 for the catalytic oxidation of C_2H_4 and of CH_4 on Pt/YSZ. As also shown in this figure, increasing Φ also causes a linear variation in activation energy E_A:

$$E_A = E_A^o + \alpha_H \Delta\Phi \tag{4.50}$$

where α_H is a constant which is usually negative for electrophobic reactions.

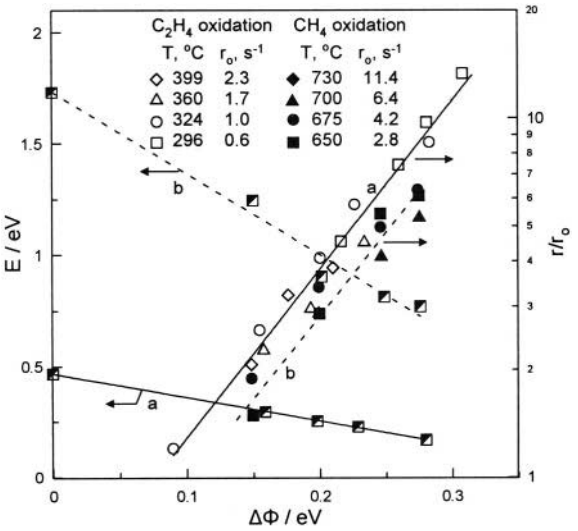

Figure 4.28. Electrophobic behaviour: Effect of catalyst work function Φ on the activation energy E and catalytic rate enhancement ratio r/r_0 for C_2H_4 oxidation on Pt; p_{O_2}=4.8 kPa, $p_{C_2H_4}$=0.4 kPa (a) and CH_4 oxidation on Pt; p_{O_2} =2.0 kPa, p_{CH_4} =2.0 kPa (b).[114] Reprinted with permission from Elsevier Science.

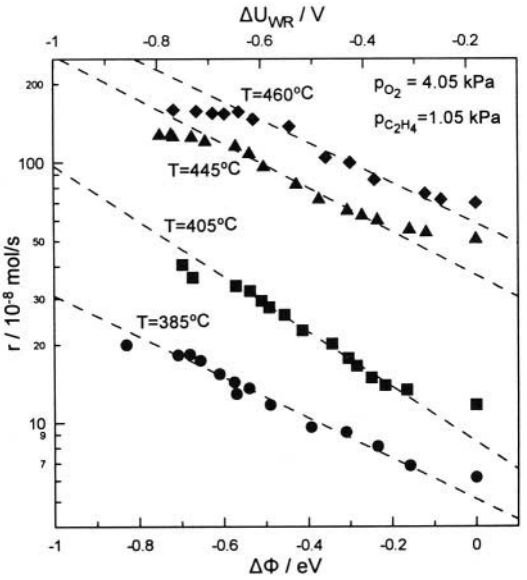

Figure 4.29. Electrophilic behaviour: Effect of catalyst potential and work function change $\Delta\Phi$ on the rate of C_2H_4 oxidation on a Pt film deposited on $CaZr_{0.9}In_{0.1}O_{3-\alpha}$ which is a H^+ conductor.[104] Reprinted with permission from the Institute for Ionics.

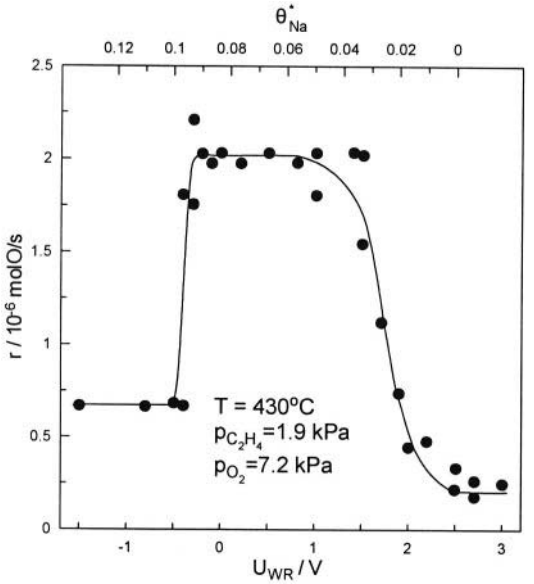

Figure 4.30. Volcano-type behaviour: Effect of catalyst potential U_{WR} on the rate of ethylene oxidation on a Pt film deposited on NASICON ($Na_3Zr_2Si_2PO_{12}$), a Na^+ conductor: T=430°C, p_{O2} =7.2 kPa, p_{C2H4}=1.9 kPa.[102] Reproduced by permission of The Electrochemical Society.

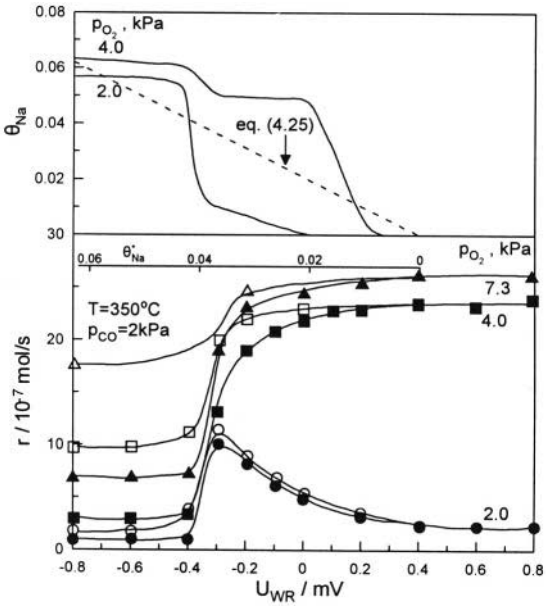

Figure 4.31. Transition from volcano-type behaviour at low p_{O_2} to electrophobic behaviour at high p_{O_2} during CO oxidation on Pt/β″-Al_2O_3.[51] Effect of U_{WR} and linearized[51] Na coverage θ^*_{Na} on the rate of CO oxidation on Pt/β″-Al_2O_3 at varying p_{O_2}. Other conditions: p_{CO}=2 kPa, T=350°C. The top part of the figure shows the corresponding variation of the actual[51] Na coverage, θ_{Na}, with U_{WR}. Reprinted with permission from Academic Press.

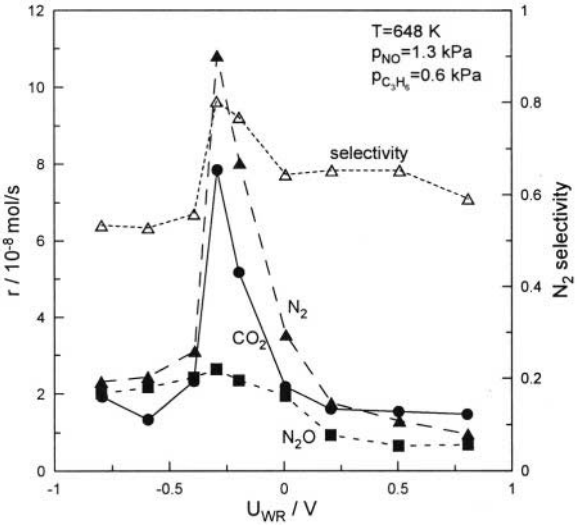

Figure 4.32. Volcano type behaviour. Effect of U_{WR} on the rates of CO_2, N_2, N_2O formation and on the selectivity to N_2 during NO reduction by propene on Pt/β"-Al_2O_3.[98,99] Reprinted from ref. 98 with permission from Elsevier Science.

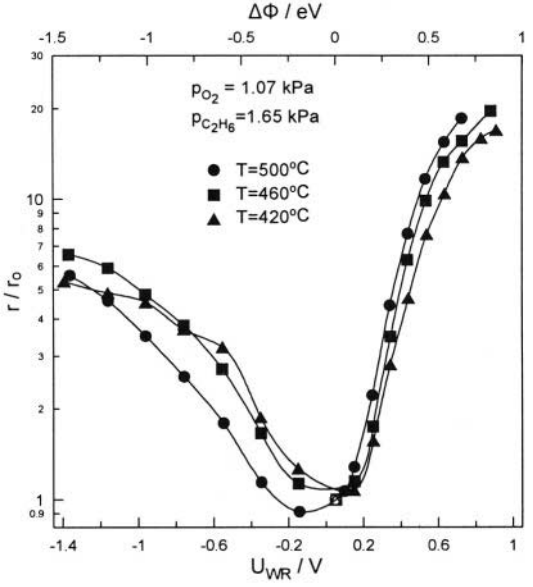

Figure 4.33. Inverted volcano behaviour. Effect of catalyst potential and work function on the rate of C_2H_6 oxidation on Pt/YSZ. p_{O_2} =1.07 kPa, $p_{C_2H_6}$ =1.65 kPa; ●, T=500°C; ■, T=460°C; ▲, T=420°C.[24] Reprinted with permission from Academic Press.

Electrophilic reactions also frequently conform to Eq. (4.49) with $\alpha<0$. An example is shown in Fig. 4.29 for the case of C_2H_4 oxidation on Pt supported on $CaIn_{0.1}Zr_{0.9}O_{3-\alpha}$, a H^+ conductor. At a first glance it is surprising that the

same reaction, i.e. ethylene oxidation on Pt, can exhibit both electrophobic and electrophilic behaviour depending on the solid electrolyte and on the experimental conditions. As analyzed in detail in Chapter 6 this is not too uncommon, since the electrophobicity or electrophilicity of a reaction depends on the work function of the film, which is influenced by the solid electrolyte via ion backspillover and this is turn affects the chemisorptive propensity of the electron acceptor (O_2) and electron donor (C_2H_4) reactants in a different way.

Actually, as shown in Fig. 4.30, C_2H_4 oxidation on $Pt/Na_3Zr_2Si_2PO_{12}$, where $Na_3Zr_2Si_2PO_{12}$ (NASICON) is a Na^+ conductor, can exhibit *volcano-type* behaviour, i.e. electrophobic behaviour at low potentials followed by electrophilic behaviour at higher potentials.

The transition from *volcano-type* behaviour to electrophobic behaviour upon changing p_{O_2} is shown in Fig. 4.31 for the case of CO oxidation on $Pt/\beta''\text{-}Al_2O_3$. Another example of volcano-type behaviour is shown in Fig. 4.32 for the case of NO reduction by C_3H_6 on $Pt/\beta''\text{-}Al_2O_3$.[98,99]

A fourth important case of r vs Φ dependence is the *inverted volcano* behaviour depicted in Figure 4.33 for the case of C_2H_6 oxidation on Pt/YSZ.[24] The rate is enhanced by a factor of 7 for negative potentials and by a factor of 20 for positive ones.

4.5.6.2 Local and Global r vs Φ Dependence

In view of the previous section and of Figs. 4.28 to 4.33 one may conclude the following:

When examining the r vs Φ behaviour of a catalytic system at a *local* level, i.e. for small (<0.1 eV) variations in work function Φ there are two types of behaviour (Fig. 4.34a):

1. Electrophobic, i.e. $\partial r/\partial\Phi > 0$.
2. Electrophilic, i.e. $\partial r/\partial\Phi < 0$.

When examining the r vs Φ behaviour at a *global* level, i.e. over the entire experimentally accessible Φ range (typically over 1.5 to 2eV) then there are four types of behaviour (Fig. 4.34b).

1. Purely electrophobic, i.e. $\partial r/\partial\Phi > 0$
2. Purely electrophilic, i.e. $\partial r/\partial\Phi < 0$
3. Volcano-type, i.e. $\partial r/\partial\Phi > 0$ followed by $\partial r/\partial\Phi < 0$
4. Inverted volcano-type, i.e. $\partial r/\partial\Phi < 0$ followed by $\partial r/\partial\Phi > 0$.

Table 4.2 classifies the catalytic reactions of Table 4.1 on the basis of reaction type and shows their global r vs Φ behaviour. In Chapter 6 we will provide simple rules which enable one to rationalize and predict the behaviour of any given catalytic reaction both at the local and at the global level. Table 4.2, which classifies the 58 catalytic reactions of Table 4.1 on the basis of reaction type, also provides two additional pieces of information for each reaction:

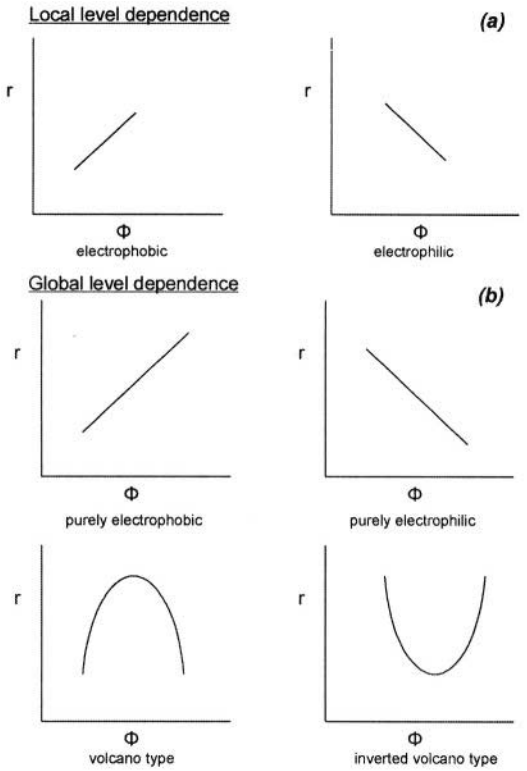

Figure 4.34. The types of local (a) and global (b) rate-work function dependence.

(a) The investigated range of the ratio, p_A/p_D of partial pressures of the electron acceptor (A) and of the electron donor (D) reactant. As we shall see in Chapter 6 this information is quite useful.

(b) The type of *global* r vs Φ dependence observed (purely electrophobic, purely electrophilic, volcano, inverted-volcano). One may notice that all four types of global behaviour are equally common.

Is there any way to predict the local or global r vs Φ behaviour of a catalytic reaction? The picture which emerges from Table 4.2 is, at a first glance, rather discouraging. Even for the same reaction and same metal catalyst the r vs Φ behaviour often changes from one type to the other upon changing the solid electrolyte support or the gaseous composition. There is no clear pattern formation regarding the r vs Φ behaviour except for some limiting observations, e.g. that C_2H_4 oxidation is always electrophobic at very high p_A/p_D ($=p_{O_2}/p_{C_2H_4}$) ratios.[59]

It is a recent discovery, presented in Chapter 6, that behind the apparent chaos of Table 4.2 there are some simple regularities which enable one to predict the r vs Φ local and global behaviour on the basis of the open-circuit

catalytic kinetics, i.e. on the basis of the unpromoted catalyst r vs p_A and r vs p_D dependency.[115-117]

Thus in Table 4.3 we add to Table 4.2 the last, but quite important, available piece of information, i.e. the observed kinetic order (positive order, negative order or zero order) of the catalytic reaction with respect to the electron donor (D) and the electron acceptor (A) reactant. We then invite the reader to share with us the joy of discovering the rules of electrochemical promotion (and as we will see in Chapter 6 the rules of promotion in general), i.e. the rules which enable one to predict the global r vs Φ dependence (purely electrophobic, purely electrophilic, volcano, inverted volcano) or the basis of the r vs p_A and r vs p_D dependencies.

If an additional hint is needed the reader may jump to Table 6.1 in Section 6.2. Table 6.1 is the same with Table 4.3, except that the reactions are there listed on the basis of their r vs Φ global behaviour.

Table 4.2. Classification of electrochemical promotion studies on the basis of catalytic reaction.

Ethylene oxidation: **Reactants: C_2H_4 (D), O_2 (A).**

Catalyst	Solid Electrolyte	p_A/p_D	T (°C)	$\rho_{max}(>1)$ or $\rho_{min}(<1)$	Global r vs Φ behaviour	Ref
Pt	$ZrO_2(Y_2O_3)$	12-16	260-450	55	Purely electrophobic	4,59,60
Pt	β''-Al_2O_3	238	180-300	0.25	Purely electrophobic	19,36
Pt	$Na_3Zr_2Si_2PO_{12}$	1.3-3.8	430	10	Volcano type	102
Pt	$CaZr_{0.9}In_{0.1}O_{3-a}$	4.8	385-470	5	Purely electrophilic	104
Pt	TiO_2	(a) 3.5-12 *(oxidizing conditions)* (b) 0.2-0.3 *(reducing conditions)*	450-600	20	Purely electrophobic Inverted volcano	90
Pt	CeO_2	1.6-3.7	500	3	Purely electrophilic	91
Pt	YZTi10	3	400-475	2	Purely electrophilic	92
Rh	$ZrO_2(Y_2O_3)$	0.05-2.6	250-400	90	Purely electrophobic	50,68,69
Pd	$ZrO_2(Y_2O_3)$	0.2-10	290-360	2	Purely electrophobic	14
Ag	$ZrO_2(Y_2O_3)$	0.2-1.1	320-470	30	Purely electrophobic	11,12,49,77
Ag	β''-Al_2O_3	0.3-0.4	240-280	3	Purely electrophilic	101
IrO_2	$ZrO_2(Y_2O_3)$	300	350-400	6	Purely electrophobic	87,88
RuO_2	$ZrO_2(Y_2O_3)$	155	240-500	115	Purely electrophobic	23

CO oxidation: **Reactants: CO (D), O_2 (A).**

Catalyst	Solid Electrolyte	p_A/p_D	T (°C)	$\rho_{max}(>1)$ or $\rho_{min}(<1)$	Global r vs Φ behaviour	Ref
Pt	$ZrO_2(Y_2O_3)$	0.2-55	468-558	5	Volcano type	19,63,64
Pt	β''-Al_2O_3	0.5-20	300-450	8	Volcano type	19,51
Pt	CaF_2	11-17	500-700	2.5	Purely electrophobic	19,89
Pd	$ZrO_2(Y_2O_3)$	500	400-550	2	Purely electrophobic	19,66
Ag	$ZrO_2(Y_2O_3)$	0.6-14	350-450	15	Inverted volcano	19,80
Ag	β''-Al_2O_3	0.1-10	360-420	2	Purely electrophilic	19
Ag-Pd alloy	$ZrO_2(Y_2O_3)$	3.5-12.5	450-500	5	Inverted volcano	84
Au	$ZrO_2(Y_2O_3)$	3-53	450-600	3	Inverted volcano	82,83

Other oxidation reactions.

Catalyst	Solid Electrolyte	Reactants (D)	Reactants (A)	p_A/p_D	T (°C)	$\rho_{max}(>1)$ or $\rho_{min}(<1)$	Global r vs Φ behaviour	Ref
Pt	$ZrO_2(Y_2O_3)$	C_2H_6	O_2	0.06-7	270-500	20	Inverted volcano	24
Pt	$ZrO_2(Y_2O_3)$	CH_4	O_2	0.02-7	600-750	70	Inverted volcano	19,61
Pt	$ZrO_2(Y_2O_3)$	CH_3OH	O_2	3-45	300-500	4,15	Inverted volcano	19,65
Pt	$ZrO_2(Y_2O_3)$	C_3H_6	O_2	0.9-55	350-480	6	Purely electrophilic	25
Pt	YZTi10	C_3H_6	O_2	5	400-500	2.4	Inverted volcano	92
Pt	Nafion	H_2	O_2	0.2-5	25	6	Volcano type	108
Pt	H_2O - 0.1N KOH	H_2	O_2	0.3-3	25-50	6	Purely electrophobic	19,110, 111
Pt	V_2O_5-$K_2S_2O_7$	SO_2	O_2	1.8	350-450	6	Volcano type	112
Pd	$ZrO_2(Y_2O_3)$	CH_4	O_2	0.2-4.8	380-440	90	Purely electrophobic	14,74
Ag	$ZrO_2(Y_2O_3)$	C_3H_6	O_2	20-120	320-420	2	Purely electrophobic	19,78
Ag	$ZrO_2(Y_2O_3)$	CH_4	O_2	0.02-2	650-850	30	Purely electrophobic	19,79
Ag	$ZrO_2(Y_2O_3)$	CH_3OH	O_2	0-2	500	2	Purely electrophilic	10
Au	$ZrO_2(Y_2O_3)$	CH_4	O_2	0.1-0.7	700-750	3	Purely electrophilic	82,83,86

Nitrogen oxide reduction reactions.

Catalyst	Solid Electrolyte	Reactants (D)	Reactants (A)	p_A/p_D	T (°C)	$\rho_{max}(>1)$ or $\rho_{min}(<1)$	Global r vs Φ behaviour	Ref
Pt	$ZrO_2(Y_2O_3)$	C_2H_4	NO	0.2-10	380-500	7	Purely electrophilic	67
Pt	β''-Al_2O_3	C_2H_4	NO	0.1-1.1	280-400	∞	Purely electrophilic	32
Pt	β''-Al_2O_3	C_3H_6	NO	2-70	375	10	Volcano type	97-99
Pt	β''-Al_2O_3	CO	NO	0.3-5	320-400	13	Purely electrophilic	96-98

Pt	β''-Al_2O_3	H_2	NO	0.3-6	360-400	30	Volcano type	52
Rh	$ZrO_2(Y_2O_3)$	C_3H_6	NO,O_2	0.08-8*	250-450	150	Inverted volcano	70
Rh	$ZrO_2(Y_2O_3)$	CO	NO,O_2	0.33*	250-450	20	Inverted volcano	71
Pd	$ZrO_2(Y_2O_3)$	CO	NO	0.5-6.5	320-480	3	Purely electrophilic	75, 76
Pd	$ZrO_2(Y_2O_3)$	CO	N_2O	2-50	440	2	Purely electrophilic	75

(*) *p_A/p_D denotes the ratio $p_{NO}/p_{C_3H_6}$ or p_{NO}/p_{CO}. The p_{O_2} range is 0 – 6 kPa.*

Hydrogenation and dehydrogenation reactions.

Catalyst	Solid Electrolyte	Reactants (D)	Reactants (A)	p_A/p_D	T (°C)	$\rho_{max}(>1)$ or $\rho_{min}(<1)$	Global r vs Φ behaviour	Ref
Pt	β''-Al_2O_3	C_6H_6	H_2	0.02-0.12	100-150	~0	Purely electrophobic	93,94
Pt	β''-Al_2O_3	C_2H_2	H_2	1.7-9	100-300	-	Purely electrophobic	95
Rh	$ZrO_2(Y_2O_3)$	H_2	CO_2	0.03-0.7	300-450	3	Purely electrophobic	19
Pd	$ZrO_2(Y_2O_3)$	H_2	CO	0.1-6	300-370	3	Mixed behaviour, depending on the product	19
Pd	$ZrO_2(Y_2O_3)$	H_2	CO_2	0.2-1.1	500-590	10	Inverted volcano	19,66
Pd	β''-Al_2O_3	H_2	C_2H_2, C_2H_4	0.1-5.9#	70-100	0.13	Purely electrophobic	100
Fe	$CaZr_{0.9}In_{0.1}O_{3-a}$	H_2	N_2	0-3	440	12	Purely electrophilic	105
Ni	$CsHSO_4$	H_2	C_2H_4	1	150-170	2	Purely electrophilic	19, 107
Pt	$ZrO_2(Y_2O_3)$	CH_3OH	-	---	400-500	3	Purely electrophilic	65,66
Pt	$ZrO_2(Y_2O_3)$	H_2S	-	---	600-750	11	Purely electrophobic	19,73
Ag	$ZrO_2(Y_2O_3)$	CH_3OH	-	0-6 kPa	550-750	6	Purely electrophilic	19,81
Ag	$SrCe_{0.95}Yb_{0.05}O_3$	CH_4	-	---	750	8	Purely electrophobic	19, 106
Fe	$CaZr_{0.9}In_{0.1}O_{3-a}$	NH_3	-	4-12kPa	530-600	3.6	Purely electrophobic	103
Fe	$K_2YZr(PO_4)_3$	NH_3	-	4-12kPa	500-700	4.5	Purely electrophobic	103

(#) *$p_D = p_{C_2H_2} + p_{C_2H_4}$*

Other catalytic reactions.

Catalyst	Solid Electrolyte	Reactants (D)	Reactants (A)	p_A/p_D	T (°C)	$\rho_{max}(>1)$ or $\rho_{min}(<1)$	Global r vs Φ behaviour	Ref
Pd	Nafion	1-butene		---	70	~40	Purely electrophilic	109
Ni	$ZrO_2(Y_2O_3)$	CH_4	H_2O	0.05-3.5	600-900	2	Purely electrophobic	19,85

Table 4.3. Classification of Electrochemical Promotion studies on the basis of catalytic reaction, showing the observed kinetic order with respect to the electron donor (D) and electron acceptor (A) reactant and the corresponding global r vs Φ behaviour.

: Purely electrophobic, : Purely electrophilic, : Volcano-type, : Inverted volcano-type
+ : Positive order, - : Negative order, 0 : Zeroth order, ? : Not measured

Ethylene oxidation: **Reactants: C_2H_4 (D), O_2 (A).**

Catalyst	Solid Electrolyte	p_A/p_D	T (°C)	Kinetics in D $\partial r/\partial p_D)_\Phi$	Kinetics in A $\partial r/\partial p_A)_\Phi$	Global r vs Φ behaviour	Ref
Pt	$ZrO_2(Y_2O_3)$	12-16	260-450	+	0		4,59,60
Pt	β''-Al_2O_3	238	180-300	+	0		19,36
Pt	$Na_3Zr_2Si_2PO_{12}$	1.3-3.8	430	-	+		102
Pt	$CaZr_{0.9}In_{0.1}O_{3-a}$	4.8	385-470	-	+		104
Pt	TiO_2	(a) 3.5-12	450-600	+	0		90
		(b) 0.2-0.3		+	+		
Pt	CeO_2	1.6-3.7	500	-	+		91
Pt	YZTi10	3	400-475	?	?		92
Rh	$ZrO_2(Y_2O_3)$	0.05-2.6	250-400	+	0		50,68,69
Pd	$ZrO_2(Y_2O_3)$	0.2-10	290-360	+	≤0		14
Ag	$ZrO_2(Y_2O_3)$	0.2-1.1	320-470	+	0		11,12,49,77
Ag	β''-Al_2O_3	0.3-0.4	240-280	-	+		101
IrO_2	$ZrO_2(Y_2O_3)$	300	350-400	+	0		87,88
RuO_2	$ZrO_2(Y_2O_3)$	155	240-500	+	≤0		23

CO oxidation: **Reactants: CO (D), O_2 (A).**

Catalyst	Solid Electrolyte	p_A/p_D	T (°C)	Kinetics in D $\partial r/\partial p_D)_\Phi$	Kinetics in A $\partial r/\partial p_A)_\Phi$	Global r vs Φ behaviour	Ref
Pt	$ZrO_2(Y_2O_3)$	0.2-55	468-558	+	-		19,63,64
Pt	β''-Al_2O_3	0.5-20	300-450	-	+		19,51
Pt	CaF_2	11-17	500-700	+	0		19,89
Pd	$ZrO_2(Y_2O_3)$	500	400-550	?	?		19,66
Ag	$ZrO_2(Y_2O_3)$	0.6-14	350-450	+	+		19,80
Ag	β''-Al_2O_3	0.1-10	360-420	0	+		19

Ag-Pd alloy	$ZrO_2(Y_2O_3)$	3.5-12.5	450-500	+	+		84
Au	$ZrO_2(Y_2O_3)$	3-53	450-600	+	≥0		82,83

Other oxidation reactions

Catalyst	Solid Electrolyte	Reactants (D)	Reactants (A)	p_A/p_D	T (°C)	Kinetics in D $\partial r/\partial p_D)_\Phi$	Kinetics in A $\partial r/\partial p_A)_\Phi$	Global r vs Φ behaviour	Ref
Pt	$ZrO_2(Y_2O_3)$	C_2H_6	O_2	0.06-7	270-500	+	+		24
Pt	$ZrO_2(Y_2O_3)$	CH_4	O_2	0.02-7	600-750	+	+		19,61
Pt	$ZrO_2(Y_2O_3)$	CH_3OH	O_2	3-45	300-500	+	?		19,65
Pt	$ZrO_2(Y_2O_3)$	C_3H_6	O_2	0.9-55	350-480	≤0	+		25
Pt	YZTi10	C_3H_6	O_2	5	400-500	?	?		92
Pt	Nafion	H_2	O_2	0.2-5	25	+	-		108
Pt	H_2O - 0.1N KOH	H_2	O_2	0.3-3	25-50	+	-		19,110, 111
Pt	V_2O_5-$K_2S_2O_7$	SO_2	O_2	1.8	350-450	?	?		112
Pd	$ZrO_2(Y_2O_3)$	CH_4	O_2	0.2-4.8	380-440	+	0		14,74
Ag	$ZrO_2(Y_2O_3)$	C_3H_6	O_2	20-120	320-420	+	≤0		19,78
Ag	$ZrO_2(Y_2O_3)$	CH_4	O_2	0.02-2	650-850	+	0		19,79
Ag	$ZrO_2(Y_2O_3)$	CH_3OH	O_2	0-2	500	?	+		10
Au	$ZrO_2(Y_2O_3)$	CH_4	O_2	0.1-0.7	700-750	0	+		82,83, 86

Nitrogen oxide reduction reactions.

Catalyst	Solid Electrolyte	Reactants (D)	Reactants (A)	p_A/p_D	T (°C)	Kinetics in D $\partial r/\partial p_D)_\Phi$	Kinetics in A $\partial r/\partial p_A)_\Phi$	Global r vs Φ behaviour	Ref
Pt	$ZrO_2(Y_2O_3)$	C_2H_4	NO	0.2-10	380-500	0	+		67
Pt	β″-Al_2O_3	C_2H_4	NO	0.1-1.1	280-400	?	?		32
Pt	β″-Al_2O_3	C_3H_6	NO	2-70	375	-	+		97-99
Pt	β″-Al_2O_3	CO	NO	0.3-5	320-400	≤0	+		96-98
Pt	β″-Al_2O_3	H_2	NO	0.3-6	360-400	-	+		52
Rh	$ZrO_2(Y_2O_3)$	C_3H_6	NO,O_2	0.08-8*	250-450	+	NO: + O_2: 0		70
Rh	$ZrO_2(Y_2O_3)$	CO	NO,O_2	0.33*	250-450	+	NO: + O_2: 0		71

Pd	$ZrO_2(Y_2O_3)$	CO	NO	0.5-6.5	320-480	~0	+		75,76
Pd	$ZrO_2(Y_2O_3)$	CO	N_2O	2-50	440	-	+		75

(*) *p_A/p_D denotes the ratio $p_{NO}/p_{C_3H_6}$ or p_{NO}/p_{CO}. The p_{O_2} range is 0 – 6 kPa.*

Hydrogenation and dehydrogenation reactions.

Cata-lyst	Solid Electrolyte	Reactants (D)	Reactants (A)	p_A/p_D	T (°C)	Kinetics in D $\partial r/\partial p_D)_\Phi$	Kinetics in A $\partial r/\partial p_A)_\Phi$	Global r vs Φ behaviour	Ref
Pt	β''-Al_2O_3	C_6H_6	H_2	0.02-0.12	100-150	≥0	~0		93, 94
Pt	β''-Al_2O_3	C_2H_2	H_2	1.7-9	100-300	?	?		95
Rh	$ZrO_2(Y_2O_3)$	H_2	CO_2	0.03-0.7	300-450	+	0		19
Pd	$ZrO_2(Y_2O_3)$	H_2	CO	0.1-6	300-370			Mixed behaviour, depending on the product	19
Pd	$ZrO_2(Y_2O_3)$	H_2	CO_2	0.2-1.1	500-590	+	+		19, 66
Pd	β''-Al_2O_3	H_2	C_2H_2, C_2H_4	0.1-5.9#	70-100	≥0	0		100
Fe	$CaZr_{0.9}In_{0.1}O_{3-a}$	H_2	N_2	0-3	440	?	?		105
Ni	$CsHSO_4$	H_2	C_2H_4	1	150-170	?	?		19, 107
Pt	$ZrO_2(Y_2O_3)$	CH_3OH	-	---	400-500		?		65, 66
Pt	$ZrO_2(Y_2O_3)$	H_2S	-	---	600-750	?			19, 73
Ag	$ZrO_2(Y_2O_3)$	CH_3OH	-	0-6 kPa	550-750		+		19, 81
Ag	$SrCe_{0.95}Yb_{0.05}O_3$	CH_4	-	---	750	?			19, 106
Fe	$CaZr_{0.9}In_{0.1}O_{3-a}$	NH_3	-	4-12kPa	530-600	+			103
Fe	$K_2YZr(PO_4)_3$	NH_3	-	4-12kPa	500-700	+			103

(#) *$p_D = p_{C_2H_2} + p_{C_2H_4}$*

Other catalytic reactions.

Catalyst	Solid Electrolyte	Reactants (D)	Reactants (A)	p_A/p_D	T (°C)	Kinetics in D $\partial r/\partial p_D)_\Phi$	Kinetics in A $\partial r/\partial p_A)_\Phi$	Global r vs Φ behaviour	Ref
Pd	Nafion	1-C_4H_8		---	70		?		109
Ni	$ZrO_2(Y_2O_3)$	CH_4	H_2O	0.05-3.5	600-900	+	≤0		19, 85

4.5.7 Activation Energy and Preexponential Factor Dependence on Work Function

It has been known since the early days of electrochemical promotion that upon varying U_{WR} and thus Φ, not only the catalytic rates, r, are changing in a frequently dramatic manner, but also the activation energy of the catalytic reaction is also significantly affected. An example was already presented in Fig. 4.28 which shows that both C_2H_4 and CH_4 oxidation on Pt/YSZ conform to equation (4.50) with α_H values of -1 and -3, respectively.

This linear variation in catalytic activation energy with potential and work function is quite noteworthy and, as we will see in the next sections and in Chapters 5 and 6, is intimately linked to the corresponding linear variation of heats of chemisorption with potential and work function. More specifically we will see that the linear decrease in the activation energies of ethylene and methane oxidation is due to the concomitant linear decrease in the heat of chemisorption of oxygen with increasing catalyst potential and work function.

Such linear or near-linear variations in activation energy E with work function as the one shown in Fig. 4.28 but also in Figures 4.35 to 4.37 are quite common in electrochemical promotion studies and are usually accompanied by a concomitant linear variation in the logarithm of the preexponential factor, r^o, defined from:

$$r = r^o \exp(-E/k_bT) \tag{4.51}$$

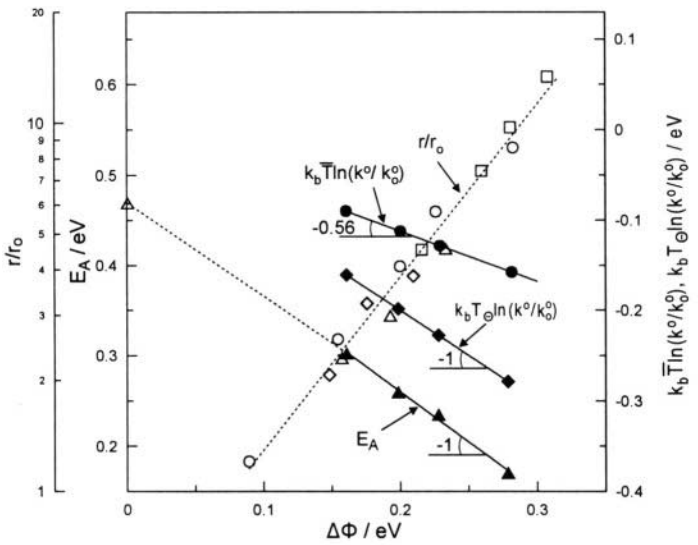

Figure 4.35. Effect of catalyst work function Φ on the activation energy E_A, preexponential factor k^o and catalytic rate enhancement ratio r/r_0 for C_2H_4 oxidation on Pt/YSZ;[4] p_{O_2}=4.8 kPa, $p_{C_2H_4}$=0.4 kPa.[4,54] k^o_o is the open-circuit preexponential factor, $\overline{T}$ is the mean temperature of the kinetic investigation, 375°C.[4] T_Θ is the (experimentally inaccessible) isokinetic temperature, 886°C.[4,25,50]

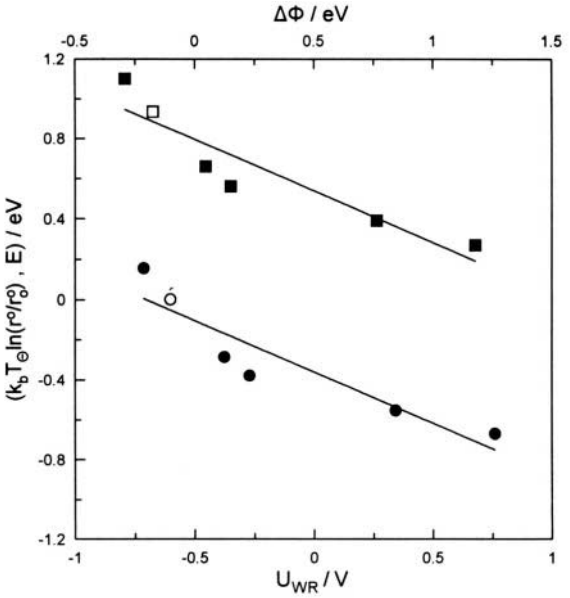

Figure 4.36. Effect of catalyst potential U_{WR} and work function Φ on the activation energy E (squares) and preexponential factor r^o (circles) of C_2H_4 oxidation on Rh/YSZ. open symbols: open-circuit conditions. T_Θ is the isokinetic temperature 372°C and r_0^o is the open-circuit preexponential factor. Conditions: p_{O_2}=1.3 kPa, $p_{C_2H_4}$ =7.4 kPa.[50] Reprinted with permission from Academic Press.

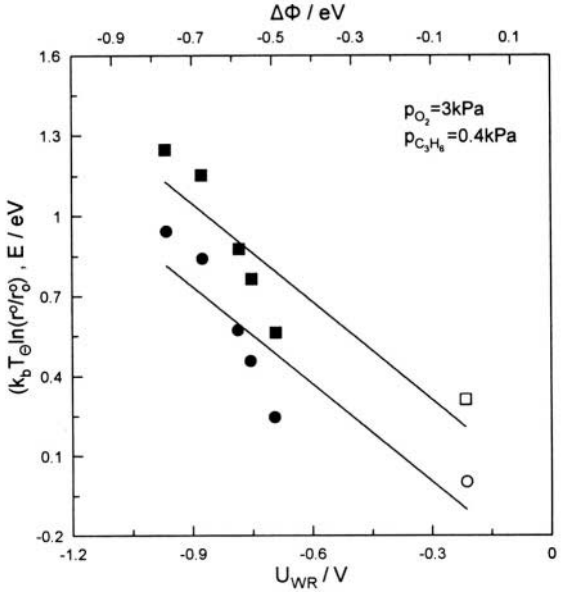

Figure 4.37. Effect of catalyst potential U_{WR} and work function Φ on the activation energy E (squares) and preexponential factor r^0 (circles) of C_3H_6 oxidation on Pt/YSZ. open symbols: open-circuit conditions. T_Θ is the isokinetic temperature 398°C and r_0^o is the open-circuit preexponential factor. Conditions: p_{O2} =3 kPa, p_{C3H6} =0.4 kPa.[25] Reprinted with permission from Academic Press.

as shown in Figures 4.35 to 4.37 for the cases of C_2H_4 oxidation on Pt/YSZ,[4] C_2H_4 oxidation on Rh/YSZ[50] and C_3H_6 oxidation on Pt/YSZ,[25] respectively.

It is quite interesting that $\ln(r^o/r_0^o)$, where r_0^o is the open-circuit preexponential factor, also varies linearly with U_{WR} and Φ (Figs. 4.35 to 4.37) and in fact, when plotted as $k_bT_\Theta\ln(r^o/r_0^o)$ where T_Θ is the isokinetic temperature discussed below, with the same slope as E_A. This decrease in apparent preexponential factor with increasing Φ can be attributed to the reduced binding strength and thus enhanced mobility of chemisorbed oxygen on the catalyst surface.

4.5.7.1 Compensation Effect

The observed linear variation in activation energy, E, and in the preexponential factor r^o/r_0^o (Figs. 4.35 to 4.37), which conform to the equations:

$$E=E^o+\alpha_H\Delta\Phi \tag{4.50}$$

$$k_bT_\Theta\ln(r^o/r_0^o)=\alpha_H\Delta\Phi \tag{4.52}$$

leads to the appearance of the well-known *compensation effect* (Fig. 4.38 and 4.39), where T_Θ is the *isokinetic temperature,* i.e. the temperature where the rate is the same for all imposed potentials and corresponding work functions. At this temperature (Figs. 4.38 and 4.39) the NEMCA effect disappears as the rate, r, does not depend on U_{WR} and Φ. Also note that a reaction which is electrophobic below T_Θ becomes electrophilic above it (Figs. 4.38 and 4.39). This is because at lower temperatures the enthalpic term dominates, i.e. the decrease in activation energy, while for $T>T_\Theta$ the entropic term becomes dominant, i.e. the decrease in preexponential factor with increasing U_{WR} and Φ.

All this is nicely described by the following equation, derived easily via mathematical manipulation of equations (4.49) to (4.52), which relates the NEMCA coefficient α (eq. 4.49) with the enthalpic parameter α_H (eq. 4.50):

$$\alpha=(-\alpha_H)\cdot\frac{(T_\Theta/T)-1}{(T_\Theta/T)} \tag{4.53}$$

Normally in heterogeneous catalysis compensation effect behaviour is obtained either for the same reaction upon using differently prepared catalysts of the same type, or with the same catalyst upon using a homologous set of reactants. In the case of electrochemical promotion (Figs. 4.38 and 4.39) one has the same catalyst and the same reaction but various potentials, i.e. various amounts of promoter on the catalyst surface.

As shown in Figs. 4.38 and 4.39 there can be no doubt that the effect is real. As well known from the heterogeneous catalysis literature its existence

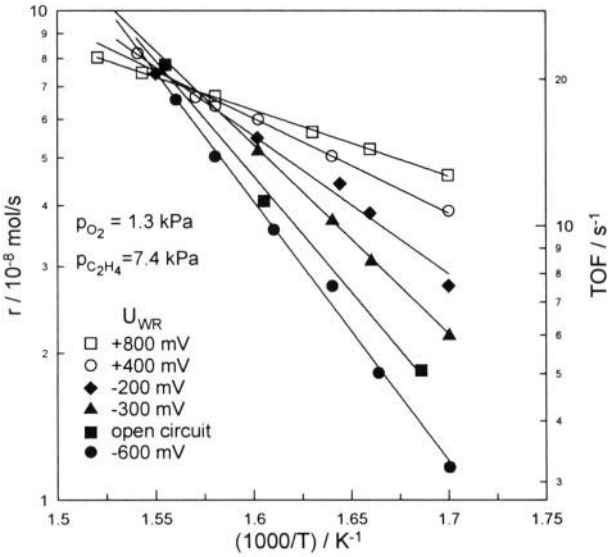

Figure 4.38. NEMCA-induced compensation effect in the isokinetic point for C_2H_4 oxidation on Rh/YSZ. Conditions: p_{O_2} = 1.3 kPa, $p_{C_2H_4}$ =7.4 kPa.[50] Reprinted with permission from Academic Press.

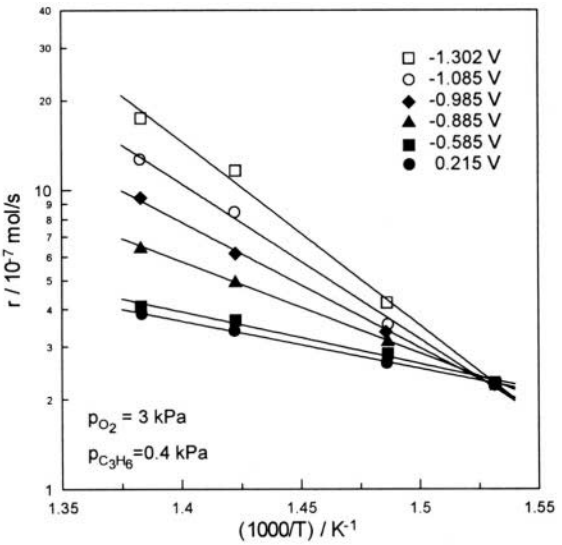

Figure 4.39. NEMCA-induced compensation effect in the isokinetic point for C_3H_6 oxidation on Pt/YSZ. Conditions: p_{O_2}=3 kPa, $p_{C_3H_6}$=0.4 kPa.[25] Reprinted with permission from Academic Press.

implies a linear relation between activation energy and log of preexponential factor or, equivalently, enthalpy and entropy of activation. The experimental equations (4.50) and (4.52) give us one additional piece of

information, i.e. that both activation energy and log of preexponential factor vary linearly with catalyst work function. The cause of this linear variation, at least for the enthalpic part, can be understood both in terms of rigorous quantum-mechanical calculations (Chapter 5) and in terms of simple electrostatic considerations (section 4.5.9.2).

It is worth noting that the linear variation in E and $\log r^o$ with Φ is a more general phenomenon than the actual appearance of an isokinetic point. The reason is that when equations 4.50 and 4.52 are satisfied (Figs. 4.35 to 4.37) this guarantees mathematically the existence of an isokinetic T_Θ, but this T_Θ may lie in the T region of the investigation (Figs. 4.38 and 4.39, appearance of an isokinetic temperature) or may lie outside the region of the investigation (e.g. C_2H_4 oxidation on Pt/YSZ, Fig. 4.35).

4.5.8 Selectivity Modification

One of the most promising features of electrochemical promotion is in product selectivity modification. A dramatic demonstration of selectivity modification with varying Φ was shown already in Fig. 4.18 for the case of NO reduction by H_2 on Pt/β″-Al_2O_3.[52] The selectivity to the desired product, N_2, increases from 35% on the unpromoted surface ($U_{WR} > 0$) to more than 70% on the Na-promoted surface ($U_{WR} < 0$). Similar is the behaviour when using CO instead of H_2 as the reductant[96] (Fig. 4.40). Upon decreasing the U_{WR} and Φ of the Pt/β″-Al_2O_3 catalyst, S_{N_2} increases from 15% to 60%. Thus Pt becomes as selective as Rh for the reduction of NO to N_2.

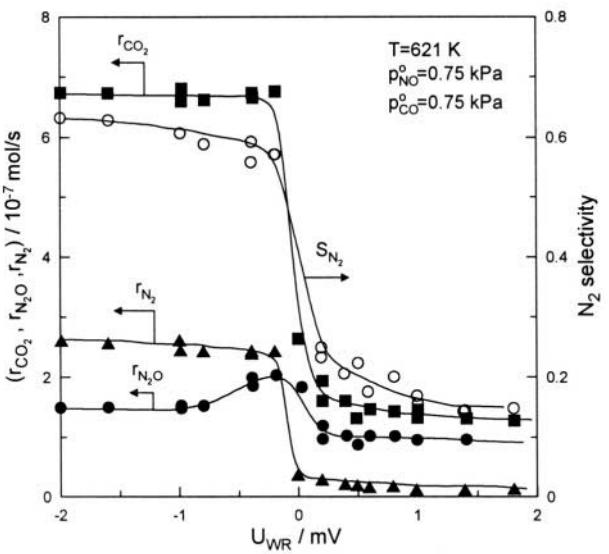

Figure 4.40. Effect of catalyst potential on the rates of formation of CO_2, N_2 and N_2O and on the selectivity to N_2 during NO reduction by CO on Pt/β″-Al_2O_3.[96] Reprinted with permission from Academic Press.

Two more examples regarding the epoxidation of ethylene on Ag are shown in Figs 4.41 and 4.42. In the former case[77] the Ag film is supported on YSZ. For $U_{WR} > 0$ ethylene oxide and CO_2 are the only products and the selectivity to ethylene oxide is 55%. Decreasing the catalyst potential to U_{WR}=-0.6 V causes a dramatic shift in selectivity. The selectivity to ethylene oxide drops to 0% and acetaldehyde becomes the dominant product with a selectivity of 55%. Note in Figure 4.41 that the presense of chlorinated hydrocarbon moderator ($C_2H_4Cl_2$), as also done in industry, stabilizes the selectivity to C_2H_4O to high values almost regardless of the applied potential. This is because Cl, acting as an electronegative classical promoter, counterbalances the decrease in Φ induced by the applied potential.

In the latter case[101] (Fig. 4.42) the Ag catalyst is supported on β''-Al_2O_3 and traces of $C_2H_4Cl_2$ "moderator" are added again to the gas phase.[101] Ethylene oxide and CO_2 are the only products. The figure shows the combined effect of the partial pressure of $C_2H_4Cl_2$ and of the catalyst potential on the selectivity to ethylene oxide. For U_{WR}=0 and -0.4 V the Na coverage is nil and 0.04 respectively. As shown in the figure there is an optimal combination of $U_{WR}(\theta_{Na})$ and $p_{C_2H_4Cl_2}$ leading to a selectivity to ethylene oxide of 88%. This is one of the highest values reported for the epoxidation of ethylene. Figures 4.18, 4.41 and 4.42 exemplify how *in situ* controlled promotion can be used for a systematic investigation of the role of promoters in technologically important systems.

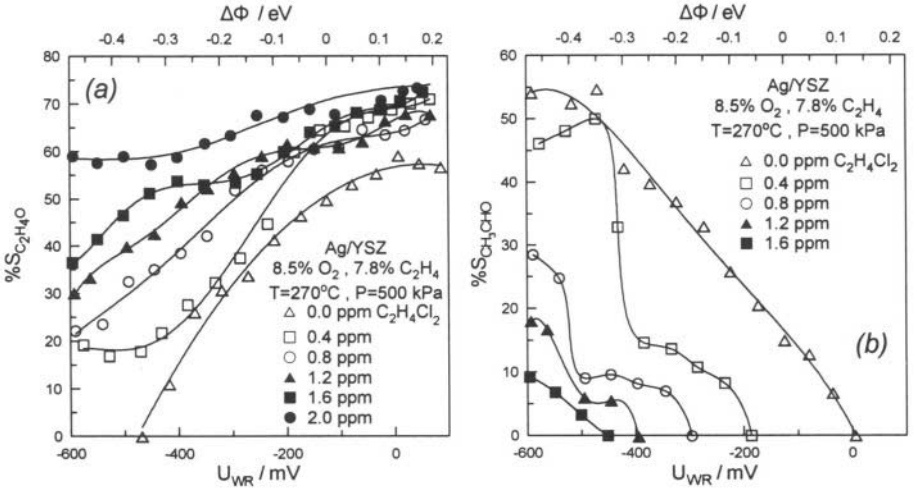

Figure 4.41. Effect of Ag/YSZ catalyst potential, work function and feed partial pressure of dichloroethane on the selectivity to ethylene oxide (a) and to acetaldehyde (b). T=270°C, P=500 kPa, 8.5% O_2, 7.8% C_2H_4.[77] Reprinted with permission from Academic Press.

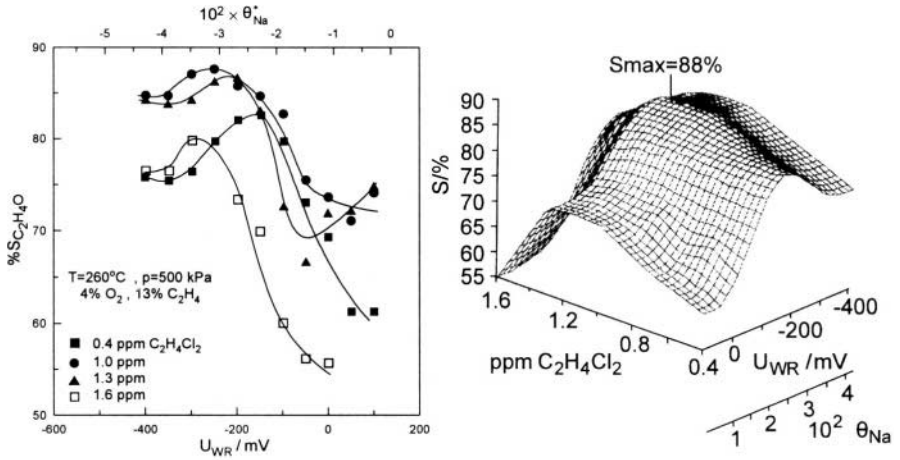

Figure 4.42. Ethylene epoxidation on Ag/β″-Al_2O_3.[101] Steady-state effect of catalyst potential on the selectivity to ethylene oxide at various levels of gas-phase dichloroethane (a) and 3-dimensional representation of the effect of dichloroethane concentration, catalyst potential and corresponding Na coverage on the selectivity to ethylene oxide (b).[101] Reprinted with permission from Academic Press.

4.5.9 Promotional Effects on Chemisorption

4.5.9.1 Experimental Results

As already noted the strength of chemisorptive bonds can be varied in situ via electrochemical promotion. This is the essence of the NEMCA effect. Following initial studies of oxygen chemisorption on Ag at atmospheric pressure, using isothermal titration, which showed that negative potentials causes up to a six-fold decrease in the rate of O_2 desorption,[11] temperature programmed desorption (TPD) was first used to investigate NEMCA.[29]

The power of electrochemistry to affect chemisorption on metals interfaced with solid electrolytes can be appreciated from figure 4.43[29] which shows oxygen temperature programmed desorption (TPD) spectra obtained upon electrochemically supplying O^{2-} to the Pt/YSZ catalyst surface during a galvanostatic transient (I=15μA) following previous exposure to gaseous O_2. The corresponding U_{WR} values are also indicated in the figure. The TPD spectrum labeled "0 s" corresponds to gaseous O_2 chemisorption. As well known from the surface science literature a single peak is obtained above room T, centered at ~730 K and corresponding to dissociatively chemisorbed atomic oxygen.

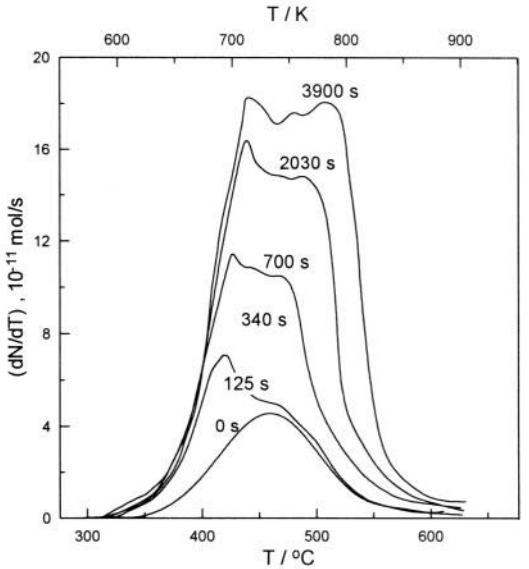

Figure 4.43. Thermal desorption spectra after gaseous oxygen adsorption on a Pt film deposited on YSZ at 673 K and an O_2 pressure of 4×10^{-6} Torr for 1800 s (7.2 kL) followed by electrochemical O^{2-} supply (I=+15 μA) for various time periods.[29,30] Reprinted from ref. 30 with permission from Academic Press.

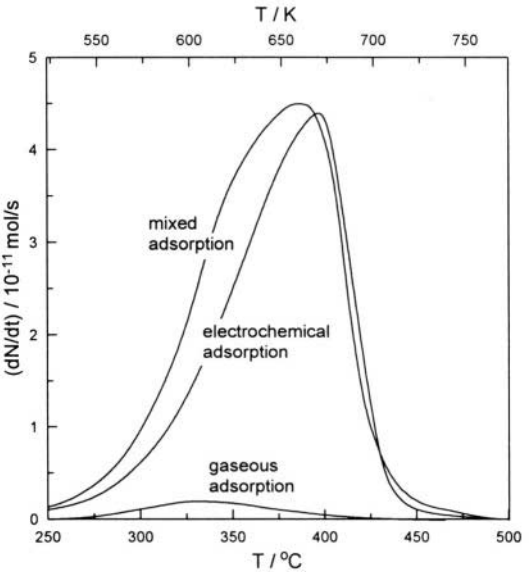

Figure 4.44. Comparison of the oxygen TPD spectra from Ag deposited on YSZ obtained with the three different modes of adsorption, gaseous, electrochemical and mixed, under the same conditions: T_{ads}=300°C, 5.4 kL of oxygen exposure (for gaseous and mixed adsorption), and 4.6×10^{-9} mol O of electrochemically supplied oxygen (for electrochemical and mixed adsorption), i.e. 5 μA for 180 s. (U_{WR}=+0.7 V, $\Delta\Phi$=+1.3 eV).[31] Reprinted with permission from Academic Press.

Upon electrochemically supplying O^{2-} onto the catalyst surface and thus increasing U_{WR} and Φ (Fig. 4.43) the oxygen TPD spectrum grows dramatically with the appearance of a weakly bonded state (peak desorption temperature, T_P, at ~680-700 K) and in addition of a strongly bonded one (T_P~780K) which develops at higher potentials over a time period $2FN_G/I$, i.e. the time required to form a monolayer of atomic oxygen on the Pt catalyst surface. What figure 4.43 and also 4.44 show conclusively it that:

1. Massive oxygen backspillover from the solid electrolyte onto the catalyst surface takes place under electrochemical promotion conditions.
2. Increasing catalyst potential and work function leads to a pronounced increase in total oxygen coverage (which approaches unity even at elevated temperatures) and causes the appearance of new chemisorption states. At least two such states are created on Pt/YSZ (Fig. 4.43): A strongly bonded one which, as discussed in Chapter 5, acts as a sacrificial promoter during catalytic oxidations, and a weakly bonded one which is highly reactive and causes the observed dramatic increase in catalytic rate.

These important conclusions are not limited to Pt/YSZ only. Similar is the behaviour of Ag/YSZ[31,119] (Fig. 4.44) and Au/YSZ.[119] In the last case actually gaseous oxygen adsorption is negligible.[119]

When all the oxygen is supplied on the metal (Pt, Ag) catalyst electrochemically, i.e. without previous gaseous adsorption, then at relatively low coverages only the weakly bonded highly reactive oxygen chemisorption state forms (Fig. 4.45). The T_P of this state depends significantly on the potential U^*_{WR} applied to the catalyst during the electrochemical O^{2-} supply (Fig. 4.45 and 4.46, inset) which is very close to U_{WR} during the TPD run (Fig. 4.45, top). Thus by varying the electrochemical adsorption temperature and the adsorption time one can obtain TPD spectra of oxygen at near constant coverage which, nevertheless correspond to different potentials and work functions on the catalyst surface (Figs. 4.45 and 4.46). Consequently one can study the dependence of T_P on U_{WR} (Fig. 4.45, 4.46 inset). Furthermore by varying the heating rate β (K/s) during the TPD runs and using the modified Redhead equation of Falconer and Madix[118]:

$$\ln(\beta/T_p)^2 = \ln(R\nu\theta_0^{n-1}/E_d) - (E_d/R)(1/T_p) \qquad (2.22)$$

where ν is the preexponential factor and θ_0 is the initial coverage, one can obtain directly the activation energy of oxygen desorption, E_d, corresponding to diffent U_{WR} values. In Chapter 5 we will see several such Redhead plots, i.e., $\ln(\beta/T_P^2)$ vs T_P^{-1} obtained at different U_{WR} values in a very detailed investigation of O_2 chemisorption on Pt/YSZ,[30] but here we can see the final results of this investigation (Fig. 4.47): E_d, which for nonactivated oxygen

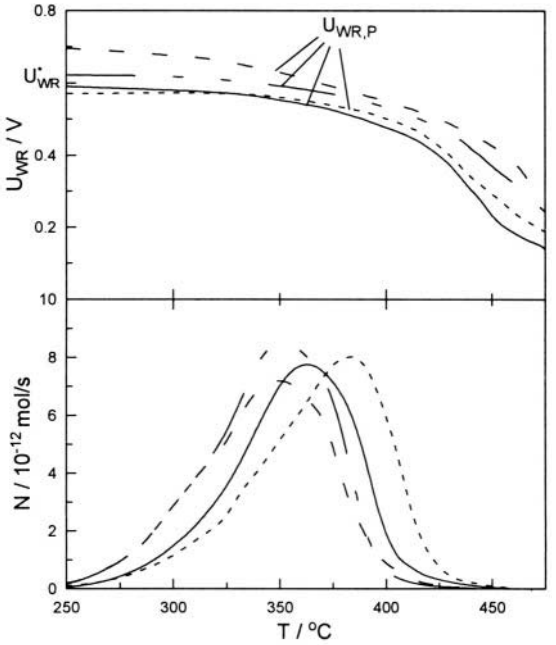

Figure 4.45. Thermal desorption spectra (bottom) and corresponding catalyst potential variation (top) after electrochemical O^{2-} supply to Ag/YSZ at 260-320°C at various initial potentials U^*_{WR}. Each curve corresponds to different adsorption temperature and current, thus different values of U^*_{WR}, in order to achieve nearly constant initial oxygen coverage.[31] Reprinted with permission from Academic Press.

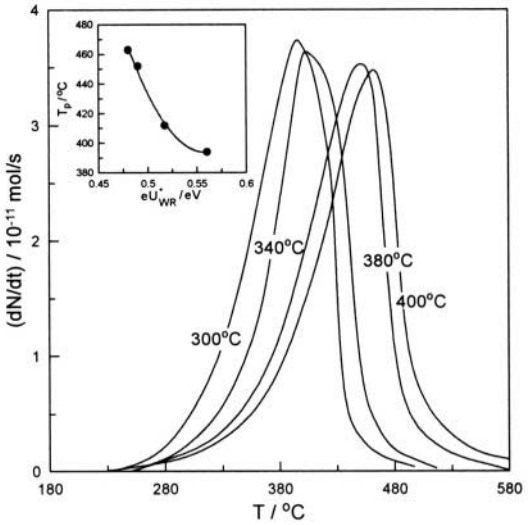

Figure 4.46. Thermal desorption spectra after electrochemical O^{2-} supply to Ag/YSZ through the electrolyte for 10 min. Each curve corresponds to different adsorption temperature and current in order to achieve nearly constant initial coverage. Desorption was performed with linear heating rate, β=1 K/s (Inset) Effect of potential on peak temperature.[31] Reprinted with permission from Academic Press.

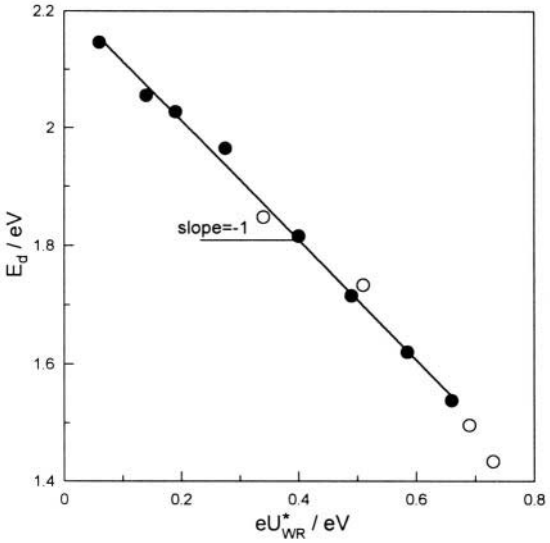

Figure 4.47. Effect of catalyst potential on the desorption activation energy of O_2 from Pt/YSZ calculated from the modified Redhead analysis (●) and from the initial slope of the TPD spectra (○).[30] Reprinted with permission from Academic Press.

chemisorption also equals the isosteric (constant coverage) *heat of adsorption* of O on the Pt surface, decreases *significantly,* and in fact *linearly,* with U^*_{WR} and Φ and in fact with a slope of–1!

As discussed in detail in Chapter 5 this is not a coincidence. Similar is the behaviour of oxygen chemisorption on Ag[31,119] and on Au[119] and the E_d vs Φ slopes are –1 and –4 respectively. Furthermore such a linear decrease in E_d with Φ is in agreement with rigorous cluster quantum mechanical calculations.[120,121]

It is important to notice that the observed linear decrease in E_d with Φ with a slope of–1 in the case of oxygen chemisorption on Pt is in excellent agreement with the observed linear decrease in activation energy, E, with Φ in the Pt catalyzed oxidation of C_2H_4 and CH_4 (figs. 4.28 and 4.35). In fact in the case of C_2H_4 oxidation where the temperature range of the investigation was similar to that of the TPD studies the E_d vs Φ slope is –1.

This is an important result and shows that the dramatic decrease in catalytic activation energy, E_A, upon increasing Φ is due to the decrease in E_d and concomitant weakening of the Pt=O chemisorptive bond upon increasing U_{WR} and Φ.

But why linearly and why with a slope of–1, or something thereabout, the reader may righteously ask. In anticipation of the quantum mechanical treatment in Chapter 5 we can briefly discuss here a simple electrostatic model which fully accounts for the observed behaviour. After all, as the detailed quantum mechanical treatment has shown, direct electrostatic

"through the vacuum" forces between coadsorbates account for more than 80% of the observed decrease in E_d with Φ.

4.5.9.2 Electrostatic Interactions of Adsorbates in a Double Layer

We can consider now the adsorbates examined in Fig. 4.20 in presence of the double layer formed by the backspillover ions on the catalyst surface (Fig. 4.48). The double layer will be assumed homogeneous with a thickness d and a uniform field strength $\tilde{E}$ which can be computed from:

$$\tilde{E} = (\Delta\Phi/ed)\,\tilde{n} \tag{4.54}$$

where $\Delta\Phi(=\Phi-\Phi_o)$ is the work function difference between that of the actual surface and that of the surface at its point of zero charge (pzc) where $\Phi=\Phi_o$, and $\tilde{n}$ is the unit vector normal to the surface and pointing to the vacuum.

It is clear that the change ΔH in the potential energy, and thus internal energy and enthalpy of the adsorbed molecule, j, with dipole moment $\tilde{P}_j$ due to the presence of the field is:

$$\Delta H_j = \tilde{E}\cdot\tilde{P}_j \tag{4.55}$$

thus

$$\Delta H_j = \Delta\Phi\left(\frac{q_j}{e}\right)\left(\frac{\ell}{2d}\right)\cos\omega \tag{4.56}$$

An increase in the enthalpy, H, of the adsorbate causes an equal decrease in its activation energy for desorption, E_d, i.e. $\Delta H = -\Delta E_d$, thus:

$$\Delta E_{d,j} = -\,\Delta\Phi\left(\frac{q_j}{e}\right)\left(\frac{\ell}{2d}\right)\cos\omega \tag{4.57}$$

Thus for the case of O chemisorbed on Pt one may reasonably assume $\cos\omega=1$ and $\ell=d$ to obtain:

$$\Delta E_{d,j} = -\left(\frac{n_j}{2e}\right)\Delta\Phi; \qquad \Delta E_{d,j} = \frac{\lambda_j}{2}\Delta\Phi \tag{4.58}$$

where $\lambda_j(=n_j/e)$ is the partial charge transfer parameter of adsorbate j, which is positive for an electron donor and negative for an electron acceptor.

Equation (4.58) is in excellent agreement with experiment (Fig. 4.47) and allows one to speculate that the partial change transfer λ_O is near –2 for the case of O chemisorption on Pt. In fact equation 4.58 can even account for

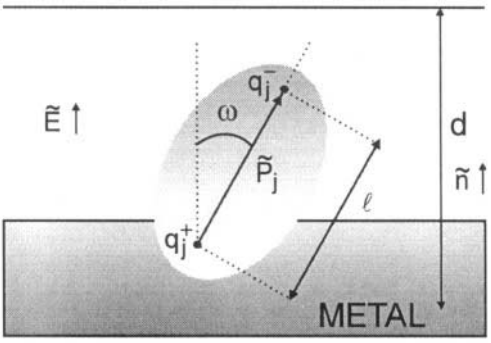

Figure 4.48. Schematic of an adsorbed molecule, modeled as a dipole, in the electric field of the metal-gas effective double layer.

the decrease in the ΔE vs Φ slope from (-1 to –4) as one goes from C_2H_4 oxidation on Pt (T~600-700 K) to CH_4 oxidation on Pt (T~800-900 K) (Fig. 4.28) where the effective thickness d of the double layer can be reasonably assumed to be smaller. The same applies for the decrease in the ΔE_d vs Φ plots upon going from Pt and Ag (slope≈-1) to Au (slope≈-4), to be discussed in Chapter 5 (Figure 5.26), where again d can be reasonably expected to be smaller on Au than on Pt or Ag due to the sparse O^{2-} adsorption layer on Au.[122]

As already noted in Chapter 2 (eq. 2.23), equations (4.56) and (4.58) are in good qualitative agreement with the classical promotion literature as well. This type of equation was first discussed as an empirical observation by Boudart many year ago.[123] Today we see that both experiment and theory support it.

4.5.10 "Permanent NEMCA"

One of the most interesting and potentially important from a practical viewpoint aspect of electrochemical promotion is the "permanent NEMCA" effect first discovered and studied by Comninellis and coworkers at Lausanne.

A typical example is shown in figure 4.49 which depicts a galvanostatic NEMCA transient during C_2H_4 oxidation on IrO_2.[22,87,88] The authors, in addition to monitoring the rate, r, and the catalyst potential U_{WR}, were also in situ moni-toring via a Kelvin probe the change, $\Delta\Phi$, in the IrO_2 surface work function which at steady-state nicely conforms to the fundamental equation 4.30.

Upon positive current application the rate of C_2H_4 oxidation increases by a factor of 13 (ρ=14) with a Λ value of the order of 100. The important aspect of the figure is that upon current interruption neither the rate nor Φ return to their initial open- circuit values (Fig. 4.49). There is a permanent

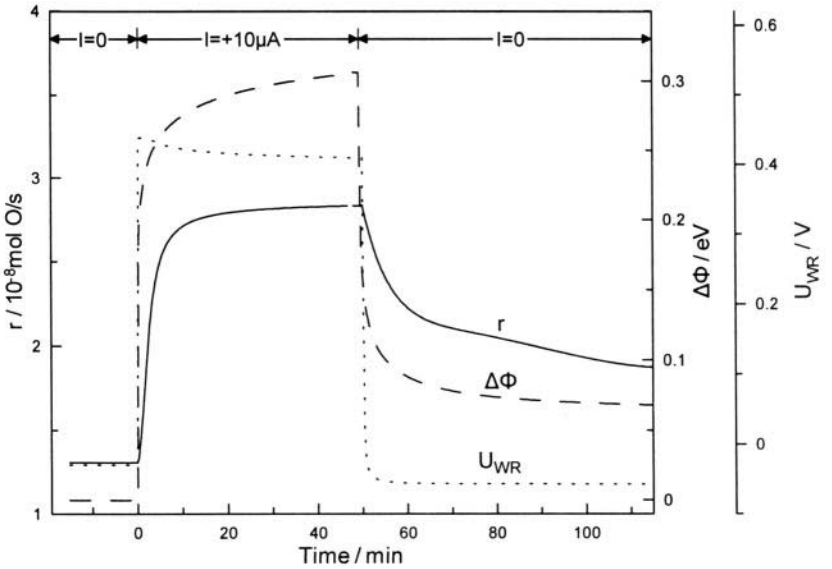

Figure 4.49. Transient effect of constant applied current (I=+10 μA) on the rate (r) of C_2H_4 oxidation on IrO_2/YSZ, on catalyst work function (ΔΦ) and on catalyst potential (U_{WR}). Conditions: T=380°C, p_{O_2} =15 kPa and $p_{C_2H_4}$ =0.05 kPa.[88] Reprinted with permission of The Electrochemical Society.

rate enhancement, accompanied by a permanent change in Φ. Comninellis and coworkers[87,88] defined a "permanent" rate enhancement ratio γ from:

$$\gamma = r_{per}/r_0 \tag{4.59}$$

which in the case of Fig. 4.49 equals 3.

Other examples of permanent NEMCA behaviour are shown in Fig. 4.50 for the case of C_2H_4 oxidation on IrO_2-TiO_2 mixtures[124] deposited on YSZ, the first NEMCA study utilizing an oxide catalyst (IrO_2) and in fact in contact with a mixed electronic-ionic conductor (TiO_2). As we shall see in Chapter 11 these measurement of Nicole[124] provided the first basis for establishing the mechanistic equivalence of NEMCA and metal-support interactions.[125]

Permanent NEMCA behaviour has been also observed in the case of NO reduction by propene[70,71] or CO[71] in presence of O_2 on Rh/YSZ, a system of great technological interest (Figs. 4.51 and 4.52). In the former case[70] (C_3H_6, T=380°C) ρ is 52 and γ is 6 (Fig. 4.51) but in the latter case (CO, T=270°C) ρ is 17 but γ is near 14. There is a very pronounced permanent enhancement of the Rh catalyst activity and selectivity. This could lead to practical applications utilizing NEMCA during catalyst preparation.

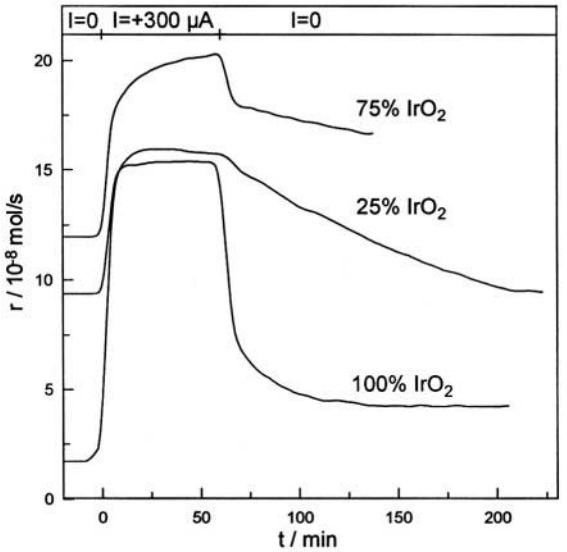

Figure 4.50. Transient effect of constant applied current (I=+300 μA) on the rate of C_2H_4 oxidation on IrO_2 and on 75mol% IrO_2 - 25%TiO_2 and 25% IrO_2 - 75%TiO_2 composite catalysts deposited on YSZ. Note the decrease in ρ upon increasing the TiO_2 content and the appearance of permanent NEMCA in all cases.[124]

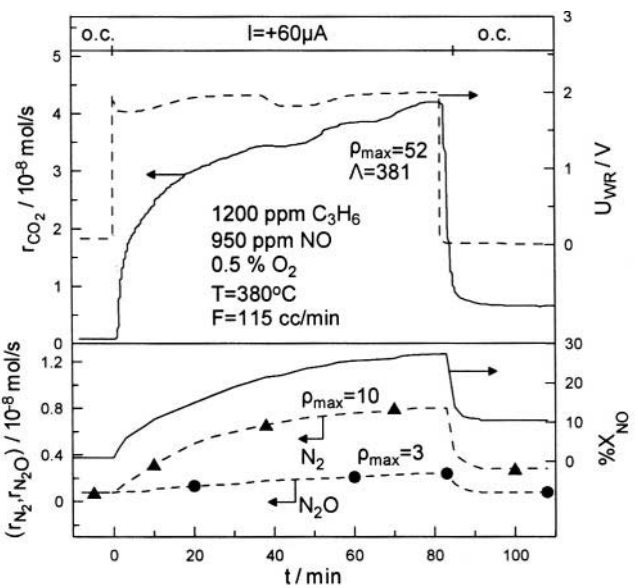

Figure 4.51. Transient effect of a constant applied current on the rates of CO_2, N_2 and N_2O production, on NO conversion (X_{NO}) and on catalyst potential (U_{WR}) during NO reduction by propene in presence of gaseous O_2 on Rh/YSZ.[70] Reprinted with permission from Elsevier Science.

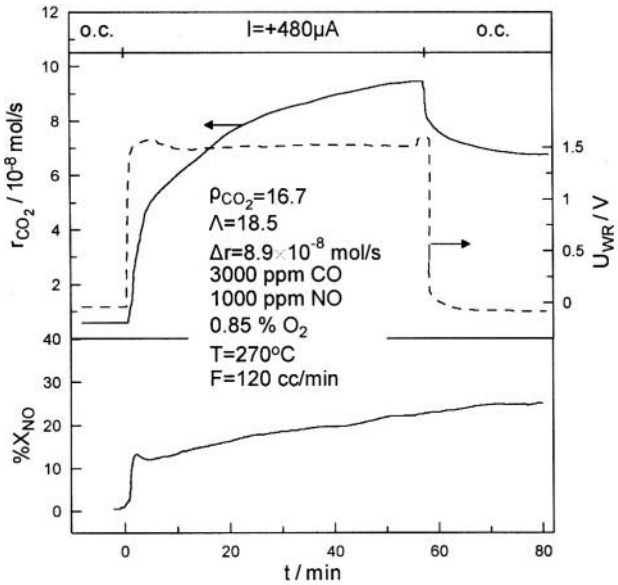

Figure 4.52. Transient effect of a constant applied current on the reaction rate of $CO/NO/O_2$ reaction and on the NO conversion on Rh/YSZ[71]; GHSV=25000 h^{-1}.[71] Reprinted with permission from the Institute for Ionics.

What is the cause of permanent NEMCA? Comninellis and coworkers have found strong evidence that it is due to the electrochemical creation and stabilization of a promoting superoxide on the catalyst surface. This is supported by the fact that permanent NEMCA appears to be more frequent with metal oxides where the metal has multiple valence states, thus the ability to form several different oxides. It is also supported by the observation that the initial catalyst activity and work function can be restored only after prolonged catalyst exposure to the reacting gas mixture.[70,71] It is possible that the initial state corresponds to surface Rh_2O_3,[50] the high activity NEMCA state corresponds to O^{2-} -decorated reduced Rh[50] and the permanent NEMCA state corresponds to O^{2-} decorated surface Rh_2O_3. This interesting subject is certainly worth further investigation.

4.6 PREDICTION OF THE MAGNITUDE OF THE FARADAIC EFFICIENCY Λ

One of the first steps in understanding electrochemical promotion was the observation[1] that the absolute value $|\Lambda|$ of the Faradaic efficiency Λ of different catalytic reactions could be approximated by (Fig. 4.23)

$$|\Lambda| \approx 2Fr_0/I_0 \tag{4.20}$$

It was also quickly observed[1] that for a given catalytic reaction, Λ decreases with increasing temperature (Fig. 4.53) and approaches unity at temperatures where the reactants do not chemisorb any more on the catalyst surface. The latter (Fig. 4.53, C_2H_4 oxidation) is easy to understand in view of the oxygen TPD spectra of Figures 4.43, 4.45 and 4.46: Above 650°C there is practically no oxygen, chemisorbed or backspillover, on the catalyst electrode surface, thus no chemisorbed double layer and thus no electrochemical promotion. Simple mass balance considerations dictate that at this limit (no gaseous O_2 adsorption) only electrochemically supplied oxygen will react, thus Λ=1 as experimentally observed (Fig. 4.53). Equation 4.20 is also easy to understand in view of the very commonly observedcatalytic rate dependence on potential and work function (Eq. 4.51):

$$\ln(r/r_0) = \alpha(\Phi-\Phi^*)/k_bT \tag{4.49}$$

taken in conjunction the high field approximation of the Butler-Volmer equation:

$$\ln(I/I_0) = \alpha_A e\Delta U_{WR}/k_bT \tag{4.13}$$

and the potential-work function equivalence of solid state electrochemistry (Eq. 4.30):

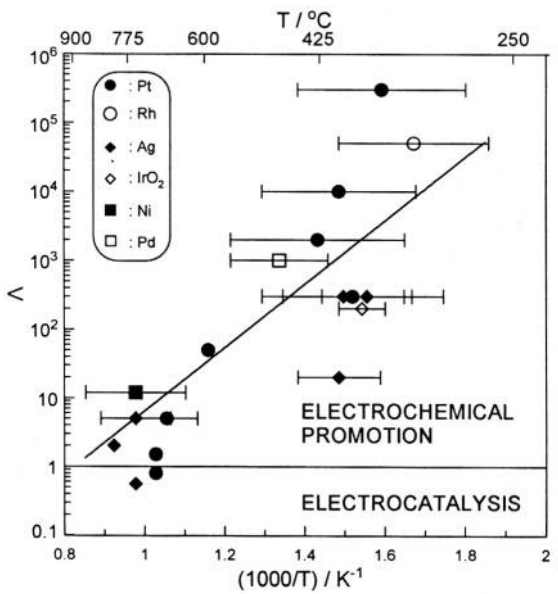

Figure 4.53. Effect of temperature on the faradaic efficiency, Λ, values measured in electrochemical promotion (NEMCA) studies of C_2H_4 oxidation on various metals.[30] Reprinted with permission from Academic Press.

$$\Delta\Phi = e\Delta U_{WR} \tag{4.30}$$

which combined lead to the dimensionless equation:

$$\frac{2Fr}{I} = \frac{2Fr_0}{I_0}\exp\frac{(\alpha-\alpha_A)\Delta\Phi}{k_bT} \tag{4.60}$$

Thus if $\rho \gg 1$, so that $\Delta r \approx r$ the left hand side (1hs) of eq. (4.60) is Λ and if $\alpha \approx \alpha_A$, as frequently observed in practice,[1] then equation (4.60) reduces to the experimental equation (4.20) (Fig. 4.23). The absolute magnitude sign (| |) of Eq. 4.20 is still necessary since during the first years of electrochemical promotion research, and until very recently[115,116] no safe predictions could be made about the electrophobicity ($\Lambda>1$) or electrophilicity ($\Lambda<-1$) of a catalytic reaction. Now the situation is changing, as will be surveyed in chapter 6 where, for the first time, rigorous promotional rules are presented. Nevertheless one should keep in mind that equation (4.20), despite its frequently impressive success, is only an approximation which can only serve to predict the order of magnitude of Λ for different catalytic systems provided the open-circuit catalytic rate, r_0, and the exchange current I_0 are known.

4.7 SYNOPSIS OF THE PHENOMENOLOGY: REACTIONS STUDIED SO FAR

In this chapter we have surveyed the key phenomenological aspects of electrochemical promotion.

These are:

a. The rate enhancement with current and potential which is described by the parameters Λ (Faradaic efficiency), ρ (rate enhancement ratio), PI_j (promotion index of the promoting ion) and, for the case of permanent NEMCA, γ (permanent rate enhancement ratio).
b. The selectivity modification with current and potential
c. The work function variation with potential
d. The activation energy modification with potential and work function.
e. The chemisorptive bond strength variation with potential and work function
f. The local electrophobicity or electrophilicity of different catalytic reactions, which lead to the four types of global r vs Φ behaviour (i.e. purely electrophobic, purely electrophilic, volcano and inverted volcano).

These features are common regardless of the type of solid electrolyte and promoting ion used. It is also in general noteworthy that the electrophobicity or electrophilicity of a reaction studied under the same experimental conditions sometimes changes upon changing the solid electrolyte.

Nevertheless there are some reactions which never change. Thus NO reduction on noble metals, a very important catalytic reaction, is in the vast majority of cases electrophilic, regardless of the type of solid electrolyte used (YSZ or β''-Al_2O_3). And practically all oxidations are electrophobic under fuel lean conditions, regardless of the type of solid electrolyte used (YSZ, β''-Al_2O_3, proton conductors, even alkaline aqueous solutions).

Table 4.1 summarizes the catalytic systems studied so far in terms of the solid electrolyte used and shows the measured Λ, ρ and PI_j values.

Table 4.2 lists the same catalytic systems but now grouped in terms of different reaction types (oxidations, hydrogenations, reductions and others). In this table and in subsequent chapters the subscript "D" denotes and electron donor reactant while the subscript "A" denotes an electron acceptor reactant. The table also lists the temperature and gas composition range of each investigation in terms of the parameter p_A/p_D which as subsequently shown plays an important role on the observed r vs Φ global behaviour. Table 4.3 is the same as Table 4.2 but also provides additional information regarding the open-circuit catalytic kinetics, whenever available. Table 4.3 is useful for extracting the promotional rules discussed Chapter 6.

In Chapters 8 to 10 we will have the opportunity to examine in some more detail the specific characteristics of each catalytic system presented in Tables 4.1, 4.2 and 4.3.

REFERENCES

1. C.G. Vayenas, S. Bebelis, I.V. Yentekakis, and H.-G. Lintz, Non-Faradaic Electrochemical Modification of Catalytic Activity: A Status Report (Review Paper), *Catalysis Today* **11**(3), 303-442 (1992).
2. I.V. Yentekakis, and S. Bebelis, Study of the NEMCA effect in a single-pellet catalytic reactor, *J. Catal.* **137**, 278-283 (1992).
3. C. Cavalca, G. Larsen, C.G. Vayenas, and G. Haller, Electrochemical Modification of CH_3OH oxidation selectivity and activity on a Pt single-pellet catalytic reactor, *J. Phys. Chem.* **97**, 6115-6119 (1993).
4. S. Bebelis, and C.G. Vayenas, Non-Faradaic Electrochemical Modification of Catalytic Activity: 1. The case of Ethylene Oxidation on Pt, *J. Catal.* **118**, 125-146 (1989).
5. D.Y. Wang, and A.S. Nowick, Cathodic and anodic polarization phenomena at platinum electrodes with doped CeO_2 as electrolyte. I. Steady-state overpotential, *J. Electrochem. Soc.* **126**(7), 1155-1165 (1979).
6. D.Y. Wang, and A.S. Nowick, Cathodic and anodic polarization phenomena at platinum electrodes with doped CeO_2 as electrolyte. II. Transient overpotential and A-C Impedance, *J. Electrochem. Soc.* **126**(7), 1166-1172 (1979).
7. D.Y. Wang, and A.S. Nowick, Diffusion-controlled polarization of Pt, Ag, and Au electrodes with doped ceria electrolyte, *J. Electrochem. Soc.* **128**(1), 55-63 (1981).
8. C.G. Vayenas, A. loannides, and S. Bebelis, Solid Electrolyte Cyclic Voltammetry for in situ Investigation of Catalyst Surfaces, *J. Catal.* **129**, 67-87 (1991).
9. P.J. Gellings, and H.J.M. Bouwmeester, eds., *The CRCHandbook of Solid State Electrochemistry,* CRC Press, Boca Raton (1997).

10. J.K. Hong, I.-H. Oh, S.-A. Hong, and W.Y. Lee, Electrochemical Oxidation of Methanol over a Silver Electrode Deposited on Yttria-Stabilized Zirconia Electrolyte, *J. Catal.* **163**, 95-105 (1996).
11. S. Bebelis, and C.G. Vayenas, Non-Faradaic Electrochemical Modification of Catalytic Activity: 5. Oxygen Chemisorption on Silver, *J. Catal.* **138**, 570-587 (1992).
12. S. Bebelis, and C.G. Vayenas, Non-Faradaic Electrochemical Modification of Catalytic Activity: 6. The epoxidation of Ethylene on Ag/ZrO_2(8mol%)Y_2O_3, *J. Catal.* **138**, 588-610 (1992).
13. E.J.L. Schouler, and M. Kleitz, Electrocatalysis and inductive effects at the gas, Pt/Stabilized Zirconia Interface, *J. Electrochem. Soc.* **134**(5), 1045-1050 (1987).
14. A.D. Frantzis, S. Bebelis, and C.G. Vayenas, Electrochemical promotion (NEMCA) of CH_4 and C_2H_4 oxidation on Pd/YSZ and investigation of the origin of NEMCA via AC impedance spectroscopy, *Solid State Ionics* **136-137**, 863 (2000).
15. C.G. Vayenas, On the work function of the gas exposed electrode surfaces in solid state electrochemistry, *J. Electroanal. Chem.* **486**, 85-90 (2000).
16. C.G. Vayenas, and D. Tsiplakides, On the work function of the gas-exposed electrode surfaces in solid state electrolyte cells, *Surf. Sci.* **467**, 23-34 (2000).
17. D. Tsiplakides, and C.G. Vayenas, Electrode work function and absolute potential scale in solid state electrochemistry. *J. Electrochem. Soc.* **148**(5), E189-E202 (2001).
18. I. Riess, and C.G. Vayenas, Fermi level and potential distribution in solid electrolyte cells with and without ion spillover, *Solid State Ionics,* in press (2001).
19. C.G. Vayenas, M.M. Jaksic, S. Bebelis, and S.G. Neophytides, The Electrochemical Activation of Catalysis, in *Modern Aspects of Electrochemistry,* J.O.M. Bockris, B.E. Conway, and R.E. White, eds., Kluwer Academic/Plenum Publishers, New York (1996), pp. 57-202.
20. B.C.H. Steele. Dense Ceramic ion conducting membranes in *Oxygen ion and mixed conductors and their technological applications,* (1997) Erice, Italy: Kluwer.
21. H.-H. Hildenbrand, and H.-G. Lintz, Solid electrolyte potentiometry aided study of the influence of promotors on the phase transitions in copper-oxide catalysts under working conditions, *Catalysis Today* **9**, 153-160 (1991).
22. J. Nicole, and C. Comninellis, Electrochemical promotion of IrO_2 catalyst activity for the gas phase combustion of ethylene, *J. Appl. Electrochem.* **28**, 223-226 (1998).
23. S. Wodiunig, and C. Comninellis, Electrochemical Promotion of RuO_2 Catalysts for the Gas Phase Combustion of C_2H_4, *Journal of the European Ceramic Society* **19**, 931 -934 (1999).
24. A. Kaloyannis, and C.G. Vayenas, Non-Faradaic Electrochemical Modification of Catalytic Activity. 11. Ethane Oxidation on Pt, *J. Catal.* **171**, 148-159 (1997).
25. A. Kaloyannis, and C.G. Vayenas, Non-Faradaic electrochemical modification of catalytic activity. 12: Propylene oxidation on Pt, *J. Catal.* **182**, 37-47 (1999).
26. M. Stoukides, and C.G. Vayenas, Solid Electrolyte Aided Study of the Oxidation of Ethylene Oxide on Silver, *J. Catal.* **64**, 18-28 (1980).
27. M. Stoukides, and C.G. Vayenas, Solid Electrolyte-Aided Study of the Ethylene Oxidation on Polycrystalline Silver, *J. Catal.* **69**, 18-31 (1981).
28. S. Ladas, S. Kennou, S. Bebelis, and C.G. Vayenas, Origin of Non-Faradaic Electrochemical Modification of Catalytic Activity, *J. Phys. Chem.* **97**, 8845-8847 (1993).
29. S.G. Neophytides, and C.G. Vayenas, TPD and Cyclic Voltammetric Investigation of the Origin of Electrochemical Promotion in Catalysis, *J. Phys. Chem.* **99**, 17063-17067 (1995).

30. S. Neophytides, D. Tsiplakides, and C.G. Vayenas, Temperature-Programmed Desorption of Oxygen from Pt-films Interfaced with Y_2O_3-Doped ZrO_2, *J. Catal.* **178,** 414-428 (1998).
31. D. Tsiplakides, and C.G. Vayenas, Temperature Programmed Desorption of Oxygen from Ag films interfaced with Y_2O_3-doped ZrO_2, *J. Catal.* **185**, 237-251 (1999).
32. I. Harkness, and R.M. Lambert, Electrochemical Promotion of the NO + Ethylene Reaction over Platinum, *J. Catal.* **152**, 211-214 (1995).
33. M. Makri, C.G. Vayenas, S. Bebelis, K.H. Besocke, and C. Cavalca, Atomic resolution STM imaging of Electrochemically Controlled Reversible Promoter Dosing of Catalysts, *Surf. Sci.* **369**, 351-359 (1996).
34. C.G. Vayenas, B.Lee, and J. Michaels, Kinetics, Limit Cycles and Mechanism of Ethylene Oxidation on Pt, *J. Catal.* **66**, 36-48 (1980).
35. C.G. Vayenas, C.Georgakis, J. Michaels, and J. Tormo, The role of PtOx in the isothermal rate and oxygen activity oscillations of the Ethylene Oxidation on Pt, *J. Catal.* **67**, 348-361 (1981).
36. C.G. Vayenas, S. Bebelis, and S. Despotopoulou, Non-Faradaic Electrochemical Modification of Catalytic Activity: 4. The use of β''-Al_2O_3 as the solid electrolyte, *J. Catal.* **128**,415-435 (1991).
37. J. Tafel, in Z. *Phys. Chem. (Leipzig),* (1905), p. 641.
38. J.A.V. Butler, Studies in heterogeneous equilibria. Part II: The kinetic interpretation of the Nernst theory of electromotive force, *Transactions of the Faraday Society* **19**, 729-733 (1924).
39. T. Erdey-Gruz, and M. Volmer, Zur Theorie der Wasserstoffüberspannung, in Z. *Phys. Chem. (Leipzig),* (1930), p. 203.
40. J.O' M. Bockris, and A.K.N. Reddy, *Modern Electrochemistry,* Plenum Press, New York (1970), pp. 1-5.
41. J.O' M. Bockris, and S.U.M. Khan, *Surface Electrochemistry: A Molecular Level Approach,* Plenum Press, New York (1993).
42. J. Newman, in *Electrochemical Systems,* Prentice Hall (1973).
43. M. Manton, *PhD Thesis,* MIT (1986).
44. C.G. Vayenas, and J. Michaels, On the Stability Limit of Surface Platinum Oxide and its role in the oscillatory behavior of Platinum Catalyzed Oxidations, *Surf. Sci.* **120**, L405-L408 (1982).
45. M. Peuckert, and H.P. Bonzel, Characterization of oxidized platinum surfaces by X-ray photoelectron spectroscopy, *Surf. Sci.* **145**, 239-259 (1984).
46. M. Peuckert, and H. Ibach, Vibrational spectra of an oxidized platinum electrode, *Surf. Sci.* **136**, 319-326(1984).
47. J. Yi, A. Kaloyannis, and C.G. Vayenas, High Temperature cyclic voltammetry of Pt electrodes in solid electrolyte cells, *Electrochim. Acta* **38**(17), 2533-2539 (1993).
48. M. Boudart, and G. Djega-Mariadassou, *Kinetics of Heterogeneous Catalytic Reactions,* Princeton Univ. Press, Princeton, NJ (1984).
49. M. Stoukides, and C.G. Vayenas, The effect of Electrochemical Oxygen Pumping on the Rate and Selectivity of Ethylene Oxidation on Polycrystalline Silver, *J. Catal.* **70**, 137-146 (1981).
50. C. Pliangos, I.V. Yentekakis, X.E. Verykios, and C.G. Vayenas, Non-Faradaic Electrochemical Modification of Catalytic Activity: 8. Rh-catalyzed C_2H_4 oxidation, *J. Catal.* **154**, 124-136 (1995).
51. I.V. Yentekakis, G. Moggridge, C.G. Vayenas, and R.M. Lambert, In situ controlled promotion of catalyst surfaces via NEMCA: The effect of Na on the Pt-catalyzed CO oxidation, *J. Catal.* **146**, 292-305 (1994).

52. O.A. Mar'ina, I.V. Yentekakis, C.G. Vayenas, A. Palermo, and R.M. Lambert, In situ controlled Promotion of Catalyst Surfaces via NEMCA: The effect of Na on the Pt-catalyzed NO Reduction by H_2, *J. Catal.* **166**, 218-228 (1997).
53. H.L. Skriver, and N.M. Rosengaard, Ab initio work function of elemental metals, *Physical Review B* **45**(16), 9410-9412 (1992).
54. C.G. Vayenas, S. Bebelis, and S. Ladas, Dependence of Catalytic Rates on Catalyst Work Function, *Nature* **343**, 625-627 (1990).
55. S. Ladas, S. Bebelis, and C.G. Vayenas, Work Function Measurements on Catalyst Films subject to in-situ Electrochemical Promotion, *Surf. Sci.* **251/252**, 1062-1068 (1991).
56. P.M. Gundry, and F.C. Tompkins, in *Experimental Methods in Catalyst Research,* R.B.Anderson, ed. Academic Press, New York (1968), pp. 100-168.
57. W. Zipprich, H.-D. Wiemhöfer, U. Vöhrer, and W. Göpel, In-situ Photoelectron-Spectroscopy of Oxygen Electrodes on Stabilized Zirconia, *Ber. Buns. Phys. Chem.* **99**, 1406-1413 (1995).
58. J. Poppe, A. Schaak, J. Janek, and R. Imbihl, Electrochemically Induced Surface Changes on Microstructured Pt Films on a solid YSZ Electrolyte, *Ber. Buns. Phys. Chem.* **102**, 1019-1022 (1998).
59. S. Bebelis, M. Makri, A. Buekenhoudt, J. Luyten, S. Brosda, P. Petrolekas, C. Pliangos, and C.G. Vayenas, Electrochemical activation of catalytic reactions using anionic, cationic and mixed conductors, *Solid State Ionics* **129**, 33-46 (2000).
60. C.G. Vayenas, S. Bebelis, and S. Neophytides, Non-Faradaic Electrochemical Modification of Catalytic Activity, J. *Phys. Chem.* **92**, 5083-5085 (1988).
61. P. Tsiakaras, and C.G. Vayenas, Non-Faradaic Electrochemical Modification of Catalytic Activity: 7. The oxidation of CH_4 on Pt, *J. Catal.* **140**, 53-70 (1993).
62. C.G. Vayenas, S. Bebelis, I.V. Yentekakis, P. Tsiakaras, and H. Karasali, Non-Faradaic Electrochemical Modification of Catalytic Activity on Pt Metals, *Platinum Metals Review* **34**(3), 122-130 (1990).
63. I.V. Yentekakis, and C.G. Vayenas, The Effect of Electrochemical O^{2-} Pumping on the Steady State and Oscillatory Behavior of CO oxidation on Polycrystalline Pt, *J. Catal.* **111**, 170-188 (1988).
64. H. Karasali, and C.G. Vayenas, NEMCA: The Oxidation of CO on Pt, *Materials Science Forum* **76**, 171-174 (1991).
65. C.G. Vayenas, and S. Neophytides, Non-Faradaic Electrochemical Modification of Catalytic Activity: 3. The Case of Methanol Oxidation on Pt, *J. Catal.* **127**, 645-664 (1991).
66. C.G. Vayenas, and S. Neophytides, Electrochemical Activation of Catalysis: In situ controlled promotion of catalyst surfaces, in *Catalysis-Special periodical Report,* Royal Society of Chemistry, Cambridge (1996), pp. 199-253.
67. M. Marwood, A. Kaloyannis, and C.G. Vayenas, Electrochemical Promotion of the NO reduction by C_2H_4 on Pt/YSZ and by CO on Pd/YSZ, *Ionics* **2**, 302-311 (1996).
68. C.G. Vayenas, and I.V. Yentekakis, Electrochemical Modification of Catalytic Activity, in *Handbook of Catalysis,* G. ErtI, H. Knötzinger, and J. Weitcamp, eds., VCH Publishers, Weinheim (1997), pp. 1310-1338.
69. C.G. Vayenas, and S. Bebelis, Electrochemical Promotion of heterogeneous catalysis, *Catalysis Today* **51**, 581-594 (1999).
70. C. Pliangos, C. Raptis, T. Badas, and C.G. Vayenas, Electrochemical promotion of NO reduction by C_3H_6 on Rh/YSZ catalyst-electrodes, *Solid State Ionics* **136/137**, 767-773 (2000).

71. C. Pliangos, C. Raptis, T. Badas, and C.G. Vayenas, Electrochemical Promotion of NO Reduction by C_3H_6 and CO on Rh/YSZ Catalyst - Electrodes, *Ionics* **6**, 119-126 (2000).
72. K. Yiokari, and S. Bebelis, In situ controlled electrochemical promotion of catalyst surfaces: Pd-catalysed ethylene oxidation, *J. Appl. Electrochem.* **30**, 1277-1283 (2000).
73. H. Alqahtany, P.M. Chiang, P. Eng, M. Stoukides, and A.R. Robbat, Electrocatalytic decomposition of hydrogen sulfide, *Catal. Lett.* **13**, 289-296 (1992).
74. A. Giannikos, A.D. Frantzis, C. Pliangos, S. Bebelis, and C.G. Vayenas, Electrochemical Promotion of CH_4 oxidation on Pd, *Ionics* **4**, 53-60 (1998).
75. M. Marwood, and C.G. Vayenas, Electrochemical Promotion of the Catalytic Reduction of NO by CO on Palladium, *J. Catal.* **170**, 275-284 (1997).
76. G.L. Haller, and S. Kim. *ACS Petroleum Division Preprints, Symposium in Catalytic Combustion* in *213th National ACS Meeting,* 155-158 (1997, April 13-17) San Francisco, CA.
77. C. Karavasilis, S. Bebelis, and C.G. Vayenas, Non-Faradaic Electrochemical Modification of Catalytic Activity: 10. Ethylene epoxidation on Ag deposited on stabilized Zr02 in presence of chlorine moderators, J. *Catal.* **160**, 190-204 (1996).
78. M. Stoukides, and C.G. Vayenas, The effect of electrochemical oxygen pumping on the Rate and Selectivity of Propylene Oxidation on Silver in a Solid Electrolyte Cell, *J. Electrochem. Soc.* **131**(4), 839-845 (1984).
79. P. Tsiakaras, and C.G. Vayenas, Oxidative Coupling of CH_4 on Ag catalyst-electrodes deposited on ZrO_2(8mol% Y_2O_3), *J. Catal.* **144**, 333-347 (1993).
80. C. Karavasilis, S. Bebelis, and C.G. Vayenas, NEMCA: The Oxidation of CO on Ag, *Materials Science Forum* **76**, 175-178 (1991).
81. S. Neophytides, and C.G. Vayenas, Non-Faradaic Electrochemical Modification of Catalytic Activity: 2. The case of Methanol Dehydrogenation and Decomposition on Ag, J. *Catal.* **118**, 147-163 (1989).
82. O.A. Mar'ina, and V.A. Sobyanin, The effect of electrochemical oxygen pumping on the rate of CO oxidation on Au electrode-catalyst, *Catal. Lett.* **13**, 61-70 (1992).
83. O.A. Mar'ina, V.A. Sobyanin, V.D. Belyaev, and V.N. Parmon, The effect of electrochemical oxygen pumping on catalytic properties of Ag and Au electrodes at gas-phase oxidation of CH_4, *Catalysis Today* **13**, 567-570 (1992).
84. T.I. Politova, G.G. Gal'vita, V.D. Belyaev, and V.A. Sobyanin, Non-Faradaic catalysis: the case of CO oxidation over Ag-Pd electrode in a solid oxide electrolyte cell, *Catal. Lett.* **44**, 75-81 (1997).
85. I.V. Yentekakis, Y. Jiang, S. Neophytides, S. Bebelis, and C.G. Vayenas, Catalysis, Electrocatalysis and Electrochemical Promotion of the Steam Reforming of Methane over Ni Film and Ni-YSZ cermet Anodes, *Ionics* **1**, 491-498 (1995).
86. O.A. Mar'ina, V.A. Sobyanin, V.D. Belyaev, and V.N. Parmon, The effect of electrochemical pumping of oxygen on catalytic behaviour of metal electrodes in methane oxidation, in *New Aspects of Spillover Effect in Catalysis for Development of Highly Active Catalysts,* Stud. Surf. Sci. Catal. **77** (T. Inui, K. Fujimoto, T. Uchijima, M. Masai, eds.), pp. 337-340, Elsevier Science Publishers B.V. (1993).
87. E. Varkaraki, J. Nicole, E. Plattner, C. Comninellis, and C.G. Vayenas, Electrochemical Promotion of IrO_2 catalyst for the gas phase combustion of ethylene, *J. Appl. Electrochem.* **25**, 978-981 (1995).
88. D. Tsiplakides, J. Nicole, C.G. Vayenas, and C. Comninellis, Work function and catalytic activity measurements of an IrO_2 film deposited on YSZ subjected to in situ electrochemical promotion, *J. Electrochem. Soc.* **145**(3), 905-908 (1998).
89. I.V. Yentekakis, and C.G. Vayenas, In situ controlled promotion of Pt for CO oxidation via NEMCA using CaF_2 as the solid electrolyte, *J. Catal.* **149**, 238-242 (1994).

90. C. Pliangos, I.V. Yentekakis, S. Ladas, and C.G. Vayenas, Non-Faradaic Electrochemical Modification of Catalytic Activity: 9. Ethylene oxidation on Pt deposited on TiO_2, *J. Catal.* **159**, 189-203 (1996).
91. P.D. Petrolekas, S. Balomenou, and C.G. Vayenas, Electrochemical promotion of Ethylene Oxidation on Pt Catalyst Films deposited on CeO_2, *J. Electrochem. Soc.* **145**(4), 1202-1206 (1998).
92. P. Beatrice, C. Pliangos, W.L. Worrell, and C.G. Vayenas, The electrochemical promotion of ethylene and propylene oxidation on Pt deposited on Yttria-Titania-Zirconia, *Solid State Ionics* **136-137**, 833-837 (2000).
93. C.A. Cavalca, and G.L. Mailer, Solid Electrolytes as Active Catalyst Supports: Electrochemical Modification of Benzene Hydrogenation Activity on $Pt/\beta''(Na)Al_2O_3$, *J. Catal.* **177**, 389-395 (1998).
94. C.A. Cavalca, *PhD Thesis,* Yale University (1995).
95. S. Tracey, A. Palermo, J.P.H. Vazquez, and R.M. Lambert, In Situ Electrochemical Promotion by Sodium of the Selective Hydrogenation of Acetylene over Platinum, *J. Catal.* **179**, 231-240 (1998).
96. A. Palermo, R.M. Lambert, I.R. Harkness, I.V. Yentekakis, O. Mar'ina, and C.G. Vayenas, Electrochemical promotion by Na of the Platinum catalyzed reaction between CO and NO, *J. Catal.* **161**, 471-479 (1996).
97. A. Palermo, M.S. Tikhov, N.C. Filkin, R.M. Lambert, I.V. Yentekakis, and C.G. Vayenas, Electrochemical Promotion of NO reduction by CO and by Propene, *Ionics* **1**, 366-372 (1995).
98. A. Palermo, M.S. Tikhov, N.C. Filkin, R.M. Lambert, I.V. Yentekakis, and C.G. Vayenas, Electrochemical Promotion of NO Reduction by CO and by Propene, *Stud. Surf. Sci. Catal.* **101**, 513-522 (1996).
99. R.M. Lambert, M. Tikhov, A. Palermo, I.V. Yentekakis, and C.G. Vayenas, Electrochemical Promotion of Environmentally Important Catalytic Reactions, *Ionics* **1**, 366-376 (1995).
100. A. Giannikos, P. Petrolekas, C. Pliangos, A. Frenzel, C.G. Vayenas, and H. Putter, Electrochemical promotion of Pd for the Hydrogenation of C_2H_2, *Ionics* **4**, 161-169 (1998).
101. C. Karavasilis, S. Bebelis, and C.G. Vayenas, In Situ Controlled Promotion of Catalyst Surfaces via NEMCA: The Effect of Na on the Ag-Catalyzed Ethylene Epoxidation in the Presence of Chlorine Moderators, *J. Catal.* **160**, 205-213 (1996).
102. P.D. Petrolekas, S. Brosda, and C.G. Vayenas, Electrochemical promotion of Pt catalyst-electrodes deposited on $Na_3Zr_2Si_2PO_{12}$ during Ethylene Oxidation, *J. Electrochem. Soc.* **145**(5), 1469-1477 (1998).
103. G. Pitselis, P. Petrolekas, and C.G. Vayenas, Electrochemical Promotion of NH_3 decomposition on Fe using H^+, Na^+ and K^+ conductors, *Ionics* **3**, 110-117 (1997).
104. M. Makri, A. Buekenhoudt, J. Luyten, and C.G. Vayenas, Non-Faradaic Electrochemical Modification of the Catalytic Activity of Pt using a $CaZr_{0.9}In_{0.1}O_{3-\alpha}$ Proton Conductor, *Ionics* **2**, 282-288 (1996).
105. C.G. Yiokari, G.E. Pitselis, D.G. Polydoros, A.D. Katsaounis, and C.G. Vayenas, High pressure electrochemical promotion of ammonia synthesis over an industrial iron catalyst, *J. Phys. Chem.* **104**, 10600-10602 (2000).
106. P.H. Chiang, D. Eng, and M. Stoukides, Solid electrolyte aided direct coupling of methane, *J. Catal.* **139**, 683-687 (1993).
107. T.I. Politova, V.A. Sobyanin, and V.D. Belyaev, Ethylene hydrogenation in electrochemical cell with solid proton-conducting electrolyte, *Reaction Kinetics and Catalysis Letters* **41(2)**, 321-326 (1990).

108. D. Tsiplakides, S. Neophytides, O. Enea, M.M. Jaksic, and C.G. Vayenas, Non-faradaic Electrochemical Modification of Catalytic Activity (NEMCA) of Pt Black Electrodes Deposited on Nafion 117 Solid Polymer Electrolyte, *J. Electrochem. Soc.* **144**(6), 2072-2088 (1997).
109. L. Ploense, M. Salazar, B. Gurau, and E.S. Smotkin, Proton Spillover Promoted Isomerization of n-Butylenes on Pt-black Cathodes/Nafion 117, *JACS* **119**, 11550-11551 (1997).
110. S. Neophytides, D. Tsiplakides, P. Stonehart, M. Jaksic, and C.G. Vayenas, Electrochemical enhancement of a catalytic reaction in aqueous solution, *Nature* **370**, 292-294 (1994).
111. S. Neophytides, D. Tsiplakides, P. Stonehart, M.M. Jaksic, and C.G. Vayenas, Non-Faradaic Electrochemical enhancement of H_2 oxidation in alkaline solutions, *J. Phys. Chem.* **100**, 14803-14814 (1996).
112. I.M. Petrushina, V.A. Bandur, F. Cappeln, and N.J. Bjerrum, Electrochemical Promotion of Sulfur Dioxide Catalytic Oxidation, *J. Electrochem. Soc.* **147(8)**, 3010-3013 (2000).
113. T. Wolkenstein, *Elektronentheorie der Katalyse an Halbleitern,* VEB Deutscher Verlag der Wissenschaften, Berlin (1964).
114. C.G. Vayenas, S. Ladas, S, Bebelis, I.V. Yentekakis, S. Neophytides, J. Yi, C. Karavasilis, and C. Pliangos, Electrochemical promotion in catalysis: Non-Faradaic electrochemical modification of catalytic activity, *Electrochim. Acta* **39**(11/12), 1849-1855 (1994).
115. C.G. Vayenas, S. Brosda, and C. Pliangos, Rules and Mathematical Modeling of Electrochemical and Chemical Promotion: 1. Reaction Classification and Promotional Rules, *J. Catal.,* in press (2001).
116. C.G. Vayenas, and S. Brosda, Electrochemical promotion: Experiment, rules and mathematical modeling, *Solid State Ionics,* submitted (2001).
117. C.G. Vayenas, and S. Brosda, Spillover-modified catalysis: Experiment and mathematical modeling, *Stud. Surf. Sci. Catal.* in press, (2001).
118. J.L. Falconer, and R.J. Madix, Flash desorption activation energies: DCOOH decomposition and CO desorption from Ni(110), *Surf. Sci.* **48**, 393-405 (1975).
119. D. Tsiplakides, S. Neophytides, and C.G. Vayenas, Thermal Desorption Study of Oxygen Adsorption on Pt, Ag and Au films Deposited on YSZ, *Ionics* **3**, 201-208 (1997).
120. G. Pacchioni, F. Illas, S. Neophytides, and C.G. Vayenas, Quantum-Chemical Study of Electrochemical Promotion in Catalysis, *J. Phys. Chem.* **100**, 16653-16661 (1996).
121. G. Pacchioni, J.R. Lomas, and F. Illas, Electric field effects in heterogeneous catalysis, *Molecular Catalysis A: Chemical* **119**, 263-273 (1997).
122. D. Tsiplakides, S. Neophytides, and C.G. Vayenas, Investigation of the state of the electrochemically generated adsorbed O species on Au films interfaced with Y_2O_3-doped-ZrO_2, *Ionics,* submitted (2001).
123. M. Boudart, Heterogeneity of Metal Surfaces, *JACS* **74**, 3556-3561 (1952).
124. J. Nicole, *PhD Thesis,* EPFL (1999).
125. J. Nicole, D. Tsiplakides, C. Pliangos, X.E. Verykios, C. Comninellis, and C.G. Vayenas, Electrochemical Promotion and Metal-support interactions, *J. Catal.,* in press (2001).

CHAPTER 5

ORIGIN OF NEMCA

"The strong long-range effect implied by the correlation of work-function change with activation-energy change found by Vayenas et al in the presence of electrochemically induced promotion is therefore particularly intriguing. So too is the nature of the electrochemically induced oxygen species that is believed to cause the increase in work function and catalytic promotion, yet which is less reactive than the adsorbed oxygen reactant that covers most of the surface. There is clearly much surface chemistry to be explored and it will be interesting to see how general the work function effect proves to be. In any case, the ability to vary the concentration of promoters by electrochemical control while under reaction conditions is a valuable development in catalytic research, and one can expect it to be rapidly exploited in conjunction with other in situ techniques of surface analysis."

J. Pritchard, Nature, 1990

5.1 PROBLEMS AND METHODS

After reading the review of the phenomenology of electrochemical promotion (or NEMCA) in Chapter 4 the reader may righteously ask: What is taking place at the molecular level on a catalyst electrode surface under electrochemical promotion conditions such as e.g. the galvanostatic transients shown in Figs. 4.13 to 4.15? What is the physical meaning of faradaic efficiency, A, values up to 300,000 such as the ones shown in these Figures (e.g. Fig. 4.13) and Table 4.1? Does electrochemical promotion really violate Faraday's law? Are there limitations, other than possible economic ones, for its practical utilization?

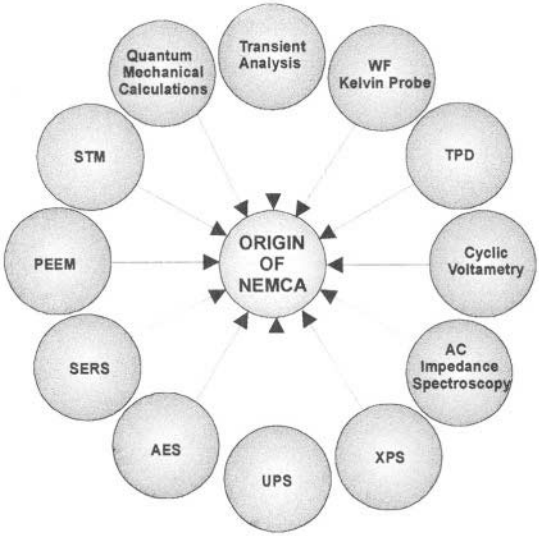

Figure 5.1. Surface science, catalytic and electrochemical techniques employed during the last few years to determine the origin of electrochemical promotion.

To answer these questions, and many others, a whole arsenal of surface science, catalytic and electrochemical techniques have been employed during the last few years (Fig. 5.1). These include:

a) Analysis of time constants during galvanostatic NEMCA transients.
b) Work function measurements via the Kelvin probe technique and via UPS (Ultra violet Photoelectron Spectroscopy) experiments.
c) Temperature Programmed Desorption (TPD)
d) Cyclic voltammetric investigations.
e) AC Impedance spectroscopic investigations.
f) XPS (X-ray Photoelectron Spectroscopy) investigations.
g) UPS investigations.
h) AES (Auger Electron Spectroscopic) investigations
i) SERS (Surface Enhanced Raman Spectroscopy) investigations.
j) PEEM (Photoelectron Emission Microscopy) investigations.
k) Scanning Tunneling Microscopy (STM) investigations.
l) Ab initio quantum mechanical calculations.

All these techniques have provided a unanimous answer to the above questions. A combination of the results of any two or three of them would have sufficed to put together the puzzle. But each one of them has something new to offer, some new facet of the surface chemistry to reveal. So each of them will be discussed in this chapter in a sequence which in many cases coincides with the chronological order in which they were employed in order to solve the puzzle and understand the origin of electrochemical promotion.

As J. Prichard[1] had correctly predicted in his 1990 Nature editorial on NEMCA[2] *"there is clearly much surface chemistry to be explored."* Indeed there was and there is quite a lot.

Before discussing the results obtained by each of the above techniques individually, it is useful first to discuss the galvanostatic transient of Figure 4.13 in light of parallel TPD and cyclic voltammetry investigations of Pt deposited on YSZ (Fig. 5.2). These two techniques are very well understood among surface scientists and electrochemists, respectively, and thus Fig. 5.2 can help every reader to grasp immediately the underlying molecular phenomena.

5.2 A GALVANOSTATIC NEMCA TRANSIENT REVISITED

We can now concentrate on Figure 5.2 which shows a galvanostatic catalytic rate transient during ethylene oxidation on Pt/YSZ at 370°C (Fig. 5.2a)[3] together with (a) oxygen TPD spectra obtained on Pt/YSZ[4] upon exposure at 400°C to $p_{O2}=4\times10^{-6}$ Torr for 1800 s (7.2 kilolangmuirs) followed by electrochemical O^{2-} supply (I=15 μA) for various time periods t_I, rapid cooling to 300°C followed by a linear increase in T at a heating rate β (K/s) *under open-circuit* to obtain the TPD spectra of Figure 5.2b. (b) Cyclic voltammograms obtained at 400°C and various holding times at a positive potential (U_{WR} = 0.8 V) under uhv conditions[4] (Fig. 5.2c).

In comparing Figures 5.2a, 5.2b and 5.2c it is worth noting that 5.2b and 5.2c have been obtained with a Pt film having a true surface area $N_G=2\times10^{-7}$ mol Pt[4] while Fig. 5.2a has been obtained on a Pt film with true surface area $N_G=4.2\times10^{-9}$ mol Pt.[3] Thus for the three different experiments of Figs. 5.2a, 5.2b and 5.2c the NEMCA time constants τ (= $2FN_G/I$) are 800 s, 2500 s and 1200 s respectively, i.e. they are of the same order of magnitude.

Both the TPD spectra (Fig. 5.2b) and the cyclic voltammograms (Fig. 5.2c) show clearly the creation of *two* distrinct oxygen adsorption states on the Pt surface (vs. *only one state* formed upon gas phase O_2 adsorption, Fig. 5.2b, t=0).

The weakly bonded O adsorption state is populated almost immediately (Figs. 5.2b and 5.2c). The strongly bonded O adsorption state is populated over a time period of the order $2FN_G/I$. This is exactly the time period which the catalytic rate needs to reach its electrochemically promoted value (Fig. 5.2a).

One can then ask: What is the rate at which the strongly bonded state is populated during the TPD and cyclic voltammetric experiments of Figures 5.2b and 5.2c? The answer is clear: It is the rate of O^{2-} supply to the catalyst, i.e. I/2F.

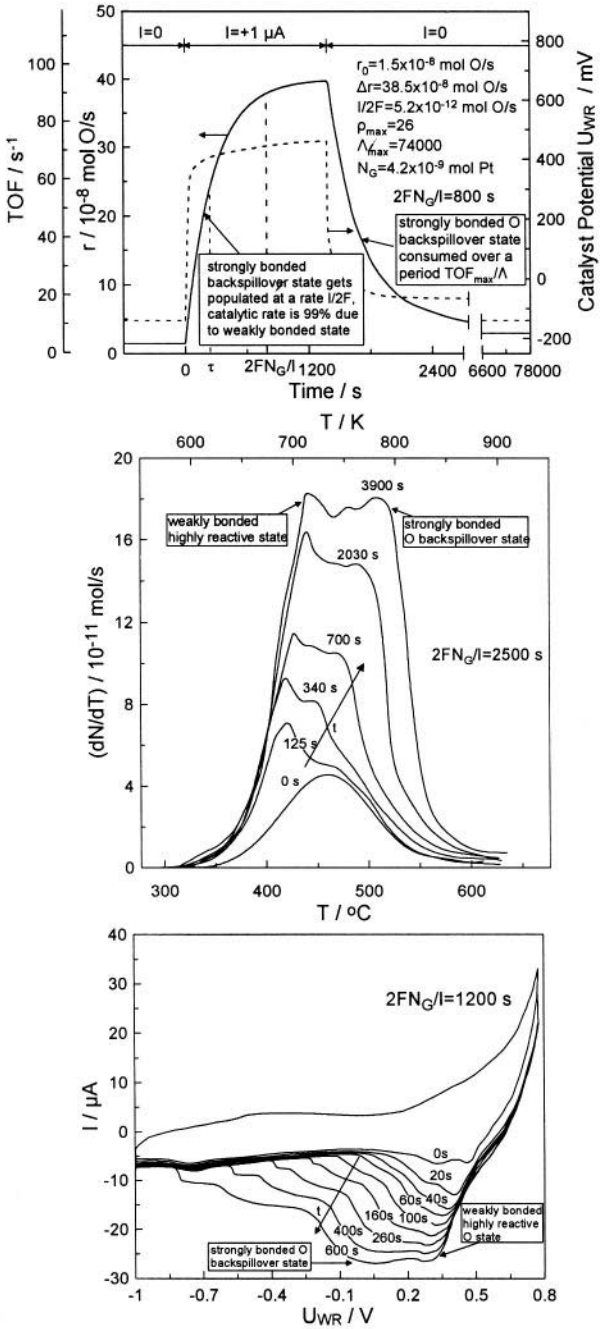

Figure 5.2. NEMCA and its origin on Pt/YSZ catalyst electrodes. Transient effect of the application of a constant current (a, b) or constant potential U_{WR} (c) on (a) the rate, r, of C_2H_4 oxidation on Pt/YSZ (also showing the corresponding U_{WR} transient)[3] (b) the O_2 TPD spectrum on Pt/YSZ[4,7] after current (I = 15 μA) application for various times t. (c) the cyclic voltammogram of Pt/YSZ[4,7] after holding the potential at U_{WR} = 0.8 V for various times t.

The next question is: What is the rate at which the strongly bonded state of oxygen is supplied and populated during the catalytic transient of Figure 5.2a? Clearly it is again of the order I/2F, since in Figs. 5.2a, 5.2b and 5.2c the time constants are all similar, i.e. $2FN_G/I$.

Finally one may ask: What is the rate at which the strongly bonded oxygen state is removed from the catalyst surface at steady state, i.e. when the rate has reached its maximum value? It clearly has also to equal I/2F. What removes the strongly bonded state from the catalyst surface? Clearly it is reaction with C_2H_4 (although desorption to the gas phase also plays a role which can become dominant in absence of C_2H_4). Consequently at steady state the strongly bonded oxygen state reacts with C_2H_4 at a rate I/2F.

At this point (steady-state) the weakly bonded oxygen is reacting with ethylene at a rate $r - I/2F \approx r$ ($= 3.85 \cdot 10^{-7}$ mol O/s) which is 74,000 ($= \Lambda$) times larger than I/2F. So what is the physical meaning of the faradaic efficiency Λ? It is simply the ratio of the reactivity (with C_2H_4) of the weakly bonded and strongly bonded oxygen state.[5]

The latter acts as a *sacrificial promoter*. It is a promoter, as it forces oxygen to populate the weakly bonded (and highly reactive) oxygen adsorption state. It is also "sacrificed" as it is consumed by C_2H_4 at a rate I/2F, equal to its rate of supply.

In view of the above physical meaning of Λ it is clear why Λ can approach "infinite" values when Na^+ is used as the "sacrificial promoter" (e.g. when using β''-Al_2O_3 as the solid electrolyte) to promote reactions such as CO oxidation (Fig. 4.15) or NO reduction by H_2 (Fig. 4.17). In this case Na on the catalyst surface is not consumed by a catalytic reaction and the only way it can be lost from the surface is via evaporation. Evaporation is very slow below 400°C (see Chapter 9) so Λ can approach "infinite" values.

Returning to the Figure 5.2a we can further discuss the physical meaning of Λ to gain some more physical insight and to prove the validity of the "sacrificial promoter" concept.

Since Λ expresses the ratio of the rates of consumption of the two oxygen states by C_2H_4, one has:

$$\Lambda = \frac{r_1}{r_2} = \left(= \frac{\Delta r}{(I/2F)} \right) = \frac{TOF_1}{TOF_2} \tag{5.1}$$

where TOF_1 and TOF_2 are the turnover frequencies of the two reactions (s^{-1}), both based on the total Pt catalyst surface area or maximum oxygen uptake ($N_G = 4.2 \cdot 10^{-9}$ mol Pt). The value of the two TOF at steady state in Fig. 5.2a are:

$$TOF_1 = 95.2\ s^{-1}\ (= r_1/N_G) \tag{5.2a}$$

$$TOF_2 = 1.2 \cdot 10^{-3}\ s^{-1}\ (= r_2/N_G) \tag{5.2b}$$

The inverse of these numbers express roughly the average lifetimes of oxygen at the two adsorption states at steady state, i.e.

$$\tau_1 \approx 0.01\ s;\ \tau_2 \approx 1000\ s \tag{5.2c}$$

Can these two oxygen adsorption states, clearly manifest by TPD and cyclic voltammetry in Figures 5.2b and 5.2c, have indeed such different reactivities with C_2H_4? A look at Figure 5.3 can convince us about this: The figure shows how the population of the two states evolves in time, in absence of C_2H_4, if we just let oxygen desorb by stopping the applied current, i.e. if we see the results of isothermal desorption.[4,7] It is clear that the weakly bonded state desorbs much faster, at least 50 times faster, than the strongly bonded one. It is thus also reasonable to expect that it will react with C_2H_4 much faster than the strongly bonded one.

Can we identify the strongly bonded oxygen state as the "backspillover" oxygen originating from the solid electrolyte? Since the strongly bonded state is occupied over a time period $2FN_G/I$ (Fig. 5.2) the answer is, for all practical purposes, yes. But we should also keep in mind that oxygen atoms can exchange between the two states: At 400°C and in presence of gaseous

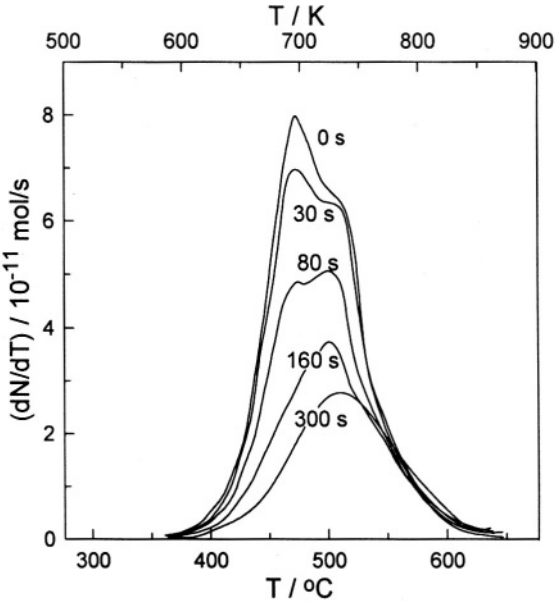

Figure 5.3. Oxygen thermal desorption spectra after electrochemical O^{2-} supply to Pt/YSZ at 673 K (I = +12 μA for 1800 s) followed by isothermal desorption at the same temperature at various times as indicated on each curve.[4,7] Reprinted from ref. 7 with permission from Academic Press.

$^{18}O_2$, ^{18}O tracer experiments have shown isotopic scrambling between the two states to be almost complete after 30 s.

A straightforward, qualitative, but strong, confirmation of the electrochemical promotion mechanism described above conies when we try to predict what will happen to the promoted catalytic rate after the current is interrupted (Fig. 5.2a): If the average lifetime of the promoting strongly bonded oxygen species is indeed 1000 s ($= TOF_2^{-1} = (r_2/N_G)^{-1}$) then one would expect that upon current interruption the promoted catalytic rate will decay to its unpromoted (open-circuit) values within a time τ_D of roughly 1000s. This is exactly what Figure 5.2a shows upon current interruption. Thus by simply knowing the TOF of the electrochemically promoted catalytic reaction ($\approx TOF_1$) and estimating the TOF of the reaction of the promoting species ($= TOF_2$) from the time decay of the rate upon current interruption, one can estimate the Faradaic efficiency Λ from :

$$\Lambda = TOF_1/TOF_2 = \tau_D/(r_1/N_G) \tag{5.3}$$

without knowing the value of the applied current I!

A more rigorous mathematical analysis is presented in section 5.3, but the reader is invited to check the validity of Eq. (5.3) with all galvanostatic transients presented in this book.

Thus the picture which emerges is quite clear (Fig. 5.4): At steady state, before potential (or current) application, the Pt catalyst surface is covered, to a significant extent, by chemisorbed O and C_2H_4. Then upon current (and thus also potential) application O^{2-} ions arriving from the solid electrolyte at the tpb at a rate I/2F react at the tpb to form a backspillover ionically strongly bonded species

$$O^{2-}(YSZ) \rightarrow [O^{\delta-} - \delta+] (Pt) + 2e^- \tag{5.4}$$

The exact value of δ is not yet known but useful information can be extracted from the surface spectroscopic techniques described in the continuation of this chapter. Both XPS[6] and dipole moment measurements[7] suggest $\delta \approx 2$, so that $O^{\delta-}$ is O^{2-}, at least for Pt.[8] Nevertheless it is still safer to maintain the symbolism $O^{\delta-}$. The symbolism $[O^{\delta-} - \delta+]$ emphasizes that the backspillover oxygen species is overall neutral, as it is accompanied by its compensating image charge in the metal ($\delta+$). At the same time the applied potential and concomitant high oxygen chemical potential creates on the Pt surface two new oxygen adsorption states. A strongly bonded one and weakly bonded one. The backspillover $[O^{\delta-}-\delta+]$ species migrate over the entire Pt catalyst surface. Due to the repulsive interaction of the $[O^{\delta-}-\delta+]$ dipoles, diffusion on the Pt surface is fast and the rate of spreading of the $[O^{\delta-} - \delta+]$ species on the Pt surface is controlled by the rate, I/2F, of their creation at the tpb and not by their surface diffusivity.[5,8]

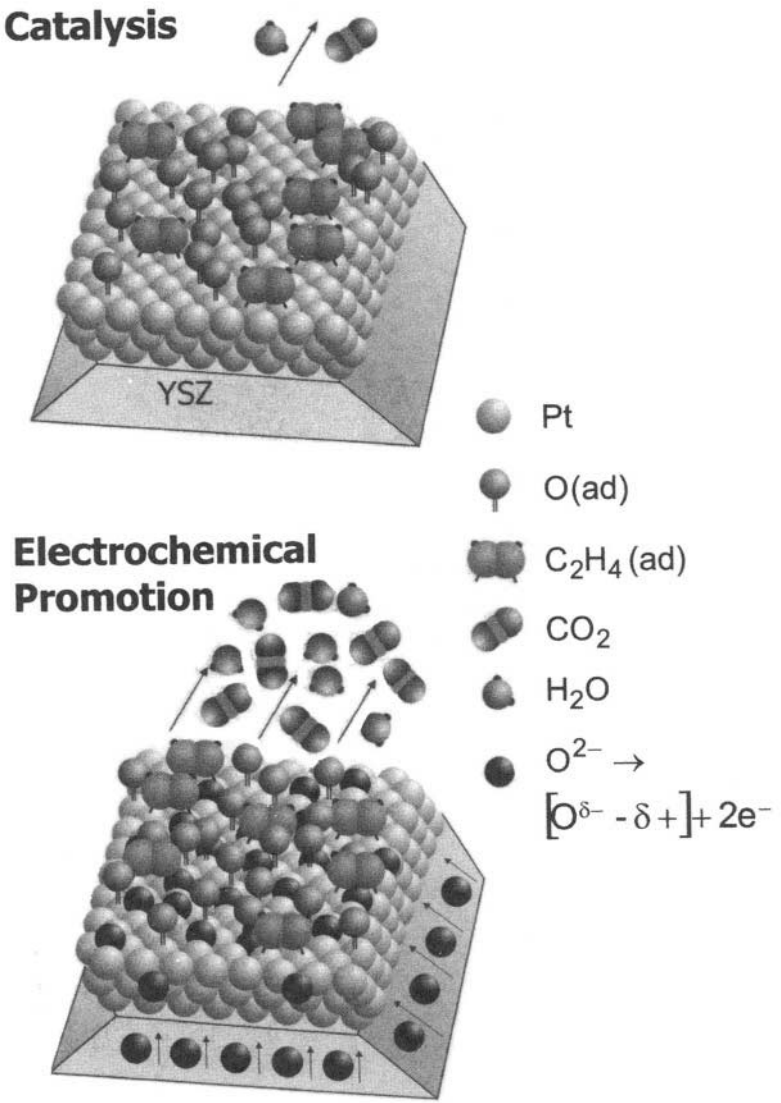

Figure 5.4. Atomic visualization of NEMCA during ethylene C_2H_4 on Pt/YSZ. The backspillover $[O^{\delta-} - \delta+]$ species forces O(ad) to a more weakly bonded and more reactive state.

The backspillover oxygen species occupies primarily the strongly bonded oxygen chemisorption state. Oxygen adsorbing from the gas phase is forced to populate primarily the weakly bonded (and highly reactive) state (Fig. 5.4). Consequently the catalytic rate starts increasing dramatically up to the point where a steady-state coverage is established for the strongly bonded oxygen. At this point the (electrochemically promoted) catalytic rate is at its

new steady-state value (Figs 5.2 and 5.4).

Which surface sites are occupied by the strongly bonded oxygen state? This is not known yet. It is likely that they correspond to threefold hollow sites while the weakly bonded state corresponds to bridge-bonded or even on-top sites. This is only a proposition at this time but STM should be able to provide soon useful information. The point is that, as shown by the TPD spectra of Fig. 5.2b, electrochemical promotion forces large amounts of oxygen (near monolayer coverages) to remain adsorbed on the catalyst surface under conditions where gaseous adsorption (many kilolangmuirs) leads to coverages of the order of 0.05 (Fig. 5.2b).

The same figure proves unambiguously that electrochemically controlled backspillover of oxygen from the solid electrolyte onto the catalyst surface takes place and is the cause of NEMCA.

Figure 5.2b, as well as 5.2c, also demonstrates the enormous power of electrochemistry to create new adsorption states on a catalyst surface.

There are several questions which may still exist in the reader's mind:

1. In the hypothetical case that electrochemistry (i.e. the application of potential at the metal-electrolyte interface) and the concomitantly imposed very high oxygen chemical potential did not lead to the creation of (at least) two oxygen adsorption states, at least on Pt, would electrochemical promotion ($|\Lambda| > 1$) still exist? The answer is probably not, but it is not easy to see how oxygen adsorbing at the electrochemically imposed huge oxygen chemical potential could be accommodated in the same oxygen adsorption sites occupied via gaseous oxygen adsorption.
2. Is the application of an anodic overpotential $\eta (= U_{WR} - U^{o}_{WR})$ equivalent to the application of a huge oxygen pressure $p_{O_2,NERNST}$ computable from the Nernst equation:

$$p_{O_2,NERNST} = p_{O_2,R} \exp(4F\eta/RT) \tag{5.5}$$

where $p_{O_2,R}$ is the open-circuit surface oxygen activity, or equivalent oxygen partial pressure?

This for the conditions of Fig. 5.2a gives at steady state $p_{O_2,NERNST} = 5 \cdot 10^{15}$ bar. The answer is again nontrivial. If η is a purely concentration overpotential,[9,10] then Eq. (5.5) is valid. But if η also contains an activation overpotential, this must be subtracted from η and thus $p_{O_2,NERNST}$ can decrease substantially from this enormous value. A more rigorous analysis of and answer to this important question is given in Chapter 6.

5.3 ANALYSIS OF RATE TIME CONSTANTS DURING GALVANOSTATIC TRANSIENTS

5.3.1 Introduction

The first indication that NEMCA is due to electrochemically induced ion backspillover from solid electrolytes to catalyst surfaces came together with the very first reports of NEMCA: Upon constant current application, i.e. during a galvanostatic transient, e.g. Fig. 5.2, the catalytic rate does not reach instantaneously its new electrochemically promoted value, but increases slowly and approaches asymptotically this new value over a time period which can vary from many seconds to a few hours, but is typically on the order of several minutes (Figure 5.2, galvanostatic transients of Chapters 4 and 8.)

This observation immediately rules out the possibility that NEMCA is an electrocatalytic phenomenon causing only a local acceleration of the catalytic rate at the three-phase-boundaries (tpb) metal-solid electrolyte-gas. In such a case the rate increase would obviously be instantaneous during a galvanostatic transient.

It was quickly observed that the catalytic rate response during galvanostatic transients can be reasonably well approximated by the response of a first order system, i.e. by:

$$\Delta r/\Delta r_{max} = 1 - \exp(-t/\tau) \tag{4.31}$$

where the characteristic time constant τ, denoted NEMCA time constant, and expressing the time required for the rate increase to reach 63% of its final maximum value, can be approximated quite well by the expression:

$$\tau \approx 2FN_G/I \tag{4.32}$$

where N_G(mol) is the, independently measured, reactive oxygen uptake of the catalyst surface which expresses, approximately, the mols of surface metal catalyst. This observation was already made in 1981 by Stoukides and Vayenas[11] who experimented with nine different Ag catalyst electrode samples deposited on YSZ and differing in their gas exposed catalyst electrode surface area N_G (Figure 5.5).

The physical meaning of the parameter $2FN_G/I$ is obvious: It expresses the time required to form a monolayer of oxide ions on a surface with N_G adsorption sites when the oxide ions are supplied at a rate I/2F. This proves that NEMCA is a surface phenomenon (not a bulk phenomenon and not a phenomenon at the tpb) taking place over the entire gas-exposed catalyst electrode surface.

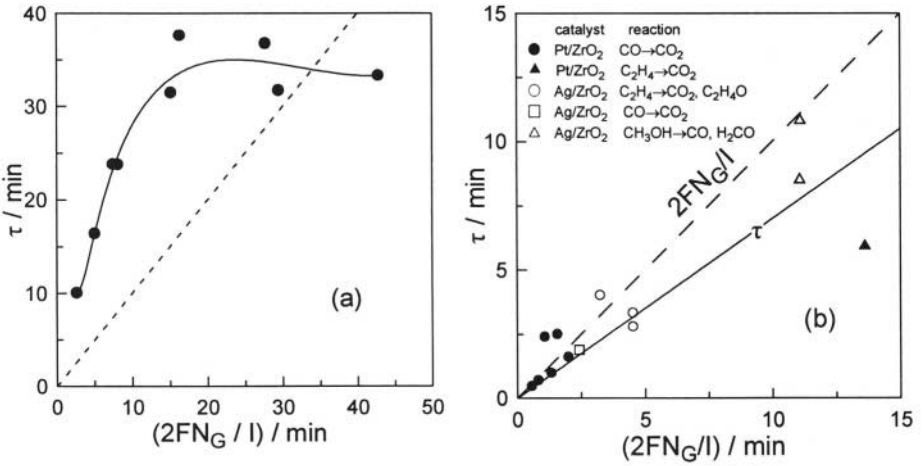

Figure 5.5. (a) Dependence of the NEMCA relaxation time constant τ on $2FN_G/I$ for C_2H_4 epoxidation on Ag[11] and (b) for CO, C_2H_4 and CH_3OH oxidation on Pt and Ag.[12] Adapted from ref. 11 and reprinted from ref. 12 with permission from the American Chemical Society and from Elsevier Science respectively.

It also shows that electrochemical promotion is due to electrochemically controlled migration (backspillover) of ions (acting as promoters) from the solid electrolyte to the gas-exposed catalytically active catalyst-electrode surface.

Equations 4.31 and 4.32 also suggest another important fact regarding NEMCA on noble metal surfaces: The rate limiting step for the backspillover of ions from the solid electrolyte over the entire gas exposed catalyst surface is <u>not</u> their surface diffusion, in which case the surface diffusivity D_S would appear in Eq. 4.32, but rather their creation at the three-phase-boundaries (tpb). Since the surface diffusion length, L, in typical NEMCA catalyst-electrode film is of the order of 2 μm and the observed NEMCA time constants τ are typically of the order of 1000 s, this suggests surface diffusivity values, D_S, of at least L^2/τ, i.e. of at least $4 \cdot 10^{-11}$ cm^2/s. Such values are reasonable, in view of the surface science literature for O on Pt(111).[13,14] For example this is exactly the value computed for the surface diffusivity of O on Pt(111) and Pt(100) at 400°C from the experimental results of Lewis and Gomer[14] which they described by the equation:

$$D_s = \alpha^2 \nu \exp(\Delta S/R)\exp(-E/RT) \qquad (5.6)$$

with $\alpha = 3$Å, $\Delta S = 17$ cal/mol·K, $\nu = 10^{12}$ s^{-1} and $E = 34.1$ kcal/mol.

Furthermore it is logical to expect that partly ionic species such as $O^{\delta-}$ or $Na^{\delta+}$ will have even higher diffusivities on metal surfaces than less ionic adsorbates due to their strong electrostatic repulsion which forces them to migrate over the entire gas-exposed electrode surface.

5.3.2 Time Constants During Galvanostatic Transients and Faradaic Efficiency

The faradaic efficiency, Λ, can be computed in every NEMCA experiment from its definition, i.e.:

$$\Lambda = \Delta r/(I/2F) \tag{4.19}$$

where r is expressed in mol O/s, or more generally, from :

$$\Lambda = \Delta r/(I/F) \tag{5.7}$$

where r is expressed in g-equiv/s.

There exists, however, a second, approximate, way of estimating Λ on the basis of galvanostatic rate transients as outlined in section 5.2 and shown in Figure 5.6a. This approximate method is useful for gaining additional physical insight on the meaning of the faradaic efficiency Λ and for checking the internal consistency of experimental data with the ion backspillover mechanism.

This method is based on two observations:

a) Upon current interruption the catalytic rate decays to its initial (unpromoted) value over a time period τ_D, which is often comparable to $2FN_G/I$, and which reflects the kinetics (TOF_2) of consumption of the backspillover species from the catalyst surface ($\tau_D \approx TOF_2^{-1}$).
b) In the fully promoted steady state the faradaic efficiency Λ, as also discussed in section 5.2, expresses the ratio of the catalytic rate (TOF_1) divided by the rate of consumption of the backspillover species (TOF_2):

$$\Lambda = TOF_1/TOF_2 = \tau_D/(r_1/N_G) \tag{5.3}$$

Thus by simply measuring τ_D, r_1 and N_G one can estimate Λ. The thus computed values are always in excellent qualitative agreement with those accurately computed from Eq. (4.19). The interested reader can check this with all galvanostatic transients presented in this book.

Another use of Eq. (5.3) is that by measuring τ_D and r_1 and computing Λ via Eq. (4.19) one can estimate the catalyst surface area N_G. Alternatively this also can be done by comparing the parameter $2FN_G/I$ with the experimentally measured time constant τ via Eq. (4.32).

5.3.3 Transient Analysis and Promotion Index

As previously noted, determination of the promotion index $PI_{O^{\delta-}}$ of the promoting oxide ions $O^{\delta-}$ requires knowledge of the coverage of $O^{\delta-}$ on the

catalyst surface. This can be done by using the rate transient analysis upon current interruption.[15] We first consider the mass balance of $O^{\delta-}$ during current application ($0 \le t \le t_0$):

$$N_G \frac{d\theta_{O^{\delta-}}}{dt} = (I/2F) - N_G f(\theta_{O^{\delta-}}) \tag{5.8}$$

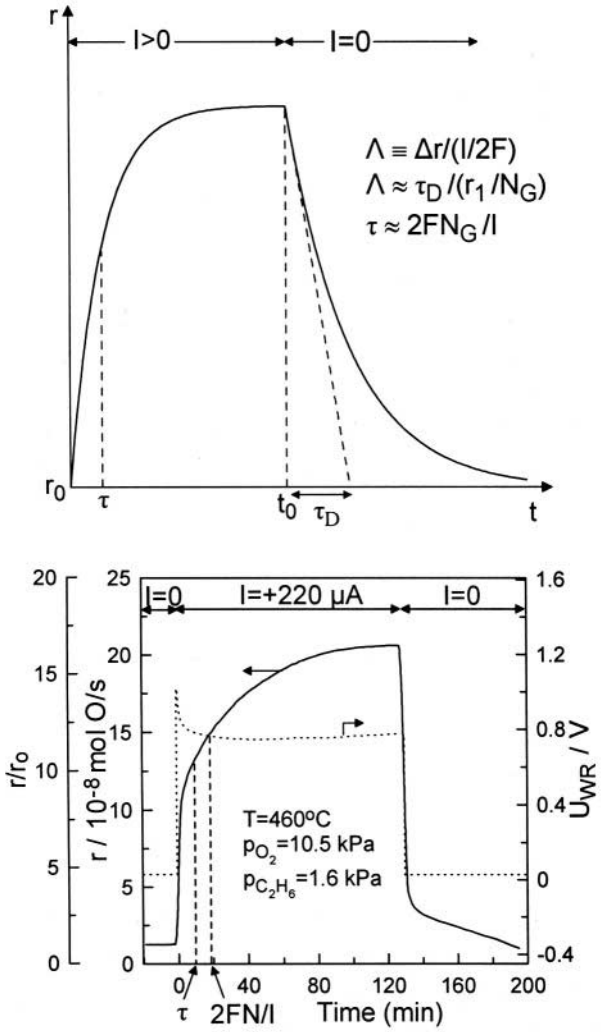

Figure 5.6. (a) Galvanostatic transient analysis: Definitions of τ, τ_D and estimation of the faradaic efficiency Λ which also expresses the ratio of the average lifetimes of the promoting species (τ_D) and of the reactants (N_G/r_1) on the catalyst surface. (b) Galvanostatic transient of the catalytic rate (continuous line) and of the catalyst potential (dotted line) during C_2H_6 oxidation on Pt/YSZ[15]; r_0=1.25×10^{-8} mol O/s, N_G=1.1×10^{-6} mol O. Reprinted with permission from Academic Press.

where $f(\theta_{O^{\delta-}})$ is the rate of consumption of $O^{\delta-}$ on the catalyst surface, due to catalytic reaction or desorption. We then note that in the region of positive potentials the catalytic rate is exponentially dependent on $\Delta\Phi$,[15] conforming to Eq. 4.49 with positive α (electrophobic behaviour). The change in work function Φ, $\Delta\Phi$, is linearly related to $\theta_{O^{\delta-}}$, provided the dipole moment of $O^{\delta-}$ is constant with coverage. On the basis of this assumption one can write:

$$r = r_0 \exp(c\,\theta_{O^{\delta-}}) \tag{5.9}$$

where c is a constant. It follows then from Eq. (5.8) and the initial condition ($t = 0$, $\theta_{O^{\delta-}} = 0$) that:

$$cN_G \left.\frac{d\theta_{O^{\delta-}}}{dt}\right|_{t=0} = N_G \left.\frac{d\ln(r/r_0)}{dt}\right|_{t=0} = c(I/2F) \tag{5.10}$$

Consequently c can be obtained from the initial slope of $\ln(r/r_0)$ vs t. For the rate transient upon current imposition (Fig. 5.6b) one can estimate a c value of 6.5.

We then note that at steady-state (I/2F) equals $N_G f(\theta_{O^{\delta-}})$, Eq. 5.8, and we apply Eq. 5.8 for $t>t_0$, thus I=0 (Fig. 5.6a). Taking the derivative at $t=t_0^+$:

$$N_G \left.\frac{d\theta_{O^{\delta-}}}{dt}\right|_{t=t_0^+} = -N_G f(\theta_{O^{\delta-}}) = -(I/2F) \tag{5.11}$$

where I is the previously applied current and the last equality holds because of the previously established steady state.

In view of Eq. (5.9) one has:

$$N_G \left.\frac{d\ln(r/r_0)}{dt}\right|_{t=t_0^+} = -c(I/2F) \tag{5.12}$$

which implies that a second estimate of c can also be obtained from the initial rate slope upon current interruption. From the transient upon current interruption of Fig. 5.6(b) one obtains c = 5.6, in reasonable agreement with the value estimated upon current imposition.

Once c has been estimated, one can then compute $\theta_{O^{\delta-}}$ from Eq. (5.9) for any time t from the corresponding r/r_0 value, i.e.:

$$\theta_{O^{\delta-}} = \frac{1}{c}\ln(r/r_0) \tag{5.13}$$

The maximum $\theta_{O^{\delta-}}$ value is thus computed for the transient of Fig. 5.6b to be $\theta_{O^{\delta-}} \approx 0.5$. This, in view of the definition of the promotion index, PI, (Chapter 4) and the observed ρ value ($\rho \approx 16.5$) gives a $PI_{O^{\delta-}}$ value of the order of 30, in good qualitative agreement with $PI_{O^{\delta-}}$ values for other Pt catalyzed oxidations.[5]

5.4 WORK FUNCTION AND ELECTROCHEMICAL PROMOTION

5.4.1 Work Function, Fermi Level, Vacuum Level, Galvani and Volta Potentials, Dipole Moments

The work function, Φ, of a solid surface (in eV) is the minimum energy required to extract an electron from that (neutral) surface.[9,10,16-23] The parameter Φ/e (in V) is usually called the extraction potential.

To be more precise Φ refers to the energy required to extract an electron from the bulk of the solid through that surface and at a distance of a few μm from the surface so that the image charge forces are at this point negligible. Energetically the electron is initially at the Fermi level, E_F, of the solid or, equivalently, at the electrochemical potential $\bar{\mu}$ of the electrons in the solid.[18,19] It is well established that $\bar{\mu} = E_F$ for any solid. In the absence of any net charge on the surface of the metal the work function Φ is the energy required to bring an electron from the Fermi level of the solid to its ground state in vacuum at an "infinite" distance from the solid (Fig. 5.7). More generally when the surface carries a net charge, q, then the outer or Volta potential, Ψ, and the three energies $\bar{\mu}$ (= E_F), Φ and $e\Psi$ are related via:

$$-\bar{\mu} = \Phi + e\Psi \tag{5.14}$$

The energy $e\Psi$ is known to surface physicists as the "vacuum level." Eq. (5.14) presents the surface science approach of counting the energy difference between the zero energy state of electrons (always taken in this book as the energy of an electron at its ground state and at "infinite" distance from any solid). There is a second, electrochemical, way of counting this energy difference:

$$\bar{\mu} = \mu + (-e)\varphi \tag{5.15}$$

where μ is the chemical potential of electrons in the metal and the inner or Galvani potential, φ, is the electrostatic potential of electrons in the solid. The situation is depicted schematically in Figure 5.7.

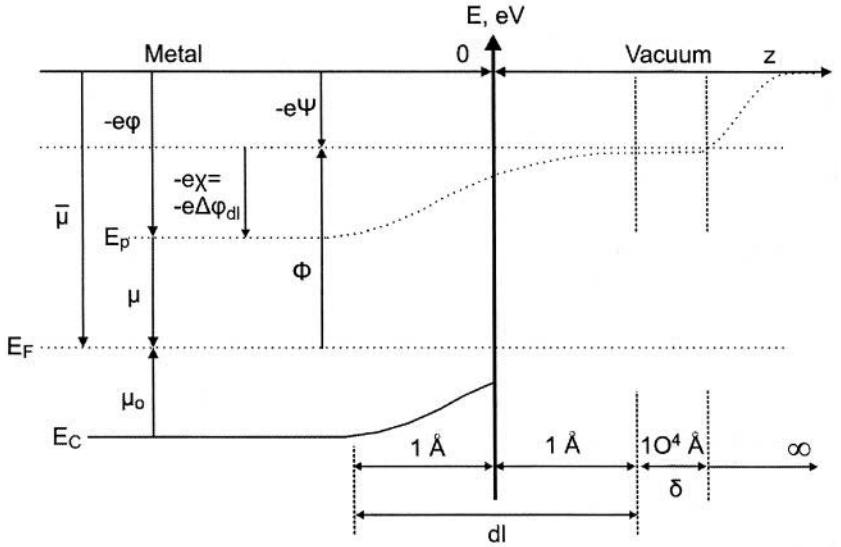

Figure 5.7. Schematic representation of the definitions of work function Φ, chemical potential of electrons μ, electrochemical potential of electrons or Fermi level $\bar{\mu} = E_F$, surface potential χ, Galvani (or inner) potential φ, Volta (or outer) potential Ψ, Fermi energy μ_o and of the variation in the mean effective potential energy E_P of electrons in the vicinity of a metal-vacuum interface according to the jellium model. E_C is the bottom of the conduction band and dl denotes the double layer at the metal/vacuum interface.

The surface science approach (Eq. 5.14) has the important advantage that both Φ and Ψ are measurable quantities. This is not the case for the electrochemical approach (Eq. 5.15) since neither the chemical potential μ nor the Galvani potential φ are measurable quantities. Only changes in φ are measurable.

The quantities $\bar{\mu}_e$, μ_e, φ are bulk properties of the metal. The quantities Φ, and of course Ψ, are surface properties which can vary on a metal surface from one crystallographic plane to the other. Such variations are typically on the order of 0.1 eV but can be as high as 0.5 V. The measured work function Φ, of a polycrystalline metal is an average of the Φ values on different crystallographic planes.

The work function of clean metal surfaces, which we denote throughout this book by Φ_0, varies between 2 eV for alkalis up to 5.5 eV for transition metals such as Pt. In general it increases as one moves to the right on the periodic table but deviations exist (Figure 4.19 in Chapter 4).

When atoms or molecules adsorb on a metal surface they change its work function. Electronegative (electron acceptor) adsorbates such as O or Cl can increase the Φ of a metal surface up to 1 eV. Electropositive (electron donor) adsorbates such as H or, particularly, alkalis can decrease the Φ of a metal surface by up to 3 eV.

The variation in Φ of a metal M with the coverage θ_i of an adsorbate, i, is given by the Helmholz equation:

$$\Delta\Phi = \frac{eN_M}{\varepsilon_o}\Delta(P_j\theta_j) \tag{5.16}$$

where e is the electron charge ($1.6\cdot10^{-19}$ C), N_M is the surface atom density (atom/m^2), ε_o is the electric permeability of vacuum (ε_o=$8.85\cdot10^{-12}$ C^2/Jm) and P_j is the dipole moment of the adsorbate, j, in the adsorbed state. Typically P_j values are in the order of 10^{-29} Cm or 3D (Debye). The Debye unit, D, equals $3.36\cdot10^{-10}$ Cm. Dipole moments of adsorbates, P_j, are taken in this book by convention negative when the positive side of the adsorbate dipole is pointing towards the vacuum (e.g. $Na^{\delta+}$ on Pt) and positive when the negative side of the adsorbate dipole is pointing toward the vacuum (e.g. $O^{\delta-}$ on Pt). According to Eq. (5.16) in the former case one has a decrease in Φ while in the latter case one has an increase in Φ.

5.4.2 The Work Function of Catalyst Films Deposited on Solid Electrolytes

5.4.2.1 Experimental Results

Work function, a quantity of great importance in surface science and catalysis, plays a key role in solid state electrochemistry and in electrochemical promotion. As will be shown in Chapter 7 the work function of the gas-exposed surface of an electrode in a solid electrolyte cell can be used to define an absolute potential scale in solid state electrochemistry.

In this chapter, however, we will first examine how the work function Φ of the gas exposed surface of a catalyst-electrode changes with gaseous composition and catalyst potential U_{WR}. That Φ will change with varying gaseous composition over the catalyst-electrode should be no surprise, in view of Eq. (5.16), since the coverages of adsorbed reactants and products on the catalyst-electrode surface depend on gaseous composition. The observation, however that Φ changes with varying catalyst potential U_{WR} and in fact in a very simple one-to-one manner came as a surprise when first reported[2] although such a variation had been anticipated and predicted on the basis of the very first NEMCA studies.[3]

What was found experimentally[2,24-29] and explained theoretically[30,33] was that:

1. Solid electrolyte cells can be used to alter significantly the work function Φ of the gas-exposed, i.e., catalytically active, catalyst electrode surface by polarizing the catalyst-solid electrolyte interface.

$$e\Delta U_{WR} \neq 0 \Rightarrow \Delta\Phi \neq 0 \tag{5.17}$$

2. Over a wide range of conditions (i.e. as long as ion backspillover from the solid electrolyte forms a double layer at the metal/gas interface)[30-33]

solid electrolyte cells are *work function probes and work function controllers* for the gas-exposed, catalytically active catalyst-electrode surfaces, i.e. the change $\Delta\Phi$ in catalyst surface average work function Φ is equal to $e\Delta U_{WR}$. The catalyst potential U_{WR} with respect to a reference electrode can be varied both by changing the gaseous composition and/or by polarizing the catalyst-solid electrolyte interface.

$$e\Delta U_{WR} = \Delta\Phi_W \tag{5.18}$$

This is shown in Figures 5.8 to 5.13 which demonstrate (Figures 5.10 to 5.12) that Eq. (5.18) is also valid to a good approximation not only at steady state but also during transients.

3. Over a wide range of conditions (again i.e., as long as ion backspillover from the solid electrolyte forms a double layer at the metal/gas interface)[30-33] the potential difference eU_{WR} is equal to the difference in work functions between the two electrodes

$$eU_{WR} = \Phi_W - \Phi_R \tag{5.19}$$

This amazing result is shown in Figure 5.14 to 5.16 and is discussed in detail in Chapter 7.

Equation (5.18) plays a key role in understanding and interpreting the NEMCA effect and it is therefore important to discuss it in some detail. Equation (5.19) is discussed in detail in Chapter 7 in connection with the absolute potential scale of solid state electrochemistry.

5.4.2.2 Implications of the Experimental Results

We start by considering a schematic representation of a porous metal film deposited on a solid electrolyte, e.g., on Y_2O_3-stabilized-ZrO_2 (Fig. 5.17). The catalyst surface is divided in two distinct parts: One part, with a surface area A_E is in contact with the electrolyte. The other with a surface area A_G is not in contact with the electrolyte. It constitutes the gas-exposed, i.e., catalytically active film surface area. *Catalytic reactions* take place on this surface only. In the subsequent discussion we will use the subscripts E (for electrolyte) and G (for gas), respectively, to denote these two distinct parts of the catalyst film surface. Regions E and G are separated by the three-phase-boundaries (tpb) where *electrocatalytic reactions* take place. Since, as previously discussed, electrocatalytic reactions can also take place to, usually,a minor extent on region E, one may consider the tpb to be part of region E as well. It will become apparent below that the essence of NEMCA is the following: One uses electrochemistry (i.e. a slow electrocatalytic reaction) to alter the electronic properties of the metal-solid electrolyte interface E.

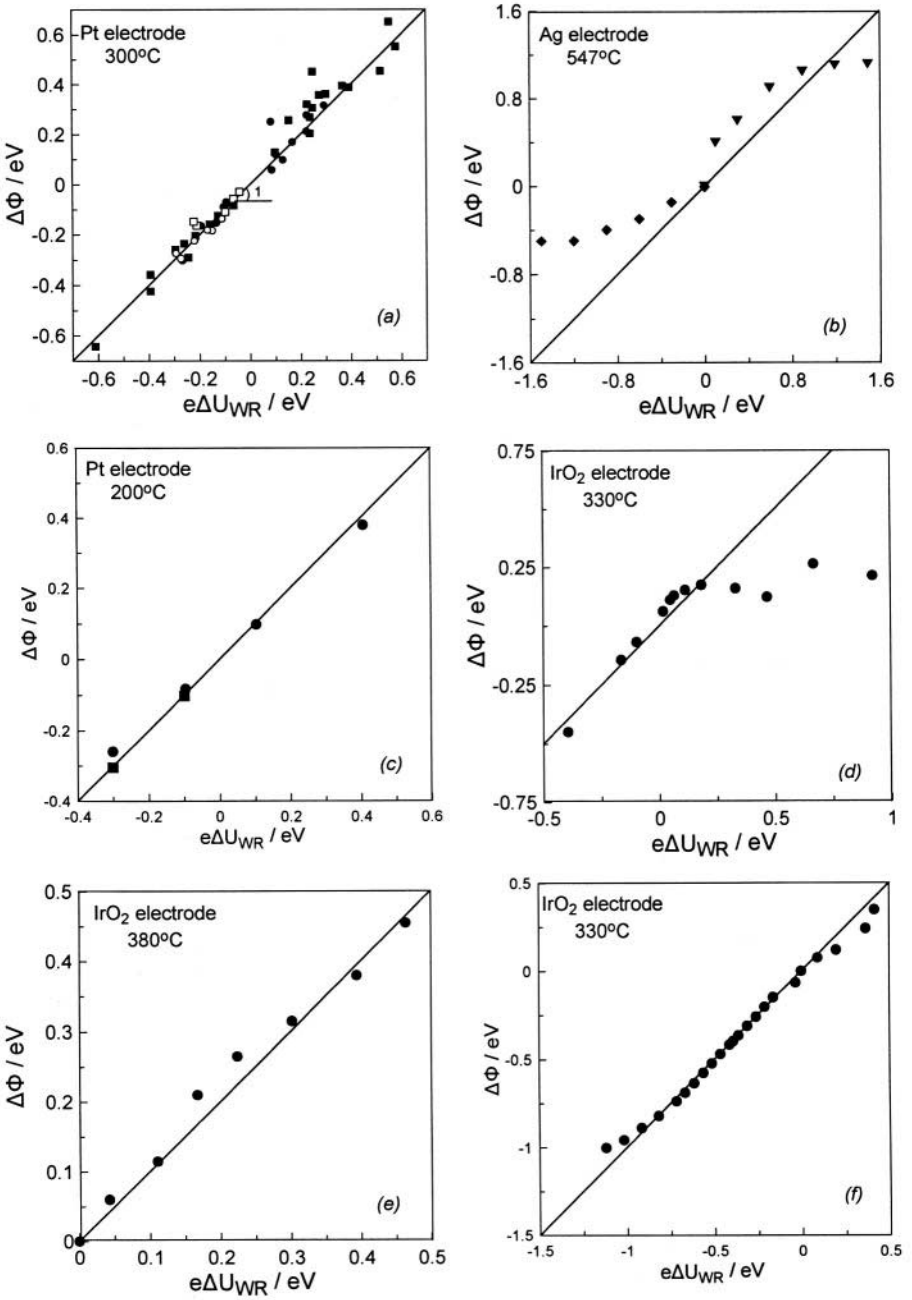

Figure 5.8. Effect of catalyst-electrode potential U_{WR} on the work function Φ of the gas exposed catalyst-electrode surface (a) Pt/YSZ, T = 300°C (squares), Pt/β″-Al_2O_3, T = 240°C (circles), filled symbols: closed-circuit operation, open symbols: open-circuit operation, O_2, C_2H_4/O_2 and NH_3/O_2 mixtures.[2,26] (b) Ag/YSZ, T = 547°C,[24] (c) Pt/β″-Al_2O_3, T = 200°C,[25] (d) IrO_2/YSZ, T = 330°C, air,[27] (e) IrO_2/YSZ, T = 380°C, p_{O_2} = 15 kPa, $p_{C_2H_4} = 5 \cdot 10^{-2}$ kPa,[27] (f) IrO_2/ β″-Al_2O_3, T = 330°C, air.[27]

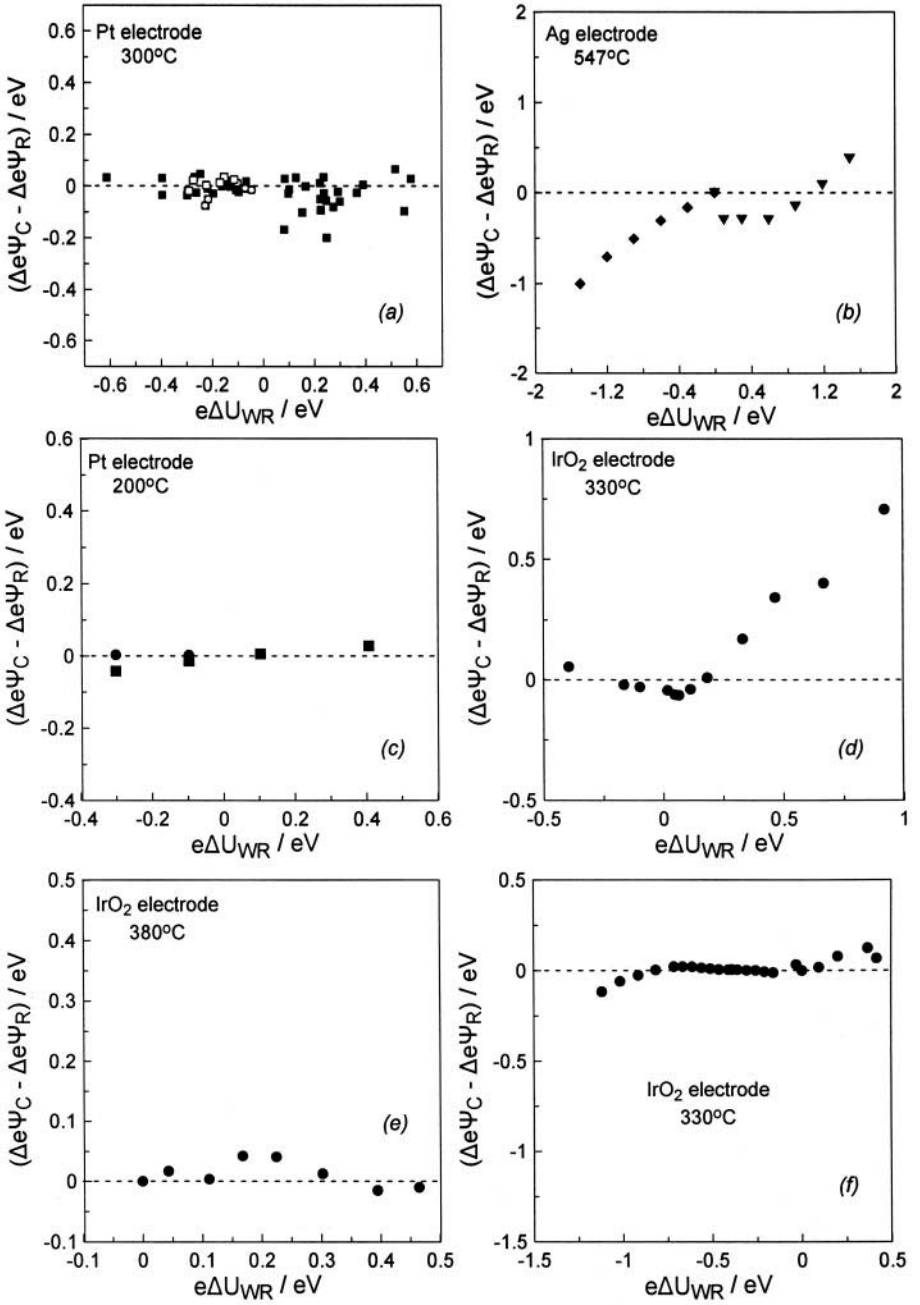

Figure 5.9. Effect of catalyst-electrode potential U_{WR} on $e\Delta\Psi_c$-$e\Delta\Psi_R$ which equals by definition (and $\Delta\Phi_R = 0$) to $\Delta\Phi_c$-$e\Delta U_{WR}$ for (a) Pt/YSZ, T = 300°C (squares), Pt/β″-Al_2O_3, T = 240°C (circles), filled symbols: closed-circuit operation, open symbols: open-circuit operation, O_2, C_2H_4/O_2 and NH_3/O_2 mixtures,[2,26] (b) Ag/YSZ, T = 547°C,[24] (c) Pt/β″-Al_2O_3, T = 200°C[25], (d) IrO_2/YSZ, T = 330°C, air,[27] (e) IrO_2/YSZ, T = 380°C, p_{O_2} = 15 kPa, $p_{C_2H_4}$ = $5\cdot10^{-2}$ kPa,[27] (f) IrO_2/β″-Al_2O_3, T = 330°C, air.[27]

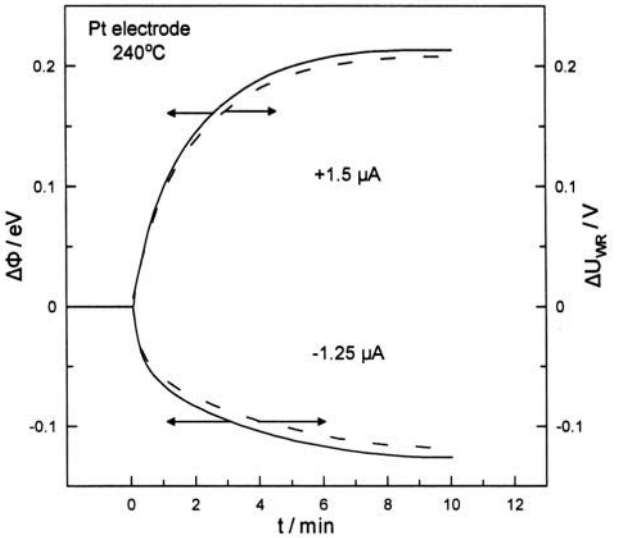

Figure 5.10. Transient response of catalyst work function Φ and potential U_{WR} upon imposition of constant currents I between the Pt catalyst (labeled[26] C2) and the Pt counter electrode; β"-Al_2O_3 solid electrolyte; T = 240°C, p_{O2} = 21 kPa; Na ions are pumped to (I<0) or from (I>0) the catalyst surface at a rate I/F.[26] Reprinted with permission from Elsevier Science.

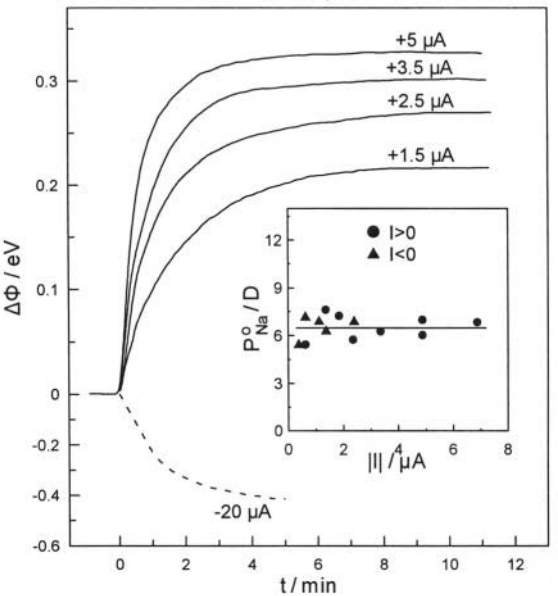

Figure 5.11. Effect of applied current on induced work function change on Pt/β"-Al_2O_3;[26] dashed line: catalyst labeled[26] C1, T = 291°C, p_{O2} = 5 kPa, p_{C2H4} = 2.1x10^{-2} kPa; solid lines: catalyst labeled[26] C2, T = 240°C, p_{O2} = 21 kPa, Inset: Effect of applied current on computed initial dipole moment of Na on Pt; (●): I>0, (▲): I<0.[26] Reprinted with permission from Elsevier Science.

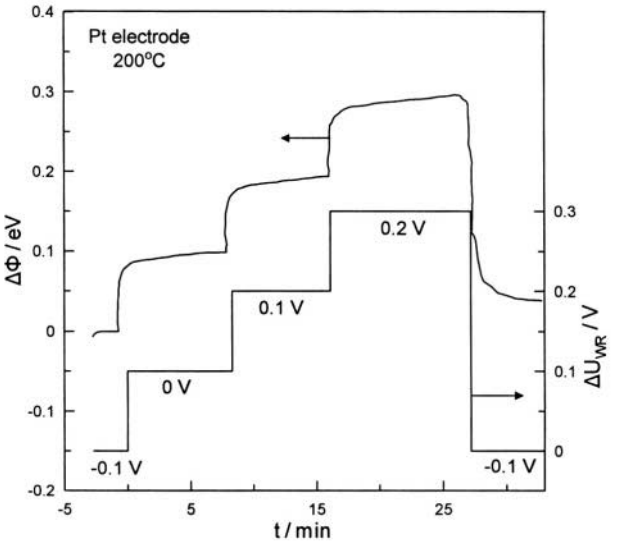

Figure 5.12. Time evolution of catalyst potential and work function for Pt/β″-Al_2O_3 during potentiostatic transients, T = 200°C, $p_{O_2} = 10^{-10}$ Pa.[25]

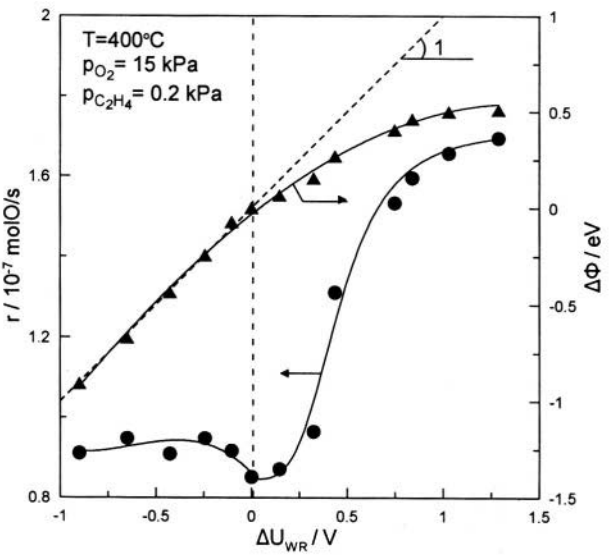

Figure 5.13. Effect of catalyst overpotential, ΔU_{WR}, on catalytic rate and on catalyst work function changes, $\Delta\Phi$, during ethylene oxidation on Pt/YSZ at 400°C.[34]Reprinted with permission from Elsevier Science.

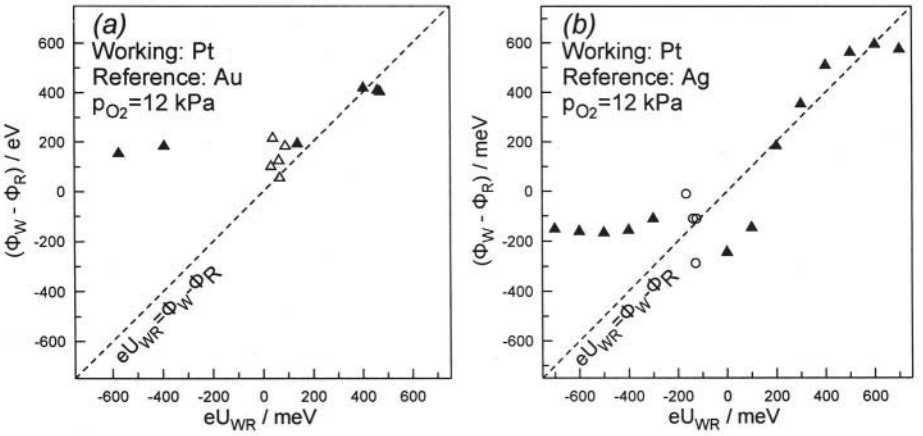

Figure 5.14. Dependence of Φ_W-Φ_R on catalyst potential eU_{WR} for the systems (a) Pt(W)-Au(R) and (b) Pt(W)-Ag(R) at T=400°C. Open symbols: Open-circuit operation in O_2-He mixtures. Filled symbols: Closed circuit operation at p_{O_2}=12 kPa.[32] Reprinted by permission of The Electrochemical Society.

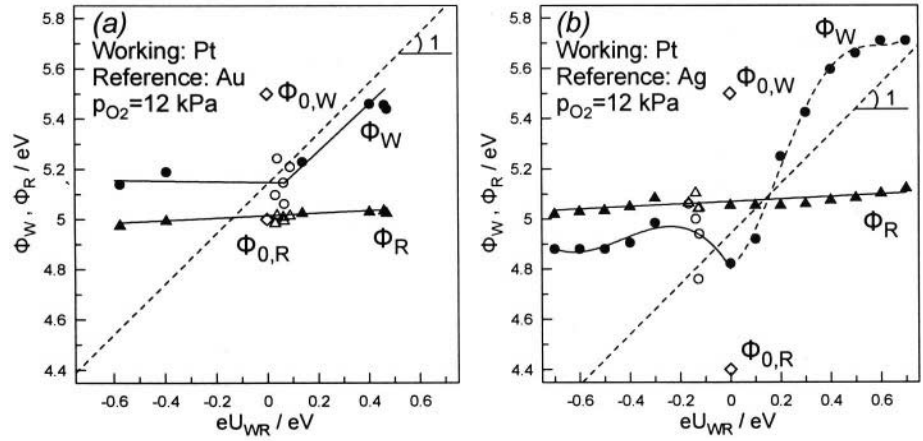

Figure 5.15. Work function of working (W) and reference (R) electrode, Φ_W and Φ_R, as a function of catalyst potential eU_{WR} for the systems (a) Pt(W)-Au(R) and (b) Pt(W)-Ag(R). Symbols and conditions as in Fig. 5.14.[32] Reproduced by permission of The Electrochemical Society.

This perturbation is then propagated via the spatial constancy of the Fermi level E_F throughout the metal film to the metal-gas interface G, altering its electronic properties thus causing ion migration and thus influencing catalysis, i.e. catalytic reactions taking place on the metal-gas interface G.

We then concentrate on the meaning of U_{WR}, that is, of the (ohmic-drop-free) potential difference between the catalyst film (W, for working electrode) and the reference film (R). The measured (by a voltmeter),

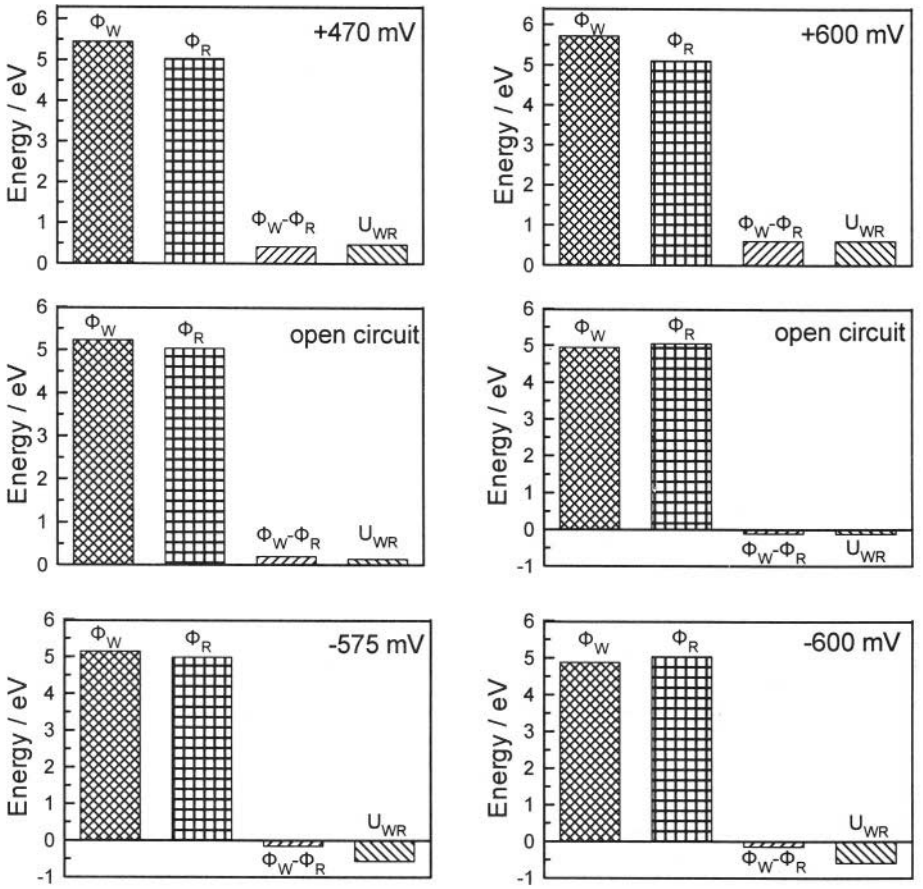

Figure 5.16. Bar charts of Φ_W, Φ_R, Φ_W-Φ_R and U_{WR} at +470 mV, open circuit (U^o_{WR} = 68 mV) and –575 mV for the system Pt(W)-Au(R) (left) and at +600 mV, open circuit (U^o_{WR} = –124 mV) and –600 mV for the system Pt(W)-Ag(R) (right) at T=400°C and p_{O_2}=12 kPa.[32] Reproduced by permission of The Electrochemical Society.

potential difference U_{WR} is, by definition,[33,35] the difference between electrochemical potentials $\bar{\mu}$ of the two electrodes:

$$eU_{WR} = \bar{\mu}_R - \bar{\mu}_W \tag{5.20}$$

As already noted the electrochemical potential of electrons in a metal, $\bar{\mu}$, is related to the Galvani potential φ via:

$$\bar{\mu} = \mu + (-e)\varphi \tag{5.15}$$

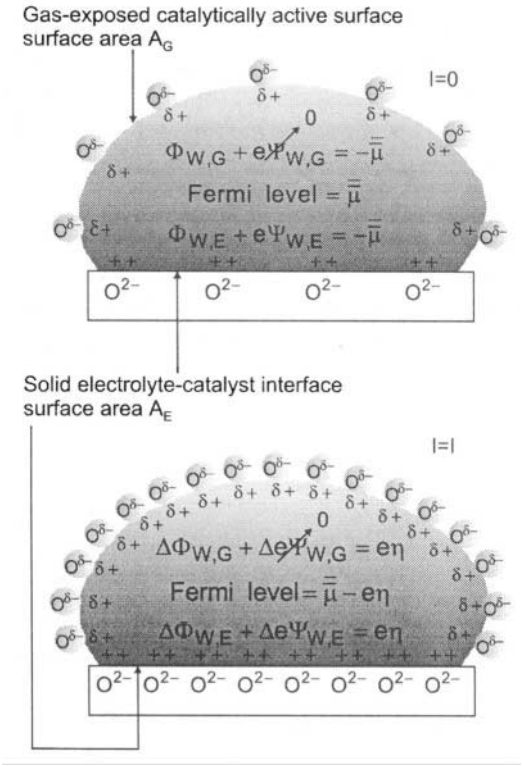

Figure 5.17. Schematic representation of a metal crystallite deposited on YSZ and of the changes induced in its electronic properties upon polarizing the catalyst-solid electrolyte interface and changing the Fermi level (or electrochemical potential of electrons) from an initial value $\bar{\bar{\mu}}$ to a new value $\bar{\bar{\mu}}$ -eη.[30,31] Reprinted with permission from Elsevier Science.

where μ is the chemical potential of electrons in the metal, a purely bulk property and the Galvani potential φ is the electrostatic potential of electrons inside the metal film. It is also worth reminding that $\bar{\bar{\mu}}$ can be shown[18,19] to be identical with the Fermi level E_F in the metal (Fig. 5.7, 5.18, and refs. [9,10,16-22] which provide an excellent introduction to the meaning of the various potentials discussed here). In view of Eq. (5.15) one can rewrite Eq. (5.20) as:

$$eU_{WR} = (\mu_R - \mu_W) - e(\varphi_R - \varphi_W) \tag{5.21}$$

Equation (5.21) is based on the electrochemical way of counting the energy difference between zero (defined throughout this book as the potential energy of an electron at its ground state at "infinite" distance from the metal) and the Fermi level E_F (Eq. 5.15). The latter quantity must not be confused with the Fermi energy μ_o which is the energy difference between

the Fermi level and the energy at the bottom of the conduction band and provides a measure of the average kinetic energy of electrons at the Fermi level (Fig. 5.7). The electrochemical way of splitting the energy difference from zero to E_F is a conceptual one, as the absolute values of φ and μ are not accessible to direct experimental measurement. Even the separatability of μ and φ has been disputed.

Therefore it is much more useful to use the second way of splitting the energy difference between zero and $\bar{\mu}$, which is common in the area of surface science, i.e. to consider $-\bar{\mu}$ as the sum of the work function Φ and of $e\Psi$, where Ψ is the outer (or Volta) potential or vacuum level of the surface under consideration:

$$-\bar{\mu} = \Phi + e\Psi \tag{5.14}$$

As previously noted the work function Φ is the work required to bring an electron from the Fermi level of the metal to a point outside the metal where the image forces are negligible, i.e., typically 1 to 0.1 μm outside the metal surface.[9,10,16-22] The Volta potential Ψ at this point is defined so that the energy required to bring an electron from that point to an "infinite" distance from the metal surface is $e\Psi$.

It is important to emphasize again that Φ and Ψ (which are both accessible to experimental measurement)[16-22] are not, in general, spatially uniform over the metal surface. Different crystallographic planes are well known to have different Φ values and thus non-trivial variations in Φ and $e\Psi$ are to be expected on the surface of polycrystalline samples. It is important, however, to notice that their sum is always spatially uniform (Eq. 5.14) since the electrochemical potential $\bar{\mu}$ or, equivalently, Fermi level E_F is spatially uniform. This is true even when an electrical current is passing through the metal film under consideration, provided that the ohmic drop in the film is negligible (less than a few mV) which is always the case with the conductive metal films and low currents employed in NEMCA studies. It is also important to notice that, by definition, Ψ vanishes if there is no <u>net</u> charge on the metal surface under consideration. This is a direct consequence of Gauss's fundamental law in electrostatics, provided the surface under consideration is not the interior of a hollow conductor.

One can then combine Eqs. (5.20) and (5.14) to obtain:

$$eU_{WR} = \Phi_W - \Phi_R + e(\Psi_W - \Psi_R) \tag{5.22}$$

It is worth emphasizing that Eq. (5.22) is valid under both open-circuit and closed-circuit conditions and that it holds for *any* part of the surfaces of the catalyst and the reference electrodes. Thus, referring to the metal electrode surfaces in contact with the electrolyte (region E) it is:

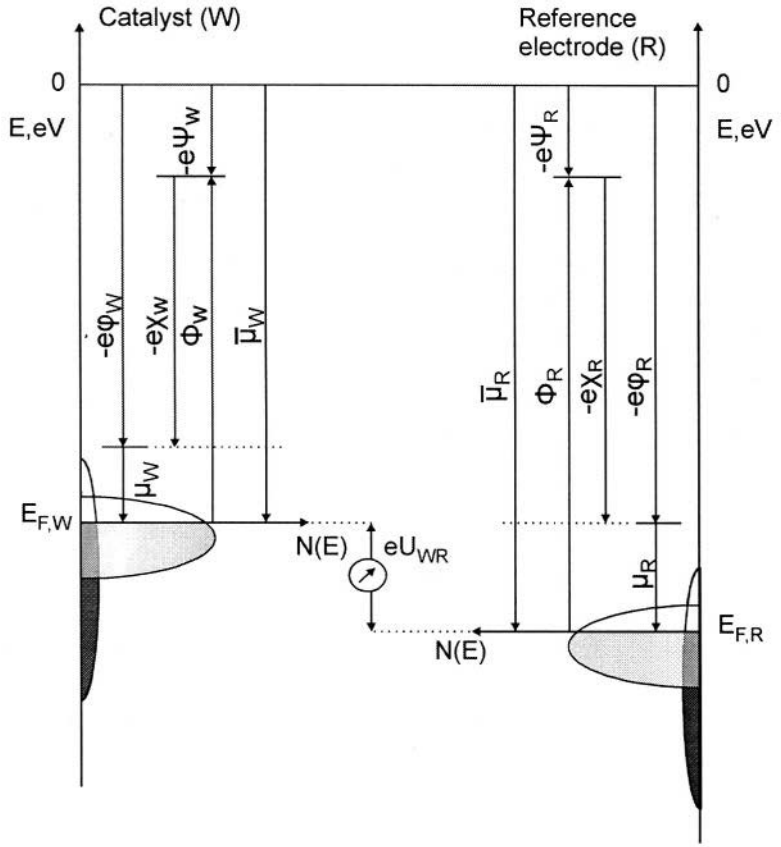

Figure 5.18. Schematic representation of the density of states N(E) in the conduction band and of the definitions of work function Φ, chemical potential of electrons μ, electrochemical potential of electrons or Fermi level $\bar{\mu}$, surface potential χ, Galvani (or inner) potential φ and Volta (or outer) potential Ψ for the catalyst (W) and for the reference electrode (R). The measured potential difference U_{WR} is by definition the difference in Fermi levels; φ, μ and $\bar{\mu}$ are spatially uniform; Φ and Ψ can vary locally on the metal sample surfaces; and the Ψ potentials vanish, on the average, for the (effective double layer covered) gas-exposed catalyst and reference electrode surfaces.[32] Reprinted with permission from The Electrochemical Society.

$$eU_{WR} = \Phi_{W,E} - \Phi_{R,E} + e(\Psi_{W,E} - \Psi_{R,E}) \tag{5.23}$$

while for the gas-exposed, i.e., catalytically active electrode surfaces (region G) it is:

$$eU_{WR} = \Phi_{W,G} - \Phi_{R,G} + e(\Psi_{W,G} - \Psi_{R,G}) \tag{5.24}$$

In order to discuss the origin of NEMCA one needs to concentrate only on Eq. (5.24) which refers to the gas-exposed, catalytically active, film

surface. As already stated, different crystallographic planes will, in general, have different Φ values, thus, even over region G the work function Φ needs not to be spatially uniform. These local spatial variations in Φ and Ψ are not expected to be significant in polycrystalline films with large (~1 μm) crystallites such as the ones used in most NEMCA studies[5] since the surface consists primarily of low Miller index crystallographic planes, e.g. of the (111) plane in the case of Pt films.[5] This is supported by recent STM information, e.g. Fig. 4.3. We can thus first reasonably assume that Φ and Ψ are spatially uniform over region G and will treat the more general case below. Returning to Eq. (5.24) we note that when U_{WR} is changed by varying the gaseous composition over the catalyst or by polarizing by means of a current the catalyst-solid electrolyte interface, then the properties of the reference electrode remain unaffected[31,32] and thus:

$$e\Delta U_{WR} = \Delta\Phi_{W,G} + e\Delta\Psi_{W,G} \tag{5.25}$$

It must be emphasized that Equations (5.24) and (5.25) stem from the definitions of Fermi level, work function and Volta potential and are *generally valid* for any electrochemical cell, solid state or aqueous. We can now compare these equations with the corresponding *experimental* equations (5.18) and (5.19) found to hold, under rather broad temperature, gaseous composition and overpotential conditions (Figs. 5.8 to 5.16), in solid state electrochemistry:

$$eU_{WR}=\Phi_{W,G}-\Phi_{R,G} \tag{5.19}$$

$$e\Delta U_{WR} = \Delta\Phi_{W} \tag{5.18}$$

What do we learn from this comparison of the *general theoretical* equations (5.24) and (5.25) with the *specific experimental* equations (5.19) and (5.18) of solid state electrochemistry? The answer is mathematically obvious and physically important. In solid state electrochemistry one has:

$$\Psi_{W,G}-\Psi_{R,G}=0 \tag{5.26}$$

$$\Delta\Psi_{W,G}=0;\ \Psi_{W,G}=C \tag{5.27}$$

Furthermore, to the extent that the entire solid electrolyte cell under consideration is overall neutral, i.e. carries no net charge, one can show using Gauss's law of electrostatics, that the constant C in Eq. (5.27) is zero, i.e. that:

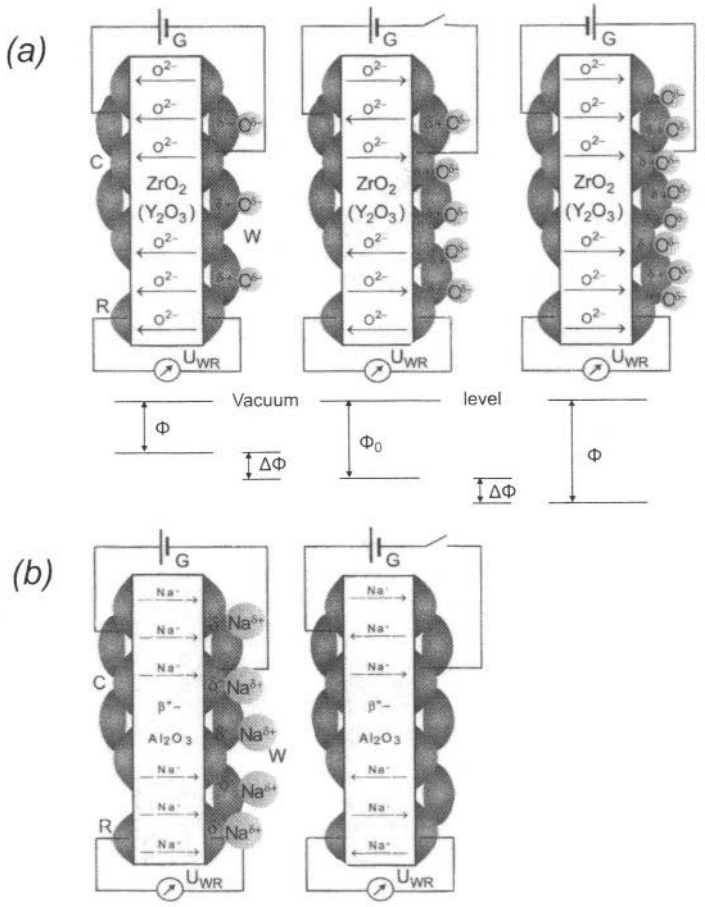

Figure 5.19. The physical origin of NEMCA: When a metal counter electrode (C) is used in conjunction with a galvanostat (G) to supply or remove ions [O^{2-} for the doped ZrO_2 (a), Na^+ for β"-Al_2O_3 (b)] to or from the polarizable solid electrolyte/catalyst (or working electrode, W) interface, backspillover ions [$O^{\delta-}$ in (a), $Na^{\delta+}$ in (b)] together with their compensating charge in the metal are produced or consumed at the tpb between the three phases solid electrolyte/catalyst/gas. This causes an increase (right) or decrease (left) in the work function Φ of the gas-exposed catalyst surface. In all cases $\Delta\Phi = e\Delta U_{WR}$ where ΔU_{WR} is the overpotential measured between the catalyst and the reference electrode (R).

$$\Psi_{W,G}=\Psi_{R,G}=0 \tag{5.28}$$

What is the physical implication of the experimental equations (5.26) to (5.28)? They simply reflect the fact that the effective double layer formed (via ion spillover) at the metal/gas interface is, as every double layer, overall neutral.

The implications of equations (5.26) to (5.28) and of their, mathematically and physically equivalent, equations (5.19) and (5.18) are simple, direct and important.

Equation (5.19) shows that the emf eU^{o}_{WR} of solid electrolyte cells provides a direct measure of the difference in work function of the two gas-exposed, i.e., catalytically active, electrode surfaces. Thus, solid electrolyte cells are work function probes for their gas exposed electrode surfaces. This was shown in Figures 5.15 and 5.16.

Equation (5.18) is equally important, as it shows that the work function of the catalytically active catalyst electrode surface can be varied at will by varying the (ohmic-drop-free) catalyst potential. This can be done either by varying the gaseous composition over the catalyst or by using a potentiostat. Catalytic chemists are familiar with the former mode: When the gaseous composition changes, then surface coverages will change with a concomitant change in work function. But what about the latter? For the work function to change the coverages and/or dipole moments of species already adsorbed on the surface must change, or new species must get adsorbed. As discussed in this chapter, it is now firmly established that the induced work function change on the surface is predominantly due to the migration (backspillover) of ions originating from the solid electrolyte. (We use the term "backspillover" instead of "spillover" for the following reason: In catalysis the term "spillover" denotes migration of adsorbates from a supported metal catalyst to an oxide carrier (support). The term "backspillover" denotes migration of species in the opposite direction i.e., from the support to the metal catalyst, as is the case here). These backspillover ions (oxygen anions for the case of doped ZrO_2, partly ionized Na for the case of β''-Al_2O_3) accompanied by their compensating charge in the metal, thus forming spillover dipoles, spread over the catalytically active surface altering its work function and catalytic properties (Fig. 5.19).

5.4.3 The Work Function of Catalyst Films Deposited on Solid Electrolytes: Rationalization of the Potential–Work Function Equivalence

The key experimental observations:

$$e\Delta U_{WR} = \Delta\Phi_W \tag{5.18}$$

$$eU_{WR} = \Phi_W - \Phi_R \tag{5.19}$$

$$\Psi_W = \Psi_R = 0 \tag{5.29}$$

are due to ion spillover on the electrode surfaces and to the formation there of the effective electrochemical double layer. This double layer neutralizes any net electrostatic charge residing on the gas exposed electrode surface (surface charge density $\sigma = 0$, $\Psi = 0$) as follows:

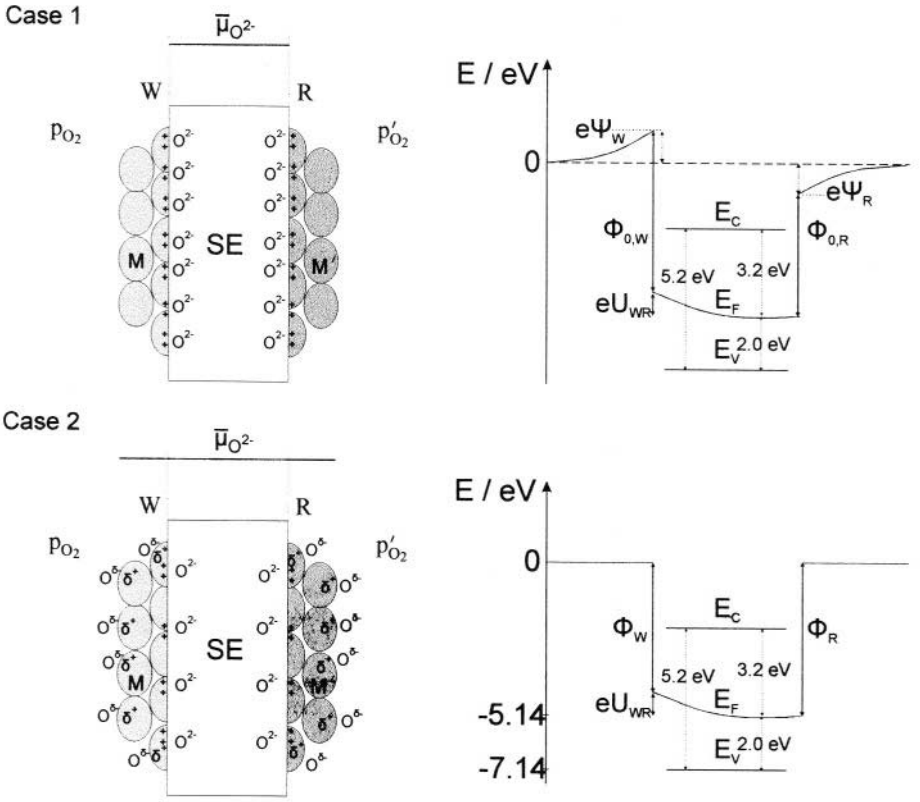

Figure 5.20. Left: Schematic of an O^{2-} conducting solid electrolyte cell with fixed p_{O_2} and p'_{O_2} values at the porous working (W) and reference (R) electrodes *without* (top) and *with* (bottom) ion backspillover on the gas exposed electrodes surfaces, showing also the range of spatial constancy of the electrochemical potential, $\bar{\mu}_{O^{2-}}$, of O^{2-}. Right: Corresponding spatial variation in the electrochemical potential of electrons, $\bar{\mu}_e (= E_F)$; U_{WR} is fixed in both cases to the value (RT/4F)ln(p_{O_2} / p'_{O_2}); also shown in the relative position of the valence band, E_V, and of the bottom of the conduction band, E_C, in the solid electrolyte (SE); numerical values correspond to 8 mol% Y_2O_3-stabilized-ZrO_2, $p_{O_2} = 10^{-6}$ bar, $p'_{O_2} = 1$ bar and T=673 K.[32] Reproduced by permission of The Electrochemical Society.

Consider the solid electrolyte cell shown in Figure 5.20. For simplicity we consider only a working (W) and reference (R) electrode deposited on a solid electrolyte, such as YSZ or β''-Al_2O_3. The two electrodes are made of the same metal or of two different metals, M and M′. The partial pressures of O_2 on the two sides of the cell are p_{O_2} and p'_{O_2} . Oxygen may chemisorb on the metal surfaces so that the workfunctions Φ_W and Φ_R of the two gas-exposed electrode surfaces are $\Phi_W(p_{O_2})$ and $\Phi_R(p'_{O_2})$.

We consider now the following cases[30-33]:

1. The temperature is low so that ionic mobility on the electrode surfaces is negligible, i.e. *there is no spillover.*

One always has by definition:

$$eU_{WR} = -(\bar{\mu}_W - \bar{\mu}_R) = \Phi_W - \Phi_R + e\Psi_W - e\Psi_R \tag{5.30}$$

Also due to the establishment of the equilibrium:

$$O_2(g) + 4e^- \leftrightarrow 2O^{2-} \tag{5.31}$$

at the metal-gas-solid electrolyte three-phase-boundaries, one has:

$$\mu_{O_2} + 4\bar{\mu}_W = 2\bar{\mu}_{O^{2-}} = \mu'_{O_2} + 4\bar{\mu}_R \tag{5.32}$$

and from Eq. (5.30):

$$eU_{WR} = (1/4F)(\mu_{O_2} - \mu'_{O_2}) = (RT/4F)\ln(p_{O_2}/p'_{O_2}) \tag{5.33}$$

Thus upon comparing Eqs. (5.23) and (5.33) one has:

$$e\Psi_W - e\Psi_R = \underset{\text{fixed}}{eU_{WR}} + \underset{\text{fixed}}{\Phi_R(p'_{O_2})} - \underset{\text{fixed}}{\Phi_W(p_{O_2})} \tag{5.34}$$

Since p_{O_2} and p'_{O_2} are fixed, U_{WR} is fixed and also, since there is no spillover, $\Phi_R(p'_{O_2})$ and $\Phi_W(p_{O_2})$ are also fixed. Thus in case 1 (*no ion spillover*) $e\Psi_W$-$e\Psi_R$ is fixed to an (in general) *nonzero value.*

In fact, consider as an example of application of Eq. (5.34) the case $p_{O_2} = p'_{O_2}$, thus $U_{WR} = 0$. Then one has:

$$e\Psi_W - e\Psi_R = \Phi_R(p'_{O_2}) - \Phi_W(p_{O_2}) \neq 0 \tag{5.35}$$

Thus if the working and counter electrodes are made of different metals, then Eq. (5.35) gives the *cpd* (contact potential difference) of the two metals:

$$cpd = e\Psi_W - e\Psi_R = \Phi_{M'} - \Phi_M \tag{5.36}$$

The same result as in the case $p_{O_2} = p'_{O_2}$ is obtained if the electrolyte is not present but the two metals are brought in direct contact so that $\bar{\mu}_W = \bar{\mu}_R$, from which Eq. (5.36) is directly derived.

The non-zero value of $e\Psi_W$-$e\Psi_R$ in Eq. (5.35) implies that there are net surface charges on the gas exposed electrode surfaces. These charges (q_+,q_-) have to be opposite and equal as the cell is overall electrically neutral and all other charges are located at the metal-solid electrolyte interfaces to maintain their electroneutrality. The charges $q_+ = -q_-$ are quite small in relation to the charges, Q, stored at the metal-electrolyte interface but nevertheless the

system has, due to their presence, an excess electrostatic energy:

$$E_C = (\Psi_W - \Psi_R)\, q_+ \tag{5.37}$$

The positive charge is on the electrode with the lower work function.

2. The temperature is now increased to the point that the ionic mobility on the electrode surfaces is high, so that now *there is ion spillover.*

Oxygen anions are thus now attracted to the electrode with the positive charge or the electrode which has been made positive by anodic polarization. Backspillover will continue untill the charge is neutralized. Similarly oxygen anions will be repelled from the negatively charged or cathodically polarized electrode to enter into the YSZ structure. The charges q_+ and q_- thus disappear and thus Ψ_W and Ψ_R vanish.

To prove this formally one has to examine again Eq. (5.34):

$$e\Psi_W - e\Psi_R = \underset{\text{fixed}}{eU_{WR}} + \underset{\text{variable}}{\Phi_R} - \underset{\text{variable}}{\Phi_W} \tag{5.38}$$

Now eU_{WR} is still fixed by Eq. (5.33) but Φ_R and Φ_W are *variables.* They can change due to the spillover of ions. They will change in such a way as to minimize the excess electrostatic energy of the system

$$E_C = (\Psi_W - \Psi_R)\, q_+ = 0 \tag{5.39}$$

This can be done when $\Psi_W = \Psi_R$, which implies that $q_+ = q_- = 0$ *for an overall neutral system,* i.e. $\Psi_W = \Psi_R = 0$. But note that even for an *overall charged system,* i.e. a system where a net charge q has been introduced via, e.g. a van de Graaf machine, the excess electrostatic energy is:

$$E_C = (\Psi_W - \Psi_R)\, q \tag{5.40}$$

and is minimized by

$$\Psi_W = \Psi_R \tag{5.41}$$

Thus even in this case, where q cannot vanish, Eq. (5.41) is satisfied.

It therefore follows from Eqs. (5.38) and (5.41) that:

$$eU_{WR} = \Phi_W - \Phi_R \tag{5.42}$$

$$\Psi_W = \Psi_R = 0 \quad \text{(overall neutral cell)} \tag{5.43}$$

$$\Psi_W = \Psi_R \quad \text{(overall charged cell)} \tag{5.44}$$

5.4.4 Spatial Variations

One can then address the question of the meaning of Eqs. (5.18) and (5.19) in the case of significant spatial variations in the work function Φ of the polycrystalline catalyst surface. In this case, due to the constancy of the Fermi level, slightly different nonzero excess free charge densities will exist on different planes with different Φ, causing local variations in Ψ. Surface physicists would refer to this as a local variation in the "vacuum level" $e\Psi$. In this case the average surface work function Φ is defined from[5,16-21] .

$$\Phi = \sum_j f_j \Phi_j \tag{5.45}$$

where f_j is the total catalyst surface fraction corresponding to a crystallographic plane with a work function Φ_j. One can then apply Eq. (5.24) to each crystallographic plane j:

$$eU_{WR} = \Phi_{W,G\,j} - \Phi_{R,G} + e(\Psi_{W,G\,j} - \Psi_{R,G}) \tag{5.46}$$

By multiplying Eq. (5.46) by f_j, summing for all planes and noting that $\Psi_{R,G} = 0$, for overall neutral cell under conditions of spillover, one obtains:

$$eU_{WR} = \sum_j f_j \Phi_{W,G,j} - \Phi_{R,G} + \sum_j f_j e\Psi_{W,G,j} \tag{5.47}$$

Since Ψ is via Gauss's Law of electrodynamics proportional to the local excess free charge it follows that the term $\Sigma f_j e\Psi_{W,G,j}$ is proportional to the net charge stored in the metal in region G. This net charge, however, was shown above to be zero, due to the electroneutrality of the backspillover-formed effective double layer at the metal/gas interface and thus $\Sigma f_j e\Psi_{W,G,j}$ must also vanish. Consequently Eq. (5.47) takes the same form with Eq. (5.19) where, now, Φ stands for the average surface work function. The same holds for Eq. (5.18).

As already shown on Figures 5.8 and 5.11, Eqs. (5.18) and (5.19) have been obtained experimentally with polycrystalline Pt, Ag and Au catalyst electrodes deposited on YSZ and β''-Al_2O_3.

As an example Figure 5.8a shows that the change, $\Delta\Phi$ in the work function of the polycrystalline gas-exposed (that is, catalytically active) surface of the catalyst equals $e\Delta U_{WR}$, both under closed- and open-circuit conditions. In the former case U_{WR} was varied by changing the polarizing current with the catalyst exposed to air or to $NH_3/O_2/He$ and $CO/O_2/He$ mixtures, whereas in the latter only the gaseous composition was varied. Both doped ZrO_2 and β''-Al_2O_3 solid electrolytes have been used and several laboratories have confirmed this important finding.[2,24-29] The validity of Eq. (5.19) has been recently confirmed using two Kelvin probes to measure Φ_W and Φ_R independently. (Figs. 5.15 & 5.16).[32]

5.4.5 Transients and Measurement of Dipole Moments

As already shown in Figures 5.10 and 5.11 the equality $\Delta\Phi = e\Delta U_{WR}$ also holds to a good approximation during transients. In this case a constant current is applied at t = 0 between the catalyst and the counter electrode and one follows the time evolution of U_{WR} by a voltmeter and of Φ by a Kelvin probe.

Work function transients of the type shown on Figures 5.10 and 5.11 can be used to estimate initial dipole moments of the spillover dipoles on the catalyst surface.[5,36,37]

Thus referring to Na supply onto a Pt catalyst surface with surface area A_G via a β''-Al_2O_3 solid electrolyte (Fig. 5.10), one can use Faraday's law to obtain:

$$\frac{d\theta_{Na}}{dt} = -\frac{N_{AV}(I/F)}{A_G N_{Pt}} \tag{5.48}$$

where N_{AV} is Avogadro's number and $N_{Pt} = 1.53 \cdot 10^{19}$ atoms/m^2 is the surface Pt atom concentration on the Pt(111) plane. One can then combine Eq. (5.48) with the definition of the Na coverage $\theta_{Na}(=N_{Na}/N_{Pt})$ and with the differential form of the Helmholz equation:

$$\frac{d\Phi}{dt} = -\frac{e|P^o_{Na}|}{\varepsilon_o} \cdot \frac{dN_{Na}}{dt} \tag{5.49}$$

where N_{Na} denotes adsorbed Na atoms/m^2, $\varepsilon_o = 8.85 \cdot 10^{-12}$ C^2/J·m and $|P^o_{Na}|$ is the absolute value of the initial dipole moment of Na on Pt to obtain:

$$\frac{d\Phi}{dt} = \frac{|P^o_{Na}|I}{\varepsilon_o A_G} \tag{5.50}$$

Using Eq. (5.50) and the initial slope in Fig. 5.11 one computes the absolute value of initial dipole moment P^o_{Na} of Na on Pt to be $2.15 \cdot 10^{-29}$ C·m or 6.5 D, i.e., 22% higher than the literature value of 5.3 D for Na on a clean Pt(111) surface.[21] This is excellent agreement, in view of the fact that in the case of Fig. 5.11 the Pt surface is essentially saturated in oxygen,[26] which has been shown for systems like Cs/W(110) and Cs/Ni(100)[21] to give P° values typically 20-30% higher than on the clean metal surface. As shown on Fig. 5.11 the computed P° value is independent of the magnitude and sign of the applied current, which confirms the validity of the approach. One additional conclusion which may be drawn is that Na introduced on metal surfaces via β''-Al_2O_3 to induce NEMCA is not different from Na introduced as a dopant using standard metal dispenser sources. This has been confirmed more recently by Lambert

using XPS.[38] An important advantage, however, in using the electrochemical approach, i.e. in employing a solid electrolyte as the dopant donor, is that the doping is reversible, i.e. the dopant can be removed electrochemically. Furthermore the amount and coverage of the dopant on the surface can be accurately determined by integrating Eq. (5.48), i.e., by using Faraday's law.

When doped ZrO_2 is used as the ion donor then the situation is somehow more complicated, as the backspillover oxygen anions can also form chemisorbed oxygen and desorb or react with the reactants, albeit at a slower rate.[5] Consequently the coverage of backspillover oxygen anions is more difficult to measure. Aside from direct measurement by XPS or TPD in ultra-high-vacuum (UHV) or by cyclic voltammetry under NEMCA conditions[39] an alternative method for measuring the backspillover oxide ion coverage, $\theta_O^{\delta-}$, via analysis of the catalytic rate response upon current interruption was discussed in section 5.3.3. It appears that the coverage of the backspillover $O^{\delta-}$ species can approach values near unity and that its dipole moment is 1-2 D, depending on coverage.

It is worth noting that in general:

$$e\Delta U_{WR} = \Delta\Phi = \frac{eN_M}{\varepsilon_o}\sum_j \Delta(P_j \cdot \theta_j) \tag{5.16}$$

where N_M is the surface metal atom concentration (atoms/m^2) and j stands for all adsorbed species on the catalyst surface, including the backspillover promoters but also the adsorbed reactants and intermediate species (P_j is taken always negative for electropositive species and positive for electronegative ones). Consequently upon varying U_{WR} and thus Φ it follows that the coverages and/or dipole moments of adsorbed reactants and intermediates may also change, although the effect of promoting ions (Na^+, $O^{\delta-}$) is usually dominant due to their large positive or negative dipole moments. In the case that no backspillover ions are supplied to the catalyst surface (e.g. negative current application to metal/YSZ systems which, as shown in Chapter 4, also leads frequently to pronounced NEMCA behaviour) the imposed $e\Delta U_{WR}$ and $\Delta\Phi$ change is accommodated again (Eq. 5.16) by changes in the coverages and dipole moments both of the promoting ions and of the other adsorbates.

5.4.6 Deviations from the Equality in the Changes of Extraction Potential and Electrode Potential

In section 5.4.3 we have discussed the physical meaning and range of validity of the potential-work function equivalence equations of solid state electrochemistry:

$$eU_{WR} = \Phi_W - \Phi_R \tag{5.19}$$

$$e\Delta U_{WR} = \Delta\Phi_W \tag{5.18}$$

and of their equivalent:

$$\Psi_W - \Psi_R = 0 \tag{5.51}$$

Very simply these equations are valid as long as ion backspillover from the solid electrolyte onto the gas-exposed electrode surfaces is fast relative to other processes involving these ionic species (desorption, reaction) and thus spillover-backspillover is at equilibrium, so that the electrochemical potential of these ionic species is the same in the solid electrolyte and on the gas exposed electrode surface. As long as this is the case, equation (5.29) and its consequent Eqs. (5.18) and (5.19) simply reflect the fact that an overall neutral double layer is established at the metal/gas interface.

This does not imply that this double layer is at its point of zero charge (pzc). On the contrary, as with every other double layer in electrochemistry, there exists for every metal/solid electrolyte combination one and only one U_{WR} value for which this metal/gas double layer is at its point of zero charge. These critical U_{WR} values can be determined by measuring the dependency on U_{WR} of the double layer capacitance, C_d, of the effective double layer at the metal/gas interface via AC Impedance Spectroscopy as discussed in Chapter 5.7.

Equations (5.18) and (5.19), particularly the latter, have only recently been reported and are quite important for solid state electrochemistry. Some of their consequences are not so obvious. For example consider a solid electrolyte cell Pt/YSZ/Ag with both electrodes exposed to the same p_{O2}, so that $U^0_{WR} = 0$. Equation (5.19) implies that, although the work functions of a clean Pt and a clean Ag surface are quite different (roughly 5.3 eV vs 4.7 eV respectively) ion backspillover from the solid electrolyte onto the gas exposed electrode surfaces will take place in such a way as to equalize the work functions on the two surfaces. This was already shown in Figs. 5.14 and 5.15.

As also already shown in Figures 5.8 to 5.16 the validity of Eqs. (5.18) and (5.19) has been confirmed by several laboratories using the Kelvin probe technique, as well as UPS (via electron cutoff energy) and in a semiquantitative manner via the PEEM technique. Experiment has also clearly shown that the validity of these equations, which include only thermodynamic properties, does not depend on which, if any, electrode is grounded.[31] The same is clearly true for electrochemical promotion in general, as should be obvious to every electrochemist reader.

As also intuitively obvious to electrochemists and as shown in Figures 5.8 to 5.16 the U_{WR} range of validity of Equation (5.18) is typically 1 V, although wider U_{WR} ranges of validity have also been reported.[29] At high anodic or cathodic overpotentials significant deviations from Eq. (5.18) are observed and this is due to the destruction at one end and saturation at the other end of the effective backspillover ion double layer at the metal/gas interface.

Although so far only one group has reported, for reasons described below, significant deviations from Eq. (5.18),[40] it is useful due to the importance of Eqs. (5.18) and (5.19) to understand the reasons for such deviations.

There are two reasons for experimental deviations from Eqs. (5.18) and (5.19).

1. Artificial reasons due to (a) improper choice of the electrode morphology (reversible vs blocking electrode) and (b) inaccurate measurement of U_{WR}.
2. Real reasons due to (a) the occurance of very fast (and therefore in most cases diffusion controlled) *catalytic* reactions on the electrode surface. (b) Formation of non-conducting carbonaceous or oxidic layers on the catalyst electrode surface.

We discuss the artificial reasons first:

(1) Measurement of any potential in aqueous or solid electrochemistry requires some finite reversibility of both electrodes. The electrodes *must not be blocking*. They must allow for easy access of reactants and removal of products to/from the metal-solution interface (aqueous electrochemistry) or to the three-phase-boundaries (solid state electrochemistry). Simple inspection of the SEM of the Pt electrode used in the only report of significant deviations from Eq. (5.18)[40] exemplifies the case (vs e.g. the SEMs of non-blocking Pt electrodes used in solid state electrochemistry and NEMCA, Figs. 4.3, 4.5 and 4.6). It is surprising that some change in Φ with potential (up to 15% of the value predicted by Eq. (5.18)) was obtained even with the non-porous blocking Pt electrode used[40] which implies that some O^{2-} was able to find its way through microcracks and reach the electrode surface where the work function was measured.

(2) The measurement of U_{WR} has always to be made with a differential voltmeter or at least with a good, high internal impedance, voltmeter. When current is applied one must take care of substracting from the measured U'_{WR} value the parasitic $\eta_{ohmic,WR}$ drop between the working and reference electrode as already described in Chapter 4. As also discussed in Chapter 4, for an ideal reference electrode this $\eta_{ohmic,WR}$ drop vanishes. But for any real reference electrode, $\eta_{ohmic,WR}$ must be determined via current interruption using a fast recorder or an oscilloscope or via AC Impedance spectroscopy and subtracted from U'_{WR} to obtain the true U_{WR} value.

We then discuss real reasons for deviations from Eq. (5.18). Such real deviations are exemplified in Figs. 5.8 to 5.16. Two types of deviations can be observed:

(a) Deviations at very high or very low imposed U_{WR} values (Figs. 5.8d, 5.13-5.15).

(b) Deviations due to the simultaneous occurance of a fast catalytic reaction which consumes fast the backspillover ions.

The deviations of type (a) are similar to these observed with emersed

electrodes in aqueous electrochemistry where an equation identical with Eq. (5.18) has been established,[41,42] in which case ΔU_{WR} is the overpotential applied in the immersed state and $\Delta\Phi$ is the work function change measured in the emersed state. The implication in aqueous electrochemistry is that the double layer retains its structure after emersion. The corresponding implication in solid state electrochemistry is *that the double layer* (due to ion back-spillover) *extends itself over the entire gas-exposed electrode surface.*

In aqueous electrochemistry the explanation of deviations from Eq. (5.18) at high and low overpotential is associated with the "destruction of the double layer". Similar is the explanation in solid electrochemistry for cathodic overpotential in which case Φ is limited to the value, Φ_0, of the bare metal surface. At high anodic overpotentials the saturation limit of the metal surface with backspillover ions is reached thus Φ is again limited. The range of validity of Eqs. (5.18) and (5.19) is about 1eV in both aqueous and solid electrochemistry.

(b) The deviations of type (b) are quite interesting and easy to rationalize. If a very fast catalytic reaction e.g. ethylene or CO oxidation is taking place on the gas-exposed catalyst-electrode surface then its rate reaches the limit of mass-transfer control. Under such conditions the reactant coverages on the gas exposed electrode surface vanish and even the backspillover species (e.g. $O^{\delta-}$) which are less reactive, are eventually consumed. Consequently the catalyst-electrode work function Φ cannot respond anymore to the imposed value of $e\Delta U_{WR}$. It must be emphasized that, under conditions of mass-transfer control, electrochemical promotion itself is not operative anymore since the catalytic rate is controlled by gaseous diffusion rather than by the surface kinetics. The Carberry number:[43]

$$Ca = r/k_g a[A_b] \tag{5.52}$$

provides a direct measure of the extent to which a catalytic reaction is mass-transfer controlled. Here r is the measured catalytic rate (mol/s), k_g is the mass transfer coefficient (m/s, directly computable for any geometry by standard mass transfer expressions,[43] e.g. $k_g \sim D_A/\ell$, where D_A is the diffusivity of key reactant A and ℓ is the thickness of the hydrodynamic boundary layer), a is the superficial gas exposed catalyst-electrode surface area, and $[A_b]$ is the gaseous bulk concentration of A. The advantage of the Carberry number (which is dimensionless) is that it consists only of *measurable* quantities. Kinetic measurements should be taken only with Ca < 0.01. At the limit of complete mass transfer control it is Ca = 1. Practically speaking for a 1% C_2H_4 or CO bulk mol percent in the gas phase, the catalytic rates must be smaller than 10^{-7} mol/s for the kinetics to be reliable. Thus when a very fast and mass-transfer-controlled catalytic reaction takes place on a catalyst-electrode it is likely that even the backspillover species (which are Λ times less reactive than the key reactants) will be consumed and thus

deviations from Eq. (5.18) will be observed. The interested reader will find a mathematical analysis of promoter diffusion and reaction in Section 11.3.

There is a third real reason for deviations from Eq. (5.18) in the case that a non-conductive insulating product layer is built via a catalytic reaction on the catalyst electrode surface (e.g. an insulating carbonaceous or oxidic layer). This is manifest by the fact that C_2H_4 oxidation under fuel-rich conditions has been found to cause deviations from Eq. (5.18) while H_2 oxidation does not. A non-conducting layer can store electric charge and thus the basic Eq. 5.29 (which is equivalent to Eq. (5.18)) breaks down.

In conclusion: When no catalytic reaction is taking place on the gas-exposed electrode surface, only poor experimentation (blocking electrodes, inaccurate measurement of U_{WR}, and of course Φ) can cause deviations from Eq. (5.18) in presence of ion backspillover. In presence of a catalytic reaction Eq. (5.18) still holds unless the reaction is severely mass transfer controlled or an insulating layer is built on the catalyst surface.

5.5 TEMPERATURE PROGRAMMED DESORPTION(TPD)

The technique of temperature programmed desorption (TPD) is one of the oldest and strongest tools of surface science to investigate adsorption on single crystal or polycrystalline catalyst samples. In recent years it has been used[4,7,44-47] to investigate the origin of the electrochemical activation of catalysis for the systems Pt/YSZ, Ag/YSZ and Au/YSZ. To this end oxygen adsorption was investigated on polycrystalline Pt, Ag and Au catalyst films deposited on YSZ as a function of catalyst potential under ultrahigh vacuum conditions and temperatures of 600 – 900 K. Oxygen was supplied both via the gas phase and electrochemically, as O^{2-}, via current application between the Pt or Ag catalyst film and a Au counter electrode.

Some of the key results[4,7] for the case of Pt are shown in Figures 5.21, 5.22 and 5.23. Figure 5.21 shows the experimental setup and oxygen TPD spectra after gaseous O_2 dosing at 673 K. As is well established from previous TPD studies on polycrystalline Pt films[4] a single adsorption state is obtained with a peak desorption temperature T_P at 720 to 740 K.

Figure 5.22 reveals the ability of solid state electrochemistry to create new types of adsorption on metal catalyst electrodes. Here oxygen has been supplied not from the gas phase but electrochemically, as O^{2-}, via current application for a time, denoted t_I, of $I=15\ \mu A$ at 673 K, i.e. at the same temperature used for gaseous O_2 adsorption (Fig. 5.21). Figure 5.23 shows the effect of mixed gaseous-electrochemical adsorption. The Pt surface has been initially exposed to $p_{O_2}=4\times10^{-6}$ Torr for 1800 s (7.2 kL) followed by electrochemical O^{2-} supply ($I=15\ \mu A$) for various time periods t_I shown on the figure, in order to simulate NEMCA conditions.

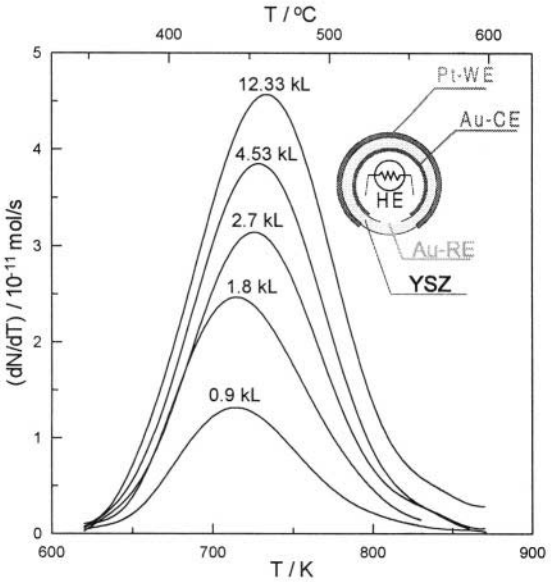

Figure 5.21. Experimental setup (inset) showing the location of the working (WE), counter (CE) and reference (RE) electrodes and of the heating element (HE); thermal desorption spectra after gaseous oxygen dosing at 673 K and an O_2 pressure of 4×10^{-6} Torr on Pt deposited on YSZ for various exposure times. Oxygen exposure is expressed in kilo-langmuirs (1 kL=10^{-3} Torr·s). Desorption was performed with linear heating rate, β=1 K/s.[4,5] Reprinted with permission from Academic Press.

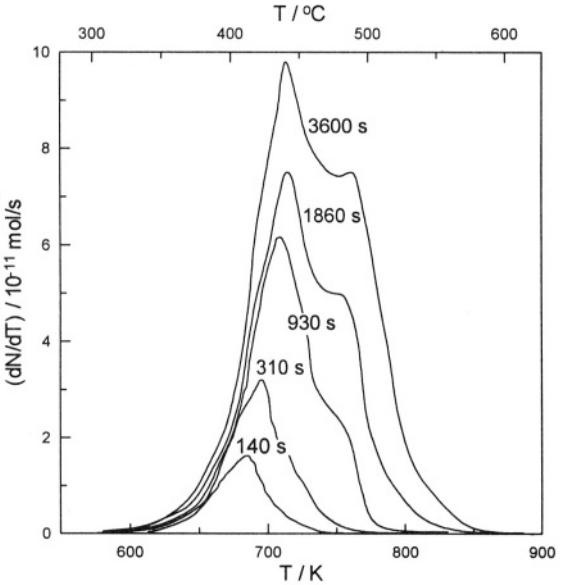

Figure 5.22. Thermal desorption spectra after electrochemical O^{2-} supply on Pt deposited on YSZ[4,5] at 673 K. The different curves correspond to various times of current application; I=+15 μA. Desorption was performed with linear heating rate, β=1 K/s; $2FN_G/I$=2570 s.[4,7] Reprinted from ref. 7 with permission from Academic Press.

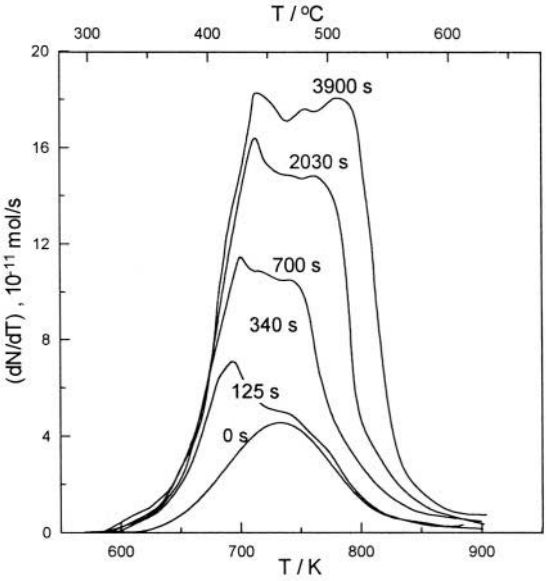

Figure 5.23. Thermal desorption spectra of oxygen on a Pt film deposited on YSZ[4,7] after gaseous oxygen adsorption at 673 K and an O_2 pressure of 4×10^{-6} Torr for 1800 s (7.2 kL) followed by electrochemical O^{2-} supply (I=+15 μA) for various time periods. Desorption was performed with linear heating rate, β=1 K/s, $2FN_G/I$=2570 s. Reprinted from ref. 7 with permission from Academic Press.

The creation of at least two distinct oxygen adsorption states is clear in Figs. 5.22 and 5.23. The weakly bonded state (T_P~675-685 K) desorbs some 40-50K lower than the state formed via gaseous adsorption. The strongly bonded state (T_P~750-780 K) desorbs some 30 K higher than the state formed via gaseous adsorption. It fully develops only after prolonged current application, i.e. when the electrochemically supplied oxygen is comparable to $2FN_G/I$ (=2570 s for the experiment of Figure 5.23). This provides strong evidence that the strongly bonded state, populated by the backspillover O^{2-} originating from the solid electrolyte, is the same ionic species with the species with low Ols binding energy (E_b=528.8 eV) observed in the XPS studies discussed in section 5.8 and with the ionic species developing at long holding times and reduced at more negative potentials in the cyclic voltammetric investigations discussed in section 5.6.

By varying the temperature of electrochemical O^{2-} supply or the magnitude of the applied current one can vary the potential, U^*_{WR}, at the start of the TPD run at near constant initial oxygen coverage. Figure 5.24 shows the *effect of* U^*_{WR} *on the peak desorption temperature,* T_p, *of the weakly bonded* oxygen state for three different heating rates, β, during the TPD run. It can be seen that by increasing eU^*_{WR} by 0.6 eV one causes a 120 K decrease in T_p. This indicates a pronounced weakening in the Pt = O bond.

One can then use the standard Redhead analysis to the data of Fig. 5.24. To this end one uses the Redhead equation in its generalized form derived by Falconer and Madix:[48]

$$\ln(\beta/T_p^2) = \ln(Rv\theta_o^{n-1}/E_d) - (E_d/RT_p) \tag{5.53}$$

where β (K/s) is the heating (or ramp) rate, R is the gas constant, v is the preexponential factor, n is the desorption rate reaction order and E_d is the activation energy for desorption. Thus by plotting $\ln(\beta/T_p^2)$ vs T_p^{-1} one directly extracts E_d, which for non-activated adsorption, as is the case here, expresses the binding strength of atomic O on the Pt surface (Fig. 5.25).

The resulting E_d dependence on eU_{WR} is shown in Fig. 5.26 for Pt, as well as for Ag and Au.[44-47] The results are striking: In all three cases E_d decreases linearly with increasing U_{WR}:

$$\Delta E_{d,Pt=O} = \alpha_{Pt=O}\Delta eU_{WR} \tag{5.54}$$

$$\Delta E_{d,Ag=O} = \alpha_{Ag=O}\Delta eU_{WR} \tag{5.55}$$

$$\Delta E_{d,Au=O} = \alpha_{Au=O}\Delta eU_{WR} \tag{5.56}$$

with $\alpha_{Pt=O}$=-1, $\alpha_{Ag=O}$=-1 and $\alpha_{Au=O}$=-4.

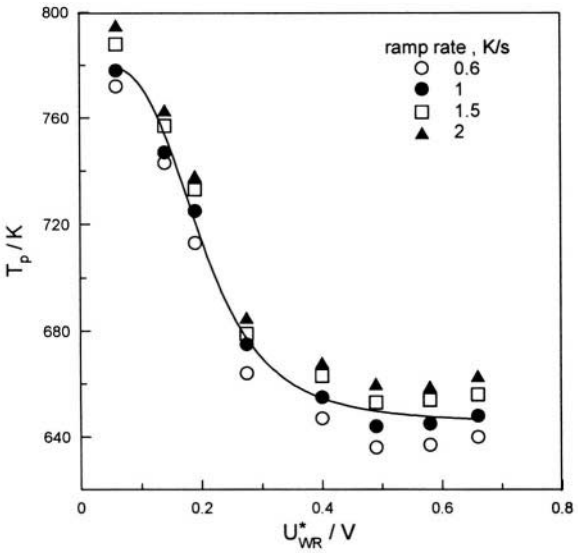

Figure 5.24. Effect of catalyst potential, U^*_{WR}, on oxygen peak desorption temperature, T_p during O_2 TPD from Pt/YSZ.[4,5] The exact definition of U^*_{WR} has been given in Figure 4.45. It is the U_{WR} value at the beginning of the TPD run and differs little (<0.1 V) from the U_{WR} value at T_p.[4,7] Reprinted with permission from the American Chemical Society.

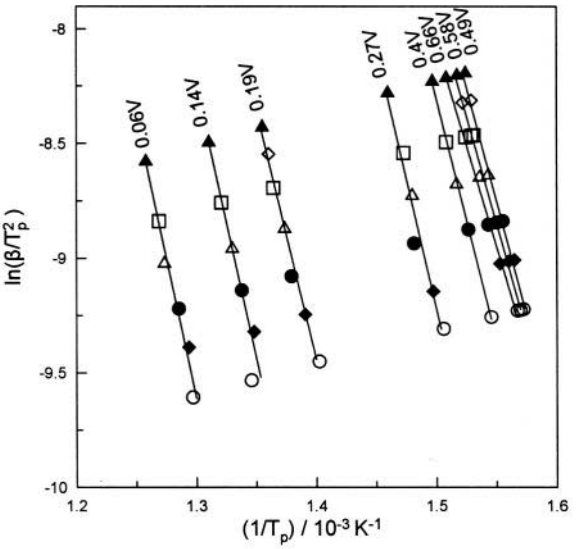

Figure 5.25. Redhead plot for oxygen desorption from a Pt film deposited on YSZ for various catalyst film potentials vs Au reference electrode. The slope of each line is equal to E_d/R.[7] Reprinted with permission from Academic Press.

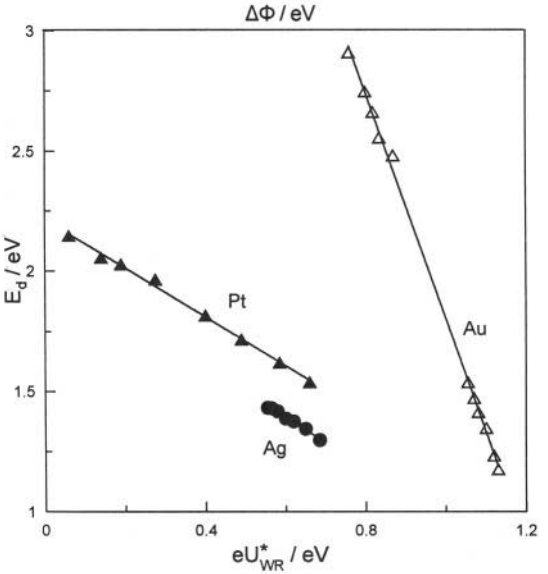

Figure 5.26. Effect of catalyst potential on the oxygen desorption activation energy, E_d, calculated from the modified Redhead analysis for Pt, Ag and Au electrodes deposited on YSZ.[44,46] Reprinted from ref. 44 with permission from the Institute for Ionics.

In view of the potential-work function equivalence of solid state electrochemistry (Eq. 4.30 or 5.18) and of the fact that for non-activated adsorption, $\Delta E_{d,Pt-O}=\Delta|\Delta H_{O,Pt}|$, where $\Delta H_{O,Pt}$ is the enthalpy of chemisorption of O on Pt, these equations can also be written as:

$$\Delta|\Delta H_{O,Pt}| = \alpha_{Pt-O}\Delta\Phi_{Pt} \tag{5.57}$$

$$\Delta|\Delta H_{O,Ag}| = \alpha_{Ag-O}\Delta\Phi_{Ag} \tag{5.58}$$

$$\Delta|\Delta H_{O,Au}| = \alpha_{Au-O}\Delta\Phi_{Au} \tag{5.59}$$

which conform nicely to the general equation (2.24) expressing the linear variation of heats of adsorption with Φ. These linear variations are intimately related to the linear variations of activation energies of catalytic reactions, E, with Φ, Equation (4.50).

The above results establish that the binding strength of oxygen, which is an electron acceptor, decreases with increasing catalyst potential and work function. Intuitively one can understand this important result as being primarily due to the strong lateral repulsive interactions of adsorbed O with coadsorbed O^{2-} ("through the vacuum" interaction). As shown in section 5.13, rigorous quantum mechanical calculations using Pt clusters have confirmed these important results (Eqs. 5.54 and 5.57) and have shown that the through the vacuum interactions are quite dominant.

5.6 SOLID ELECTROLYTE CYCLIC VOLTAMMETRY

5.6.1 Detection of Adsorbed Species

Cyclic voltammetry is one of the most common techniques in aqueous electrochemistry to study adsorbed species and reaction kinetics,[9,10,49] but has only recently and to a limited extent been used in solid state electrochemistry.[4,39,50-52] With appropriate choice of the scan rate, υ, and other operating conditions one can obtain useful information about the state of species adsorbed on metal electrodes in contact with solid electrolytes. Several examples are shown in Figs. 5.27 and 5.28 for the case of oxygen adsorption on Pt deposited on YSZ. Oxygen adsorption takes place during the anodic scan (I>0) and oxygen reduction (to O^{2-} which migrates in the YSZ) during the cathodic scan (I<0). The time numbers on the figures indicate the value of the holding time at positive potential and current.

The creation of two types of chemisorbed oxygen on Pt and Ag surfaces subject to NEMCA conditions is clearly shown by cyclic voltammetry (Fig. 5.27)[39,50,52] or by the similar Potential-Programmed-Reduction (PPR) technique[53] (Fig. 5.28). This is a variation of cyclic voltammetry in which all

oxygen adsorption takes place during the holding time at a positive current and potential. The high-U_{WR} oxygen reduction peak corresponds to normally chemisorbed atomic oxygen and the low-U_{WR} peak, which develops only after prolonged positive current application,[52] corresponds to backspillover oxygen originating from the YSZ solid electrolyte. Figure 5.27 has been obtained at atmospheric pressure (a) at ultra high vacuum (b) and at $p_{O_2}=4\times10^{-6}$ Torr (c).

Figure 5.28a (bottom) has been obtained at $p_{O_2}=0.1$ kPa. The behaviour is qualitatively the same, regardless of the oxygen pressure. The creation of the

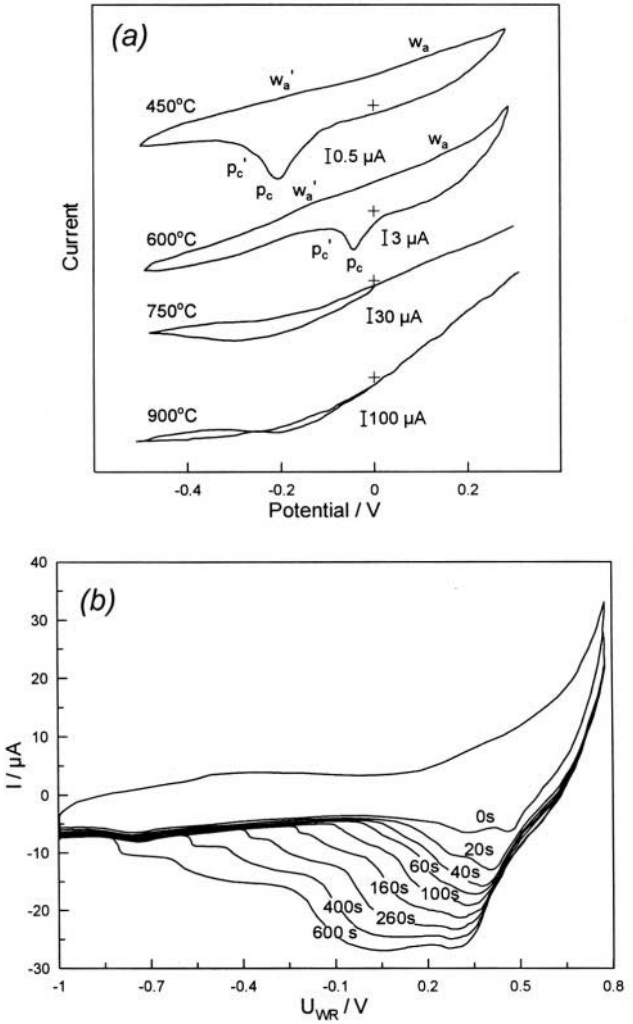

Figure 5.27. Cyclic voltammograms of Pt/YSZ electrodes in air at different temperatures at 50 mV/s (a).[50] Cyclic voltammograms of a Pt/YSZ film at 673 K and various holding times under (b) UHV[4] and (c) $P_{O_2}=4\times10^{-6}$ Torr[4]. Holding potential: 0.8 V; scan rate: 50 mV/s.Reprinted with permission from the American Chemical Society.

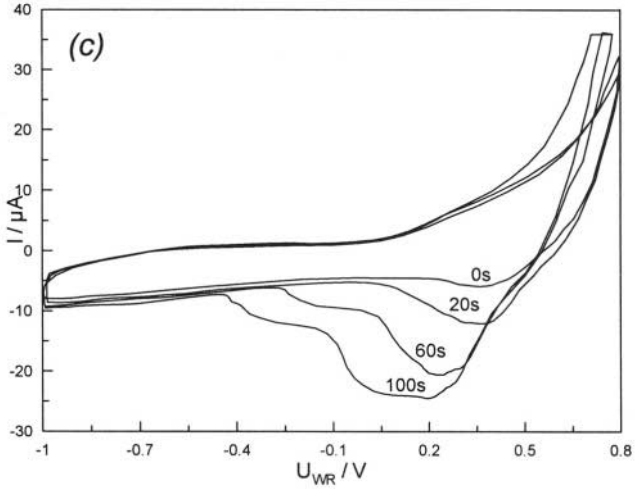

Figure 5.27. (continued)

two oxygen states on Ag/YSZ subject to anodic polarization is shown clearly in Figure 5.28b via potential-programmed reduction.[53]

Note that upon increasing the time of O_2 desorption, denoted t_{He}, the peak A, corresponding to chemisorbed O, decreases much faster than the back-spillover oxygen peak B. Similarly upon increasing the holding time, t_H, of positive potential application (U_{WR}=0.2 V) peak A reaches saturation first, followed by a gradual approach to saturation of the backspillover oxygen peak B.

One interesting feature of Figure 5.27 is that the anodic oxygen peak is missing. This is very common in solid state electrochemistry and can be understood easily as follows: The, thermodynamically favoured, oxygen adsorption takes place in a catalytic (no net charge transfer) step, thus no anodic peak appears. Oxygen reduction to O^{2-} is a net charge transfer process, thus only the cathodic (adsorbed oxygen reduction) peak(s) appear.

The "thickness" δI of a cyclic voltammogram at a fixed U_{WR} value also conveys useful information. It is related to the scan rate υ and to the capacitance C_d of the electrode-electrolyte interface via:

$$C_d = \delta I/2\upsilon \tag{5.60}$$

One can thus use the voltammograms of Figs. 5.27 and 5.28 to estimate C_d values of the order of 200 $\mu F/cm^2$ of solid electrolyte.

If only the three-phase-boundaries (tpb) were electrocatalytically active one would expect C_d values of the order of 10 $\mu F/cm^2$. The thus measured high C_d values also provide evidence that the charge transfer zone is extended over the entire gas-exposed electrode surface, i.e. that an effective double layer is formed over the entire gas exposed electrode surface.

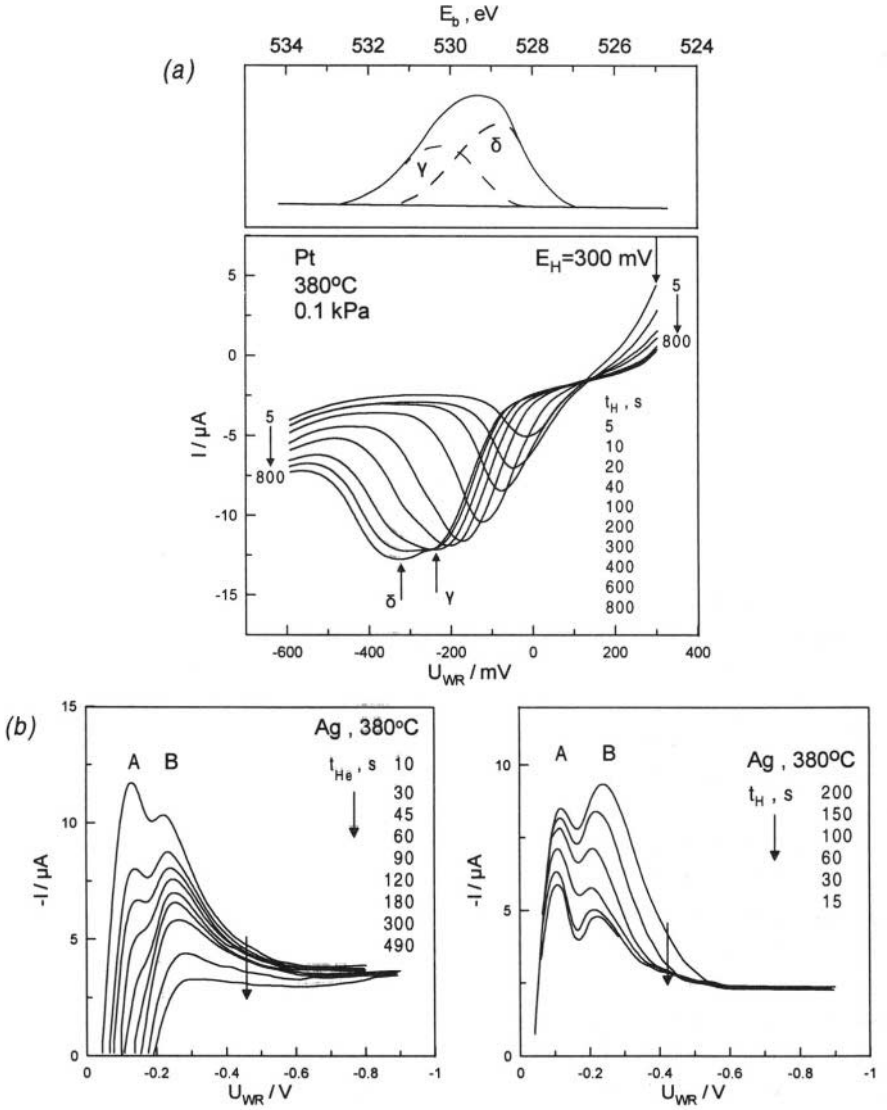

Figure 5.28.(a) Top: O1s photoelectron spectrum of oxygen adsorbed on a Pt electrode supported on YSZ under UHV conditions after applying a constant overpotential ΔU_{WR}=1.2 V corresponding to a steady state current I=40 μA for 15 min at 400°C.[6] The γ-state is normally chemisorbed atomic oxygen (E_b=530.2 eV) and the δ-state is backspillover oxidic oxygen (E_b=528.8 eV).[6] Reprinted with permission of the American Chemical Society. Bottom: Linear potential sweep voltammogram obtained at T=380°C and p_{O_2}=0.1 kPa on a Pt electrode supported on YSZ showing the effect of holding time t_H at U_{WR}=300 mV on the reduction of the γ- and δ-states of adsorbed oxygen; sweep rate: 30 mV/s.[52] Reprinted with permission from Elsevier Science (b) Potential programmed reduction (PPR) of oxygen on Ag/YSZ catalyst electrodes;[53] (left): effect of desorption time, t_{He}, on the PPR spectrum of oxygen on Ag after electrochemical supply of oxygen (U_{WR}=0.2 V) for 60s; υ=10 mV/s, $F_{v,He}$=100 cm^3 STP/min; (right): effect of potential holding time, t_H, at U_{WR}=0.2 V; t_{He}=10 s, υ=5 mV/s, $F_{v,He}$=100 cm^3 STP/min. Reprinted with permission from Academic Press.[53]

5.6.2 Potential Programmed Reduction

The interesting related technique of Potential Programmed Reduction (PPR) or linear sweep voltammetry was discussed in the previous section (Figure 5.28b). In this technique the catalyst electrode under consideration is kept at an anodic holding potential for a time t_H and the potential U_{WR} is then swept linearly in time in the cathodic direction with simultaneous recording of the cathodic current (Fig. 5.28b). In this way one gets interesting information on the coverage but also, in principle, on the chemical potential of adsorbed species, provided the sweep rate υ is sufficiently small so that the peak potentials E_P are insensitive to υ. In this way the standard chemical potential of adsorbed and backspillover oxygen on Ag deposited on YSZ can be estimated to be -22.2 kJ/mol O and -46 kJ/mol O respectively (Fig. 5.28b).[53]

5.7 AC IMPEDANCE SPECTROSCOPY

5.7.1 General Features

The technique of AC Impedance Spectroscopy is one of the most commonly used techniques in electrochemistry, both aqueous and solid.[49] A small amplitude AC voltage of frequency f is applied between the working and reference electrode, superimposed to the catalyst potential U_{WR}, and both the real (Z_{Re}) and imaginary (Z_{Im}) part of the impedance Z ($=dU_{WR}/dI=Z_{Re}+iZ_{Im}$)[9,10] are obtained as a function of f (Bode plot, Fig. 5.29a). Upon crossplotting Z_{Im} vs Z_{Re}, a Nyquist plot is obtained (Fig. 5.29b). One can also obtain Nyquist plots for various imposed U_{WR} values as shown in subsequent figures.

Due to the small amplitude of the superimposed voltage or current, the current-voltage relationship is linear and thus even charge-transfer reactions, which normally give rise to an exponential current-potential dependence (Chapter 4), appear as resistances, usually coupled with a capacitance. Thus any real ohmic resistance associated with the electrode will appear as a single point, while a charge transfer reaction (e.g. taking place at the tpb) will appear ideally as a semicircle, i.e. a combination of a resistor and capacitor connected in parallel (Fig. 5.29).

Figures 5.29a and 5.29b show the Bode and Nyquist plot for a resistor, R_0, connected in series with a resistor, R_1, and capacitor, C_1, connected in parallel. This is the simplest model which can be used for a metal-solid electrolyte interface. Note in figure 5.29b how the first intersect of the semicircle with the real axis gives R_0 and how the second intersect gives R_0+R_1. Also note how the capacitance, C_1, can be computed from the frequency value, f_m, at the top of the semicircle (summit frequency), via $C_1=1/2\pi f_m R_1$.

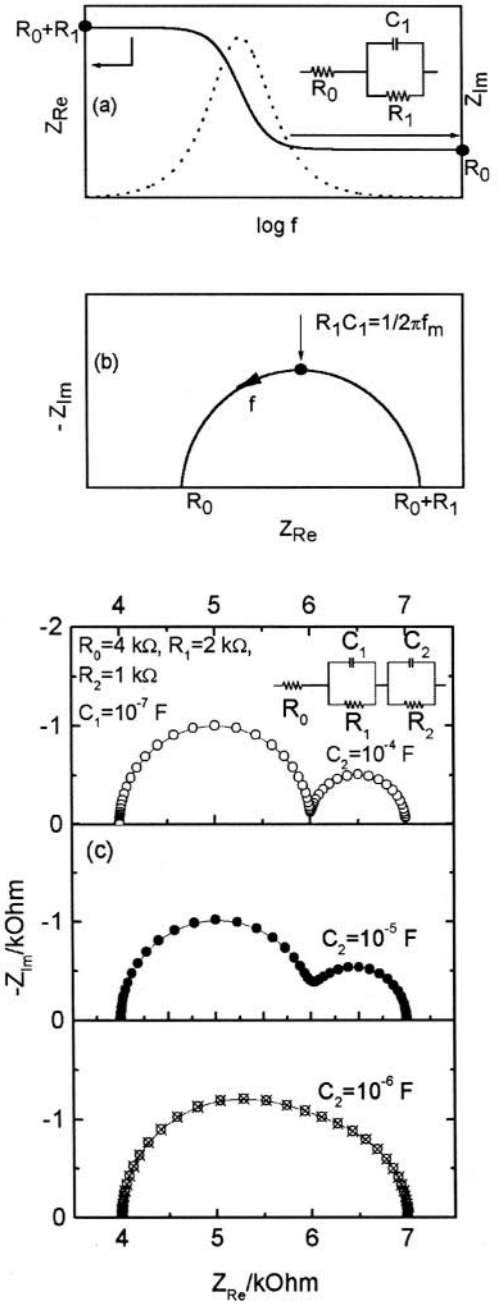

Figure 5.29. Bode (a) and corresponding Nyquist plot (b) of the circuit shown in inset which is frequently used to model a metal/solid electrolyte interface. Effect (c) of capacitance C_2 on the Nyquist plot at fixed R_0, R_1 and R_2.

Figure 5.29c shows Nyquist plots corresponding to a more complex resistor-capacitor network which is frequently found to describe well the behaviour of metal-solid electrolyte interfaces under electrochemical promotion conditions. The left, high frequency, semicircle simulates the charge transfer reaction at the tpb, the second (right) low frequency semicircle simulates the charge transfer reaction over the entire gas exposed electrode surface. Figure 5.29c shows that the second semicircle appears clearly only when C_2 exceeds C_1 by two orders of magnitude.

Figure 5.30 exemplifies such a behaviour of a Pd catalyst electrode deposited on YSZ and exposed to CH_4/O_2 mixtures.[54] The resistance R_0 is associated with the ohmic resistance of the electrode while the semicircles labeled C_1 and $C_{1'}$ are associated with the charge transfer reaction

$$O^{2-} \rightleftharpoons O(a)+2e^- \qquad (5.61)$$

at the tpb; $C_{1'}$ most likely corresponds to tpb covered with PdO while C_1 corresponds to tpb covered with reduced Pd. They correspond to capacitance values $C_{d,1}$ and $C_{d,1'}$ computed from $C_{d,i}=1/2\pi f_{m,i}R_i$ where i=(1,1′) and $f_{m,i}$ is the frequency at the peak of semicircle i. It is $C_{d,1} \approx 0.1\mu F/cm^2$ and $C_{d,1'} \approx 0.1$ to 10 $\mu F/cm^2$ (Fig. 5.30b).p

The third semicircle labeled C_2 is the "backspillover oxygen semicircle". It appears only at positive imposed U_{WR} values, i.e. when O^{2-} is supplied to the catalyst surface. It corresponds to a capacitance $C_{d,2}$ again computed from $C_{d,2} = 1/2\pi f_{m,2}R_2$ and gives a $C_{d,2}$ value of 200 $\mu F/cm^2$. It is due to the charge transfer reaction (5.61) now taking place over the entire gas-exposed electrode surface area. The dependency of $C_{d,1}$, $C_{d,1'}$ and $C_{d,2}$ (and of the corresponding frequencies $f_{m,1}$, $f_{m,1'}$, $f_{m,2}$) on potential is shown in Figure 5.30b and c.

Similar is the behaviour when the Pd catalyst electrode deposited on YSZ is exposed to C_2H_4/O_2 mixtures (Figs. 5.31). Here the $C_{1'}$ semicircle (corresponding to tpb covered with PdO) is missing (due to the higher reducing propensity of C_2H_4 vs CH_4) but the features regarding the "tpb semicircle" C_1 and the "backspillover semicircle" C_2 remain the same. The metal-gas double layer capacitance $C_{d,2}$ is now somehow lower (~100 $\mu F/cm^2$) due to the higher reactivity of the backspillover O^{2-} species with C_2H_4.

For the experiments shown in Fig. 5.30 the ratio $C_{d,2}/C_{d,1}$ is on the average 2500, very close to the ratio N_G/N_{tpb} (≈3570)[54] where N_G is the gas-exposed electrode surface area and N_{tpb} is the "surface area" of the three phase boundaries. These quantities were measured via surface titration and via SEM and the techniques described in section 5.7.2, respectively. Thus once N_G has been measured, AC Impedance spectroscopy allows for an estimation of the three-phase-boundary (tpb) length via:

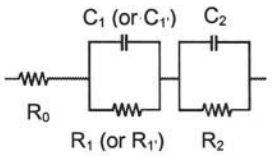

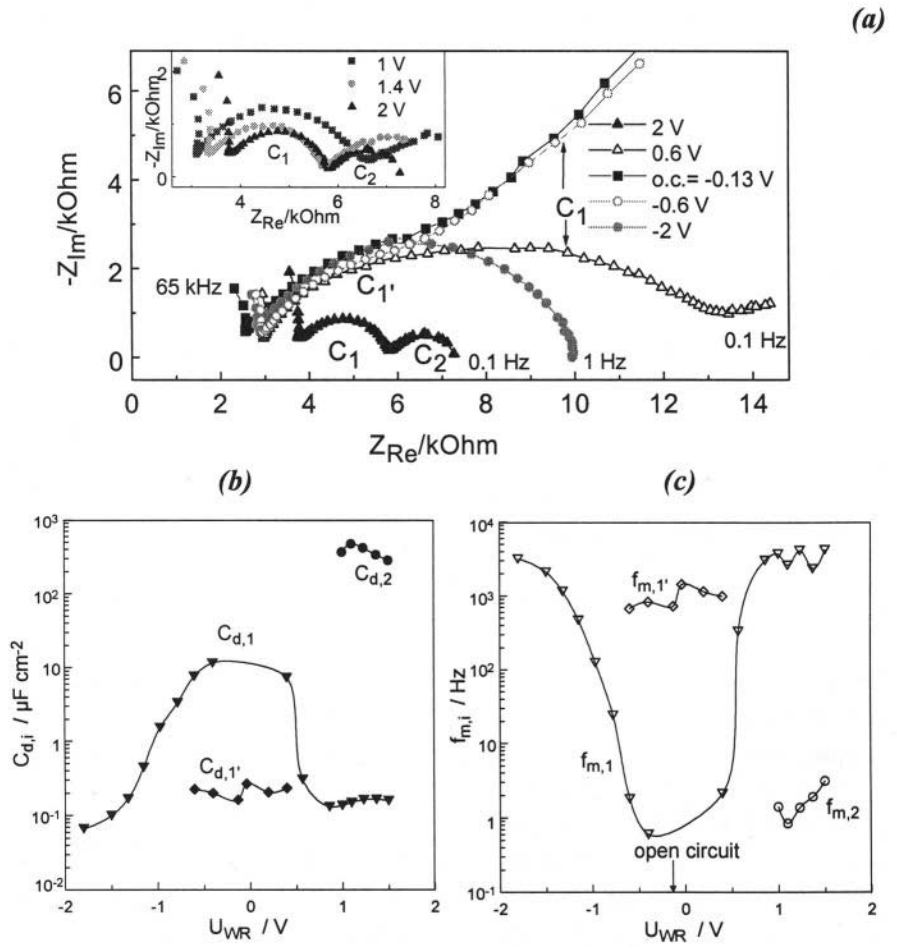

Figure 5.30. (a) Complex impedance spectra (Nyquist plots) of the CH_4, O_2, Pd|YSZ system at different Pd catalyst potentials. Open circuit potential U^{o}_{WR} =-0.13 V. Dependence on catalyst potential of the individual capacitances, $C_{d,i}$ (b) and of the corresponding frequencies, $f_{m,i}$, at maximum absolute negative part of impedance (c).[54] Reprinted with permission from Elsevier Science.

$$\frac{N_{tpb}}{N_G} = \frac{C_{d,1}}{C_{d,2}} \tag{5.62}$$

Similar are the conclusions from the work of Kek, Pejonic and Mogensen[55] who were first to use AC Impedance spectroscopy for the detailed investigation of Pt, Au and Ni films deposited in YSZ and exposed

to mildly reducing environments (Figs. 5.32 and 5.33). The low frequency capacitance of the metal/YSZ interface is up to **300 μF/cm²**, manifesting the presence of a double layer at the metal/gas interface even under mildly reducing conditions **(~1% H_2)** (Fig. 5.33). This double layer is stabilized even on Au via prolonged anodic polarization (Fig. 5.32d).

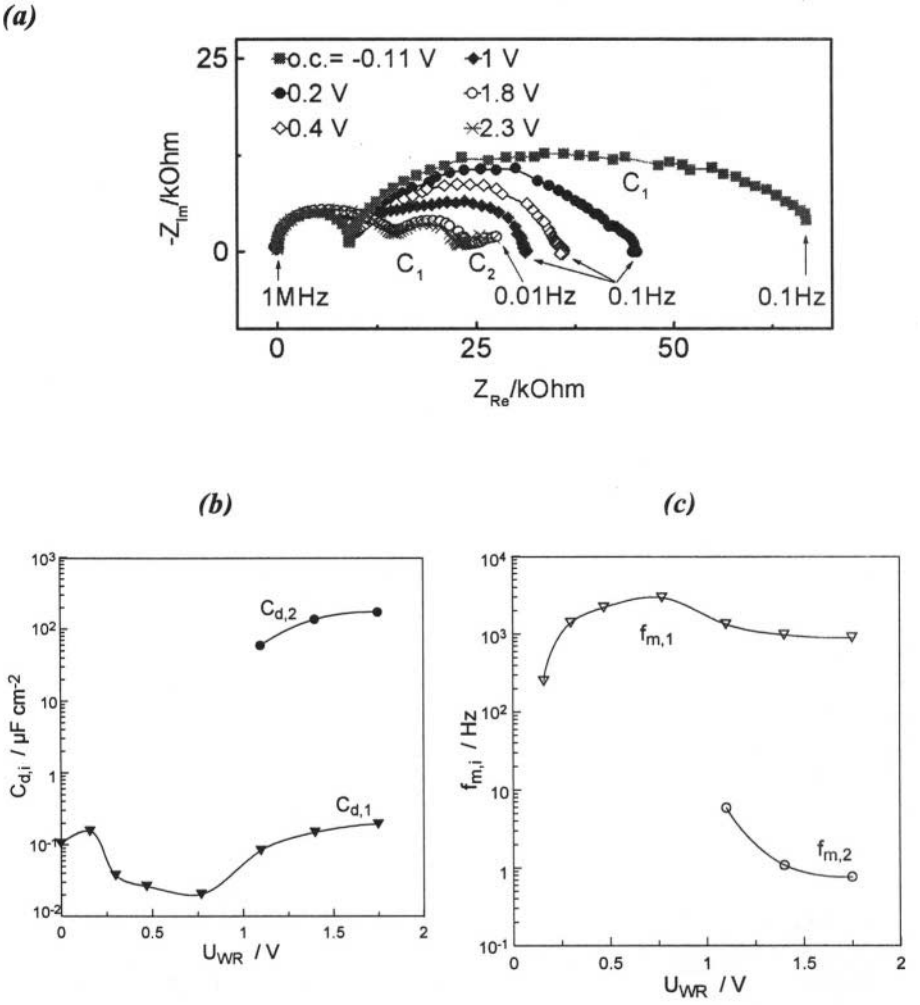

Figure 5.31. (a) Complex impedance spectra (Nyquist plots) of the C_2H_4, O_2, Pd|YSZ system at different Pd catalyst potentials. Open circuit potential U^o_{WR} =-0.11 V. Dependence on catalyst potential of the individual capacitances, $C_{d,i}$ (b) and of the corresponding frequencies, $f_{m,i}$, at maximum absolute negative part of impedance (c).[54] Reprinted with permission from Elsevier Science.

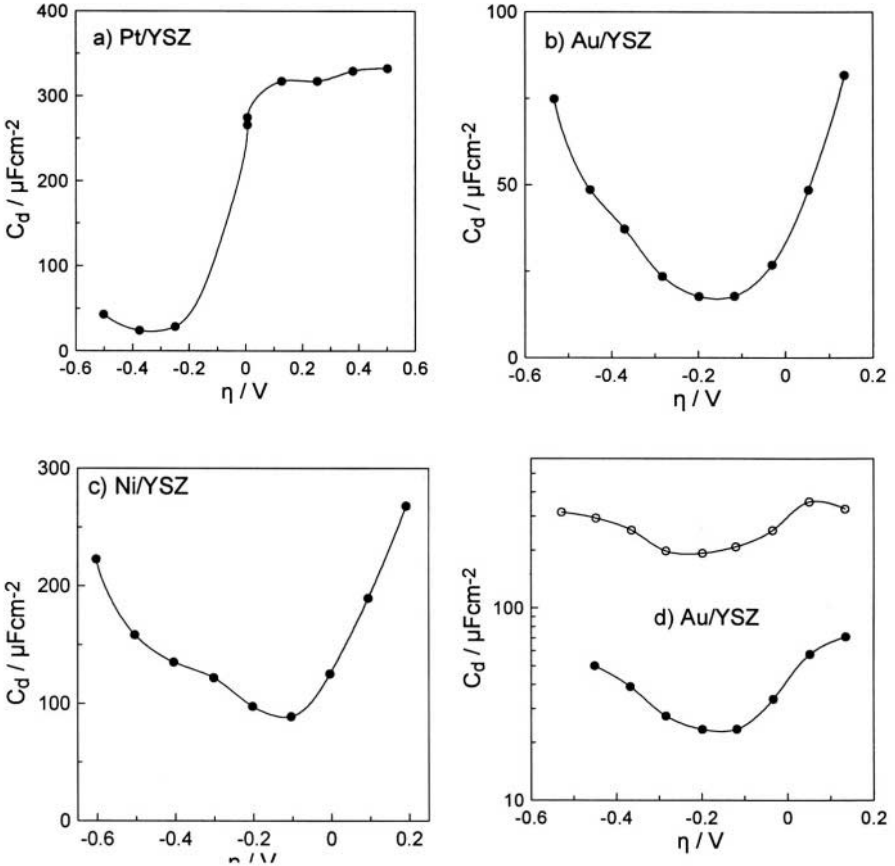

Figure 5.32. Double layer capacitance as a function of overpotential of the system a) Pt/YSZ, b) Au/YSZ, c) Ni/YSZ and d) Au/YSZ before (●) and after (○) prolonged anodic overpotential application.[55] Reprinted with permission from the National Institute of Chemistry, Ljubljana, Slovenia.

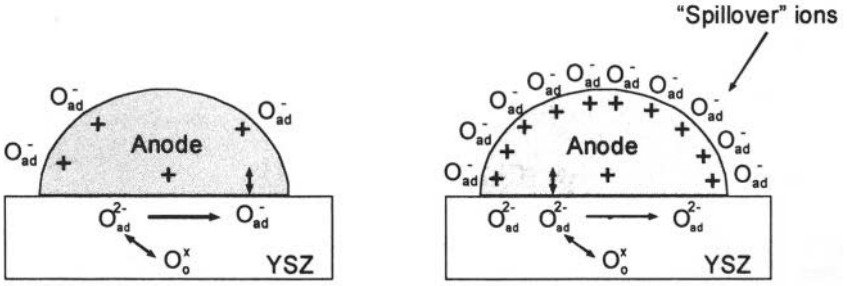

Figure 5.33. Schematic of the state of the metal/YSZ and metal/gas interfaces a) at zero overpotential; b) after applied anodic overpotential.[55] Reprinted with permission from the National Institute of Chemistry, Ljubljana, Slovenia.

In summary AC impedance spectroscopy provides concrete evidence for the formation of an effective electrochemical double layer over the entire gas-exposed electrode surface. The capacitance of this metal/gas double layer is of the order of 100-300 $\mu F/cm^2$, comparable to that corresponding to the metal/solid electrolyte double layer. Furthermore it permits estimation of the three-phase-boundary length via Eq. 5.62 once the gas exposed electrode surface area N_G is known.

5.7.2 Measurement of the tpb Length

Several approaches have been proposed to measure the three phase boundary (tpb) length, N_{tpb}, in solid state electrochemistry. The parameter N_{tpb} expresses the mol of metal electrode in contact both with the solid electrolyte and with the gas phase. More commonly one is interested in the tpb length normalized with respect to the surface area, A, of the electrolyte. This normalized tpb length, denoted by $N_{tpb,n}$ equals N_{tpb}/A.

It is also common to express the tpb length as an actual length, ℓ_{tpb}, computed from $\ell_{tpb} = N_{tpb} d_M N_{AV}$, or $\ell_{tpb,n} = N_{tpb,n} d_M N_{AV}$ where d_M is the atomic diameter of the metal (electrode) and N_{AV} is Avogadro's number.

A first approximate approach for estimating $N_{tpb,n}$ or $\ell_{tpb,n}$ is to use scanning electron microscopy to estimate the average grain size, d, of the electrode. One then assumes spherical grains for the electrode film and semispherical grains in contact with the solid electrolyte to obtain:

$$N_{tpb,n} = \pi/(d d_M N_{AV}) \; ; \; \ell_{tpb,n} = \pi/d \tag{5.63}$$

Thus for $d = 0.1\ \mu m$ one has $N_{tpb,n} = 2 \cdot 10^{-11}$ mol/cm^2 and $\ell_{tpb,n} = 3 \cdot 10^5$ cm^{-1}, i.e. 3 km/cm^2! A disadvantage of this simple model is that it does not account for the "roughness" of the tpb at the atomic level.

The second approach, followed by Vayenas et al[39] is direct measurement of N_{tpb} and $N_{tpb,n}$ using cyclic voltammetry, as in aqueous electrochemistry,[49] and measuring the height, I_p, or the area $\int I dt$ of the cathodic oxygen reduction peak (Fig. 5.28a). Then N_{tpb} can be estimated from:

$$N_{tpb,n} = \frac{2.72 R T I_p}{n \alpha_c n_c F^2 \upsilon A} \left(\frac{d_M}{\delta} \right) \text{ or } N_{tpb,n} = \frac{\int I dt}{2FA} \left(\frac{d_M}{\delta} \right) \tag{5.64}$$

where n(=2) is the total number of transferred electrons, $\alpha_c(=1)$ is the cathodic transfer coefficient, $n_c(=1)$ is the number of electrons transferred in the rate limiting step of the cathodic charge transfer reaction, υ is the sweep rate (V/s), A is the solid electrolyte surface area and δ (m) is the thickness of

the spreading of the tpd zone on the electrode surface. The latter can be computed from:

$$\delta=(D_s RT/F\upsilon)^{1/2} \tag{5.65}$$

where D_s is the surface diffusivity of species being reduced (e.g. O (Pt)). For the case of Pt electrodes D_s can be computed from Equation (5.6). No sufficient data exist for other metals and this is the disadvantage of this approach, which for the case of Pt electrodes gives good qualitative agreement with the simple spherical model equation (5.63).[39] It should be noted that equations similar to (5.64) but without the corrective term (d_m/δ) are used routinely in aqueous electrochemistry to measure the electrocatalytically active surface area. However it has been clearly shown[39] that inclusion of this term is necessary in solid state electrochemistry due to the spreading of the electrochemically active zone on the electrode surface. Omission of this term leads to gross overestimation of $N_{tpb,n}$ and $\ell_{tpb,n}$. The same work[39] has shown experimentally the, intuitively obvious, proportionality between $N_{tpb,n}$, $\ell_{tpb,n}$ and the exchange current density i_0.

Thus, due to the lack of sufficient D_s data for most metals, other than Pt, the most reliable method for measuring N_{tpb} and $N_{tpb,n}$ is based on AC Impedance spectroscopy as outlined in the previous section and using equation (5.62), i.e.

$$\frac{N_{tpb}}{N_G}=\frac{C_{d,1}}{C_{d,2}} \tag{5.62}$$

Typical $N_{tpb,n}$ values are of the order of 10^{-9}-10^{-10} mol metal/cm^2 electrolyte i.e. typically a factor 10^2-10^3 smaller than N_G. This still corresponds to a "length" $\ell_{tpb,n}$ of several km per cm^2 of solid electrolyte.

5.8 XPS INVESTIGATIONS

5.8.1 XPS in Catalysis and Solid State Electrochemistry

X-ray photoelectron spectroscopy (XPS), which is synonymous with ESCA (Electron Spectroscopy for Chemical Analysis), is one of the most powerful surface science techniques as it allows not only for qualitative and quantitative analysis of surfaces (more precisely of the top 3-5 monolayers at a surface) but also provides additional information on the chemical environment of species via the observed core level electron shifts. The basic principle is shown schematically in Fig. 5.34.

There are several factors affecting these core level shifts and both initial state and final state effects play a role.[20] Yet the dominant factor affecting such "chemical" shifts is the oxidation state of the element under consideration. A negative charge on an element (e.g. O) will in general cause a decrease in the binding energy of core level electrons (such as for example the O1s core level electrons) while a positive charge on an element (e.g. Na) will cause an increase in the binding energy of core level electrons (e.g. the Na 1s core level electrons). Thus the observed (up to ±2 eV) chemical shifts can provide useful information on the oxidation state of an element in its local environment.

When carrying out XPS experiments to study in situ the electrodes of solid electrolyte cells one must be aware not only of the above "chemical" shifts but also of "electrochemical" shifts.[6,56-62] The electron binding energies are always measured with respect to the Fermi level of the grounded XPS detector (monochromator). Thus if the sample (e.g. the electrode under consideration) is also grounded then the electron binding energies of the elements of the electrode (e.g. Pt) and of the elements of species adsorbed on that electrode, are properly measured. If, however, one examines with XPS the reference electrode, one finds that the binding energies, $E_{b,R}$, of the core level electrons of its elements are shifted by:

$$\Delta E_{b,R} = -eU_{WR} = \bar{\mu}_W - \bar{\mu}_R \tag{5.66}$$

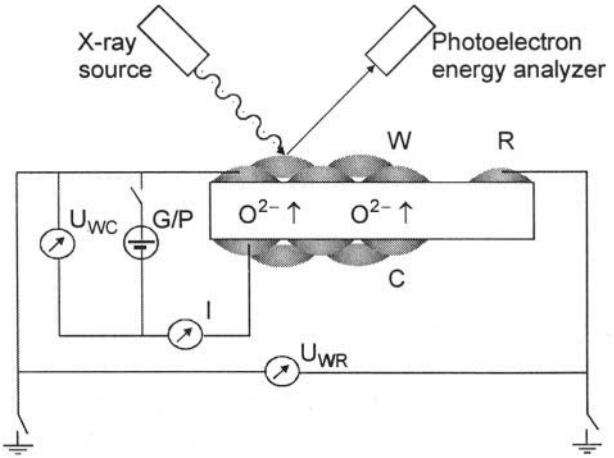

Figure 5.34. Schematic of the experimental setup for using X-ray photoelectron spectroscopy (XPS) to investigate the catalyst-electrode surface.[6] Reprinted with permission from the American Chemical Society.

This is called *electrochemical shift* and simply stems from the fact that the Fermi level of the reference electrode is not equal to that of the working electrode and thus to the Fermi level of the detector. Furthermore if one changes U_{WR} via a potentiostat the core level electron binding energies of species associated with the reference electrode will shift according to Eq. (5.66), i.e. the XPS analyzer acts also as a (very expensive) voltmeter.

What happens if, with the working electrode always grounded, one looks at elements on the solid electrolyte surface in the vicinity of the working electrode? Can one, using an equation similar to Eq. (5.66), measure the Galvani potential difference $\Delta\varphi$ between the working electrode and the solid electrolyte, which is one of the "unresolved" problems in electrochemistry, solid and aqueous? The answer is we could if it was somehow possible to eliminate chemical shifts, i.e. if we could have the same species (e.g. Zr) with the same chemical environment, both in the solid electrolyte and on the working electrode surface. This does not appear to be feasible. Nevertheless as one varies U_{WR} by ΔU_{WR} one again observes that the core level binding energies of the elements of the solid electrolyte, $E_{b,EL}$, also shift according to:

$$\Delta E_{b,EL} = -e\Delta U_{WR} = \Delta(\bar{\mu}_W - \bar{\mu}_R) \tag{5.67}$$

i.e., again there is an "electrochemical" shift and again the XPS detector provides the same information as a good voltmeter, i.e. it measures in this case the working electrode overpotential.

When doing in situ XPS in solid state electrochemistry one must be aware of the following experimental realities:[6,56-62]

1. The working electrode, assuming it is the electrode under observation, should preferably be grounded. If the reference electrode is grounded instead, one should be constantly aware of the above electrochemical shifts.
2. The sample temperature should be sufficiently high to ensure sufficient conductivity of the solid electrolyte and thus avoid "charging" of the solid electrolyte. This means temperatures above 300°C for YSZ and above 100°C for β''-Al_2O_3.
3. The solid electrolyte is always "visible" to the XPS through microcracks of the metal films. As already discussed, some porosity of the metal film is necessary to guarantee enough tpb and thus the ability to induce electrochemical promotion. In order, however, to have sufficient signal from species adsorbed on the metal it is recommended to use films with relatively small porosity (crack surface area 10-25% of the superficial film surface area).

X-ray photoelectron spectroscopic (XPS) studies of Ag[63,64] and Pt[6,56-62] films deposited on YSZ under positive current application conditions have confirmed the proposition[2-4] that NEMCA with oxide ion conducting solid electrolytes is due to an electrochemically induced and controlled backspillover of oxide ions on the catalyst surface.

The early studies of Arakawa et al.[63,64] focused on Ag films. Upon positive current application chemisorbed atomic oxygen is immediately formed (O 1s binding energy at 532.6 eV) followed by the gradual appearance of anionic oxygen (O 1s at 529.2 eV) which eventually causes a small decrease in the amount of chemisorbed atomic oxygen. This transient behaviour is in good qualitative agreement with catalytic rate transients during ethylene epoxidation on Ag under similar temperature and imposed current conditions at atmospheric pressure.[65] More recently Göpel and coworkers used XPS, UPS and EELS (electron energy loss spectroscopy) to study Ag/YSZ surfaces under NEMCA conditions.[24] Their XPS spectra are similar to those of Arakawa et al.[63,64]

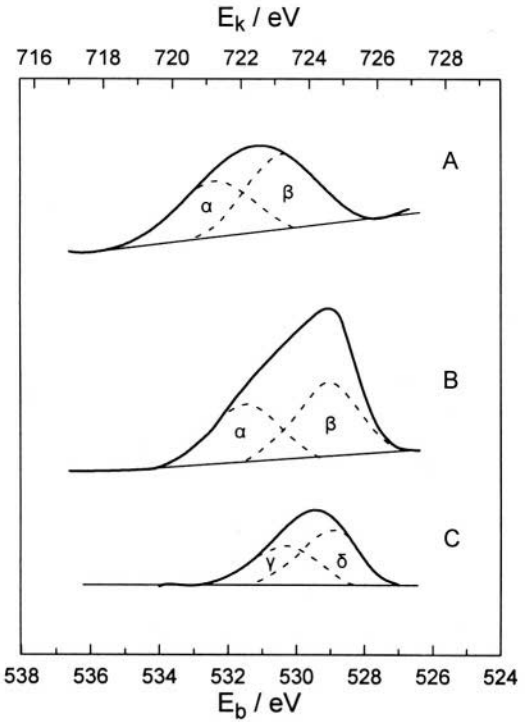

Figure 5.35. Effect of electrochemical O^{2-} pumping on the O 1s spectrum of Pt/YSZ[6] (A-C). XPS spectra at 400°C (A) ΔU_{WR}=0, I=0; (B) ΔU_{WR}=1.2 V, I=40 μA; (C) O 1s difference spectrum.[6] Reprinted with permission from the American Chemical Society.

A subsequent detailed XPS study of Pt films interfaced with YSZ[6] (Figs 5.35 to 5.37) has shown that:

a) Upon positive overpotential application ($\Delta U_{WR}>0$) backspillover of oxygen takes place from the solid electrolyte onto the Pt catalyst surface. This is manifest by the pronounced increase in the total area of the O1s peak (Fig. 5.35). This backspillover oxygen has a very low binding energy (~ 528.8 eV), i.e. it is very oxidic, it carries a strong negative charge (δ-state in Fig. 5.35).
b) Normally chemisorbed atomic oxygen (O 1s at 530.2 eV) is also formed with applied current (peak γ in Fig. 5.35). The maximum coverages of the γ and δ states of oxygen (based on the number of surface Pt atoms) are comparable and of the order of 0.5 each.[6]
c) Backspillover oxide ions (O 1s at 528.8 eV) are generated on the Pt surface with a time constant of $2FN_G/I$ (Eq. 4.32) where I is the applied current (peak δ in Fig. 5.35).
d) Oxidic backspillover oxygen (δ-state) is much less reactive than normally chemisorbed oxygen (γ-state) with the reducing (H_2 and CO) UHV background.[6]

The above observations provide a straightforward explanation for the physicochemical origin of NEMCA, or electrochemical promotion, when using O^{2-} conducting solid electrolytes, such as YSZ: Backspillover oxide ions $O^{\delta-}$ (O 1s at 528.8 eV) generated at the tpb upon electrochemical O^{2-} pumping to the catalyst spread over the gas-exposed catalyst surface. They are accompanied by their compensating (screening) charge in the metal, thus forming surface dipoles. An "effective electrochemical double layer"[66] is thus established on the catalyst surface (Fig. 1.4) which increases the work function of the metal and affects the strength of chemisorptive bonds such as that of normally chemisorbed oxygen via through-the-metal or through-the-vacuum interactions. The change in chemisorptive bond strengths causes the observed dramatic changes in catalytic rates.

The creation of an "effective double layer" is also supported by the following observation during the XPS experiments (Fig. 5.36): As the grounded Pt electrode is polarized via application of a potential ΔU_{WR}, the Zr $3d_{5/2}$ spectrum shifts by $e\Delta U_{WR}$ and the same applies for the O1s spectrum of β-oxygen which corresponds to the lattice YSZ oxygen. Thus the XPS shift of the components of the solid electrolyte provide a direct measure of the electrode overpotential (Eq. 5.67). An interesting observation is that the δ state of oxygen (backspillover oxygen) and the, electrochemically shifted, β-state (YSZ) are both at practically the same binding energy during potential application of ~1 V (Fig. 5.35). Thus the entire Pt electrode appears to be surrounded on all sides, i.e. at the metal/gas and near the metal/solid electrolyte interface, from energetically indistinguishable oxygen, i.e. oxygen ions with the same core level shift, thus practically identical charge.

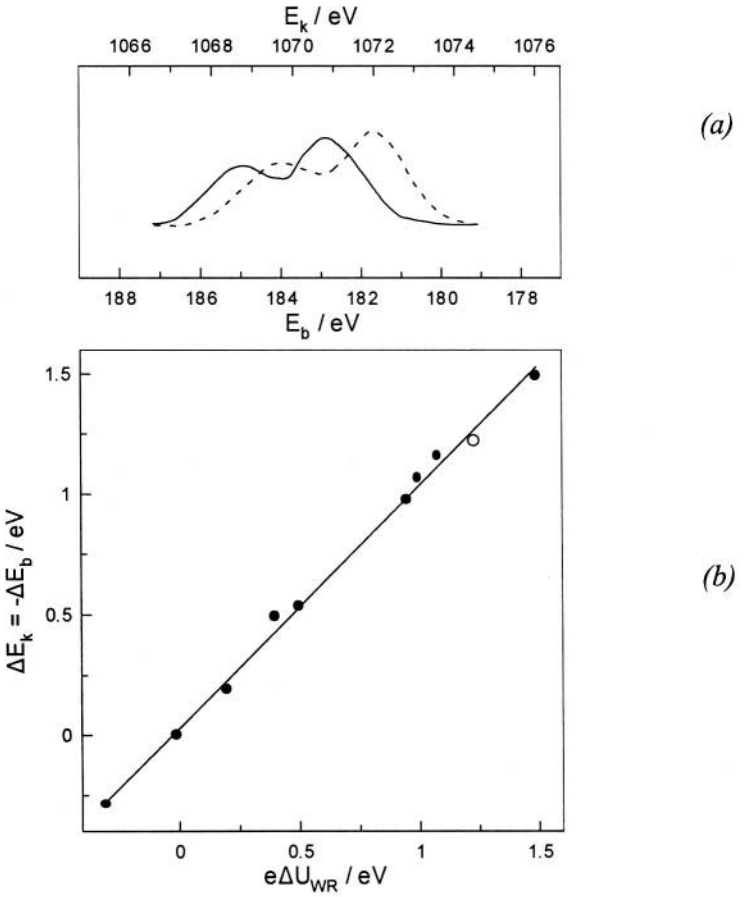

Figure 5.36. Effect of electrochemical O^{2-} pumping on the Zr $3d_{5/2}$ XPS spectra of Pt/YSZ at 400°C; (a) Zr $3d_{5/2}$ spectrum shift from $\Delta U_{WR}=0$ (solid curve) to $\Delta U_{WR}=1.2$ V (dashed curve) (b) effect of overpotential ΔU_{WR} on the binding energy, E_b, and kinetic energy, E_k, ($\Delta E_k=-\Delta E_b$) shifts of Zr $3d_{5/2}$ (filled circles, working electrode grounded) and Pt $4f_{7/2}$ (open circle, reference electrode grounded).[6] Reprinted with permission from the American Chemical Society.

Chemical and electrochemical shifts have merged into one and all oxygen ions surrounding the metal electrode have the same electrochemical potential. One can thus say that the electrode "floats in a sea" of oxygen ions which are present both on the YSZ side and on the gas-exposed electrode side. As already discussed in section 5.4 the ionic oxygen which migrates (backspillover oxygen) on the gas-exposed electrode surface under the influence of the applied positive overpotential ΔU_{WR} increases the work function, Φ, of the gas exposed electrode surface by $\Delta\Phi = e\Delta U_{WR}$.

Figure 5.36 shows the excellent agreement between Eq. (5.67) and the measured "electrochemical" core level shifts of the Zr $3d_{5/2}$ electrons of the solid electrolyte, with the Pt working electrode grounded, and of the Pt $4f_{7/2}$

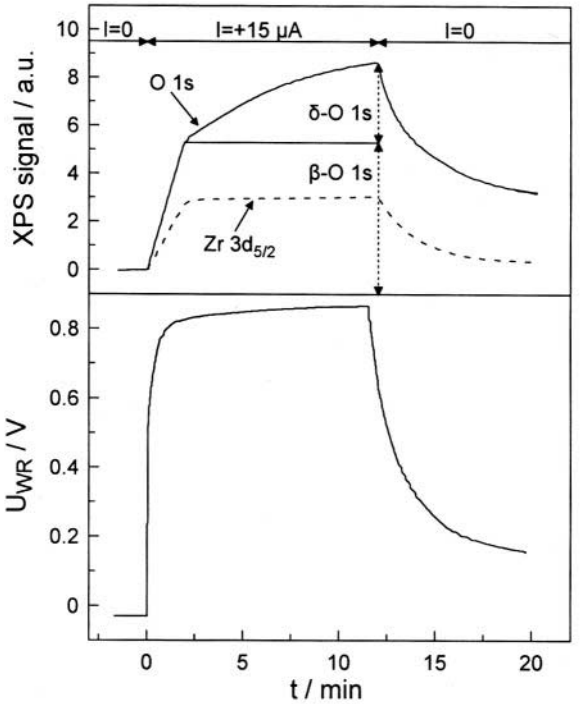

Figure 5.37. Transient effect of constant current application and interruption on the Pt/YSZ catalyst potential U_{WR} and on the XPS signal at E_b = 528.8 eV (location of δ-O 1s peak) and at E_b = 181.7 eV (electrochemically shifted position of the Zr $3d_{5/2}$ peak).[6] Reprinted with permission from the American Chemical Society.

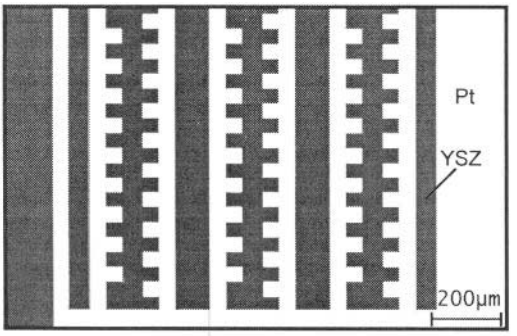

Figure 5.38. Optical micrograph of a representative structure of the microstructured Pt film on single crystalline YSZ used for SPEM experiments.[67] Reprinted with permission from Elsevier Science.

electrons of the working electrode, with the reference electrode grounded, during the experiments of Fig. 5.35.

Figure 5.37 reveals some additional interesting, although well expected, features and provides additional proof for the oxygen ion backspillover mechanism: Upon anodic galvanostatic polarization, the Zr $3d_{5/2}$ electron

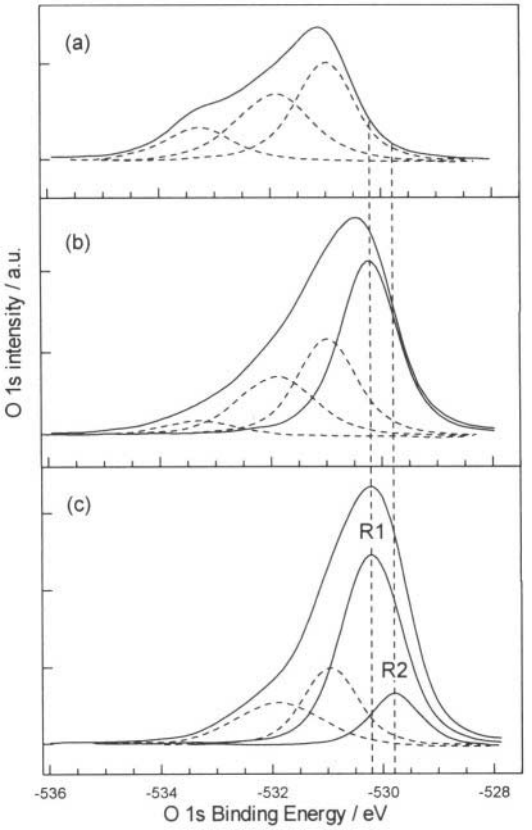

Figure 5.39. Characterization of the spillover species by photoelectron spectra of the O1s region taken from a ~0.02 μm^2 spot on the Pt surface: (a) The residual O 1s spectrum after the cleaning cycles; (b) The O1s spectrum measured in O_2 atmosphere (p_{O_2}=1×10^{-6} mbar); (c) The O1s spectrum obtained during electrochemical pumping in vacuum with U_{WR} = 1.1 V. R1 and R2 are the components which are formed by adsorption from the gas phase and by electrochemical pumping. The fitting components of the residual oxygen are shown with dashed lines. Photon energy = 643.2 eV, T≈350-400°C.[67] Reprinted with permission from Elsevier Science.

shift transient follows exactly the potential U_{WR} transient and so does also the shift of the O 1s electrons of the β-O state. This is quite logical as both signals originate from core level electrons in the solid electrolyte. The O 1s electrons shift transient, however, of the δ-O state (backspillover oxygen) has a much longer time constant, of the order of $2FN_G/I$, as discussed in Section 5.2. It corresponds to the backspillover oxygen on the Pt electrode.

Imbihl, Kiskinova, Janek and coworkers[67] have also used XPS and spatially-resolved photoelectron emission microscopy (SPEM) to investigate oxygen backspillover between YSZ and evaporated microstructured Pt films prepared using microlithographic techniques (Figure 5.38).

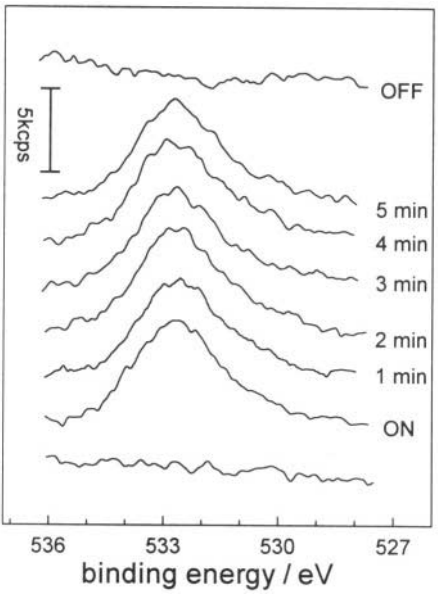

Figure 5.40. O1s spectra from a Ag/YSZ electrode at 598 K following application of an anodic current.[63,64] Reprinted with permission from Elsevier Science.

The technique of SPEM allows one to obtain XPS spectra from extremely small (~0.02 μm^2) surface areas and thus one can study O 1s spectra obtained from small (~0.02 μm^2) spots on the Pt surface.[67]

Figure 5.39a shows the residual O 1s spectrum obtained in ultra-high-vacuum after repeated cleaning cycle at 350-400°C. It is clear that there is a significant amount of residual O on the Pt surface which cannot be removed with conventional cleaning procedures. This by itself suffices to prove the presence of the omnipresent backspillover-formed effective double layer on the vacuum exposed Pt surface.

Figure 5.39 b shows the O 1s spectrum measured in an O_2 atmosphere ($p_{O_2}=10^{-6}$ mbar). It is clear that the oxygen present on the Pt surface increases and the broad O 1s spectrum peak shifts to 530.5 eV.

Figure 5.39 c shows the O 1s spectrum obtained during electrochemical O^{2-} pumping in vacuum at U_{WR} 1.1V. The spectrum clearly proves massive electrochemically controlled O^{2-} backspillover onto the Pt catalyst surface with a concomitant shift of the broad O 1s spectrum peak maximum to ~530 eV.

It is interesting to notice again the merging of the chemical and of the electrochemical shift upon anodic (ΔU_{WR}=1.1 V) polarization (Fig. 5.39c).[67] The backspillover $O^{\delta-}$ species on the Pt surface have an O 1s binding energy 1.1 eV lower than on the same surface under open-circuit conditions. The Pt catalyst-electrode is surrounded by isoenergetic oxygen species both at the Pt/YSZ and at the Pt/vacuum interfaces.[67]

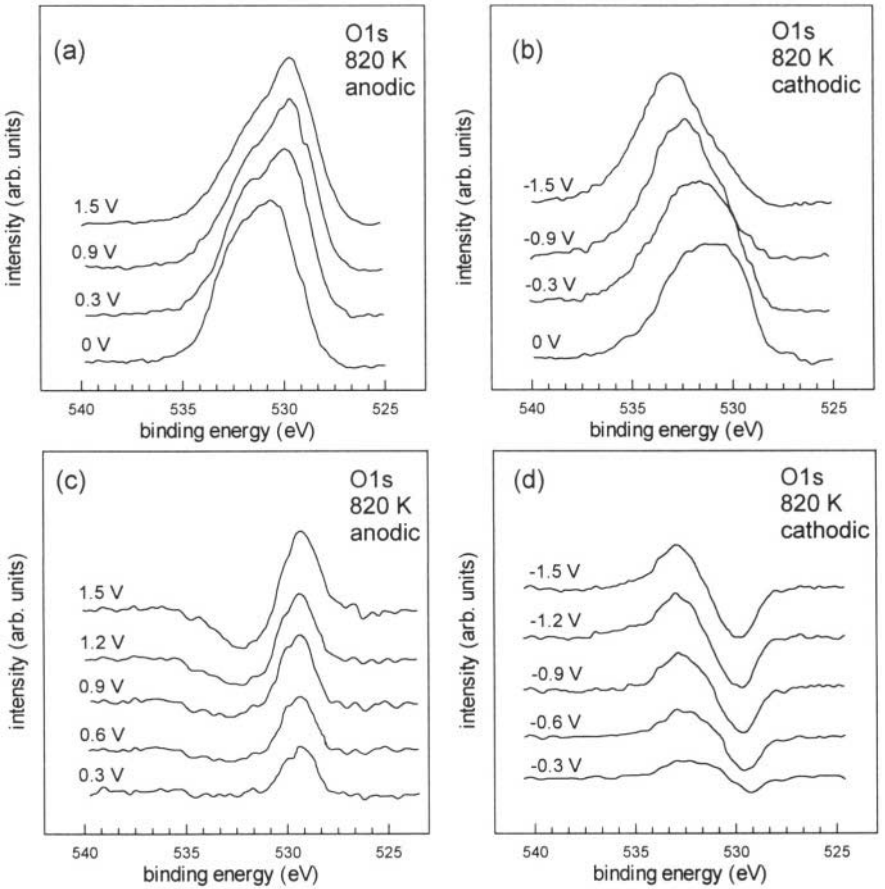

Figure 5.41. O 1s spectra from a Ag/YSZ electrode (in a Ag|YSZ|Pd,PdO cell) under (a) anodic and (b) cathodic polarization at 820 K and the corresponding difference spectra of the O1s signal for (c) anodic and (d) cathodic polarization.[24,68] Reprinted from ref. 24 with permission from Wiley-VCH.

Similar is the behaviour with Ag electrodes deposited on YSZ as shown in Figures 5.40 and 5.41.[68] The oxygen ion backspillover mechanism of electrochemical promotion is confirmed quite conclusively.

In summary in situ XPS with metal/YSZ catalyst-electrodes has positively confirmed the O backspillover mechanism as the cause of NEMCA and has provided very interesting information about the strongly anionic state of the backspillover oxygen species. *On the basis of the energetic indistinguishability of the backspillover* $O^{\delta-}$ *on the Pt surface and* O^{2-} *in the YSZ revealed by XPS, it appears almost certain that* $O^{\delta-}$ *is* O^{2-}. Nevertheless and in anticipation of further confirmation we have chosen to use the symbol $O^{\delta-}$, rather than O^{2-} for this, most effective, albeit relatively short-lived anionic promoter.

5.8.2 XPS Studies of Metals Supported on Na^+ Conductors

Reversible sodium backspillover as the origin of electrochemical promotion when using Na^+ conductors, such as β''-Al_2O_3, as the solid electrolyte has been confirmed by the in situ XPS work of Lambert and coworkers.[56-61]

A lucid example is shown in Fig. 5.42. The Na 1s spectrum corresponding to U_{WR}=600 mV corresponds to an electrochemically cleaned Pt surface, thus all the Na 1s signal originates from Na^+ in the β''-Al_2O_3, visible through microcracks of the Pt film. Upon decreasing U_{WR} one clearly observes:

An increase in the total Na 1s peak, positively confirming Na backspillover on the catalyst surface.

An electrochemical shift, as expected, of the Na 1s peak corresponding to the Na^+ of the β''-Al_2O_3 to higher binding energies, according to Eq. (5.67).

The creation of a new peak, at 1072.8 eV, corresponding to Na present on the Pt surface. Lambert and coworkers[56-60] have also shown that the same Na species forms on the catalyst surface via gas phase Na adsorption and that this species can then be pumped electrochemically into the β''-Al_2O_3 solid electrolyte via positive U_{WR} application.

The same observations made during XPS studies of Pt/YSZ regarding the almost identical core level shifts of O^{2-} in the YSZ and on the gas exposed Pt electrode surface, can be made here (Fig. 5.42) regarding the core level shifts of the Na 1s electrons: Upon cathodic polarization by –1V (i.e. from 0.6 V to –0.4 V) the Na 1s signal of the Na^+ in the β''-Al_2O_3 lattice shifts to a higher by 1 eV binding energy as expected from Eq. (5.67). But at the same time the backspillover $Na^{\delta+}$ species which appears on the Pt surface (Fig. 5.42) has the binding energy of its Na 1s electrons at practically the same value, as the two peaks are indistinguishable. Once again, as in the case of O^{2-} in Pt/YSZ, electrochemical and chemical shifts have merged into one, and all Na ions surrounding the metal electrode have practically the same core level shift, i.e. are energetically indistinguishable. Once again one can say that the Pt electrode "floats in a sea" of Na^+ which are present both on the β''-Al_2O_3 side and on the gas exposed electrode size.

Subsequent elegant work by Lambert and coworkers[61] has shown that, while under UHV conditions the electropumped Na is indistinguishable from Na adsorbed by vacuum deposition, under electrochemical reaction conditions the electrochemically supplied Na can form surface compounds (e.g. Na nitrite/nitrate during NO reduction by CO, carbonate during NO reduction by C_2H_4). These compounds (nitrates, carbonates) can be effectively decomposed via positive potential application. Furthermore the large dipole moment of Na (~5D) dominates the U_{WR} and Φ behaviour of the catalyst-electrode even when such surface compounds are formed.

Similar observations confirming the reversible Na spillover-backspillover mechanism of electrochemical promotion have been made by Lambert and coworkers using AES (Auger Electron Spectroscopy).[61]

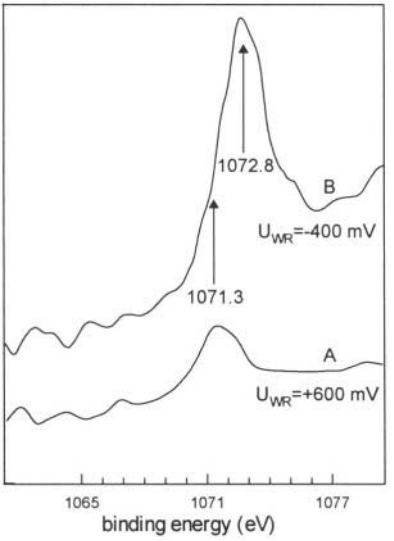

Figure 5.42. XPS of Pt/β"-alumina acquired under fixed potential application at 227°C. A) cleaned surface, B) Na-promoted surface.[58] Reprinted with permission from the Institute for Ionics.

5.9 UPS INVESTIGATIONS

Significant observations regarding the origin of NEMCA have been also made using Ultra-violet Photoelectron Spectroscopy (UPS) with Pt and Ag electrodes deposited on YSZ. In this case the work function of the electrode can be determined from the cutoff energy of secondary electrons (Fig. 5.43).[24,68] As shown in Fig. 5.8b the change in the work function of the gas-exposed Ag surface is very close to the imposed electrode potential change ΔU_{WR}.

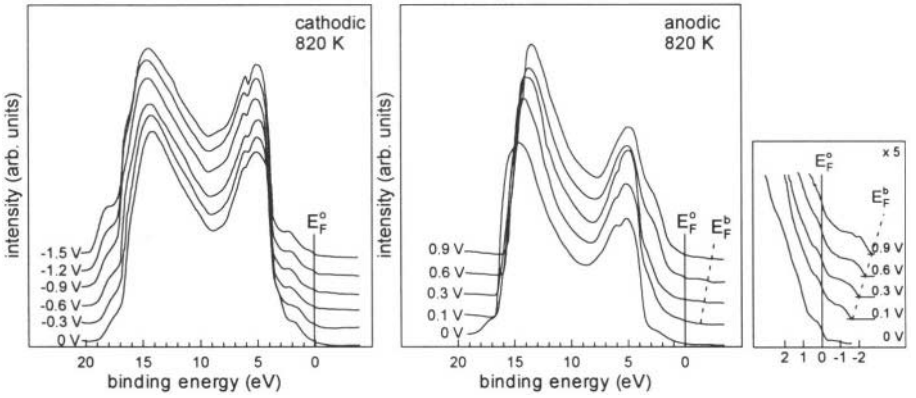

Figure 5.43. UP-spectra of Ag|YSZ electrodes for (a) cathodic and (b) anodic polarization of the galvanic cell Ag|YSZ|Pd,PdO at 547°C. In (b), the shift of the Fermi edge of the small silver particles on YSZ under anodic polarization is shown enlarged (5x).[24] Reprinted with permission from Wiley-VCH.

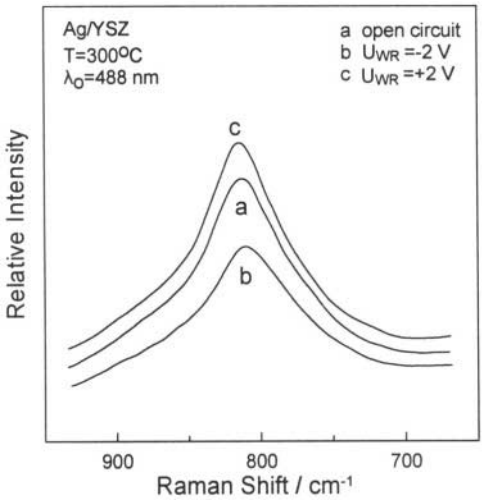

Figure 5.44. In situ SERS spectra[69] of oxygen adsorbed on Ag/YSZ at 300°C under (a) open circuit conditions and with the cell operating in the potentiostatic mode with (b) U_{WR} = -2 V and (c) U_{WR} = +2 V. Spectra (b) and (c) were obtained after the system had reached steady state. w = 200 mW, photon counter time constant, τ = 2 s, ssw = 2 cm^{-1}. Reprinted with permission from WILEY-VCH.

For the case of Ag it was found that both anodic and cathodic polarization lead to the creation of small insulated particles on the YSZ surface. Both the Fermi level and the work function of the insulated Ag particles was found to change with Ag electrode overpotential but the changes are smaller than on the continuous Ag film.[24]

5.10 SERS INVESTIGATIONS

Evidence for the potential-controlled spillover-backspillover of oxygen between YSZ and Ag has also been obtained using surface-enhanced-Raman spectroscopy (SERS).[69] As shown in Fig. 5.44 anodic polarization causes an increase in the coverage of oxygen on the Ag surface as manifest by the increase in the area of the O-related peak at 815 cm^{-1} which is the dominant freature of SERS spectra of oxygen covered Ag films deposited on YSZ.[69,70] It is likely that this frequency corresponds to O-O stretching of O atoms adsorbed in the troughs of Ag(110) which is usually the dominant crystallographic plane on polycrystalline Ag surfaces. Recent work by Savinova and Doblhofer indicates that this band may correspond to O-H bending. In any case it has been shown that the O species responsible for the peak at 815 cm^{-1} is a spectator species[69,70] which is consistent with the notion that it is related to the backspillover oxygen species. As also shown in Figure 5.44 there is also a small shift to higher frequencies, upon anodic potential application of the peak associated with

the Raman-active adsorbed oxygen species. Haller and co-workers[71] have observed the appearance of a low frequency band $\nu \sim 200\ cm^{-1}$, presumably corresponding to the Ag-O stretch of ionically bonded O under anodic polarization conditions.

5.11 PEEM INVESTIGATIONS

The technique of photoemission electron spectroscopy (PEEM) is a particularly attractive and important one for spatially resolved work function measurements, as both the Kelvin probe technique and UPS are integral methods with very poor (~mm) spatial resolution. The PEEM technique, pioneered in the area of catalysis by Ertl,[72-74] Block[75,76] and Imbihl,[28] has been used successfully to study catalytic oscillatory phenomena on noble metal surfaces.[74,75]

It has also been recently employed to investigate NEMCA by Imbihl and coworkers.[28] Both porous Pt paste films and evaporated microstructured Pt electrodes prepared by microlithography were investigated. These microstructured electrodes were typically 500 Å thick.

With both types of electrodes Imbihl and coworkers[28,29] found good agreement with the work function-change potential-change equality

$$\Delta\Phi = e\Delta U_{WR} \tag{5.18}$$

previously obtained via Kelvin probe and UPS measurements (Fig. 5.15). They also found variations in the Fermi level of the YSZ upon potential application, which is an important and quite logical observation, since the Fermi level of YSZ in the vicinity of the metal electrode is pinned to the Fermi level of the electrode as discussed in Chapter 7.

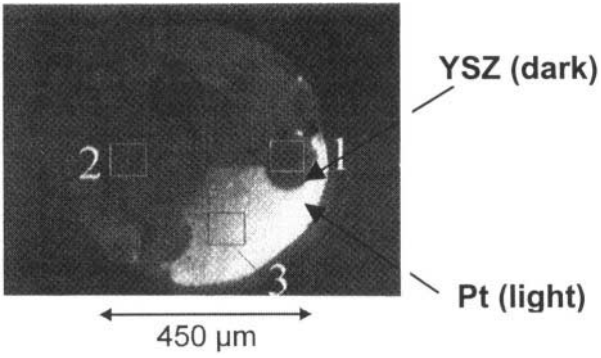

Figure 5.45. PEEM image of the Pt/YSZ microstructure showing three circular YSZ domains connected via channels which are surrounded by a Pt film. Inside the window marked from 1-3 the digitized PEEM intensity has been integrated for the measurements displayed in Fig. 5.46.[28] Reprinted with permission from Wiley-VCH.

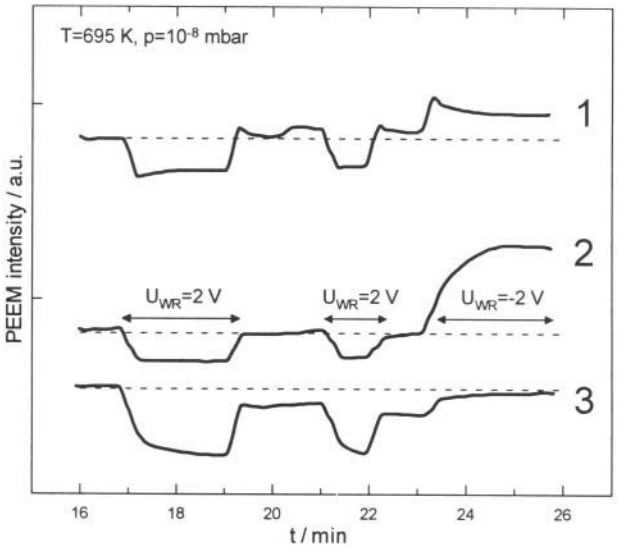

Figure 5.46. Local brightness variations in the three windows marked in Fig. 5.45 during electrochemical pumping at T = 695 K.[28] Reprinted with permission from WILEY-VCH.

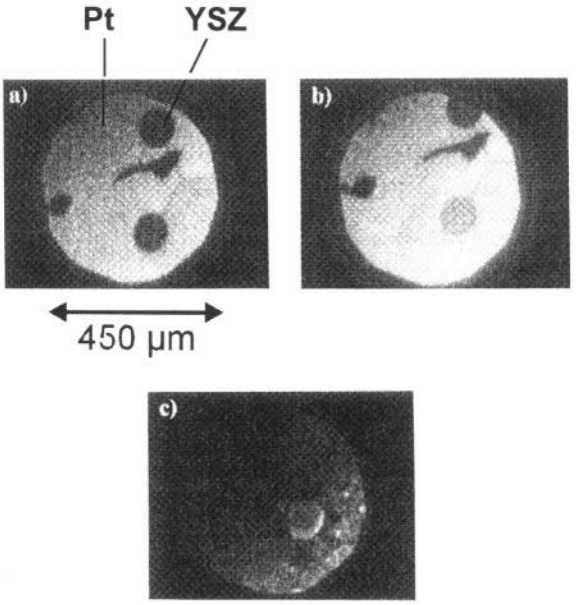

Figure 5.47. a) PEEM image at U_{WR} = 0 V and T = 695 K. The irregularly shaped island close to the upper YSZ circle represents probably a defect in the Pt film. b) Surface after electrochemical pumping with U_{WR}= -2 V for 2 min. c) Surface during electrochemical pumping with U_{WR} = 2 V for 2 min at T = 737 K.[28] Note the pronounced increase/decrease in brightness in (b) and (c) caused by the applied negative/positive potential on the grounded Pt electrode manifesting the pronounced decrease/increase in the work function Φ not only of the Pt surface but also of the YSZ solid electrolyte due to the Fermi level pinning at the Pt/YSZ interface. Reprinted with permission from WILEY-VCH.

Figure 5.45 shows a Pt electrode (light) deposited on YSZ (dark). There are three circular areas of bare YSZ connected via very narrow bare YSZ channels. The rest of the surface is Pt. Note that, as will be discussed in Chapter 7, the Fermi levels of the Pt film and of the YSZ solid electrolyte in the vicinity of the Pt film are equal. The YSZ, however, appears in the PEEM images much darker than the Pt film since YSZ has a negligible density of states at its Fermi level in comparison to a metal like Pt.

Figure 5.46 shows clearly how the application of potential changes the brightness and thus the workfunction Φ, of the *grounded* Pt catalyst-electrode (windows 2 and 3) and of the YSZ surface, (window 1), in accordance to the above discussed alignment (pinning) of the two Fermi levels.

The figure shows the observed variations in local work function within the three marked squares (1 is mostly on YSZ, 2 and 3 are on Pt). As shown in this figure and also in Fig. 5.47 the local work function (which increases with decreasing local brightness) follows the imposed variation in U_{WR}.

Increasing U_{WR} increases Φ, according to Eq. (5.18), thus causes local darkening (less electrons are emitted) as expected (Fig. 5.47c). Decreasing U_{WR} decreases Φ, again according to Eq. (5.18) as expected (Fig. 5.47b).

In that pioneering study[28] it was not possible to obtain a time resolved distribution of the backspillover oxygen species despite the fast, 40 ms, time resolution of the video-frames. If the spillover distance is 100 μm, this implies surface spillover oxygen diffusivities as high as 10^{-3} cm^2/s. If, however, microcracks exist in the film, which is very likely, then the spillover distance is much shorter and thus much lower diffusivities would suffice to escape time-dependent detection.

The significant point is that PEEM, as clearly presented in Figures 5.45 to 5.47, has shown conclusively that Φ follows reversibly the applied potential and has provided the basis for space-and time-resolved ion spillover studies of electrochemical promotion. It has also shown that the Fermi level and work function of the solid electrolyte in the vicinity of the metal electrode follows the Fermi level and work function of the metal electrode, which is an important point as analyzed in Chapter 7.

5.12 SCANNING TUNELLING MICROSCOPY

5.12.1 Direct Atomic Scale Observation of Electrochemically Controlled Spillover/Backspillover

Since the pioneering work of Rohrer and Binning,[77] scanning tunelling microscopy (STM) has been used to image atomic-scale features of electrically conductive surfaces under ultra-high-vacuum but also at atmospheric pressure and in aqueous electrochemical environments. The ability of STM to image chemisorption and surface reconstruction is well

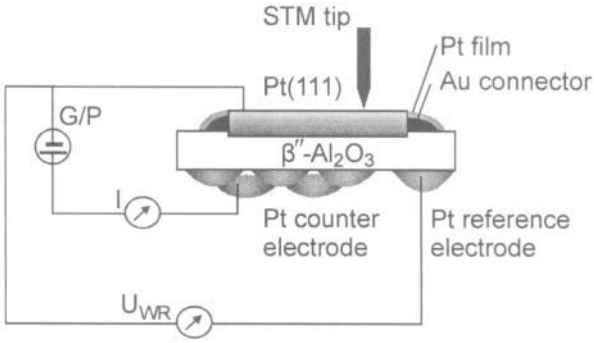

Figure 5.48. Schematic of the experimental setup for using Scanning Tunelling Microscopy (STM) to investigate a Pt(111) catalyst-electrode surface.[78] Reprinted with permission from Elsevier Science.

documented and of paramount importance in the fields of surface science, heterogeneous catalysis and electrochemistry.

Can one use STM to study spillover/backspillover phenomena and to confirm the origin of electrochemical promotion? The answer is positive and the experimental setup used for the first demonstration of electrochemically controlled spillover/backspillover between a catalyst-electrode (Pt) and a solid electrolyte (β''-Al_2O_3) is shown in Figure 5.48.[78,79] A polished Pt(111) single crystal (10mm×10mm×1mm) was mounted on an appropriately carved polycrystalline β''-Al_2O_3 sample (20mm×20mm×3mm).

Good mechanical and electrical contact between the metal and the solid electrolyte was established by coating a thin (~10μm) Au layer around the perimeter of the Pt crystal. The Au layer was covered by a porous Pt film (thickness ~10 μm) similar to those used in electrochemical promotion experiments. The Au and Pt films were prepared using thin coatings of unfluxed Au and Pt pastes followed by calcination at 850°C as described in Section 4.1. This design permits the same type of interfacing between single-crystal metal surfaces (which allow for relatively easy atomic-scale STM observation) and solid electrolyte components as that between polycrystalline metal films and solid electrolytes used in electrochemical promotion experiments. This electrical interfacing between the Pt single crystal and the solid electrolyte provides a significant "area" $N_{Pt,tpb}$ of three-phase-boundaries (tpb) between the solid electrolyte the metal catalyst-electrode and the gas phase. These three-phase-boundaries contain the active sites for the charge-transfer (electrocatalytic) reaction:

$$Na^+(\beta''\text{-}Al_2O_3) + e^- \leftrightarrow Na(a) \tag{5.68}$$

where Na(a) is Na adsorbed on the Pt surface. Reaction (5.68) proceeds to the right upon negative current or potential application.

The experiments were carried out in ambient air.[78,79] STM images were obtained at 300 K following current, I, or potential, U_{WR}, application in ambient air at 550 K. Figure 5.49 shows an unfiltered atomic resolution image of the Pt (111) surface after assembling the solid electrolyte cell before any current or potential application.

As expected, the Pt(111) surface is covered under ambient conditions by the well-known Pt(111)-(2×2)-O adlattice which corresponds to $\theta_O^{Pt} = 0.25$ where the superscript "Pt" denotes that the coverage is based on the total surface Pt atoms. The measured interatomic distance of 5.61 Å (Fig. 5.49a) is in excellent agreement with literature for the Pt(111)-(2×2)-O adlatice. As manifest by the Fourier transform spectrum (Fig. 5.49b) of the surface image of Fig. 5.49a there exists on the surface a second hexagonally ordered adlattice,

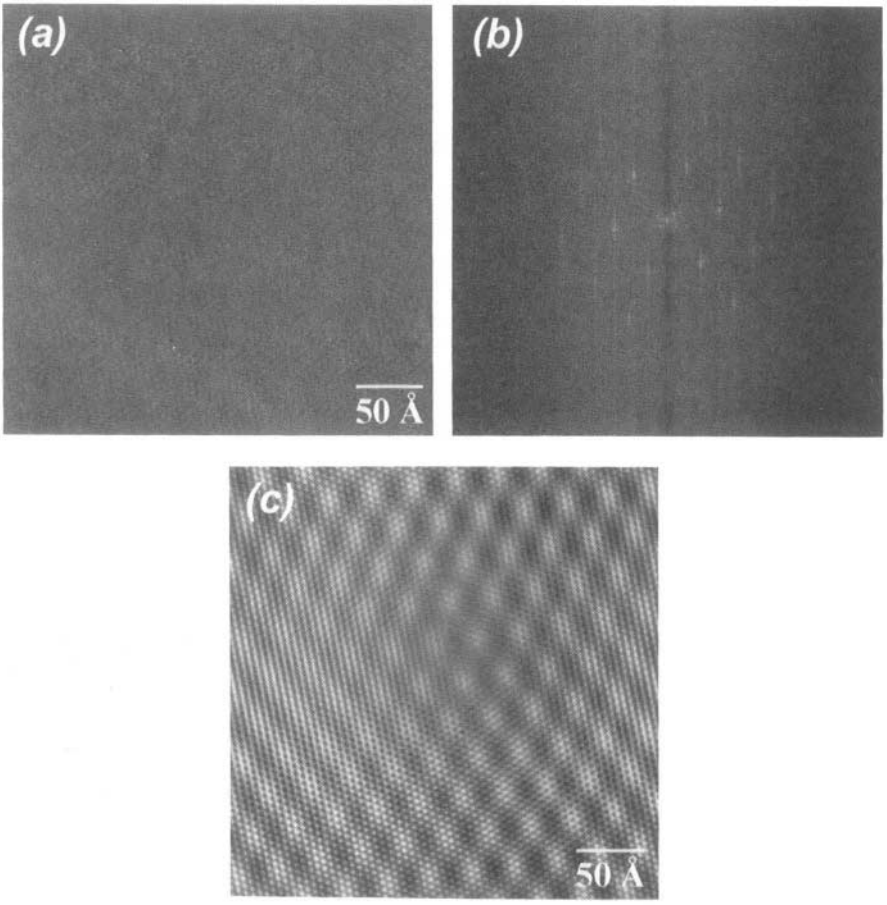

Figure 5.49. (a) STM image (unfiltered) of the initially sodium-contaminated Pt(111)-(2×2)-O adlattice (b) corresponding Fourier transform spectrum (c) Fourier-filtered STM image of the overlapping Pt(111)-(2×2)-O and Pt(111)-(12×12)-Na adlayers (bias U_t = 80 mV, tunelling current I_t = 10 nA, total scan size 319 Å).[78] Reprinted with permission from Elsevier Science.

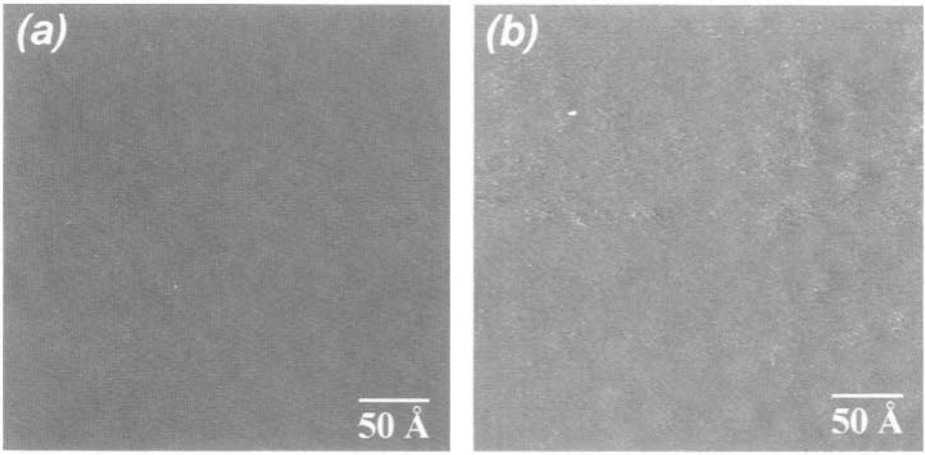

Figure 5.50. STM images (unfiltered) of the (a) sodium-cleaned and (b) sodium-dosed Pt(111)-(2x2)-O adlattice showing the reversible appearance of the Pt(111)-(12×12)-Na adlayer (U_t = +100 mV, I_t = 1.8 nA, total scan size 319 Å).[78] Reprinted with permission from Elsevier Science.

superimposed on the Pt(111)-(2×2)-O adlattice, which is also shown in the Fourier-filtered image of the surface (Fig. 5.49c). As shown below this second adlattice, which is visible in the lower part of Fig. 5.49a and has an interatomic distance of 33.6 Å is formed by sodium which has thermally migrated on the Pt(111) surface from the β''-Al_2O_3 solid electrolyte during sample calcination.

Upon application of positive potential (U_{WR}=0.4V) for 10 min the surface is cleaned from sodium and one obtains the image of Fig. 5.50a which shows only the Pt(111)-(2×2)-O adlattice.

Subsequent application of negative current (I = -1 μA for t=1400 s at 550 K) corresponding to the electrochemical supply of $-It/F=1.5\times10^{-8}$ mol Na with a concomitant final 1 V decrease in U_{WR} (U_{WR} = -0.6 V) and 1 eV decrease in Φ, causes the appearance of the Pt(111)-(12×12)-Na overlayer (Fig. 5.50b).

The same reversible appearance and disappearance of the Pt(111)-(12×12)-Na overlayer is shown in Figure 5.51, together with the corresponding two-dimensional Fourier-transform spectra and also in Fig. 5.52, which shows smaller areas of the sodium-free and sodium doped Pt(111) surface. The reversible electrochemically controlled spillover/backspillover of sodium between the solid electrolyte and the Pt(111) surface is clearly proven.

It is worth noting that each Na atom appears to perturb the electron density of the Pt(111) surface over large (~12) atomic distances. This can explain nicely the observed long-range promotional effect of Na on Pt surfaces. It is strongly reminiscent of the IR spectroscopic work of Yates and coworkers who showed that a single adsorbed alkali atom can affect the IR spectra of up to 27 coadsorbed CO molecules.[80]

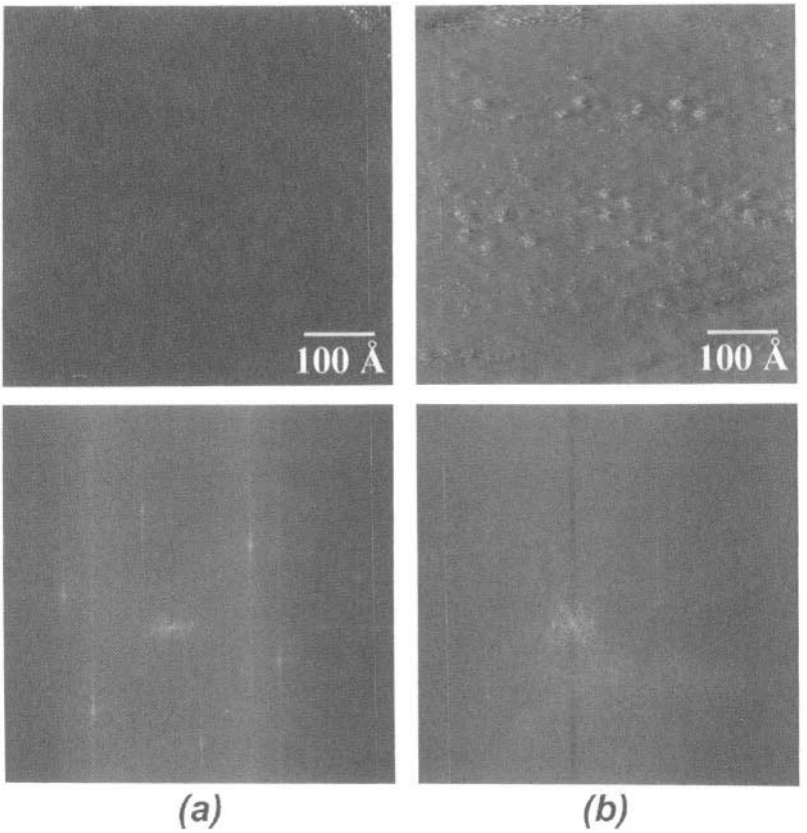

Figure 5.51. STM images (unfiltered) and corresponding Fourier spectra of the (a) sodium-cleaned and (b) sodium-dosed Pt(111)-(2×2)-O adlattice. Total scan size 638 Å, other conditions as in Figure 5.50.[78] Reprinted with permission from Elsevier Science.

The Pt(111)-(12×12)-Na adlattice, which as also shown in Figure 5.50 to 5.52 and in the corresponding Fourier spectra, can coexist with the Pt(111)-(2×2)-O adlayer, was found to be present over atomically enormous domains of the Pt(111) surface (Fig. 5.53a). No patches of the Pt(111) surface not covered by the Pt(111)-(12×l2)-Na adlattice could be found.[78,79] At higher Na coverages (~3%) more complex and geometrically more interesting ordered Na structures appear (Fig. 5.53b).[81]

Figures 5.49 to 5.53 show conclusively that:

1. Spillover-backspillover phenomena can take place over enormous (~mm) atomic distances.
2. Electrochemically induced and controlled Na backspillover is the origin of electrochemical promotion on metals interfaced with β''-Al_2O_3 solid electrolytes.
3. Promoters, such as sodium, tend to form ordered structures on catalyst surfaces.

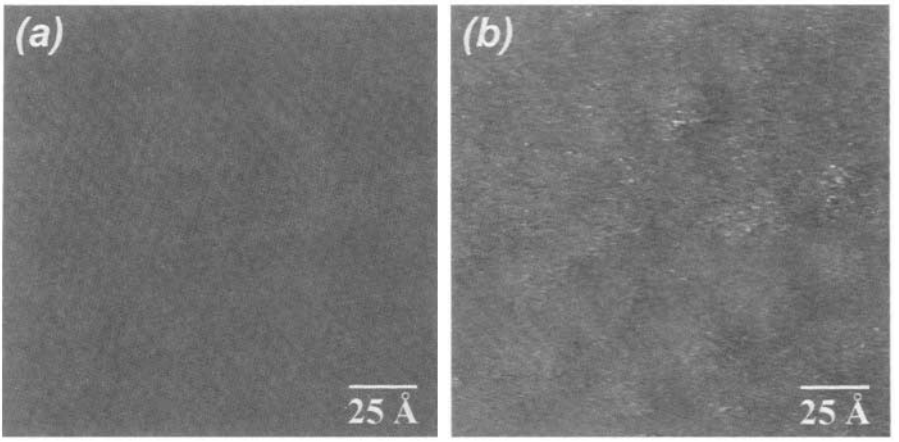

Figure 5.52. Low scanning-area STM images (unfiltered) of the (a) sodium-cleaned and (b) sodium-dosed Pt(111)-(2×2)-O adlattice. Total scan size 159 Å, other conditions as in Figure 5.50. Reprinted with permission from Elsevier Science.

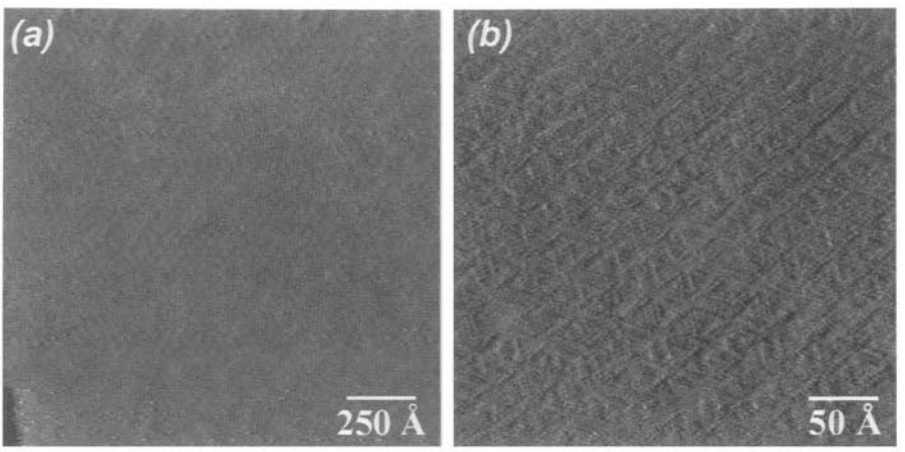

Figure 5.53. (a) Large scanning-area STM image (unfiltered) of the Pt(111)-(12×12)-Na adlattice. U_t = 500 mV, I_t = 2.5 nA, total scan size 1275 Å.[78] (b) STM image (unfiltered) of ordered Na adlattice formed on the Pt(111) – (2×2) – O surface at higher (~3%) Na coverage.[81]

5.12.2 Ordered Promoter Adlattices and Electrochemical Promotion

The electrochemically induced creation of the Pt(111)-(12×12)-Na adlayer, manifest by STM at low Na coverages, is strongly corroborated by the corresponding catalyst potential U_{WR} and work function Φ response to galvanostatic transients in electrochemical promotion experiments utilizing polycrystalline Pt films exposed to air and deposited on β''-Al_2O_3.[36,37] Early exploratory STM studies had shown that the surface of these films is largely composed of low Miller index Pt(111) planes.[5]

Two examples of the observed U_{WR} variation with sodium coverage on the Pt catalyst surface are shown in Fig. 5.54, together with the concomitant variation in the rates of CO[37] and C_2H_4[36] oxidation. In these experiments the Na coverage θ^{O}_{Na} was varied via galvanostatic negative current application, corresponding to the supply of (-It/F) mol Na onto Pt catalysts of measured maximum reactive oxygen uptake N_G (mol of O). Consequently the resulting Na coverage, θ^{O}_{Na}, based on the maximum number of surface oxygen atoms, can be computed from:[36,37]

$$\theta^{O}_{Na} = -It/FN_G \tag{5.69}$$

Assuming that the reactive oxygen corresponds to the oxygen which forms the well-known Pt(111)-(2×2)-O structure,[82] one can define the second Na coverage scale, θ^{Pt}_{Na}, shown in Figure 5.54, which is based on the number of surface Pt atoms, and equals

$$\theta^{Pt}_{Na} = (0.25)\,\theta^{O}_{Na} \tag{5.70}$$

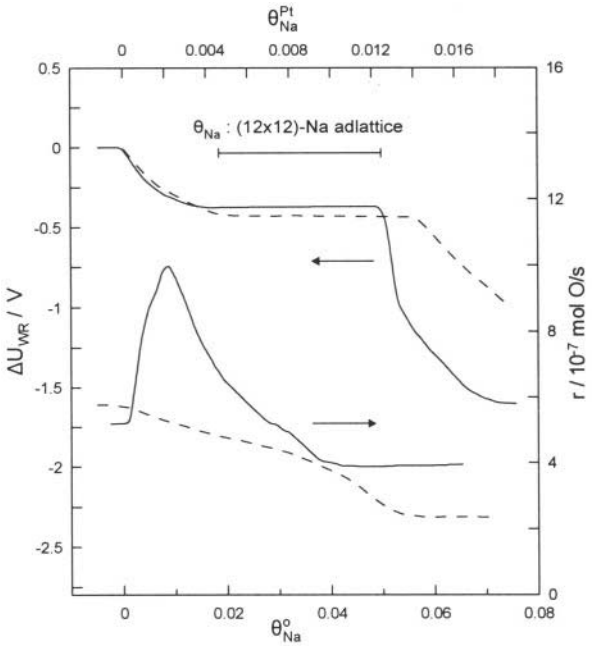

Figure 5.54. Effect of sodium coverage on the change ΔU_{WR} of polycrystalline Pt catalyst potential U_{WR} and on the catalytic rates of CO oxidation (solid lines[37]) and C_2H_4 oxidation (dashed lines[36]). Comparison with the theoretical Na coverage required to form the Pt(111)-(12×12)-Na adlayer; θ^{Pt}_{Na} is based on the number of surface Pt atoms; θ^{O}_{Na} is based on the number of surface O atoms corresponding to the Pt(111)-(2×2)-O adlattice.[78] Reprinted from ref. 78 with permission from Elsevier Science.

As shown in Figure 5.54 increasing sodium coverage causes initially ($\theta^{O}_{Na} < 0.01$) a decrease in catalyst potential U_{WR} (and thus work function $e\Phi$) followed by a rather wide sodium coverage region ($\Delta\theta^{O}_{Na} \approx 0.035$) where U_{WR} remains practically constant. The constancy of ΔU_{WR} with changing Na coverage indicates strongly the formation of an ordered structure whose chemical potential is independent of coverage. The observed $\Delta\theta^{O}_{Na}$ and $\Delta\theta^{Pt}_{Na}$ values over which U_{WR} remains constant (0.035 and 0.00875 respectively) are in excellent agreement with the corresponding theoretical geometric Na coverages ($\Delta\theta^{O}_{Na} = 1/36 = 0.0278$; $\Delta\theta^{Pt}_{Na} = 1/144 = 0.00695$) required to form the Pt(111)-(12×12)-Na adlattice (Fig. 5.54).

It is worth noting that for both systems the observed ΔU_{WR} value corresponding to the onset of the formation of the ordered Na adlattice is practically the same, which strongly supports the idea that this ΔU_{WR} value is characteristic of the chemical potential of this structure. The fact that a small but not negligible Na coverage ($\theta^{O}_{Na} < 0.015$) preceeds the formation of the ordered Na structure on the surface of polycrystalline Pt samples (Fig. 5.54) may indicate preferential Na adsorption on stepped surfaces before Na adsorption on Pt(111) starts taking place.

It should be noted that in that study[78] Na backspillover takes place not only on the surface of the Pt(111) single crystal (surface area $1 cm^2$, thus 1.53×10^{15} surface Pt atoms or 2.54×10^{-9} surface Pt mol) but also on the surface of the connecting porous Pt film along the perimeter of the Pt(111) monocrystal. Therefore only a small fraction (1.76×10^{-11} mol Na i.e. roughly 0.12% of the totally supplied Na) creates the (12×12)-Na adlayer on the single crystal surface and the rest is used to establish an equivalent Na coverage on the connecting porous Pt film of surface area ~800 cm^2. It is worth emphasizing that the measured change $\Delta U_{WR} = -1$ V in the Pt(111) catalyst potential during electrochemical Na supply and the concomitant decrease of 1 eV in the work function of the Pt(111) surface, is consistent, in view of Fig. 5.54, with the completion of the (12×12)-Na adlattice, i.e. with a θ^{O}_{Na} value in excess of 0.05.

As previously noted the constancy of catalyst potential U_{WR} during the formation of the Pt-(12×12)-Na adlayer, followed by a rapid decrease in catalyst potential and work function when more Na is forced to adsorb on the surface, (Fig. 5.54) is thermodynamically consistent with the formation of an ordered layer whose chemical potential is independent of coverage.

The formation of the ordered Pt-(12×12)-Na structure over the entire Pt(111) surface shows that the repulsive dipole-dipole interactions of the partly ionized Na atoms (which are accompanied by their image charges in the metal) overbalances the attractive Madelung-type attraction between the Na adlayer and the underlying (2×2)-O adlattice. This is corroborated by the fact that the catalytic rate relaxation time constant τ during galvanostatic transients in electrochemical promotion studies utilizing Pt/Na-β''-Al_2O_3 has

been found to be given by:[36,37]

$$\tau = FN_G \theta^{O}_{Na} / I \tag{5.71}$$

where N_G is the catalyst surface area expressed in mol adsorbed O. Equation (5.71) could suggest that electrochemically supplied Na spreads at the macroscopic level more or less uniformly everywhere on the gas exposed catalyst surface due to the dominating repulsive dipole-dipole interactions of Na adatoms, although the constancy of U_{WR} during formation of the Pt-(12×12)-Na adlayer (Fig. 5.54) suggests local island formation of the (12×12) structure due to local Madelung-type attraction.

It should be clear that, as well known from the surface science literature (Chapter 2) and from the XPS studies of Lambert and coworkers with Pt/β″-Al_2O_3 (section 5.8), the Na adatoms on the Pt surface have a strong cationic character, $Na^{\delta+}$-δ+, where δ+ is coverage dependent but can reach values up to unity. This is particularly true in presence of other coadsorbates, such as O, H_2O, CO_2 or NO, leading to formation of surface sodium oxides, hydroxides, carbonates or nitrates, which may form ordered adlattices as discussed in that section. What is important to remember is that the work function change induced by such adlayers is, regardless of the exact nature of the counter ion, dominated by the large (~5D) dipole moment of the, predominantly cationic, Na adatom.

5.13 QUANTUM MECHANICAL CALCULATIONS

The previous sections of this chapter have established that NEMCA, or Electrochemical Promotion, is caused by the electrochemically controlled backspillover of ionic species onto the catalyst surface and by the concomitant change on catalyst work function and adsorption binding energies. Although the latter may be considered as a consequence of the former, experiment has shown some surprisingly simple relationships between change ΔΦ in catalyst work function and change in chemisorptive bond strengths E_{ads}, catalytic activation energies E_{act} and catalytic rates:

$$\Delta E_{ads} = \alpha_{ads}\Delta\Phi \qquad \alpha_{ads}<0 \text{ for electron acceptor adsorbates} \tag{5.72}$$
$$\alpha_{ads}>0 \text{ for electron donor adsorbates}$$

$$\Delta E_{act} = \alpha_{act}\Delta\Phi \qquad \alpha_{act}<0 \text{ for electrophobic reactions} \tag{5.73}$$
$$\alpha_{act}>0 \text{ for electrophilic reactions}$$

$$\ln(r/r_o) = \alpha\Delta\Phi/k_bT \qquad \alpha>0 \text{ for electrophobic reactions} \tag{5.74}$$
$$\alpha<0 \text{ for electrophilic reactions}$$

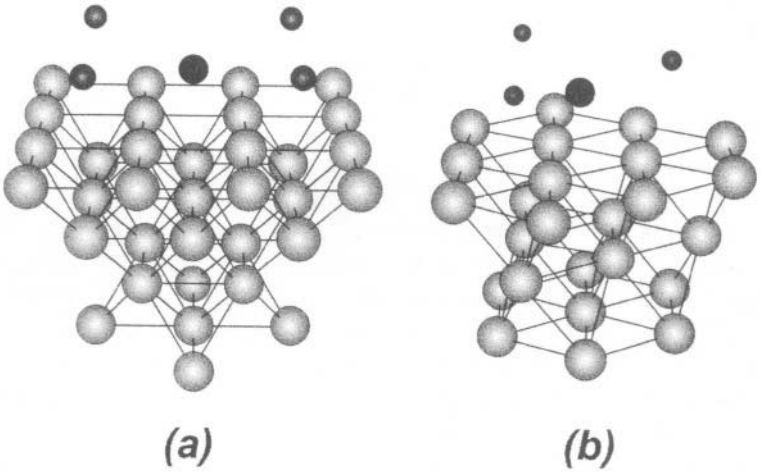

Figure 5.55. (a) Cu_{34} cluster used to model the Cu(100) surface. Oxygen has been adsorbed on the central 4-fold hollow site. (b) Pt_{25} cluster used to model the Pt(111) surface. Oxygen has been adsorbed on the central 3-fold hollow site. The position of the adsorbed ions (or point charges) is also shown.[83,84] Reprinted with permission from the American Chemical Society.

One of the most striking results is that of C_2H_4 oxidation on Pt[5] where $\alpha_{ads,O} = \alpha_{act} = -1$, i.e. the decreases in reaction activation energy and in the chemisorptive bond strength of oxygen induced by increasing work function Φ are equal to each other and equal to the increase in Φ. Similar is the case for ethylene epoxidation and deep oxidation on Ag.[5]

Although the range of validity of such simple expressions may not be too wide (typically 0.3-1eV) still it is quite important to try to analyze and understand them as rigorously as possible.

To this end quantum mechanical calculations have been carried out[83,84] using cluster models of the Pt(111) surface, as well as of the Cu(100) surface, with various representations of the adsorbed ions on the catalyst surface (Fig. 5.55).

In this section we will concentrate on the results obtained with the cluster model of the Pt(111) surface. The results with Cu(100) are qualitatively similar and have shown that point charges provide a very good approximation to the effect of coadsorbed ions.[83,84]

The basic idea is that a positive (negative) ion adsorbed on the surface induces a polarization of the substrate metal with formation of an image charge in such a way that the electric field within the metal is zero.[83] The substrate electron redistribution can be represented by an effective, or image, charge below the surface of opposite sign compared with the "test" charge above the surface. This charge pair (dipole) generates a nonuniform electric field above the surface which will affect the properties of an adsorbed atom (chemisorbed oxygen in the present case). Thus ions and image charges can be modeled as point charges.[83]

However, uniform electric fields, normal to the cluster surface, were also investigated.[83] In both cases (point charges and uniform fields) two effects were examined:

a) How the oxygen adsorption energy varies with the change of the point charge or with the strength of the field.
b) How the position of the cluster Fermi level (the cluster HOMO, highest occupied molecular orbital) varies with the charge of the point charge or with the strength of the field. Since the cluster is overall neutral and its adsorbing surface carries no net charge, it follows that the cluster Fermi level coincides with the work function, Φ, of its adsorbing surface.

To model the coadsorption of an oxygen atom and positively or negatively charged ions on the surface of metal catalysts, Pacchioni and Illas computed cluster model Hartree-Fock (HF) wave functions. The Pt(111) surface was simulated by using a Pt_{25} (12,6,7) cluster (Figure 5.55). The three Pt atoms defining the 3-fold hollow site were treated with a 10-electron relativistic effective core potential (ECP) which includes explicitly the valence of the $5d^9$ and $6s^1$ electrons. The remaining 22 Pt atoms were described with a 1-electron relativistic ECP. The different s, p, d, and f potentials were obtained from an all-electron relativistic self-consistent field (SCF) calculation carried out in a very large basis set of Slater type orbitals for the Pt-atom. The calculations were performed using the HONDO 8.5 and HONDO-CIPSI program packages.[83]

Figure 5.56 shows the effect of point charge value on the position of the HOMO in Pt_{25} and of the Pt_{25}/O adsorption energy, E_{ads}, at the Stark and full

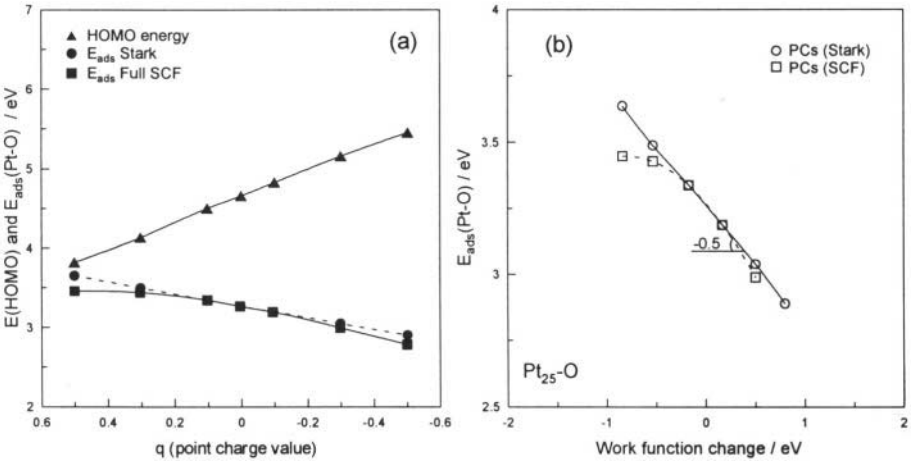

Figure 5.56. (a) Dependence of the position of the HOMO in Pt_{25} and of the Pt_{25}/O adsorption energy, E_{ads}, at the Stark and full self-consistent field (SCF) levels, as a function of the presence of point charge q above and below the cluster first layer.(b) Oxygen adsorption energy, E_{ads}, vs work function change, as measured by the cluster HOMO, for Pt_{25}/O. The curves refer to the cluster with point charges (PC). Both Stark and full SCF curves are shown.[83] Reprinted with permission from the American Chemical Society.

SCF levels as a function of the presence of point charges ±q above and below the cluster first layer. The presence of positive (negative) charges above the surface causes a near-linear decrease (increase) in the HOMO, and thus Φ, of the cluster. They also cause a near linear increase (decrease) in the adsorption energy, E_{ads}, of atomic oxygen. The change in E_{ads} is not accompanied by a significant change in the oxygen vertical height.[83] The change in E_{ads} caused by the point charges is similar at the Stark and self-consistent field (SCF) levels. This confirms that with Pt (as well as with Cu) the variation in the strength of the chemisorptive bond has a predominantly electrostatic "through the vacuum" origin.

Upon crossplotting E_{ads} vs HOMO (thus vs E_F and Φ) change one obtains Figure 5.56b. In excellent qualitative agreement with experiment (Figs. 5.26 and 4.47) there is a near-linear decrease in E_{ads} with increasing Φ. The slope is -0.5 (vs -1.0 for the experimental E_{ads} vs Φ relationship obtained via TPD (Fig. 5.26 and 4.47) and with -1 for the experimental activation energy dependence of C_2H_4 oxidation, E_{act}, vs Φ) (Fig. 4.35).

Consequently one of the key experimental observations of electrochemical promotion obtains a firm theoretical quantum mechanical confirmation: The binding energy of electron acceptors (such as O) decreases (increases) with increasing (decreasing) work function in a linear fashion and this is primarily due to repulsive (attractive) dipole-dipole interactions between O and coadsorbed negative (positive) ionically bonded species. These interactions are primarily "through the vacuum" and to a lesser extent "through the metal".

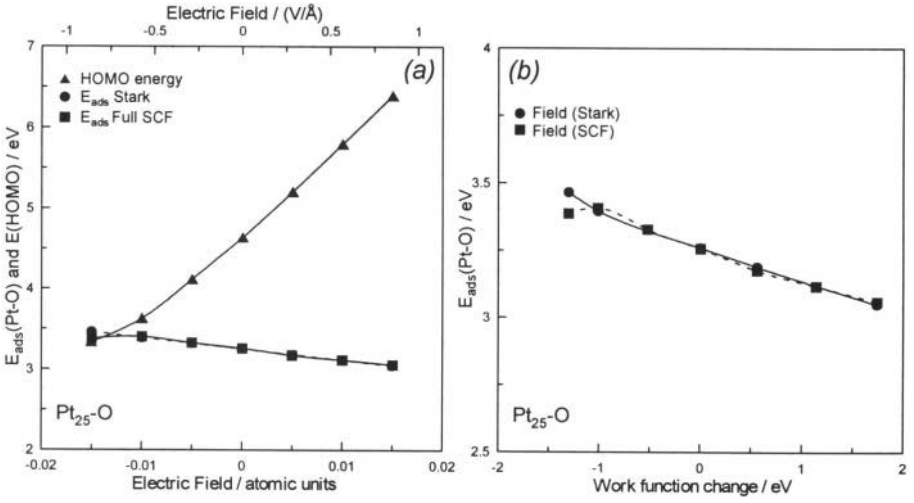

Figure 5.57. (a) Dependence of the position of the HOMO in Pt_{25} and of the Pt_{25}/O adsorption energy, E_{ads}, at the Stark and full SCF levels, as a function of the presence of an external electric field normal to the cluster surface.(b) Oxygen adsorption energy, E_{ads}, vs work function change, as measured by the cluster HOMO, for Pt_{25}/O.[83] Reprinted with permission from the American Chemical Society.

To further examine this point, Pacchioni and Illas replaced the point charges with a field, $\tilde{E}$, vertical to the surface.[83] The field strength was varied from ±0.005 to ±0.02 au (1 atomic unit au=5.7×10^9 V/cm), i.e. of the order of magnitude as the fields inside the double layer at electrode-electrolyte interfaces and as the fields experienced by valence electrons in atoms and molecules (1 V/Å). The results are presented in Figures 5.57a and 5.57b.As shown in Figure 5.57a the situation is qualitatively similar to that obtained with point charges: Increasing the negative (positive) field strength (which is similar to placing a positive (negative) point charge above the surface) causes a pronounced near-linear decrease in the cluster HOMO and a more moderate increase in the adsorption energy of oxygen. Upon crossplotting E_{ads} vs Δ(HOMO) or $\Delta\Phi$ one obtains Figure 5.57b. Again electrostatic interactions dominate (as manifest of the close agreement between Stark and full SCF results) and again a near-linear dependence is obtained. The slope is -0.14.

It thus appears that point charges provide a much better simulation of electrochemical promotion than uniform electric fields.

For comparison, in the case of O adsorption on a Cu_{34} cluster, simulating the Cu(100) surface, the corresponding computed ΔE_{ads} vs $\Delta\Phi$ slopes are -2.5 when using ions or point charges and -0.23 when using uniform electric fields.[83] It will be truly interesting to compare these theoretically predicted values with experiment. We note that the experimental values are -1 for O adsorption on polycrystalline Pt and Ag and -4 for O adsorption on Au (Fig. 5.26).

In conclusion, quantum mechanical cluster model calculations[83,84] provide a general basis for the understanding of electrochemical promotion (and also classical promotion) in catalysis. The existence of a near-linear relationship between change in work function and change in chemisorption energy of oxygen is confirmed. The mechanism has a predominantly electrostatic ("through the vacuum" interaction) nature. Local field inhomogeneity plays an important role. Coadsorbed ions and point charges simulate the actual behaviour much better than homogeneous electric fields.

5.14 THE EFFECTIVE DOUBLE LAYER

The picture which emerges from all the catalytic, electrochemical and surface science techniques reviewed in this Chapter is clear (Fig. 5.58). At sufficiently high temperatures for ionic motion in the solid electrolyte, the entire gas exposed surface of the metal electrodes is covered, to a significant extent, by ionic species which migrate there from the solid electrolyte. These ionic species ($O^{\delta-}$, $Na^{\delta+}$) are accompanied by their compensating (screening) charge in the metal, thus an overall neutral dipole layer is formed. This dipole layer has practically all the properties of the metal-solid electrolyte double-layer. It can thus be termed "effective double layer" to distinguish it

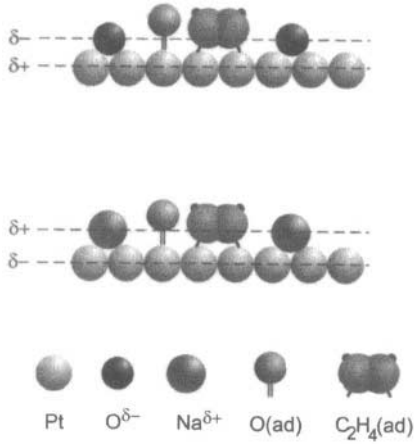

Figure 5.58. Schematic of the effective double layer during C_2H_4 oxidation on Pt/YSZ (top) and Pt/β″-Al_2O_3.

from the classical metal-solid electrolyte double layer and from the even more classical metal-aqueous electrolyte double layer. Like in every double layer, the field strength, $\tilde{E}$, within the effective double layer, is typically of the order 1V/Å. This parameter which equals $d\varphi/dz$ within the double layer, plays an important role in describing electrochemical promotion as analyzed in the next section.

The obvious question then arises as to whether the effective double layer exists before current or potential application. Both XPS and STM have shown that this is indeed the case due to thermal diffusion during electrode deposition at elevated temperatures. It is important to remember that most solid electrolytes, including YSZ and β″-Al_2O_3, are non-stoichiometric compounds. The non-stoichiometry, δ, is usually small ($< 10^{-4}$)[85] and temperature dependent, but nevertheless sufficiently large to provide enough ions to form an effective double-layer on both electrodes without any significant change in the solid electrolyte non-stoichiometry. This open-circuit effective double layer must, however, be relatively sparse in most circumstances. The effective double layer on the catalyst-electrode becomes dense only upon anodic potential application in the case of anionic conductors and cathodic potential application in the case of cationic conductors.

In a broad sense similar effective double layers can be formed via gaseous adsorption or evaporation (e.g. Na evaporated on Pt electrodes deposited on β″-Al_2O_3 has been shown to behave similarly to electrochemically supplied Na). In other cases, such as the effective double layer formed upon anodic polarization of Pt deposited on YSZ, the electrochemically created effective double layer appears to be unique and cannot be formed via gaseous oxygen adsorption at least under realistic (<300 bar) oxygen pressure conditions.

An interesting observation about this effective double layer came from XPS, i.e. that the backspillover oxygen ions on the Pt surface are isoenergetic with the O^{2-} ions of the YSZ in the vicinity of the Pt electrode. The Pt electrode is surrounded from all sides by oxide ions, O^{2-}, which are adsorbed on the Pt electrode with apparently the same binding energy. The electrochemical shift of the O^{2-} of the YSZ and the chemical shift of the $O^{\delta-}$ on the Pt surface lead to practically the same absolute O1s binding energy with respect to the grounded Pt electrode. This merging of XPS chemical and electrochemical shifts manifests the identical binding energy and indistinguishability of the oxide ions surrounding the Pt electrode.

The unique characteristic of the "effective double layer" is that it is directly accessible to gaseous reactants. Thus electrochemical promotion is *catalysis in the presence of a controllable* (via current and potential) *electrochemical double layer.* The theoretical implications and practical opportunities are obvious and numerous.

REFERENCES

1. J. Pritchard, Electrochemical Promotion, *Nature* **343**, 592 (1990).
2. C.G. Vayenas, S. Bebelis, and S. Ladas, Dependence of Catalytic Rates on Catalyst Work Function, *Nature* **343**, 625-627 (1990).
3. S. Bebelis, and C.G. Vayenas, Non-Faradaic Electrochemical Modification of Catalytic Activity: 1. The case of Ethylene Oxidation on Pt, *J. Catal.* **118**, 125-146 (1989).
4. S.G. Neophytides, and C.G. Vayenas, TPD and Cyclic Voltammetric Investigation of the Origin of Electrochemical Promotion in Catalysis, J. *Phys. Chem.* **99**, 17063-17067 (1995).
5. C.G. Vayenas, M.M. Jaksic, S. Bebelis, and S.G. Neophytides, The Electrochemical Activation of Catalysis, in *Modern Aspects of Electrochemistry,* J.O.M. Bockris, B.E. Conway, and R.E. White, eds., Kluwer Academic/Plenum Publishers, New York (1996), pp. 57-202.
6. S. Ladas, S. Kennou, S. Bebelis, and C.G. Vayenas, Origin of Non-Faradaic Electrochemical Modification of Catalytic Activity, *J. Phys. Chem.* **97**, 8845-8847 (1993).
7. S. Neophytides, D. Tsiplakides, and C.G. Vayenas, Temperature-Programmed Desorption of Oxygen from Pt-films Interfaced with Y_2O_3-Doped ZrO_2, *J. Catal.* **178**, 414-428(1998).
8. C.G. Vayenas, and G. Pitselis, Mathematical Modeling of Electrochemical Promotion and of Metal-Support Interactions, *I&EC Research* **40**(20), 4209-4215 (2001).
9. J.O' M. Bockris, and A.K.N. Reddy, *Modern Electrochemistry,* Plenum Press, New York (1970), pp. 1-5.
10. J.O' M. Bockris, and S.U.M. Khan, *Surface Electrochemistry: A Molecular Level Approach,* Plenum Press, New York (1993).
11. M. Stoukides, and C.G. Vayenas, Transient and steady-state vapor phase electrocatalytic ethylene epoxidation, ACS Symposium Series **178** ("Catalysis under transient conditions") A.T. Bell and L.L. Hegedus, Eds., pp. 181-202 (1982).
12. C.G. Vayenas, S. Bebelis, I.V. Yentekakis, and H.-G. Lintz, Non-Faradaic Electrochemical Modification of Catalytic Activity: A Status Report (Review Paper), *Catalysis Today* **11**(3), 303-442 (1992).

13. J.V. Barth, Transport of adsorbates at metal surfaces: from thermal migration to hot precursors, *Surf. Sci. Rep.* **40**, 75-149 (2000).
14. R. Lewis, and R. Gomer, Adsorption of Oxygen on Platinum, *Surf. Sci.* **12**, 157-176 (1968).
15. A. Kaloyannis, and C.G. Vayenas, Non-Faradaic Electrochemical Modification of Catalytic Activity. 11. Ethane Oxidation on Pt, *J. Catal.* **171**, 148-159 (1997).
16. Electrodes of conductive metallic oxides, in *Studies in Physical and Theoretical Chemistry,* S. Trasatti, ed. Elsevier Scientific Publishing Company, Amsterdam (1980), pp. 123-125.
17. B.E. Conway, Bicentennial of Alessandro Volta's Invention of the "Electric Pile": Discovery of the Electrical Basis of Chemistry, *Canadian Chemical News,* 15-17 (2000).
18. H. Reiss, The Fermi level and the Redox potential, *J. Phys. Chem.* **89**, 3783-3791 (1985).
19. H.J. Reiss, The Absolute Electrode Potential. Tying the Loose Ends, *J. Electrochem. Soc.* **135**, 247C-258C (1988).
20. P.M. Gundry, and F.C. Tompkins, in *Experimental Methods in Catalyst Research,* R.B.Anderson, ed. Academic Press, New York (1968), pp. 100-168.
21. J. Hölzl, and F.K.Schulte, Work Function of Metals, in *Solid Surface Physics,* Springer-Verlag, Berlin (1979), pp. 1-150.
22. S. Trasatti, The Work Function in Electrochemistry, in *Advances in Electrochemistry and Electrochemical Engineering,* H. Gerisher, and C.W. Tobias, eds., Journal Wiley and Sons (1977).
23. N. Sato, *Electrochemistry at metal and semiconductor electrodes,* Elsevier, Amsterdam (1998).
24. W. Zipprich, H.-D. Wiemhöfer, U. Vöhrer, and W. Göpel, In-situ Photoelectron-Spectroscopy of Oxygen Electrodes on Stabilized Zirconia, *Ber. Buns. Phys. Chem.* **99**, 1406-1413(1995).
25. C.A. Cavalca, *PhD Thesis,* Yale University (1995).
26. S. Ladas, S. Bebelis, and C.G. Vayenas, Work Function Measurements on Catalyst Films subject to in-situ Electrochemical Promotion, *Surf. Sci.* **251/252**, 1062-1068 (1991).
27. J. Nicole, *PhD Thesis,* EPFL (1999).
28. J. Poppe, A. Schaak, J. Janek, and R. Imbihl, Electrochemically Induced Surface Changes on Microstructured Pt Films on a solid YSZ Electrolyte, *Ber. Buns. Phys. Chem.* **102**, 1019-1022(1998).
29. J. Poppe, S. Voelkening, A. Schaak, E. Schuetz, J. Janek, and R. Imbihl, Electrochemical promotion of catalytic CO oxidation on Pt/YSZ catalysts under low pressure conditions, *Phys. Chem. Chem. Phys.* **1**, 5241-5249 (1999).
30. C.G. Vayenas, On the work function of the gas exposed electrode surfaces in solid state electrochemistry, *J. Electroanal. Chem.* **486**, 85-90 (2000).
31. C.G. Vayenas, and D. Tsiplakides, On the work function of the gas-exposed electrode surfaces in solid state electrolyte cells, *Surf. Sci.* **467**, 23-34 (2000).
32. D. Tsiplakides, and C.G. Vayenas, Electrode work function and absolute potential scale in solid state electrochemistry, *J. Electrochem. Soc.* **148**(5), E189-E202 (2001).
33. I. Riess, and C.G. Vayenas, Fermi level and potential distribution in solid electrolyte cells with and without ion spillover, *Solid State Ionics* **in press**, (2001).
34. D. Tsiplakides, S. Neophytides, and C.G. Vayenas, Investigation of electrochemical promotion using temperature programmed desorption and work function measurements, *Solid State Ionics* **136-137**, 839-847 (2000).

35. I. Riess, What does a voltmeter measure?, *Solid State Ionics* **95**, 327-328 (1997).
36. C.G. Vayenas, S. Bebelis, and S. Despotopoulou, Non-Faradaic Electrochemical Modification of Catalytic Activity: 4. The use of β''-Al_2O_3 as the solid electrolyte, *J. Catal.* **128**, 415-435 (1991).
37. I.V. Yentekakis, G. Moggridge, C.G. Vayenas, and R.M. Lambert, In situ controlled promotion of catalyst surfaces via NEMCA: The effect of Na on the Pt-catalyzed CO oxidation, *J. Catal.* **146**, 292-305 (1994).
38. S. Tracey, A. Palermo, J.P.H. Vazquez, and R.M. Lambert, In Situ Electrochemical Promotion by Sodium of the Selective Hydrogenation of Acetylene over Platinum, *J. Catal.* **179**, 231-240 (1998).
39. C.G. Vayenas, A. Ioannides, and S. Bebelis, Solid Electrolyte Cyclic Voltammetry for in situ Investigation of Catalyst Surfaces, *J. Catal.* **129**, 67-87 (1991).
40. D.A. Emery, P.H. Middleton, and I.S. Metcalfe, The effect of electrochemical current pumping on the work function of solid electrolyte supported catalysts, *Surf. Sci.* **405**, 308-315 (1998); Electrochemical enhancement of CO oxidation over YSZ supported Pt catalysts I&II, *J. Electrochem. Soc.* **146**(6), 2188-2193 (1999), ibid **146**(6), 2194-2198 (1999).
41. E.R. Koetz, H. Neff, and K. Mueller, A UPS, XPS and work function study of emersed silver, platinum and gold electrodes, *J. Electroanal. Chem.* **215**, 331-344 (1986).
42. Z. Samec, B.W. Johnson, and K. Doblhofer, The absolute electrode potential of metal electrodes emersed from liquid electrolytes, *Surf. Sci.* **264**, 440-448 (1992).
43. G.F. Froment, and K.B. Bischoff, *Chemical Reactor Analysis and Design,* John Wiley & Sons, New York (1979).
44. D. Tsiplakides, S. Neophytides, and C.G. Vayenas, Thermal Desorption Study of Oxygen Adsorption on Pt, Ag and Au films Deposited on YSZ, *Ionics* **3**, 201-208 (1997).
45. D. Tsiplakides, and C.G. Vayenas, Temperature Programmed Desorption of Oxygen from Ag films interfaced with Y_2O_3-doped ZrO_2, *J. Catal.* **185**, 237-251 (1999).
46. D. Tsiplakides, S. Neophytides, and C.G. Vayenas, Investigation of Electrochemical Promotion using Temperature-Programmed-Desorption and Work Function measurements, *Solid State Ionics* **136-137**, 839-847 (2000).
47. D. Tsiplakides, S. Neophytides, and C.G. Vayenas, Investigation of the state of the electrochemically generated adsorbed O species on Au films interfaced with Y_2O_3-doped-ZrO_2, *Ionics,* submitted (2001).
48. J.L. Falconer, and R.J. Madix, Flash desorption activation energies: DCOOH decomposition and CO desorption from Ni(110), *Surf. Sci.* **48**, 393-405 (1975).
49. A.J. Bard, and L.R. Faulkner, *Electrochemical Methods. Fundamentals and Applications,* John Wiley & Sons, Inc., New York (2001).
50. T. Chao, K.J. Walsh, and P.S. Fedkiw, Cyclic voltammetric study of the electrochemical formation of platinum oxide in a Pt/yttria-stabilized zirconia cell, *Solid State Ionics* **47**, 277-285 (1991).
51. C.G. Vayenas, S. Bebelis, I.V. Yentekakis, and S. Neophytides, Electrocatalysis and Electrochemical Reactors, in *CRC Handbook on Solid State Ionics,* P.J. Gellings, and H.J.M. Bouwmeester, eds., CRC Press, Inc., Boca Raton (1997), pp. 445-480.
52. Y. Jiang, A. Kaloyannis, and C.G. Vayenas, High Temperature cyclic voltammetry of Pt electrodes in solid electrolyte cells, *Electrochim. Acta* **38**(17), 2533-2539 (1993).
53. Y. Jiang, I.V. Yentekakis, and C.G. Vayenas, Potential-programmed reduction: A new technique for investigating chemisorption on catalysts supported on solid electrolytes, *J. Catal.* **148**, 240-251 (1994).
54. A.D. Frantzis, S. Bebelis, and C.G. Vayenas, Electrochemical promotion (NEMCA) of

CH_4 and C_2H_4 oxidation on Pd/YSZ and investigation of the origin of NEMCA via AC impedance spectroscopy, *Solid State Ionics* **136-137**, 863-872 (2000).

55. D. Kek, M. Mogensen, and S. Pejovnik, A Study of Metal (Ni, Pt, Au)/Yttria-Stabilized Zirconia Interface in Hydrogen Atmosphere at Elevated Temperature, *J. Electrochem. Soc.* **148**(8), A878-A886 (2001).
56. I. Harkness, and R.M. Lambert, Electrochemical Promotion of the NO + Ethylene Reaction over Platinum, *J. Catal.* **152**, 211-214 (1995).
57. R.M. Lambert, I.R.Harkness, I.V. Yentekakis, and C.G. Vayenas, Electrochemical Promotion in Emission Control Catalysis, *Ionics* **1**, 29-32 (1995).
58. R.M. Lambert, M. Tikhov, A. Palermo, I.V. Yentekakis, and C.G. Vayenas, Electrochemical Promotion of Environmentally Important Catalytic Reactions, *Ionics* **1**, 366-376 (1995).
59. O.A. Mar'ina, I.V. Yentekakis, C.G. Vayenas, A. Palermo, and R.M. Lambert, In situ controlled Promotion of Catalyst Surfaces via NEMCA: The effect of Na on the Pt-catalyzed NO Reduction by H_2, *J. Catal.* **166**, 218-228 (1997).
60. I.R. Harkness, C. Hardacre, R.M. Lambert, I.V. Yentekakis, and C.G. Vayenas, Ethylene oxidation over Platinum: In situ electrochemical promotion using β''-Al_2O_3 and studies with a Pt(111)/Na model catalyst, *J. Catal.* **160**, 19-26 (1996).
61. R.M. Lambert, F. Williams, A. Palermo, and M.S. Tikhov, Modelling alkali promotion in heterogeneous catalysis: in situ electrochemical control of catalytic reactions, *Topics in Catalysis* **13**, 91-98 (2000).
62. C. Pliangos, I.V. Yentekakis, S. Ladas, and C.G. Vayenas, Non-Faradaic Electrochemical Modification of Catalytic Activity: 9. Ethylene oxidation on Pt deposited on TiO_2, *J. Catal.* **159**, 189-203 (1996).
63. T. Arakawa, A. Saito, and J. Shiokawa, Surface study of a Ag electrode on a solid electrolyte used as oxygen sensor, *Applications of Surface Science* **16**, 365-372 (1983).
64. T. Arakawa, A. Saito, and J. Shiokawa, XPS for in situ observation of an Ag electrode on a solid electrolyte used as oxygen sensor, *Chem. Phys. Lett.* **94**, 250-252 (1983).
65. S. Bebelis, and C.G. Vayenas, Non-Faradaic Electrochemical Modification of Catalytic Activity: 6. The epoxidation of Ethylene on $Ag/ZrO_2(8mol\%)Y_2O_3$, *J. Catal.* **138**, 588-610(1992).
66. C. Cavalca, G. Larsen, C.G. Vayenas, and G. Haller, Electrochemical Modification of CH_3OH oxidation selectivity and activity on a Pt single-pellet catalytic reactor, *J. Phys. Chem.* **97**, 6115-6119 (1993).
67. B. Luerssen, S. Günther, H. Marbach, M. Kiskinova, J. Janek, and R. Imbihl, Photoelectron spectromicroscopy of electrochemically induced oxygen spillover at the Pt/YSZ interface, *Chem. Phys. Lett.* **316**, 331-335 (2000).
68. U. Vöhrer, *PhD Thesis,* University of Tuebingen (1992).
69. D.I. Kondarides, G.N. Papatheodorou, C.G. Vayenas, and X.E. Verykios, In situ High Temperature SERS study of Oxygen adsorbed on Ag: Support and Electrochemical Promotion Effects, *Ber. Buns. Phys. Chem.* **97**, 709-720 (1993).
70. S. Boghosian, S. Bebelis, C.G. Vayenas, and G.N. Papatheodorou, In Situ High Temperature SERS on Ag Catalysts and Electrodes during Ethylene Epoxidation, *J. Catal.* **117**, 561-565 (1989).
71. L. Basini, C.A. Cavalca, and G.L. Haller, Electrochemical Promotion of Oxygen Atom Back-Spillover from Yttria-Stabilized Zirconia onto a Porous Platinum Electrode: Detection of SERS Signals, *J. Phys. Chem.* **98**, 10853-10856 (1994).
72. A.van Oertzen, A. Mikhailov, H.-H. Rotermund, and G. Ertl, Subsurface oxygen formation on the Pt(110) surface: experiment and mathematical modeling, *Surf. Sci.* **350**, 259-270 (1996).

73. K. Asakura, J. Lanterbach, H.H. Rothermund, and G. Ertl, Spatio-temporal pattern formation during catalytic CO oxidation on a Pt(100) surface modified with submonolayers of Au, *Surf. Sci.* **374**, 125-141 (1997).
74. S. Kelling, S. Cerasari, H.H. Rotermund, G. Ertl, and D.A. King, A photoemission electron microscopy (PEEM) study of the effect of surface acoustic waves on catalytic CO oxidation over Pt(110), *Chem. Phys. Lett.* **293**, 325-330 (1998).
75. M. Kolodzejczyk, R.E.R. Colen, B. Delmon, and J.H. Block, Interaction between Cu and Pt(111) in the reaction $CO+O_2$ modification by Cu sub-monolayers and cooperation between pure and Cu-modified Pt(111), *Appl. Surf. Sci.* **121/122**, 480-483 (1997).
76. R.E.R. Colen, M. Kolodziejczyk, B. Delmon, and J.H. Block, Kinetic study of CO oxidation on copper modified Pt(111), *Surf. Sci.* **412/413**, 447-457 (1998).
77. G. Binning, H. Rohrer, C. Gerber, and E. Weibel, Surface Studies by Scanning Tunneling Microscopy, *Physical Review Letters* **49**(1), 57-61 (1982).
78. M. Makri, C.G. Vayenas, S. Bebelis, K.H. Besocke, and C. Cavalca, Atomic resolution STM imaging of Electrochemically Controlled Reversible Promoter Dosing of Catalysts, *Surf. Sci.* **369**, 351-359 (1996).
79. M. Makri, C.G. Vayenas, S. Bebelis, K.H. Besocke, and C. Cavalca, Atomic Resolution Scanning Tunneling Microscopy Imaging of Pt Electrodes Intefaced with β''-Al_2O_3, *Ionics* **2**, 248-253 (1996).
80. K.J. Uram, L. Ng, and J.R.Yates Jr., Electrostatic effects between adsorbed species-The K-CO interaction on Ni(111) as studied by infrared reflection - absorption spectroscopy, *Surf. Sci.* **177**, 253-277 (1986).
81. A. Frantzis, and C.G. Vayenas, in preparation (2001).
82. C.T. Campbell, G. Ertl, H. Kuipers, and J. Segner, A molecular beam study of the adsorption and desorption of oxygen from a Pt(111) surface, *Surf. Sci.* **107**, 220-236 (1981).
83. G. Pacchioni, F. Illas, S. Neophytides, and C.G. Vayenas, Quantum-Chemical Study of Electrochemical Promotion in Catalysis, *J. Phys. Chem.* **100**, 16653-16661 (1996).
84. G. Pacchioni, J.R. Lomas, and F. Illas, Electric field effects in heterogeneous catalysis, *Molecular Catalysis A: Chemical* **119**, 263-273 (1997).
85. J. Xue, and R. Dieckmann. Oxygen partial pressure dependence of the oxygen content of zirconia-based electrolytes in *Ionic and Mixed Conducting Ceramics Second International Symposium* **94-12**, 191-208 (1994) ES Meeting San Francisco, California.

CHAPTER 6

RULES AND MODELING OF PROMOTION

"The notions of the electronic theory of catalysis developed in the 1950s by the Russian school of Wolkenstein and Roginskii, and revived by Vayenas..... should also be reexamined in an attempt to couple the collective properties of catalysts to the nature and structure of active surface species "
B. Grzybowska-Swierkosz and J. Haber, Annual Reports on Chemistry, 1994[1]

6.1 ELECTRON ACCEPTOR AND ELECTRON DONOR ADSORBATES

The chemisorptive bond is a chemical bond. The nature of this bond can be covalent or can have a strong ionic character. The formation of the chemisorptive bond in general involves either donation of electrons from the adsorbate to the metal (donation) or donation of electrons from the metal to the adsorbate (backdonation).[2] In the former case the adsorbate is termed electron donor, in the latter case it is termed electron acceptor.[3] In many cases both donation and backdonation of electrons is involved in chemisorptive bond formation and the adsorbate behaves both as an electron acceptor and as an electron donor. A typical example is the chemisorption of CO on transition metals where, according to the model first described by Blyholder,[4] the chemisorptive bond formation involves both donation of electrons from the π orbitals of CO to the metal and backdonation of electrons from the metal to the antibonding π^* orbitals of CO.

In all cases the adsorbate forms a dipole with the metal. The adsorbate is overall neutral as it is always accompanied by its compensating (screening) charge in the metal.[5-7] Thus the presence of an adsorbate on a metal surface will affect, in general, the work function of the surface.[5]

Electron acceptor adsorbates, such as atomic oxygen, increase in general

the work function of the substrate. The dipole formed by the chemisorbed oxygen atom has its negative end pointing to the vacuum. This implies an additional difficulty in the extraction of electrons from the metal, thus an increase in Φ.

Electron donor adsorbates, such as atomic H or alkalis or olefins, decrease in general the work function of the substrate. The dipole formed by the adsorbate has its positive end pointing to the vacuum. This facilitates electron extraction from the metal, thus decreases Φ.

In both cases the variation of work function with the coverage θ_j of an adsorbate, j, is described by the Helmholz equation[7,8]:

$$\Delta\Phi = \frac{eN_M}{\varepsilon_o}\Delta(P_j\theta_j) \tag{5.16}$$

where N_M is the surface metal atom concentration (atom/m^2), $e=1.6\cdot10^{-19}$ C, $\varepsilon_o=8.85\cdot10^{-12}$ C^2/Jm and P_j is the (average) dipole moment of the adsorbate j in Cm. Dipole moments, P_j, are also frequently expressed in D (Debye) where $1D=3.36\cdot10^{-30}$ Cm. As already noted P_j is taken in this book by convention negative for electropositive (electron donor) adsorbates, since the vector $\tilde{P}_j$ is pointing towards the surface, i.e. opposite to ñ and positive for electronegative (electron acceptor) adsorbates.

The electron acceptor or electron donor character of adsorbates plays a very important role in their catalytic properties. It also plays a crucial role in their electrochemical promotion behaviour. This is to be expected since electrochemical promotion is catalysis in presence of a controllable double layer which interacts strongly with the adsorbate dipoles.

The electron acceptor or electron donor character of an adsorbate, a good measure of which is its dipole moment P_j, can be easily determined in the

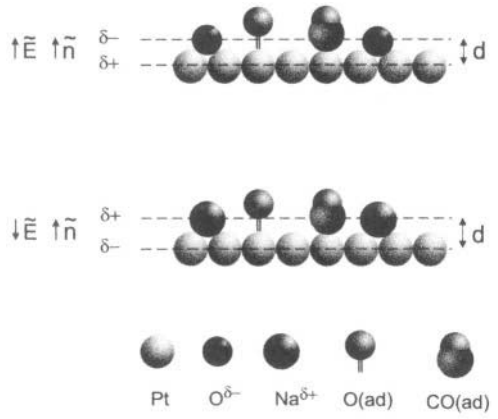

Figure 6.1. Effective double layer during CO oxidation on Pt/YSZ (top) and Pt/β″-Al_2O_3 (bottom).

experimental setup used for electrochemical promotion studies by just examining the effect of the adsorbate on U_{WR}. Electropositive (electron donor) adsorbates tend to decrease U_{WR} (thus Φ) while electronegative adsorbates cause an increase in U_{WR} and Φ.

As shown in Fig. 6.1 the effective double layer can be approximately described by two parameters[9]: The double layer thickness, d, and the field strength $\tilde{E}$. The latter equals $(d\varphi/dz)\tilde{n}$, where φ is the electrical potential in the double layer, z is the distance normal to the surface and $\tilde{n}$ is the unit vector normal to the surface. It is important to note that when the metal-gas interface is at its point of zero charge (pzc)[10] then $d\varphi/dz=0$. At this point it is also $\Phi=\Phi_{pzc}$, where Φ_{pzc} is the work function at the pzc. Defining $\Delta\Phi$ $(=\Phi-\Phi_{pzc})$ as the change in the surface work function induced by the presence of the double layer, it follows[9] that $d\varphi/dz=\Delta\Phi/ed$. Thus the field strength $\tilde{E}$ can be computed from $(\Delta\Phi/ed)\tilde{n}$ where $\Delta\Phi$ is the change in the surface work function induced by the presence of the effective double layer.

6.2 ELECTROPHOBIC, ELECTROPHILIC, VOLCANO AND INVERTED VOLCANO REACTIONS: RATIONALIZATION, RULES, AND PREDICTIONS

In sections 4.5.5 and 4.5.6 we have seen how the catalyst potential and work function affect the rates of catalytic reactions. We discussed in particular the r vs Φ dependence first at the local level (i.e. for small, e.g. 0.1-0.2 eV variations in eU_{WR} and Φ) and then at the global level (i.e. for eU_{WR} and Φ variations as wide as the experimentally available eU_{WR} range, typically 1.5-2 eV).

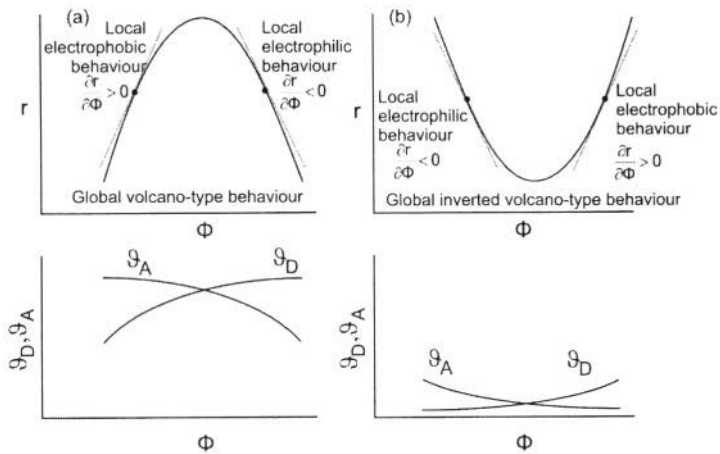

Figure 6.2. (Top) Definitions of local electrophobic and local electrophilic behaviour for two reactions exhibiting global volcano-type behaviour (a) and global inverted-volcano-type behaviour (b). (Bottom): Corresponding variations in surface coverages of adsorbed electron donor (D) and electron acceptor (A) reactants. As shown in this chapter volcano-type behaviour corresponds in general to high reactant coverages, inverted-volcano-type behaviour corresponds in general to low reactant coverages.

We saw that there are two types of *local* behaviour, i.e. electrophobic ($\partial r/\partial U_{WR}>0$) and electrophilic ($\partial r/\partial U_{WR} < 0$) (Fig. 6.2) and four main types of *global* r vs U_{WR}, or equivalently r vs Φ, behaviour (Fig. 6.3)[9,11] :

1. Purely electrophobic behaviour, i.e. $\partial r/\partial U_{WR} > 0$, $\partial r/\partial \Phi > 0$.
2. Purely electrophilic behaviour, i.e. $\partial r/\partial U_{WR} < 0$, $\partial r/\partial \Phi < 0$.
3. Volcano type behaviour, i.e. electrophobic behaviour followed by electrophilic one.
4. Inverted volcano (or V-type) behaviour, i.e. electrophilic behaviour followed by electrophobic one.

After the discovery of electrochemical promotion in the 1980's[12,13] it took only a short time[6] to find the means (i.e. Eq. (4.20)) for rationalizing and predicting the magnitude of the absolute value of Faradaic efficiency Λ, i.e. $|\Lambda|$. However, rationalization and prediction of the magnitude of ρ and of the four types of r vs Φ behaviour described above appeared at that time as a very distant goal. Today this goal has been achieved in a semi-quantitative manner on the basis of some rigorous and surprisingly simple rules.[9,11]

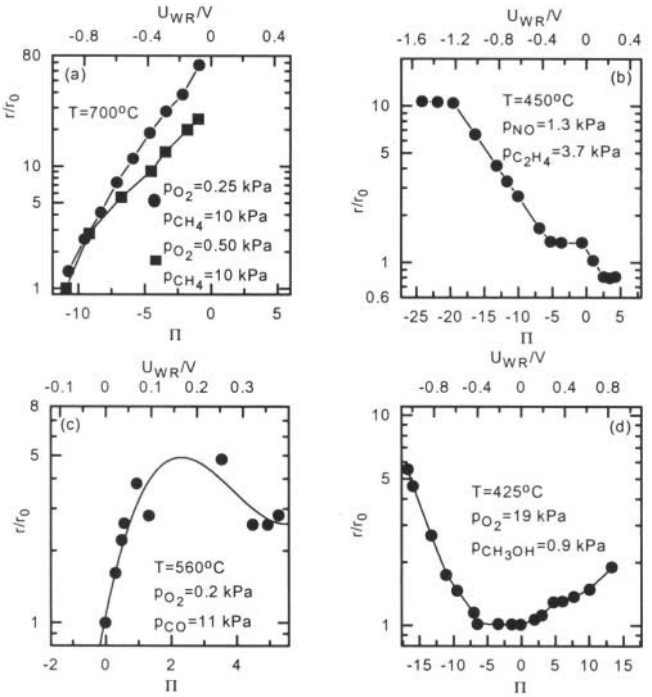

Figure 6.3. Examples for the four types of global electrochemical promotion behaviour: (a) electrophobic, (b) electrophilic, (c) volcano-type, (d) inverted volcano-type. (a) Effect of catalyst potential and work function change (vs I = 0) for high (20:1) and (40:1) CH_4 to O_2 feed ratios, Pt/YSZ[14] (b) Effect of catalyst potential on the rate enhancement ratio for the rate of NO reduction by C_2H_4 consumption on Pt/YSZ[15] (c) NEMCA generated volcano plots during CO oxidation on Pt/YSZ[16] (d) Effect of dimensionless catalyst potential on the rate constant of H_2CO formation, Pt/YSZ.[17] $\Pi=FU_{WR}/RT$ ($=\Delta\Phi/k_bT$).

These rules were gradually established on the basis of experimental observations on the plethora of electrochemical promotion studies outlined in Tables 4.1 to 4.3 of Chapter 4 and described in more detail in Chapters 8 to 10 of this book. They correspond to some 60 reactions, using a variety of metals and solid electrolytes. There is every reason to believe that these rules apply not only to electrochemical promotion but also to chemical promotion in general. There is already strong experimental evidence for this as discussed below.

6.2.1 Similarities and Differences Between Electrochemical and Classical Promotion

As already analysed in Chapter 5, once the backspillover species originating from the solid electrolyte have migrated at the metal/gas interface, then they act as normal (chemical) promoters for catalytic reactions. For example, Lambert and coworkers via elegant use of XPS[18] have shown that the state of sodium introduced via evaporation on a Pt surface interfaced with β''-Al_2O_3 is indistinguishable from $Na^{\delta+}$ introduced on the same Pt surface via negative (cathodic) potential application.

Thus the only real difference between electrochemical and classical promotion is that in the former case one can control in situ the amount of promoter on the catalyst surface. This implies that if the promoting species has a short lifetime (e.g. 10-10^3 s) on the catalyst surface (e.g. O^{2-} originating from YSZ)[7] it can still be used as a promoter since its coverage on the catalyst surface can be fixed by appropriate setting of the potential U_{WR}. *The difference between electrochemical and classical promotion is thus operational and not functional.*

Despite the functional identity of classical and electrochemical promotion, the usefulness of the latter is not to be deemphasized. For example, more than fifty electrochemical promotion studies utilizing YSZ or TiO_2 as the promoter donor on Pt, Rh, Pd, Ag, IrO_2, RuO_2, Au and Ni surfaces (ref. 7 and Chapter 8) have revealed the great importance of $O^{\delta-}$ (probably O^{2-}) as an extremely effective promoting species for most catalytic oxidations. This promoting species was hitherto unknown from classical (chemical) promotion studies since its controlled formation on a metal surface without using an O^{2-} conducting solid electrolyte is very difficult experimentally and, most importantly, because its lifetime, τ, on a metal catalyst surface under real oxidation reaction conditions at atmospheric pressure is typically 50-500 s,[7] i.e. too short for any realistic practical catalyst application unless it is continuously replenished on the catalyst surface, as is the case in electrochemical promotion (NEMCA) studies utilizing O^{2-} conductors.

Another important operational advantage of electrochemical promotion is the direct possibility of controlling *in situ* the coverage of the promoting species on the catalyst surface (via current, I, or potential, U_{WR}, control).

This allows for direct examination of the effect of promoter coverage and of Φ on the catalytic reaction kinetics. Such examples are shown in Figures 6.3[14-17] and 6.4[19-22] for the four main types of experimentally observed catalytic rate, r, vs work function, Φ, dependence, i.e.

1. Electrophobic $(\partial r/\partial\Phi)_{p_A,p_D} > 0$
2. Electrophilic $(\partial r/\partial\Phi)_{p_A,p_D} < 0$
3. Volcano-type (r exhibits a maximum with respect to Φ)
4. Inverted volcano-type (r exhibits a minimum with respect to Φ).

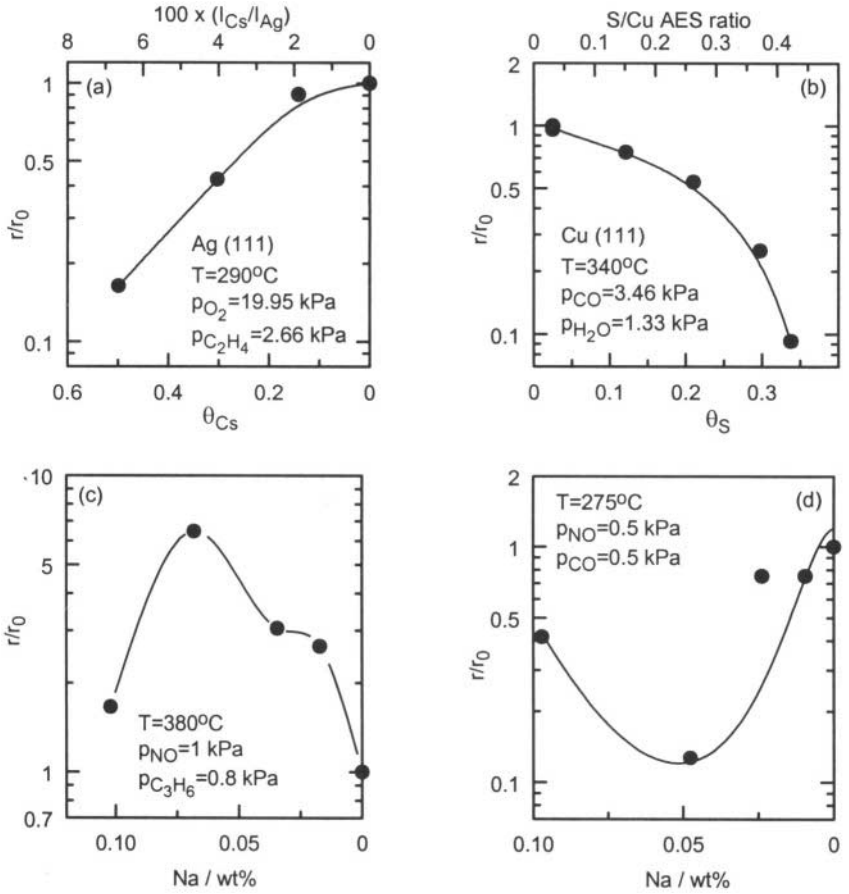

Figure 6.4. Examples for the four types of global classical promotion behaviour. Work function increases with the x-axis. (a) Steady-state (low conversion) rates of ethylene oxide (EtO) and CO_2 production from a mixture of 20 torr of ethylene and 150 torr of O_2 for various Cs predosed coverages on Ag(111) at 563 K[19] (b) Rate of water-gas shift reaction over Cu(111) as a function of sulphur coverage at 612 K, 26 Torr CO and 10 Torr H_2O[20] (c) Effect of sodium loading on NO reduction to N_2 by C_3H_6 on Pd supported on YSZ[21] at T=380°C (d) Effect of sodium loading on the rate of NO reduction by CO on Na-promoted 0.5 wt% Rh supported on TiO_2(4% WO_3).[22]

Thus although the rules presented here are applicable both for classical (Fig. 6.4) and electrochemical (Fig. 6.3) promotion, their extraction became possible only due to the systematic r vs Φ (as well as r vs p_A and r vs p_D at constant Φ) studies that electrochemical promotion enables one to perform efficiently and reversibly.

In Table 4.3 we had classified all published electrochemical promotion studies on the basis of the catalytic reaction and had provided the observed global r vs Φ behaviour together with the observed r vs p_D and r vs p_A open-circuit kinetic behaviour. We had then invited the reader to use Table 4.3 in order to derive the rules of promotion. As a further step we present here in Table 6.1 the same information given in Table 4.3 with only one difference: In Table 6.1 the 58 catalytic reactions are grouped in terms of their global r vs Φ behaviour.

6.2.2 Promotional Rules

The rules of electrochemical promotion follow directly from Table 6.1: For example, as shown in Table 6.1 all purely electrophobic reactions are positive order in D and zero or negative order in A. All purely electrophilic reactions are positive order in A and zero or negative order in D. Volcano-type reactions are always positive order in one reactant and purely negative order in the other. Inverted volcano-type reactions are positive order in both reactants.

Thus the following promotional rules can be formulated:

6.2.2.1 Electrophobic Reactions:

Inspection of Table 6.1 shows the following rule for electrophobic reactions:

Rule G1: A reaction exhibits purely electrophobic behaviour ($(\partial r/\partial\Phi)_{p_A,p_D} > 0$) *when the kinetics are positive order in the electron donor (D) reactant and negative or zero order in the electron acceptor (A) reactant.*

Table 6.1 provides 21 such examples. There appear to be no exceptions. Some typical examples from the literature[23-25] are shown in Figures 6.5 and 6.6.

An equivalent formulation of rule G1 is the following:

Rule G1': A reaction exhibits purely electrophobic behaviour ($(\partial r/\partial\Phi)_{p_A,p_D} > 0$) *when the electron acceptor reactant (A) is strongly adsorbed and much more strongly adsorbed on the catalyst surface than the electron donor reactant (D).*

In the context of Langmuir-Hinshelwood type kinetics the latter can be expressed as:

$$k_A p_A >> 1 \text{ and } k_A p_A >> k_D p_D \quad \Rightarrow \quad (\partial r/\partial\Phi)_{p_A,p_D} > 0 \qquad (6.1)$$

where k_A, k_D are the adsorption equilibrium constants of A and D on the catalyst surface. The dependence of k_A, k_D on work function Φ is discussed in section 6.4.

Table 6.1. Classification of Electrochemical Promotion studies on the basis of global r vs. Φ behaviour.

A. Purely electrophobic reactions

Reactants (D)	(A)	Catalyst	Solid Electrolyte	p_A/p_D	T (°C)	Kinetics in D $\partial r/\partial p_D)_\Phi$	Kinetics in A $\partial r/\partial p_A)_\Phi$	Rule	Ref
C_2H_4	O_2	Pt	$ZrO_2(Y_2O_3)$	12-16	260-450	+	0	G1	13,23,26
C_2H_4	O_2	Pt	β''-Al_2O_3	238	180-300	+	0	G1	7,27
C_2H_4	O_2	Pt	TiO_2	3.5-12	450-600	+	0	G1	28
C_2H_4	O_2	Rh	$ZrO_2(Y_2O_3)$	0.05-2.6	250-400	+	0	G1	29-31
C_2H_4	O_2	Pd	$ZrO_2(Y_2O_3)$	0.2-10	290-360	+	≤0	G1	32
C_2H_4	O_2	Ag	$ZrO_2(Y_2O_3)$	0.2-1.1	320-470	+	0	G1	12,33-35
C_2H_4	O_2	IrO_2	$ZrO_2(Y_2O_3)$	300	350-400	+	0	G1	36,37
C_2H_4	O_2	RuO_2	$ZrO_2(Y_2O_3)$	155	240-500	+	≤0	G1	38
CO	O_2	Pt	CaF_2	11-17	500-700	+	0	G1	7,39
CO	O_2	Pd	$ZrO_2(Y_2O_3)$	500	400-550	?	?	?	7,40
CH_4	O_2	Pd	$ZrO_2(Y_2O_3)$	0.2-4.8	380-440	+	0	G1	32,41
C_3H_6	O_2	Ag	$ZrO_2(Y_2O_3)$	20-120	320-420	+	≤0	G1	7,42
CH_4	O_2	Ag	$ZrO_2(Y_2O_3)$	0.02-2	650-850	+	0	G1	7,43
C_6H_6	H_2	Pt	β''-Al_2O_3	0.02-0.12	100-150	≥0	~0	G1	24,25
C_2H_2	H_2	Pt	β''-Al_2O_3	1.7-9	100-300	?	?	?	44
H_2	CO_2	Rh	$ZrO_2(Y_2O_3)$	0.03-0.7	300-450	+	0	G1	7
H_2	C_2H_2, C_2H_4	Pd	β''-Al_2O_3	0.1-5.9[#]	70-100	≥0	0	G1	45
H_2S	-	Pt	$ZrO_2(Y_2O_3)$	---	600-750	?		?	*7,46*
CH_4	-	Ag	$SrCe_{0.95}Yb_{0.05}O_3$	---	750	?		?	7,47
NH_3	-	Fe	$CaZr_{0.9}In_{0.1}O_{3-\alpha}$	4-12kPa	530-600	+		G1	*48*
NH_3	-	Fe	$K_2YZr(PO_4)_3$	4-12kPa	500-700	+		G1	*48*
CH_4	H_2O	Ni	$ZrO_2(Y_2O_3)$	0.05-3.5	600-900	+	≤0	G1	7,49

(#) $p_D = p_{C_2H_2} + p_{C_2H_4}$

B. Purely electrophilic reactions

Reactants (D)	(A)	Catalyst	Solid Electrolyte	p_A/p_D	T (°C)	Kinetics in D $\partial r/\partial p_D)_\Phi$	Kinetics in A $\partial r/\partial p_A)_\Phi$	Rule	Ref
C_2H_4	O_2	Pt	$CaZr_{0.9}In_{0.1}O_{3-a}$	4.8	385-470	-	+	G2	50
C_2H_4	O_2	Pt	CeO_2	1.6-3.7	500	-	+	G2	51
C_2H_4	O_2	Pt	YZTi10	3	400-475	?	?	?	52
C_2H_4	O_2	Ag	β''-Al_2O_3	0.3-0.4	240-280	-	+	G2	53
CO	O_2	Ag	β''-Al_2O_3	0.1-10	360-420	0	+	G2	7
C_3H_6	O_2	Pt	$ZrO_2(Y_2O_3)$	0.9-55	350-480	≤0	+	G2	7,54
CH_3OH	O_2	Ag	$ZrO_2(Y_2O_3)$	0-2	500	?	+	G2	55
CH_4	O_2	Au	$ZrO_2(Y_2O_3)$	0.1-0.7	700-750	0	+	G2	56-58
H_2	N_2	Fe	$CaZr_{0.9}In_{0.1}O_{3-\alpha}$	0-3	440	?	?	?	59
H_2	C_2H_4	Ni	$CsHSO_4$	1	150-170	?	?	?	7,60
	CH_3OH	Pt	$ZrO_2(Y_2O_3)$	---	400-500		?	?	7,17
	CH_3OH	Ag	$ZrO_2(Y_2O_3)$	0-6 kPa	550-750		+	G2	7,61
C_2H_4	NO	Pt	$ZrO_2(Y_2O_3)$	0.2-10	380-500	0	+	G2	15

C_2H_4	NO	Pt	β''-Al_2O_3	0.1-1.1	280-400	?	?	?	18
CO	NO	Pt	β''-Al_2O_3	0.3-5	320-400	≤0	+	G2	62-64
CO	NO	Pd	$ZrO_2(Y_2O_3)$	0.5-6.5	320-480	~0	+	G2	65,66
CO	N_2O	Pd	$ZrO_2(Y_2O_3)$	2-50	440	-	+	G2	65
	1-C_4H_8	Pd	Nafion	---	70		?	G2	67

C. Volcano type reactions

Reactants (D)	(A)	Catalyst	Solid Electrolyte	p_A/p_D	T (°C)	Kinetics in D $\partial r/\partial p_D)_\Phi$	Kinetics in A $\partial r/\partial p_A)_\Phi$	Rule	Ref
C_2H_4	O_2	Pt	$Na_3Zr_2Si_2PO_{12}$	1.3-3.8	430	-	+	G3	68
CO	O_2	Pt	$ZrO_2(Y_2O_3)$	0.2-55	468-558	+	-	G3	7,69, 70
CO	O_2	Pt	β''-Al_2O_3	0.5-20	300-450	-	+	G3	7,71
H_2	O_2	Pt	H_2O-0.1N KOH	0.3-3	25-50	+	-	G3	7,72, 73
H_2	O_2	Pt	Nafion	0.2-5	25	+	-	G3	74
SO_2	O_2	Pt	V_2O_5-$K_2S_2O_7$	1.8	350-450	?	?	?	75
C_3H_6	NO	Pt	β''-Al_2O_3	2-70	375	-	+	G3	63,64, 76
H_2	NO	Pt	β''-Al_2O_3	0.3-6	360-400	-	+	G3	77

D. Inverted Volcano reactions

Reactants (D)	(A)	Catalyst	Solid Electrolyte	p_A/p_D	T (°C)	Kinetics in D $\partial r/\partial p_D)_\Phi$	Kinetics in A $\partial r/\partial p_A)_\Phi$	*Rule*	Ref
C_2H_4	O_2	Pt	TiO_2	0.2-0.3#	450-600	+	+	G4	28
C_3H_6	O_2	Pt	YZTi10	5	400-500	?	?	?	52
CO	O_2	Ag	$ZrO_2(Y_2O_3)$	0.6-14	350-450	+	+	G4	7,78
CO	O_2	Ag-Pd alloy	$ZrO_2(Y_2O_3)$	3.5-12.5	450-500	+	+	G4	79
CO	O_2	Au	$ZrO_2(Y_2O_3)$	3-53	450-600	+	≥0	G4	56,57
C_2H_6	O_2	Pt	$ZrO_2(Y_2O_3)$	0.06-7	270-500	+	+	G4	80
CH_4	O_2	Pt	$ZrO_2(Y_2O_3)$	0.02-7	600-750	+	+	G4	7,14
CH_3OH	O_2	Pt	$ZrO_2(Y_2O_3)$	3-45	300-500	+	?	?	7,17
H_2	CO_2	Pd	$ZrO_2(Y_2O_3)$	0.2-1.1	500-590	+	+	G4	7,40
C_3H_6	NO,O_2	Rh	$ZrO_2(Y_2O_3)$	0.08-8$	250-450	+	*NO:* + *O_2:* 0	G4	81
CO	NO,O_2	Rh	$ZrO_2(Y_2O_3)$	0.33$	250-450	+	*NO:* + *O_2:* 0	G4	82

($) : p_A/p_D is the ratio $p_{NO}/p_{C_3H_6}$ and p_{NO}/p_{CO}. The p_{O_2} range is between 0 – 6 kPa., (#) : low p_A, p_D region, (?) : *No data available.*

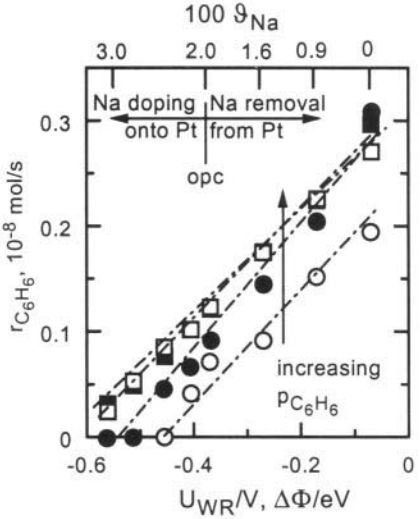

Figure 6.5. Example of rule G1 (electrophobic behaviour): Effect of Na coverage and concomitant work function change on the rate of C_6H_6 hydrogenation on Pt deposited on β″-Al_2O_3 at 130°C. Note that the rate is positive order in C_6H_6 (D). It is also near zero order in H_2.[24,25]

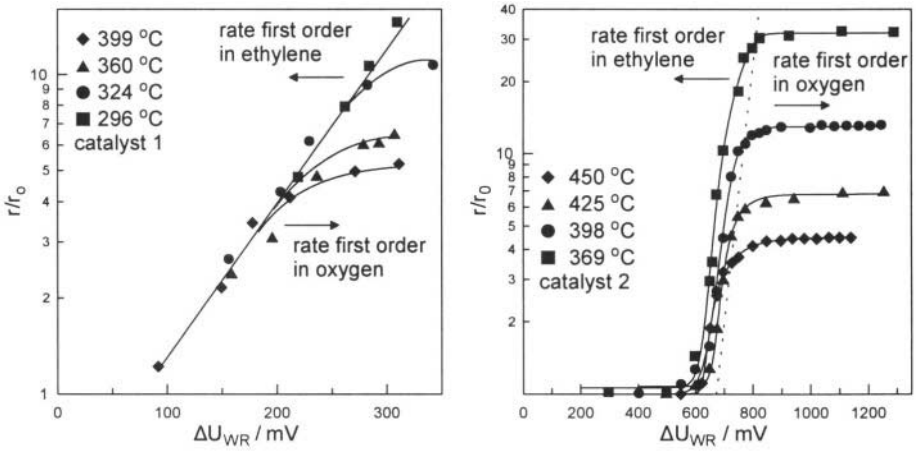

Figure 6.6. Example of rule G1 (electrophobic behaviour): Effect of ΔU_{WR} and $\Delta\Phi$ on the rate of C_2H_4 oxidation on Pt deposited on YSZ.[23] Electrophobic behaviour is obtained only when the rate is first order in C_2H_4.[23] The r vs Φ dependence traces the r vs $p_{C_2H_4}$(=p_D) dependence. Reprinted with permission from Academic Press.

6.2.2.2 Electrophilic Reactions:

Inspection of Table 6.1 shows the following rule for electrophilic reactions:

Rule G2: A reaction exhibits purely electrophilic behaviour $((\partial r/\partial\Phi)_{p_A,p_D} < 0)$ *when the kinetics are positive order in the electron acceptor (A) reactant and negative or zero order in the electron donor (D) reactant.*

Table 6.1 provides 18 such examples and no exceptions. Some typical examples from the electrochemical promotion literature[50] are shown in Figure 6.7.

An equivalent formulation of rule G2 is the following:

Rule G2': A reaction exhibits purely electrophilic behaviour $((\partial r/\partial\Phi)_{p_A,p_D} < 0)$ *when the electron donor reactant (D) is strongly adsorbed and much more strongly adsorbed on the catalyst surface than the electron acceptor reactant (A).*

In the context of Langmuir-Hinshelwood type kinetics the latter can be expressed as:

$$1 \ll k_D p_D \text{ and } k_A p_A \ll k_D p_D \quad \Rightarrow \quad (\partial r/\partial\Phi)_{p_A,p_D} < 0 \qquad (6.2)$$

6.2.2.3 Volcano-Type Reactions

Inspection of Table 6.1 shows that reactions exhibiting volcano-type (maximum type) behaviour with respect to Φ are those where the kinetics also exhibit a maximum with respect to A and D so that the rate is always positive order in A or D and at the same time negative (not zero) order in D or A respectively.

Thus the following rule is derived:

Rule G3: A reaction exhibits volcano-type behaviour when both the electron donor D and electron acceptor A are strongly adsorbed on the catalyst surface.

Table 6.1 provides 8 such examples and no exceptions. Some typical examples from the literature[72,73] are shown in Figure 6.8.

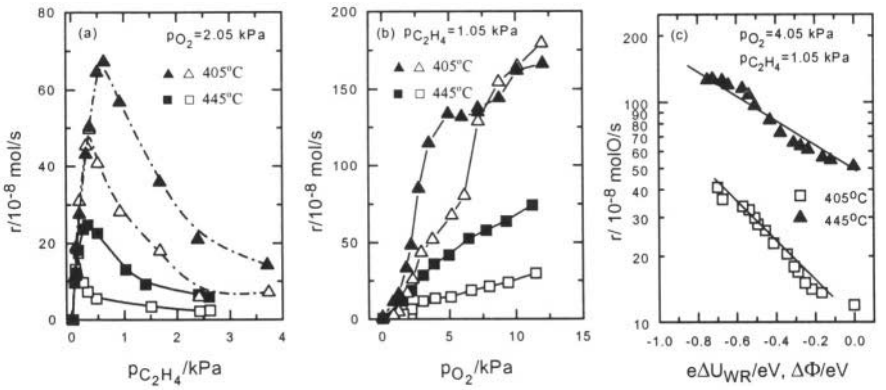

Figure 6.7. Example of rule G2 (electrophilic behaviour): Effect of $p_{C_2H_4}$(=p_D) (a), p_{O_2} (=p_A) (b) and $\Delta\Phi$ (c) on the rate of C_2H_4 oxidation on Pt films interfaced with $CaZr_{0.9}In_{0.1}O_{3-\alpha}$, a H^+-conductor.[50] Note that Fig. 6.7c is obtained under gaseous composition where the rate is positive order in O_2 and negative order in C_2H_4 (Figs. 6.7a, 6.7b). Reprinted with permission from the Institute for Ionics.

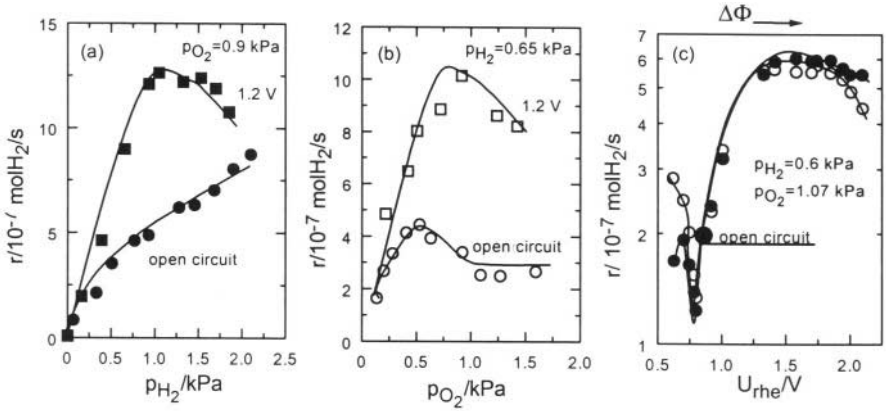

Figure 6.8. Example of rule G3 (volcano-type behaviour): Effect of p_{H_2}(=p_D) (a), p_{O_2} (=p_A) (b) and of potential U_{WR} and $\Delta\Phi$ (c) on the rate of H_2 oxidation on Pt /graphite (a and b) and Pt/black (c) in aqueous 0.1 M KOH solutions.[72,73] Note that under the p_{H_2}, p_{O_2} conditions of Fig. 6.7c the open-circuit rate is positive order in H_2 (Fig. 6.8a) and negative order in O_2 (Fig. 6.8b) and that the orders are reversed with the applied positive potential (U_{WR}=1.2 V). At this potential the rate passes through its maximum (volcano) value (Fig. 6.8c). Reprinted with permission from McMillan Magazines Ltd (ref. 72) and from the American Chemical Society (ref. 73).

In the context of Langmuir-Hinshelwood type kinetics, Rule G3 can be expressed as:

$$k_A p_A, k_D p_D >> 1 \Rightarrow \begin{cases} (\partial r/\partial\Phi)_{p_A,p_D} > 0; & \Phi < \Phi_M \\ (\partial r/\partial\Phi)_{p_A,p_D} = 0; & \Phi = \Phi_M \\ (\partial r/\partial\Phi)_{p_A,p_D} < 0; & \Phi > \Phi_M \end{cases} \tag{6.3}$$

where Φ_M is the work function value at the rate maximum (volcano-maximum).

6.2.2.4 Inverted Volcano (Minimum) Type Reactions

Inspection of Table 6.1 shows the following rule for inverted volcano type reactions:

Rule G4: A reaction exhibits inverted volcano (minimum rate) type behaviour when the kinetics are positive order in both the electron acceptor (A) and electron donor (D) reactant.

Table 6.1 provides 11 such examples and no exceptions. Some typical examples from the literature[78] are shown in Figure 6.9.

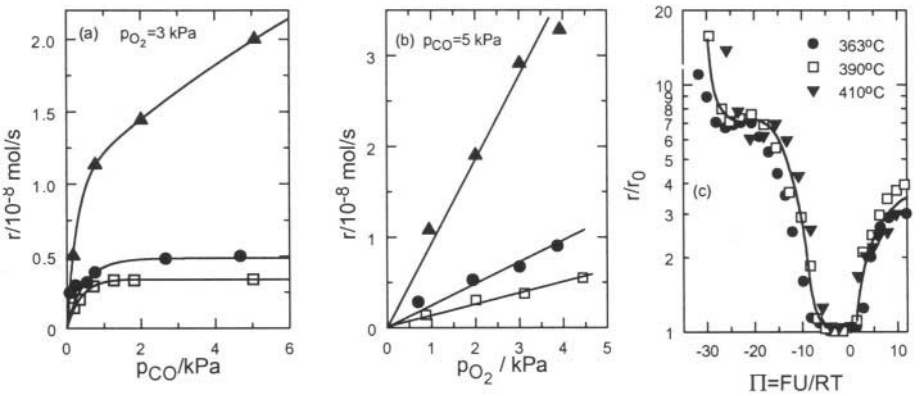

Figure 6.9. Example of rule G4 (inverted volcano-type behaviour): Effect of p_{CO} (=p_D) (a), p_{O_2}(=p_A) (b) and $\Delta\Phi$ and dimensionless work function $\Pi(=\Delta\Phi/k_bT)$ (c) on the rate of CO oxidation on Ag films deposited on YSZ;[6,78] T=415°C. (a): p_{O_2}= 3 kPa, □: open-circuit, ●: U_{WR}=475 mV, ▲:U_{WR}=-1300 mV. (b): p_{CO}= 5 kPa, □: open-circuit, ●: U_{WR}=475 mV, ▲:U_{WR}=-1300 mV. (c): p_{O_2}= 3 kPa, p_{CO}= 5 kPa, ●: T=363°C, r_0=2.7 nmol O/s, □: T=390°C, r_0=3.4 nmol O/s, ▼: T=410°C, r_0=5.5 nmol O/s. Reprinted with permission from Elsevier Science (ref. 6) and Trans. Tech. Publications (ref. 78).

In the context of Langmuir-Hinshelwood type kinetics, Rule G4 can be expressed as:

$$k_A p_A, k_D p_D << 1 \Rightarrow \begin{cases} (\partial r/\partial\Phi)_{p_A,p_D} < 0; & \Phi < \Phi_m \\ (\partial r/\partial\Phi)_{p_A,p_D} = 0; & \Phi = \Phi_m \\ (\partial r/\partial\Phi)_{p_A,p_D} > 0; & \Phi > \Phi_m \end{cases} \tag{6.4}$$

where Φ_m is the work function value at the rate minimum.

Three additional rules, also derived from experiment can be formulated:

Rule G5: The above rules G1-G4 apply also when D and A are both electron acceptors or electron donors. In this case D is always the stronger electron donor or weaker electron acceptor and A is always the weaker electron donor or stronger electron acceptor.

Rule G6: A monomolecular reaction is electrophobic for an electron donor adsorbate and electrophilic for an electron acceptor adsorbate.

Rule G7: The maximum rate modification (ρ_{max}/ρ_{min}) *obtained under electrochemical promotion conditions increases for every fixed overpotential with increasing difference in the electron acceptor-electron donor character of the two reactants.*

On the basis of the published literature on NEMCA or Electrochemical promotion up to now (2001) *there appear to be no exceptions to the above local and global rules.*

This is shown in Table 6.1.

These rules are not limited to electrochemical promotion only. To the best of our knowledge they are also in good qualitative agreement with the results of classical chemical promotion (electropositive or electronegative promoters) on the rates of catalytic reactions. Several examples are shown in this chapter.

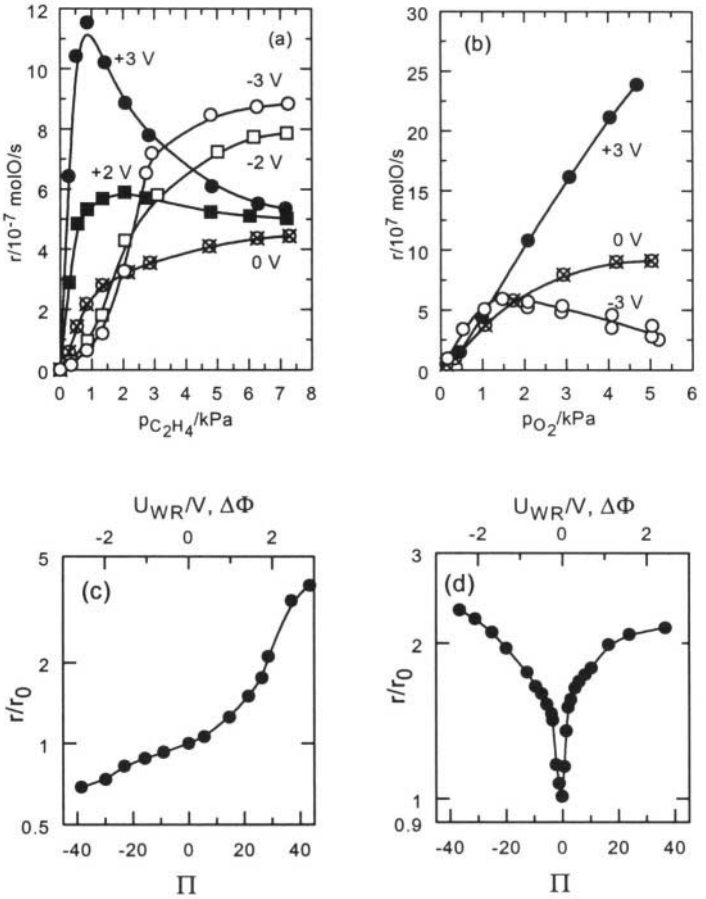

Figure 6.10. Example of rules G1 and G4: Effect of $p_{C_2H_4}$ (=p_D) (a), p_{O_2}(=p_A) (b) and $\Delta\Phi$ and Π(=$e\Delta U_{WR}/k_bT$) (c) and (d) on the rate of C_2H_4 oxidation on Pt films deposited on TiO_2.[28] Numbers (V) refer to ΔU_{WR} which is a factor of 10 larger than $\Delta\Phi$.[28] (a) : p_{O_2}= 1.45 kPa, ● : +3 V, ■ : +2V, ⊗ : open-circuit, □ : -2 V, ○ : -3V. (b) : p_{CO} = 3 kPa, ● : +3 V, ⊗ : open-circuit, ○ : -3V. (c): $p_{C_2H_4}$=0.6 kPa, p_{O_2}= 1.45 kPa, rule G1. (d): $p_{C_2H_4}$=5.6 kPa, p_{O_2}= 1.45 kPa, rule G4. Reprinted with permission from Academic Press.

6.2.2.5 More Complex Examples

The excellent agreement between the above rules and the classical and electrochemical promotion literature can also be appreciated from Figures 6.10 to 6.13 which show some more complex examples which nevertheless can be fully described by the above rules:

Figure 6.10 refers to C_2H_4 oxidation on Pt/TiO_2.[28] The kinetics change dramatically with potential (Figs. 6.10a and 6.10b). For high potential U_{WR} and thus Φ values the rate is positive order in O_2 (A) and negative order in C_2H_4 (D). For low Φ values the rate is positive order in C_2H_4 (D) and even becomes negative order in O_2(A) for high p_{O2} values (Fig. 6.10b). But in all cases the above rules G1 to G4 apply. For example for low $p_{O_2}(=p_A)$ to $p_{C_2H_4}(=p_D)$ ratios (e.g. p_{O_2}=1.45 kPa, $p_{C_2H_4}$=5.6 kPa) the open-circuit rate is positive order both in A and in D (Figs, 6.10a, 6.10b), thus inverted volcano behaviour is obtained, according to rule G4, (Fig. 6.10c, right). For high $p_{O_2}(=p_A)$ to $p_{C_2H_4}(=p_D)$ ratios (e.g. p_{O_2}=1.45 kPa, $p_{C_2H_4}$=0.6 kPa) the open-circuit rate becomes near zero order in O_2 (=A) and positive order in C_2H_4(=D) (Fig. 6.10a, 6.10b), thus purely electrophobic behaviour is obtained (rule G1, Fig. 6.10c left).

Figure 6.11 comes from the classical promotion literature and refers to CO oxidation on Pt(111) promoted with Li.[83] As with every alkali promoter,

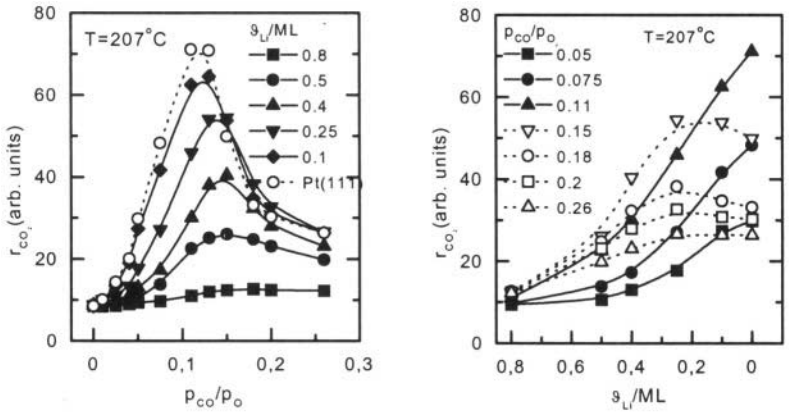

Figure 6.11. Effect of p_{CO}/p_{O_2} ratio at fixed Li coverage (left) and of Li coverage at fixed p_{CO}/p_{O_2} ratio (right) on the rate of CO oxidation on Pt(111).[83] Reprinted with permission from Elsevier Science.

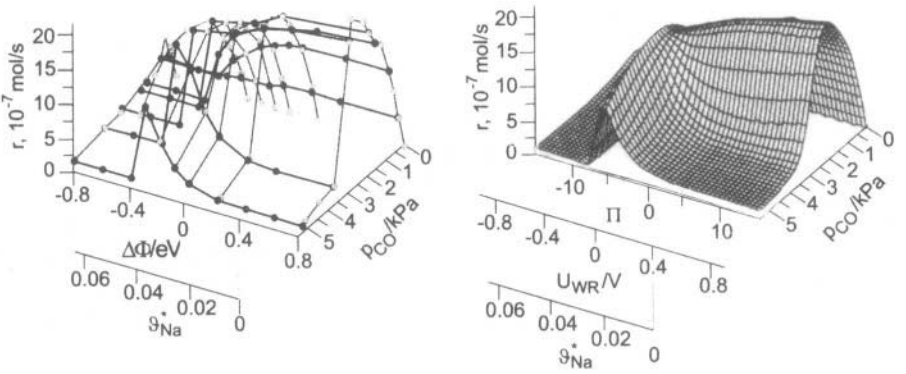

Figure 6.12. Example of rules G1, G2 and G3: Effect of p_{CO} (=p_D) and of Na coverage and corresponding U_{WR} and $\Delta\Phi$ values on the rate of CO oxidation on Pt films deposited on β″-Al_2O_3 at fixed p_{O_2}=6 kPa [71] Note that $\partial r/\partial\Phi$(= $\partial r/e\partial U_{WR}$) always traces $\partial r/\partial p_{CO}$ for negative, positive and zero (volcano peak) values. In the right figure the raw data (left) have been fitted to a polynomial expression.[71] Reprinted with permission from Academic Press.

decreasing Li content on the catalyst surface corresponds to increasing Φ.[83] Here O_2 is the electron acceptor (A) and CO plays the role of the electron donor (D). For low p_{CO}/p_{O_2} (=p_D/p_A) ratios where the rate is positive order in CO the rate is dramatically enhanced with increasing Φ, i.e. with decreasing Li coverage (Fig. 6.11 left, rule G1). For high p_{CO}/p_{O_2} ratios, where the rate is negative order in CO, electrophilic behaviour is observed for low Li coverages (Fig. 6.11, rule G2).

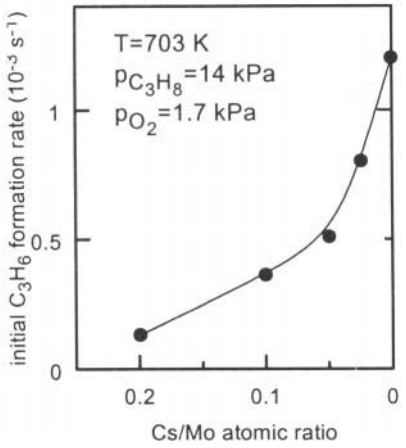

Figure 6.13. Dependence of initial propene formation rate on Cs:Mo atomic ratio for Cs-Mo/Zr catalyst samples (703K, 14 kPa, C_3H_8, 1.7 kPa O_2, balance He).[84] Reprinted with permission from Academic Press.

The behaviour is qualitatively similar for CO oxidation on Pt deposited on β''-Al_2O_3, a Na^+ conductor and promoter donor,[71] as shown in Fig. 6.12 which comes from the electrochemical promotion literature.[71] Here when the rate is negative order in CO (=D) electrophilic behaviour ($\partial r/\partial\Phi<0$) is obtained (Fig. 6.12, rule G2). When the rate is positive order in CO a weak electrophobic behaviour is observed (Fig. 6.12, rule G1). Note that the rate exhibits volcano-type behaviour both with respect to Φ and to p_{CO} (Rule G3). The present rules enable one to model mathematically the data of Fig. 6.12 in a semiquantitive manner as shown in the next section.

Another, and simpler, manifestation of rule G1 coming from the classical promotion literature is shown in Fig. 6.13. The rate of the oxidative dehydrogenation of C_3H_8 to C_3H_6 is first order in propane and near zero order in O_2.[84] As expected from rule G1 the reaction exhibits electrophobic behaviour.

6.2.3 Connection Between Φ and Adsorbate Coverage:

As already discussed (see e.g. Fig. 6.12) the work function Φ is directly related to the coverage, θ_i, of the promoting ion via the Helmholtz equation[7,8]:

$$\Delta\Phi = \frac{eN_M}{\varepsilon_0} P_i \Delta\theta_i \tag{6.5}$$

where e is the unit electron charge ($1.6\cdot10^{-19}$ C/atom), N_M is the surface atom density of the catalyst surface (atom/m^2), $\varepsilon_0=8.85\cdot10^{-12}$ C^2/J·m and P_i (C·m) is the dipole moment of the promoting species i. Typically P_i is of the order of 1-5 D (1 D (Debye) $=3.36\cdot10^{-30}$ C·m).

In general P_i is coverage-dependent and also the Helmholtz equation has to be written in its general form:

$$\Delta\Phi = \frac{eN_M}{\varepsilon_0} \sum_j P_j \Delta\theta_j \tag{6.6}$$

where the summation extends over all adsorbed reactants, intermediates and promoters (j=i). This is because when the coverage, θ_i, of a promoting species, i, is varied in an electrochemical (or classical) promotion experiment, it is reasonable to expect that the coverages of coadsorbed reactants, $\theta_{j\neq i}$, will also change. Since, however, the dipole moment, P_i, of electropositive ($P_i<0$) or electronegative ($P_i>0$) promoters, such as $Na^{\delta+}$ or O^{2-}, is typically a factor of five larger than the dipole moments of more covalently adsorbed reactants and intermediates,[7,8] experiment has shown that equation (6.5) rather than its more general form (6.6) can be used to a good approximation.

This enables one to formulate the above promotional rules G1 to G4 (eqs. 6.1 to 6.4) also in terms of promoter coverage by simply replacing $\partial\Phi$ by $\partial\theta_i$ (for electronegative promoters i) and by $-\partial\theta_i$ (for electropositive promoters i).

6.2.4 Local Promotional Rules

When examining the rate dependence on Φ at any fixed work function Φ value, two possibilities exist:

$$(\partial r/\partial\Phi)_{p_A,p_D} > 0 \text{ (electrophobic behaviour)} \tag{6.7}$$

$$(\partial r/\partial\Phi)_{p_A,p_D} < 0 \text{ (electrophilic behaviour)} \tag{6.8}$$

On the basis of the above global promotional rules the following two very simple local (L) rules can be directly derived:

Rule L1: When the electron acceptor reactant (A) is more strongly adsorbed than the electron donor reactant (D) then the reaction exhibits local electrophobic behaviour.

Mathematically this is expressed as:

$$k_A p_A >> k_D p_D \Rightarrow (\partial r/\partial\Phi)_{p_A,p_D} > 0 \tag{6.9}$$

Rule L2: When the electron acceptor reactant (A) is more weakly adsorbed than the electron donor reactant (D) then the reaction exhibits local electrophilic behaviour.

Mathematically this is expressed as:

$$k_A p_A << k_D p_D \Rightarrow (\partial r/\partial\Phi)_{p_A,p_D} < 0 \tag{6.10}$$

The local rules L1 and L2 can also be expressed in the following equivalent way:

Rule L1': When the rate is negative or zero order in the electron acceptor A and positive order in the electron donor D then the reaction exhibits electrophobic behaviour.

Rule L2': When the rate is positive order in the electron acceptor A and negative or zero order in the electron donor D then the reaction exhibits electrophilic behaviour.

Rules L1 and L2 (or L1′ and L2′) are exemplified in Table 6.1 and all Figures 6.3 to 6.8 and 6.10 to 6.12.

It is also clear that the global promotional rules G1 to G3 stem directly from rules L1 and L2, so that if rules L1 and L2 can be rationalized at the

molecular level, then rules G1 to G3 can also be rationalized.

Before proceeding with this rationalization at the molecular level we first present a direct mathematical consequence of rules L1′ and L2′:

$$\left(\frac{\partial r}{\partial \Phi}\right)_{p_A,p_D}\left(\frac{\partial r}{\partial p_D}\right)_{\Phi,p_A} > 0 \tag{6.11}$$

$$\left(\frac{\partial r}{\partial \Phi}\right)_{p_A,p_D}\left(\frac{\partial r}{\partial p_A}\right)_{\Phi,p_D} < 0 \tag{6.12}$$

These surprisingly simple inequalities contain mathematically not only the local rules L1 and L2 but also the global rules G1 to G3. This is also clear from Table 6.1 and from all figures 6.5 to 6.12. Deviations from inequalities (6.11) and (6.12) exist only in the case of weak adsorption of both D and A (rule G4) in which case both $(\partial r/\partial p_D)$ and $(\partial r/\partial p_A)$ are positive. In this case they are simply replaced by:

$$(\Phi - \Phi_m)\left(\frac{\partial r}{\partial \Phi}\right)_{p_A,p_D} > 0 \tag{6.13}$$

which is rule G4, (Fig. 6.9) and has been discussed and derived from first principles recently.[9,11]

Inequality 6.11 dictates that (unless both A and D are very weakly adsorbed, rule G4) *the r vs Φ dependence always follows (has the same sign with) the r vs p_D behaviour.*

This again can be confirmed from Table 6.1 and all Figures 6.3 to 6.8 as well as from the more complex ones Figures 6.9 to 6.12 which show the transition from one global behaviour to another as p_A and p_D are varied. Note, for example in Figure 6.12 that *when a reaction exhibits a maximum in the* r vs p_D $(=p_{CO})$ *behaviour, it also exhibits a maximum (volcano) in the r vs Φ behaviour.*

One might righteously ask why this close and preferential connection exists between the r vs Φ and the r vs p_D dependencies. The answer is straightforward and has simply to do with the definitions of Φ and Fermi level E_F (or electrochemical potential of electrons $\bar{\mu}$ $(=E_F)$)[7] which are connected via:

$$-\bar{\mu} = \Phi + e\Psi \tag{5.14}$$

where Ψ is the outer (or Volta) potential of the catalyst surface. For an overall neutral catalyst surface (as is usually the case, e.g. when it is covered by the effective double layer, Fig. 6.1) it is $\Psi = 0$[85-87] and thus:

$$-\bar{\mu} = \Phi \;;\; -E_F = \Phi \tag{6.14}$$

Consequently the generalized promotional rules (6.11) and (6.12) can also be written as:

$$\left(\frac{\partial r}{\partial E_F}\right)_{p_A,p_D}\left(\frac{\partial r}{\partial p_D}\right)_{E_F,p_A} < 0 \tag{6.15}$$

$$\left(\frac{\partial r}{\partial E_F}\right)_{p_A,p_D}\left(\frac{\partial r}{\partial p_A}\right)_{E_F,p_D} > 0 \tag{6.16}$$

$$(E_F - E_{F,m})\left(\frac{\partial r}{\partial E_F}\right)_{p_A,p_D} > 0 \tag{6.17}$$

and now one sees from Eqs. (6.15) and (6.16) that the r vs E_F dependence follows the r vs p_A (electron acceptor) dependence. So $(\partial r/\partial \Phi)$ traces $(\partial r/\partial p_D)$, Eq. (6.11), and $(\partial r/\partial E_F)$ traces $(\partial r/\partial p_A)$, eq. (6.16).

6.2.5 Practical Considerations

The above global and local promotional rules suggest, in a straightforward manner, the following three practical rules for promoter selection with respect to rate maximization[9,11]:

Rule P1: If a catalyst surface is predominantly covered by an electron acceptor adsorbate, then an electron acceptor (electronegative) promoter is to be recommended.

Rule P2: If a catalyst surface is predominantly covered by an electron donor adsorbate, then an electron donor (electropositive) promoter is to be recommended.

Rule P3: If a catalyst surface has very low coverages of both electron acceptor and electron donor adsorbates then both an electron acceptor and electron donor promoter will enhance the rate.

Needless to remind that the above practical promotional rules are applicable for modest (e.g. <0.2) coverages of the promoting species so that site-blocking by the promoter does not become the dominant factor limiting the catalytic rate.

6.3 RATIONALIZATION OF THE PROMOTIONAL RULES

Electrochemical promotion studies have used from the beginning[5-7] two very simple qualitative rules in order to explain all the observed effects of varying potential U_{WR} or work function Φ on the reaction kinetics:

F1. Increasing work function Φ (e.g. via addition of electronegative promoters) strengthens the chemisorptive bond of electron donor adsorbates (D) and weakens the chemisorptive bond of electron acceptor adsorbates (A).

F2. Decreasing work function Φ (e.g. via addition of electropositive promoters) weakens the chemisorptive bond of electron donor adsorbates (D) and strengthens the chemisorptive bond of electron acceptor adsorbates (A).

These two complementary rules are intuitively obvious, e.g. can be simply derived by considering the lateral attractive and repulsive interactions of coadsorbed reactants and promoters as already shown in section 4.5.9.2. They can explain all the observed promotionally induced kinetics for more than sixty different catalytic systems (Table 6.1). As an example these two rules can explain all the observed changes in kinetics orders with Φ shown in Figures 6.8, 6.9, 6.10, 6.11 and 6.12 in a straightforward manner.

We are not aware of any exceptions to these rules even in cases where they lead at a first glance to surprising predictions e.g. that addition of O^{2-} on a Rh surface destabilizes formation of surface Rh_2O_3[29] or that anodic ($\Delta U_{WR}>0$) polarization of Pt both on solid electrolyte surfaces[7] and in aqueous media[72,73] weakens the Pt=O chemisorptive bond and leads to massive O_2 desorption[88] or that alkali addition on transition metal surfaces enhances O chemisorption and thus promotes hydrocarbon oxidation under fuel-rich conditions.[53,71] All these predictions have been confirmed experimentally[7,29,53,71-73,88] and, for many cases, also theoretically via rigorous quantum-mechanical calculations using metal clusters.[89,90]

It therefore becomes important to discuss:

How the "fundamental" rules F1 and F2 lead to the experimentally observed promotional rules L1, L2 and G1 to G4.

How the "fundamental" rules F1 and F2 follow from fundamental first principles.

6.3.1 Derivation of the experimental local rules L1 and L2 from the fundamental rules F1 and F2

The two "fundamental" rules F1 and F2 can be expressed mathematically as:

$$\left(\frac{\partial\theta_D}{\partial\Phi}\right)_{p_A,p_D} \geq 0 \qquad (6.18)$$

$$\left(\frac{\partial\theta_A}{\partial\Phi}\right)_{pA,pD} \leq 0 \tag{6.19}$$

As shown recently[11] these two "fundamental" rules lead directly mathematically to the experimental rules L1 and L2 (Eqs. 6.11, 6.12 and, for low coverages, to rule G4, eq. 6.13). Henceforth the global rules G1 to G4 are all derived on the basis of the "fundamental" rules F1 and F2.

6.3.2 Experimental Confirmation and First Principle Rationalization of Rules F1 and F2:

The variation in the enthalpy of adsorption of electron acceptor (e.g. O), electron donor (e.g. C_2H_4) and amphoteric (e.g. H, CO) adsorbates with varying promoter coverage and thus work function Φ has been studied experimentally using mostly the technique of temperature programmed desorption (TPD) both for classical[91] and for electrochemical[88,89,92] promotion. As already discussed in Chapter 2 (Figs. 2.6, 2.15 and 2.22) and also in Chapter 5 (Fig. 5.26) it is always found that electropositive promoters increase the binding energy of electron acceptor adsorbates and decrease the binding energy of electron donor adsorbates. Conversely, electronegative adsorbates decrease the binding energy of electron acceptor adsorbates and increase the binding energy of electron donor adsorbates.

As already shown in Figures 2.6, 2.15, 2.22 and 5.26 very often it is found that the binding energy, $E_{b,j}$, or enthalpy of adsorption, ΔH_j, is related linearly to the change in work function Φ:

$$\Delta|\Delta H_j| \approx \alpha_{H,j} \cdot \Delta\Phi \tag{6.20}$$

where the parameter $\alpha_{H,j}$ ($|\alpha_{H,j}| \approx 0.2\text{-}1$) is positive for electropositive (electron donor) adsorbates and negative for electronegative (electron acceptor) adsorbates. This correlation is similar in form to that proposed by Boudart many years ago,[93] has a firm electrostatic (section 4.5.9.2) and quantum mechanical[89,90] basis and as shown in Figures 2.6, 2.15, 2.22 and 5.26 provides an excellent description for the adsorption of alkalis on Ru(00l),[94] CO on alkali (Na, K, Cs) – modified $Ru(10\bar{1}0)$,[95,96] H on alkali modified Ni(111)[97] and O on polycrystalline Pt, Ag and Au surface interfaced with YSZ and modified by O^{2-}.[88,89,92] We do not imply that equation (6.20) is a general fundamental equation, although, as shown in Chapter 5 the ab initio quantum mechanical calculations of Pacchioni and Illas[89,90] are in excellent agreement with it and although it can be rigorously derived on the basis of a simple electrostatic model which accounts only for through-the-vacuum adsorbate interactions as shown in section 4.5.9.2, which also provides a simple physical meaning to the parameter $\alpha_{H,j}$ on the basis of the dipole moment P_j of adsorbate j.

Although we do not wish to imply that equation (6.20) is a general fundamental equation, we are also not aware of any published exceptions to the physical meaning it conveys, i.e. that the enthalpy of adsorption and thus, according to any isotherm, the coverage of an electron acceptor/donor adsorbate decreases/ increases with increasing work function Φ and thus decreasing Fermi level E_F.

As shown in Figures 2.6, 2.15 and 5.25 the experimental $\alpha_{H,i}$ values are ~0.2 for alkalis on Ru(001), ~ -0.2 for CO on Na-modified $Ru(10\bar{1}0)$ (here CO behaves as an electron acceptor as is very often the case[7]), -1 for O on Pt and Ag and –4 for O on Au. These values imply dipole moment, P_j, values on the order of 1-5 D, in good agreement with the literature as also discussed in section 4.5.9.2.

Equation (6.20) and the semiquantitative trends it conveys, can be rationalized not only on the basis of lateral coadsorbate interactions (section 4.5.9.2) and rigorous quantum mechanical calculations on clusters[89] (which have shown that 80% of the repulsive O^{2-} - O interaction is indeed an electrostatic (Stark) through-the-vacuum interaction) but also by considering the band structure of a transition metal (Fig. 6.14) and the changes induced by varying Φ (or E_F) on the chemisorption of a molecule such as CO which exhibits both electron acceptor and electron donor characteristics. This example has been adapted from some rigorous recent quantum mechanical calculations of Koper and van Santen.[98]

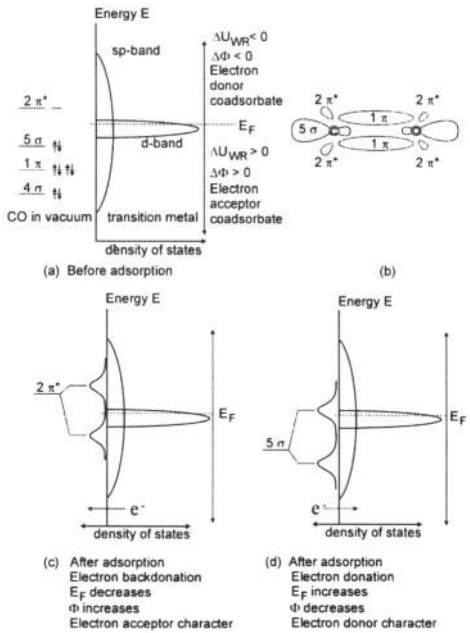

Figure 6.14. CO chemisorption on a transition metal. Molecular orbitals and density of states before (a,b) and after (c and d) adsorption. Effect of varying Φ and E_F on electron backdonation (c) and donation (d). Based on Fig. 4 of ref. 98. See text for discussion. Reprinted with permission from Elsevier Science.

Figure 6.14a shows the sp and d bands of a transition metal (e.g. Pt), i.e. the density of states (DOS) as a function of electron energy E. It also shows the outer orbital energy levels of a gaseous CO molecule. Orbitals 4σ, 1π and 5σ are occupied, as indicated by the arrows, orbital $2\pi^*$ is empty. The geometry of these molecular orbitals is shown in Figure 6.14b.

Figures 6.14c and 6.14d show the energy and density of states of the resonances (adsorbed molecular orbitals) formed upon CO adsorption due to the interaction of the $2\pi^*$ orbitals (Fig. 6.14c) and 5σ orbitals (Fig. 6.14d) with the metal surface. As Koper and van Santen, who have performed these intriguing calculations,[98] point out, these resonances are rather broad due to the influence of the broad sp-band.

Figure 6.14c shows the electron backdonation interaction (electrons are transferred from the Fermi level of the metal to the hybridized $2\pi^*$ molecular orbital which was originally empty, thus this is, by definition, a backdonation interaction).

Figure 6.14d shows the electron donation interaction (electrons are transferred from the initially fully occupied 5σ molecular orbitals to the Fermi level of the metal, thus this is an electron donation interaction). Blyholder was first to discuss that CO chemisorption on transition metal involves both donation and backdonation of electrons.[4] We now know both experimentally[7] and theoretically[96,98] that the electron backdonation mechanism is usually predominant, so that CO behaves on most transition metal surfaces as an overall electron acceptor.

Electrochemical or classical promotion enables one to vary the Fermi level E_F of a metal and thus to also vary Φ (Fig. 6.14). It is clear from Fig. 6.14c that lowering the work function Φ (or equivalently increasing the Fermi level E_F) enhances electron backdonation to the $2\pi^*$ orbitals and diminishes electron donation from the 5σ orbitals (which were originally fully occupied). The enhanced backdonation of electrons to the $2\pi^*$ orbitals results to a significant strengthening of the Pt=CO bond,[98] in qualitative agreement with Eq. (6.20), which eventually, i.e. for strongly negative $\Delta\Phi$ values, leads to CO disproportionation due to the concomitant weakening in the C=O bond.[4,98]

6.3.3 Summary of Promotional Rules

Tables 6.2 to 6.9 summarize all local (Table 6.2), global (Tables 6.3 to 6.7), fundamental (Table 6.8) and practical (Table 6.9) promotional rules. Tables 6.6 and 6.7 provide some obvious extensions to monomolecular reactions, also in good agreement with experiment. All the rules can be summarized by the inequalities 6.11, 6.12 and 6.13:

$$\left(\frac{\partial r}{\partial \Phi}\right)_{p_A,p_D}\left(\frac{\partial r}{\partial p_D}\right)_{\Phi,p_A}>0\,;\left(\frac{\partial r}{\partial \Phi}\right)_{p_A,p_D}\left(\frac{\partial r}{\partial p_A}\right)_{\Phi,p_D}<0\,;(\Phi-\Phi_m)\left(\frac{\partial r}{\partial \Phi}\right)_{p_A,p_D}>0$$

Table 6.2. **Local Electrochemical Promotion Rules (Langmuir-Hinshelwood mechanisms)**

TYPE OF REACTION	D + A → products			
Donicity of reactants	D: Electron donor $\partial\Phi/\partial\theta_D<0$		A: Electron acceptor $\partial\Phi/\partial\theta_A>0$	
Kinetics	Rate positive order in D $\partial r/\partial p_D>0$	Rate negative order in A $\partial r/\partial p_A<0$	Rate negative order in D $\partial r/\partial p_D<0$	Rate positive order in A $\partial r/\partial p_A>0$
Predicted NEMCA behaviour	RULE L1 **Electrophobic behaviour** $\partial r/\partial\Phi>0$, $\Lambda>1$		RULE L2 **Electrophilic behaviour** $\partial r/\partial\Phi<0$, $\Lambda<-1$	

Table 6.3. **Global Electrochemical Promotion Rules – Rules G1 & G2**

TYPE OF REACTION	D + A → products			
Donicity of reactants	D: Electron donor $\partial\Phi/\partial\theta_D<0$		A: Electron acceptor $\partial\Phi/\partial\theta_A>0$	
Open-circuit kinetics and strength of adsorption	Rate positive order in D $\partial r/\partial p_D>0$	Rate zeroth or negative order in A $\partial r/\partial p_A\leq 0$	Rate zeroth or negative order in D $\partial r/\partial p_D\leq 0$	Rate positive order in A $\partial r/\partial p_A>0$
	D strongly adsorbed A weakly adsorbed $k_Dp_D \ll k_Ap_A$ & $1 \ll k_Ap_A$		D weakly adsorbed A strongly adsorbed $k_Dp_D \gg k_Ap_A$ & $k_Dp_D \gg 1$	
Predicted NEMCA behaviour	**Purely electrophobic behaviour** $\partial r/\partial\Phi > 0$		**Purely electrophilic behaviour** $\partial r/\partial\Phi < 0$	

Table 6.4. **Global Electrochemical Promotion Rules - Rule G3**

TYPE OF REACTION	D + A → products			
Donicity of reactants	Electron donor $\partial\Phi/\partial\theta_D<0$		Electron acceptor $\partial\Phi/\partial\theta_A>0$	
Open-circuit kinetics and strength of adsorption	Strong adsorption Rate positive order in D $\partial r/\partial p_D>0$	Strong adsorption Rate negative order in A $\partial r/\partial p_A\leq 0$	Strong adsorption Rate negative order in D $\partial r/\partial p_D<0$	Strong adsorption Rate positive order in A $\partial r/\partial p_A>0$
	D and A strongly adsorbed			
	$k_Ap_A > k_Dp_D > 1$		$k_Dp_D > k_Ap_A > 1$	
Predicted NEMCA behaviour	**Volcano type behaviour**			

Table 6.5. **Global Electrochemical Promotion Rules - Rule G4**

TYPE OF REACTION	D + A → products	
Donicity of Reactants	Electron donor $\partial\Phi/\partial\theta_D<0$	Electron acceptor $\partial\Phi/\partial\theta_A>0$
Open-circuit kinetics and strength of adsorption	Weak adsorption Rate positive order in D $\partial r/\partial p_D>0$	Weak adsorption Rate positive order in A $\partial r/\partial p_A>0$
Predicted NEMCA behaviour	**Inverted Volcano type behaviour**	

Table 6.6. **Global Electrochemical Promotion Rules - Rules G6**

TYPE OF REACTION	D → products A → products	
Donicity of Reactants	D: Electron donor $\partial\Phi/\partial\theta_D<0$	A: Electron acceptor $\partial\Phi/\partial\theta_A>0$
Open-circuit kinetics and strength of adsorption	Rate positive order in D $\partial r/\partial p_D>0$	Rate positive order in A $\partial r/\partial p_A>0$
Predicted NEMCA behaviour	**Purely electrophobic behaviour**	**Purely electrophilic behaviour**

Table 6.7. **Fundamental rules F1 and F2**

$$\left(\frac{\partial\theta_D}{\partial\Phi}\right)_{p_A,p_D} \geq 0$$

$$\left(\frac{\partial\theta_A}{\partial\Phi}\right)_{p_A,p_D} \leq 0$$

Table 6.8. **Practical rules**

P1: $\theta_A \rightarrow 1 \Rightarrow$ Electronegative promoter recommended

P2: $\theta_D \rightarrow 1 \Rightarrow$ Electropositive promoter recommended

P3: $\theta_A,\theta_D << 1 \Rightarrow$ Electropositive or electronegative promoter recommended

6.4 MATHEMATICAL MODELLING OF ELECTROCHEMICAL PROMOTION AND CLASSICAL PROMOTION

6.4.1 Introduction

In the previous section it was shown that the global electrochemical promotion rules G1 to G7 cover not only all cases of electrochemical promotion studied up to date but also the general trends observed with classical chemical promotion.

In this section we will see how all these rules can be described mathematically by a single and simple kinetic model based on fundamental thermodynamic and catalytic principles.[99]

Such a model should be as simple as possible, without however missing any of the underlying thermodynamic and physicochemical factors which cause electrochemical promotion. In particular it will be shown that even the use of Langmuir-type adsorption isotherms, appropriately modified due to the application of potential (or equivalently by the presense of promoters) suffice to describe *all* the experimentally observed rules G1 to G7 as well as practically all other observations regarding electrochemical promotion including the effect of potential on heats of adsorption as well as on kinetics and reaction orders.

Thus for an arbitrary catalytic reaction:

$$D + A \rightarrow \text{products} \tag{6.21}$$

where D is an electron donor (e.g. C_2H_4 or H_2) and A is an electron acceptor (e.g. O_2) we develop a general rate expression

$$r = r(k_R, k_D, k_A, p_D, p_A, \Phi, T) \tag{6.22}$$

where k_R is the surface reaction rate constant between chemisorbed D and A and k_D and k_A are the adsorption equilibrium constants of D and A, respectively, which is able to describe:

a) The dependence of r on $\Phi(=eU_{WR})$ for fixed p_D and p_A (purely electrophobic, purely electrophilic, volcano, inverted volcano).
b) The dependence of r on p_D (or p_A) at fixed p_D (or p_A) and Φ (positive and negative order kinetics and transition between positive and negative order kinetics).

The problem posed by Eq. (6.22), without the additional complication of the Φ dependence, is a classical problem in heterogeneous catalysis. The usual approach it to use Langmuir isotherms to describe reactant (and sometimes product) adsorption. This leads to the well known Langmuir-Hinshelwood-Hougen-Watson (LHHW) kinetics.[3] The advantage of this approach is

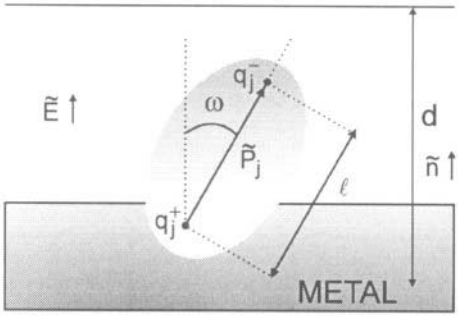

Figure 6.15. Schematic of an adsorbate, modeled as a dipole, in the presence of the metal/gas effective double layer.

mathematical simplicity, the weakness is inherent in the assumptions and limitations of the Langmuir isotherm. Thus LHHW kinetics usually provide only a qualitative and, in several instances, semiquantitative description of actual experimental kinetics. More realistic isotherms (Temkin, Freundlich, Guggenheim) lead to large numbers of adjustable parameters and mathematically intractable expressions.

Consequently the only realistic approach to the problem posed by Eq. (6.22) is a Langmuirian approach in which, however, one describes explicitly the dependence of k_R, k_D and k_A on catalyst potential U_{WR} or, equivalently, work function Φ.

6.4.2 Adsorption in Presence of a Double Layer

We consider the adsorption of a single molecule, j, on a metal film M. The film is deposited on a solid electrolyte, e.g. YSZ, or is partly covered by a promoter, or simply has a significant coverage of adsorbed reactants and products on its surface, so that we may consider (Chapter 5) that an *effective double layer* is present at the the metal-gas interface (Fig. 6.15).

The double layer is described by its effective thickness, d, and by its field strength $\tilde{E}$ (Fig. 6.15). The adsorbed molecule has a dipole moment $\tilde{P}$. It is well documented[100] that the local field strength $\tilde{E}$ can affect strongly not only the chemisorptive bond strength but also the preferred orientation of the adsorbate (Fig. 6.16).

In the case of electrochemically promoted (NEMCA) catalysts we concentrate on the adsorption on the gas-exposed electrode surface and not at the three-phase-boundaries (tpb). The "surface area," N_{tpb}, of the three-phase-boundaries is usually at least a factor of 100 smaller than the gas-exposed catalyst-electrode surface area N_G. Adsorption at the tpb plays an important role in the electrocatalysis at the tpb, which can affect indirectly the NEMCA behaviour of the electrode. But it contributes little directly to the measured catalytic rate and thus can be neglected. Its effect is built in U_{WR} and Φ.

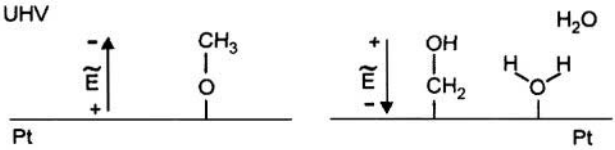

Figure 6.16. Different modes of adsorption of CH_3OH on Pt under ultra-high vacuum (left) and in aqueous solutions (right) showing the effect of local electrostatic field and surface work function on the mode of adsorption.[100] Reprinted with permission from the American Chemical Society.

We first assume Langmuir-type adsorption ($\tilde{E}=0$ or $\tilde{P}_j=0$) which implies negligible lateral interactions between adsorbed molecules and negligible inherent or induced heterogeneity of the catalyst-electrode surface:

$$k_j p_j = \theta_j/(1-\theta_j) \tag{6.23}$$

Equation (6.23) is obtained assuming equilibrium between gaseous and adsorbed species S_j:

$$S_j(g) \rightleftharpoons S_j(ad) \tag{6.24}$$

thus

$$\mu_j(g) = \mu_j(ad) \tag{6.25}$$

or equivalently:

$$\mu_j^o(g) + RT\ln p_j = \mu_j^o(ad) + RT\ln(\theta_j/(1-\theta_j)) \tag{6.26}$$

where the standard chemical potential, $\mu_j^o(ad)$, of adsorbed j corresponds to a standard state of $\theta_j = 0.5$. The Langmuir isotherm (6.23) is directly obtained from Eq. (6.26) with:

$$k_j = \exp((\mu_j^o(g) - \mu_j^o(ad))/RT) \tag{6.27}$$

The larger the value of k_j, the stronger is the adsorption of j on the catalyst-electrode surface. More generally the Langmuir isotherm (6.23) can be written as:

$$k_j a_j = \theta_j/(1-\theta_j) \tag{6.28}$$

where a_j is the activity of j on the catalyst surface. The latter is defined using the gaseous j standard state:

$$\mu_j = \mu_j^o(g) + RT\ln a_j \tag{6.29}$$

It should be noted that within the context of the Langmuir isotherm (energetically equivalent adsorption sites, no lateral interactions) Eq. (6.28), which relates *two surface properties,* i.e. a_j and θ_j, remains valid even when the surface activity of S_j, a_j, is different from the gaseous activity, p_j, i.e. when $\mu_j(g) \neq \mu_j(ad)$.

We start by noting that the Langmuir isotherm approach does not take into account the electrostatic interaction between the dipole of the adsorbate and the field of the double layer. This interaction however is quite important as already shown in section 4.5.9.2. In order to account explicitly for this interaction one can write the adsorption equilibrium (Eq. 6.24) in the form:

$$S_j(g) \rightleftharpoons [S_j^{\lambda_j^+} - \lambda_j e^-] \tag{6.30}$$

where the partial charge transfer parameter λ_j is the net number of electrons donated by the adsorbate to the metal during chemisorptive bond formation (Fig. 6.15). The right hand side (rhs) of Eq. (6.30) represents the overall neutral dipole adsorbate formed on the catalyst surface and accounts explicitly for partial charge transfer between the adsorbate and the metal. The quantity λ_j is zero for a truly covalent chemisorptive bond, positive for an electron donor adsorbate and negative for an electron acceptor adsorbate.

The partial electron transfer parameter λ_j is directly related to the dipole moment, P_j, of adsorbed j via:

$$P_j = -q_j \ell /2 = -\lambda_j e \ell /2 \tag{6.31}$$

where ℓ is the distance between the centers of the positive and negative charges in the adsorbed dipole.

We then write the equilibrium condition for reaction (6.30):

$$\bar{\mu}_j(g) = \bar{\mu}_j(ad)\text{, i.e. } \mu_j(g) = \bar{\mu}_j(ad) \tag{6.32}$$

where now the use of the electrochemical potential $\bar{\mu}_j(ad)$ of the adsorbed species is necessary since the adsorbate dipole interacts electrostatically with its surroundings.

In view of the assumed lack of individual lateral adsorbate-adsorbate interactions the only electrostatic energy to be accounted for in expressing the electrochemical potential, $\bar{\mu}_j$, of the adsorbate is the electrostatic energy of interaction of the adsorbate dipole with the effective double layer field. This is accounted for by:

$$\bar{\mu}_j(ad) = \mu_j(ad) + \tilde{P}_j \cdot \tilde{E}\, N_{AV} \tag{6.33}$$

where $\tilde{P}_j$, here taken as a vector, is the adsorbate dipole, $\tilde{E}$ is the field strength and N_{AV} is Avogadro's number. Equation (6.33) shows that the electrochemical potential of an adsorbate is increased when its dipole moment is in the same orientation with the double layer field (dipole repulsion) and is decreased when it is in the opposite direction with the field (dipole attraction). As already noted $\tilde{E} = (\Delta\Phi/ed)\tilde{n}$ and thus in view of equation (6.31) one can rewrite Equation (6.33) in the form:

$$\bar{\mu}_{j,ad} = \mu_{j(ad)} - \lambda_j \frac{\ell}{2d} \cos\omega \Delta\Phi \, N_{AV} \tag{6.34}$$

where ω is the angle formed between the adsorbate dipole and the field (Fig. 6.15).

Equation 6.34 expresses the fact that the electrochemical potential of an electron donor ($\lambda_j>0$) is lowered with anodic ($U_{WR}>0$) potential or with increasing work function ($\Delta\Phi>0$). This favours adsorption. Similarly for an electron acceptor adsorbate ($\lambda_j<0$) anodic potential ($U_{WR}>0$) or increasing work function ($\Delta\Phi>0$) increases the electrochemical potential of the adsorbate. This hinders adsorption.

Upon combining Eqs. (6.32) and (6.33) one obtains:

$$\mu_j^o(g) + RT\ln p_j = \mu_j^o(ad) + RT\ln(\theta_j/(1-\theta_j)) - \lambda_j \frac{\ell}{2d} \cos\omega \Delta\Phi \, N_{AV} \tag{6.35}$$

The above equation reduces to the one used to derive the Langmuir isotherm (Eq. 6.26) when $\lambda_j=0$ or $\Delta\Phi=0$.

Upon rearranging one obtains:

$$k_j p_j = (\theta_j/(1-\theta_j))\exp(-\lambda_j \Pi) \tag{6.36}$$

with

$$\Pi = \Delta\Phi\left(\frac{\ell}{2d}\cos\omega\right)/k_b T \tag{6.37}$$

$$k_j = \exp((\mu_j^o(g) - \mu_j^o(ad))/RT) \tag{6.38}$$

which is identical with Eq. (6.27) and thus the adsorption equilibrium constant k_j retains the same meaning as in the absence of an applied potential. The standard state of the adsorbed phase is always that corresponding to $\theta_j=0.5$ and $\Delta\Phi=0$. Equation (6.36) is formally identical with the electrochemical Langmuir isotherm.[101] Its dimensionless potential term, Π, however has a somehow different, surface science, meaning as it reflects the interaction between the adsorbate dipole moment and the effective double layer present on the catalyst surface. We can thus term it

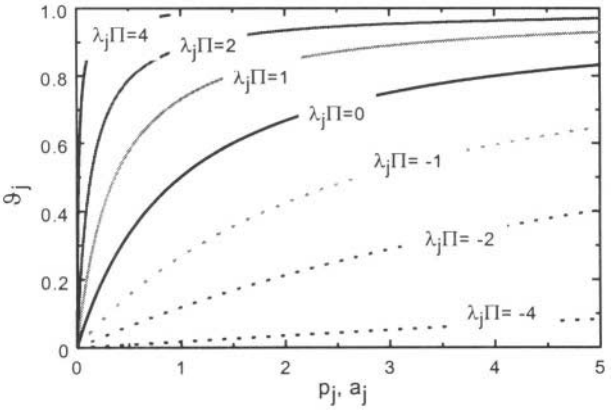

Figure 6.17. Effective double layer adsorption equilibrium isotherms for k_j=1 and various values of the parameter $\lambda_j\Pi$.

effective double layer (EDL) isotherm. Note that the EDL isotherm is mathematically very simple (like the electrochemical Langmuir isotherm) as long as Π and $\Delta\Phi$ (Eq. 6.37) can be treated as independently controllable variables (e.g. by fixing $\Delta\Phi$ via a promoter or via potentiostatic imposition of ΔU_{WR} in NEMCA systems). When this is not the case and $\Delta\Phi$, thus Π, is determined by θ_j, one obtains more complex, Frumkin type,[101] isotherms as we shall see in section 6.4.3.

Using equation (6.34) and the definition of the isosteric heat of adsorption $H_{ad}=T^2(\partial(\bar{\mu}_{j(ad)}/T)p_j,\theta_j$ one can show easily that the isosteric heat of adsorption, $\Delta H_{ad,j}$, is given by:

$$\Delta H_{ad,j} = \Delta H^{o}_{ad,j} + \lambda_j \frac{\ell}{2d} \cdot \Delta\Phi \tag{6.39}$$

where $\Delta H^{o}_{ad,j}$ is the heat of adsorption for $\Delta\Phi$=0. Also, if one assumes $\ell \approx d$:

$$\Delta H_{ad,j} \approx \Delta H^{o}_{ad,j} + (\lambda_j/2)\Delta\Phi \tag{6.40}$$

Thus for an electron acceptor adsorbate (λ_j<0) Eqs. 6.39 and 6.40 predict a linear decrease in ΔH_{ad} with increasing $\Delta\Phi$, while for electron donor adsorbates (λ_j>0) they predict a linear decrease in ΔH_{ad} with decreasing $\Delta\Phi$. Both predictions are in excellent agreement with experiment.

As shown in Figure 5.26 and also Figs. 2.6 and 2.15 there is excellent agreement between Eq. (6.40) and experiment. Equation 6.40 is also in excellent qualitative agreement with rigorous quantum mechanical calculations (Fig. 5.56). This provides solid support for the effective double layer isotherm (Eq. 6.36).

Figure 6.17 shows the isotherms resulting from Eq. (6.36) for various values of the dimensionless work function Π and of the partial electron transfer paramenter λ_j.

Equation (6.36) can be written in the form:

$$\theta_j/(1-\theta_j) = k_j p_j \exp(\lambda_j \Pi) \tag{6.41}$$

or equivalently:

$$\theta_j/(1-\theta_j) = k_j a_j \exp(\lambda_j \Pi) \tag{6.42}$$

thus figure 6.17 shows the isotherms resulting from equation (6.41) or (6.42) for various values of the papameter $\lambda_j\Pi$. It should be noted that $\lambda_j\Pi<0$ implies repulsive electrostatic interactions between the adsorbate j and the double layer while $\lambda_j\Pi>0$ corresponds to *attractive* interactions. Thus $\lambda_j\Pi<0$ causes a decrease in θ_j, for any fixed P_j (or λ_j) in relation to the value it would have in absence of the double layer (Π=0, Figure 6.17). The opposite hold for $\lambda_j\Pi>0$.

Conversely Figure 6.17 shows that when $\lambda_j\Pi<0$, then for any fixed θ_j one has an increase in p_j, or surface activity a_j, in relation to the p_j or a_j value corresponding to Π=0. In fact, denoting by p_j^o or a_j^o the activity of species j in absence of the double layer (Π=0), then one obtains from equations (6.41) or (6.42) *for any fixed θ_j:*

$$p_j = p_j^o \exp(-\lambda_j \Pi) \tag{6.43}$$

$$a_j = a_j^o \exp(-\lambda_j \Pi) \tag{6.44}$$

Thus for the case of O chemisorption ($\lambda_O<0$) equations (6.43) and (6.44) imply an increase in oxygen activity with increasing Π (or Φ or U_{WR}) for any fixed oxygen coverage. This is due to the increasing strength of repulsive lateral interactions between chemisorbed O and the double layer. If oxygen is chemisorbed on the metal surface as O^{2-} (λ_O=-2) then in view of $\Delta\Phi=e\Delta U_{WR}$ and provided ℓ =d, cosω=1 one obtains from equation (6.44)

$$a_O = a_O^o \exp(2e\Delta U_{WR}/k_bT) = a_O^o \exp(2F\Delta U_{WR}/RT) \tag{6.45}$$

and taking into account the dissociative oxygen chemisorption equilibrium condition ($a_O^2 = p_{O_2}$) one obtains:

$$p_{O_2} = p_{O_2}^o \exp(4e\Delta U_{WR}/k_bT) = p_{O_2}^o \exp(4F\Delta U_{WR}/RT) \tag{6.46}$$

$$a_{O_2} = a_{O_2}^o \exp(4e\Delta U_{WR}/k_bT) = a_{O_2}^o \exp(4F\Delta U_{WR}/RT) \tag{6.47}$$

which are the equations commonly used to describe the variation is surface oxygen activity on an electrode deposited on YSZ due to the application of an overpotential ΔU_{WR}. These equations are equivalent to:

$$\mu_{O_2}(ad) = \mu^{o}_{O_2}(ad) + 4F\Delta U_{WR} \tag{6.48}$$

where $\mu^{o}_{O_2}(ad)$ is the chemical potential of oxygen on the electrode in absence of an applied overpotential ΔU_{WR}. But it is worth noting that these equations, as well as equations (6.46) and (6.47) *are only valid for fixed coverage (any fixed coverage) of the adsorbate on the electrode surface.*

This point is important to remember for the following reason which is significant when modeling catalytic kinetics in presence of a double layer. When θ_j is not fixed, but instead a_j (or p_j) is fixed due to equilibrium with gaseous S_j (a_j=p_j) then for λ_j<0 (e.g. O chemisorption) upon *increasing* Π (or $\Delta\Phi$ or ΔU_{WR}) the surface coverage θ_j *decreases* (Fig. 6.17). This is perhaps at the beginning somehow not intuitively obvious (e.g. how an increase in catalyst-electrode potential causes a *decrease* in O coverage) but is in excellent agreement with all catalytic oxidation promotional kinetics, both electrochemical and classical, and of course, with the modified electrochemical Langmuir isotherm described by Eq. (6.36). The reason is the increasing electrochemical potential of electron acceptor adsorbates with increasing Φ or U_{WR} due to repulsive lateral interactions with the double layer (Eqs. 6.33 or 6.36).

Stricktly speaking the partial charge transfer parameter λ_j which appears in the modified electrochemical Langmuir isotherm (6.36) or (6.41) is not a constant but may vary with θ_j or Π. This because, in view of Eq. (6.31) λ_j is given by:

$$\lambda_j = -\frac{2P_j}{e\ell} \tag{6.49}$$

and both P_j and ℓ may be, to some extent, coverage dependent.

6.4.3 Adsorption in Absence of Coadsorbing Species

In the previous section we have assumed that $\Delta\Phi$, thus Π, is an independently controllable variable, such as p_j. This is true both in electrochemical promotion experiments, since $\Delta\Phi$=$e\Delta U_{WR}$ and in classical promotion experiments where $\Delta\Phi$ can largely controlled, albeit not in situ, by the amount of promoter species deposited on the catalyst surface.

We now examine what happens to the modified electrochemical Langmuir isotherm (Eq. 6.36) when $\Delta\Phi$ is created only by the presence of the adsorbate j, i.e. in absence of any coadsorbing ionic species. Substituting equation (6.49) into equation (6.36) and expressing $\Delta\Phi$ via the Helmholz equation (5.16) one obtains:

$$k_j p_j = (\theta_j/(1-\theta_j))\exp\left(\frac{N_M \cos\omega}{\varepsilon_o d k_b T} P_j^2 \theta_j\right) \tag{6.50}$$

which is a Frumkin or Fowler-Guggenheim type isotherm [101-106] and the exponential term accounts for the lateral repulsive interactions between the adsorbed j molecules.

More precisely, and accounting for the possible variation of P_j with θ_j, one can write equation (6.50) in the form:

$$k_j p_j = \theta_j/(1-\theta_j)\exp\left(\frac{N_M \cos\omega}{\varepsilon_o d k_b T} \int_0^{\theta_j} P_j^2(\theta_j) d\theta_j'\right) \tag{6.51}$$

To the extent that P_j may be assumed constant one can then show that the variation in the isosteric heat of adsorption $\Delta H_{ad,j}$, with coverage θ_j is given by:

$$\Delta H_{ad,j} = \Delta H^o_{ad,j} - \frac{N_M \cos\omega}{\varepsilon_o d} P_j^2 \theta_j \tag{6.52}$$

where $\Delta H^o_{ad,j}$ refers again to $\theta_j=0$, $\Delta\Phi=0$. As noted in Chapter 2 equation (6.52) is often found to be in good agreement with experiment.

In view of eqs. (6.51) and (6.52) one can now appreciate the advantages of the effective medium double layer approach used to derive Equation (6.36). Even with the simpler Frumkin or Fowler-Guggenheim approach (Eqs. 6.50 and 6.52), treating the coadsorption and surface reaction of different adsorbates leads immediately to mathematically intractable expressions and to the introduction of new parameters, whereas equation (6.36) leads to mathematical simple catalytic rate expressions, as will be shown in the next sections.

6.4.4 Adsorption Isotherms, Nernst Equation and Potential-Work Function Equivalence

Before presenting the catalytic promotional kinetics to which the modified electrochemical Langmuir or effective double layer isotherm (Eq. 6.36) leads, it is interesting to examine the following point which relates to the dual meaning of the potential U_{WR} of solid electrolyte cells. We consider a solid electrolyte which is a $j^{\pm}$-ion conductor (e.g. $j^{\pm}=O^{2-}$, Na^+) and two reversible, working and reference, metal electrodes made of the same material deposited on it. Let p_j and p_j' be the partial pressures or activities of species j (e.g. $j=O_2$, Na) in equilibrium with the working and reference electrode. The open-circuit potential, U^o_{WR}, of the cell is then given by the Nernst Equation:

$$eU_{WR}=\frac{k_bT}{n_j}\ln(p_j/p'_j) \tag{6.53}$$

where n_j is the number of electrons involved in the reduction/oxidation of $j^{\pm}$ to j. On the other hand the potential-work function equivalence of solid-state electrochemistry (Eq. 5.19) dictates:

$$eU_{WR} = \Phi(p_j) - \Phi(p'_j) \tag{6.54}$$

where $\Phi(p_j) - \Phi(p'_j)$ are the work function values of the working and reference electrode surfaces exposed to p_j and p'_j respectively.

Both equations are valid. The question is to find what type of adsorption isotherms for j are consistent with both equations (6.53) and (6.54).

Consistency with both equations implies that

$$\int_0^{\theta_j} P_j(\theta_j)d\theta'_j = \frac{\varepsilon_o k_b T}{n_j e N_M}\ln p_j + C(T) \tag{6.55}$$

where C(T) is a constant. With constant P_j equation (6.55) is the Temkin isotherm which is derived assuming a linear decrease in $\Delta H_{ad,j}$ with θ_j, which is consistent with Eq. (6.52), thus with the modified Fowler-Guggenheim isotherm and with the modified electrochemical Langmuir isotherm from which it was derived. More precisely the simultaneous validity of Eqs. (6.53) and (6.54) implies:

$$d\Phi(p_j)=\frac{k_bT}{n_j}d\ln p_j \tag{6.56}$$

thus, using the Helmholz equation:

$$P_j = \frac{\varepsilon_o k_b T}{n_j e N_M}\cdot\frac{d\ln p_j}{d\theta_j} \tag{6.57}$$

Differentiation of Eq. (6.50) and substitution into equation (6.57) with $\cos\omega=1$ leads to:

$$P_j=\frac{\varepsilon_o k_b T}{eN_M n_j}\left[\frac{1}{\theta_j}+\frac{1}{1-\theta_j}+\frac{N_M}{k_bTd\varepsilon_o}P_j^2\right] \tag{6.58}$$

which reduces to $P_j = en_jd$ for θ_j not near 0 or 1. Thus when P_j satisfies Eq. (6.58) then Eqs. (6.53) and (6.54) are satisfied simultaneously over the entire

P_j and θ_j range. Substitution of Eq. (6.57) into Eq. (6.58) gives the following isotherm:

$$k_j p_j = \theta_j/(1-\theta_j)\exp\left[\frac{\varepsilon_o k_b T\cos\omega}{n_j^2 e^2 N_M d}\int_0^{\theta_j}\left(\frac{d\ln p_j}{d\theta_j'}\right)^2 d\theta_j'\right] \tag{6.59}$$

This isotherm is consistent with the modified electrochemical Langmuir isotherm, the Nernst equation and the potential-work function equivalence. For intermediate θ_j and p_j values the isotherm of Eq. (6.58) is well approximated both by the Fowler-Guggenheim and by the Temkin isotherms.

6.4.5 Catalytic Kinetics in Presence of a Double Layer

So far we have established that the modified electrochemical Langmuir or effective double layer isotherm (Eq. 6.41)

$$\theta_j/(1-\theta_j) = k_j p_j \exp(\lambda_j \Pi) \tag{6.41}$$

is consistent with the main experimental finding regarding the effect of promotion on adsorption i.e. with the observed linear variation of heats of adsorption with $\Delta\Phi$ (Eq. 6.40)

$$\Delta H_{ad,j} = \Delta H^o_{ad,j} + (\lambda_j/2)\Delta\Phi \tag{6.40}$$

The crucial task remains of examining to what extent it can also describe the effect of promotion, electrochemical or classical, on catalytic reaction kinetics. More specifically we will examine to what extent it can predict the four main types of global r vs Φ dependence and all the associated local and global electrochemical and chemical promotional rules.

We thus consider an arbitrary catalytic reaction between an electron donor D ($\lambda_D>0$) and an electron acceptor A ($\lambda_A<0$):

$$D + A \rightarrow \text{products} \tag{6.21}$$

We also assume that adsorbed D and A are in equilibrium with gaseous D and A respectively ($\mu_D(g) = \mu_D(ad)$, $\mu_A(g) = \mu_A(ad)$) and that product adsorption is relatively weak and their desorption fast, so that the reaction between adsorbed D and A is rate limiting.

We start by noting that when D and A coadsorb, their adsorption isotherms are given by:

$$\theta_D/\theta_v = k_D p_D \exp(\lambda_D \Pi)\ ;\ \theta_D/\theta_v = k_A p_A \exp(\lambda_A \Pi) \tag{6.60}$$

where θ_v is the coverage of vacant sites on the catalyst surface. Adding these equations and noting that $\theta_A+\theta_R+\theta_v = 1$ one obtains:

$$(1-\theta_v)/\theta_v = k_D p_D \exp(\lambda_D \Pi) + k_A p_A \exp(\lambda_A \Pi) \tag{6.61}$$

therefore:

$$\theta_v = 1/(1+k_D p_D \exp(\lambda_D \Pi) + k_A p_A \exp(\lambda_A \Pi)) \tag{6.62}$$

combining with equation (6.60) one obtains:

$$\theta_D = \frac{k_D p_D \exp(\lambda_D \Pi)}{1 + k_D p_D \exp(\lambda_D \Pi) + k_A p_A \exp(\lambda_A \Pi)} \tag{6.63}$$

$$\theta_A = \frac{k_A p_A \exp(\lambda_A \Pi)}{1 + k_D p_D \exp(\lambda_D \Pi) + k_A p_A \exp(\lambda_A \Pi)} \tag{6.64}$$

$$r = k_R \theta_D \theta_A = \frac{k_R k_A p_D p_A \exp[(\lambda_D + \lambda_A)\Pi]}{(1 + k_D p_D \exp(\lambda_D \Pi) + k_A p_A \exp(\lambda_A \Pi))^2} \tag{6.65}$$

where the surface reaction rate constant k_R can in general be expressed as

$$k_R = k_R^o \exp(\lambda_R \Pi) \tag{6.66}$$

Metcalfe[107,108] has recently modeled electrochemical promotion using O^{2-} conductors and derived[108] equation (6.66) using transition state theory and the concept of a partially charged transition state.[108] Despite this interesting theoretical study,[108] which is consistent with the basic experimental electrochemical promotion observations Eqs. (4.49) and (4.50) little is still known, experimentally or theoretically about the parameter λ_R and its possible relationship to λ_D and λ_A. Consequently, and in order not to introduce adjustable parameters, we will set λ_R equal to zero in the subsequent analysis and will show[99] that it is possible to derive all local and global promotional rules in terms of only four parameters

a. The two adsorption coefficients k_D and k_A which quantify the chemisorptive bond strength of D and A at the point of zero charge of the double layer.

b. The two partial charge transfer parameters λ_D (>0) and λ_A (<0) which describe the electron donicity of the reactants. The values of λ_D and λ_A will

be considered fixed except for the case of very weak adsorption ($k_D p_D$, $k_A p_A < 10^{-2}$) where λ_D and λ_A are assumed to vanish in the Π range of repulsive interactions ($\Pi<0$ and $\Pi>0$ respectively). This means that in the region of low coverages (θ_D, $\theta_A < 10^{-2}$) repulsive interactions are neglected. All four parameters are amenable to direct experimental measurement.

The mathematical model of equations (6.63) to (6.65) is in excellent qualitative agreement with experiment as shown in Figures 6.18 to 6.25. It describes in a semiquantitative manner all electrochemical promotion studies up to date and predicts all the local and global electrochemical and classical promotion rules L1, L2 and G1 to G7.

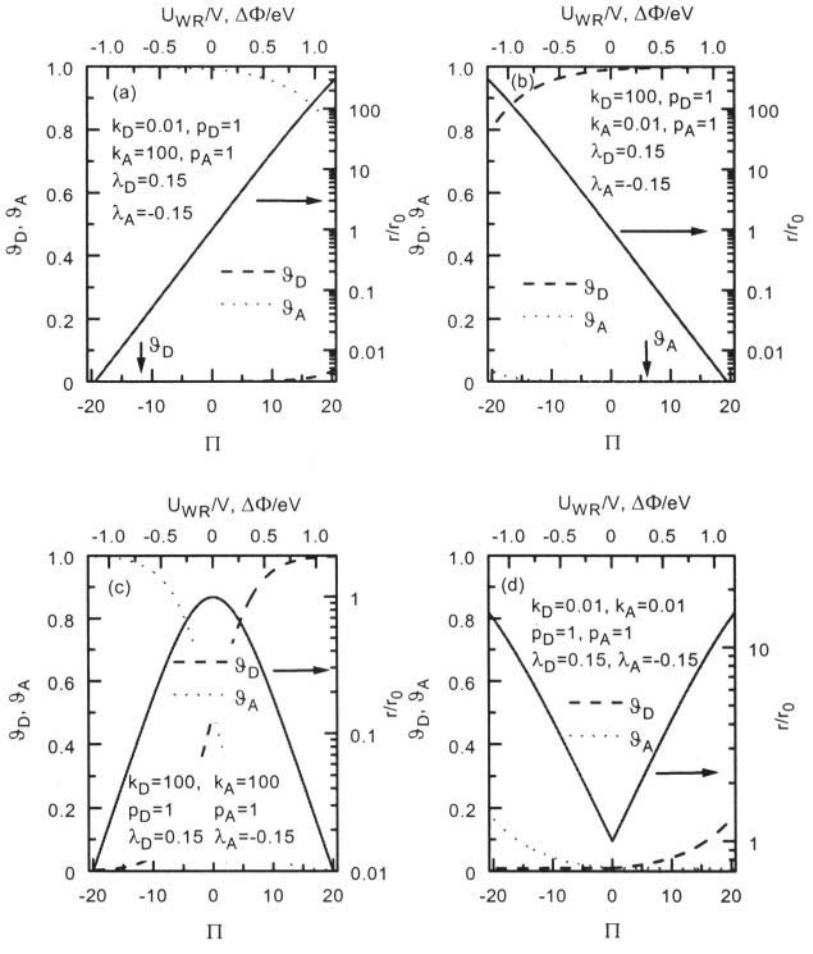

Figure 6.18. Model predicted electrochemical promotion behaviour: (a) electrophobic, (b) electrophilic, (c) volcano-type, (d) inverted volcano-type.

Figure 6.18 shows how the model predicts the four main types of r vs Φ global behaviour (electrophobic, electrophilic, volcano, inverted volcano) for fixed λ_D and λ_A, p_D and p_A, by just varying the adsorption equilibrium constants k_D and k_A. Note that in Figure 6.18 and till the end of this chapter we omit the units of p_D and p_A (e.g. kPa) and k_D,k_A (e.g. kPa^{-1}), unless we refer to experimental data. This is because one is free to use any consistent set of units, since only the dimensionless products k_Ap_A and k_Dp_D enter the calculations.

a. In figure 6.18a it is $k_Dp_D \ll k_Ap_A$ i.e. strong adsorption of A and weak adsorption of D. This leads to *purely electrophobic* behaviour. As also shown in Figures 6.19a and 6.19b with these parameter values ($k_D=10^{-2}$, $k_A=10^2$) the rate is 1st order in D for every Φ (or ΔU_{WR}) value. It is also negative order in A (for $p_A>10^{-2}$) for every Φ (or ΔU_{WR}) value. Thus *rule G1* is *predicted exactly.*

To gain some additional insight we note that the general rate expression (6.65) is now reduced to:

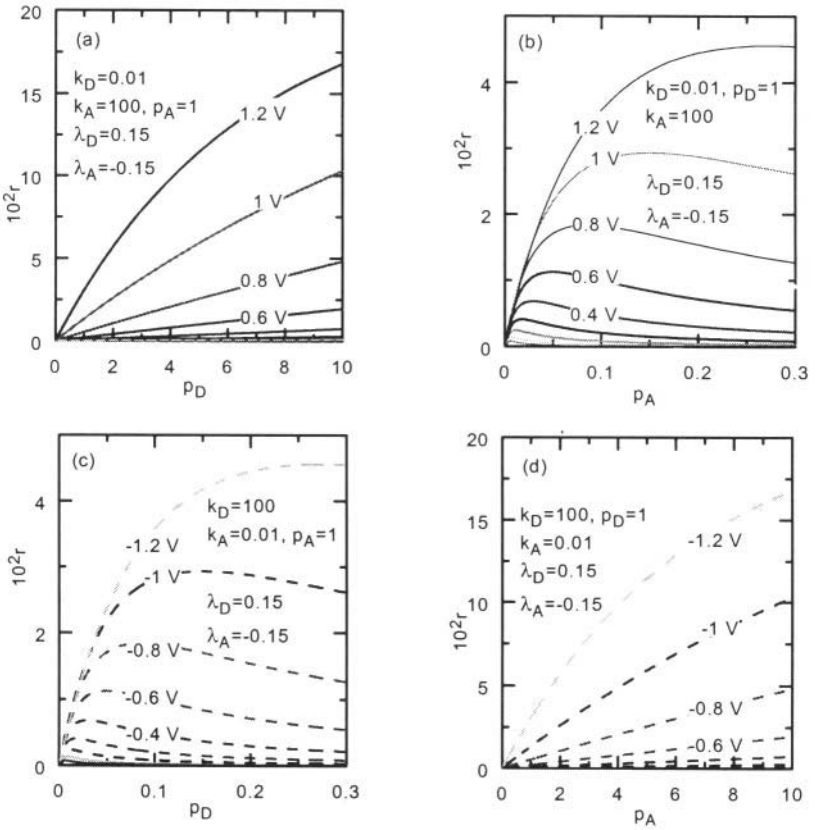

Figure 6.19. Model predicted electrochemical promotion kinetic behaviour: (a) and (b) electrophobic reaction, (c) and (d) electrophilic reaction.

$$r \approx k_R \frac{k_D p_D}{k_A p_A} \exp[(\lambda_D - \lambda_A)\Pi] \tag{6.67}$$

where, since $\lambda_D > 0$ and $\lambda_A < 0$, $\lambda_D - \lambda_A > 0$. Thus the slope in the lnr vs Π line in Fig. 6.18a is $\lambda_D - \lambda_A$. Note also that Eq. (6,67) explains the experimentally observed exponential dependence of r on Φ (Eq. 4.51).

$$\ln(r/r_o)=\alpha(\Phi-\Phi^*)/k_bT \tag{4.51}$$

and provides the following physical meaning to the NEMCA coefficient α:

$$\alpha = \frac{\ell}{2d}(\cos\omega_D\lambda_D - \cos\omega_A\lambda_A) \tag{6.68}$$

which for the case of non-zero λ_R in eq. (6.66) becomes:

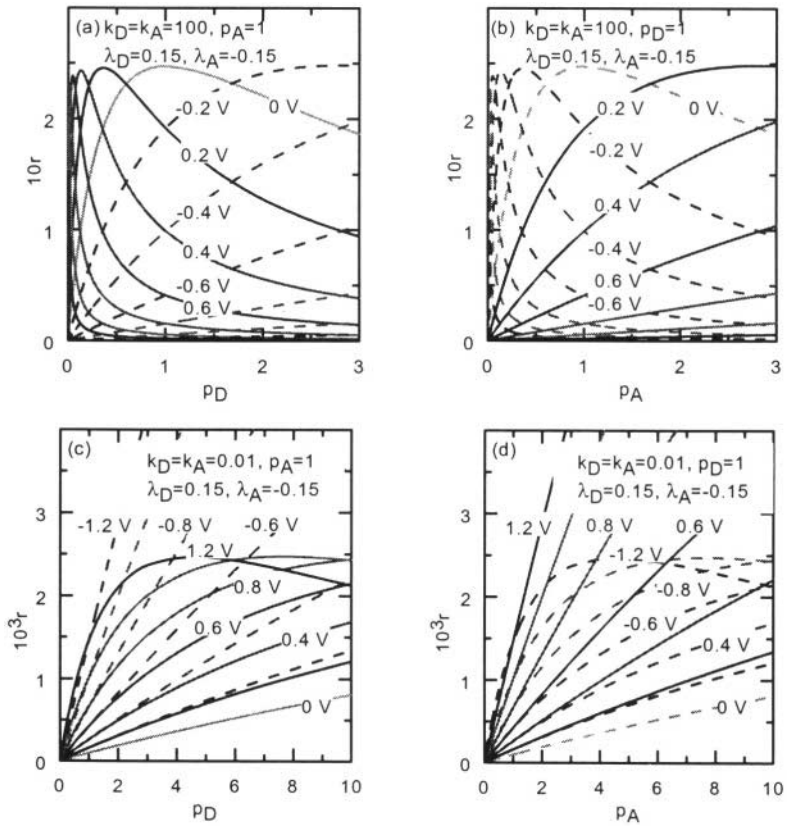

Figure 6.20. Model predicted electrochemical promotion kinetic behaviour: (a) and (b) volcano-type reaction, (c) and (d) inverted volcano-type reaction.

$$\alpha = \frac{\ell}{2d}(\lambda_R + \cos\omega_D\lambda_D - \cos\omega_A\lambda_A) \tag{6.69}$$

or approximately

$$\alpha \approx \lambda_R + \lambda_D - \lambda_A \tag{6.70}$$

b. In figure 6.18b it is $k_D p_D \gg 1 \gg k_A p_A$, i.e. strong adsorption of the electron donor D and weak adsorption of the electron acceptor A. This leads to *purely electrophilic behaviour.* As also shown in Figure 6.19c and 6.19d with these parameter values ($k_D=10^2$, $k_A=10^{-2}$) the rate is negative order D (for $p_D>10^{-2}$) for every Φ value. It is also first order in A for every Φ value. Thus *rule G2* is *predicted exactly.*

The general rate expression (6.65) now reduces to:

$$r = k_R \frac{k_A p_A}{k_D p_D} \exp[(\lambda_A - \lambda_D)\Pi] \tag{6.71}$$

where $\lambda_A - \lambda_D < 0$. This is the slope value in Fig. 6.18b. The experimental equation (4.51) is also nicely predicted while the (negative for electrophilic reactions) NEMCA coefficient α is given by:

$$\alpha = \frac{\ell}{2d}[\lambda_A \cos\omega_A - \lambda_D \cos\omega_D] \tag{6.72}$$

or more generally by

$$\alpha = \frac{\ell}{2d}[\lambda_R + \lambda_A \cos\omega_A - \lambda_D \cos\omega_D] \tag{6.73}$$

or approximately

$$\alpha = \lambda_R + \lambda_A - \lambda_D \tag{6.74}$$

c. Next we examine strong adsorption of both D and A ($k_D p_D = k_A p_A = 10^2$). This leads to volcano behaviour! (Fig. 6.18c) The rate dependence of r on p_D and p_A (Fig. 6.20a and 6.20b) shifts from negative order in D and positive order in A at high positive Φ values to positive order in D and negative order in A at low (negative) Φ values. The similarity with the r vs p_{H_2} and r vs p_{O_2} behaviour during H_2 oxidation on Pt in alkaline solutions which exhibits volcano r vs Φ behaviour (Table 6.1 and section 10) is truly excellent. *Rule G3* is *predicted exactly.*

The general rate expression (6.65) now reduces to:

$$r = k_R \frac{\frac{k_D p_D}{k_A p_A} \exp[(\lambda_D - \lambda_A)\Pi]}{\left[1 + \frac{k_D p_D}{k_A p_A} \exp[(\lambda_D - \lambda_A)\Pi]\right]^2} \tag{6.75}$$

thus the asymptotes in the volcano lnr vs Π plot (Fig. 6.18c) are λ_D-λ_A (>0) for low Π and $\lambda_A - \lambda_D$ (<0) for high Π.

Furthermore simple differentiation of equation (6.75) shows that the rate is maximized (θ_D=θ_A) when

$$\frac{k_D p_D}{k_A p_A} \exp[(\lambda_D - \lambda_A)\Pi] \approx 1 \tag{6.76}$$

This equation, solved in terms of p_D, for fixed p_A and Π (or $\Delta\Phi$), gives the-location of the rate maxima in Fig. 6.20a. When solved in terms of p_A, for fixed p_D and Π (or $\Delta\Phi$) it gives the location of the rate maxima in Fig. 6.20b. And when solved in terms of Π(or $\Delta\Phi$) for fixed p_D and p_A it gives the location of the volcano peak (Fig. 6.18c).

d. Last we examine the case of weak adsorption of both D and A ($k_D p_D$=$k_A p_A$=10^{-2}). In this case, since as previously noted only attractive interactions are considered and the repulsive interactions are neglected, the coverage equations (6.63) and (6.64) take the form:

$$\theta_D = \frac{k_D p_D \exp[\max(0, \lambda_D \Pi)]}{1 + k_D p_D \exp[\max(0, \lambda_D \Pi)] + k_A p_A \exp[\max(0, \lambda_A \Pi)]} \tag{6.77}$$

$$\theta_A = \frac{k_A p_A \exp[\max(0, \lambda_A \Pi)]}{1 + k_D p_D \exp[\max(0, \lambda_D \Pi)] + k_A p_A \exp[\max(0, \lambda_A \Pi)]} \tag{6.78}$$

where the symbol max(α,β) denotes α when α>β, β when α<β and α(or β) when α=β.

The resulting r vs Π behaviour is shown in Fig. 6.18d. In excellent agreement with *global rule G4 inverted volcano* behaviour is predicted with a minimum at the point of zero charge. Furthermore the r vs p_D behaviour shifts from 1st order in D for negative $\Delta\Phi$ to Langmuir-type or even negative order in D for high Φ (Fig. 6.20c).

Conversely the r vs p_A behaviour (Fig. 6.20d) shifts from 1st order in A for positive $\Delta\Phi$ to Langmuir-type or even negative order in A for very low Φ.

Thus global rule G4 is confirmed exactly.

Monomolecular reactions: Two case have to be examined here:

$$D \rightarrow \text{products} \tag{6.79}$$

$$A \rightarrow \text{products} \tag{6.80}$$

In both cases the rate expression is:

$$r = k_R \theta_j = k_R \frac{k_j p_j \exp(\lambda_j \Pi)}{1 + k_j p_j \exp(\lambda_j \Pi)} \tag{6.81}$$

where j stands for D or A and in the former case $\lambda_D > 0$ where in the latter $\lambda_A < 0$. The resulting r vs Π and r vs p_D (or p_A) behaviour is shown in Figures 6.21 and 6.22.

In the former case ($\lambda_D > 0$) the r vs Φ behaviour is electrophobic and the reaction order with respect to p_D decreases with increasing Φ. This confirms rule G6.
In the latter case ($\lambda_A < 0$) the r vs Φ behaviour is electrophilic and the reaction order increases with increasing Φ. This also confirms rule G6.

Effect of partial electron transfer parameter: Figure 6.23 depicts the effect of the value of the partial charge transfer parameter λ_D for fixed $\lambda_A(=-0.15)$ on the rate enhancement ratio $\rho(=r/r_o)$ for the four main types of promotional behaviour, i.e., electrophobic, electrophilic, volcano and inverted volcano. The main feature of the Figure is that it confirms in general the global rule

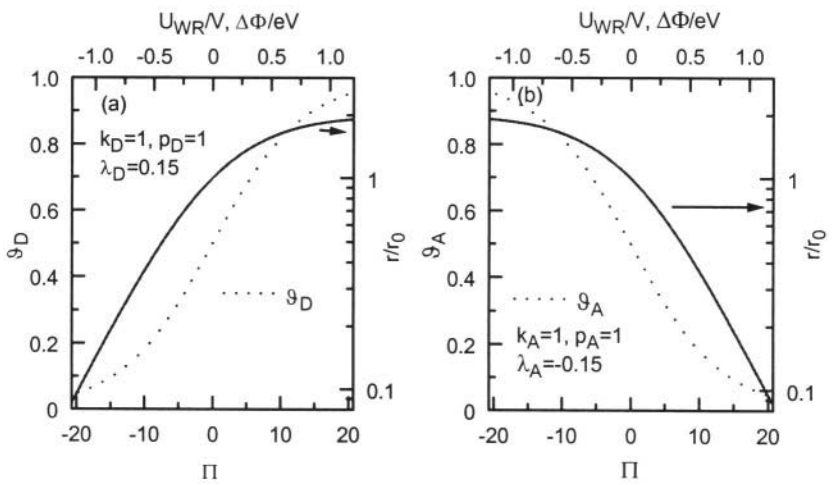

Figure 6.21. Model predicted electrochemical promotion behaviour for a monomolecular reaction (a) electrophobic (b) electrophilic.

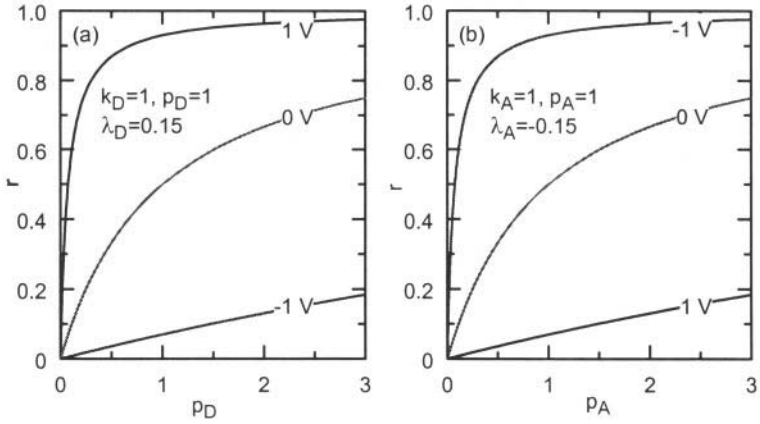

Figure 6.22. Model predicted electrochemical promotion kinetic behaviour for a monomolecular reaction of an electron donor (left) and an electron acceptor (right) absorbate.

G5 and G7. Regarding global rule G5 it can be seen in Figs. 6.23a,b and c that as long as $\lambda_D > \lambda_A$ rules Gl to G3 remain valid regardless of the sign of λ_D with some deviations predicted only for rule G4 in the case of positive Π (in this case a shift from inverted volcano to electrophilic behaviour is predicted when both λ_A and λ_D are negative (Fig. 6.23d)).

With respect to rule G7 Figs. 6.23a,b and c shows that indeed, the larger the value of $|\lambda_D - \lambda_A|$ is, the stronger is the rate dependence on potential and thus the larger is the maximum obtainable $\rho(=r/r_0)$ value. Some deviations are again predicted for the case of inverted volcano reactions (Fig. 6.23d) where it is the value of λ_D (at fixed λ_A) and not the difference $|\lambda_D - \lambda_A|$ which dictates the maximum $\rho(=r/r_0)$ value.

In the case of strong adsorption of A (Fig. 6.23a) ρ $(=r/r_0)$ is an increasing function of λ_D except for very high λ_D where volcano type behaviour is predicted. This is because in this case the coverage of A decreases significantly at very positive potentials. When λ_D also becomes negative (like λ_A) then volcano type behaviour is again predicted (Fig. 6.23a).

For strong adsorption of D (Fig. 6.23b), ρ is again an increasing function of λ_D and for negative λ_D values a transition to inverted-volcano type behaviour is predicted.

Rules G5 and G7 are also predicted for the case of strong adsorption of both D and A (Fig. 6.23c), i.e. for the case of volcano behaviour. In the case of weak adsorption of D and A (Fig. 6.23d) a transition from inverted volcano to purely electrophilic behaviour is predicted when λ_D is negative as already noted.

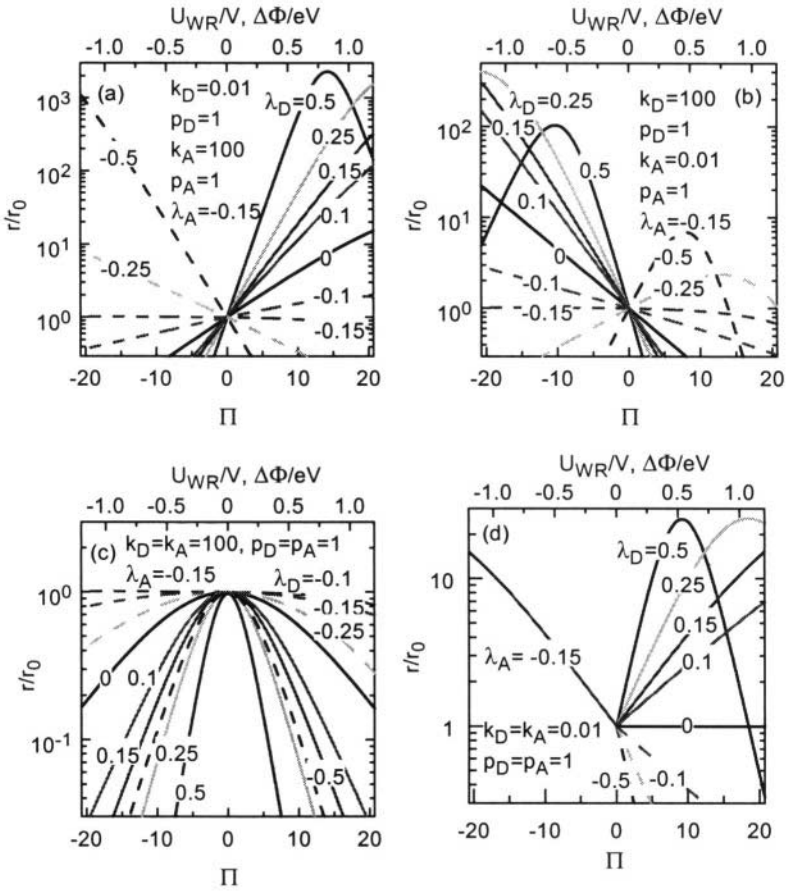

Figure 6.23. Effect of partial charge transfer coefficient λ_D on catalyst performance for fixed λ_A depending on dimensionless potential Π, (a) electrophobic, (b) electrophilic, (c) volcano-type, (d) inverted volcano-type.

The excellent prediction by the model of all global promotion rules is not only qualitative. The predicted ρ values ($\sim 10^2$ for 1V variation in U_{WR}, Fig. 6.18a) is in excellent agreement with experiment (e.g. Fig. 4.24). Also the ρ_{max} values (~10-20) predicted for *volcano* and *inverted volcano* behaviour are in very good agreement with experiment. Finally the λ_D, λ_A which are used (± 0.15) are physically very reasonable. For example for U_{WR}=1 V at 673 K it is $\Pi \approx 17$, thus the λ_D and λ_A values used in the simulations , which are physically very reasonable, give $\exp(\lambda_j \Pi)$, and thus ρ, values between 10^{-2} and 10^2 in good qualitative agreement with experiment.

The success of the model can be appreciated from Figure 6.24 which compares model predictions (top, Fig. 6.24a and b) with some truly interesting and complex experimental results (bottom, Fig. 6.24c and d) obtained during C_2H_4 oxidation on Pt/TiO_2.[28] As shown in Figure 6.24c and d (bottom) the rate dependence on U_{WR} and Π shifts from inverted volcano (Fig. 6.24c) to purely electrophobic (Fig. 6.24d) as $p_{C_2H_4}(=p_D)$ is decreased by a factor of 10 at fixed p_{O_2}.

As shown in Figure 6.24a and b (top) the model predicts the shift in global behaviour in a truly impressive semiquantitative manner and in fact with very reasonable λ_D and λ_A values ($\lambda_D > 0$, $\lambda_A < 0$).

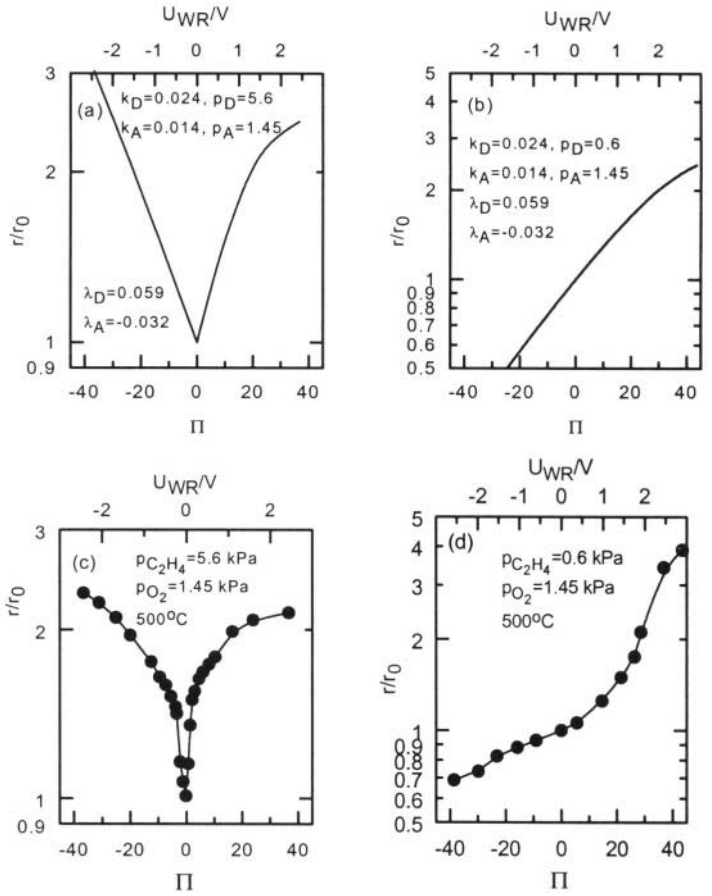

Figure 6.24. Experimentally observed (bottom) and model predicted (top) transition from inverted volcano to electrophobic behaviour upon increasing the O_2 to ethylene (i.e. A/D) ratio by a factor of 10, C_2H_4 oxidation on Pt/TiO_2.[28] Reprinted with permission from Academic Press.

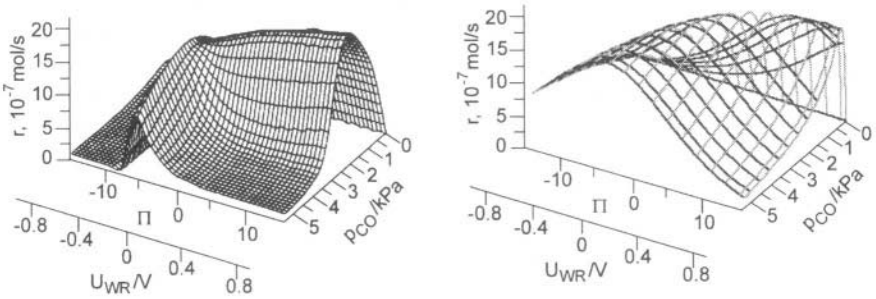

Figure 6.25. Experimental[71] (left) and modelled simulated[99] (right) dependence of the rate of CO oxidation on Pt deposited on β″-Al_2O_3 as a function of p_{CO}, catalyst potential U_{WR} and dimensionless catalyst work function $\Pi(=\Delta\Phi/k_bT)$ at p_{O_2}=6 kPa.[71] Parameters used in equations (6.65) and (6.66): k_A=9.133, k_D=8.715, λ_A=-0.08, λ_D=0.09, λ_R=0, k_R=6.19·10^{-6}. Reprinted with permission from Academic Press.

Finally the success of the model can be judged from Figures 6.25a and b which show the experimental and model-predicted rate dependence on p_{CO} and work function during CO oxidation on Pt/β″-Al_2O_3.[71] Note the transition from a classical Langmuir-Hinshelwood to a positive order rate dependence on p_{CO} with decreasing work function. Also notice that on every point of the experimental or model predicted rate dependence, the basic promotional rule:

$$\left(\frac{\partial r}{\partial \Phi}\right)_{p_A,p_D}\left(\frac{\partial r}{\partial p_D}\right)_{\Phi,p_A} > 0 \qquad (6.11)$$

is strictly obeyed. The optimal λ_D and λ_A values are again quite reasonable (λ_D >0, λ_A<0). The large optimal k_A and k_D values (~9) are also quite reasonable as they indicate strong adsorption of both CO (=D) and oxygen (=A) which is the necessary and sufficient condition (Rule G3) for the appearance of volcano-type behaviour.

In general Figures 6.18 to 6.25, and in particular figures 6.18, 6.19, 6.20, 6.24 and 6.25 show, beyond any reasonable doubt, that the effective double layer model of promotion, expressed mathematically by Equations 6.65 and 6.66, grasps the essence of promotional kinetics.

REFERENCES

1. B. Grzybowska-Swierkosz and J. Haber, *Annual Reports on the Progress of Chemistry,* The Royal Society of Chemistry, Cambridge (1994), p. 395.
2. T. Wolkenstein, *Elektronentheorie der Katalyse an Halbleitern,* VEB Deutscher Verlag der Wissenschaften, Berlin (1964).
3. L.L. Hegedus, R. Aris, A.T. Bell, M. Boudart, N.Y. Chen, B.C. Gates, W.O. Haag, G.A. Somorjai, and J. Wei, *Catalyst design: Progress and Perspectives,* John Wiley & sons, New York (1987).
4. G. Blyholder, Molecular Orbital View of Chemisorbed Carbon Monoxide, *J. Phys. Chem.* **68**, 27-72 (1964).
5. C.G. Vayenas, S. Bebelis, and S. Ladas, Dependence of Catalytic Rates on Catalyst Work Function, *Nature* **343**, 625-627 (1990).
6. C.G. Vayenas, S. Bebelis, I.V. Yentekakis, and H.-G. Lintz, Non-Faradaic Electrochemical Modification of Catalytic Activity: A Status Report (Review Paper), *Catalysis Today* **11**(3), 303-442 (1992).
7. C.G. Vayenas, M.M. Jaksic, S. Bebelis, and S.G. Neophytides, The Electrochemical Activation of Catalysis, in *Modern Aspects of Electrochemistry,* J.O.M. Bockris, B.E. Conway, and R.E. White, eds., Kluwer Academic/Plenum Publishers, New York (1996), pp. 57-202.
8. J. Hoelzl, and F.K. Schulte, *Solid Surface Physics,* Springer-Verlag, Berlin (1979), pp. 1-150.
9. C.G. Vayenas, and S. Brosda, Spillover-modified catalysis: Experiment and mathematical modeling, *Stud. Surf. Sci. Catal,* in press (2001).
10. J.O' M. Bockris, and S.U.M. Khan, *Surface Electrochemistry: A Molecular Level Approach,* Plenum Press, New York (1993).
11. C.G. Vayenas, S. Brosda, and C. Pliangos, Rules and Mathematical Modeling of Electrochemical and Chemical Promotion: 1. Reaction Classification and Promotional Rules, *J. Catal.,* in press (2001).
12. M. Stoukides, and C.G. Vayenas, The effect of Electrochemical Oxygen Pumping on the Rate and Selectivity of Ethylene Oxidation on Polycrystalline Silver, *J. Catal.* **70**, 137-146 (1981).
13. C.G. Vayenas, S. Bebelis, and S. Neophytides, Non-Faradaic Electrochemical Modification of Catalytic Activity, *J. Phys. Chem.* **92**, 5083-5085 (1988).
14. P. Tsiakaras, and C.G. Vayenas, Non-Faradaic Electrochemical Modification of Catalytic Activity: 7. The oxidation of CH_4 on Pt, *J. Catal.* **140**, 53-70 (1993).
15. M. Marwood, A. Kaloyannis, and C.G. Vayenas, Electrochemical Promotion of the NO reduction by C_2H_4 on Pt/YSZ and by CO on Pd/YSZ, *Ionics* **2**, 302-311(1996).
16. C.G. Vayenas, S. Bebelis, I.V. Yentekakis, P. Tsiakaras, and H. Karasali, Non-Faradaic Electrochemical Modification of Catalytic Activity on Pt Metals, *Platinum Metals Review* **34**(3), 122-130 (1990).
17. C.G. Vayenas, and S. Neophytides, Non-Faradaic Electrochemical Modification of Catalytic Activity: 3. The Case of Methanol Oxidation on Pt, *J. Catal.* **127**, 645-664 (1991).
18. I. Harkness, and R.M. Lambert, Electrochemical Promotion of the NO + Ethylene Reaction over Platinum, *J. Catal.* **152**, 211-214 (1995).
19. C.T. Campbell, Cs promoted Ag(111): Model studies of selective ethylene oxidation catalysts, *J. Phys. Chem.* **89**(26), 5789-5795 (1985).
20. C.T. Campbell, and B.E. Koel, H_2S/Cu(111): A model study of sulfur poisoning of water-gas shift catalysts, *Surf. Sci.* **183**, 100-112 (1987).

21. I.V. Yentekakis, R.M. Lambert, M.S. Tikhov, M. Konsolakis, and V. Kiousis, Promotion by sodium in emission control catalysis: A kinetic and spectroscopic study of the Pd-catalyzed reduction on NO by propene, *J. Catal.* **176**, 82-92 (1998).
22. F.A. Alexandrou, V.G. Papadakis, X.E. Verykios, and C.G. Vayenas. *The promotional effect of Na on the NO reduction by CO on supported Pt, Pd and Rh catalysts* in *Proc. 4th Intnl. Congress on Catalysis and Automotive Pollution Control* **2**, 1-16 (1997).
23. S. Bebelis, and C.G. Vayenas, Non-Faradaic Electrochemical Modification of Catalytic Activity: 1. The case of Ethylene Oxidation on Pt, *J. Catal.* **118**, 125-146 (1989).
24. C.A. Cavalca, *PhD Thesis,* Yale University (1995).
25. C.A. Cavalca, and G.L. Haller, Solid Electrolytes as Active Catalyst Supports: Electrochemical Modification of Benzene Hydrogenation Activity on $Pt/\beta''(Na)Al_2O_3$, *J. Catal.* **177**, 389-395 (1998).
26. S. Bebelis, M. Makri, A. Buekenhoudt, J. Luyten, S. Brosda, P. Petrolekas, C. Pliangos, and C.G. Vayenas, Electrochemical activation of catalytic reactions using anionic, cationic and mixed conductors, *Solid State Ionics* **129**, 33-46 (2000).
27. C.G. Vayenas, S. Bebelis, and S. Despotopoulou, Non-Faradaic Electrochemical Modification of Catalytic Activity: 4. The use of β''-Al_2O_3 as the solid electrolyte, *J. Catal.* **128**, 415-435 (1991).
28. C. Pliangos, I.V. Yentekakis, S. Ladas, and C.G. Vayenas, Non-Faradaic Electrochemical Modification of Catalytic Activity: 9. Ethylene oxidation on Pt deposited on TiO_2, *J. Catal.* **159**, 189-203 (1996).
29. C. Pliangos, I.V. Yentekakis, X.E. Verykios, and C.G. Vayenas, Non-Faradaic Electrochemical Modification of Catalytic Activity: 8. Rh-catalyzed C_2H_4 oxidation, *J. Catal.* **154**, 124-136(1995).
30. C.G. Vayenas, and I.V. Yentekakis, Electrochemical Modification of Catalytic Activity, in *Handbook of Catalysis,* G. Ertl, H. Knötzinger, and J. Weitcamp, eds., VCH Publishers, Weinheim (1997), pp. 1310-1338.
31. C.G. Vayenas, and S. Bebelis, Electrochemical Promotion of heterogeneous catalysis, *Catalysis Today* **51**, 581-594 (1999).
32. A.D. Frantzis, S. Bebelis, and C.G. Vayenas, Electrochemical promotion (NEMCA) of CH_4 and C_2H_4 oxidation on Pd/YSZ and investigation of the origin of NEMCA via AC impedance spectroscopy, *Solid State Ionics* **136-137**, 863-872 (2000).
33. S. Bebelis, and C.G. Vayenas, Non-Faradaic Electrochemical Modification of Catalytic Activity: 5. Oxygen Chemisorption on Silver, *J. Catal.* **138**, 570-587 (1992).
34. S. Bebelis, and C.G. Vayenas, Non-Faradaic Electrochemical Modification of Catalytic Activity: 6. The epoxidation of Ethylene on Ag/ZrO_2(8mol%)Y_2O_3, *J. Catal.* **138**, 588-610 (1992).
35. C. Karavasilis, S. Bebelis, and C.G. Vayenas, Non-Faradaic Electrochemical Modification of Catalytic Activity: 10. Ethylene epoxidation on Ag deposited on stabilized ZrO_2 in presence of chlorine moderators, *J. Catal.* **160**, 190-204 (1996).
36. E. Varkaraki, J. Nicole, E. Plattner, C. Comninellis, and C.G. Vayenas, Electrochemical Promotion of IrO_2 catalyst for the gas phase combustion of ethylene, *J. Appl. Electrochem.* **25**, 978-981 (1995).
37. D. Tsiplakides, J. Nicole, C.G. Vayenas, and C. Comninellis, Work function and catalytic activity measurements of an IrO_2 film deposited on YSZ subjected to in situ electrochemical promotion, *J. Electrochem. Soc.* **145**(3), 905-908 (1998).
38. S. Wodiunig, and C. Comninellis, Electrochemical Promotion of RuO_2 Catalysts for the Gas Phase Combustion of C_2H_4, *Journal of the European Ceramic Society* **19**, 931-934 (1999).
39. I.V. Yentekakis, and C.G. Vayenas, In situ controlled promotion of Pt for CO oxidation

via NEMCA using CaF_2 as the solid electrolyte, *J. Catal.* **149**, 238-242 (1994).

40. C.G. Vayenas, and S. Neophytides, Electrochemical Activation of Catalysis: In situ controlled promotion of catalyst surfaces, in *Catalysis-Special periodical Report,* Royal Society of Chemistry, Cambridge (1996), pp. 199-253.
41. A. Giannikos, A.D. Frantzis, C. Pliangos, S. Bebelis, and C.G. Vayenas, Electrochemical Promotion of CH_4 oxidation on Pd, *Ionics* **4**, 53-60 (1998).
42. M. Stoukides, and C.G. Vayenas, The effect of electrochemical oxygen pumping on the Rate and Selectivity of Propylene Oxidation on Silver in a Solid Electrolyte Cell, *J. Electrochem. Soc.* **131**(4), 839-845 (1984).
43. P. Tsiakaras, and C.G. Vayenas, Oxidative Coupling of CH_4 on Ag catalyst-electrodes deposited on ZrO_2(8mol% Y_2O_3), *J. Catal.* **144**, 333-347 (1993).
44. S. Tracey, A. Palermo, J.P.H. Vazquez, and R.M. Lambert, In Situ Electrochemical Promotion by Sodium of the Selective Hydrogenation of Acetylene over Platinum, *J. Catal.* **179**, 231-240 (1998).
45. A. Giannikos, P. Petrolekas, C. Pliangos, A. Frenzel, C.G. Vayenas, and H. Putter, Electrochemical promotion of Pd for the Hydrogenation of C_2H_2, *Ionics* **4**, 161-169 (1998).
46. H. Alqahtany, P.H. Chiang, P. Eng, M. Stoukides, and A.R. Robbat, Electrocatalytic decomposition of hydrogen sulfide, *Catal. Lett.* **13**, 289-296 (1992).
47. P.H. Chiang, D. Eng, and M. Stoukides, Solid electrolyte aided direct coupling of methane, *J. Catal.* **139**, 683-687 (1993).
48. G. Pitselis, P. Petrolekas, and C.G. Vayenas, Electrochemical Promotion of NH_3 decomposition on Fe using H^+, Na^+ and K^+ conductors, *Ionics* **3**, 110-117 (1997).
49. I.V. Yentekakis, Y. Jiang, S. Neophytides, S. Bebelis, and C.G. Vayenas, Catalysis, Electrocatalysis and Electrochemical Promotion of the Steam Reforming of Methane over Ni Film and Ni-YSZ cermet Anodes, *Ionics* **1**, 491-498 (1995).
50. M. Makri, A. Buekenhoudt, J. Luyten, and C.G. Vayenas, Non-Faradaic Electrochemical Modification of the Catalytic Activity of Pt using a $CaZr_{0.9}In_{0.1}O_{3-\alpha}$ Proton Conductor, *Ionics* **2**, 282-288 (1996).
51. P.D. Petrolekas, S. Balomenou, and C.G. Vayenas, Electrochemical promotion of Ethylene Oxidation on Pt Catalyst Films deposited on CeO_2, *J. Electrochem. Soc.* **145**(4), 1202-1206 (1998).
52. P. Beatrice, C. Pliangos, W.L. Worrell, and C.G. Vayenas, The electrochemical promotion of ethylene and propylene oxidation on Pt deposited on Yttria-Titania-Zirconia, *Solid State Ionics* **136-137**, 833-837 (2000).
53. C. Karavasilis, S. Bebelis, and C.G. Vayenas, In Situ Controlled Promotion of Catalyst Surfaces via NEMCA: The Effect of Na on the Ag-Catalyzed Ethylene Epoxidation in the Presence of Chlorine Moderators, *J. Catal.* **160**, 205-213 (1996).
54. A. Kaloyannis, and C.G. Vayenas, Non-Faradaic electrochemical modification of catalytic activity. 12: Propylene oxidation on Pt, *J. Catal.* **182**, 37-47 (1998).
55. J.K. Hong, I.-H. Oh, S.-A. Hong, and W.Y. Lee, Electrochemical Oxidation of Methanol over a Silver Electrode Deposited on Yttria-Stabilized Zirconia Electrolyte, *J. Catal.* **163**, 95-105 (1996).
56. O.A. Mar'ina, and V.A. Sobyanin, The effect of electrochemical oxygen pumping on the rate of CO oxidation on Au electrode-catalyst, *Catal. Lett.* **13**, 61-70 (1992).
57. O.A. Mar'ina, V.A. Sobyanin, V.D. Belyaev, and V.N. Parmon, The effect of electrochemical oxygen pumping on catalytic properties of Ag and Au electrodes at gas-phase oxidation of CH_4, *Catalysis Today* **13**, 567-570 (1992).
58. O.A. Mar'ina, V.A. Sobyanin, V.D. Belyaev, and V.N. Parmon, The effect of electrochemical pumping of oxygen on catalytic behaviour of metal electrodes in

methane oxidation, in *New Aspects of Spillover Effect in Catalysis for Development of Highly Active Catalysts,* Stud. Surf. Sci. Catal. **77**, T. Inui, K. Fujimoto, T. Uchijima and M. Masai, Eds., pp. 337-340, Elsevier Science Publishers B.V. (1993).

59. C.G. Yiokari, G.E. Pitselis, D.G. Polydoros, A.D. Katsaounis, and C.G. Vayenas, High pressure electrochemical promotion of ammonia synthesis over an industrial iron catalyst, *J. Phys. Chem.* **104**, 10600-10602 (2000).
60. T.I. Politova, V.A. Sobyanin, and V.D. Belyaev, Ethylene hydrogenation in electrochemical cell with solid proton-conducting electrolyte, *Reaction Kinetics and Catalysis Letters* **41**(2), 321-326 (1990).
61. S. Neophytides, and C.G. Vayenas, Non-Faradaic Electrochemical Modification of Catalytic Activity: 2. The case of Methanol Dehydrogenation and Decomposition on Ag, *J. Catal.* **118**, 147-163 (1989).
62. A. Palermo, R.M. Lambert, I.R. Harkness, I.V. Yentekakis, O. Mar'ina, and C.G. Vayenas, Electrochemical promotion by Na of the Platinum catalyzed reaction between CO and NO, *J. Catal.* **161**, 471-479 (1996).
63. A. Palermo, M.S. Tikhov, N.C. Filkin, R.M. Lambert, I.V. Yentekakis, and C.G. Vayenas, Electrochemical Promotion of NO Reduction by CO and by Propene, *Stud. Surf. Sci. Catal.* **101**, 513-522 (1996).
64. A. Palermo, M.S. Tikhov, N.C. Filkin, R.M. Lambert, I.V. Yentekakis, and C.G. Vayenas, Electrochemical Promotion of NO reduction by CO and by Propene, *Ionics* **1**, 366-372 (1995).
65. M. Marwood, and C.G. Vayenas, Electrochemical Promotion of the Catalytic Reduction of NO by CO on Palladium, *J. Catal.* **170**, 275-284 (1997).
66. G.L. Haller, and S. Kim. *ACS Petroleum Division Preprints, Symposium in Catalytic Combustion* in *213th National ACS Meeting,* 155-158 (1997, April 13-17) San Francisco, CA.
67. L. Ploense, M. Salazar, B. Gurau, and E.S. Smotkin, Proton Spillover Promoted Isomerization of n-Butylenes on Pt-black Cathodes/Nafion 117, *JACS* **119**, 11550-11551 (1997).
68. P.D. Petrolekas, S. Brosda, and C.G. Vayenas, Electrochemical promotion of Pt catalyst-electrodes deposited on $Na_3Zr_2Si_2PO_{12}$ during Ethylene Oxidation, *J. Electrochem. Soc.* **145**(5), 1469-1477 (1998).
69. I.V. Yentekakis, and C.G. Vayenas, The Effect of Electrochemical O^{2-} Pumping on the Steady State and Oscillatory Behavior of CO oxidation on Polycrystalline Pt, *J. Catal.* **111**, 170-188 (1988).
70. H. Karasali, and C.G. Vayenas, NEMCA: The Oxidation of CO on Pt, *Materials Science Forum* **76**,171-174 (1991).
71. I.V. Yentekakis, G. Moggridge, C.G. Vayenas, and R.M. Lambert, In situ controlled promotion of catalyst surfaces via NEMCA: The effect of Na on the Pt-catalyzed CO oxidation, *J. Catal.* **146**, 292-305 (1994).
72. S. Neophytides, D. Tsiplakides, P. Stonehart, M. Jaksic, and C.G. Vayenas, Electrochemical enhancement of a catalytic reaction in aqueous solution, *Nature* **370**, 292-294 (1994).
73. S. Neophytides, D. Tsiplakides, P. Stonehart, M.M. Jaksic, and C.G. Vayenas, Non-Faradaic Electrochemical enhancement of H_2 oxidation in alkaline solutions, *J. Phys. Chem.* **100**, 14803-14814 (1996).
74. D. Tsiplakides, S. Neophytides, O. Enea, M.M. Jaksic, and C.G. Vayenas, Non-Faradaic Electrochemical Modification of Catalytic Activity (NEMCA) of Pt Black Electrodes Deposited on Nafion 117 Solid Polymer Electrolyte, *J. Electrochem. Soc.* **144**(6), 2072-2088 (1997).

75. I.M. Petrushina, V.A. Bandur, F. Cappeln, and N.J. Bjerrum, Electrochemical Promotion of Sulfur Dioxide Catalytic Oxidation, *J. Electrochem. Soc.* **147(8)**, 3010-3013 (2000).
76. R.M. Lambert, M. Tikhov, A. Palermo, I.V. Yentekakis, and C.G. Vayenas, Electrochemical Promotion of Environmentally Important Catalytic Reactions, *Ionics* **1**, 366-376 (1995).
77. O.A. Mar'ina, I.V. Yentekakis, C.G. Vayenas, A. Palermo, and R.M. Lambert, In situ controlled Promotion of Catalyst Surfaces via NEMCA: The effect of Na on the Pt-catalyzed NO Reduction by H_2, *J. Catal.* **166**, 218-228 (1997).
78. C. Karavasilis, S. Bebelis, and C.G. Vayenas, NEMCA: The Oxidation of CO on Ag, *Materials Science Forum* **76**, 175-178 (1991).
79. T.I. Politova, G.G. Gal'vita, V.D. Belyaev, and V.A. Sobyanin, Non-Faradaic catalysis: the case of CO oxidation over Ag-Pd electrode in a solid oxide electrolyte cell, *Catal. Lett.* **44**, 75-81 (1997).
80. A. Kaloyannis, and C.G. Vayenas, Non-Faradaic Electrochemical Modification of Catalytic Activity. 11. Ethane Oxidation on Pt, *J. Catal.* **171**, 148-159 (1997).
81. C. Pliangos, C. Raptis, T. Badas, and C.G. Vayenas, Electrochemical promotion of NO reduction by C_3H_6 on Rh/YSZ catalyst-electrodes, *Solid State Ionics* **136/137**, 767-773 (2000).
82. C. Pliangos, C. Raptis, T. Badas, and C.G. Vayenas, Electrochemical Promotion of NO Reduction by C_3H_6 and CO on Rh/YSZ Catalyst - Electrodes, *Ionics* **6**, 119-126 (2000).
83. I.N. Yakovkin, V.I. Chernyi, and A.G. Naumovetz, Oxidation of CO on Li-precovered Pt, *Surf. Sci.* **442**, 81-89 (1999).
84. K. Chen, S. Xie, A.T. Bell, and E. Iglesia, Alkali effects of molybdenum oxide catalysts for the oxidative dehydrogenation of propane, *J. Catal.* **195**, 244-252 (2000).
85. C.G. Vayenas, On the work function of the gas exposed electrode surfaces in solid state electrochemistry, *J. Electroanal. Chem.* **486**, 85-90 (2000).
86. C.G. Vayenas, and D. Tsiplakides, On the work function of the gas-exposed electrode surfaces in solid state electrolyte cells, *Surf. Sci.* **467**, 23-34 (2000).
87. D. Tsiplakides, and C.G. Vayenas, Electrode work function and absolute potential scale in solid state electrochemistry, *J. Electrochem. Soc.* **148**(5), E189-E202 (2001).
88. S. Neophytides, D. Tsiplakides, and C.G. Vayenas, Temperature-Programmed Desorption of Oxygen from Pt-films Interfaced with Y_2O_3-Doped ZrO_2, *J. Catal.* **178**, 414-428 (1998).
89. G. Pacchiont, F. Illas, S. Neophytides, and C.G. Vayenas, Quantum-Chemical Study of Electrochemical Promotion in Catalysis, *J. Phys. Chem.* **100**, 16653-16661 (1996).
90. G. Pacchioni, J.R. Lomas, and F. Illas, Electric field effects in heterogeneous catalysis, *Molecular Catalysis A: Chemical* **119**, 263-273 (1997).
91. M. Kiskinova, Poisoning and Promotion in Catalysis based on Surface Science Concepts and Experiments, in *Stud. Surf. Sci. Catal.* **70**, Elsevier, Amsterdam (1992).
92. D. Tsiplakides, S. Neophytides, and C.G. Vayenas, Thermal Desorption Study of Oxygen Adsorption on Pt, Ag and Au films Deposited on YSZ, *Ionics* **3**, 201-208 (1997).
93. M. Boudart, Heterogeneity of Metal Surfaces, *JACS* **74**, 3556-3561 (1952).
94. G. Rangelov, and L. Surnev, Alkali Metal Adsorption on Ru(001), *Surf. Sci.* **185**, 457-468 (1987).
95. M. Kiskinova, Interactions of CO and sodium coadsorbed on Ru(10 $\bar{1}$ 0), *Surf. Sci.* **182**, 150-160 (1987).
96. M. Kiskinova, and M. Tikhov, Adsorption of CO on Ru(10 $\bar{1}$ 0) doped with different amounts of K and Cs, *Surf. Sci.* **194**, 379-396 (1988).

97. A.-M Lanzillotto, M.J. Dresser, M.D. Alvey, and J.T.Yates Jr., Alkali sensitization of H^+ electron stimulated desorption from H adsorbed on Ni(111), *J. Phys. Chem.* **89**(1), 570-576 (1988).
98. M.T.M. Koper, and R.A.van Santen, Electric field effects on CO and NO adsorption at the Pt(111) surface, *J. Electroanal. Chem.* **476**, 64-70 (1999).
99. S. Brosda, and C.G. Vayenas, *J. Catal.,* submitted (2001).
100. K. Franaszczuk, E. Herrero, P. Zelenay, A. Wieckowski, J. Wang, and R.I. Masel, A comparison of electrochemical and gas-phase decomposition of methanol on platinum surfaces, *J. Phys. Chem.* **96**(21), 8509-8516 (1992).
101. E. Gileadi, *Electrode kinetics: for chemists, chemical engineers, and materials scientists,* Wiley-VCH, Weinheim (1993).
102. G.A. Somorjai, *Chemistry in Two Dimensions:* Surfaces, Cornell University Press (1981).
103. A.W. Adamson, *Physical Chemistry of Surfaces,* John Wiley & Sons, Inc., New York (1990).
104. W. Rudinski, and D.H. Everett, *Adsorption of gases on heterogeneous surfaces,* Academic Press, London (1992).
105. I. Rubinstein, ed., *Physical Electrochemistry.* Principles, Methods, and Applications, Marcel Dekker, Inc., New York (1995).
106. J.O' M. Bockris, A.K.M. Reddy, and M. Gamboa-Aldeco, *Modern Electrochemistry,* Kluwer Academic/Plenum Publishers, New York, (2000).
107. I. Metcalfe, Electrochemical Promotion of Catalysis I: Thermodynamic considerations, *J. Catal.* **199**, 247-258 (2001).
108. I. Metcalfe, Electrochemical Promotion of Catalysis II: The role of stable spillover species and prediction of reaction rate modification, *J. Catal.* **199**, 259-272 (2001).

CHAPTER 7

THE ABSOLUTE POTENTIAL

7.1 INTRODUCTION

The concept of «absolute» electrode potential still appeals strongly to the interest of electrochemists and solid state physicists. Prominent scientists including Bockris,[1,2] Frukmin,[3,4] Riess, Gileadi,[1] Kanevsky,[5] Reiss,[6] Parsons,[7] Gomer,[8] Hansen,[9] Gerischer,[10] Kolb[11,12] and Trasatti[13-16] have made important contributions in this area.

One basic reason which made the absolute electron potential problem so complicated to solve in aqueous electrochemistry is the experimental difficulty of measuring work functions on metal surfaces covered with liquid films or in contact with liquids and their vapours.

For reasons which will become apparent below, such experimental problems are minimized in solid state electrochemistry so that both the definition and the direct measurement of «absolute» electrode potentials is rather straightforward.

It will also be shown that the absolute electrode potential is not a property of the electrode but is a property of the electrolyte, aqueous or solid, and of the gaseous composition. It expresses the energy of "solvation" of an electron at the Fermi level of the electrolyte. As such it is a very important property of the electrolyte or mixed conductor. Since several solid electrolytes or mixed conductors based on ZrO_2, CeO_2 or TiO_2 are used as conventional catalyst supports in commercial dispersed catalysts, it follows that the concept of absolute potential is a very important one not only for further enhancing and quantifying our understanding of electrochemical promotion (NEMCA) but also for understanding the effect of metal-support interaction on commercial supported catalysts.

7.2 ABSOLUTE POTENTIAL SCALES IN AQUEOUS ELECTROCHEMISTRY

Trasatti[14-16] has done a very thorough and lucid work in clarifying the concept of absolute electrode potentials in aqueous electrochemistry. He has pointed out that at least four different absolute, or "single", electron potentials can be defined, depending on the choice of the reference state of electrons.

We start by noting that an electrode potential, U_{WR}, as measured with respect to a reference electrode R, is a relative measure (in volts) of the energy of electrons at the Fermi level of the metal constituting the electrode:

$$eU_{WR}=-(\bar{\mu}_e^W - \bar{\mu}_e^R) \tag{7.1}$$

This can be expressed also as follows:

$$U_{WR}=U_W(she)-U_R(she)=U_W(abs)-U_R(abs) \tag{7.2}$$

where U(she) is electrode potential with respect to the she (standard hydrogen electrode) scale and U(abs) are so-called "absolute" (or single) electrode potentials, i.e. electrode potentials not referred to another electrode system but to a given reference electronic energy taken as zero. In particular:

$$U_W(she)=U_W(abs)- U^o_{H_2}(abs) \tag{7.3}$$

where $U^o_{H_2}(abs)$ is the "absolute" electrode potential of the standard hydrogen electrode, which is taken as the universal zero for electrode potentials in aqueous solutions.

Thus when using the she scale one chooses as the reference state of electrons (and assigns the zero value to it) the state of an electron at the Fermi level of a metal electrode in equilibrium with an aqueous solution of pH=0 and $p_{H_2}=1$ atm at 25°C.

This is a thermodynamically legitimate choice of the zero energy level and she potentials are the ones most commonly used in aqueous electrochemistry. But in reality one would like to choose the zero level for the electronic energy in such a way that the energy scale of electrochemical systems can be directly compared with that of solid/gas or solid/vacuum interfaces.[17]

Trasatti[14-16] has discussed the zero level choice thoroughly and has shown that the best choice is that of an electron in vacuum close to the surface of the solution:

$$U_W(abs) = - \bar{\mu}_W /e - \Psi_S \tag{7.4}$$

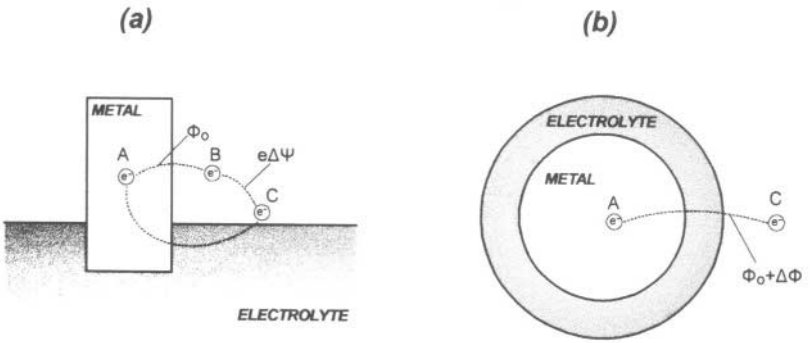

Figure 7.1. Definition of absolute electron potential in aqueous electrochemistry according to Trasatti[16] in a classical (a) and liquid covered (b) electrode geometry. Point C corresponds to the zero energy level. Φ_0 is the work function of the bare electrode surface and $\Delta\Phi(=e\Delta\Psi)$ is the work function modification induced by the presence of the electrolyte layer (b). Reprinted with permission from Elsevier Science.

where Ψ_s is the outer (Volta) potential of the solution. In view of the fact that for any metal:

$$-\bar{\mu}_M = \Phi_M + e\Psi_M \tag{7.5}$$

one has also:

$$eU_W(abs) = \Phi_{W,0} + e(\Psi_W - \Psi_s) \tag{7.6}$$

where $\Phi_{W,0}$ is the work function of the *bare* metal surface and Ψ_M-Ψ_S is the contact (Volta) potential difference (cpd) arising as an interface is formed between the working electrode and the solution (Fig. 7.1a).

Trasatti has then elegantly shown[16] that $U_W(abs)$ is also given by the equation

$$eU_W(abs) = \Phi_{W,0} + \Delta\Phi_W \tag{7.7}$$

where $\Delta\Phi_W(=e(\Psi_W-\Psi_s))$ is the modification of $\Phi_{W,0}$ induced by the contact with the solution and can be measured as the modification of $\Phi_{W,0}$ due to H_2O adsorption or due to the presence of a liquid layer covering the surface of the working metal electrode (Fig. 7. la). This suggests the use of emersed electrodes[9,11,12,18,19] and experiment has provided $U^o_{H_2}$ (abs) values varying between 4.4 and 4.85 eV in good qualitative agreement with values (4.76 eV) already calculated as early as 1968 by Bockris and Argade.[20] The IUPAC recommended value is 4.44 eV.[14]

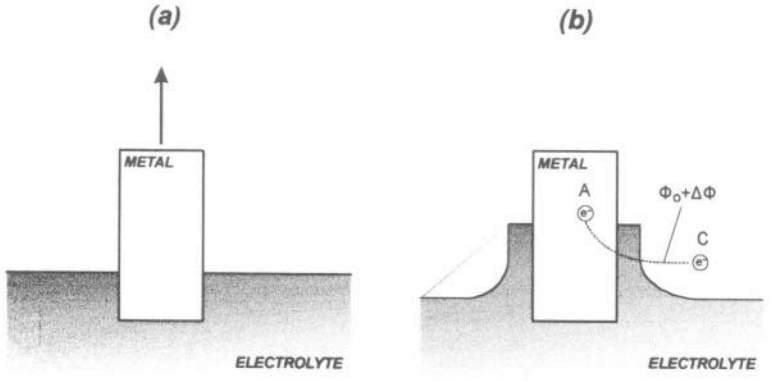

Figure 7.2. Schematic of a normal (a) and an emersed (b) electrode in aqueous electrochemistry showing the conceptual similarity of case (b) with Fig. 7.1b (adapted from Trasatti[16]). Reprinted with permission from Elsevier Science.

It is worth noting in Figures 7. 1b and 7.2b that the zero energy level choice (point C) is not only, by definition, a point in vacuum close to the surface of the solution (Fig. 7.1a, 7.2a), but also, as clearly shown by Trasatti,[16] a point in vacuum close to the surface of the emersed (liquid or adsorption covered) electrode.

One obvious but important aspect of the absolute potential defined by Eq. (7.7) is that its value does not depend on the material of the electrode. Thus, although different metals (e.g. Pt, Ag, Hg) have significantly different $\Phi_{W,0}$ values, the change $\Delta\Phi_W$ induced by the presence of the aqueous overlayer is such that $\Phi_{W,0}+\Delta\Phi_W$ ($=eU_W(abs)$) *does not depend* on the metal.

This, at first perhaps surprising fact, is important to remember as the same situation arises in solid state electrochemistry. To understand its validity it suffices to remember that the definition of the reference (zero) energy level of electrons for the she scale is simply the state of an electron at the Fermi level of *any* metal in equilibrium with an aqueous solution of pH=0 and $p_{H_2}=1$ atm at 25°C.

7.3 ABSOLUTE POTENTIAL SCALE AND ZERO ENERGY LEVEL OF ELECTRONS IN SOLID STATE ELECTROCHEMISTRY

As already discussed extensively in this book, Y_2O_3-stabilized-ZrO_2(YSZ), an O^{2-} conductor at temperatures 300°-1200°C and β''-Al_2O_3, a Na^+ conductor at temperatures 150° to 400°C are two of the most commonly used solid electrolytes. YSZ, in particular, is almost as important for solid state electrochemistry as aqueous solutions are for liquid electrolyte electrochemistry. Recently published work[21] has focused on establishing and measuring the absolute potential scale using YSZ, although extension to other solid electrolyte systems is rather straightforward.

Similarly to aqueous electrochemistry, potentials in solid state electrochemistry utilizing YSZ are expressed in terms of the potential of a reference metal electrode exposed to $p_{O_2} = 1$ atm at the temperature T of interest. Thus a standard oxygen electrode scale (soe) can be defined. Similarly to equation (7.2) one has:

$$U_{WR} = U_W(soe) - U_R(soe) = U_W(abs) - U_R(abs) \tag{7.8}$$

where U(soe) are the electrode potentials with respect to the soe (standard oxygen electrode) scale and U(abs) are the "absolute" potentials with respect to a reference (zero) electronic state not referred to another electrode system.

Before discussing the experimental results, which by themselves suggest a unique choice of the reference (zero) state of electrons in solid state electrochemistry, which is the same with the choice of Trasatti for aqueous electrochemistry,[14-16] it is useful to discuss some of the similarities and differences between aqueous and solid electrochemistry (Fig. 7.3).

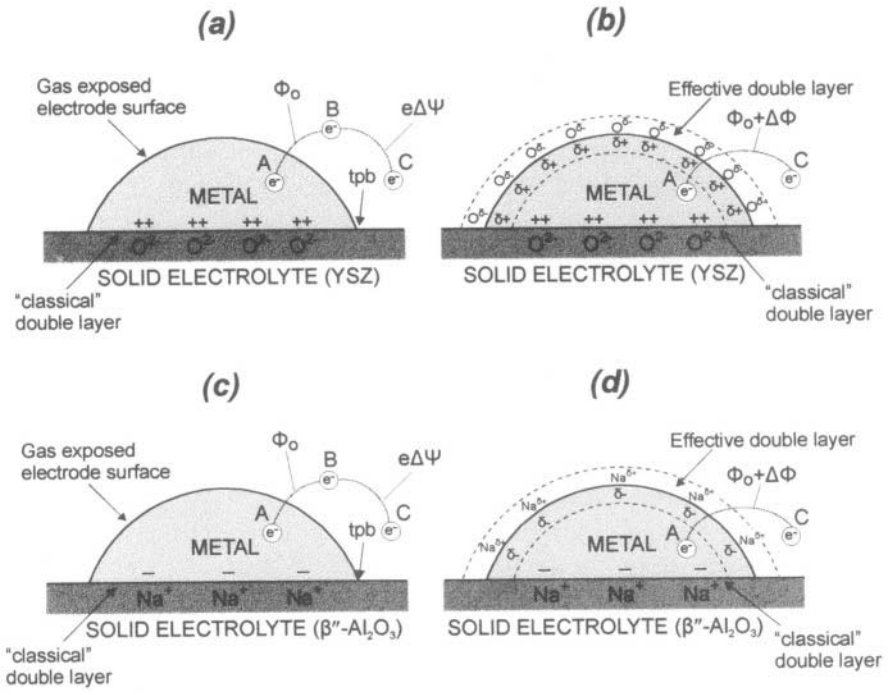

Figure 7.3. Schematic representation of a metal electrode deposited on a O^{2-} conducting (a,b) and on a Na^+-conducting (c,d) solid electrolyte, showing the location of the classical metal-electrolyte double layer and of the effective double layer (b,d) created at the metal/gas interface due to potential-controlled ion migration (backspillover).[21] Reproduced by permission of The Electrochemical Society.

In aqueous electrochemistry electrochemical (charge transfer) reactions take place over the entire metal/electrolyte interface.

In solid electrochemistry electrochemical (change transfer) reactions take place primarily at the three-phase-boundaries (tpb) metal-electrolyte-gas, e.g.:

$$O_2(g) + 4e^-(M) \rightleftharpoons 2O^{2-}(YSZ) \tag{7.9}$$

There is a (classical) double-layer at the metal-solid electrolyte interface and its point of zero charge (pzc) can be measured by similar techniques as in aqueous electrochemistry.[22] As already discussed in Chapter 5 during the last ten years it has become obvious from a variety of surface spectroscopic techniques including UPS,[23] XPS,[24,25] TPD,[26,27] STM,[28] AC Impedance spectroscopy[22,29] and PEEM[30] that there exists a second double layer which must be taken into account at the metal-gas interface (Fig. 7.3). This "effective" double layer is formed via backspillover of ions (e.g. O^{2-}, Na^+) from the solid electrolyte onto the gas exposed electrode surface. This double layer, which as AC Impedance spectroscopy has shown[22,29] has a capacitance of the order of 200 $\mu F/cm^2$, is intimately related to the effect of electrochemical promotion[31-33] and has a wide range of temperature stability, i.e. 300-600°C on metal electrodes deposited on YSZ or 150-400°C on metal electrodes deposited on β''-Al_2O_3. At lower temperatures ion backspillover is frozen, at higher temperature the backspillover species desorb.[26,27] It therefore must be emphasized that the situation depicted in Fig. 7.3 (b and d) is not a model but an experimental reality which manifests itself in all the techniques which have been used to investigate the metal/gas interface in solid state electrochemistry.

7.3.1 The Nature of the Effective Double Layer

In Chapter 5 we have discussed in detail the nature of the effective double layer formed at the metal/gas interface of metals deposited on solid electrolyte.

As an example the STM images[21,28,34] of Figure 7.4 show the $Na^{\delta+}$ backspillover double layer formed on Pt(111) surfaces interfaced with β''-Al_2O_3, a Na^+ conductor, in ambient air. Figure 7.4a depicts the O (2×2) adlattice forming on the bare Pt(111) surface which has been cleaned from $Na^{\delta+}$ via anodic potential application. Each sphere is an oxygen atom. Figure 7.4b shows the same surface after electrochemical supply of Na^+ to the Pt(111) surface up to a $Na^{\delta+}$ coverage, θ_{Na}, of roughly 0.01.[28] The $Na^{\delta+}$ adatoms form a (12×12) overlayer on top of the O (2×2) adlattice over the entire Pt/gas interface[28] as shown also in Figure 7.4c where each sphere is a $Na^{\delta+}$ adatom.[21,34] It is interesting to notice that each $Na^{\delta+}$ adatom perturbs the electronic cloud of several neighboring Pt atoms, so that the effective double layer appears "dense" even at low (0.01) $Na^{\delta+}$ coverages.

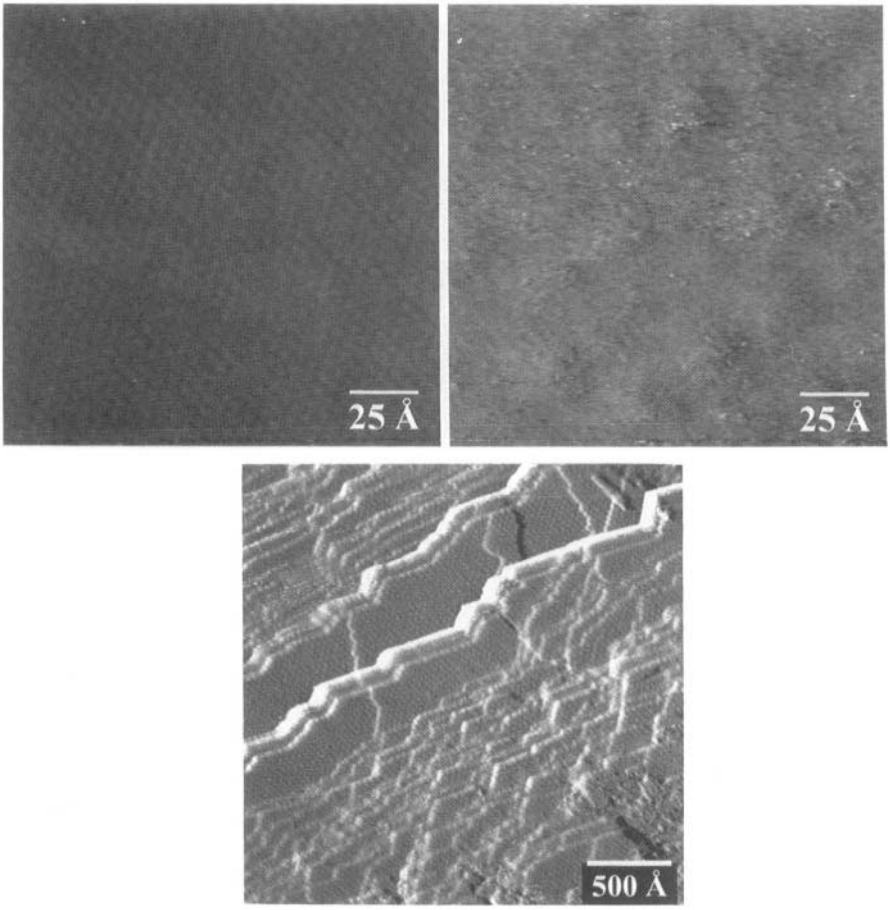

Figure 7.4. STM images (unfiltered) of a Pt(111) surface interfaced with β″-Al_2O_3[28] in ambient air showing the (a) sodium-cleaned and (b) sodium-dosed surface. Note (a) the Pt(111)-(2x2)-O adlatice and the reversible appearance (b) of the Pt(111)-(12×12)-Na adlayer (U_t = +100 mV, I_t = 1.8 nA, total scan size 319 Å).[28] Reprinted with permission from Elsevier Science (c) STM images (unfiltered) of the effective double layer formed by the $Na^{\delta+}$ (12x12) – Na adlayer on a Pt surface consisting mainly of Pt(111) planes and interfaced with β″-Al_2O_3.[21,34] Each sphere is a Na atom. Reprinted with permission from The Electrochemical Society.

It must be emphasized that the effective double layer is overall neutral, as the backspillover species ($O^{\delta-}$, $Na^{\delta+}$) are accompanied by their compensating (screening) charge in the metal.[32,33,35,36] It must also be clarified that this backspillover formed effective double layer is not in general at its pzc (point of zero charge). This happens only at a specific value of the electrode potential, as in aqueous electrochemistry.[37]

The thermodynamics of ion backspillover from the solid electrolyte to the gas exposed electrode surface have been discussed in section 3.4.3 and also

in Chapter 5. It is worth reminding that the thermodynamic driving force for migration (backspillover) from YSZ to a metal electrode surface is the difference $\bar{\mu}_{O^{2-}(YSZ)} - \bar{\mu}_{O^{2-}(M)}$, where the two terms are the electrochemical potential of O^{2-} in YSZ and on the metal (M) surface.

Regarding the kinetics of O^{2-} backspillover on metal electrodes, it has been known for years from transient electrochemical promotion experiments[35] that they are quite fast, due to the strong repulsive dipole-dipole repulsion of the O^{2-} backspillover species. A conservative estimate of the surface diffusivity, D_s, of O^{2-} on Pt(111) can be made from the surface diffusivity measurements of Gomer and Lewis[38] for O on Pt(111) and (110) near 400°C. They described their data from the equation[38]:

$$D_s = \alpha^2 \nu \exp(\Delta S/R)\exp(-E/RT) \tag{7.10}$$

with $\alpha = 3$Å, $\Delta S = 17$ cal/mol·K and, $\nu = 10^{12}$ s^{-1} and E = 34.1 kcal/mol. At 400°C this gives $D_s = 4.\cdot 10^{-11}$ cm^2/s. Thus for a typical 1 μm thick porous metal electrode used in solid electrochemistry the diffusion time is $\tau = L^2/D_s \approx 250$ s, i.e. significantly shorter than actual galvanostatic electrochemical promotion transient time constants which are typically[35] of the order of $2FN_G/I$ (500-5000 s, see Chapter 4). This confirms that surface diffusion of the backspillover species is generally faster than the rate (I/2F) of their generation at the three-phase-boundaries (tpb) so that the latter is usually the rate controling step for the formation of the effective double layer.[35]

The presence of this backspillover formed effective double layer is important not only for interpreting the effect of electrochemical promotion, but also for understanding the similarity of solid state electrochemistry depicted in Fig. 7.3 with the case of emersed electrodes in aqueous electrochemistry (Fig. 7.2) and with the "gedanken" experiment of Trasatti (Fig. 7.1) where one may consider that H_2O "spillovers" on the metal surface. This conceptual similarity also becomes apparent from the experimental results.

7.3.2 Experimental Establishment of the Absolute Potential Scale

The solid electrolyte cell shown in Figure 7.5a was used for the work function measurements which led recently to the establishment of the absolute potential scale in solid state electrochemistry.[21] It consists of an 8 mol%-Y_2O_3-stabilized-ZrO_2 (YSZ) disc. On this YSZ disc three metal electrodes, working, counter and reference were deposited (Fig. 7.5a) using thin coatings of Engelhard metal pastes for Pt and Au and GC electronics paint for Ag, followed by drying and calcination in air at 1073 K for Pt and Au and 873 K for Ag, as described elsewhere.[21] The thus deposited porous electrodes had thicknesses of the order of 5 μm.[21] By using different disks each of the three metals (Pt, Au, Ag) was tested as a working, as a counter and as a reference electrode.

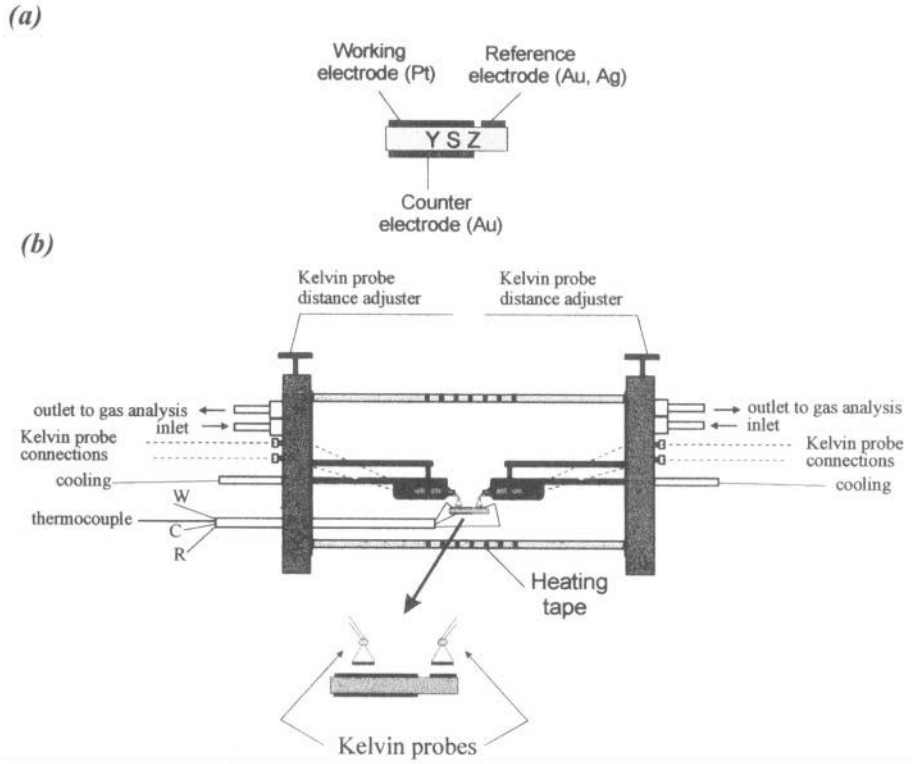

Figure 7.5. (a) Solid electrolyte cell consisting of an YSZ disk with working (Pt), reference (Au, Ag) and counter electrodes (Au). (b) Schematic diagram of the electrochemical reactor.[21] Reprinted with permission from The Electrochemical Society.

Tsiplakides and Vayenas[21] have used *two* Kelvin probes, one always facing the working and the other facing the reference electrode to measure in situ the work functions, Φ_W and Φ_R, of the gas-exposed electrode surfaces of the working and reference electrodes respectively (Figure 7.5b). It should be remembered that Φ is used to denote the actual, experimentally measured, work function of the gas exposed electrode surface and not the work function of the clean metal surface for which the symbol Φ_0 is reserved. The two Kelvin probes (Besocke/Delta Phi-Electronik, Probe "S"), with a 2.5 mm diameter gold grid vibrating electrode placed ~500 μm from the electrode surface were calibrated using Au and Ag foils at room temperature. It was verified that the work function measurements were not influenced by the exact distance of the two capacitors elements. In the Kelvin probe 'S' operation, the work function signal is drawn from the vibrating gold grid, so that the Kelvin probe lock-in amplifier circuit is entirely independent of the solid electrolyte cell circuit.[31,39,40] In this type of operation, the electrode under measure has to be grounded and thus it is not possible to measure the

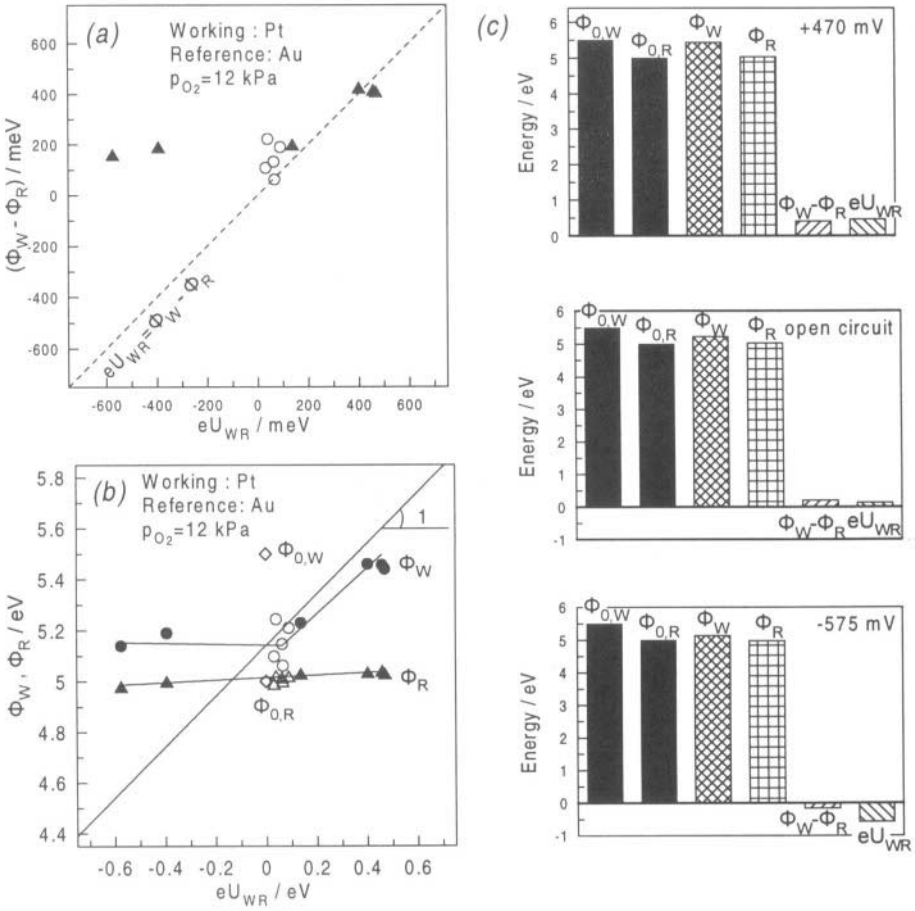

Figure 7.6. (a) Dependence of $\Phi_{W(Pt)}$-$\Phi_{R(Au)}$ on potential U_{WR} for the system Pt(W)-Au(R).[21] Open symbols: Open-circuit operation. Filled symbols: Closed circuit operation T=673 K. (b) Work function of working (W) and reference (R) electrode, Φ_W (○, ●) and Φ_R (Δ, ▲), as a function of potential U_{WR} for the system Pt(W)-Au(R). Symbols and conditions as in (a). Diamonds show the literature[41] values of $\Phi_{0,W(Pt)}$ and $\Phi_{0,R(Au)}$. (c) Bar charts of $\Phi_{0,W(Pt)}$, $\Phi_{0,R(Au)}$,[41] $\Phi_{W(Pt)}$, $\Phi_{R(Au)}$, $\Phi_{W(Pt)}$-$\Phi_{R(Au)}$ and U_{WR} at +470 mV, open circuit (U^o_{WR} = +68 mV) and −575 mV for the system Pt(W)-Au(R). Reprinted with permission from The Electrochemical Society.

work function of both electrodes, working and reference, simultaneously, but only one after the other every, e.g., 10-30 s. This, of course, does not pose any problem for steady state measurements. With appropriate water-cooled design of the two Kelvin probes, in order to keep the piezocrystal temperature below its Curie temperature of 573 K, both Kelvin probes could operate continuously at temperatures up to 673 K.[21]

Figures 7.6 and 7.7 show the dependence of $\Phi_W - \Phi_R$ (Fig. 7.6a, 7.7a), and of Φ_W and Φ_R individually (Fig. 7.6b, 7.7b) on catalyst-electrode potential U_{WR}

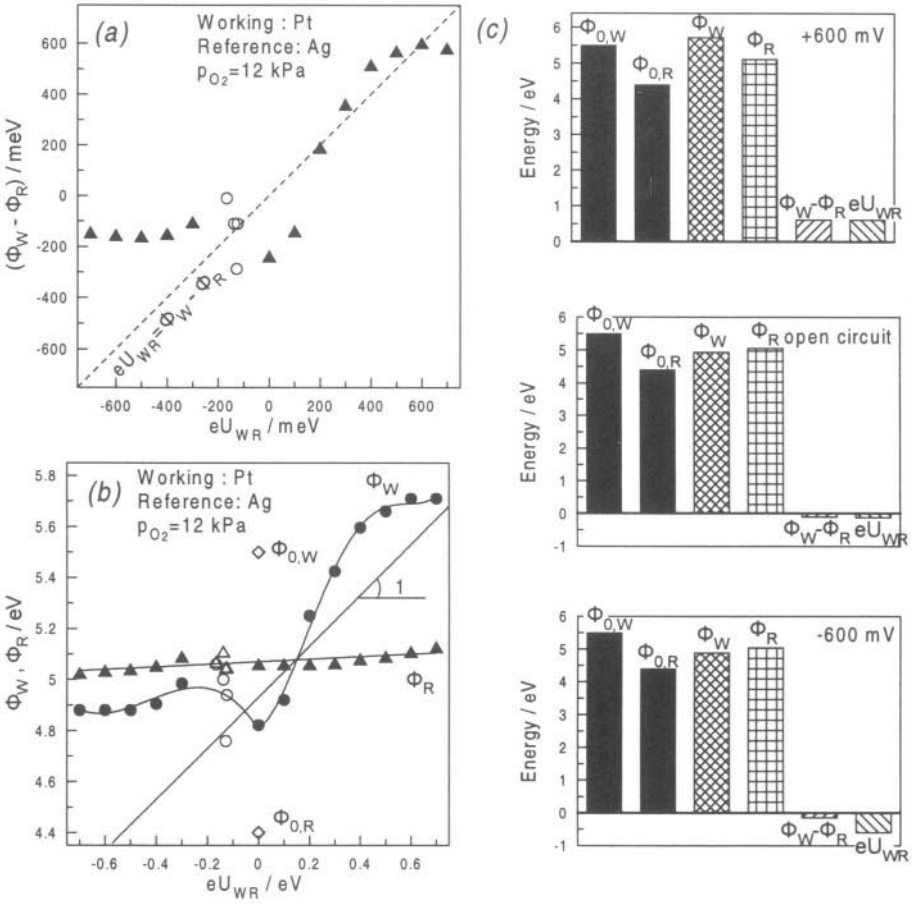

Figure 7.7. (a) Dependence of $\Phi_{W(Pt)}$-$\Phi_{R(Ag)}$ on potential U_{WR} for the system Pt(W)-Ag(R).[21] Open symbols: Open-circuit operation. Filled symbols: Closed circuit operation T=673 K. (b) Work function of working (W) and reference (R) electrode, Φ_W (○, ●) and Φ_R (Δ, ▲), as a function of potential U_{WR} for the system Pt(W)-Ag(R). Symbols and conditions as in (a). Diamonds show the literature[41] values of $\Phi_{0,W(Pt)}$ and $\Phi_{0,R(Ag)}$. (c) Bar charts of $\Phi_{0,W(Pt)}$, $\Phi_{0,R(Ag)}$,[41] $\Phi_{W(Pt)}$, $\Phi_{R(Ag)}$, $\Phi_{W(Pt)}$-$\Phi_{R(Ag)}$ and U_{WR} at +600 mV, open circuit (U^o_{WR} = -124 mV) and –600 mV for the system Pt(W)-Ag(R). Reprinted with permission from The Electrochemical Society.

for the systems Pt(W)-Au(R) (Fig. 7.6) and Pt(W)-Ag(R) (Fig. 7.7). The work functions Φ_W and Φ_R, and thus U_{WR}, were varied both by varying the gaseous composition (using O_2-He mixtures, open symbols in which case both Φ_W and Φ_R change) and by using the potentiostat to impose fixed U_{WR} values (filled symbols). In the potential range –200 to +600 mV there is good agreement with the equations:

$$eU_{WR} = \Phi_W - \Phi_R \tag{7.11}$$

$$e\Delta U_{WR}=\Delta\Phi_W \tag{7.12}$$

The constancy of Φ_R with changing potential is also remarkable, as expected for a reference electrode. The deviation from Eq. (7.11) for negative potentials is due to the removal of O^{2-} and concomitant destruction of the effective double layer.

The good agreement between experiment and Equation (7.11) can be better appreciated if one takes into account the values, Φ_0, of the bare Pt, Au and Ag surfaces ($\Phi_{0,Pt}$=5.5 eV, $\Phi_{0,Au}$=5.0 eV, $\Phi_{0,Ag}$=4.4 eV, also shown in Figs. 7.6b, 7.6c, 7.7b, 7.7c).[41] Thus in the case of the Pt(W) –Au(R) system, $\Phi_{0,W}$ and $\Phi_{0,R}$ differ by 0.5 eV on the bare surfaces (Figs. 7.6b, 7.6c) but the difference $\Phi_W - \Phi_R - eU_{WR}$ is less than 0.1 V near U_{WR}=0 (Fig. 7.6a). In the case of the Pt(W) – Ag(R) system (Figs. 7.7 and 7.8) $\Phi_{0,W}$ and $\Phi_{0,R}$ differ by 1.1 eV on the bare surfaces (Figs. 7.7b, 7.7c) but this difference vanishes near U_{WR}=0 (Figs. 7.7b, 7.7c) and even becomes negative for negative potentials (Figs. 7.7b,7.7c), i.e. the work function of Pt becomes smaller than that of Ag in this region!

Equations (7.11) and (7.12) are in very good agreement with experiment not only in chemically inert environments, but also in presence of reactive H_2-O_2 mixtures, in which case the electrode surfaces are also catalyzing the H_2 oxidation reaction. This is shown in Figures 7.8a and 7.8b with Pt working, Au counter and Ag reference electrodes. It is worth noting that although Φ_W and Φ_R both vary significantly with potential (Fig. 7.8b) their difference satisfies equation (7.11) quite well (Fig. 7.8a).

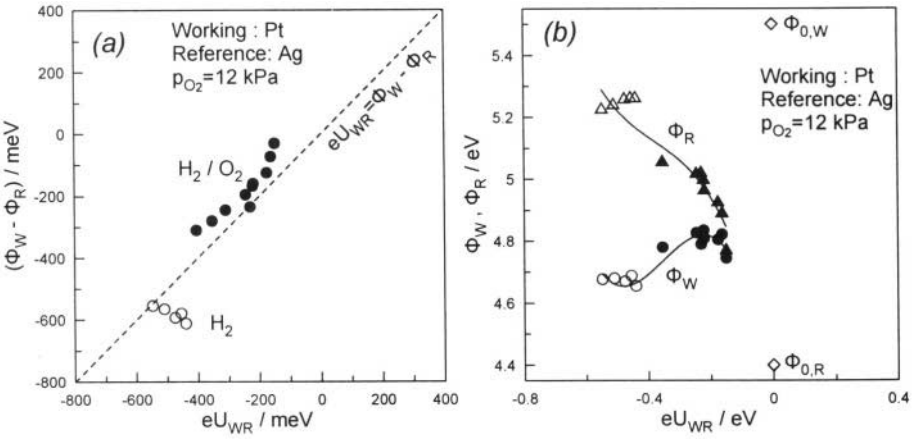

Figure 7.8. (a) Dependence of $\Phi_{W(Pt)}$-$\Phi_{R(Ag)}$ on potential U_{WR} for the system Pt(W)-Ag(R) exposed to H_2-He mixtures (open-symbols, p_{H_2} varying between 0.53 and 0.024 kPa) and H_2-O_2 mixtures (filled symbols, p_{O_2}=12 kPa, p_{H_2} varying between 0.28 and 7.8 Pa); open-circuit operation, T=673 K, Au counter electrode. (b) Work function of working (W) and reference (R) electrode as a function of open-circuit potential U_{WR}.[21] Symbols and conditions as in figure 7.8a. Diamonds show the literature[41] values of $\Phi_{0,W(Pt)}$ and $\Phi_{0,R(Ag)}$. Reprinted with permission from The Electrochemical Society.

The variation in $\Phi_{R(Ag)}$ with U_{WR} shows that Ag is not a good quasi-reference electrode in presence of reactive gas mixtures. This is due to its high catalytic activity for H_2 oxidation. Nevertheless the agreement with Eq. (7.11) is noteworthy, as is also the fact that, due to the faster catalytic reaction of H_2 on Pt than on Ag and thus due to the lower oxygen chemical potential on Pt than on Ag,[35] the work function of the Pt catalyst electrode is *lower* than that of the Ag catalyst-electrode over the entire U_{WR} range (Fig. 7.8b), although on bare surfaces Φ_0 is much higher for Pt than for Ag (Fig. 7.8b).

Equation (7.12) has been reported since 1990[31] by several groups[31,39,40,42-45] and has been confirmed using both the Kelvin probe technique and UPS, as already discussed in Chapter 5. Only one group[46] has reported significant deviations from it, but the SEMs in that work show massive blocking nonporous electrodes which apparently do not allow for ion spillover.

Equation 7.11 was proven experimentally only recently.[21] This equation had been predicted for years[35] on the basis of Eq. (7.12), but only recently *two* Kelvin probes have been used to measure the work function on both working and reference electrode to confirm its validity.[21] It is worth noting that Equation (7.12) is formally identical with that obtained with emersed electrodes in aqueous electrochemistry. In that case $\Delta\Phi_W$ is the work function change measured in the emersed state due to previous application of a potential ΔU_{WR} in the immersed state. However, in the case of emersed electrodes in aqueous electrochemistry[9,11,12,18,19] although Equation (7.12) has been found to hold, Equation (7.11) has not been reported yet. This may be due to the absence so far of studies utilizing emersed working *and* reference electrodes.

The implications of Equations (7.11) and (7.12) are quite significant. They allow for the establishment and straightforward measurement of a unique absolute electrode potential scale in solid state electrochemistry.

7.4 THE WORK FUNCTION OF CATALYST FILMS DEPOSITED ON SOLID ELECTROLYTES: RATIONALIZATION OF THE POTENTIAL –WORK FUNCTION EQUIVALENCE

As already discussed the key experimental observations:

$$eU_{WR} = \Phi_W - \Phi_R \tag{7.11}$$

$$e\Delta U_{WR} = \Delta\Phi_W \tag{7.12}$$

are due to ion spillover on the electrode surfaces and to the formation there of an effective, overall neutral, electrochemical double layer. This double

layer tends to neutralize electrostatic charges normally residing on the gas exposed electrode surfaces as analyzed below:

We start by noting that one always has by definition:

$$eU_{WR} = -(\bar{\mu}_W - \bar{\mu}_R) \tag{7.1}$$

and in view of Equation (7.5):

$$eU_{WR} = \Phi_W - \Phi_R + e\Psi_W - e\Psi_R \tag{7.13}$$

The situation is depicted schematically in Figure 7.9. It must be noted that although $\bar{\mu}$ can be split conceptually in three ways (Fig. 7.9):

$$-\bar{\mu} = \Phi + e\Psi \tag{7.5}$$

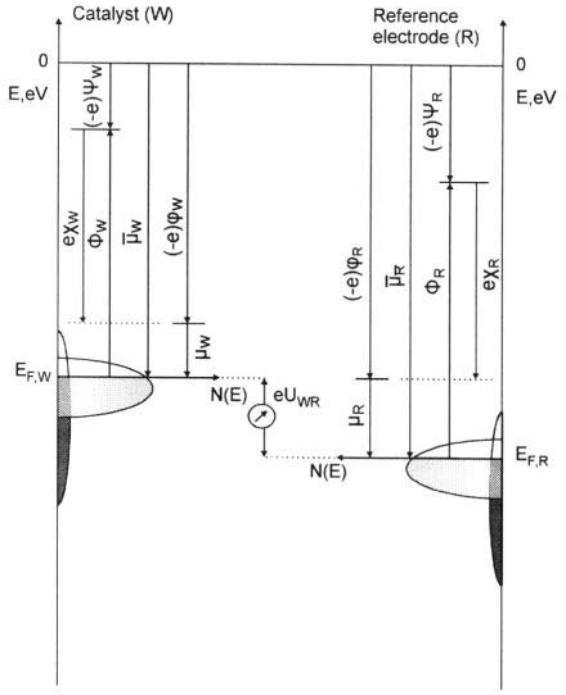

Figure 7.9. Schematic representation of the density of states N(E) in the conduction band of two transition metal electrodes (W and R) and of the definitions of work function Φ, chemical potential of electrons μ, electrochemical potential of electrons or Fermi level $\bar{\mu}$, surface potential χ, Galvani (or inner) potential φ and Volta (or outer) potential Ψ for the catalyst (W) and for the reference electrode (R). The measured potential difference U_{WR} is by definition the difference in $\bar{\mu}$; φ, μ and $\bar{\mu}$ are spatially uniform; Φ and Ψ can vary locally on the metal surfaces;[21] the Ψ terms are equal, see Fig. 5.18, for the case of fast spillover, in which case they also vanish for an overall neutral cell; Reprinted with permission from The Electrochemical Society.

$$-\bar{\mu} = -\mu + e\varphi \tag{7.13}$$

$$-\bar{\mu} = -\mu + e\chi + e\Psi \tag{7.14}$$

where μ is the chemical potential of electrons, φ is the inner (Galvani) potential, and χ is the surface potential, in Equation (7.13) and throughout this book we use only the first way of splitting $\bar{\mu}$, i.e. Eq. (7.5). This is because both Φ and Ψ are absolutely measurable quantities,[35,37,47] whereas μ, φ and χ are not.[37,47]

It must first be noted that the experimental Equation (7.11), in conjunction with the general theoretical Equation (7.13) implies directly[21,32,33]

$$\Psi_W - \Psi_R = 0 \tag{7.15}$$

This does not imply necessarily $\Psi_W = \Psi_R = 0$ or $\Psi_S = 0$, where Ψ_S is the Volta potential on the electrolyte surface. But for the subsequent analysis it is useful to notice that equation (7.15) is mathematically equivalent (in view of the general theoretical Equation (7.13) with the key experimental equation (7.11).

In order to gain some additional physical insight on how spillover leads to the experimental equations (7.11) and (7.12) we will consider the solid electrolyte cell shown in Figure 7.10a and will examine the situation in absence of spillover (Equations (7.11) and (7.12) not valid) and in presence of spillover (Equations (7.11) and (7.12) valid). For simplicity we focus on and show only the working (W) and reference (R) electrodes which are deposited on a solid electrolyte (S), such as YSZ. The two porous, thus non-blocking, electrodes are made of the same metal or of two different metals, M and M′. The partial pressures of O_2 on the two sides of the cell are p_{O_2} and p'_{O_2}. Oxygen may chemisorb on the metal surfaces so that the work functions Φ_W and Φ_R of the two gas-exposed electrode surfaces are $\Phi_W(p_{O_2})$ and $\Phi_R(p'_{O_2})$.

We consider now the following two cases:

1. No ion spillover. The temperature is first assumed low enough so that ionic mobility on the electrode surfaces is negligible, i.e. *there is no spillover.* Due to the establishment of the equilibrium

$$O_2(g) + 4e^- \rightleftharpoons 2O^{2-}(YSZ) \tag{7.9}$$

at the metal-gas-solid electrolyte three-phase-boundaries, the value of U_{WR} is fixed via the Nernst equation to:

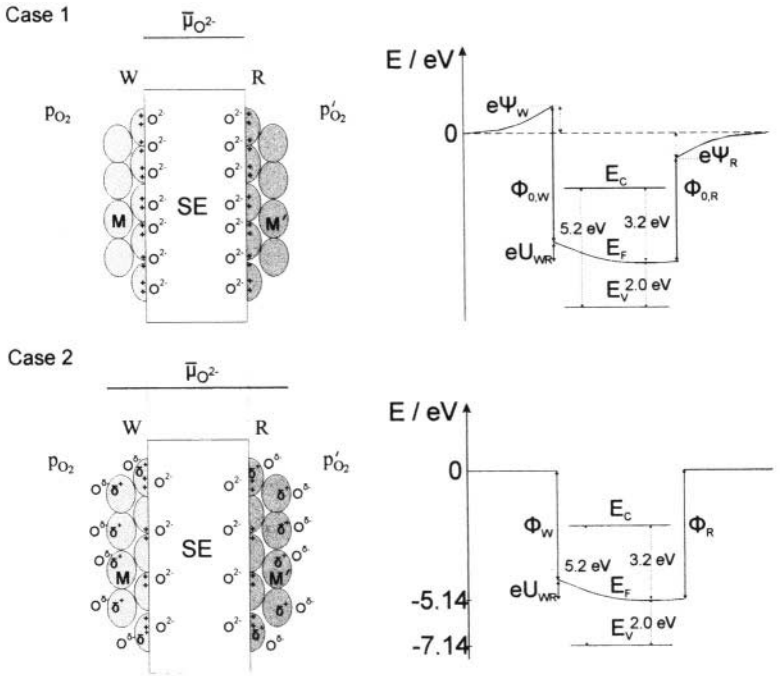

Figure 7.10. Left: Schematic of an O^{2-}conducting solid electrolyte cell with fixed p_{O_2} and p'_{O_2} values at the porous working (W) and reference (R) electrodes, *without* (top) and *with* (bottom) ion backspillover on the gas exposed electrode surfaces, showing also the range of constancy of the electrochemical potential of O^{2-}. Right: Corresponding spatial variation in the electrochemical potential of electrons, $\bar{\mu}_e$ (=E_F); U_{WR} is fixed in both cases to the value (RT/4F)·ln (p_{O_2} / p'_{O_2}); also shown is the relative position of the top of the valence band, E_V, and of the bottom of the conduction band, E_C, in the solid electrolyte (SE); numerical values correspond to 8 mol% Y_2O_3-stabilized-ZrO_2, p_{O_2} =10^{-6} bar and p'_{O_2} = 1 bar, T= 673 K.[21] Reprinted with permission from The Electrochemical Society.

$$U_{WR}=(1/4F)(\mu_{O_2}-\mu'_{O_2})=(RT/4F)\ln(p_{O_2}/p'_{O_2}) \tag{7.16}$$

regardless of the nature of the two metals and thus Equation (7.13) can be rewritten as:

$$e\Psi_W-e\Psi_R=e\underset{\text{fixed}}{U_{WR}}+\underset{\text{fixed}}{\Phi_R(p'_{O_2})}-\underset{\text{fixed}}{\Phi_W(p_{O_2})} \tag{7.17}$$

which, incidentally, in the case of negligible oxygen chemisorption on the two surfaces reduces to:

$$e\Psi_W-e\Psi_R=e\underset{\text{fixed}}{U_{WR}}+\underset{\text{fixed}}{\Phi_{0,M'}}-\underset{\text{fixed}}{\Phi_{0,M}} \tag{7.18}$$

where $\Phi_{0,M'}$ and $\Phi_{0,M}$ are the work functions of the clean surface of metals M′ and M respectively.

Since p_{O_2} and p'_{O_2} are fixed, U_{WR} is fixed and also, since there is no spillover, $\Phi_R(p'_{O_2})$ and $\Phi_W(p_{O_2})$ in equation (7.17), or $\Phi_{0,M}$ and $\Phi_{0,M'}$ in equation (7.18) are also fixed. Thus in case 1 *(no ion spillover)* $e\Psi_W$-$e\Psi_R$ is fixed to an (in general) *nonzero value.* Thus in this case equations (7.11) and (7.12) are *not* valid, since they are mathematically equivalent to Ψ_W-Ψ_R=0 as already discussed Eq. (7.15).

In fact, one may consider as an example of application of eq. (7.17), the case $p_{O_2} = p'_{O_2}$, thus from eq. (7.16) U_{WR}=0. Then one has:

$$e\Psi_W - e\Psi_R = \Phi_R(p_{O_2}) - \Phi_W(p_{O_2}) \neq 0 \tag{7.19}$$

Thus if the working and reference electrodes are made of different metals, and there is negligible adsorption of oxygen on the two metals, in which case $\Phi_R=\Phi_{0,M'}$ and $\Phi_W=e\Phi_{0,M}$ then equation (7.19) gives the *cpd* (contact potential difference) of the two metals:

$$cpd = e\Psi_W - e\Psi_R = \Phi_{0,M'} - \Phi_{0,M} \tag{7.20}$$

The same result in the case of negligible adsorption is obtained if the electrolyte is not present but the two metals are brought in direct contact so that $\bar{\mu}_W = \bar{\mu}_R$, from which equation (7.20) is directly derived.

In the case where $p_{O_2} = p'_{O_2}$ and the two electrodes are of the same material, then equation (7.18) or (7.19) gives, ofcourse, $e\Psi_W$-$e\Psi_R$=0 and $\Phi_R = \Phi_W$.

The non-zero, in general, value of $e\Psi_W$-$e\Psi_R$ in Equation (7.18) implies that there are net surface charges on the gas exposed electrode surfaces. These charges (q_+,q_-) have to be opposite and equal as the cell is overall electrically neutral and all other charges are located at the metal-solid electrolyte interfaces to maintain their electroneutrality. The charges q_+=-q_- are quite small in relation to the charges, Q, stored at the metal-electrolyte interface but nevertheless the system has, due to their presence, an excess electrostatic energy:

$$E_E = (\Psi_W - \Psi_R)q_+ \tag{7.21}$$

The positive charge is on the electrode with the lower work function.

Thus under conditions of negligible ion spillover equations (7.11) and (7.12), are not valid. This is the case in aqueous electrochemistry and can also be the case in solid state electrochemistry when the temperature is

sufficiently low to freeze ion spillover, i.e. ion migration from the solid electrolyte onto the gas exposed electrode surfaces.

2. *Ion spillover.* The temperature is now increased to the point that ionic mobility on the electrode surfaces is high, so that now *there is ion spillover.* This is the usual case in solid state electrochemistry.

Oxygen anions are thus now attracted to the working electrode with the positive charge on the electrode which has been made positive by anodic polarization. Backspillover will continue until the charge is neutralized. Similarly oxygen anions will be repelled from the negatively charged or cathodically polarized electrode to enter into the YSZ lattice (spillover). The charges q_+ and q_- thus disappear and thus Ψ_W and Ψ_R vanish.

To prove this formally one has to examine again equation (7.17):

$$e\Psi_W - e\Psi_R = \underset{\text{fixed}}{eU_{WR}} + \underset{\text{variable}}{\Phi_R} - \underset{\text{variable}}{\Phi_W} \tag{7.22}$$

Now eU_{WR} is still fixed by the Nernst Eq. 7.16 but Φ_R and Φ_W are <u>variables.</u> They can change due to the spillover of ions which can now establish a constant electrochemical potential not only in the solid electrolyte but on the gas exposed electrode surfaces as well. They will change in such a way as to minimize the excess electrostatic energy of the system

$$E_E = (\Psi_W - \Psi_R)q_+ \tag{7.21}$$

This happens when $\Psi_W = \Psi_R$. It therefore follows from Equation (7.22) that:

$$eU_{WR} = \Phi_W - \Phi_R \tag{7.11}$$

Thus the key experimental observation Equation (7.11), is satisfied in presence of spillover. When an external overpotential ΔU_{WR} is applied, with a concomitant current, I, and O^{2-} flux I/2F, although U_{WR} is not fixed anymore by the Nernst equation but by the extrernally applied potential, still the work function Φ_W will be modified and Equations (7.11) and (7.12), will remain valid as long as ion spillover is fast relative to the electrochemical charge transfer rate I/2F.[21] This is the usual case in solid state electrochemistry (Figs. 7.3b, 7.3d) as experimentally observed (Figs. 5.35, 5.23, 7.4, 7.6-7.9).

The transition from case 1 (no ion spillover) to case 2 (ion spillover) is shown in Figure 7.11 for Pt and Ag electrodes deposited on YSZ. At low temperatures (no spillover) significant deviations from Equation (7.11) are observed. As temperature is increased these deviations vanish and Equation (7.11) is satisfied.

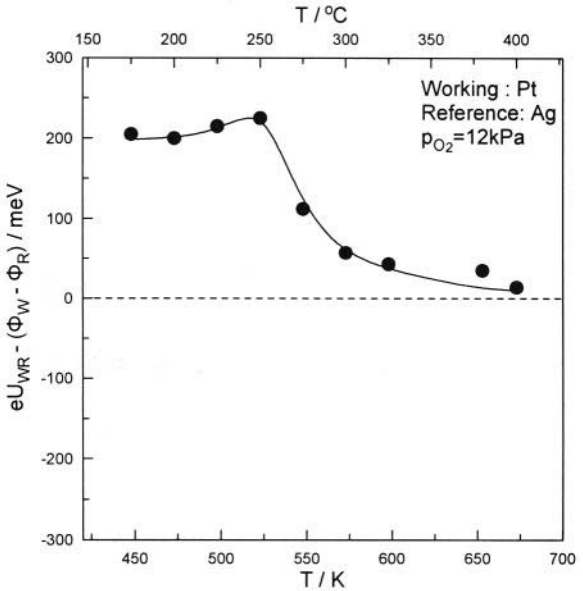

Figure 7.11. Effect of temperature on eU_{WR}-(Φ_W-Φ_R) for the system Pt(W)-Ag(R), deposited on YSZ and exposed to p_{O_2}=12 kPa, showing the transition from the T range of validity of Equation (7.11) (T>570 K, fast O^{2-} spillover-backspillover) to the T range of significant deviations from Equation (7.11) (T<550 K, slow or negligible O^{2-} spillover-backspillover).[21] Reprinted with permission from The Electrochemical Society.

7.5 DEFINITION AND PROPERTIES OF THE ABSOLUTE POTENTIAL SCALE IN SOLID ELECTROCHEMISTRY

The same conceptional approach used in aqueous electrochemistry to define "absolute" electron potentials can be used in solid state electrochemistry. Thus if one chooses as the zero level an electron just outside the solid electrolyte surface, which has been shown[14-16] by Trasatti to be the most realistic choice in aqueous electrochemistry, one has:

$$eU_W(\text{abs}) = \Phi_W + e\Psi_W - e\Psi_S \tag{7.6}$$

$$eU_W(\text{abs}) = \Phi_{W,0} + \Delta\Phi_W = \Phi_W \tag{7.7}$$

Experiment (Chapter 5 and Figs. 7.6 to 7.8) has clearly shown that for the gas exposed electrode surfaces in solid state electrochemistry one has:

$$eU_{WR} = \Phi_W - \Phi_R \tag{7.11}$$

$$\Delta(eU_{WR})=\Delta\Phi_W \tag{7.12}$$

Thus the absolute electron potential $U_W(abs)$ in solid state electrochemistry can indeed be simply defined by the equation:

$$eU_W(abs)= \Phi_W = \Phi_{W,0} + \Delta\Phi_W \tag{7.22}$$

where Φ_W is the work function of the gas exposed catalyst electrode surface. The zero energy level, as already noted, is that of an electron at rest near the electrolyte surface.

Also by the definition of the work function, Φ_W, the zero energy level is also that of an electron at rest near the surface of the gas exposed electrode surface. The observation that these two reference levels coincide underlines some of the similarities between backspillover-modified electrodes in solid state electrochemistry and emersed electrodes in aqueous electrochemistry, both leading to the experimental equation (7.12). This is not too surprising since the Debye length in solid electrolytes in contact with metals is of the order of 1 Å[35] so that a monolayer of backspillover ions on the metal/gas interface is more than sufficient to simulate the metal/solid electrolyte double layer, as also confirmed via XPS[24] from the energetic indistinguishability of O^{2-} at the metal/gas and metal/solid electrolyte interfaces (Fig. 5.35). The presence of the overall neutral effective double layer on the gas exposed electrode surface, confirmed experimentally by numerous experimental techniques including XPS, TPD and STM,[22,26-29,35,36] corresponds exactly to the "gedanken" experiment of Trasatti to define $U^o_{H_2}(abs)$ in aqueous electrochemistry[16] and to the actual emersed electrode experimental studies.[9,11,12,18,19] It is worth reminding again however some subtle differences between solid state electrochemistry and the case of emersed electrodes in aqueous electrochemistry. In the latter case equation (7.12) has been proven experimentally[9,11,12,18,19] but not equation (7.11).

In analogy with equation (7.2) one can write:

$$U'_W\ (soe)=U_W(abs)-\ U^o_{O_2}(abs) \tag{7.23}$$

by defining a "standard oxygen electron" (soe) scale which is connected to the "standard hydrogen electrode scale" (she) via the equation:

$$U'_W\ (soe)=U_W(she)+[1.236+1.69\cdot10^{-4}T-6.11\cdot10^{-5}T\ln T+1.81\cdot10^{-8}T^2-1.14\cdot10^{-12}T^3] \tag{7.24}$$

where the term in brackets is the standard open-circuit potential of a fuel cell operating on the reaction:

$$H_2(g)+1/2O_2(g) \leftrightarrow H_2O(g) \tag{7.25}$$

The use of the soe scale is more convenient than the she scale in solid state electrochemistry since YSZ (an O^{2-} conductor) is the most commonly used solid electrolyte and the metal/O_2 (p_{O_2}=1 atm)/YSZ (soe) electrode is the most commonly used reference electrode in solid state electrochemistry.

Thus in order to utilize Eq. (7.23) and to work with absolute electrode potentials, one only needs to choose a reference temperature and to know $U^o_{O_2}$(abs).

It must be emphasized that the value of $U^o_{O_2}$(abs) which is given, via Eq. (7.22) by

$$U^o_{O_2}(abs) = \Phi^o/e \tag{7.26}$$

does not depend on the choice of the metal in contact with YSZ (8mol%Y_2O_3) and p_{O_2}=1bar. Indeed as experiment has shown (Fig. 7.6 to 7.7) this is the case, at least for Pt, Au and Ag electrodes and the suggested value is:

$$U^o_{O_2}(abs) = \Phi^o/e = 5.14 \pm 0.05 \text{ V} \tag{7.27}$$

at 673 K (Figs. 7.6b, 7.7b). This value is computed from the experimental value of 5.07 ± 0.05 V obtained (Figs. 7.6b, 7.7b) for $p_{O_2}=1.2\cdot10^{-2}$ atm via the corresponding Nernst correction

$$U^o_{O_2}(abs, p = 1atm) = U^o_{O_2}(abs, p = 1.2\cdot10^{-2}\,atm) + (RT/4F)\ln(1.2\cdot10^{-2})^{-1} \tag{7.28}$$

The last term contributes 0.065 V at 673 K. It should be noted that if one wishes to use another reference temperature, then the Φ measurements of Figs. 7.6, 7.7 and 7.8 have to be repeated at this temperature but it is known that the temperature dependence of $U^o_{O_2}$(abs), and thus Φ^o, is rather weak, i.e. of the order of 0.1 V for every 500 K.[47]

There is an important point regarding the absolute standard oxygen electrode scale defined by Eq. (7.27). The $U^o_{O_2}$(abs) value is defined by the equilibrium:

$$O_2(g)(p=1atm)+4e^-(M) \rightleftharpoons 2O^{2-}(YSZ) \tag{7.29}$$

Thus the activity of O^{2-} is fixed at its value for YSZ. Contrary to aqueous electrochemistry where the activity of the H^+ can be varied (via the pH) and the she scale corresponds to p_{H_2}=1 atm and a_{H^+}=1 (pH=0), in solid state

electrochemistry the activity of O^{2-} is fixed at its value corresponding to (8mol% Y_2O_3 doped ZrO_2) YSZ. Thus if one were to use another solid electrolyte, such as CaO doped ZrO_2 (CSZ) with a different $a_{O^{2-}}$ value or even YSZ with a different level of Y_2O_3 doping, then one would observe a small shift in $U^{o}_{O_2}$(abs) and Φ^{o}.

Figure 7.12 shows the relationship between the standard oxygen electrode (soe) scale of solid state electrochemistry, the corresponding standard hydrogen electrode (she) scale of solid state electrochemistry, the standard hydrogen electrode (she) scale of aqueous electrochemistry, and the physical absolute electrode scale. The first two scales refer to a standard temperature of 673.15 K, the third to 298.15 K. In constructing Figure 7.12 we have used the she aqueous electrochemical scale as presented by Trasatti.[14]

What is the practical usefulness of the soe scale of solid state electrochemistry? As in aqueous electrochemistry, it is limited but not trivial. When a potential U_{WR} of, e.g. –300 mV is measured in an YSZ solid state cell at 673 K vs a reference electrode at $p_{O_2}=1$ atm, the implication is that the work function of the reference electrode is 5.14 eV and that of the working electrode 4.84 eV *regardless of the material of the two electrodes.*

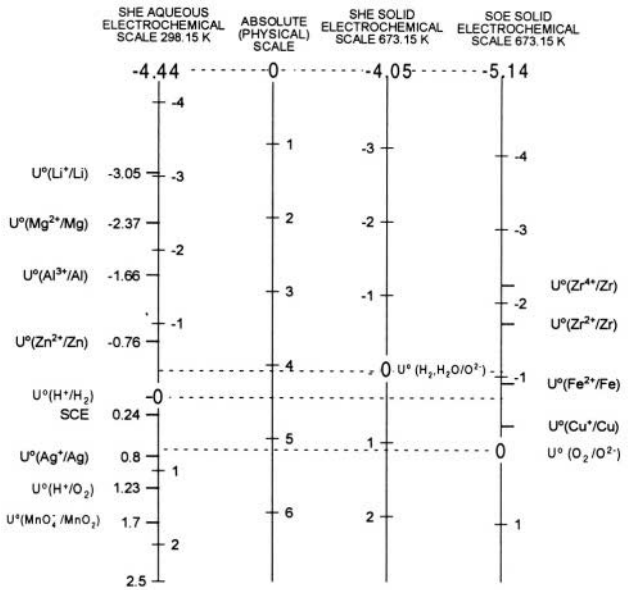

Figure 7.12. Relationship between the standard hydrogen electrode (she) scale of aqueous electrochemistry, the physical absolute electrode scale, the standard hydrogen electrode (she) scale of solid electrochemistry and the corresponding standard oxygen electrode (soe) scale of solid state (YSZ) electrochemistry.[21] Reprinted with permission from The Electrochemical Society.

It is worth emphasizing, however, that if one uses another solid electrolyte (e.g. 6 mol% Y_2O_3 doped YSZ) then the above numbers will, in general, change (because the activity of O^{2-} in the solid electrolyte will change). This is equivalent with the change in potential with pH at fixed p_{H_2} in aqueous electrochemistry. In that case the standard state is pH=0 ($a_{H^+}=1$). In the soe scale it is the activity of O^{2-} in 8mol%Y_2O_3-stabilized-ZrO_2, $a_{O^{2-}}$ (YSZ), to which one can assign, arbitrarily the value one. Then the activity of O^{2-} in other solid electrolytes can be determined by measuring the work function of electrodes deposited on them at 673 K and $p_{O_2}=1$ arm and using the equilibrium (7.29). By definition the measured work function value will always equal the absolute potential of the electrode.

It is thus clear from the previous discussion that the absolute electrode potential is not a property of the electrode material (as it does not depend on electrode material) but is a property of the solid electrolyte and of the gas composition. To the extent that equilibrium is established at the metal-solid electrolyte interface the Fermi levels in the two materials are equal (Fig. 7.10) and thus $eU^{o}_{O_2}$(abs) also expresses the energy of transfering an electron from the Fermi level of the YSZ solid electrolyte, in equilibrium with $p_{O_2}=1$ atm, to a point outside the electrolyte surface. It thus also expresses the energy of "solvation" of an electron from vacuum to the Fermi level of the solid electrolyte.

In summary, the creation via ion spillover of an effective electrochemical double layer on the gas exposed electrode surfaces in solid electrolyte cells, which is similar to the double layer of emersed electrodes in aqueous electrochemistry, and the concomitant experimentally confirmed equation

$$eU_{WR}=\Phi_W-\Phi_R \tag{7.11}$$

allows one to directly establish an experimentally accessible absolute electrode potential scale in solid state electrochemistry. The actual values of this scale can be measured directly via work function measurements of the gas exposed electrode surfaces.

Equations (7.11) and (7.12) provide a firm basis for understanding the effect of Electrochemical Promotion but also provide an additional, surface chemistry, meaning to the emf of solid electrolyte cells in addition to its usual Nerstian one.

It is important to note that equation (7.11), and thus (7.12) is valid as long as the effective double layer is present at the metal/gas interfaces. Therefore equation (7.11) is valid *not only* under open-circuit conditions (which is the case for the Nernst equation) but also under closed-circuit conditions, provided, of course, that the working electrode effective double layer is not destroyed. Consequently the importance of equation (7.11) is by no means trivial.

7.6 POTENTIAL DISTRIBUTION IN A SOLID ELECTROLYTE CELL

Having defined the absolute electrode potential in solid state electrochemistry, one can then examine the potential and corresponding electron energy distribution in a solid electrolyte cell. To this end it is useful first to review some of the basics of a vacuum-semiconductor interface (Fig. 7.13). This is important as every solid electrolyte is at the same time a semiconductor of large (4-5 eV) band gap which allows for some electronic current at high temperatures and strongly reducing conditions. Thus figure 7.13 shows the definitions of ionization potential, work function, Fermi level, conduction level, valence level and χ-potential without (a) and with (b) band bending at the semiconductor-vacuum interface.

One can then examine YSZ solid electrolyte cell with metal electrodes, M and M′, both covered by backspillover $O^{\delta-}$ ions and exposed to two different p_{O_2} values under open-circuit conditions. How do μ_{O_2}, $\bar{\mu}_{O^{2-}}$ and $\bar{\mu}$ (=E_F) vary across the cell? And how do they relate to the conduction level E_C and valence level E_V of YSZ?

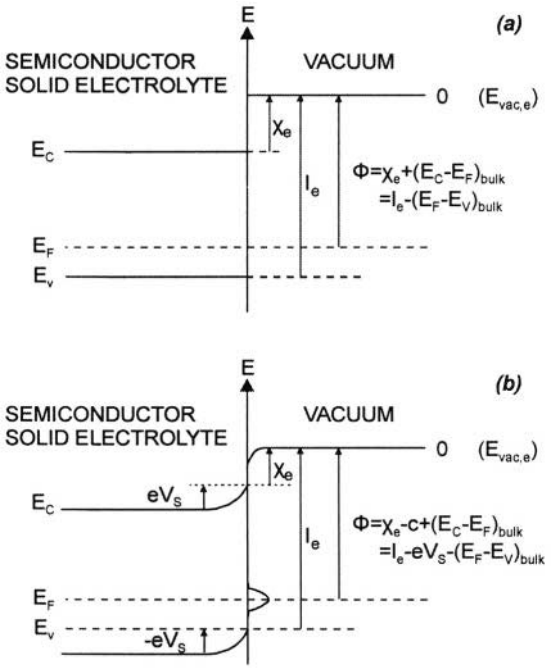

Figure 7.13. The definitions of ionization potential, I_e, work function, Φ, Fermi level, E_F, conduction level, E_C, valence level E_V, and χ-potential χ_e without (a) and with (b) band bending at the semiconductor-vacuum interface.

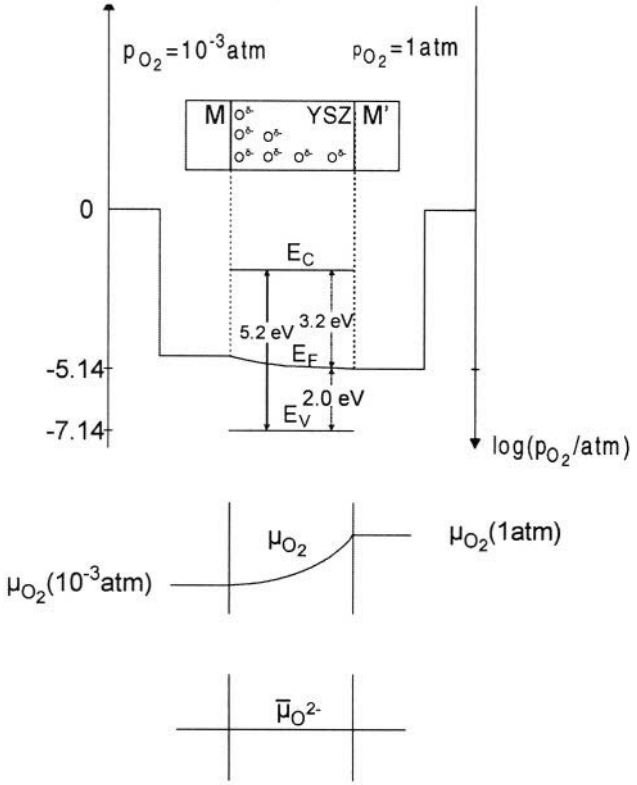

Figure 7.14. Schematic representation of the spatial variation of electrode potential, chemical potential of oxygen and electrochemical potential of O^{2-} for the cell O_2, M|YSZ|M', O_2 (=1 atm).

The answer is depicted schematically in Fig. 7.14 for the cell $O_2(p_{O_2}=10^{-3}\text{atm})$, M|YSZ|M', $O_2(p_{O_2}=1\text{atm})$.

In constructing this diagram[47-49] the following points have been taken into account:

1. The ionization energy, I_e, for YSZ is 7.14 eV. This defines the location of the valence band, E_v, in relation to the zero energy level.
2. The energy gap, E_c-E_v, between the conduction and the valence band for YSZ is 5.2 eV. This defines the location of the conduction band, E_C=-1.94 eV, again in relation to the zero energy level.
3. The Fermi level, E_F, ($=\bar{\mu}$) in YSZ is defined by the equilibrium:

$$O_2(g)+4e^- \rightleftharpoons 2O^{2-}(YSZ) \tag{7.29}$$

This implies:

$$\mu_{O_2} + 4\bar{\mu} = 2\bar{\mu}_{O^{2-}}\,(\text{YSZ}) \tag{7.30}$$

or, equivalently:

$$E_F \equiv \bar{\mu} = \left((2\bar{\mu}_{O^{2-}} - \mu^{o}_{O_2})/4\right) - (RT/4)(\ln p_{O_2}) \tag{7.31}$$

Equation 7.31 is in excellent agreement with experiment,[48-50] which has shown that:

$$\Phi_{YSZ} \equiv -E_F = C(T) + (RT/4)(\ln p_{O_2}) \tag{7.32}$$

Equation (7.29) is the same equation used to define the absolute electrode potential, thus E_F in the vicinity of the reference electrode (p_{O_2}=1 atm, Fig. 7.14) has to equal -5.14 eV at 400°C. This is indeed in good qualitative agreement with the work of Göpel and Wiemhöfer,[48-50] who used UPS in UHV to measure I_e and also (E_F-E_V) of YSZ at temperatures 800 to 1200 K and found Equation (7.31) to be valid, from which Equation (7.32) is immediately deduced. Their results indicate that the parameter C(T) in Equation (7.32) varies indeed between 5.0 and 5.35 eV, (Fig. 6 in ref. 49) as T is increased from 800 to 1200 K. This is indeed very good qualitative agreement with the value of 5.14 eV determined at atmospheric pressure[21] and measuring the work function of the electrodes rather than the E_F of YSZ itself as Göpel, Wiemhöfer and coworkers[48-50] did. Consequently at 400°C(=673 K) the value of C(T) in equation (7.32) must equal 5.14 eV, i.e. $eU^{0}_{O_2}$ (abs).

7.7 ABSOLUTE POTENTIAL OF SUPPORTED CATALYSTS

Equation (7.32) underlines the pinning of the Fermi levels of metal electrodes with the solid electrolyte and reminds the fact that the absolute electrode potential is a property of the solid electrolyte and of the gaseous composition but not of the electrode material.[21]

Consequently the absolute potential is a material property which can be used to characterize solid electrolyte materials, several of which, as discussed in Chapter 11, are used increasingly in recent years as high surface area catalyst supports. This in turn implies that the Fermi level of dispersed metal catalysts supported on such carriers will be pinned to the Fermi level (or absolute potential) of the carrier (support). As discussed in Chapter 11 this is intimately related to the effect of metal-support interactions, which is of central importance in heterogeneous catalysis.

REFERENCES

1. E. Gileadi, S.D. Argade, and J.O.M. Bockris, The Potential of Zero Charge of Platinum and its pH Dependence, *J. Phys. Chem.* **70**(6), 2044-2046 (1966).
2. J.O.M. Bockris, and S.U.M. Khan, Fermi levels in solution, *Appl. Phys. Lett.* **42**(1), 124-125 (1983).
3. A. Frumkin, and B. Damaskin, Real free solvation energy of an electron in a solution in equilibrium with the electrode and its dependence on the solvent nature, *J. Electroanal. Chem.* **79**, 259-266 (1977).
4. A.N. Frumkin, and B.B. Damaskin, Work function of solvated electrons (in Russian), *Dokl. Akad. Nauk. SSR.* **221**(2), 395-398 (1975).
5. E. Kanevsky, (in Russian), *Zhurnal Fizicheskoi Khimii (Russian Journal of Physical Chemistry)* **24**, 1511-1514 (1950).
6. H. Reiss, and A. Heller, The absolute potential of the standard hydrogen electrode: A new estimate, *J. Phys. Chem.* **89**, 4207 (1985).
7. R. Parsons, Standard potentials in aqueous solution, A.J. Bard, R. Parsons, and J. Jordan, eds., Marcel Dekker, New York (1985).
8. R. Gomer, and G. Tryson, An experimental determination of absolute half-cell emf's and single ion free energies of solvation, *J. Chem. Phys.* **66**, 4413-4424 (1977).
9. W.N. Hansen, and G.J. Hansen, Reference States for Absolute Half-Cell-Potentials, *Physical Review Letters* **59**(9), 1049-1052 (1987).
10. H. Gerischer, and W. Ekardt, Fermi levels in electrolytes and the absolute scale of redox potentials, *Appl. Phys. Lett.* **43**(4), 393-395 (1983).
11. D.L. Rath, and D.M. Kolb, Continuous work function monitoring for electrode emersion, *Surf. Sci.* **109**, 641-647 (1981).
12. D.M. Kolb, UHV Techniques in the Study of Electrode Surfaces, *Zeitschrift fuer Physikalische Chemie Neue Folge* **154**, 179-199 (1987).
13. A.D. Battisti, and S. Trasatti, *Journal of Chim. Phys.* **74**, 60 (1977).
14. S. Trasatti, The absolute electrode potential: An explanatory note, *Pure and Applied Chemistry* **58**, 955-966 (1986).
15. S. Trasatti, The "absolute" electrode potential - The end of the story, *Electrochim. Acta* **35**, 269-271 (1990).
16. S. Trasatti, Structure of the metal/electrolyte solution interface: New data for theory, *Electrochim. Acta* **36**, 1659-1667 (1991).
17. E.M. Stuve, A. Krasnopoler, and D.E. Sauer, Relating the in-situ, ex-situ, and non-situ environments in surface electrochemistry, *Surf. Sci.* **335**, 177-185 (1995).
18. E.R. Koetz, H. Neff, and K. Mueller, A UPS, XPS and work function study of emersed silver, platinum and gold electrodes, *J. Electroanal. Chem.* **215**, 331-344 (1986).
19. Z. Samec, B.W. Johnson, and K. Doblhofer, The absolute electrode potential of metal electrodes emersed from liquid electrolytes, *Surf. Sci.* **264**, 440-448 (1992).
20. J.O.M. Bockris, and S.D. Argade, Work function of metals and the potential at which they have zero charge in contact with solutions, *J. Chem. Phys.* **49**(11), 5133 (1968).
21. D. Tsiplakides, and C.G. Vayenas, Electrode work function and absolute potential scale in solid state electrochemistry, *J. Electrochem. Soc.* **148**(5), E189-E202 (2001).
22. D. Kek, M. Mogensen, and S. Pejovnik, A Study of Metal (Ni, Pt, Au)/Yttria-Stabilized Zirconia Interface in Hydrogen Atmosphere at Elevated Temperature, *J. Electrochem. Soc.* **148**(8), A878-A886 (2001).

23. W. Zipprich, H.-D. Wiemhöfer, U. Vöhrer, and W. Göpel, In-situ Photoelectron-Spectroscopy of Oxygen Electrodes on Stabilized Zirconia, *Ber. Buns. Phys. Chem.* **99**, 1406-1413 (1995).
24. S. Ladas, S. Kennou, S. Bebelis, and C.G. Vayenas, Origin of Non-Faradaic Electrochemical Modification of Catalytic Activity, *J. Phys. Chem.* **97**, 8845-8847 (1993).
25. A. Palermo, M.S. Tikhov, N.C. Filkin, R.M. Lambert, I.V. Yentekakis, and C.G. Vayenas, Electrochemical Promotion of NO Reduction by CO and by Propene, *Stud. Surf. Sci. Catal.* **101**, 513-522 (1996).
26. S.G. Neophytides, and C.G. Vayenas, TPD and Cyclic Voltammetric Investigation of the Origin of Electrochemical Promotion in Catalysis, *J. Phys. Chem.* **99**, 17063-17067 (1995).
27. D. Tsiplakides, and C.G. Vayenas, Temperature Programmed Desorption of Oxygen from Ag films interfaced with Y_2O_3-doped ZrO_2, *J. Catal.* **185**, 237-251 (1999).
28. M. Makri, C.G. Vayenas, S. Bebelis, K.H. Besocke, and C. Cavalca, Atomic resolution STM imaging of Electrochemically Controlled Reversible Promoter Dosing of Catalysts, *Surf. Sci.* **369**, 351-359 (1996).
29. A.D. Frantzis, S. Bebelis, and C.G. Vayenas, Electrochemical promotion (NEMCA) of CH_4 and C_2H_4 oxidation on Pd/YSZ and investigation of the origin of NEMCA via AC impedance spectroscopy, *Solid State Ionics* **136-137**, 863-872 (2000).
30. J. Poppe, S. Voelkening, A. Schaak, E. Schuetz, J. Janek, and R. Imbihl, Electrochemical promotion of catalytic CO oxidation on Pt/YSZ catalysts under low pressure conditions, *Phys. Chem. Chem. Phys.* **1**, 5241-5249 (1999).
31. C.G. Vayenas, S. Bebelis, and S. Ladas, Dependence of Catalytic Rates on Catalyst Work Function, *Nature* **343**, 625-627 (1990).
32. C.G. Vayenas, On the work function of the gas exposed electrode surfaces in solid state electrochemistry, *J. Electroanal. Chem.* **486**, 85-90 (2000).
33. C.G. Vayenas, and D. Tsiplakides, On the work function of the gas-exposed electrode surfaces in solid state electrolyte cells, *Surf. Sci.* **467**, 23-34 (2000).
34. A. Frantzis, and C.G. Vayenas, in preparation (2001).
35. C.G. Vayenas, M.M. Jaksic, S. Bebelis, and S.G. Neophytides, The Electrochemical Activation of Catalysis, in *Modern Aspects of Electrochemistry,* J.O.M. Bockris, B.E. Conway, and R.E. White, eds., Kluwer Academic/Plenum Publishers, New York (1996), pp. 57-202.
36. C.G. Vayenas, S. Ladas, S. Bebelis, I.V. Yentekakis, S. Neophytides, J. Yi, C. Karavasilis, and C. Pliangos, Electrochemical promotion in catalysis: Non-Faradaic electrochemical modification of catalytic activity, *Electrochim. Acta* **39**(11/12), 1849-1855 (1994).
37. J.O' M. Bockris, and S.U.M. Khan, *Surface Electrochemistry: A Molecular Level Approach,* Plenum Press, New York (1993).
38. R. Lewis, and R. Gomer, Adsorption of Oxygen on Platinum, *Surf. Sci.* **12**, 157-176 (1968).
39. S. Ladas, S. Bebelis, and C.G. Vayenas, Work Function Measurements on Catalyst Films subject to in-situ Electrochemical Promotion, *Surf. Sci.* **251/252**, 1062-1068 (1991).
40. J. Nicole, D. Tsiplakides, S. Wodiunig, and C. Comninellis, Activation of catalyst for gas-phase combustion by electrochemical pretreatment, *J. Electrochem. Soc.* **144**(12), L312-L314 (1997).
41. H.L. Skriver, and N.M. Rosengaard, Ab initio work function of elemental metals, *Physical Review B* **45**(16), 9410-9412 (1992).

42. J. Nicole, *PhD Thesis,* EPFL (1999).
43. C.A. Cavalca, *PhD Thesis,* Yale University (1995).
44. J. Poppe, A. Schaak, J. Janek, and R. Imbihl, Electrochemically Induced Surface Changes on Microstructured Pt Films on a solid YSZ Electrolyte, *Ber. Buns. Phys. Chem.* **102**, 1019-1022 (1998).
45. N.G. Torkelsen, and S. Raaen, Work function variations and oxygen conduction in a $Pt/ZrO_2(Y_2O_3)/Pt$ solid electrolyte cell, *Appl. Surf. Sci.* **93**, 199-203 (1996).
46. D.A. Emery, P.H. Middleton, and I.S. Metcalfe, The effect of electrochemical current pumping on the work function of solid electrolyte supported catalysts, *Surf. Sci.* **405**, 308-315 (1998); Electrochemical enhancement of CO oxidation over YSZ supported Pt catalysts I&II, *J. Electrochem. Soc.* **146**(6), 2188-2193 (1999), ibid **146**(6), 2194-2198 (1999).
47. I. Riess, and C.G. Vayenas, Fermi level and potential distribution in solid electrolyte cells with and without ion spillover, *Solid State Ionics,* in press (2001).
48. K. Schindler, D. Schmeisser, U. Vöhrer, H.-D. Wiemhöfer, and W. Göpel, Spectroscopic and electrical studies of Y_2O_3-stabilized-ZrO_2 for oxygen sensors, *Sensors and Actuators* **17**, 555-568 (1989).
49. W. Göpel, and H.-D. Wiemhöfer, Electrode kinetics and interface analysis of solid electrolytes for fuel cells and sensors, *Ber. Buns. Phys. Chem.* **94**, 981-987 (1990).
50. H.-D. Wiemhöfer, and U. Vöhrer, Spectroscopy and Thermodynamics of electrons in Yttria-stabilized Zirconia, *Ber. Buns. Phys. Chem.* **96**, 1646-1652 (1992).

CHAPTER 8

ELECTROCHEMICAL PROMOTION WITH O^{2-} CONDUCTORS

8.1 THE USE OF O^{2-} CONDUCTORS

Most electrochemical promotion studies have been carried out so far using 8 mol% Y_2O_3 in ZrO_2(YSZ), an O^{2-} conductor, as the solid electrolyte. The nature of the promoting species, $O^{\delta-}$, is reasonably well established via in situ XPS, TPD and cyclic voltammetric studies as analyzed in Chapter 5. This type of promotion is unique, in that the promoting species, $O^{\delta-}$, cannot form via gas phase adsorption of oxygen. The promotional action of $O^{\delta-}$ is not limited to oxidation reactions but is also important in hydrogenation and dehydrogenation reactions.

8.1.1 Complete Oxidation Reactions

8.1.1.1 Ethylene Oxidation on Pt

The kinetics and mechanism of this reaction have been studied for years on Pt films deposited on doped ZrO_2.[1-5] It has been found that at temperatures above 280°C the open-circuit catalytic kinetics can be described quantitatively by the rate expression

$$r_0 = kk_{ad}p_{C_2H_4}p_{O_2}/(kp_{C_2H_4} + k_{ad}p_{O_2}) \tag{8.1}$$

and that the activity a_O of atomic oxygen on the Pt surface is proportional to the ratio $p_{O_2}/p_{C_2H_4}$.[1,5] Both of these observations had been interpreted quantitatively by the kinetic scheme:

$$\frac{1}{2}\left\{\begin{array}{l} O_2(g) \xrightarrow{k_{ad}} O_2(a) \\ O_2(a) \rightarrow 2O(a) \end{array}\right\} \tag{8.2}$$

$$C_2H_4(g) + O(a) \xrightarrow{k} P \xrightarrow{5/2O_2} 2CO_2 + 2H_2O \tag{8.3}$$

where $O_2(a)$ is a molecularly adsorbed precursor state with a negligible coverage[1,5] and P is a reactive intermediate[1,5] which is rapidly oxidized by gaseous or adsorbed oxygen O(a).

The rates of steps (8.2) and (8.3) can be written, respectively, as:

$$r = k_{ad}\, p_{O_2}\, (1-\theta_O) \tag{8.4}$$

$$r = k\, p_{C_2H_4}\theta_O \tag{8.5}$$

where θ_O is the coverage of chemisorbed oxygen. By equating these two expressions, one obtains both the experimental rate equation (8.1) and also, assuming a Langmuir isotherm for atomic oxygen chemisorption, the proportionality between a_O and $p_{O_2}/p_{C_2H_4}$.[1,5] The oxygen coverage θ_O can be computed from:

$$\theta_O = 1/(1 + k p_{C_2H_4}/k_{ad} p_{O_2}) \tag{8.6}$$

On the fuel-lean side ($k_{ad}p_{O_2} \gg k p_{C_2H_4}$) the oxygen coverage is near unity and step (8.3) is the rate limiting step (rls). Thus equation (8.1) reduces to:

$$r_0 = k_{ad} p_{C_2H_4} \tag{8.7}$$

On the fuel-rich side ($k_{ad}p_{O_2} \ll k p_{C_2H_4}$) θ_O is near zero, the oxygen adsorption step is the rls and equation (8.1) reduces to:

$$r_0 = k_{ad} p_{O_2} \tag{8.8}$$

It turns out[1,5] that varying U_{WR} and Φ cause dramatic (up to sixty-fold) increases in k but have practically no effect on k_{ad}. Thus NEMCA is much more pronounced on the fuel-lean side, i.e. when equation (8.7) is valid. This was shown in Fig. 4.24 which depicts the effect of the $p_{O_2}/p_{C_2H_4}$ ratio in the well-mixed reactor (CSTR) on the rate under open-circuit conditions and when U_{WR} is set at +1 V. There is a sixtyfold increase in the rate for high $p_{O_2}/p_{C_2H_4}$ values.

It was found[1] that the kinetic constant k depends on Φ according to:

$$\ln(k/k_0)=\alpha e(\Phi-\Phi^*)/k_bT \quad (8.9)$$

and that the rate expression equation (8.1) remains valid under NEMCA conditions as well (Fig. 8.2) with k given from equation (8.9).

Therefore NEMCA does not induce a change in reaction mechanism, but only a pronounced increase in the rate constant k. In the context of the double layer kinetic model discussed in Chapter 6, the rate constant k is not an elementary step constant but rather equals the product $k_R k_{C_2H_4}$ where k_R is the intrinsic rate constant and $k_{C_2H_4}$ is the adsorption equilibrium constant of C_2H_4 (=D) which is a strong increasing function of Φ. For high $\Delta\Phi$ values when k has become sufficiently large, then NEMCA causes a change in the rate limiting step (rls) (Fig. 8.1), i.e., NEMCA causes oxygen adsorption to become rate limiting even under fuel-lean conditions. All this is described quantitatively by equations (8.1) and (8.9).

The fact that the oxygen adsorption kinetic constant k_{ad} is insensitive to changes in U_{WR} and Φ may provide an explanation for the oxygen isotope exchange results of Sobyanin and coworkers.[6] These authors reported that changing U_{WR} has no effect on the oxygen isotope exchange kinetics on Pt/YSZ at temperatures 450° to 510°C and p_{O_2} up to 0.05 kPa.[6] On the basis of this they questioned the variation in heats of adsorption with U_{WR} and Φ and formulated a chain mechanism to explain NEMCA.[7] As shown in Chapter 4 (Fig. 4.47) the binding strength of atomic oxygen on Pt/YSZ decreases by more than 0.6 eV with increasing U_{WR} and Φ. If, however, the rate limiting step of the oxygen exchange process is oxygen adsorption rather than desorption, as suggested by the positive order dependence of the isotope exchange rate on p_{O_2},[6] then the insensitivity of the oxygen isotope exchange rate on U_{WR} can be understood. The oxygen isotope exchange[6] is an interesting approach to study NEMCA and is certainly worth studying over broader experimental conditions.

Thus in order to rationalize the NEMCA behaviour of the ethylene oxidation system one needs only to concentrate on the kinetic constant k and on its dependence on Φ. As shown on Figure 8.3 the exponential increase in k with Φ is accompanied by a concomitant significant decrease in activation energy E and in the preexponential factor k^o defined from:

$$k=k^o\exp(-E/k_bT) \quad (8.10)$$

As shown on Figure 8.3 it is:

$$E=E^0+\alpha_H\Delta\Phi \quad (8.11)$$

and

$$k_bT\ln(k^o/k_0^o)=\alpha_S\Delta\Phi \quad (8.12)$$

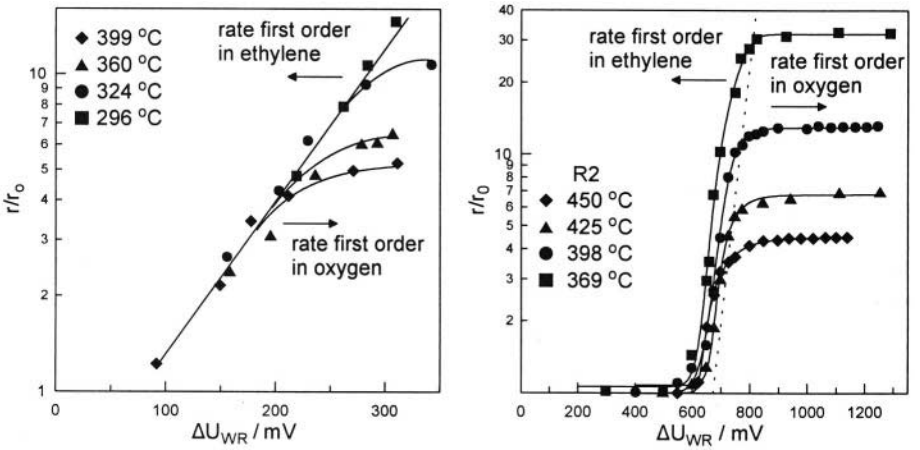

Figure 8.1. Effect of catalyst overpotential η on the rate and reaction order of C_2H_4 oxidation on two Pt catalyst films, labeled R1 and R2. For R_1, p_{O_2}=4.8 kPa and $p_{C_2H_4}$=0.4 kPa. For R_2, p_{O_2}=6.4 kPa and $p_{C_2H_4}$=0.4 kPa.[1]

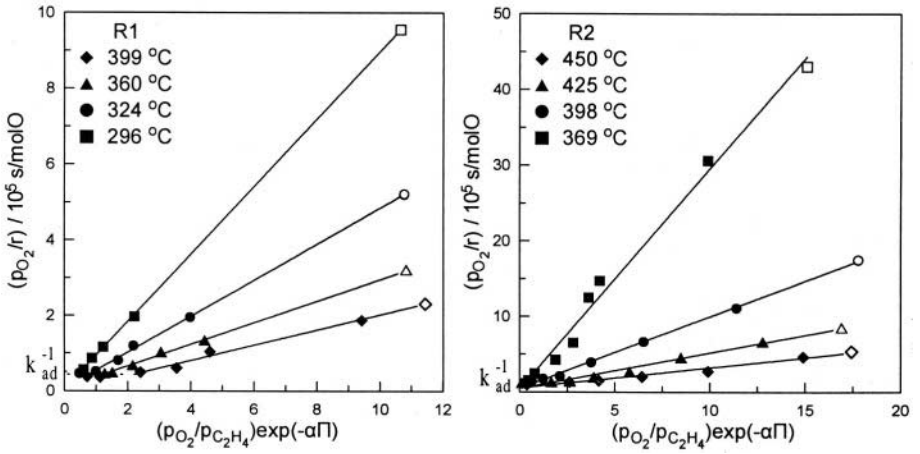

Figure 8.2. Plot of the effect of gaseous composition and of $\Pi=(\Phi-\Phi^*)/k_bT$ during C_2H_4 oxidation on two Pt catalyst films, labeled R1 and R2, showing that the rate expression given by (Eq. 8.1) is valid both under open-circuit conditions (open symbols) and also under NEMCA conditions (filled symbols).[1] Reprinted with permission from Academic Press.

where for the particular Pt catalyst film shown on the figure, α_H=-1 and α_S=-0.4. These values satisfy well the equality $\alpha=\alpha_S-\alpha_H$. Some significant variations in these values have been observed with other Pt films in the same study,[1,5] but with all films the equality $\alpha=\alpha_S-\alpha_H$ was satisfied within ±20%.

The linear decrease in activation energy with Φ and, in fact, with a slope α_H=-1 can be understood as follows: Since chemisorbed oxygen is an electron

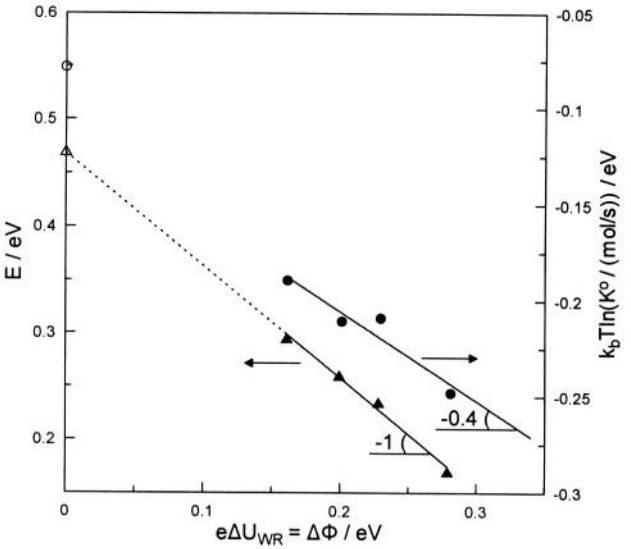

Figure 8.3. Effect of catalyst overpotential ΔU_{WR} and work function Φ on the activation energy E and preexponential factor k^o of the kinetic constant k of C_2H_4 oxidation on Pt. T is the mean operating temperature.[1] Conditions as in Fig. 8.1. Reprinted with permission from Academic Press.

acceptor, increasing Φ weakens the Pt=O chemisorptive bond and strengthens the chemisorptive bond of C_2H_4. Since the surface is predominantly covered by O, the activation energy decreases, in excellent agreement with the Polanyi principle.[8] At the same time the preexponential factor also decreases. This happens for two reasons. First because, as analyzed in Chapter 6, increasing Φ causes a decrease in the coverage of O. Second because the remaining chemisorbed oxygen becomes more mobile and weakly bonded and consequently its translational and vibrational entropy increases. This also causes a decrease in the preexponential factor according to classical transition-state theory.[8]

In order to attempt a more quantitative description one may start from the early theoretical considerations of Boudart[9] who was first to tackle the problem of predicting the change in heats of adsorption with changing work function Φ. According to his early semiempirical electrostatic model when the work function of a surface changes by $\Delta\Phi$ then the heat of adsorption, $-\Delta H_{ad}$, of covalently bonded adsorbed species should change by:

$$\Delta(-\Delta H_{ad}) = -(n/2)\Delta\Phi \tag{8.13}$$

where n is the number of valence electrons of the adatom taking part in the bonding. Since in the present case n=2, Boudart's correlation reads:

$$\Delta(-\Delta H_{ad}) = -\Delta\Phi \tag{8.14}$$

As shown in Chapter 4 (section 4.5.9.2), Equation (8.14) can also be derived via a rigorous electrostatic model which takes into account the presence of the effective double layer on the catalyst surface and gives in general:

$$\Delta E_{d,j} = \Delta(-\Delta H_{ad,j}) = (\lambda_j/2)\Delta\Phi \tag{4.58}$$

where, λ_j is the partial charge transfer parameter of adsorbate j. Thus assuming λ_j=-2 one obtains equation (8.14).

Furthermore, to the extent that the nature of the activated complex of the catalytic step involving cleavage of the Pt=O bond (equation 8.3) is not changing with varying Φ, one can use Polanyi's relationship,[8] i.e.:

$$\Delta E = \Delta(-\Delta H_{ad}) \tag{8.15}$$

which, in view of equation (8.4) yields:

$$\Delta E = -\Delta\Phi \tag{8.16}$$

which is in excellent agreement with experiment (Fig. 4.40 and equation 8.11).

Qualitatively one can reach the same conclusions, but not a linear E vs Φ relationship, via the semi-rigorous approach of Shustorovich[10] who expresses the metal-adsorbate bond strength in terms of the differences E_F-ε_A and ε_A^* - E_F, where E_F is the metal Fermi level (the variation in which is linear with Φ in NEMCA experiments), ε_A is the energy of the higher occupied (σ or π) adsorbate orbital, and ε_A^* is the energy of the lowest unoccupied (σ^* or π^*) adsorbate orbital. Both ε_A and ε_A^* refer to the adsorbing molecule before adsorption and thus before the concomitant broadening of the bonding and antibonding energy levels. Recent rigorous ab initio calculations of Pacchioni[11,12] for oxygen chemisorbed on Cu (100) and Pt(111) have shown similar linear dependence as discussed in Chapter 5.

In summary the oxidation of C_2H_4 on Pt is one of the most thoroughly studied reactions from the point of view of NEMCA and, in view of its rather simple mechanistic scheme, one of the most thoroughly understood systems. Under fuel-lean conditions the reaction is a classical example of global promotional rule G1, i.e. electrophobic behaviour.

8.1.1.2 Ethylene Oxidation on Rh

The oxidation of C_2H_4 to CO_2 on Rh has been investigated[13] at temperatures 300° to 400°C. The reaction exhibits very strong electrophobic behaviour and the rate can be reversibly enhanced by up to 10,000% by

supplying O^{2-} to the catalyst via positive potential application (up to 1.5 V). This ρ value (~100) is among the highest obtained so far with NEMCA studies utilizing YSZ.

In Figure 4.14 we have seen a typical galvanostatic transient of this system. Positive current application ($I=400\ \mu A$) causes a 88-fold increase in catalytic rate ($\rho=88$). The rate increase is 770 times larger than the rate I/2F of O^{2-} supply to the catalyst ($\Lambda=770$). The NEMCA time constant τ is 40s in good qualitative agreement with the parameter $2FN_G/I=18s$.

Figure 8.4 shows the steady-state effect of p_{O_2} and imposed catalyst potential U_{WR} on the rate of C_2H_4 oxidation and compares the results with the open-circuit kinetics. The sharp rate decline for high p_{O_2} values is due to the formation of surface Rh oxide.[13] Increasing U_{WR} causes a significant increase in the oxygen partial pressure, $p^*_{O_2}$, where oxide forms and thus causes a dramatic increase in r for intermediate (1 to 2.5 kPa) p_{O_2} values. For low p_{O_2} values (reduced surface) the effect of U_{WR} is moderate with ρ values up to 2. For high p_{O_2} values ($p_{O_2} > p^*_{O_2}$, oxidized surface) U_{WR} has practically no effect on the rate.

The effect of $p_{C_2H_4}$ and U_{WR} on the rate of C_2H_4 oxidation is shown in Fig. 8.5. Increasing U_{WR} causes a pronounced decrease in the ethylene partial pressure, $p_{C_2H_4}$, necessary to reduce the surface Rh oxide and thus a dramatic, up to 100-fold, increase in reaction rate for intermediate $p_{C_2H_4}$ values ($\rho=100$).

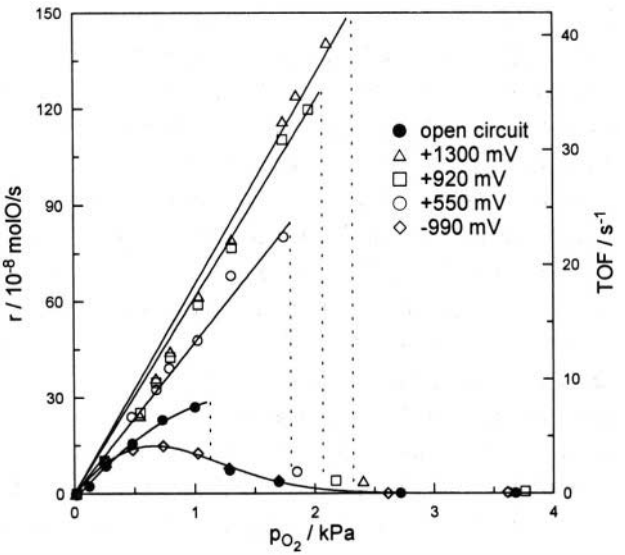

Figure 8.4. Effect of p_{O_2} and imposed catalyst potential U_{WR} on the rate of C_2H_4 oxidation on Rh/YSZ.[13] T = 350°C, $p_{C_2H_4}$=5 kPa. Reprinted with permission from Academic Press.

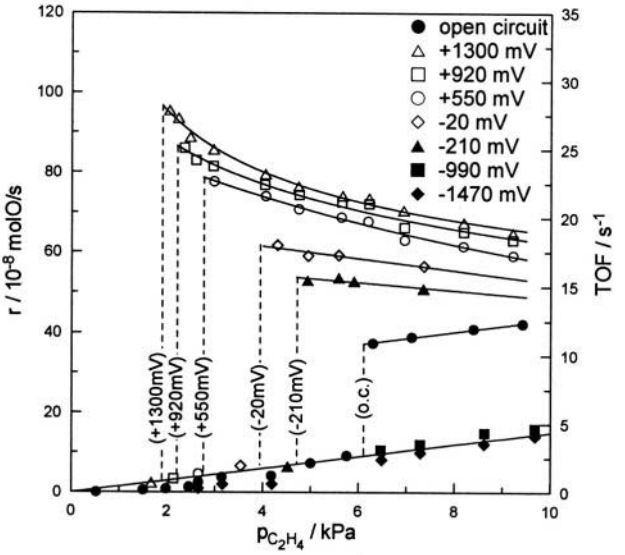

Figure 8.5. Effect of $p_{C_2H_4}$ and imposed catalyst potential U_{WR} on the rate of C_2H_4 oxidation on Rh/YSZ.[13] T=350°C, p_{O_2}=1.3 kPa. Reprinted with permission from Academic Press.

It is worth noting the change in the reaction order with respect to ethylene, from positive to negative, upon positive current application. This shows the pronounced increase in C_2H_4 coverage induced by the positive potential and concomitant destabilization of surface Rh oxide.[13]

Figures 8.6 and 8.7 show in detail the effect of U_{WR} and corresponding rate, I/2F, of O^{2-} supply at fixed gaseous composition. In the former case (Fig. 8.6) the gaseous composition was chosen such that the surface is, and remains, reduced with positive and negative current application. The rate variation is moderate as r/r_0 varies between 0.25 and 2. The Λ values are up to 15,000. In the latter case (Fig. 8.7) the gas composition is such that under open- circuit the surface is oxidized ($p_{O_2} > p^*_{O_2}$, $p_{C_2H_4} < p^*_{C_2H_4}$). At low temperatures (T=320°C) the surface remains oxidized over the whole U_{WR} range and the measured ρ and Λ values are moderate. At higher temperatures, positive currents and potentials lead to reduction of the surface Rh oxide and the rate enhancement is very pronounced, with Λ values up to 50,000 and ρ values up to 100. The observed steady-state multiplicity with respect to U_{WR} (Fig. 8.7) is due to Rh oxide decomposition in conjunction to the galvanostatic operation. Potentiostatic operation leads to steady-state multiplicity with respect to the current. Figure 8.8 shows that the activation energy E decreases linearly with U_{WR} and Φ with a slope of -0.5. The log of the preexponential factor r^o defined from:

$$r = r^o \exp(-E/k_bT) \tag{8.17}$$

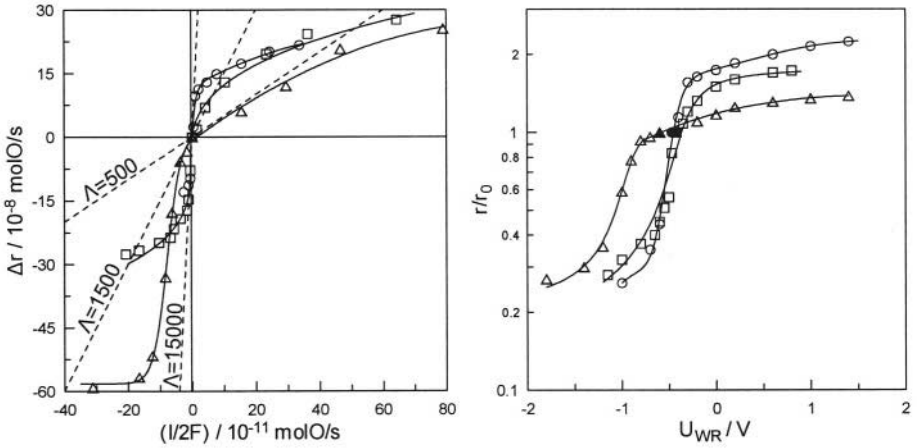

Figure 8.6. Effect of applied current (left) and corresponding catalyst potential U_{WR} (right) on the rate of C_2H_4 oxidation on a Rh surface which is reduced under open-circuit conditions.[13] p_{O_2}=1.3 kPa, $p_{C_2H_4}$=7.4 kPa. ○, T=320°C, r_0=1.74×10^{-7} mol/s; □, T=350°C, r_0=6.5×10^{-7} mol/s; △, T=370°C, r_0=8.4×10^{-7} mol/s; Filled symbols: open-circuit conditions. Reprinted with permission from Academic Press.

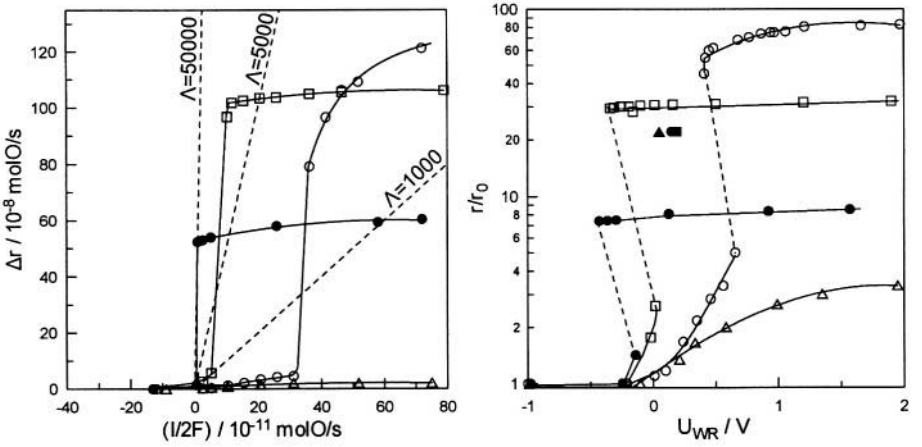

Figure 8.7. Effect of applied current (left) and corresponding catalyst potential U_{WR} (right) on the rate of C_2H_4 oxidation on a Rh surface which is oxidized under open-circuit conditions.[13] △, p_{O_2}=5 kPa, $p_{C_2H_4}$=2.5 kPa, T=320°C, r_0=0.87×10^{-8} mol/s; ○, p_{O_2}=5 kPa, $p_{C_2H_4}$=2.5 kPa, T=350°C, r_0=1.8×10^{-8} mol/s; □, p_{O_2}=5 kPa, $p_{C_2H_4}$=2.5 kPa, T=370°C, r_0=3.67×10^{-8} mol/s; ●, p_{O_2}=1.2 kPa, p_{C2H4}=3 kPa, T=350°C, r_0=9.6×10^{-8} mol/s.[13] *Reprinted with permission from* Academic Press.

also decreases linearly with U_{WR} and Φ[13] and as a result of this, in Fig. 4.38 we have seen a striking demonstration of the compensation effect with an isokinetic point at T_Θ=372°C. The compensation effect in heterogeneous catalysis has been the focal point of numerous studies and debates.[14,15] It is usually obtained from Arrhenius plots of several similar reactions on the same

catalyst or of several similar catalysts for the same reaction. In the present case it is obtained for one reaction and one catalyst by varying its potential or, equivalently, by varying the level of promoting species ($O^{\delta-}$) on its surface. Since the isokinetic point lies usually outside the temperature range of the kinetic investigation, some authors have even questioned the existence of a true compensation effect. The results of Fig. 4.38 are, consequently, rather rare and show clearly that the compensation effect is a real one.

It is worth noting that below the isokinetic point ($T < T_\Theta$) the reaction exhibits electrophobic behaviour, i.e. $\partial r/\partial U_{WR} > 0$, while for $T > T_\Theta$ the reaction becomes electrophilic. At $T = T_\Theta$ the NEMCA effect disappears (see also the curve for T=370°C in Fig. 8.6).

As shown in Fig. 8.8 the decrease in activation energy E with eU_{WR} and Φ is almost linear with a slope of -0.5. Also the logarithm of the preexponential factor r^o decreases linearly with eU_{WR} (Fig. 4.36) and upon plotting $k_bT_\Theta \ln(r^o/r_0^o)$, where r_0^o is the open-circuit preexponential factor, vs eU_{WR} the slope is again -0.5. The difference between the two parallel lines equals the open-circuit activation energy E^o, as can be shown easily.[13] As a result of Figs. 8.8 and 4.36 the logarithm of r^o increases linearly with E a slope of 18 eV^{-1} (Fig. 8.9).

The observed pronounced electrochemical promotion effect is due to the weakening of the Rh = O bond and the strengthening of the $Rh\text{-}C_2H_4$ bond with increasing U_{WR} and Φ. Increasing U_{WR} and Φ destabilizes the Rh=O bond, due to the increasing coverage of backspillover oxide ions which exert

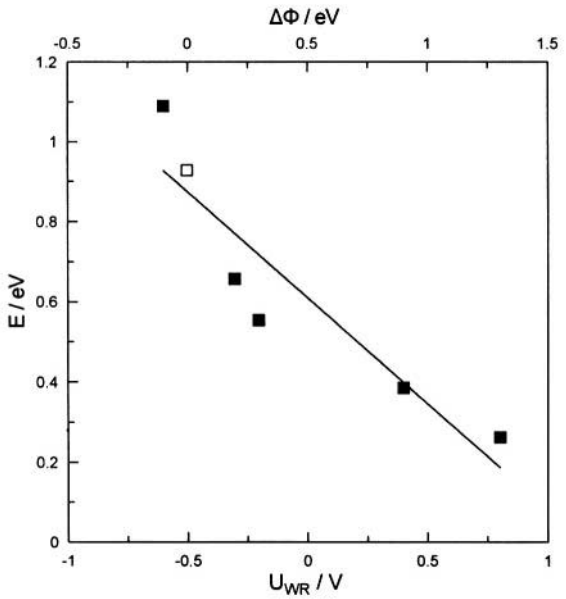

Figure 8.8. Effect of catalyst potential U_{WR} and corresponding work-function change $\Delta\Phi$ on the activation energy of C_2H_4 oxidation on Rh.[13] p_{O_2}=1.3 kPa, $p_{C_2H_4}$=7.4 kPa. Reprinted with permission from Academic Press.

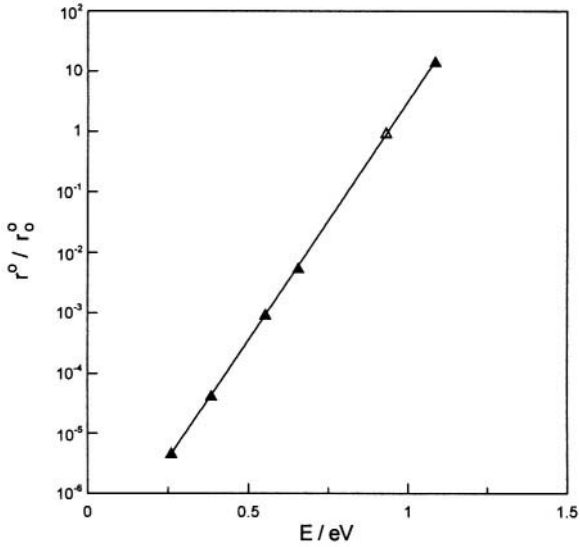

Figure 8.9. Dependence of the preexponential factor r^o on the activation energy E of C_2H_4 oxidation on Rh[13]; open symbol corresponds to open-circuit; p_{O_2}=1.3 kPa, $p_{C_2H_4}$=7.4 kPa. Reprinted with permission from Academic Press.

repulsive through-the-metal and through-the-vacuum lateral interactions with chemisorbed oxygen. Consequently higher p_{O_2} values ($p^*_{O_2}$) are required to form surface Rh (Figs. 8.4 and 8.5).

Conversely, since increasing U_{WR} and coverage of $O^{\delta-}$ stabilizes the Rh-C_2H_4 bond via enhanced π-electron donation to the metal, it follows that smaller $p_{C_2H_4}$ values ($p^*_{C_2H_4}$) are required to reduce the surface Rh oxide as experimentally observed.

These observations, which are in excellent agreement with the theory of Electrochemical Promotion regarding the effect of Φ on the binding strength of electron acceptor (e.g. O) and electron donor (e.g. C_2H_4) adsorbates (Chapter 6, global promotional rule G1) are at a first glance counterintuitive since the surface Rh oxide is destabilized by supplying O^{2-} from the solid electrolyte *to* the catalyst. This interesting and important point has been discussed in Chapter 6.

8.1.1.3 Ethylene Oxidation on Pd

In a recent study[16] Yiokari and Bebelis have investigated the electrochemical promotion of C_2H_4 oxidation on Pd films interfaced with YSZ at temperatures 290° to 360°C. Although the measured ρ values are low, typically below 2, the measured Λ values are typically $10^3 - 10^4$ and the electrochemical promotion behaviour is qualitatively similar to that of C_2H_4 oxidation on Pt and Rh, providing a nice example of rule G1: The reaction exhibits purely electrophobic behaviour only for high $p_{O_2}/p_{C_2H_4}$ ratios where the rate is first order in C_2H_4 and negative order in O_2.[16]

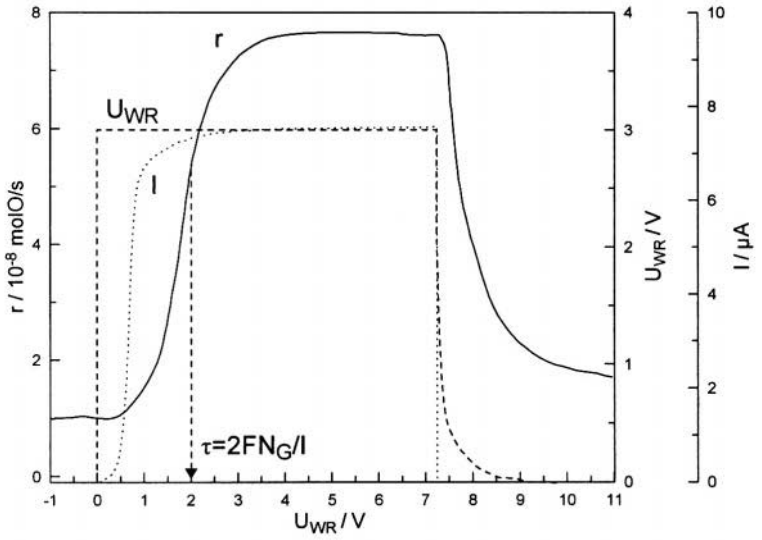

Figure 8.10. Potentiostatic and galvanostatic transient during C_2H_4 oxidation on IrO_2/YSZ;[17] $p_{C_2H_4}$=0.26 kPa; p_{O_2}=20 kPa; T=390°C; Λ≈100.

8.1.1.4 C_2H_4 Oxidation on IrO_2, RuO_2 and IrO_2-TiO_2 Mixtures: Equivalence of Metal-Support Interaction and NEMCA

Ethylene oxidation on IrO_2,[17-19] RuO_2[20-22] and IrO_2-TiO_2[19] mixtures deposited on YSZ were investigated by Comninellis and his coworkers Foti, Varkaraki, Nicole and Wodiunig at EPFL Lausanne and are truly remarkable in many aspects, including the fact that they were the first NEMCA studies on metal oxides, (Fig. 8.10).

Both IrO_2 and RuO_2 are metallic oxides with high density of states at the Fermi level. In this respect they are very similar to metals. On the other hand the fact that backspillover $O^{\delta-}$ ions originating from YSZ can migrate (backspillover) enormous (mm) atomic distances on their surface, as proven experimentally by Comninellis and coworkers, is not at all obvious.

8.1.1.4.1 Equivalence of Metal-Support Interaction and Electrochemical Promotion

The IrO_2-TiO_2 mixed catalyst system investigated by Nicole and Comninellis[19] is extremely interesting due to the well known[23] synergy of IrO_2 and TiO_2 for oxidation reactions, where TiO_2 significantly enhances the catalytic properties of IrO_2 and thus can be considered as a promoting support. Actually, in view of section 8.3.1 which shows that spectacular NEMCA behaviour for C_2H_4 oxidation can be induced with Pt films deposited on TiO_2,[24] (instead of YSZ) the promoting support action of TiO_2 in IrO_2-TiO_2 mixtures can be almost certainly attributed to a "wireless" (see Chapter 11) NEMCA effect where O^{2-} spillover from TiO_2 onto the IrO_2

surface is continuously taking place and where gaseous O_2 continuously replaces the spillover O on the TiO_2 surface (Figure 8.11).

This point is confirmed by Figure 8.12 which shows the effect of anodic polarization (I=+200μA) on the rate enhancement ρ value of C_2H_4 oxidation on IrO_2 as a function of the molar Ir content in the IrO_2-TiO_2 mixture.[19] There are three very important observations to make on this remarkable figure:

1. TiO_2 alone is not a catalyst for the reaction but it significantly promotes the catalytic activity of IrO_2, leading to a remarkable 12-fold enhancent in catalytic rate at $X_{IrO_2}=0.5$ vs $X_{IrO_2}=1$.
2. In this region of classical IrO_2 promotion by TiO_2 ($0 \leq X_{IrO_2} \leq 0.75$) the electrochemical promotion effect is negligible, as $\rho(=r/r_0)$ is below 1.5.

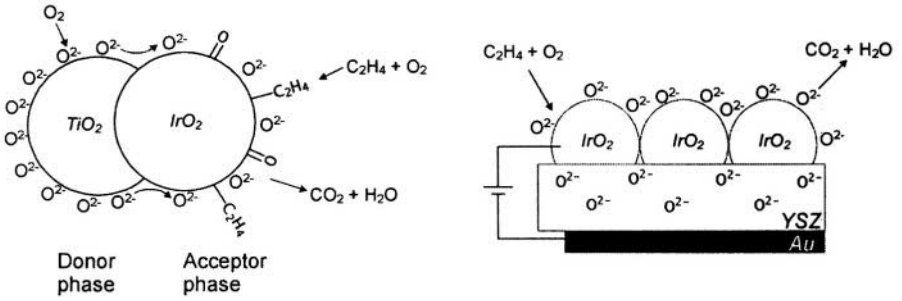

Figure 8.11. Mechanism of metal (IrO_2) – support (TiO_2) interaction (left) during ethylene oxidation on IrO_2 and of electrochemical promotion utilizing YSZ (right).

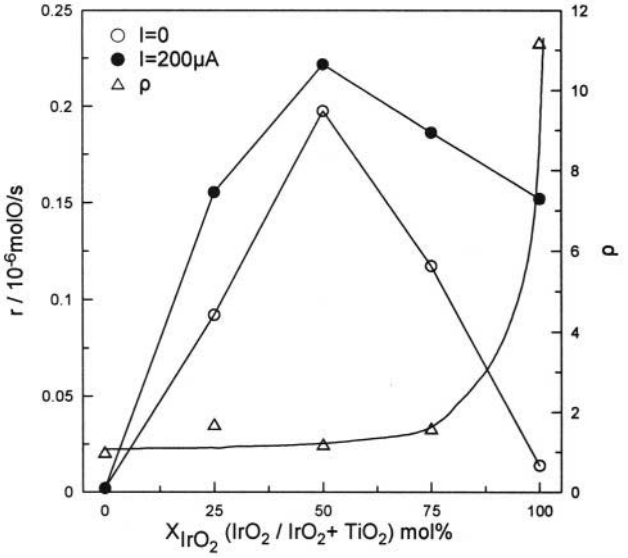

Figure 8.12. Effect of IrO_2 mol fraction in the IrO_2-TiO_2 catalyst on the open-circuit catalytic rate, r_0 of C_2H_4 oxidation (○), on the electrochemically promoted (I=200 μA) catalytic rate, r, (●) and on the corresponding rate enhancement ratio ρ (△).[19] (T=380°C, p_{O_2}=20 kPa, $p_{C_2H_4}$=0.15 kPa).

3. In absence of TiO_2 (X_{IrO_2}=1) the electrochemical promotion effect becomes dramatic with ρ values up to 11.

Thus this figure proves unambiguously the complete equivalence of "classical" metal (IrO_2)-support(TiO_2) interaction utilizing TiO_2 and electrochemical promotion utilizing YSZ. This is extremely important for understanding the mechanism of support-induced promotional activity in classical supported catalysts (Fig. 8.11) as further analyzed in Chapter 11.

8.1.1.4.2 Catalyst Film Mass and Metal-Solid Electrolyte Capacitance

In an ingeneously planned set of experiments Nicole[18] varied the IrO_2 catalyst electrode mass and examined, via detailed cyclic voltammetric analysis, the effect of catalyst mass both on the exchange current I_0 and on the capacitance C_d of the catalyst-solid electrolyte interface, which he modeled as shown in Figure 8.13a (see also Chapter 5). His results shown in Figure 8.13b demonstrate that both I_0 (which is inversely proportional to the polarization resistance, R_p (=dU_{WR}/dI)) and C_d increase strongly with increasing catalyst-electrode mass. This important result is consistent with the O^{2-} backspillover mechanism of electrochemical promotion and suggests that the charge transfer reaction zone is not limited at the tpb but extends over the entire gas exposed catalyst-electrode surface. In principle one would expect a linear variation of C_d with catalyst mass but the results of Nicole seem (Fig. 8.13) to suggest an even stronger dependence.

8.1.1.4.3 C_2H_4 Oxidation on IrO_2

The kinetics and electrochemical promotion behaviour of C_2H_4 oxidation on IrO_2/YSZ were investigated[17-19] at temperatures 350° to 450°C. As shown in Figure 8.14 for p_{O2} > 1kPa the rate is negative order in p_{O2} and positive order in $p_{C_2H_4}$. Thus, according to global rule G1 it exhibits purely electrophobic behaviour as shown already in the potentiostatic transient of Figure 8.10 and the steady state results of Figure 8.12. The ρ value is up to 12 (Fig. 8.12) and the Λ values are of the order 200 (Fig. 8.10). It is also worth noting in Figure 8.10 the good agreement between τ and $2FN_G/I$ which again confirms the O^{2-} backspillover promoting mechanism.

It is also noteworthy in Figure 8.14a that the presence of TiO_2 significantly enhances the rate in the region of oxygen inhibition. This is consistent with a weakening in the O chemisorptive bond and a strengthening in the C_2H_4 chemisorptive bond as in a classical anodic polarization NEMCA experiment. This confirms the role of TiO_2 as an O^{2-} donor.

As already discussed in Chapter 4 (Figs. 4.49 and 4.50) the IrO_2-TiO_2/YSZ system also exhibits interesting "permanent NEMCA" behaviour.

It is worth noting in Figure 4.49 that the permanent NEMCA behaviour is much more pronounced for the 25%IrO_2-75%TiO_2 catalyst, which is again consistent with the O^{2-} donor character of TiO_2.

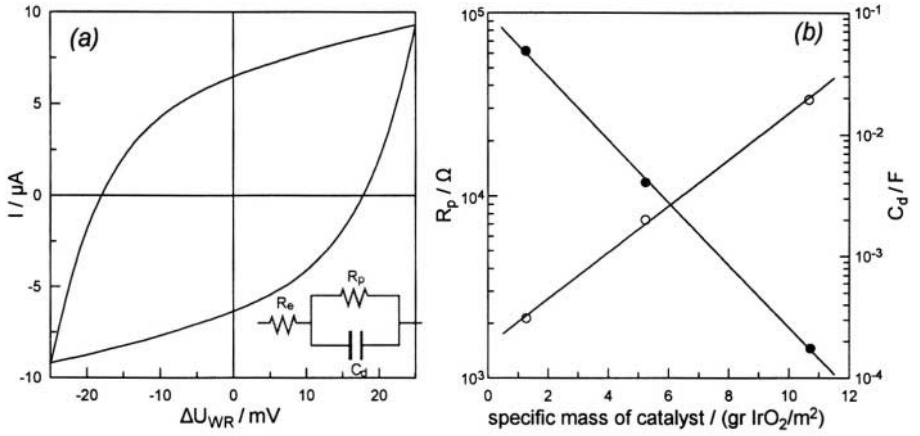

Figure 8.13. (a) Cyclic voltammetric investigation of the IrO_2/YSZ interface (inset shows the circuit used to model the data)[19] and (b) Effect of catalyst-electrode mass on the polarization resistance R_p and the double layer capacitance C_d.[19] Scan rate 20 mV/s, T=380°C, p_{O_2}=20 kPa.

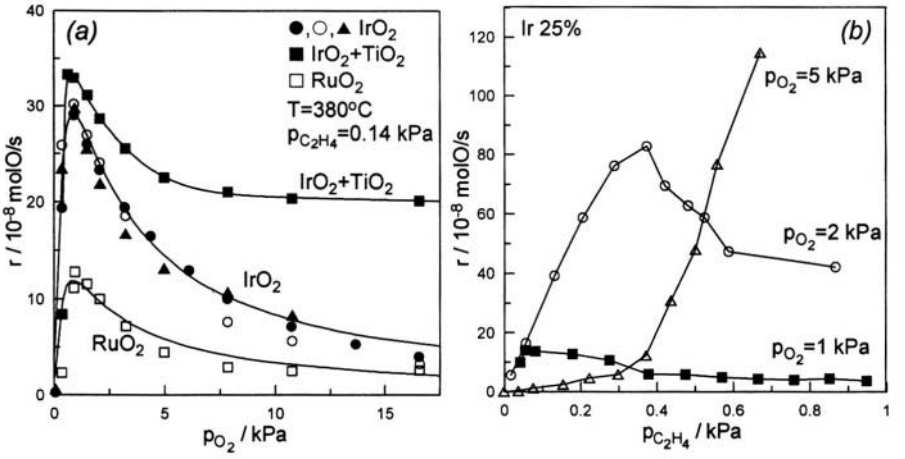

Figure 8.14. Effect of p_{O_2} (a) and $p_{C_2H_4}$ (b) on the rate of C_2H_4 oxidation on RuO_2, IrO_2 and IrO_2-TiO_2 (x_{IrO_2}=0.25) (a) and on IrO_2-TiO_2 (x_{IrO_2}=0.25) (b).[19]

8.1.1.4.4 Ethylene Oxidation on RuO_2

The oxidation of C_2H_4 on RuO_2 deposited on YSZ was studied by Wodiunig[20,21] at temperatures 250°C to 450°C. The reaction exhibits specta-cular electrophobic behaviour with ρ values up to 115 and Λ values up to 4400.

Via detailed kinetic analysis Wodiunig[20,21] showed that the open-circuit kinetics are described very well by Eq. (8.1), i.e. similar to C_2H_4 oxidation on Pt:

$$r_0 = kk_{ad}p_{C_2H_4}p_{O_2}/(kp_{C_2H_4} + k_{ad}p_{O_2}) \quad (8.1)$$

Thus for low $p_{C_2H_4}/p_{O_2}$ ratios the rate is first order in C_2H_4 and zeroth order in O_2. In excellent agreement with global rule G1, the reaction exhibits pronounced electrophobic behaviour (Fig. 8.15). The ρ value of 115 is the highest reported so far for an oxidation reaction.

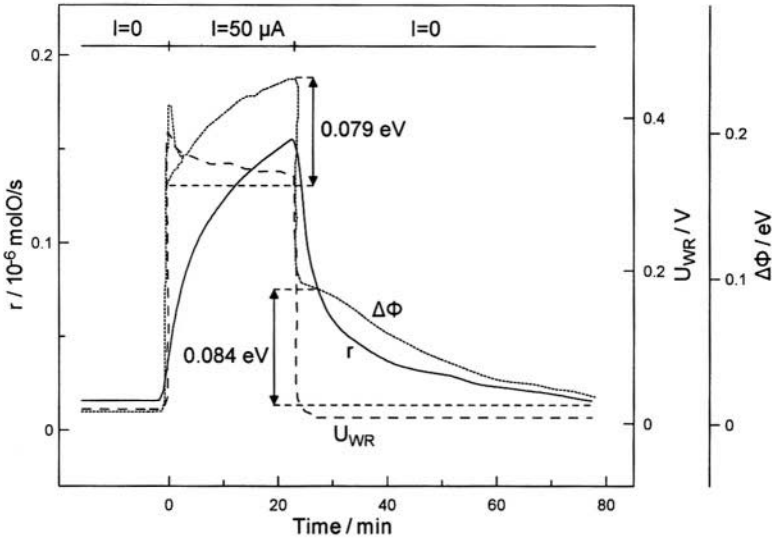

Figure 8.15. Time dependence of the work function change, ΔΦ, the reaction rate, r, and the catalyst potential, U_{WR}, following galvanostatic steps during C_2H_4 oxidation on RuO_2/YSZ.[20,21] Catalyst: RuO_2 (m=0.4 mg; A=0.5 cm^2), I=50 μA, $p_{C_2H_4}$=114 Pa, p_{O_2}=17.7 kPa, F_V=175 cm^3 STP/min, T = 380°C.[25]

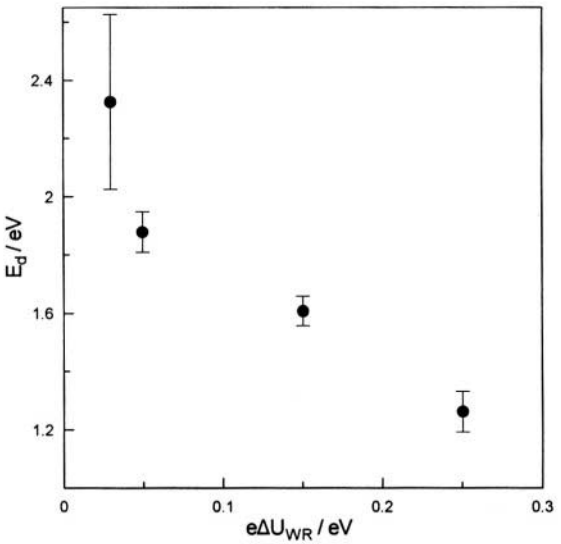

Figure 8.16. Activation energy of desorption, E_d, of O_2 from RuO_2 as a function of the applied potential,[21,25] as extracted from TPD and the modified Redhead equation of Falconer and Madix.[25,26] Reprinted from ref. 21 with permission from Elsevier Science.

Of great significance is also the detailed O_2 TPD investigation carried out by Wodiunig and Tsiplakides[25,26] (Figure 8.16). The activation energy of O_2 desorption from the RuO_2 catalyst decreases from 2.32 eV to 1.26 eV upon increasing U_{WR} and Φ. In the region 0.05 to 0.25 V the decrease in linear with a slope near -1, i.e. the same as in the case of Pt and Ag catalyst electrodes. This important result is in excellent agreement with the double layer electrostatic model presented in Chapter 4 and underlines the significance of "through the vacuum" dipole-dipole electrostatic interactions in electrochemical and classical promotion.

8.1.1.5 C_2H_6 Oxidation on Pt

The reaction has been investigated[27] in a "single-chamber" reactor at temperatures 400° to 500°C. The reaction exhibits electrophobic behaviour for positive currents ($U_{WR} > U^o_{WR}$) and electrophilic behaviour for negative currents ($U_{WR} < U^o_{WR}$) i.e. it exhibits inverted volcano behaviour (Figs. 4.33 and 8.17). In the case of positive potentials ρ is up to 20 and Λ up to 300. In the case of negative potentials ρ is up to 7 and Λ up to -100 (Figs. 4.33 and 8.17). The open-circuit kinetic behaviour indicates that the catalyst surface is predominantly covered with oxygen and that the coverage of ethane is always low.[27] However under the conditions of Figs. 4.33 and 8.17 which depict the effect of potential and current respectively on r ($p_{C_2H_6}$=1.65 kPa, p_{O_2}=1.07 kPa) the coverages of both O and C_2H_6 are low as the rate is near first order in both p_{O_2} and $p_{C_2H_6}$.[27] Consequently the observed rate enhancement with ($U_{WR} > U^o_{WR}$) can be attributed to enhanced ethane chemisorption while the rate

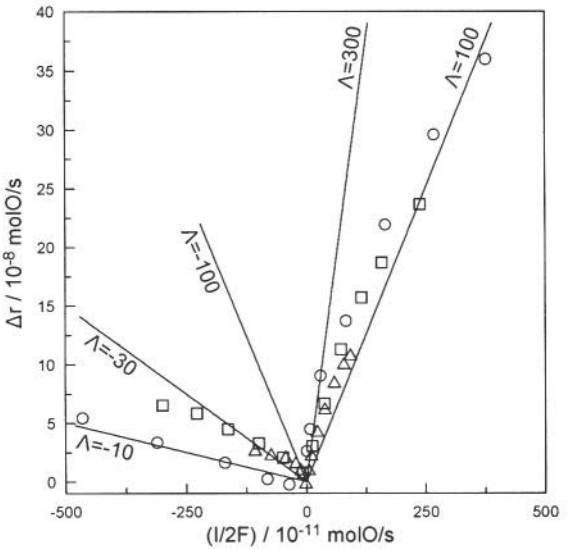

Figure 8.17. Effect of applied current on the increase in the rate of C_2H_6 oxidation;[27] $p_{C_2H_6}$=1.65 kPa, p_{O_2}=1.07 kPa; ○, T = 500°C; □, T = 460°C; △, T = 420°C. Reprinted with permission from Academic Press.

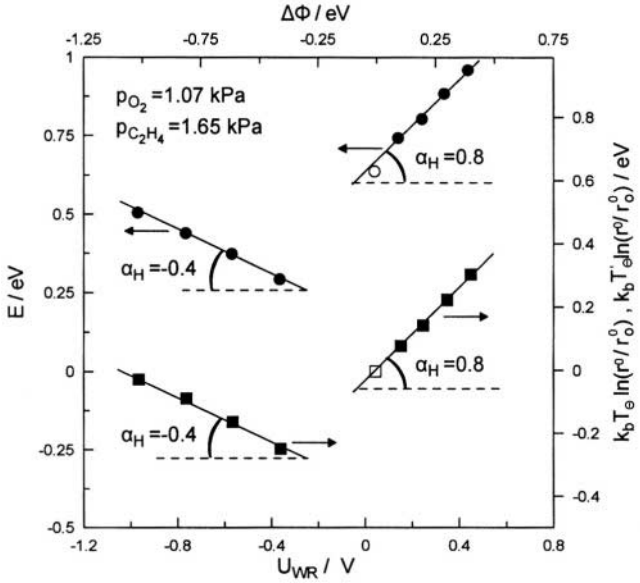

Figure 8.18. Effect of catalyst potential and work function on the apparent activation energy, E, and on the logarithm of the preexponential factor r^o; r_0^o is the open-circuit preexponential factor and T_Θ, T'_Θ are the two isokinetic points of C_2H_6 oxidation on Pt/YSZ for positive and negative potentials respectively.[27] Reprinted with permission from Academic Press.

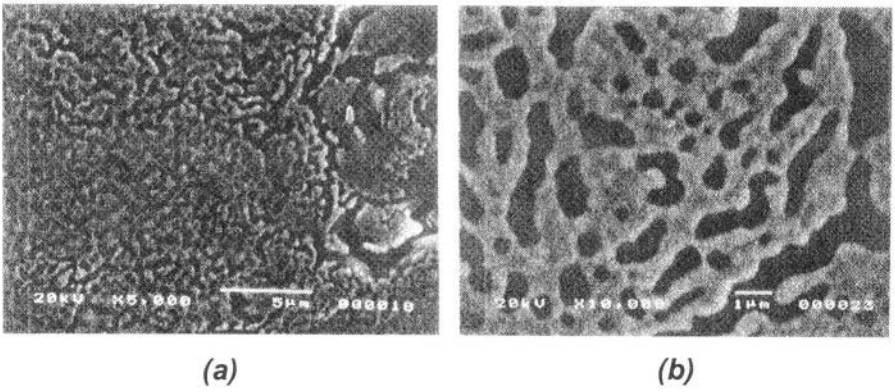

Figure 8.19. Scanning electron micrographs of the Pt-catalyst-electrode deposited on YSZ used for C_2H_6 oxidation.[27] Reprinted with permission from Academic Press.

enhancement with negative currents and potentials ($U_{WR} < U^o_{WR}$) is due to enhanced oxygen chemisorption. Therefore the observed inverted volcano behaviour is a clear demonstration of global promotional rule G4. This is also supported by the fact that the activation energy, E, of the reaction increases with both positive and negative overpotential (Fig. 8.18). Such an increase is consistent with enhanced binding of a weakly bonded, at open-circuit, reactant.

Consequently Figure 8.18 is also a nice demonstration of rule G4. As also shown in this figure the apparent preexponential factor of the catalytic reaction

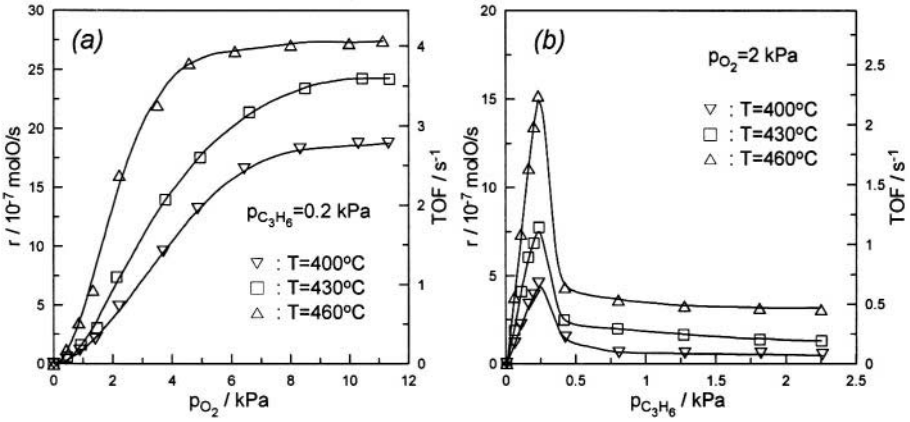

Figure 8.20. Effect of p_{O_2} (a) and $p_{C_3H_6}$ (b) on the rate and turnover frequency of propylene oxidation on Pt/YSZ.[28] Reprinted with permission from Academic Press.

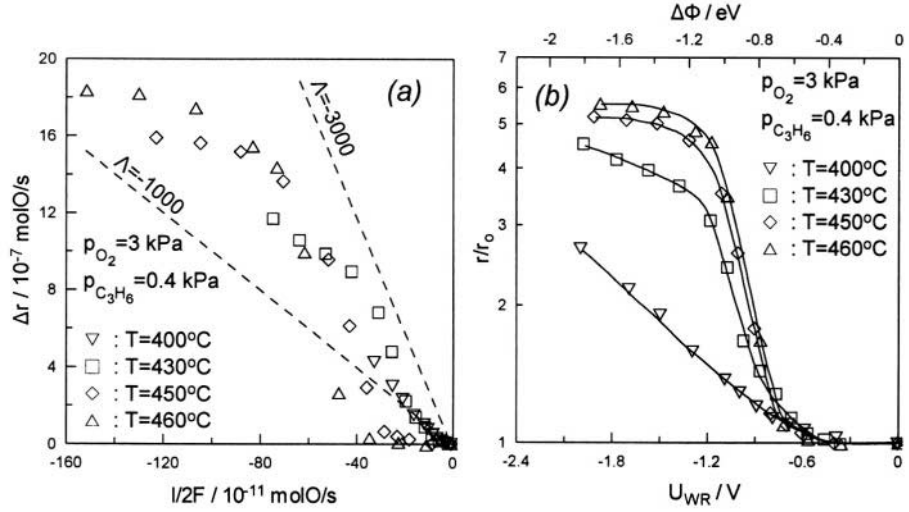

Figure 8.21. (a) Effect of the rate, I/2F, of electrochemical oxygen ion removal (I<0) on the induced increase in the rate of propylene oxidation on Pt/YSZ.[28] (b) Effect of catalyst potential and work function change on the rate enhancement ratio ρ (=r/r_0) at a fixed gaseous composition. Reprinted with permission from Academic Press.

r^o is also enhanced with both positive and negative ΔU_{WR} and $\Delta\Phi$ according to Equations (4.50) and (4.52) and this leads to the appearance of two isokinetic points.[27]

8.1.1.6 C_3H_6 Oxidation on Pt

The oxidation of propene on Pt/YSZ was studied[28] at temperatures 350° to 500°C. Figure 8.19 shows SEMs of the porous Pt/YSZ film which has a surface area corresponding to a reactive oxygen uptake N_G=6.8·10^{-7} mol O.

This is a typical example of purely electrophilic behaviour and of global promotional rule G2. As shown in Figure 8.20 the rate is positive order in p_{O_2} for p_{O_2}<4 kPa and negative order in $p_{C_3H_6}$ for $p_{C_3H_6}$>0.2 kPa. As expected from rule G2 ($\partial r/\partial P_A>0$, $\partial r/\partial P_D<0$) the reaction, within this gaseous composition, exhibits purely electrophilic behaviour (Fig. 8.21) with ρ values up to 6 and $-\Lambda$ values up to 3000.

The electrophilic behaviour is due to enhanced oxygen chemisorption with decreasing U_{WR} and Φ. This is also consistent with the observed linear increase in the apparent activation energy, E, with decreasing U_{WR} and Φ already shown in Figure 4.37 with a slope α_H=-0.9. Enhanced O binding on the catalyst surface increases the apparent activation energy but at the same time enhances the rate due to the concomitant pronounced increase in the apparent preexponential factor, r^o, as long as the operating temperature is above the isokinetic point (T_Θ=380°C, Fig. 4.39), i.e. in the region where the reaction exhibits electrophilic behaviour.

8.1.1.7 CH_4 Oxidation on Pt

Methane oxidation is another reaction exhibiting strong electrophobic behaviour for positive overpotentials and $\Delta\Phi$ both for Pt[29,30] and Pd.[31] In the case of Pt strong rate enhancement is also obtained with negative $\Delta\Phi$ leading to inverted volcano type behaviour (Figs. 8.22 and 8.23). Figure 8.23 shows the steady state effect of U_{WR} and Φ on the rate of CH_4 oxidation for a low (1:1) CH_4 to O_2 feed ratio ($p^o_{CH_4}=p^o_{O_2}=2$kPa). The rate increases exponentially with U_{WR} and Φ both with increasing and decreasing Φ. The corresponding NEMCA coefficient, α, values are α=0.7 and α=-0.37.

As shown on Fig. 8.24 changing Φ causes significant and linear variations in activation energy. The corresponding α_H values are -4.5 for $U_{WR}>U^o_{WR}$ and 1 for $U_{WR}<U^o_{WR}$. The former is qualitatively similar to the case of C_2H_4 oxidation on Pt and thus can be explained by the same reasoning. The latter is very likely due to the fact that decreasing Φ strengthens the Pt=O bond and thus enhances the activation of the C-H bond in CH_4 to form CH_3• radicals which can then be rapidly oxidized in the gas phase.[29]

The effect of U_{WR} and Φ on catalytic rate is more pronounced when high CH_4 to O_2 ratios are used. Thus for a 40:1 CH_4 to O_2 feed ratio ($p^o_{CH_4}$=10kPa, $p^o_{O_2}$=0.25 kPa, T=700°C) a seventyfold increase in catalytic rate is obtained for $e\Delta U_{WR}=\Delta\Phi$=1eV (Figure 8.25). This is due, again, to the weakening of the Pt=O bond with increasing work function. Rate enhancement factors Λ are low, typically less than five, due to the high operating temperatures and concomitantly high I_0 values (equation 4.20).[29]

In a parallel study Eng and Stoukides[30] also reported Λ values up to five for this reaction and also detected the presence of trace C_2 hydrocarbons in the effluent stream. Since YSZ is known to promote catalytically the oxidative coupling of CH_4,[32] the extent to which C_2 hydrocarbons can be found in the products is dictated by the ratio of YSZ and Pt surfaces present in the reactor.

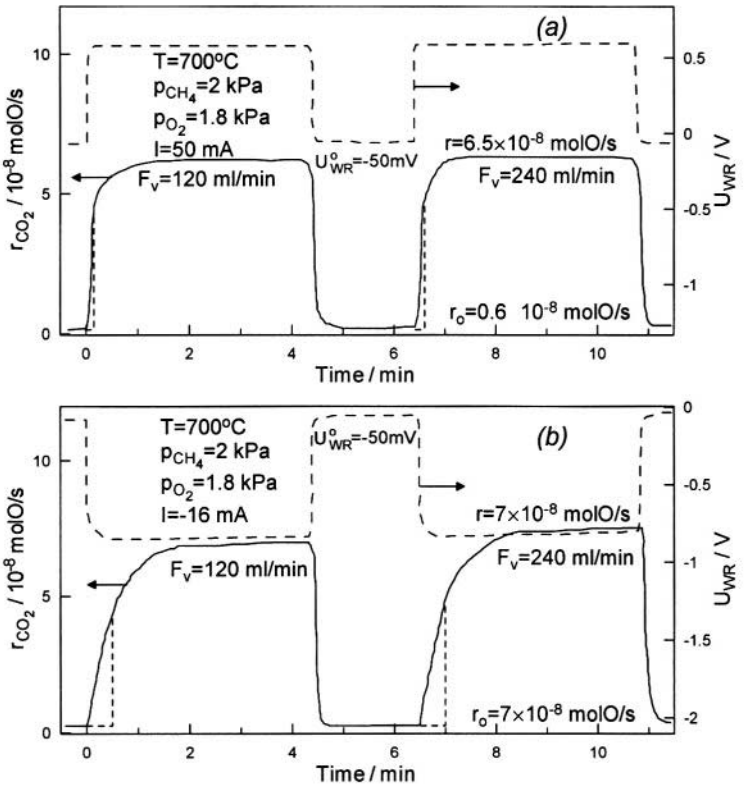

Figure 8.22. Effect of step changes in applied positive and negative currents on U_{WR} and r during CH_4 oxidation on Pt/YSZ[29] at two different volumetric flowrate F_v showing that τ is influenced by I but not by F_v.[29] Reprinted with permission from Academic Press.

The CH_4 oxidation on Pd[31] exhibits a very pronounced NEMCA behavior at much lower temperatures (380-440°C) compared with those on Pt catalysts (650-750°C). In this temperature range the reaction exhibits inverted volcano behavior.[31] For positive overpotentials the ρ values are as high as 89, with Λ values up to 105.[31] Negative overpotentials also enhance the rate[31] with ρ values up to 8.

Figure 8.26 shows the dependence of the steady-state rate on the partial pressure of methane (Fig. 8.26a) and oxygen (Fig. 8.26b) at 400°C both for open and closed circuit conditions.[31]

The rate is near first order in methane and zero order in oxygen for oxygen to methane ratios higher than 1. Also, the reaction kinetics remain unaffected upon polarization conditions. The kinetic data indicate weak bonding of methane and strong bonding of oxygen on the catalyst surface.

The pronounced rate enhancement with positive ΔU_{WR} and $\Delta\Phi$ is thus due to the weakening of the Pd=O bond according to rule L1 while the observed rate enhancement with negative ΔU_{WR} and Φ is due to enhanced binding of CH_x on the catalyst surface due to the strengthening of the Pd=O bond.

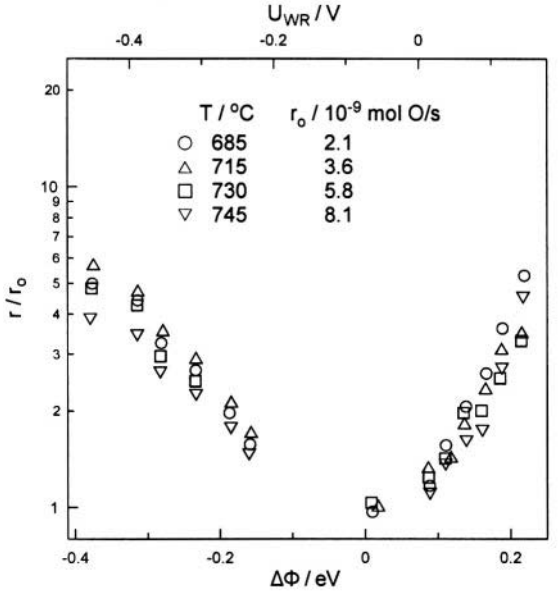

Figure 8.23. Effect of catalyst potential and work function on the rate of CH_4 oxidation to CO_2 on Pt for a low (1:1) CH_4 to O_2 feed ratio. Maximum methane conversion is 4%. p_{CH4}= p_{O2}=2 kPa, T, °C, r_0, mol O/s.[29] Reprinted with permission from Academic Press.

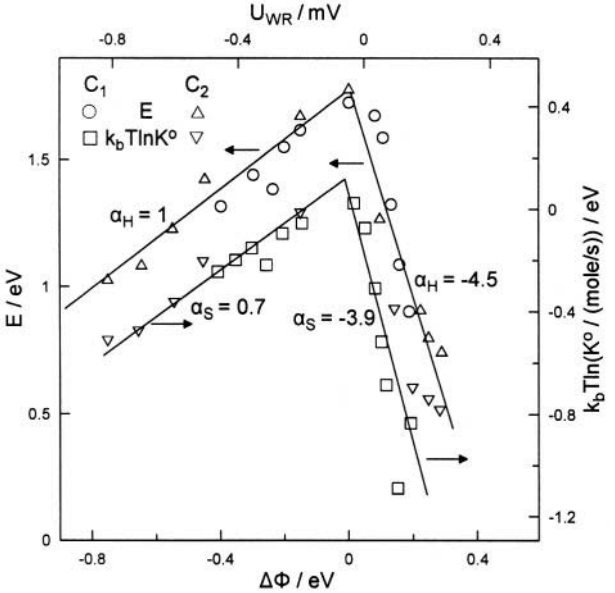

Figure 8.24. Effect of catalyst potential U_{WR} and work function change (vs I=0) on the activation energy E and preexponential factor K° of the kinetic constant K of CH_4 oxidation to CO_2; an average T value of 948 K is used in the rhs ordinate $p^o_{CH4} = p^o_{O2} = 2$ kPa .[29] Reprinted with permission from Academic Press.

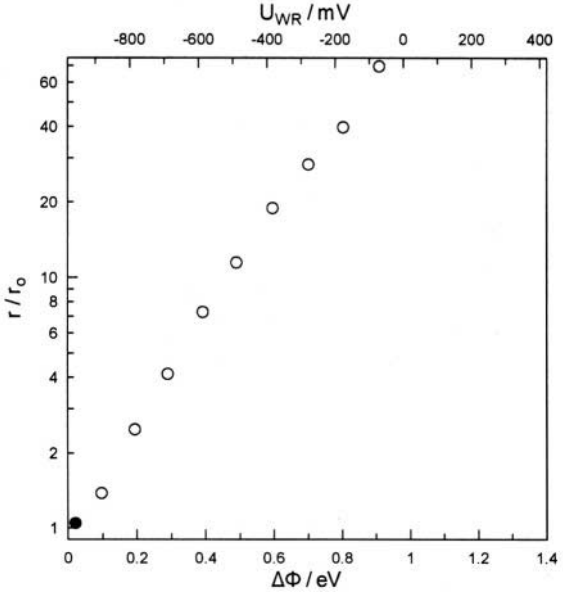

Figure 8.25. Effect of catalyst potential and work function on the rate of CH_4 oxidation to CO_2 on Pt for a high (40:1) CH_4 to O_2 feed ratio. Maximum O_2 conversion is 62%. p_{CH_4}=10 kPa, p_{O_2}=0.25 kPa, T=973 K.[5,29] Reprinted from ref. 29 with permission from Academic Press.

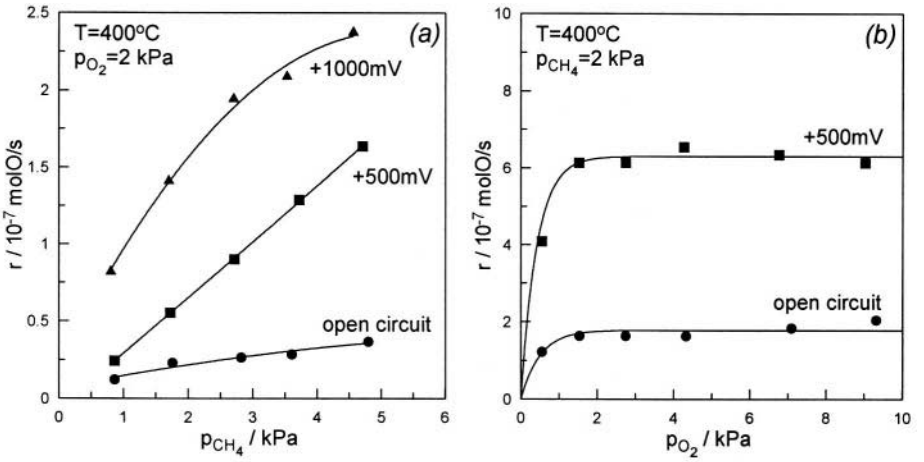

Figure 8.26. Reaction rate dependence on p_{CH_4} at constant p_{O_2} =2 kPa (a) and p_{O_2} at constant p_{CH_4}=2 kPa (b) for open circuit conditions (circles), U_{WR}=+500 mV (squares) and U_{WR}=+1000 mV (triangles) during CH_4 oxidation on Pd/YSZ[31]; T=400°C Reprinted with permission from Elsevier Science.

8.1.1.8 CO Oxidation on Pt and Pd

The CO oxidation on Pt was the second reaction, after C_2H_4 oxidation on Ag, for which a Non-Faradaic rate enhancement was observed.[33] Typical measured Λ values were of the order 10^2-10^3 while ρ was typically below five.[33]

Figure 8.27 depicts some typical galvanostatic transients which show that depending on the magnitude of the applied negative current (or overpotential) the reaction can exhibit either electrophobic behaviour (for small negative currents) or electrophilic behaviour for larger negative currents. This is also shown by the steady-state r vs U_{WR} results presented on Figure 8.28[34] which is a clear case of inverted volcano behaviour.

As shown on this Figure and also in Fig. 8.29 increasing U_{WR} and Φ above their open-circuit potential values leads to a local "volcano", i.e. the rate goes through a maximum. This is consistent with the global promotional rule G3 and the observed rate dependence on p_{CO}/p_{O_2} (Fig. 8.30) where it is interesting to observe that the rate maximum is only moderately affected by the applied potential.

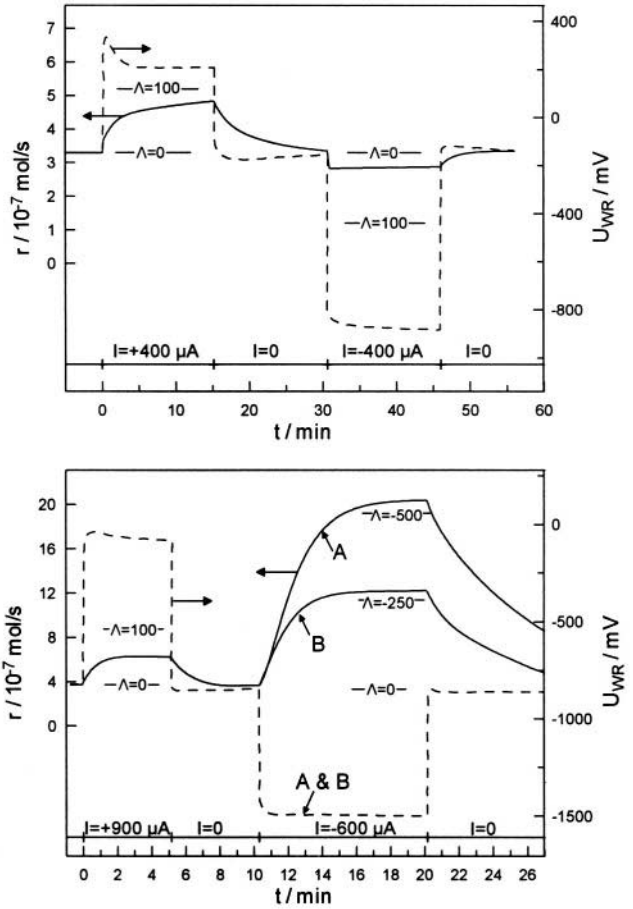

Figure 8.27. Transient effect of current on the rate of CO oxidation on Pt (solid lines) and on catalyst potential (broken lines); inlet compositions and temperatures: (a) p_{CO}=0.47 kPa, p_{O_2}=10 kPa, T=412°C; (b) p_{CO}=2.9 kPa, p_{O_2}=0.40 kPa, T=555°C.[33] Reprinted with permission from Academic Press.

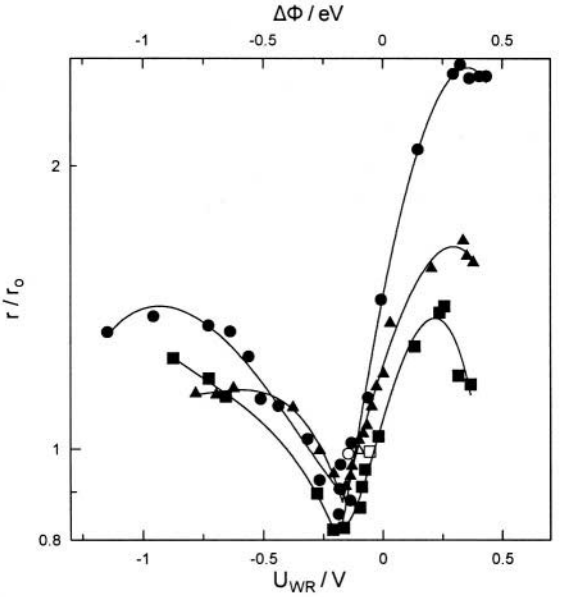

Figure 8.28. Steady-state effect of catalyst potential and work function on the rate of CO oxidation on Pt. Open symbols correspond to open-circuit conditions; ●, T=485°C, r_0=0.5×10^{-7} mol/s; ■, T=505°C, r_0=1.0×10^{-7}mol/s, ▲, T=535°C, r_0=1.5×10^{-7} mol/s. p_{CO}=0.25×10^{-2}bar, p_{O_2}=11.3×10^{-2} bar.[34] Reprinted with permission from Trans Tech Publications.

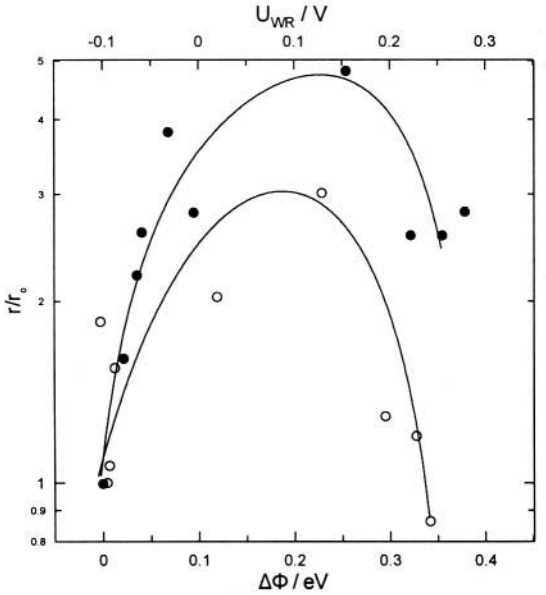

Figure 8.29. NEMCA-generated volcano plots obtained by increasing the catalyst work function above its open-circuit value during CO oxidation on Pt; p_{CO}=0.2 kPa, p_{O_2}=11 kPa, ●, T=560°C, r_0=1.5×10^{-9} mol O/s; ○, T=538°C; r_0=0.9×10^{-9} mol O/s.[36] Reprinted by permission of Platinum Metals Review.

As shown on Figs. 8.31 to 8.33 the rate and U_{WR} (or Φ) oscillations of CO oxidation can be started or stopped at will by imposition of appropriate currents.[33] Thus on Fig. 8.31 the catalyst is initially at a stable steady state. Imposition of a negative current merely decreases the rate but imposition of a positive current of 200 μA leads to an oscillatory state with a period of 80s. The effect is completely reversible and the catalyst returns to its initial steady state upon current interruption.

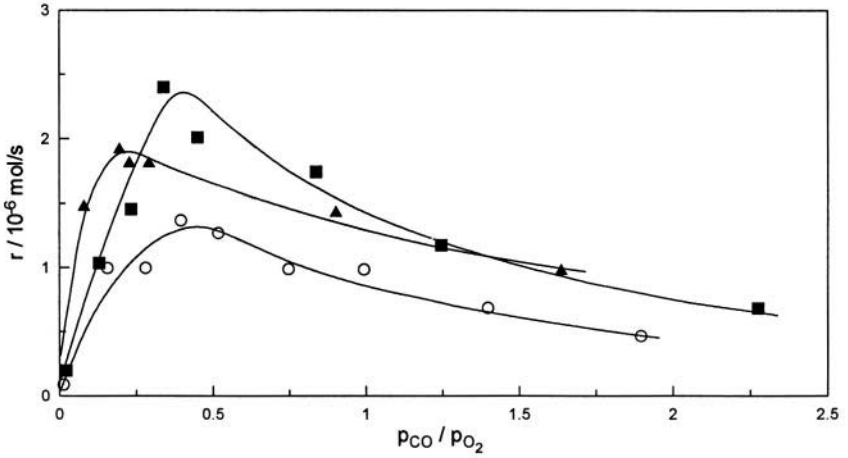

Figure 8.30. Effect of gaseous composition on the rate of CO oxidation on Pt/YSZ. T= 535°C; ○, open-circuit; ■,U_{WR}=500 mV; ▲,U_{WR}=-500 mV.[34] Reprinted with permission from Trans Tech Publications.

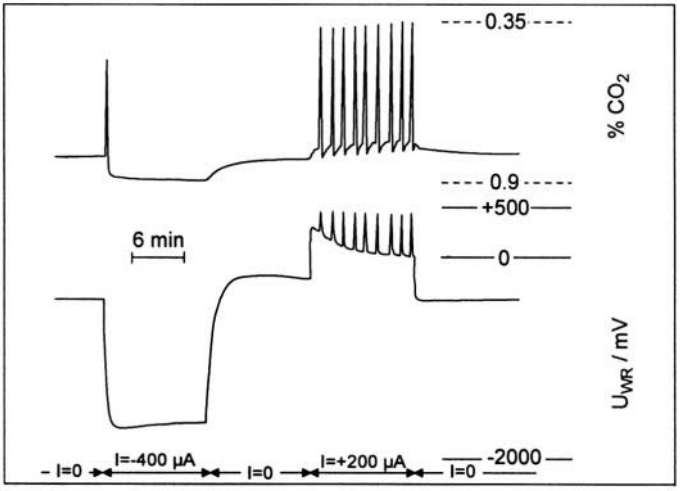

Figure 8.31. Induction of self-sustained rate and catalyst potential, or work function, oscillations by NEMCA during CO oxidation on Pt. Inlet composition: p_{CO}=0.47 kPa, p_{O_2}=16 kPa, T=297°C.[33] Reprinted with permission from Academic Press.

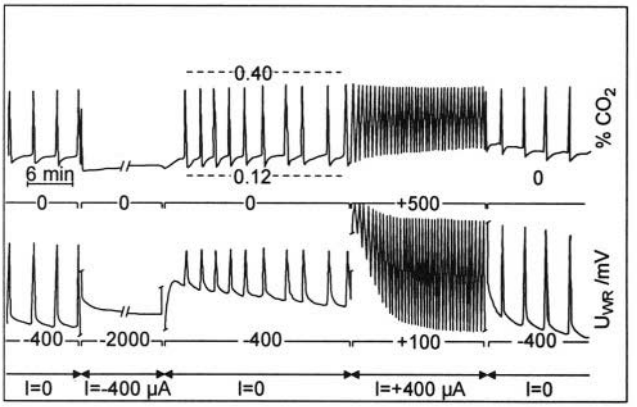

Figure 8.32. Transition from an oscillatory state to a steady state and to a higher frequency oscillatory state upon application of negative and positive current, respectively, during CO oxidation on Pt. Inlet composition: p_{CO}=0.47 kPa, p_{O_2}=16 kPa, T=332°C.[33] Reprinted with permission from Academic Press.

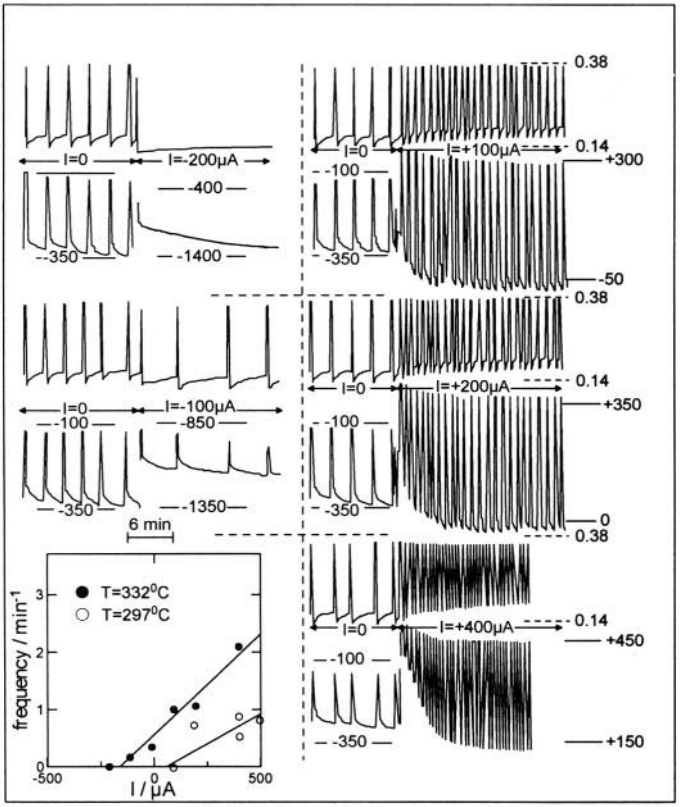

Figure 8.33. Effect of applied constant current on the frequency of the self-sustained rate and U_{WR} oscillations during CO oxidation on Pt; conditions as on Fig. 8.32; Filled circles on the frequency vs current diagram are oscillatory states of this figure; open circles include states shown on Fig. 8.31.[33] Reprinted with permission from Academic Press.

The opposite effect is depicted on Fig. 8.32 where the catalyst under open-circuit conditions exhibits stable limit cycle behaviour with a period of 184 s. Imposition of a negative current of -400 μA leads to a steady state. Upon current interruption the catalyst returns to its initial oscillatory state. Application of positive currents leads to higher frequency oscillatory states.

A striking feature of the effect of current on the CO oxidation oscillations is shown in Fig. 8.33. It can be seen that the frequency of oscillations is a linear function of the applied current. This holds not only for intrinsically oscillatory states but also for those which do not exhibit oscillations under open-circuit conditions, such as the ones shown on Fig. 8.31. This behaviour is consistent with earlier models developed to describe the oscillatory behaviour of Pt-catalyzed oxidations under atmospheric pressure conditions which are due to surface PtO_2 formation[35] as analyzed in detail elsewhere.[33]

The oxidation of CO on Pd is another reaction exhibiting NEMCA.[36] Faradaic efficiency factor Λ values of the order of 10^3 have been measured at T=290°C, $p_{CO}=3\times10^{-2}$ kPa and $p_{O_2}=15$ kPa.[36] This reaction is well known to also exhibit oscillatory behaviour[37] and deserves further examination.

8.1.1.9 CO Oxidation on Ag

Similarly to CO oxidation on Pt this reaction exhibits electrophobic ($\Lambda>0$) behaviour for high U_{WR} and Φ values and electrophilic ($\Lambda<0$) behaviour for low U_{WR} and Φ values.[38] The rate dependence on U_{WR} and Φ shown on Fig. 8.35 bears many similarities to that obtained with CO oxidation on Pt (Figure 8.28) except that the local "volcano" behaviour at high Φ is missing here, at least over the Φ range investigated. Typical Λ values are of the order of 20 in the electrophobic region and of the order of -800 in the electrophilic one.[38] Figure 8.34 shows the rate dependence on reactant partial pressures under open-circuit and NEMCA conditions. The rate remains first-order in O_2 under all conditions, while the rate dependence on CO also retains its open-circuit qualitative features under NEMCA conditions. The kinetics indicate weak to moderate bonding of the reactants on the catalyst surface, thus leading to inverted volcano behaviour (Fig. 8.35) in excellent agreement with promotional rule G4.

8.1.1.10 CO Oxidation on Ag-Pd Alloys and on Au

The oxidation of CO on Ag-25 mol%Pd alloys deposited on YSZ (Fig. 8.36) by Sobyanin and coworkers[39] was the first electrochemical promotion study utilizing an alloy catalyst. The reaction was investigated at temperatures 350° to 500°C and under open-circuit conditions was found to be first order in CO and near zeroth order in O_2 (Fig. 8.37a). The rate is significantly enhanced

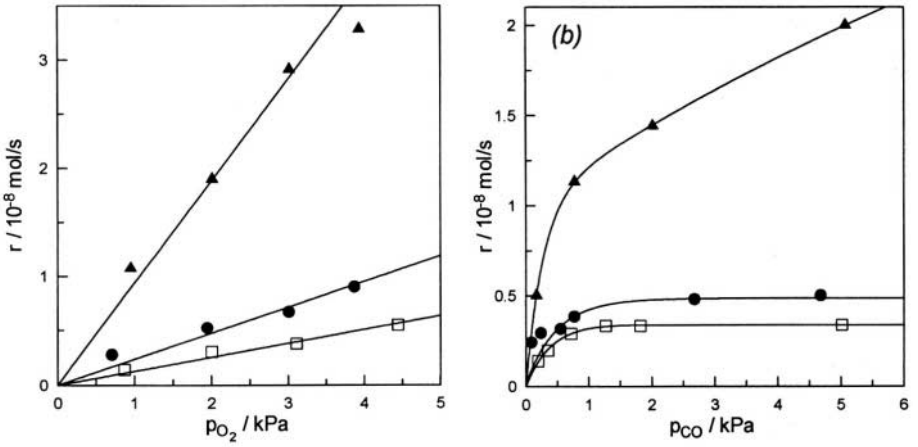

Figure 8.34. (a) Effect of p_{O_2} on regular (open-circuit) and NEMCA-induced rate of CO oxidation on Ag. T=415°C; p_{CO}=5 kPa; □, I=0; ●, U_{WR}=+475 mV; ▲, U_{WR}=-1300 mV.[38] Reprinted with permission from Trans Tech Publications. (b) Effect of p_{CO} on regular (open-circuit) and NEMCA-induced rate of CO oxidation on Ag. T=415°C; p_{O_2}=3 kPa; □, T=0; ●, U_{WR}=+475 mV; ▲, U_{WR}=-1300 mV.[2] Reprinted with permission from Elsevier Science.

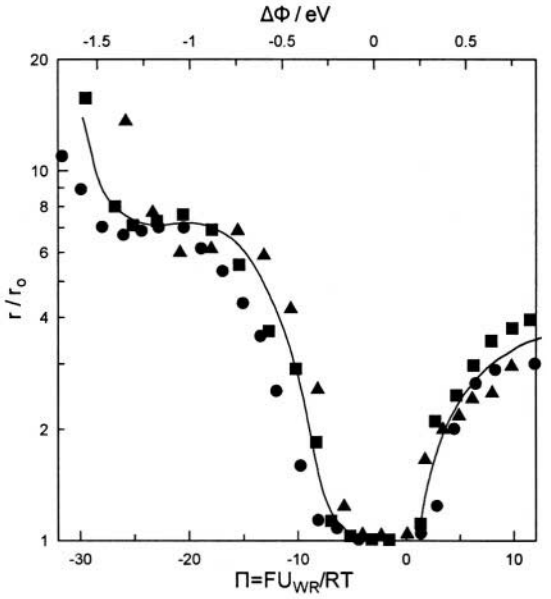

Figure 8.35. Effect of catalyst potential and work function on the rate enhancement ratio during CO oxidation on Ag. p_{O_2}=3 kPa, p_{CO}=5 kPa, ●, T=363°C, r_0=2.7×10^{-9} mol O/s; ▲, T=390°C, r_0=3.4×10^{-9} mol O/s; ■, T=410°C, r_0=5.5×10^{-9} mol O/s, ▲, T=390°C, r_0=3.4×10^{-9} mol O/s.[38] Reprinted with permission from Trans Tech Publications.

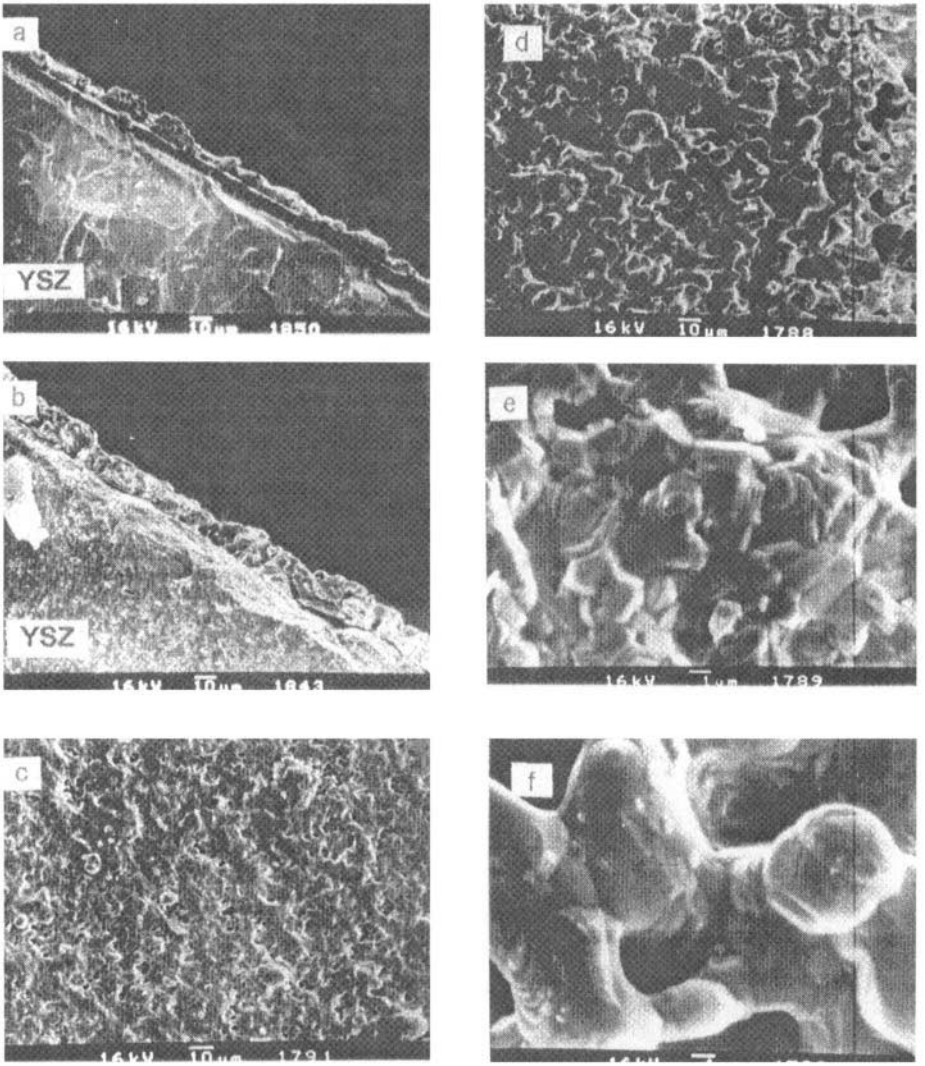

Figure 8.36. Scanning electron micrographs of an Ag-25at%Pd alloy electrode deposited on YSZ. (a,c,e) sample 1; (b, d, f) sample 2.[39]

with negative ΔU_{WR} and $\Delta\Phi$ (Fig. 8.37b) with ρ values up to 20. Positive ΔU_{WR} and $\Delta\Phi$ cause only moderate rate enhancement (Fig, 8.37b).

The observed inverted volcano behaviour, as well as the kinetic behaviour are qualitatively similar to the case of CO oxidation on Ag/YSZ (Figs. 8.34 and 8.35)[2,38] and thus present a nice example of promotional rule G4. Similar is the electrochemical promotion behaviour of CO oxidation on Au which has also been studied by Sobyanin and coworkers.[40,41]

Previous Page

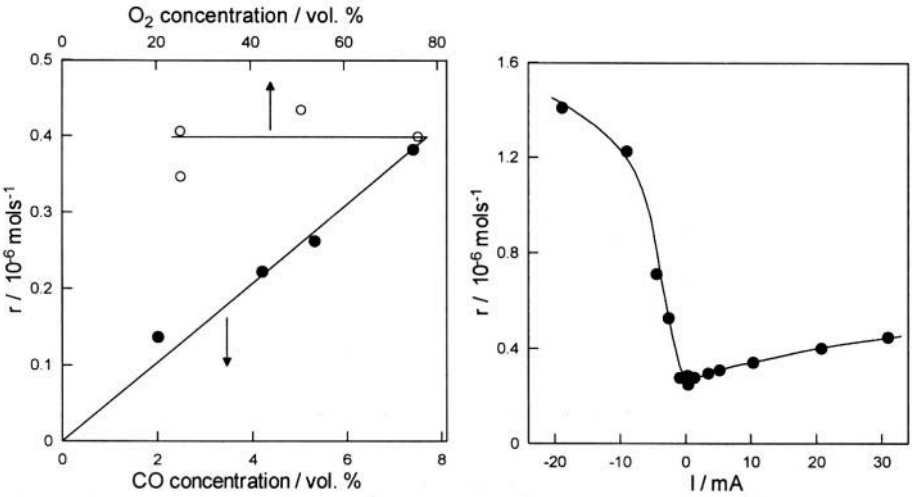

Figure 8.37. (a) Effect of gaseous compositions on the rate of CO_2 formation during CO oxidation on Ag-Pd alloys[39] under open-circuit conditions at T=450°C, (●) $[O_2]$=25 vol%, (○) [CO]=6.7 vol%. (b) Effect of applied current on the rate of CO_2 formation. Temperature and inlet composition: T=450°C, $[O_2]$=25 vol%, [CO]=6.5 vol%.[39]

8.1.2 Partial Oxidation Reactions

8.1.2.1 C_2H_4 and C_3H_6 Epoxidation on Ag

The epoxidation of ethylene was the first reaction for which a Non-Faradaic rate enhancement was found.[42] As shown on Figure 8.38 the observed increase in the rate of epoxidation r_1 and oxidation to CO_2 r_2 were typically a factor of 300 higher than the rate I/2F of supply of O^{2-} to the catalyst. A slight improvement in the selectivity to C_2H_4O (from 0.52 to 0.59) was observed with I>0 under oxidizing conditions ($p_{C_2H_4}$=1.5 kPa, p_{O_2}=10 kPa, T=400°C), while negative currents caused a decrease in selectivity from 0.52 to 0.42 (Fig. 8.39). It was observed that the rate relaxation time constants during galvanostatic transients were of the order of $2FN_G/I$, strongly indicating that the change in catalytic properties were taking place over the entire catalyst surface. No reference electrode was used in earlier studies[42] so that η and U_{WR} could not be measured.

A qualitatively similar behaviour was obtained during C_3H_6 epoxidation on Ag.[43] Enhancement factor Λ values of the order of 150 were measured.[43] Both the rates of epoxidation and oxidation to CO_2 increase with I>0 and decrease with I<0. The intrinsic selectivity to propylene oxide was very low, typically 0.03 and could be increased only up to 0.04 by using positive currents. This was again an exploratory study, as no reference electrode was used, thus η and U_{WR} could not be measured.[43]

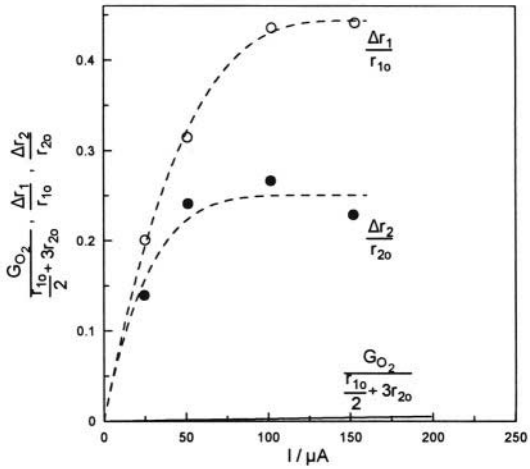

Figure 8.38. Steady state effect of current on the increase in the rates of ethylene epoxidation (r_1) and deep oxidation to CO_2 (r_2) of C_2H_4 on Ag and comparison with the rate G_{O_2}=I/4F of electrochemical oxygen supply[42]; $p_{C_2H_4}$=1.6 kPa, p_{O_2}=10 kPa, T=400°C; intrinsic (I=0) selectivity 0.5. Reprinted with permission from Academic Press.

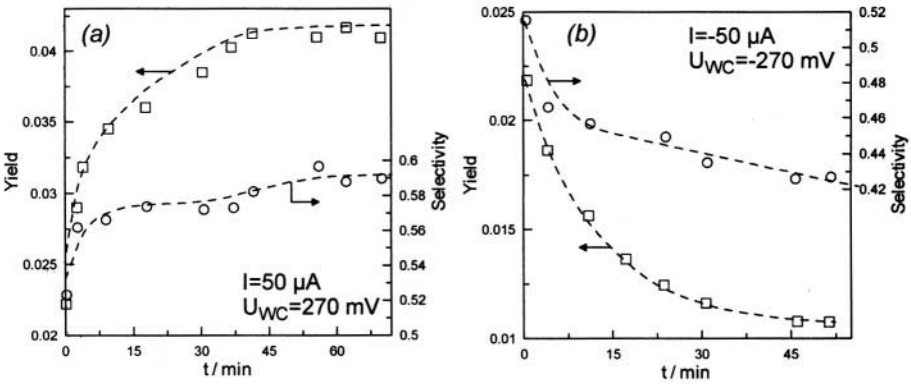

Figure 8.39. Transient effect of electrochemical O^{2-} pumping to (a) and from (b) a Ag catalyst film on selectivity and yield to ethylene oxide.[42] Current applied at t=0; $p_{C_2H_4}$=1.5 kPa, p_{O_2}=10 kPa; T=400°C. Reprinted with permission from Academic Press.

Subsequently the ethylene epoxidation system on Ag has been investigated using a proper three-electrode system utilizing both doped ZrO_2 [44,45] and β"-Al_2O_3 solid electrolytes as the ion donor.[46] These studies were extended[46,47] to examine the effect of higher operating pressures (500 kPa) and of the addition of gas-phase $C_2H_4Cl_2$ "moderator" which is known to promote the selectivity to ethylene oxide. In this section we discuss the use of doped ZrO_2.

Figure 8.40 shows some typical galvanostatic transients, one for I>0 and another for I<0. In the former case (Fig. 8.40a) both rates of C_2H_4O and CO_2 formation increase but both exhibit an initial "overshooting".

The latter case (Fig. 8.40b) is more interesting. Initially both rates decrease but at steady state the rate of epoxidation has decreased, while the rate of CO_2 formation has increased. Thus epoxidation exhibits electrophobic behaviour but oxidation to CO_2 exhibits electrophilic behaviour.[45]

Figure 8.41 shows the effect of positive overpotential, i.e. increasing work function, on the apparent activation energies E_i and preexponential factors k_i^0 of the epoxidation (i=1) and deep oxidation (i=2) reactions. After

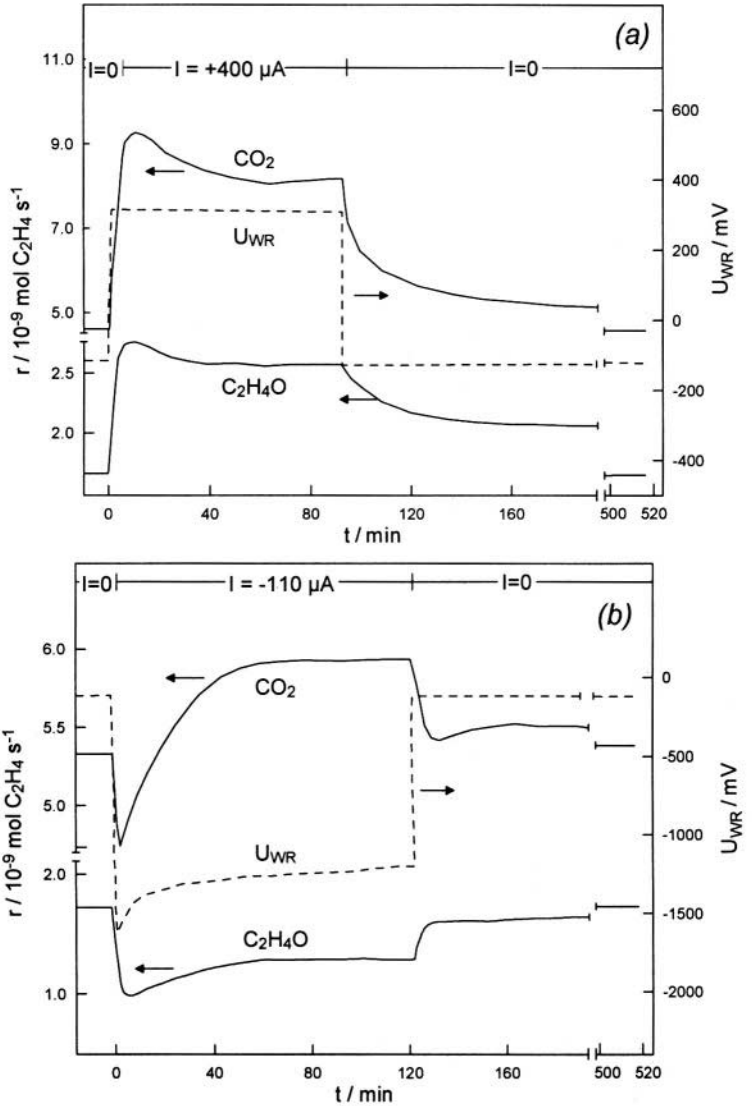

Figure 8.40. Transient effect of electrochemical O^{2-} pumping to (a) and from (b) a Ag catalyst film on selectivity and yield to ethylene oxide. Current applied at t=0; $p_{C_2H_4}$=1.5 kPa, p_{O_2}=10 kPa; T=400°C.[45] Reprinted with permission from Academic Press.

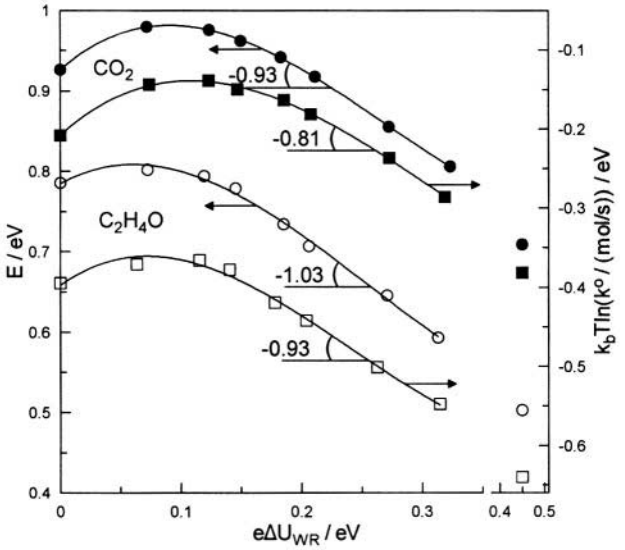

Figure 8.41. Effect of Ag/YSZ catalyst overpotential on the activation energy E and preexponential factor k^o of ethylene epoxidation (open symbols) and oxidation to CO_2 (closed symbols) $p_{C_2H_4}$=2.48 kPa, p_{O_2}≈3.15 kPa. [45] Reprinted with permission from Academic Press.

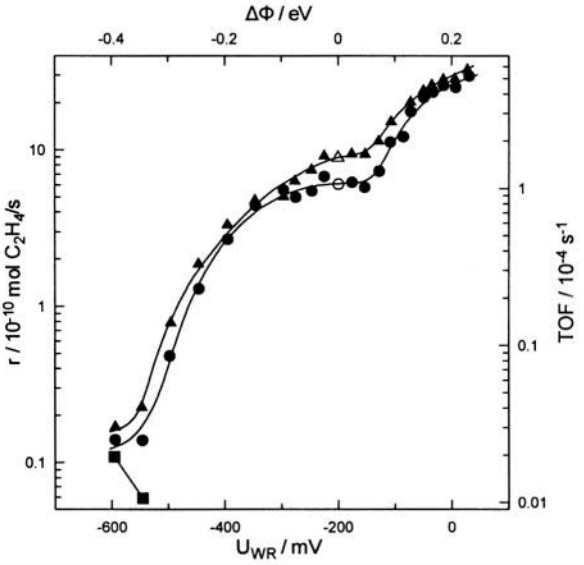

Figure 8.42. Effect of Ag/YSZ catalyst potential and work function on the rates of formation of ethylene oxide, acetaldehyde, and CO_2 at low $p_{O_2}/p_{C_2H_4}$ ratios. T=260°C; P=500 kPa; 3.5% O_2; 9.8% C_2H_4; ▲, C_2H_4O; ■, CH_3CHO; ●, CO_2.[47] Reprinted with permission from Academic Press.

a slight initial increase both E_1 and E_2 decrease substantially with increasing Φ according to:

$$\Delta E_1 = -1.03\ \Delta\Phi \tag{8.18}$$

$$\Delta E_2 = -0.93\ \Delta\Phi \tag{8.19}$$

which again conforms nicely to the linear variation of oxygen heat of adsorption and of reaction activation energy with varying work function (Eqs. 4.56 and 4.58), as already discussed for the case of C_2H_4 oxidation on Pt (section 8.1.1.1). In fact, in view of these equations it appears that the number of bonding electrons of the oxygen chemisorptive bond is n=2 which corresponds to atomically chemisorbed oxygen, in agreement with the prevailing ideas about the C_2H_4 epoxidation system.[48,49]

As expected the preexponential factors behave similarly with activation energies and $k_bT\ln k_i^0$ decreases linearly with increasing Φ (Fig. 8.41)[45]:

$$k_bT\Delta\ln k_1^0 = -0.93\ \Delta\Phi \tag{8.20a}$$

$$k_bT\Delta\ln k_2^0 = -0.81\ \Delta\Phi \tag{8.20b}$$

Similarly to the case of C_2H_4 oxidation on Pt (section 8.1.1.1) one can attribute this decrease to the increased entropy of chemisorbed atomic oxygen due to the weakening of the Ag=O bond with increasing work function Φ.

At lower temperatures (260°C) higher operating pressures (5 bar) and high C_2H_4 to O_2 ratios (Fig. 8.42) ethylene oxide formation and CO_2 formation both exhibit electrophobic behaviour over the entire U_{WR} range.[47] Both rates vary by a factor of 200 as U_{WR} is varied by 0.6 V (ρ varies between 3 and 0.015). The selectivity to ethylene oxide exhibits two local maxima.[47] More interestingly, acetaldehyde appears as a new product.[47]

At higher oxygen pressures acetaldehyde formation appears at higher potentials (Figs. 8.43 and 4.41) and the selectivity to acetaldehyde is up to 55%. Figures 4.41a and b show the effect of adding trace amounts of $C_2H_4Cl_2$ to the feed under NEMCA conditions. Dichloroethane suppresses the formation of acetaldehyde at negative potentials and leads, in conjunction to NEMCA, to ethylene oxide selectivity values up to 75% for positive potentials, (Fig. 8.44). As shown in Chapter 9, even higher ethylene oxide selectivity values can be obtained using sodium, instead of $O^{\delta-}$, as the promoting ion.

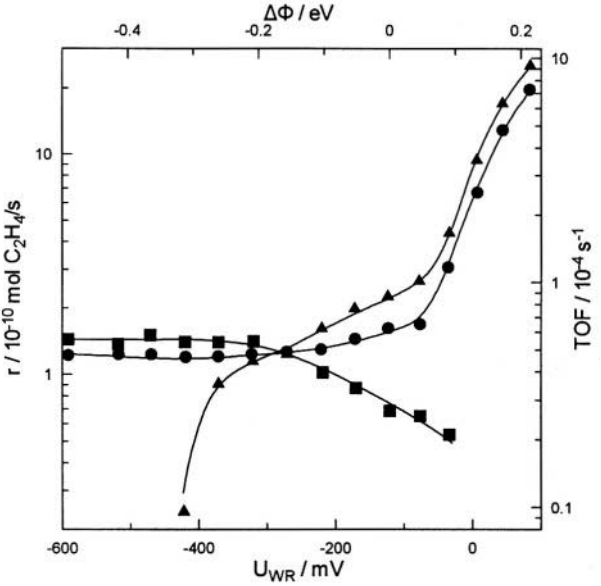

Figure 8.43. Effect of Ag/YSZ catalyst potential and work function on the rates of formation of ethylene oxide, acetaldehyde and CO_2 at high $p_{O_2}/p_{C_2H_4}$ ratios. T=270°C; P=500 kPa; 8.5% O_2; 7.8% C_2H_4; ▲, C_2H_4O; ■, CH_3CHO; ●, CO_2.[47] Reprinted with permission from Academic Press.

8.1.2.2 Methanol Oxidation on Pt and Ag

Methanol oxidation on Pt has been investigated at temperatures 350° to 650°C, CH_3OH partial pressures, p_M, between $5\cdot10^{-2}$ and 1 kPa and oxygen partial pressures, p_{O_2}, between 1 and 20 kPa.[50] Formaldehyde and CO_2 were the only products detected in measurable concentrations. The open-circuit selectivity to H_2CO is of the order of 0.5 and is practically unaffected by gas residence time over the above conditions for methanol conversions below 30%. Consequently the reactions of H_2CO and CO_2 formation can be considered kinetically as two parallel reactions.

The effect of catalyst overpotential and potential on the rates of these two reactions is shown in Figs. 8.45 and 8.46. They both exhibit electrophobic behaviour for $U_{WR} > U^{o}_{WR}$ and electrophilic behaviour for $U_{WR} < U^{o}_{WR}$, i.e. the reaction exhibits pronounced inverted volcano behaviour.

Figure 8.47 shows the effect of the dimensionless potential $\Pi = FU_{WR}/RT$, on product selectivity, S, under constant feed conditions. The selectivity to H_2CO can be varied deliberately between 0.35 and 0.60 by varying the catalyst potential.

Qualitatively similar behaviour for methanol oxidation on Pt/YSZ was reported by Cavalca, Larsen, Vayenas and Haller[51] who used the single chamber design[51] instead of the fuel-cell type design of the earlier study of Neophytides and Vayenas.[50] Cavalca et al[51] took advantage of the electrophobic

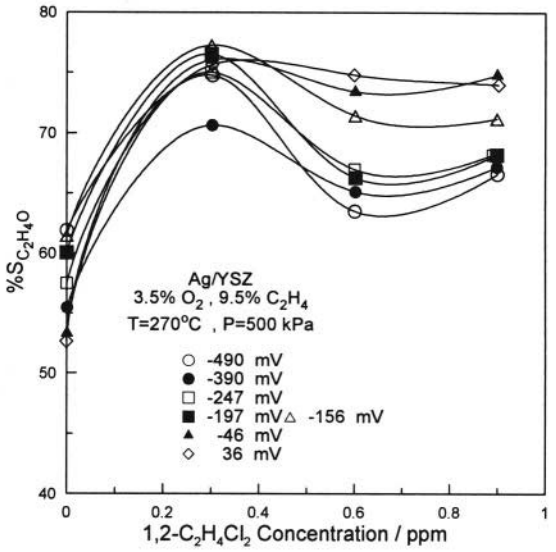

Figure 8.44. Effect of dichloroethane on the selectivity to ethylene oxide during ethylene oxidation on Ag/YSZ at various imposed catalyst potentials.[47] U^{o}_{WR} =-197 mV, T=270°C, P=500 kPa, 3.5% O_2, 9.5% C_2H_4. Reprinted with permission from Academic Press.

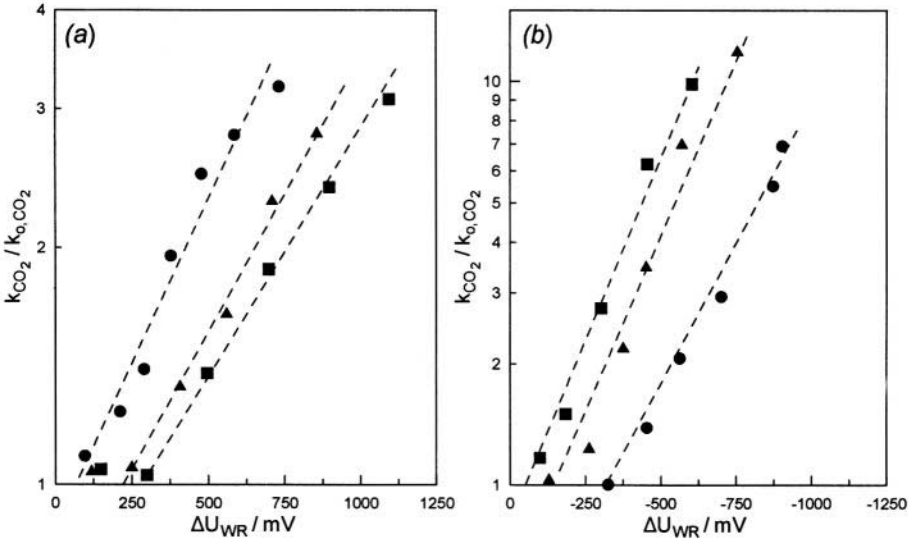

Figure 8.45. Effect of Pt catalyst overpotential on the kinetic constant of CH_3OH oxidation to CO_2 on Pt/YSZ for positive (a) and negative (b) currents. p_{CH_3OH} = 0.9 kPa, p_{O_2}=19 kPa. T=●, 698 K; ▲, 650 K; ■, 626 K; Reprinted with permission from Academic Press.[50]

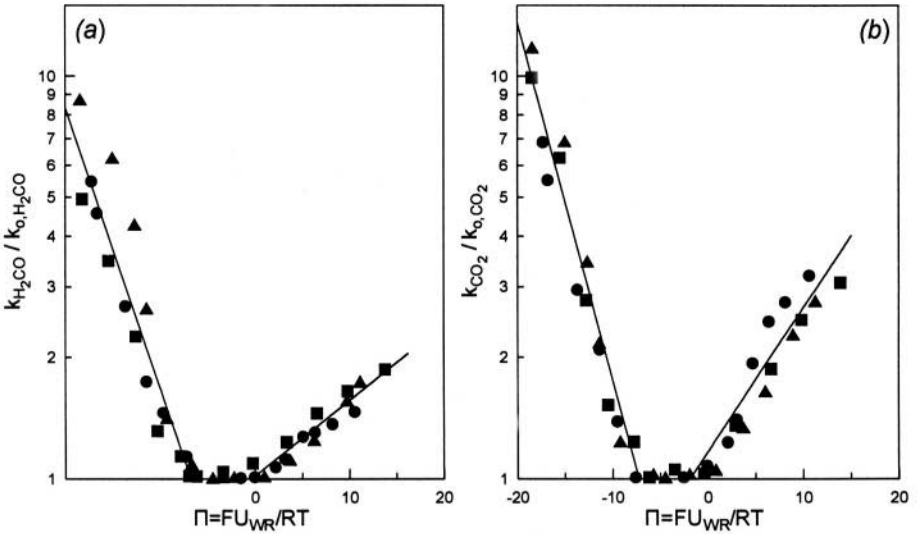

Figure 8.46. Effect of Pt catalyst dimensionless potential $\Pi=FU_{WR}/RT$ on the kinetic constants of formation of formaldehyde (a) and CO_2 (b) during CH_3OH oxidation on Pt/YSZ; Conditions as in Fig. 8.45.[50] Reprinted with permission from Academic Press.

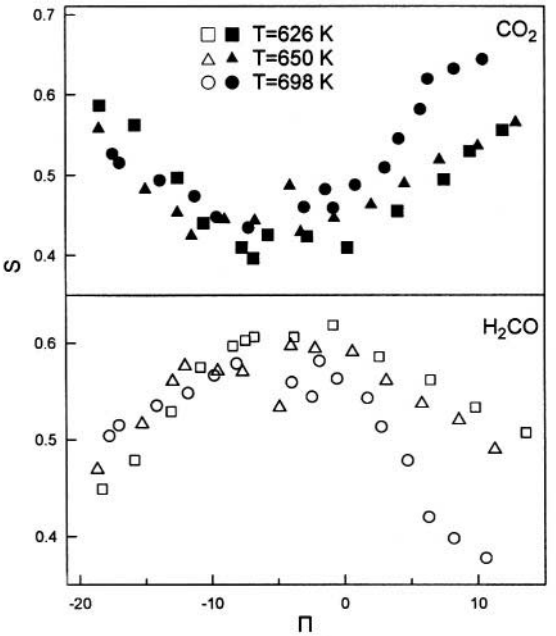

Figure 8.47. Effect of dimensionless catalyst potential $\Pi=FU_{WR}/RT$ on the selectivity to CO_2 and H_2CO during CH_3OH oxidation on Pt/YSZ; Conditions as in Fig. 8.46.[50] Reprinted with permission from Academic Press.

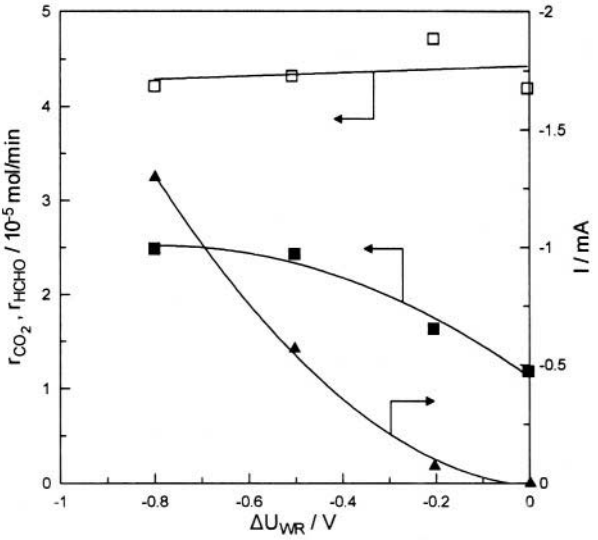

Figure 8.48. Variation of r_{CO2} (■), r_{HCHO} (□), and current (▲) with cathodic overpotential during CH_3OH oxidation on Ag/YSZ. T=500°C, inlet p_{O_2}=5 kPa, and inlet p_{CH_3OH} =5 kPa.[52] Reprinted with permission from Academic Press.

rate dependence at positive potentials (Figs. 8.45, 8.46) to induce NEMCA utilizing not an external power source but rather the potential difference U_{WC} generated between the Pt catalyst-electrode and a more inert (Ag) counter electrode which results from the reaction-induced reduction in oxygen activity on the catalyst-electrode.[51] This concept is now being used to generate power in fuel cells using the so called single-chamber design. This self-driven "wireless" type electrochemical promotion first reported by Cavalca et al.,[51] via short-circuiting the catalyst and the counter electrode, is of paramount importance for practical NEMCA applications of electrophobic reactions.

Methanol oxidation on Ag polycrystalline films interfaced with YSZ at 500°C has been in investigated by Hong et al.[52] The kinetic data in open and closed circuit conditions showed significant enhancement in the rate of CO_2 production under cathodic polarization of the silver catalyst-electrode. Similarly to CH_3OH oxidation on Pt,[50] the reaction exhibits electrophilic behavior for negative potentials. However, no enhancement of HCHO production rate was observed (Figure 8.48). The rate enhancement ratio of CO_2 production was up to 2.1, while the faradaic efficiencies for the reaction products defined from

$$\Lambda_{HCHO}=\Delta r_{HCHO}/(I/2F)\ ;\ \Lambda_{CO_2}=\Delta r_{CO_2}/(I/6F) \tag{8.21}$$

were 0 and -95, respectively.[52]

In general the oxidation of CH_3OH on Pt and Ag exhibits inverted volcano behaviour indicating weak adsorption of methoxy groups and O under the conditions of these investigations[50-52] as also corroborated by the positive-order kinetics[51] in good agreement with promotional rule G4.

8.1.2.3 CH_4 Oxidative Coupling on Ag

The oxidative coupling of CH_4 (OCM) in solid oxide fuel cells has attracted considerable attention in recent years because of the strong interest in the production of C_2 hydrocarbons from natural gas. Work in this area utilizing solid electrolytes prior to 1999 has been reviewed.[53]

It is known[32] reported that the solid electrolyte itself, i.e. Y_2O_3-doped-ZrO_2, is a reasonably selective catalyst for CH_4 conversion to C_2 hydrocarbons, i.e., ethane and ethylene[32] and this should be taken into account in studies employing stabilized ZrO_2 cells. At the same time it was found[54] that the use of Ag catalyst films leads to C_2 selectivities above 0.6 for low methane conversions.

As shown on Fig. 8.49 one can influence dramatically both the total CH_4 conversion as well as product selectivity by varying the Ag catalyst potential. Thus under open-circuit conditions ($U_{WR}= U^o_{WR}$) the CH_4 conversion is near 0.02 with a C_2 selectivity (methane molecules reacting to form C_2H_4 and C_2H_6 per total reacting CH_4 molecules) near 0.5. Increasing U_{WR} increases the methane conversion to 0.3 and decreases the selectivity to 0.23, while decreasing U_{WR} decreases the conversion to 0.01 and increases the

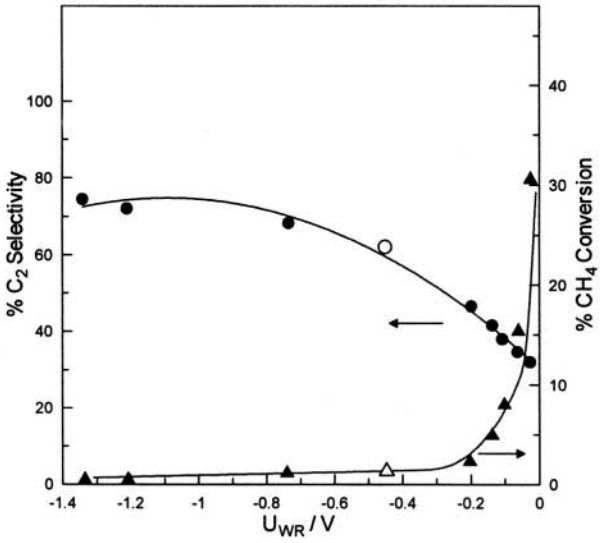

Figure 8.49. Effect of Ag/YSZ catalyst potential on CH_4 conversion and on selectivity to C_2 hydrocarbons. T=800°C, p_{O_2}=0.25 kPa, p_{CH_4}=10.13 kPa, U^o_{WR} =-0.45 V.[2,54] Open symbols correspond to open-circuit. Reprinted from ref. 2 with permission from Elsevier Science.

selectivity to 0.6. The reaction exhibits electrophobic NEMCA behaviour both for I>0 and I<0 with Λ values up to 5. The low Λ values are due to the, unavoidably, high I_0 values (equation 4.20) because of the high operating temperature. Rate enhancement ratios up to 30, 7 and 3.5 were observed for the three main products, i.e., CO_2, C_2H_4 and C_2H_6, respectively.[54]

The rates of C_2H_4, C_2H_6 and CO_2 formation depend exponentially on U_{WR} and Φ according to equation (4.49) with α values of 1.0, 0.75 and 0.4, respectively, for I>0, and of 0.15, 0.08 and 0.3, respectively for I<0. Linear decreases in activation energy with increasing Φ have been found for all three reactions.[54] It should be emphasized, however, that, due to the high operating temperatures, Λ is near unity and electrocatalysis, rather than NEMCA, plays the dominant role.

Nevertheless this system is quite interesting from a technological point of view. As shown more recently,[55] Ag and Ag-Sm_2O_3 anodes operating with pure CH_4 (no oxygen addition, chemical cogeneration mode) lead to C_2H_4 selectivities up to 100% and total C_2H_4 yields up to 85%, when using the zirconia reactor in a gas-recycle loop containing a molecular sieve adsorbent (Molecular sieve 5A) for C_2 hydrocarbon trapping.[55] This is by far the highest ethylene or C_2 hydrocarbon yield obtained so far with the OCM reaction.

Similar studies utilizing Au electrodes on YSZ showed again that the selectivity and yield of C_2 hydrocarbons can be significantly affected by applying currents or potentials to the cell.[40,41,53] The behaviour with Au appears to be qualitatively similar with that obtained with Ag electrodes although electrophilic behaviour is also reported.[40,41]

8.1.3 Dehydrogenation and Hydrogenation Reactions

8.1.3.1 Methanol Dehydrogenation on Ag and Pt

The dehydrogenation and decomposition of CH_3OH on Ag was one of the first catalytic systems for which NEMCA was studied in detail.[56] This investigation was carried out at temperatures 600 to 680°C and CH_3OH partial pressures up to 7 kPa. Total CH_3OH conversion was kept below 20% to avoid consecutive reactions. Under open-circuit conditions the main product is H_2CO (typical selectivity S_{H_2CO} is 0.85-0.90) with lesser amounts of CO (S_{CO}~.07-0.11) and CH_4 (S_{CH_4}~.03 -.05) Residence time in the CSTR had practically[56] no effect on selectivity, so that the three reactions:

$$CH_3OH \rightarrow H_2CO + H_2 \tag{8.22}$$

$$CH_3OH \rightarrow CO + 2H_2 \tag{8.23}$$

$$CH_3OH + H_2 \rightarrow CH_4 + H_2O \tag{8.24}$$

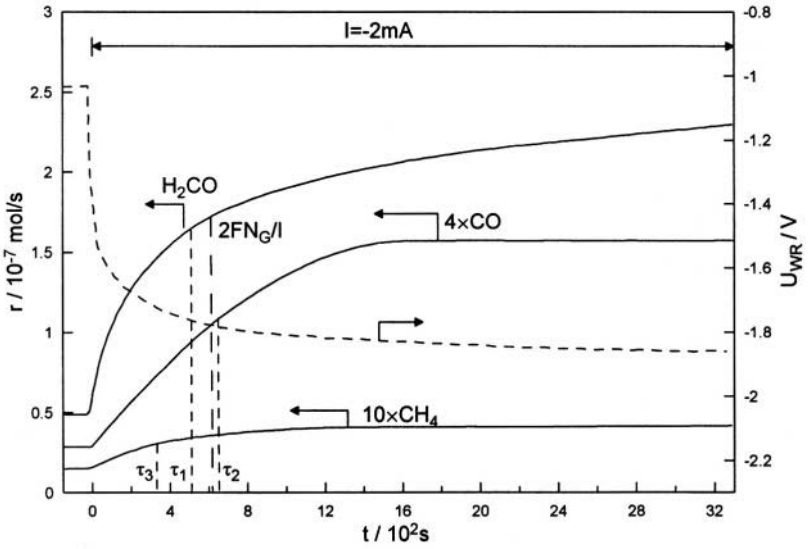

Figure 8.50. Rate and catalyst potential response to a step change in applied current during CH_3OH dehydrogenation and decomposition on Ag. The experimental time constants τ are compared with $2FN_G/I$; T=660°C, p_{CH_3OH}=5.2 kPa.[56] Reprinted with permission from Academic Press.

can be viewed macroscopically and kinetically as parallel reactions obeying simple Langmuir-type rate expressions.[56]

Figure 8.50 shows a typical galvanostatic transient. At the start of the experiment the circuit is open and the rates of H_2CO, CO and CH_4 production are $r_{0,H_2CO}=4.9\times10^{-8}$ mol/s, $r_{0,CO}=7.6\times10^{-9}$ mol/s and $r_{0,CH_4}=1.5\cdot10^{-9}$ mol/s. At t=0 a galvanostat is used to apply a current I=-2 mA with a corresponding rate of O^{2-} removal from the tpb of $I/2F=1.04\times10^{-8}$ mol/s.

This causes a 380% increase in r_{H_2CO} and a 413% increase in r_{CO}. The corresponding enhancement factors are $\Lambda_{H_2CO}=-17.5$, $\Lambda_{CO}=-3$. There is also a 190% increase in r_{CH_4} with an enhancement factor $\Lambda_{CH_4}=-0.3$, but this rate increase has been shown[56] to be Faradaic and due to the electrocatalytic reaction:

$$CH_3OH + 2e^- \rightarrow CH_4 + O^{2-} \tag{8.25}$$

taking place at the tpb. Figure 8.51 shows the effect of the dimensionless catalyst potential $\Pi=\Delta\Phi/k_bT(=FU_{WR}/RT)$ on the rates of formation of H_2CO, CO and CH_4. The α values are -0.14, -0.30 and -0.65 respectively. However, as already noted,[56] the α_{CO} value is the cathodic transfer coefficient for reaction (8.25) and is not a true NEMCA coefficient. The corresponding effect of Π on product selectivity is shown on Fig. 8.52.

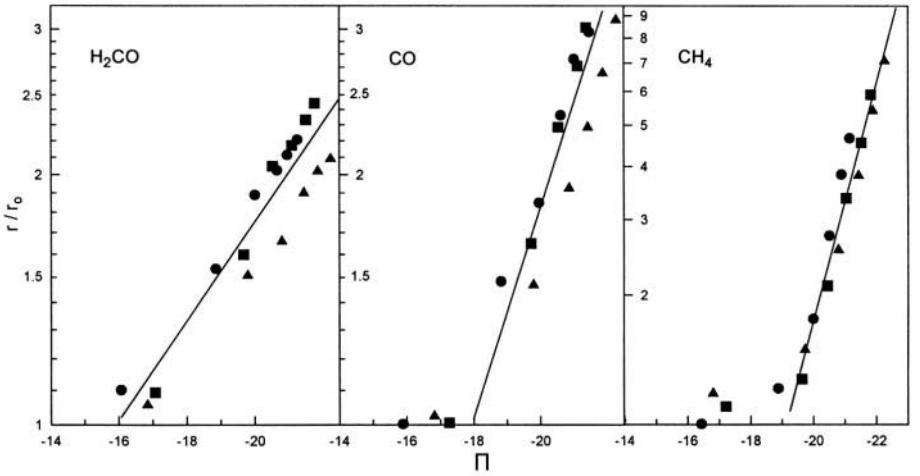

Figure 8.51. Effect of dimensionless catalyst potential $\Pi = FU_{WR}/RT$ on the rates of formation of H_2CO, CO and CH_4 during CH_3OH dehydrogenation and decomposition on Ag/YSZ; p_{CH_3OH}=5 kPa; ▲, T=620°C, ■, T=643°C, ●, T=663°C.[56] Reprinted with permission from Academic Press.

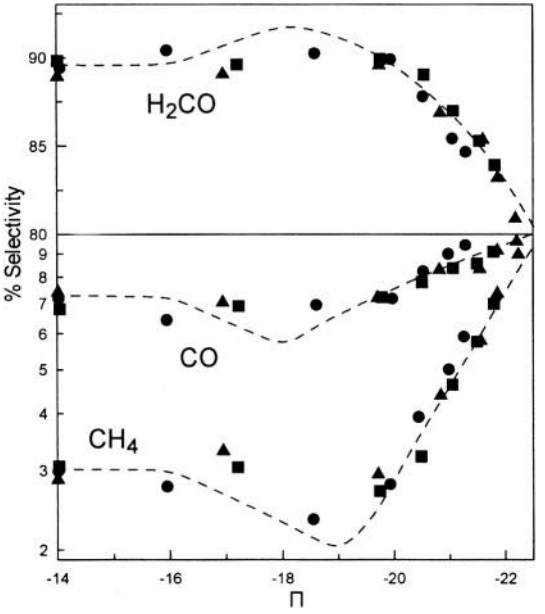

Figure 8.52. Effect of dimensionless catalyst potential $\Pi(=FU_{WR}/RT)$ on product selectivity to H_2CO, CO and CH_4 during CH_3OH dehydrogenation and decomposition on Ag. Conditions and symbols as in Fig. 8.51.[56] Reprinted with permission from Academic Press.

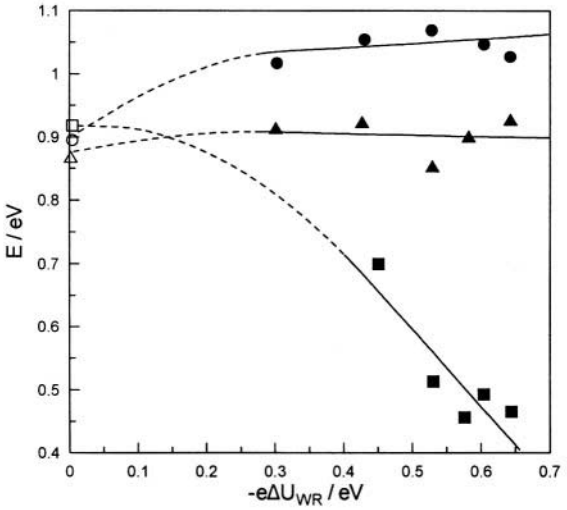

Figure 8.53. Effect of catalyst overpotential on the apparent activation energies of formation of H_2CO (●), CO (▲), and CH_4 (■) during CH_3OH dehydrogenation and decomposition on Ag.[56] Reprinted with permission from Academic Press.

The effect of overpotential ΔU_{WR} on the apparent activation energies E of this reaction system is shown on Fig. 8.53. These are extracted from lnr vs T^{-1} plots and cannot be attributed specifically to any single reaction step. The observed decrease in E_{CH_4} with increasing $|\eta|$ with a slope near -1 is in good qualitative agreement with the classical theory of electrocatalytic reactions.[57]

The observed electrophilic behaviour of the formation of H_2CO and CO has been interpreted by taking into account the strengthening of the chemisorptive bond of methoxy intermediates with decreasing catalyst work function. This strengthening in the chemisorptive bond causes, from classical bond energy bond order conservation considerations, a weakening in the intra-adsorbate C-H bonds and thus facilitates dehydrogenation.[56] More negative potentials, i.e., lower work function values, promote complete dehydrogenation, thus the selectivity to CO increases (Figure 8.52).

A qualitatively similar behaviour has been observed during CH_3OH dehydrogenation on Pt at temperatures between 400° and 500°C, where enhancement factors Λ of the order of -10 were measured.[58]

8.1.3.2 CO_2 Hydrogenation on Rh

The hydrogenation of CO and CO_2 on transition metal surfaces is a promising area for using NEMCA to affect rates and selectivities. In a recent study of CO_2 hydrogenation on Rh,[59] where the products were mainly CH_4 and CO, under atmospheric pressure and at temperatures 300 to 500°C it was found that CH_4 formation is electrophobic (Fig. 8.54a) while CO formation is electrophilic (Fig. 8.54b). Enhancement factor Λ values up to 220 were

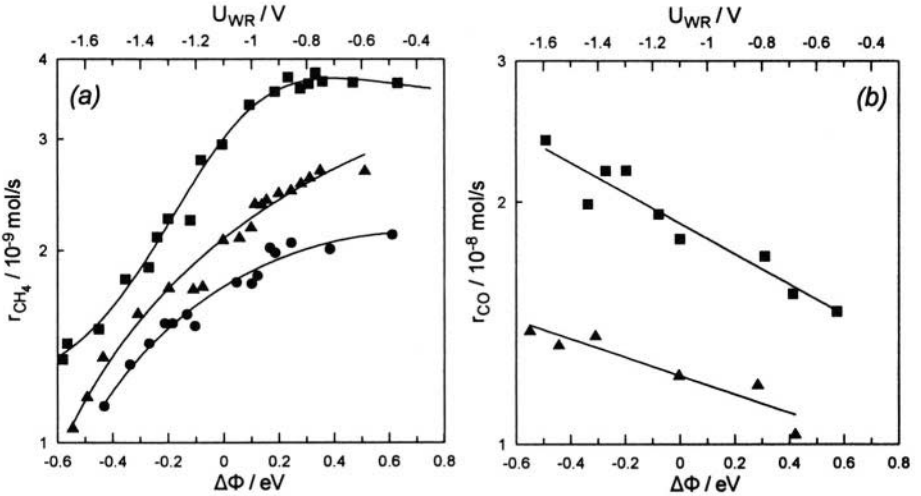

Figure 8.54. Effect of catalyst potential and work function on the rate of CH_4 (a) and CO formation (b) during CO_2 hydrogenation on Rh/YSZ.[5,59] p_{CO_2}=1 kPa; p_{H_2}=1.5 kPa; ●, T=400°C; ▲, T=451°C; ■, T=468°C.

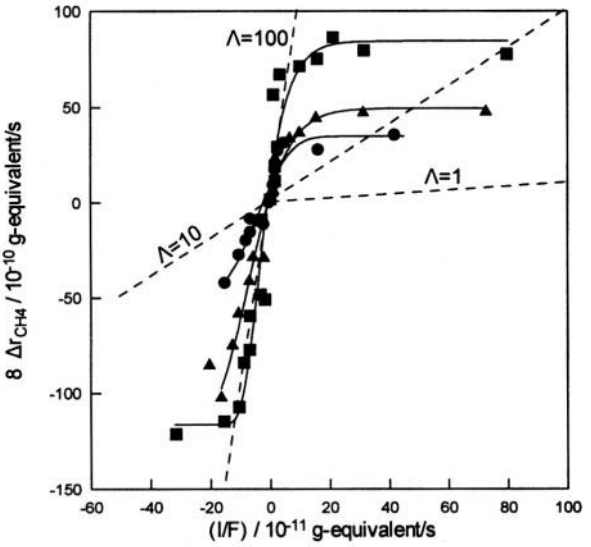

Figure 8.55. Effect of current and concomitant O^{2-} supply/removal on the change in the rate of CH_4 production during CO_2 hydrogenation on Rh/YSZ; p_{CO_2}=1 kPa; p_{H_2}=1.5 kPa; ●, T=400°C; ▲, T= 451°C; ■, T= 468°C.[5,59]

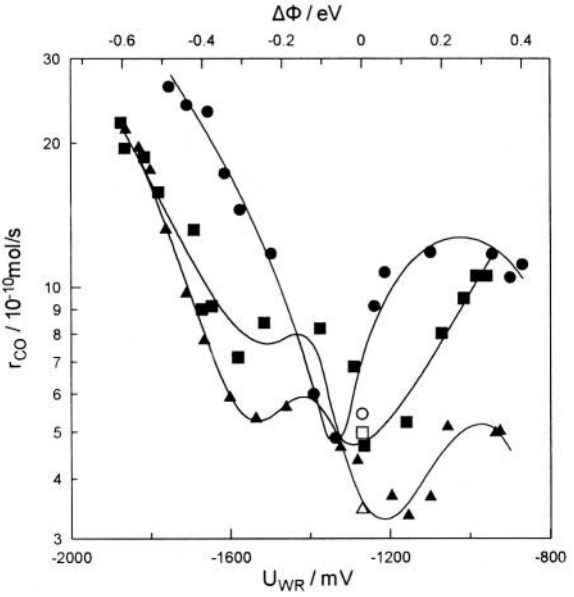

Figure 8.56. Effect of catalyst potential and work function on the rate of CO_2 hydrogenation on Pd/YSZ (reverse water-gas shift reaction). p_{CO_2}=22.5 kPa; p_{H_2}=73 kPa; ▲, T= 546°C; ■, T= 559°C; ●, T= 573°C.[59] Open symbols correspond to open-circuit.

measured (Fig. 8.55) in good agreement with the values calculated from Eq. 4.20.

The observed increase in CH_4 formation and simultaneous decrease in CO formation with increasing catalyst potential and work function i.e. with increasing supply of O^{2-} to the catalyst is remarkable and can be attributed to the preferential formation on the Rh surface of electron donor hydrogenated carbonylic species leading to formation of CH_4 and to the decreasing coverage of more electron acceptor carbonylic species resulting in CO formation.[59]

8.1.3.3 CO_2 Hydrogenation on Pd

The reaction was investigated under atmospheric pressure and at temperatures 500°C to 600°C, where the only product was CO, as Pd, contrary to Rh, does not adsorb CO_2 dissociatively.[59] This difference in reaction pathway is also reflected in the NEMCA behaviour of the system, since in the present case CO formation is enhanced (by up to 600%) not only with decreasing catalyst potential and work function, but also enhanced, although to a minor extent, via catalyst potential increase (Fig. 8.56). Enhancement factor Λ values up to 150 were measured. The reaction exhibits typical inverted volcano behaviour, which is characteristic of the weak adsorption of the reactants at the elevated temperature of this investigation, and thus of promotional rule G4.

8.1.3.4 CO Hydrogenation on Pd

This reaction is of considerable technological interest as Pd catalysts have been investigated thoroughly in recent years for the production of alcohols and other oxygenated products from synthesis gas.

The hydrogenation of CO on Pd was studied under NEMCA conditions in a single chamber YSZ cell reactor[59] at a total pressure of 12.5 bar and temperatures 330 to 370°C. Under these conditions a variety of products is obtained, including hydrocarbons (CH_4, C_2H_4, C_2H_6), alcohols (CH_3OH) and aldehydes (HCHO, CH_3CHO).The distribution of the reaction products depends strongly on temperature and space time.[59]

It was found that both the catalytic rates and the selectivity to the various products can be altered significantly (rate changes up to 250% were observed) and reversibly under NEMCA conditions. Depending on the product, electrophobic or electrophilic behaviour is observed as shown in Fig. 8.57. In addition to the selectivity modification due to the different effect on the rate of formation of each product, acetaldehyde, which is not produced under open circuit conditions is formed at negative overpotentials (Fig. 8.58). Enhancement factor Λ values up to 10 were observed in this complex system.[59]

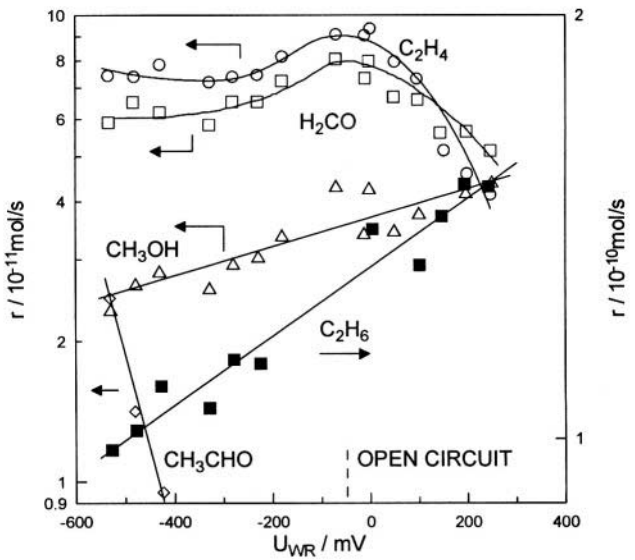

Figure 8.57. Effect of catalyst potential on the rates of formation of C_2H_6, C_2H_4, H_2CO, CH_3OH and CH_3CHO during CO hydrogenation on Pd/YSZ. The rate of CH_4 formation is of the order 10^{-9} mol/s and is only weakly affected by U_{WR}; Single pellet design; P=12.5 bar, T=350°C. p_{H_2}/p_{CO}=1.8, flowrate 85 cm^3 STP/min.[5,59]

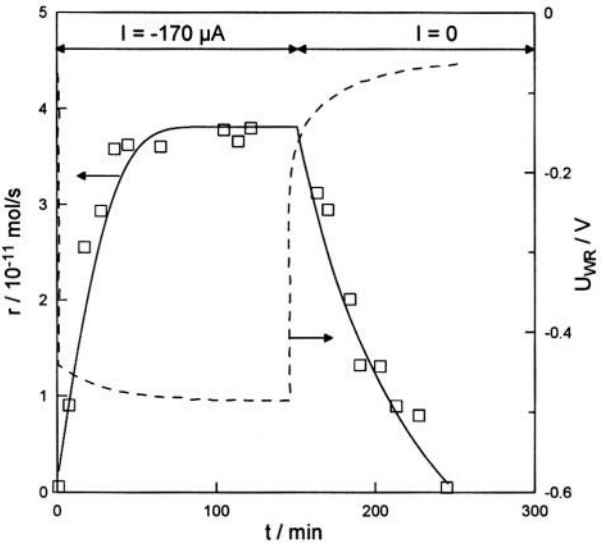

Figure 8.58. Transient effect of applied negative current on the rate of CH_3CHO formation during CO hydrogenation on Pt.[5,59] Acetaldehyde does not form under open-circuit conditions, thus ρ is nominally infinite; P=12.5 bar, T=350°C. p_{H_2}/p_{CO}=1.8, flowrate 85 cm^3 STP/min.[5,59]

8.1.3.5 Methane Reforming on Ni

This reaction is of great technological interest in the area of solid oxide fuel cells (SOFC) since it is catalyzed by the Ni surface of the Ni-stabilized ZrO_2 cermet used as the anode material in power-producing SOFC units.[60,61] The ability of SOFC units to reform methane "internally", i.e. in the anode compartment, permits the direct use of methane or natural gas as the fuel, without a separate external reformer, and thus constitutes a significant advantage of SOFC in relation to low temperature fuel cells.

The extent to which anode polarization affects the catalytic properties of the Ni surface for the methane-steam reforming reaction via NEMCA is of considerable practical interest. In a recent investigation[62] a 70 wt% Ni-YSZ cermet was used at temperatures 800° to 900°C with low steam to methane ratios, i.e., 0.2 to 0.35. At 900°C the anode characteristics were i_0=0.2 mA/cm^2, α_a=2 and α_c=1.5. Under these conditions spontaneously generated currents were of the order of 60 mA/cm^2 and catalyst overpotentials were as high as 250 mV. It was found that the rate of CH_4 consumption due to the reforming reaction increases with increasing catalyst potential, i.e., the reaction exhibits overall electrophobic NEMCA behaviour with α~0.13. Measured Λ and ρ values were of the order of 12 and 2 respectively.[62] These results show that NEMCA can play an important role in anode performance even when the anode-solid electrolyte interface is non-polarizable (high I_0 values) as is the case in fuel cell applications.

8.1.3.6 H_2S Dehydrogenation on Pt

The reaction was investigated by Stoukides and coworkers[63] at temperatures 600 to 750°C and was found to be electrophobic with ρ values up to 11. The counter and reference electrodes were placed either in a separate compartment or in the reactor (single-chamber-design). The rate of H_2S decomposition was found to increase exponentially with U_{WR} and to increase slowly during galvanostatic transients ($\tau \approx 10$ min) as in typical NEMCA experiments. However, no Λ values are reported[63] and it is likely that, due to the high operating temperature, electrocatalysis in addition to NEMCA, plays an important role.

8.1.4 NO Reduction Reactions

Reactions involving the catalytic reduction of nitrogen oxides are of major environmental importance for the removal of toxic emissions from both stationary and automotive sources. As shown in this section electrochemical promotion can affect dramatically the performance of Rh, Pd and Pt catalysts (commonly used as exhaust catalysts) interfaced with YSZ, an O^{2-} ion conductor. The main feature is strong electrophilic behaviour, i.e. enhanced rate and N_2 selectivity behaviour with decreasing U_{WR} and Φ, due to enhanced NO dissociation.

8.1.4.1 NO and N_2O Reduction by CO on Pd/YSZ

Both NO and N_2O reduction on Pd/YSZ[64-66] exhibit electrophilic NEMCA behavior with negative current or potential application. Within the temperature range of the studies[64-66] (600-750K) the catalytic activity of Pd for the reduction of NO or N_2O by CO was enhanced up to 300% and 200%, respectively, while the rate increase of NO reduction was typically more than 700 times larger than the rate of O^{2-} removal from the catalyst via negative current application.

This is shown in Fig. 8.59. Positive potentials (with respect to open circuit potential, $\Delta\Phi=0$) cause no promotional effect on the catalyst performance. On the contrary, as the catalyst potential decreases, all catalytic rates start to increase and the system exhibits electrophilic NEMCA behaviour. These changes in catalytic activity are accompanied by significant changes in nitrogen selectivity, S_{N_2}. The enhancement of the nitrogen selectivity with negative currents or potentials is due to the enhanced dissociative adsorption of NO. The formation of N_2O results from the reaction between atomic nitrogen, N(a) (originating from a dissociatively adsorbed NO) and a molecularly adsorbed NO, NO(a). Thus decreasing θ_{NO} and increasing θ_N favours the formation of N_2 vs that of N_2O.

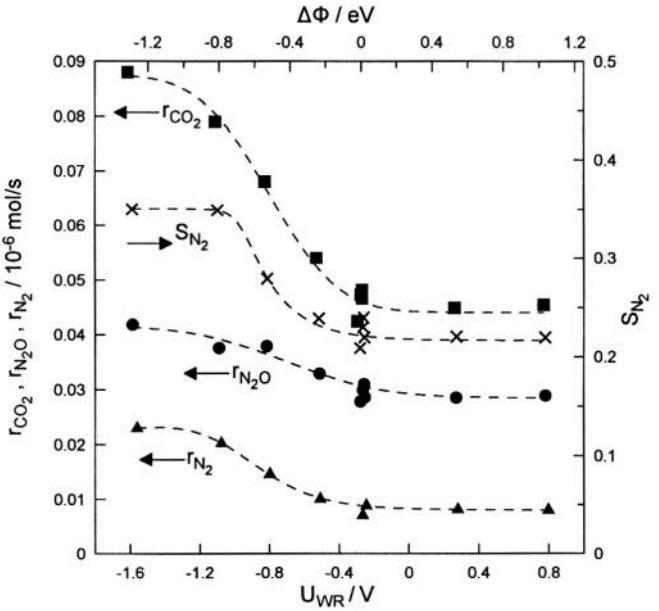

Figure 8.59. Effect of the catalyst potential (U_{WR}) on the CO_2, N_2, N_2O formation rates and the selectivity of NO reduction to N_2. Conditions: T=373°C, inlet composition: p^o_{NO}=1.34 kPa, p^o_{CO}=0.55 kPa.[65] Reprinted with permission from Academic Press.

8.1.4.2 NO Reduction by C_2H_4 on Pt/YSZ

The C_2H_4/NO reaction is a commonly studied model catalytic system for the reduction of NO by a light hydrocarbon. The kinetic and NEMCA investigation of this system was carried out on polycrystalline Pt interfaced with YSZ.[64] The reaction was studied in the temperature range of 380-500°C for gaseous compositions p_{NO}=0-2kPa and $p_{C_2H_4}$=0-4kPa.[64]

The detectable reaction products, in the absence of oxygen, were N_2, N_2O, CO and CO_2, formed according to the following overall reactions:

$$C_2H_4 + 6NO \rightarrow 2CO_2 + 3N_2 + 2H_2O\ ,\ \text{rate: } r_1 \tag{8.27}$$

$$C_2H_4 + 12NO \rightarrow 2CO_2 + 6N_2O + 2H_2O,\ \text{rate: } r_2 \tag{8.28}$$

$$C_2H_4 + 4NO \rightarrow 2CO + 2N_2 + 2H_2O,\ \text{rate: } r_3 \tag{8.29}$$

In addition to these reactions, significant carbon deposition on the Pt surface was found to take place[64] typically accounting for up to 20% of converted C_2H_4.

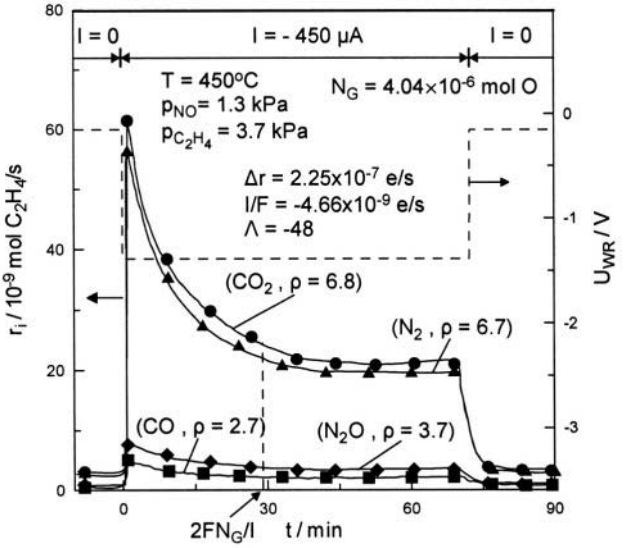

Figure 8.60. Transient effect of applied negative current on the rates of N_2, CO_2, CO and N_2O production on Pt/YSZ (solid curves) and on catalyst potential (dashed curve). Open circuit rates: r_{N_2}=2.93×10^{-9} mol C_2H_4/s, r_{CO2}=3.08×10^{-9} mol C_2H_4/s, r_{CO}=0.77×10^{-9} mol C_2H_4/s, r_{N_2O}=0.92×10^{-9} mol C_2H_4/s.[64] Reprinted with permission from the Institute for Ionics.

As already shown in Figure 6.3b the system exhibits remarkable electrophilic promotional behaviour with ρ values up to 20.[64] This is also shown in Fig. 8.60 which depicts a galvanostatic transient. Application of a negative current between the Pt catalyst-working electrode and the Au counter electrode causes a sharp increase in all reaction rates. In the new steady state of the catalyst (achieved within 1hr of current application) the catalytic rate increase of CO_2 and N_2 production is about 700%, while lesser enhancement (250-400%) is observed in the rates of CO and N_2O production. The appearance of rate maxima immediately after current application can be attributed to the reaction of NO with previously deposited carbon.[64]

The Faradaic efficiency, Λ, for this complex system can be defined from:

$$\Lambda = (12\Delta r_1 + 12\Delta r_2 + 8\Delta r_3)/(I/F) \tag{8.30}$$

since 12, 12 and 8 electrons are transferred in reactions r_1, r_2 and r_3, respectively. Thus the steady state Λ value of Fig. 8.60 is -48, which implies that each electron supplied to the Pt catalyst causes the exchange of 48 electrons due to reactions (8.27) to (8.29). As in other NO reduction NEMCA studies, the promotional action is due to enhanced adsorption and dissociation of NO with decreasing catalyst potential and work function.

8.1.4.3 NO Reduction by C_3H_6 and CO on Rh/YSZ in Presence of Oxygen

The presence of oxygen in the feed composition poses a challenging problem in NO reduction processes. Particularly, in high excess of oxygen, which is the case in lean burn or diesel engines, the high O coverage dominates the catalyst surface and blocks active sites needed for NO adsorption and dissociation. Due to the great environmental importance of such processes, the reduction of NO_x under lean burn conditions has attracted a large number of investigations during the last years.

The NEMCA behavior of NO reduction by C_3H_6 on Rh/YSZ is very pronounced[67,68] and significantly different from NO reduction in absence of gaseous O_2. Thus while in absence of O_2 the main goal of electrochemical promotion is to enhance NO dissociation, and this is achieved by lowering the work function via negative potential application, in presence of oxygen it becomes at least equally important to weaken the Rh=O chemisorptive bond thus enhance the relative NO vs O coverage. This is accomplished by increasing Φ via positive potential application (Chapters 5 and 6) since O is a stronger electron acceptor than NO.

Thus, as shown already in Fig. 4.25, the rates of N_2 and CO_2 formation are enhanced dramatically both with positive and with negative ΔU_{WR} and $\Delta\Phi$.[67,68] As also already shown in Figures 4.51 and 4.52 and also in Figure 8.61 shown here, positive potential or current application leads to rate enhancement, ρ, values up to 125 for the rate of CO_2 formation and up to 50 for the rate of N_2 formation (Figs. 4.51, 4.52 and 8.61).

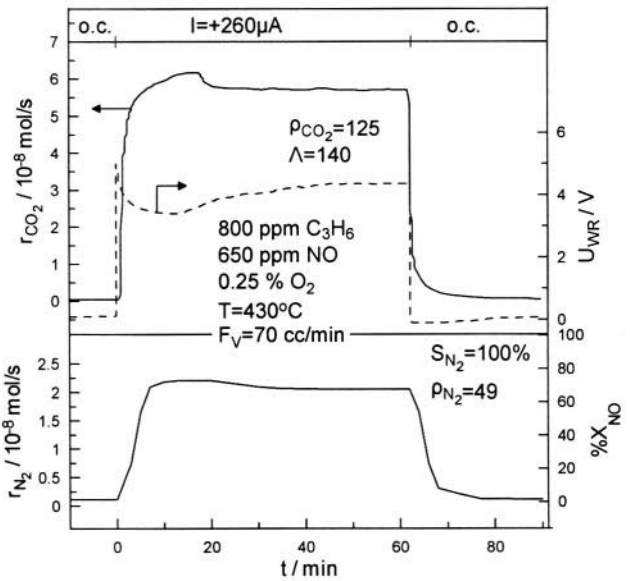

Figure 8.61. Transient effect of a constant applied current on the catalytic rates of CO_2 production, on NO conversion (X_{NO}) and on catalyst potential during NO reduction by C_3H_6 on Rh/YSZ in presence of gaseous O_2.[68] Reprinted with permission from Elsevier Science.

It is worth noting that at lower temperatures (Figs. 4.51, 4.52) positive current application leads to pronounced "permanent" NEMCA behaviour while more reversible NEMCA behaviour is obtained above 400°C (Fig. 8.61).

The ρ value of 125 is the largest one reported so far among NEMCA studies employing YSZ solid electrolyte.[68]

Figure 8.62 shows the effect of temperature and of positive potential application on the reaction rates and on the nitrogen selectivity for the $C_3H_6/NO/O_2$ reaction.[67,68] Electrochemical promotion significantly enhances both activity and N_2 selectivity (e.g. from 58% to 92% at 350°C) and causes a pronounced (60°C) decrease in the light-off temperature of NO reduction in presence of O_2. Positive potentials weaken the Rh=O bond, decrease the O coverage and thus liberate surface sites for NO adsorption and dissociation.

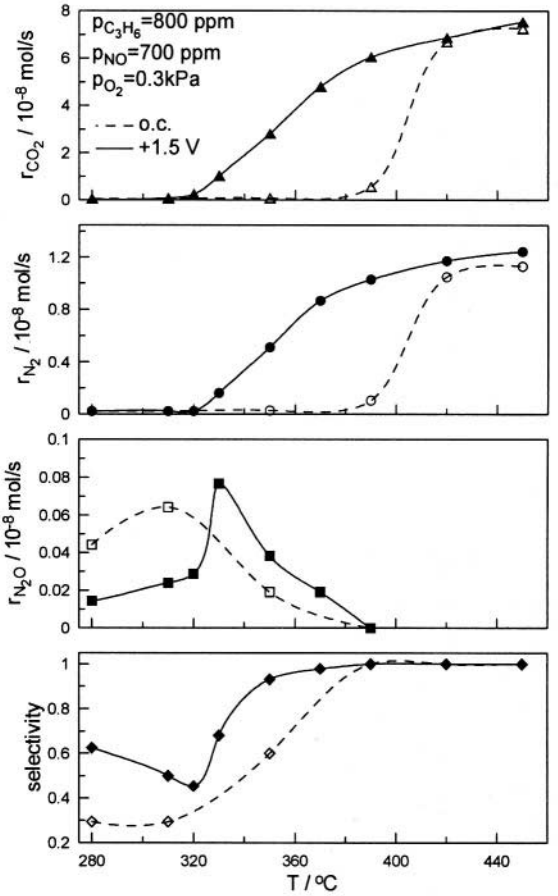

Figure 8.62. Effect of temperature on the catalytic rates of CO_2, N_2 and N_2O formation and on the corresponding N_2 selectivity, for open (unpromoted) and closed (NEMCA) circuit conditions on Rh/YSZ during NO reduction by C_3H_6.[67,68] Reprinted from ref. 68 with permission from Elsevier Science.

Negative potential application, on the other hand leads to enhanced NO dissociation and this also enhances catalytic rate and selectivity leading to the pronounced inverted volcano behaviour shown in figure 4.25.

The same Rh/YSZ catalyst film used for NO reduction by C_3H_6 in presence of O_2 (Fig. 8.63) was also used for NO reduction by CO in presence of O_2.[67,68] As shown in figures 4.52 and 8.64 the behaviour is qualitatively similar.

Positive potentials lead to ρ values up to 20. (Figure 4.52). Negative currents also enhance the rate and selectivity but to a lesser extent (Fig. 8.64). Permanent NEMCA behaviour is also observed with positive currents at lower temperatures (Fig. 4.52). Overall, however, electrochemical promotion is not as pronounced as in the case where propene is used. This can be attributed to the much stronger electron donor character of C_3H_6 relative to CO which, as already noted in this chapter, behaves predominantly as an electron acceptor. Thus positive potentials weaken CO bonding to the surface while they enhance C_3H_6 chemisorption.

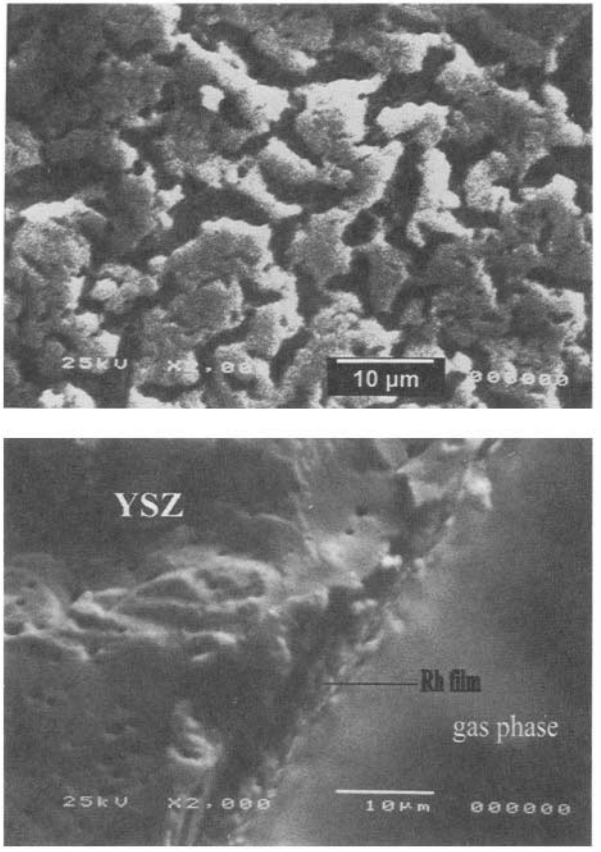

Figure 8.63. Scanning electron micrographs of the Rh/YSZ catalyst; top view (up) and a cross section of the catalyst-solid electrolyte interface (down).[67,68] Reprinted from ref. 67 with permission from the Institute for Ionics.

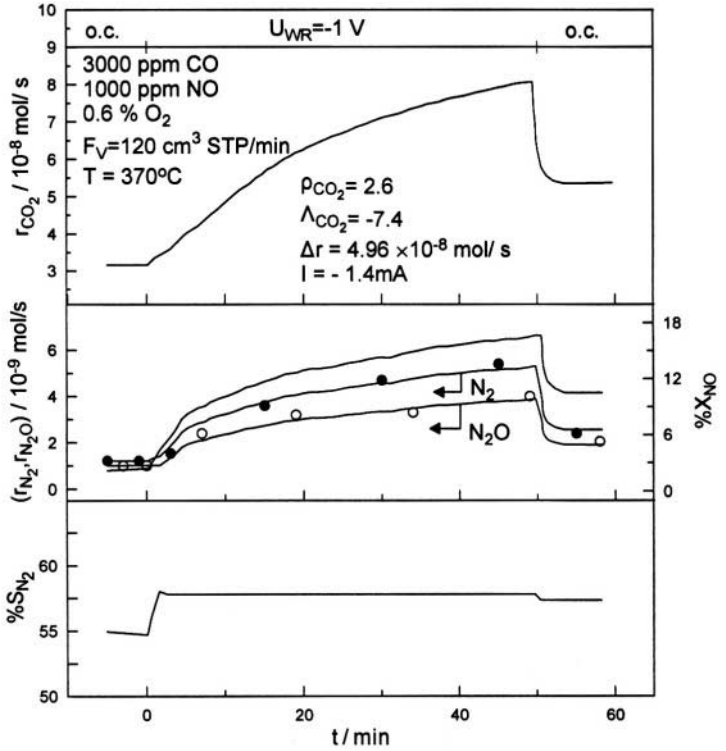

Figure 8.64. Transient effect of a constant negative applied potential on the on the rates of CO_2, N_2 and N_2O formation, on the NO conversion and nitrogen selectivity during NO reduction by CO on Rh/YSZ.[69] Reprinted with permission from Elsevier Science.

8.1.4.4 Electrochemical Promotion of a Classically Promoted Rh Catalyst for NO Reduction by CO in Presence of O_2

This case has been already discussed in Chapter 2 (Fig. 2.3).[69] The Rh film used is shown in Fig. 8.63 and exhibits inverted volcano behaviour,[67] i.e. the rate of CO_2 and N_2 formation is enhanced both with positive and with negative potentials. This is shown in Figure 8.65 and also in Figure 2.3 which depicts the r_{CO_2} and r_{N_2} dependence on T of the unpromoted and electrochemically promoted Rh catalyst. The corresponding r_{N_2O} vs T behaviour is shown in Figure 8.66.

The same Rh/YSZ film was then *classically* promoted with $Na^{\delta+}$ by depositing on its surface a θ_{Na} coverage of approximately 0.03. This was done by dry impregnation of the porous Rh film with 1 μl of a 10^{-2} N NaOH solution followed by thorough drying.[69]

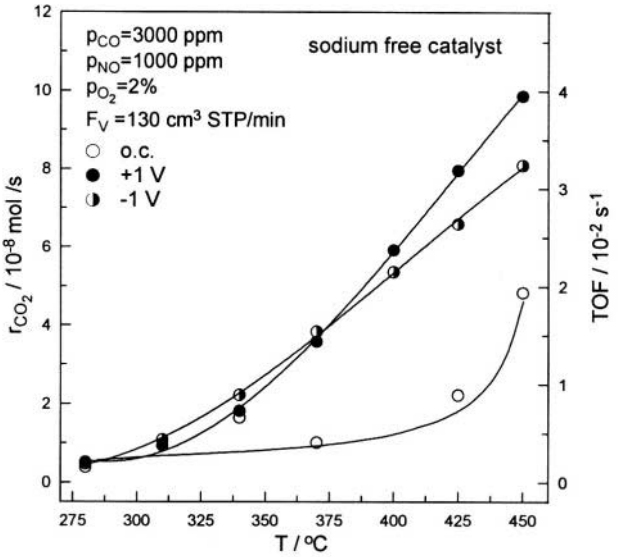

Figure 8.65. Dependence of the catalytic rates and turnover frequencies of CO_2 on the reaction temperature and on the catalyst potential for the initially sodium free Rh/YSZ catalyst (labeled C2) during NO reduction by CO in presence of gaseous O_2.[69] Reprinted with permission from Elsevier Science.

The resulting r_{CO_2}, r_{N_2}, r_{N_2O} and S_{N_2} vs T behaviour of the classically promoted Rh(Na)/YSZ film is shown in Figures 2.3, 8.66 and 8.67 (open squares). All three rates, as well as S_{N_2}, are significantly enhanced.

Subsequently this classically promoted Rh(Na)/YSZ catalyst is subject to electrochemical promotion via application of positive (1V) and negative (-1V) overpotential. The classically promoted catalyst performance is further dramatically enhanced especially in terms of r_{N_2}, r_{N_2O} and S_{N_2} (Figs. 2.3, 8.66 and 8.67) and particularly with positive overpotentials. The resulting ρ_{N_2} and ρ_{N_2O} values are on the order of 10 in the temperature range 240° to 360°C.

Figures 2.3, 8.66 and 8.67 demonstrate two important facts:

1. That a classically promoted catalyst can be further electrochemically promoted.
2. That the synergistic action of an electron donor $(Na^{\delta+})$ and electron acceptor $(O^{\delta-})$ promoter can cause dramatic enhancement in rate and selectivity. This is very likely due to the increase in the field strength, $\tilde{E}$, of the effective double layer discussed in Chapters 5 and 6 and to the concomitant enhanced interaction with the adsorbate dipoles, leading to more pronounced promotional behaviour (Chapter 6).

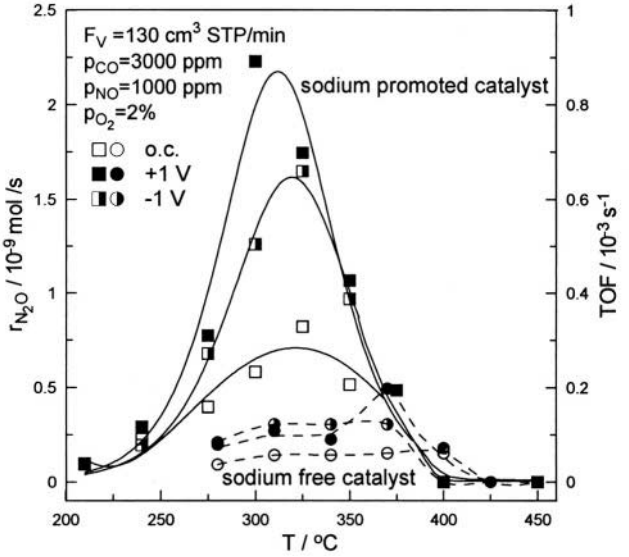

Figure 8.66. Dependence of the catalytic rates and turnover frequencies of N_2O formation of the sodium promoted Rh/YSZ catalyst (squares, continuous lines) on the reaction temperature and on the catalyst potential and comparison with the sodium free catalyst (circles, dashed lines).[69] Reprinted with permission from Elsevier Science.

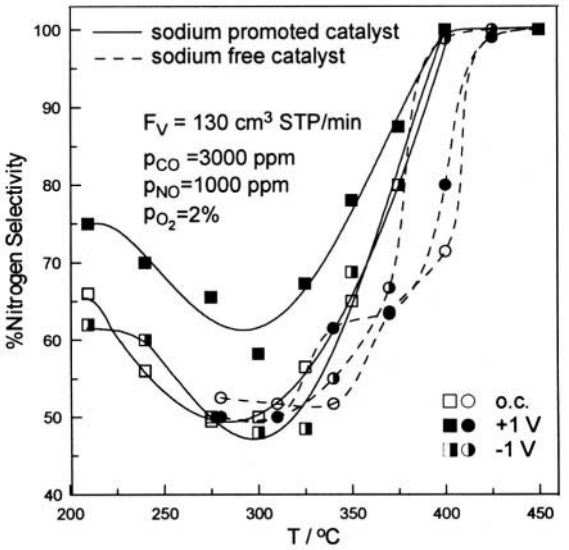

Figure 8.67. Dependence of the nitrogen selectivity on the reaction temperature and on the catalyst potential for the chemically promoted Rh/YSZ catalyst C2.[69] Reprinted with permission from Elsevier Science.

8.2 THE USE OF F^- CONDUCTORS

8.2.1 CO Oxidation on Pt/CaF_2

The oxidation of CO on a Pt film deposited on a single crystal of CaF_2 was investigated[70] at temperatures 500 to 700°C and was found to be electrophobic with ρ values up to 2.5 and Λ values up to 200. Increasing U_{WR} was found to increase the activation energy and preexponential factor, leading to the appearance of the compensation effect with an isokinetic point at 650°C. The promoting role of F^- was found to be qualitatively similar to that of O^{2-} although the ρ and P_i values are significantly smaller than in the case of O^{2-}.

8.3 THE USE OF MIXED CONDUCTORS

The induction of electrochemical promotion (NEMCA) using mixed conductors (TiO_2[24] and CeO_2[71]) which are conventional commercial dispersed catalyst supports, underlines the close similarity between electrochemical promotion and the unusual promoting action of these supports for numerous catalytic reactions.[72,73] Ceria in particular is often added as a promoter on γ-Al_2O_3 supported oxidation catalysts and it is well known for its oxygen storage capacity. TiO_2 is also a very important support which for years attracted the strong attention of the entire catalytic community due to the effect of strong metal-support interaction (SMSI) discovered by Tauster in the seventies[74] and subsequently shown to be primarily due to the migration (decoration) of the well dispersed metal (e.g. Pt) surface with TiO_x moities.[75,76]

Observing NEMCA, and actually very pronounced one, with TiO_2[24] and CeO_2[71] supports was at first surprising since TiO_2 (rutile) and CeO_2 are n-type semiconductors and their ionic (O^{2-}) conductivity is rather low so at best they can be considered as mixed electronic-ionic conductors.[77]

Nevertheless both transient rate analysis[24,71] and XPS[24] have shown that in both cases the electrochemical promotion mechanism is identical with that obtained with YSZ, i.e. electrochemically controlled migration (back-spillover) of O^{2-} onto the gas-exposed catalyst-electrode surface.[24,71]

8.3.1 C_2H_4 Oxidation on Pt/TiO_2

Ethylene oxidation on Pt/TiO_2 was investigated at temperatures 450°C to 600°C and was found to exhibit strong electrochemical promotional behaviour at temperatures near 500°C.[24]

This is a truly exciting electrochemical promotion system which can serve as an excellent example for illustrating the two local and three of the four global promotional rules described in Chapter 6. The reason is that under open-circuit conditions the reaction is positive order in both reactants, as can be seen in subsequent figures.

Thus in the case of Pt/YSZ, oxygen adsorption is favoured vs that of C_2H_4 and thus the system of C_2H_4 oxidation on Pt/YSZ exhibits electrophobic behaviour[1] (Rule L1 and G1) while in the case of Na^+ conducting solid electrolytes (β''-Al_2O_3 and NASICON) C_2H_4 adsorption is favoured vs weakly bonded reactive oxygen (except for extremely low C_2H_4 to O_2 ratios), and thus electrophilic behaviour is observed for C_2H_4 oxidation on Pt/β''-Al_2O_3 or Pt/NASICON[78] (Rule L2 and G2). But in the case of Pt/TiO_2[24] both C_2H_4 and O_2 have comparable, and rather moderate, chemisorptive propensity so that the electrochemical promotion behaviour of the system is quite interesting.

Figure 8.68 shows a typical galvanostatic transient under oxidizing gaseous conditions. The reaction rate is enhanced by a factor of 20 (ρ=21) and the faradaic efficiency Λ (=$\Delta r/(I/2F)$) is 1880. The behaviour is clearly electrophobic ($\partial r/\partial U_{WR}>0$) and strongly reminiscent of the case of C_2H_4 oxidation on Pt/YSZ (Fig. 4.13) with some small but important differences:

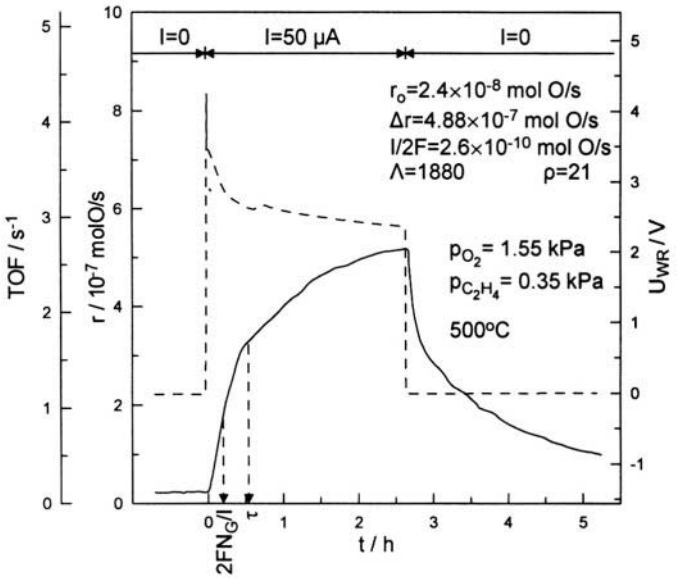

Figure 8.68. Transient effect of applied positive current on the rate and turnover frequency of C_2H_4 oxidation on Pt/TiO_2 (solid curve) and on catalyst potential (dashed curve) at high oxygen to ethylene ratios.[24] Reprinted with permission from Academic Press.

Although the ρ values are comparable (ρ=26 for Pt/YSZ, ρ=21 here) the Λ value is now a factor of 37 smaller ($\Lambda=74\cdot10^3$ for Pt/YSZ, $\Lambda\approx2\cdot10^3$ here) and now τ is a factor of 3 larger than $2FN_G/I$ (Fig. 8.68) while τ is a factor of 3 smaller than $2FN_G/I$ in the case of Pt/YSZ (e.g. Fig. 4.13), i.e. now τ is a factor of 9 longer than in the case of Pt/YSZ. Both observations, i.e. the smaller Λ and the longer τ values are consistent with the fact that only a fraction (3-15%) of the current, I, is ionic (O^{2-}) while the rest is electronic,[77] an idea also corroborated by electrical conductivity data and transient work function measurements and XPS spectra.[24]

Figure 8.69 shows that under oxidizing conditions the rate increases monotonically with I (purely electrophobic behaviour, rule G1) with Λ values of the order of 1500. However as shown in Figure 8.70 when the gaseous composition is reducing, then the reaction exhibits inverted volcano behaviour (rule G4) with Λ values as high as 2×10^3 for I>0 and as low as -2×10^3 for I<0.

Figures 8.71 and 8.72 show the same data but now in terms of catalyst potential. As already discussed in Section 6.4.5 (Fig. 6.24) this transition from purely electrophobic behaviour to inverted volcano behaviour with increasing electron donor partial pressure (i.e. from $p_{C_2H_4}$=0.4 kPa to $p_{C_2H_4}$=5.6 kPa) can be described nicely by the promotional kinetics developed in Chapter 6.

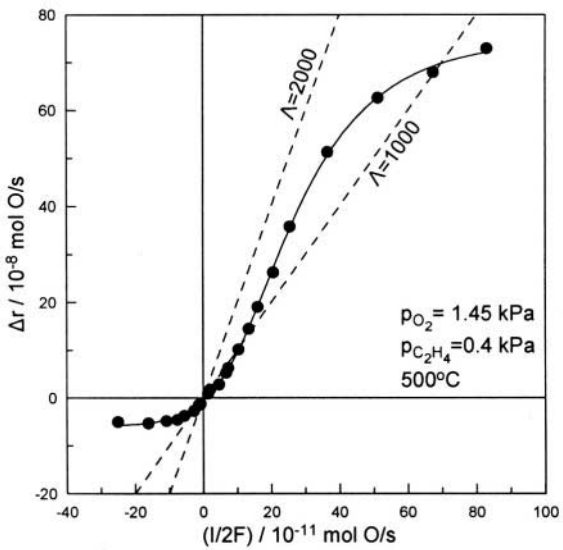

Figure 8.69. Effect of applied current on the change in the rate of C_2H_4 oxidation on Pt/TiO_2 for high oxygen to ethylene ratios. Dashed lines are constant enhancement factor (faradaic efficiency) lines.[24] Reprinted with permission from Academic Press.

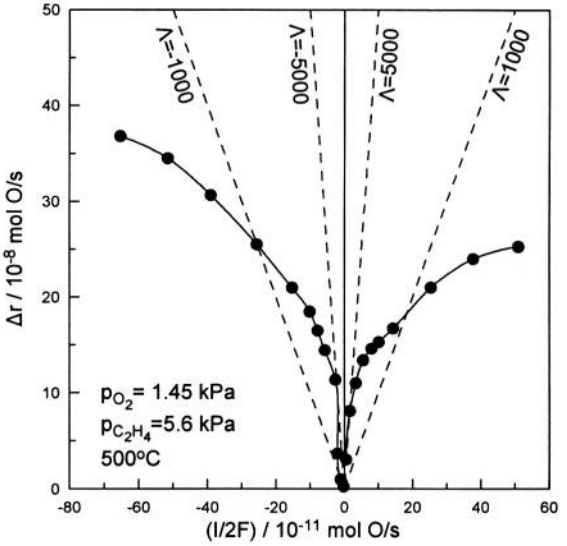

Figure 8.70. Effect of applied current on the change in the rate of C_2H_4 oxidation on Pt/TiO_2 for low oxygen to ethylene ratios. Dashed lines are constant enhancement factor (faradaic efficiency) lines.[24] Reprinted with permission from Academic Press.

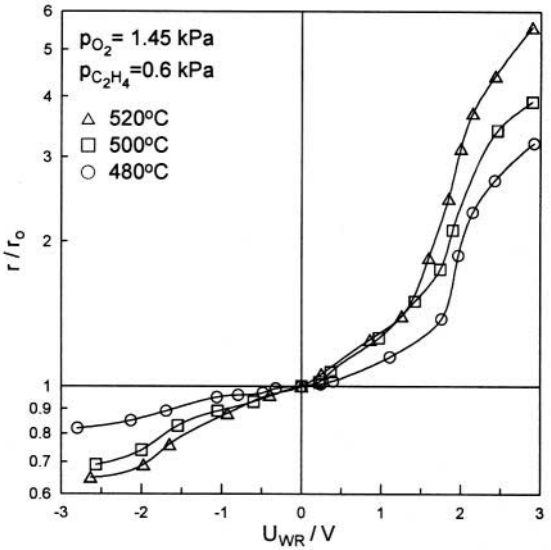

Figure 8.71. Effect of catalyst potential on the rate of C_2H_4 oxidation on Pt/TiO_2 for high oxygen to ethylene ratios.[24] Reprinted with permission from Academic Press.

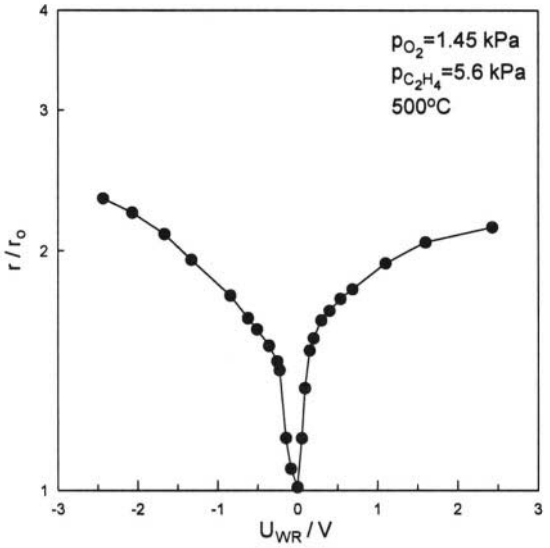

Figure 8.72. Effect of catalyst potential on the rate of C_2H_4 oxidation on Pt/TiO_2 for low oxygen to ethylene ratios.[24] Reprinted with permission from Academic Press.

The underlying surface chemistry is nicely manifest by the kinetics depicted in figs. 8.73 and 8,74. As shown in these figures, under open-circuit conditions the rate is positive order in both C_2H_4 and O_2. As shown in Fig. 8.73 for $p_{C_2H_4}$<1 kPa the rate is positive order in C_2H_4 for all potentials. In the same region the rate increases with potential, i.e. the behaviour is electrophobic. For $p_{C_2H_4}$>2 kPa the behaviour shifts to inverted volcano and at the same time the kinetics become negative order in C_2H_4 for positive potential. It is worth noticing the excellent agreement of the complex kinetics of this figure with the generalized promotional rule of Eq. (6.11):

$$\left(\frac{\partial r}{\partial U_{WR}}\right)_{p_A,p_D}\left(\frac{\partial r}{\partial p_D}\right)_{p_A,U_{WR}} > 0 \qquad (6.11)$$

It is also worth noting the transition from volcano-type kinetics to s-shape type kinetics with respect to $p_{C_2H_4}$ with decreasing potential (Fig. 8.73). Equally good agreement with the generalized promotional rule (Eq. 6.12) is shown by the kinetics with respect to p_{O2} (Fig. 8.74)

$$\left(\frac{\partial r}{\partial U_{WR}}\right)_{p_A,p_D}\left(\frac{\partial r}{\partial p_A}\right)_{p_D,U_{WR}} < 0 \qquad (6.12)$$

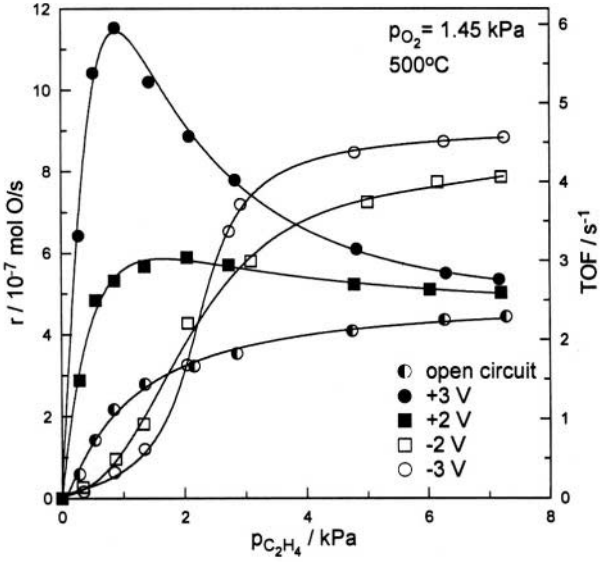

Figure 8.73. Effect of $p_{C_2H_4}$ on the rate of C_2H_4 oxidation at various catalyst potentials during C_2H_4 oxidation on Pt/TiO_2.[24] Reprinted with permission from Academic Press.

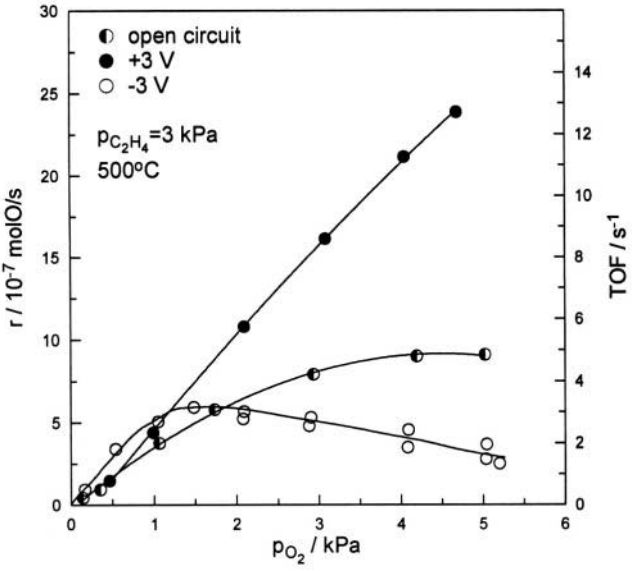

Figure 8.74. Effect of p_{O_2} on the rate of C_2H_4 oxidation at various catalyst potentials during C_2H_4 oxidation on Pt/TiO_2.[24] Reprinted with permission from Academic Press.

Here the rate is inverted volcano type for p_{O_2}<1 kPa, i.e. in the region where it is positive order in O_2 for all potentials, and shifts to purely electrophobic for higher p_{O_2} values where the rate becomes negative order in O_2 for negative potentials.

Figure 8.75 shows the dependence of the apparent activation energy E_a and of the apparent preexponential factor r°, here expressed as TOF°, on U_{WR}. Interestingly, increasing U_{WR} increases not only the catalytic rate, but also the apparent activation energy E_a from 0.3 eV (U_{WR}=-2 V) to 0.9 eV (U_{WR}=+2V). The linear variation in E_a and log (TOF°) with U_{WR} leads to the appearance of the compensation effect where, in the present case, the isokinetic point (T_Θ=300°C) lies outside the temperature range of the investigation.

Figure 8.76 shows the transient response of the work function Φ of the Pt/YSZ catalyst to step changes in applied current. Under purely reducing conditions, in presence of H_2, Φ is not affected by current or potential. This is because, in purely reducing environments, TiO_2 behaves as a purely electronic (n-type) semiconductor.[24,77] Under oxidizing conditions, however, the ionic conductivity of TiO_2 becomes significant with respect to its electronic conductivity[24,77] and thus O^{2-} spillover-backspillover takes place and consequently Φ changes, similarly to the case of Pt/YSZ. The only difference is that ΔΦ changes with U_{WR} according to:

$$\Delta\Phi = fe\Delta U_{WR} \tag{8.31}$$

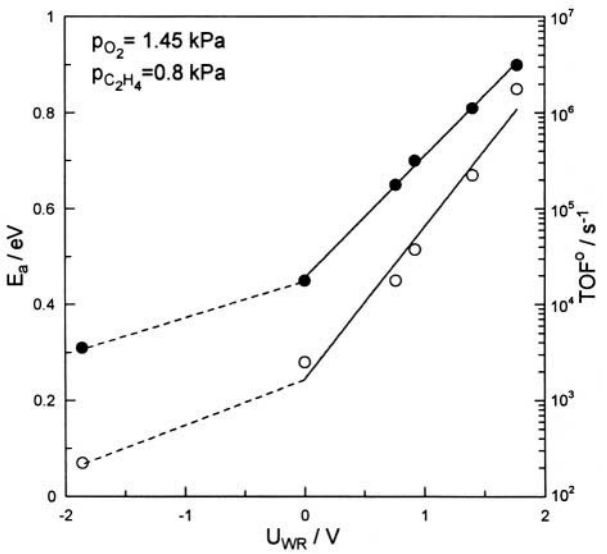

Figure 8.75. Effect of catalyst potential on the apparent activation energy (●) and preexponential factor (○) of C_2H_4 oxidation on Pt/TiO_2.[24] Reprinted with permission from Academic Press.

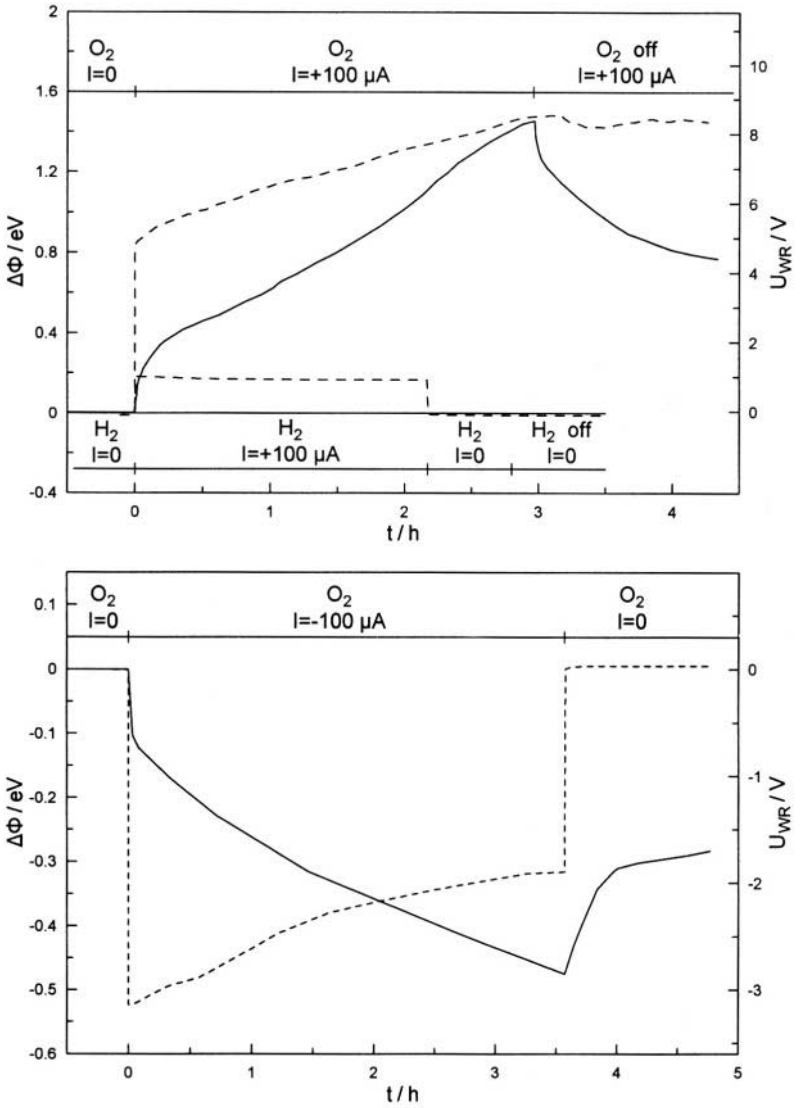

Figure 8.76. (a) Transient effect of applied positive current on the Pt/TiO_2 catalyst potential (dashed line) and on the induced change in the catalyst work function (continuous line) under oxidizing and reducing conditions. In the latter case the work function remains constant; p_{O_2}=54 mPa, p_{H_2}=30 mPa, T=500°C. (b) Transient effect of applied negative current on the catalyst potential (dashed line) and on the induced change in the catalyst work function (solid line) under oxidizing conditions. p_{O_2}=54 mPa, T=500°C.[24] Reprinted with permission from Academic Press.

with f=0.15-0.2, vs f=1 for a regular metal/solid electrolyte interface. The main reason is that only a fraction of ΔU_{WR} is a true overpotential while the remaining fraction (1-f) is a purely ohmic component.

The use of XPS[24] has shown that the O1s binding energy of the spillover $O^{\delta-}$ species is at 528.8 eV, similar to the case of Pt/YSZ. This is quite reasonable since the state of $O^{\delta-}$ on the Pt surface should not depend on the source of O^{2-} (YSZ or TiO_2).

8.3.2 C_2H_4 Oxidation on Pt/CeO_2

Ceria is another type of mixed conducting oxide which has been shown already to induce electrochemical promotion.[71] Ceria is a catalyst support of increasing technological importance.[73] Due to its nonstoichiometry and significant oxygen storage capacity it is also often used as a promoting additive on other supports (e.g. γ-Al_2O_3) in automobile exhaust catalysts.[79] It is a fluorite type oxide with predominant n-type semiconductivity. The contribution of its ionic conductivity has been estimated to be 1-3% at 350°C.[71]

Ethylene oxidation on Pt-catalyst electrodes deposited on CeO_2 can be enhanced significantly via negative current or potential application, i.e., the reaction exhibits electrophilic behavior.[71] The measured rate enhancement ratios, ρ, were up to 3, but the faradaic efficiency values, Λ, were among the largest reported so far (up to 3×10^5). An example is given in Fig. 8.77 which shows the transient effect of a negative applied potential (U_{WR}=-5V) on the reaction rate. Upon potential application the catalytic rate stabilizes to a new steady state which corresponds to a 3-fold enhancement of the catalytic activity (ρ=3). The increase in catalytic rate, Δr, is 5.2×10^4 times larger than

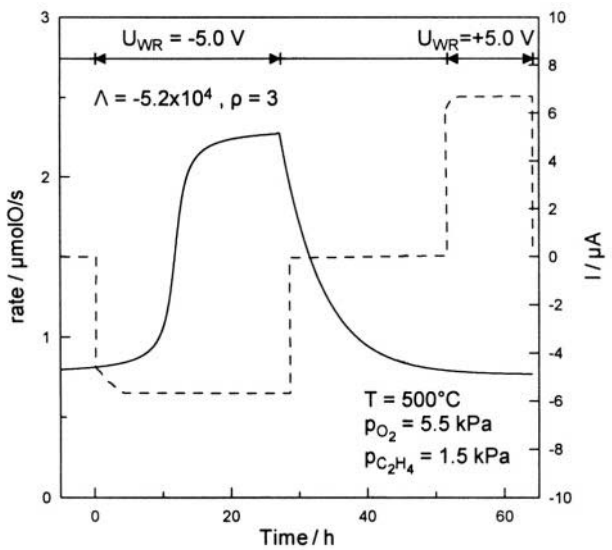

Figure 8.77. Potentiostatic transient of C_2H_4 oxidation on Pt/CeO_2. Rate and current responses to step changes in catalyst potential, U_{WR}, are plotted against time. T = 500°C, p_{O_2} = 5.5 kPa, $p_{C_2H_4}$ = 1.5 kPa.[71] Reproduced by permission of The Electrochemical Society.

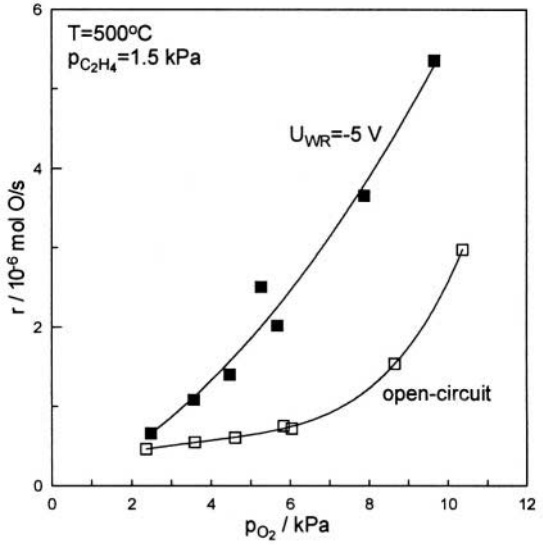

Figure 8.78. Steady-state kinetics of C_2H_4 oxidation on Pt/CeO_2 as a function of catalyst potential, U_{WR}, and oxygen partial pressure. T=500°C, $p_{C_2H_4}$=1.5 kPa.[71] Reprinted by permission of The Electrochemical Society.

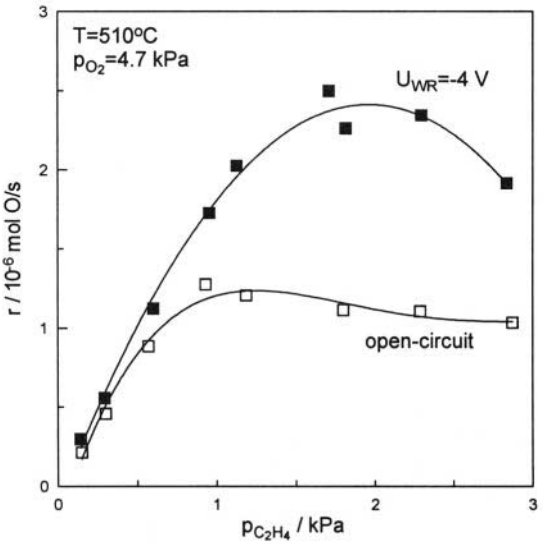

Figure 8.79. Steady-state kinetics of C_2H_4 oxidation on Pt/CeO_2 as a function of catalyst potential, U_{WR}, and ethylene partial pressure (a) catalyst A, T=500°C, p_{O_2}=5.0 kPa (b) catalyst C, T=510°C, $p_{C_2H_4}$=4.8 kPa.[71] Reprinted by permission of The Electrochemical Society.

the faradaic rate I/2F, suggesting a Λ value of -5.2×10^4, if ceria were a pure ionic conductor. But, similarly with the NEMCA investigation on Pt/TiO_2, only a small fraction of current is ionic (i.e. 3%) and therefore, the real

faradaic efficiencies are even higher than the computed Λ values.

As shown in Figure 8.78 the open-circuit rate is positive order in O_2 and, for $p_{C_2H_4}$>1 kPa, negative order in C_2H_4. Consequently, in agreement with global promotional rule G2 it exhibits electrophilic behaviour as already shown in Figure 8.77. Also, as expected, negative potential application weakens the chemisorption of ethylene vs that of oxygen, as manifest by the shift in the rate maximum in Fig. 8.79 to higher $p_{C_2H_4}$ values. Figures 8.77 to 8.79 provide a nice confirmation of global rule G2 regarding global electrophilic behaviour.

REFERENCES

1. S. Bebelis, and C.G. Vayenas, Non-Faradaic Electrochemical Modification of Catalytic Activity: 1. The case of Ethylene Oxidation on Pt, *J. Catal.* **118**, 125-146 (1989).
2. C.G. Vayenas, S. Bebelis, I.V. Yentekakis, and H.-G. Lintz, Non-Faradaic Electrochemical Modification of Catalytic Activity: A status report, *Catal. Today* **11**(3), 304-442 (1992).
3. C.G. Vayenas, S. Bebelis, I.V. Yentekakis, C. Karavasilis, and J. Yi, Non-Faradaic Electrochemical Modification of Catalytic Activity: Solid Electrolytes as Active Catalyst Supports, *Solid State Ionics* **72**, 321-327 (1994).
4. I.V. Yentekakis, and S. Bebelis, Study of the NEMCA effect in a single-pellet catalytic reactor, *J. Catal.* **137**, 278-283 (1992).
5. C.G. Vayenas, M.M. Jaksic, S. Bebelis, and S.G. Neophytides, The Electrochemical Activation of Catalysis, in *Modern Aspects of Electrochemistry,* **No. 29**, J.O' M. Bockris, B.E. Conway, and R.E. White, eds., Kluwer Academic/Plenum Publishers, New York (1996), pp. 57-202.
6. V.A. Sobyanin, V.I. Sobolev, V.D. Belyaev, O.A. Mar'ina, A.K. Demin, and A.S. Lipilin, On the origin of the Non-Faradaic electrochemical modification of catalytic activity (NEMCA) phenomena. Oxygen isotope exchange on Pt electrode in cell with solid oxide electrolyte, *Catal. Lett.* **18**, 153-164 (1993).
7. V.A. Sobyanin, and V.D. Belyaev, On the nature of Non-Faradaic catalysis on metal electrodes, *Reaction Kinetics and Catalysis Letters* **51**(2), 373-382 (1993).
8. M. Boudart, and G. Djega-Mariadassou, *Kinetics of Heterogeneous Catalytic Reactions,* Princeton Univ. Press, Princeton, NJ (1984).
9. M. Boudart, Heterogeneity of Metal Surfaces, *JACS* **74**, 3556-3561 (1952).
10. E. Shustorovich, Energetics of metal-surface reactions: Back-of-the-envelope theoretical modelling, *Journal of Molecular Catalysis* **54**, 301-311 (1989).
11. G. Pacchioni, F. Illas, S. Neophytides, and C.G. Vayenas, Quantum-Chemical Study of Electrochemical Promotion in Catalysis, *J. Phys. Chem.* **100**, 16653-16661 (1996).
12. G. Pacchioni, J.R. Lomas, and F. Illas, Electric field effects in heterogeneous catalysis, *Molecular Catalysis A: Chemical* **119**, 263-273 (1997).
13. C. Pliangos, I.V. Yentekakis, X.E. Verykios, and C.G. Vayenas, Non-Faradaic Electrochemical Modification of Catalytic Activity: 8. Rh-catalyzed C_2H_4 oxidation, *J. Catal.* **154**, 124-136 (1995).
14. E. Cremer, The Compensation Effect in Heterogeneous Catalysis, *Adv. Catal.* **7**, 75-91 (1955).
15. G.-M. Schwab, On the apparent compensation effect, *J. Catal.* **84**, 1-7 (1983).

16. K. Yiokari, and S. Bebelis, In situ controlled electrochemical promotion of catalyst surfaces: Pd-catalysed ethylene oxidation, *J. Appl. Electrochem.* **30**, 1277-1283 (2000).
17. E. Varkaraki, J. Nicole, E. Plattner, C. Comninellis, and C.G. Vayenas, Electrochemical Promotion of IrO_2 catalyst for the gas phase combustion of ethylene, *J. Appl. Electrochem.* **25**, 978-981 (1995); E. Varkaraki, *PhD Thesis,* EPFL (1995).
18. J. Nicole, and C. Comninellis, Electrochemical promotion of IrO_2 catalyst activity for the gas phase combustion of ethylene, *J. Appl. Electrochem.* **28**, 223-226 (1998).
19. J. Nicole, *PhD Thesis*, EPFL (1999).
20. S. Wodiunig, F. Bokeloh, J. Nicole, and C. Comninellis, Electrochemical Promotion of RuO_2 Catalyst Dispersed on an Yttria-Stabilized Zirconia Monolith, *Electrochemical and Solid State Letters* **2**(6), 281-283 (1999).
21. S. Wodiunig, and C. Comninellis, Electrochemical Promotion of RuO_2 Catalysts for the Gas Phase Combustion of C_2H_4, *Journal of the European Ceramic Society* **19**, 931-934 (1999).
22. G. Foti, S. Wodiunig, and C. Comninellis, Electrochemical promotion of catalysts for gas phase reactions, *Current topics in Electrochemistry* **7**, 1 -22 (2000).
23. G. Foti, D. Gandini, and C. Comninellis, Anodic oxidation of organics on thermally prepared oxide electrodes, *Current Topics in Electrochemistry* **5**, 71-91 (1997).
24. C. Pliangos, I.V. Yentekakis, S. Ladas, and C.G. Vayenas, Non-Faradaic Electrochemical Modification of Catalytic Activity: 9. Ethylene oxidation on Pt deposited on TiO_2, *J. Catal.* **159**, 189-203 (1996).
25. S. Wodiunig, *PhD Thesis,* EPFL (1999).
26. D. Tsiplakides, *PhD Thesis,* Department of Chemical Engineering, University of Patras (2001).
27. A. Kaloyannis, and C.G. Vayenas, Non-Faradaic Electrochemical Modification of Catalytic Activity. 11. Ethane Oxidation on Pt, *J. Catal.* **171**, 148-159 (1997).
28. A. Kaloyannis, and C.G. Vayenas, Non-Faradaic electrochemical modification of catalytic activity. 12: Propylene oxidation on Pt, *J. Catal.* **182**, 37-47 (1998).
29. P. Tsiakaras, and C.G. Vayenas, Non-Faradaic Electrochemical Modification of Catalytic Activity: 7. The oxidation of CH_4 on Pt, *J. Catal.* **140**, 53-70 (1993).
30. D. Eng, and M. Stoukides, Catalytic and electrochemical oxidation of methane on platinum, J. *Catal.* **130**, 306-309 (1991).
31. A.D. Frantzis, S. Bebelis, and C.G. Vayenas, Electrochemical promotion (NEMCA) of CH_4 and C_2H_4 oxidation on Pd/YSZ and investigation of the origin of NEMCA via AC impedance spectroscopy, *Solid State Ionics* **136-137**, 863 (2000).
32. S. Seimanides, P. Tsiakaras, X.E. Verykios, and C.G. Vayenas, Oxidative Coupling of Methane over Yttria-doped Zirconia Solid Electrolyte, *Appl. Catal.* **68**, 41-53 (1991).
33. I.V. Yentekakis, and C.G. Vayenas, The Effect of Electrochemical O^{2-} Pumping on the Steady State and Oscillatory Behavior of CO oxidation on Polycrystalline Pt, *J. Catal.* **111**, 170-188(1988).
34. H. Karasali, and C.G. Vayenas, NEMCA: The Oxidation of CO on Pt, *Materials Science Forum* **76**, 171-174 (1991).
35. C.G. Vayenas, C. Georgakis, and J. Michaels, Response to Comments on the Model of Isothermal Oscillations of Ethylene Oxidation on Pt, *J. Catal.* **73**, 201-206 (1982).
36. C.G. Vayenas, S. Bebelis, I.V. Yentekakis, P. Tsiakaras, and H. Karasali, Non-Faradaic Electrochemical Modification of Catalytic Activity on Pt Metals, *Platinum Metals Review* **34**(3), 122-130 (1990).
37. S. Ladas, R. Imbihl, and G. Ertl, Kinetic Oszillatotions during the catalytic CO oxidation on Pd(110): The role of subsurface oxygen, *Surf. Sci.* **219**, 88-106 (1989).

38. C. Karavasilis, S. Bebelis, and C.G. Vayenas, NEMCA: The Oxidation of CO on Ag, *Materials Science Forum* **76**, 175-178 (1991).
39. T.I. Politova, G.G. Gal'vita, V.D. Belyaev, and V.A. Sobyanin, Non-Faradaic catalysis: the case of CO oxidation over Ag-Pd electrode in a solid oxide electrolyte cell, *Catal. Lett.* **44**, 75-81 (1997).
40. O.A. Mar'ina, and V.A. Sobyanin, The effect of electrochemical oxygen pumping on the rate of CO oxidation on Au electrode-catalyst, *Catal. Lett.* **13**, 61-70 (1992).
41. O.A. Mar'ina, V.A. Sobyanin, V.D. Belyaev, and V.N. Parmon, The effect of electrochemical oxygen pumping on catalytic properties of Ag and Au electrodes at gas-phase oxidation of CH_4, *Catalysis Today* **13**, 567-570 (1992).
42. M. Stoukides, and C.G. Vayenas, The effect of Electrochemical Oxygen Pumping on the Rate and Selectivity of Ethylene Oxidation on Polycrystalline Silver, *J. Catal.* **70**, 137-146(1981).
43. M. Stoukides, and C.G. Vayenas, The effect of electrochemical oxygen pumping on the Rate and Selectivity of Propylene Oxidation on Silver in a Solid Electrolyte Cell, *J. Electrochem. Soc.* **131**(4), 839-845 (1984).
44. S. Bebelis, and C.G. Vayenas, Non-Faradaic Electrochemical Modification of Catalytic Activity: 5. Oxygen Chemisorption on Silver, *J. Catal.* **138**, 570-587 (1992).
45. S. Bebelis, and C.G. Vayenas, Non-Faradaic Electrochemical Modification of Catalytic Activity: 6. The epoxidation of Ethylene on $Ag/ZrO_2(8mol\%)Y_2O_3$, *J. Catal.* **138**, 588-610(1992).
46. C. Karavasilis, S. Bebelis, and C.G. Vayenas, Selectivity Maximization of Ethylene Epoxidation via NEMCA with Zirconia and β''-Al_2O_3 Solid Electrolytes, *Ionics* **1**, 85-91 (1995).
47. C. Karavasilis, S. Bebelis, and C.G. Vayenas, Non-Faradaic Electrochemical Modification of Catalytic Activity: 10. Ethylene epoxidation on Ag deposited on stabilized ZrO2 in presence of chlorine moderators, *J. Catal.* **160**, 190-204 (1996).
48. R.A.van Santen, and H.P.C.E. Kuipers, The mechanism of ethylene epoxidation, *Adv. Catal.* **35**, 265-321 (1987).
49. R.B. Grant, and R.M. Lambert, A single crystal study of the silver-catalyzed selective oxidation and total oxidation of ethylene, *J. Catal.* **92**, 364-375 (1985).
50. C.G. Vayenas, and S. Neophytides, Non-Faradaic Electrochemical Modification of Catalytic Activity: 3. The Case of Methanol Oxidation on Pt, *J. Catal.* **127**, 645-664 (1991).
51. C. Cavalca, G. Larsen, C.G. Vayenas, and G. Haller, Electrochemical Modification of CH_3OH oxidation selectivity and activity on a Pt single-pellet catalytic reactor, *J. Phys. Chem.* **97**, 6115-6119(1993).
52. J.K. Hong, I.-H. Oh, S.-A. Hong, and W.Y. Lee, Electrochemical Oxidation of Methanol over a Silver Electrode Deposited on Yttria-Stabilized Zirconia Electrolyte, J. *Catal.* **163**, 95-105 (1996).
53. M. Stoukides, Solid-Electrolyte Membrane reactors: Current experience and future outlook, *Catalysis Reviews - Science and Engineering* **42**(1&2), 1-70 (2000).
54. P. Tsiakaras, and C.G. Vayenas, Oxidative Coupling of CH_4 on Ag catalyst-electrodes deposited on $ZrO_2(8mol\%\ Y_2O_3)$, *J. Catal.* **144**, 333-347 (1993).
55. Y. Jiang, I.V. Yentekakis, and C.G. Vayenas, Methane to Ethylene with 85% Yield in a Gas-Recycle Electrocatalytic Reactor-separator, *Science* **264**, 1583-1586 (1994).
56. S. Neophytides, and C.G. Vayenas, Non-Faradaic Electrochemical Modification of Catalytic Activity: 2. The case of Methanol Dehydrogenation and Decomposition on Ag, *J. Catal.* **118**, 147-163 (1989).

57. J.O.M. Bockris, and A.K.N. Reddy, *Modern Electrochemistry,* Plenum Press, New York (1970), pp. 1-5.
58. S. Neophytides, *PhD Thesis,* Department of Chemical Engineering, University of Patras (1988).
59. H. Karasali, *PhD Thesis,* Department of Chemical Engineering, University of Patras (1994).
60. O. Yamamoto, Solid oxide fuel cells: fundamental aspects and prospects, *Electrochim. Acta* **45**, 2423-2435 (2000).
61. S.C. Singhal, Advances in solid oxide fuel cell technology, *Solid State Ionics* **135**, 305-313 (2000).
62. I.V. Yentekakis, Y. Jiang, S. Neophytides, S. Bebelis, and C.G. Vayenas, Catalysis, Electrocatalysis and Electrochemical Promotion of the Steam Reforming of Methane over Ni Film and Ni-YSZ cermet Anodes, *Ionics* **1**, 491-498 (1995).
63. H. Alqahtany, P.H. Chiang, P. Eng, M. Stoukides, and A.R. Robbat, Electrocatalytic decomposition of hydrogen sulfide, *Catal. Lett.* **13**, 289 (1992).
64. M. Marwood, A. Kaloyannis, and C.G. Vayenas, Electrochemical Promotion of the NO reduction by C_2H_4 on Pt/YSZ and by CO on Pd/YSZ, *Ionics* **2**, 302-311 (1996).
65. M. Marwood, and C.G. Vayenas, Electrochemical Promotion of the Catalytic Reduction of NO by CO on Palladium, *J. Catal.* **170**, 275-284 (1997).
66. G.L. Haller, and S. Kim. *ACS Petroleum Division Preprints, Symposium in Catalytic Combustion* in *213th National ACS Meeting,* 155-158 (1997, April 13-17) San Francisco, CA.
67. C. Pliangos, C. Raptis, T. Badas, and C.G. Vayenas, Electrochemical Promotion of NO Reduction by C_3H_6 and CO on Rh/YSZ Catalyst - Electrodes, *Ionics* **6**, 119-126 (2000).
68. C. Pliangos, C. Raptis, T. Badas, and C.G. Vayenas, Electrochemical promotion of NO reduction by C_3H_6 on Rh/YSZ catalyst-electrodes, *Solid State Ionics* **136/137**, 767-773 (2000).
69. C. Pliangos, C. Raptis, T. Badas, D. Tsiplakides, and C.G. Vayenas, Electrochemical Promotion of a Classically Promoted Rh catalyst for the Reduction of NO, *Electrochim. Acta* **46**, 331-339(2000).
70. I.V. Yentekakis, and C.G. Vayenas, In situ controlled promotion of Pt for CO oxidation via NEMCA using CaF_2 as the solid electrolyte, *J. Catal.* **149**, 238-242(1994).
71. P.D. Petrolekas, S. Balomenou, and C.G. Vayenas, Electrochemical promotion of Ethylene Oxidation on Pt Catalyst Films deposited on CeO_2, *J. Electrochem. Soc.* **145**(4), 1202-1206(1998).
72. T. Beutel, O.S. Alekseev, Y.A. Ryndin, V.A. Likholobov, and H. Knözinger, FTIR Spectroscopic Study and CO Hydrogenation on V, Nb, and Ta Oxide Promoted Rh/SiO_2 Catalysts, *J. Catal.* **169**, 132-142 (1997).
73. S. Rossignol, C. Micheaud-Especel, and D. Duprez, Structural and catalytic properties of Zr-Ce-O mixed oxides. Role of the anionic vacancies, *Stud. Surf. Sci. Catal.* **130**, 3327-3332 (2000).
74. S.J. Tauster, S.C. Fung, and R.L. Garten, Strong metal-support interactions. Group 8 noble metals supported on TiO_2, *JACS* **100**, 170-175 (1978).
75. G.L. Haller, and D.E. Resasco, Metal-Support Interaction: Group VIII Metals and Reducible Oxides, *Advances in Catalysis* **36**, 173-235 (1989).
76. L.L. Hegedus, R. Aris, A.T. Bell, M. Boudart, N.Y. Chen, B.C. Gates, W.O. Haag, G.A. Somorjai, and J. Wei, *Catalyst design: Progress and Perspectives,* John Wiley & sons, New York (1987).
77. P. Kofstad, *Nonstoichiometry, Diffusion and Electrical Conductivity in Binary Metal Oxides,* Wiley Interscience, New York (1972).

78. S. Bebelis, M. Makri, A. Buekenhoudt, J. Luyten, S. Brosda, P. Petrolekas, C. Pliangos, and C.G. Vayenas, Electrochemical activation of catalytic reactions using anionic, cationic and mixed conductors, *Solid State Ionics* **129**, 33-46 (2000).
79. R.J. Farrauto, and C.H. Bartholomew, *Fundamentals of industrial catalytic processes,* Chapman & Hall, London (1997).

CHAPTER 9

ELECTROCHEMICAL PROMOTION WITH CATIONIC CONDUCTORS

9.1 THE USE OF ALKALI ION CONDUCTORS

It has been known since 1991[1] that β''-Al_2O_3, a Na^+ conductor,[2,3] can also induce pronounced electrochemical promotion (NEMCA) behaviour on metal surfaces. Here the dominant electrocatalytic reaction is :

$$Na^+(\beta''\text{-}Al_2O_3) + e^- \rightarrow Na(a) \tag{9.1}$$

where Na(a) stands for Na adsorbed on the metal catalyst film surface. An attractive feature of using β''-Al_2O_3 or other cation donors is that one can compute coulometrically, via Faraday's law, the amount and coverage of alkali dopant introduced onto the catalyst surface. Furthermore, as already described in Chapter 4, one can then compare computed dipole moments with those obtained in classical promotional studies (Chapter 2).

9.1.1 Ethylene Oxidation on Pt/β''-Al_2O_3

Ethylene oxidation on Pt/β''-Al_2O_3 was studied[1] at temperatures 150° to 300°C, but most of the NEMCA experiments were carried out at 290°C. Experimental details about the cell can be found in ref. 1. The open-circuit kinetic behaviour was found to be similar to the case of C_2H_4 oxidation on Pt/YSZ (Chapter 8), i.e. the rate expression:

$$r_0 = kk_{ad}p_{C_2H_4}p_{O_2}/(kp_{C_2H_4} + k_{ad}p_{O_2}) \tag{9.2}$$

was found to provide a quantitative fit to the data at temperatures above 250°C, i.e., when the coverage of C_2H_4 becomes negligible.[1] However, and despite the similarity in turnover frequency values measured under similar T and gas composition conditions, it was found that the open-circuit k values are significantly higher, by a factor of 20, and the k_{ad} values are significantly lower, by a factor of 100, than in the case[4,5] of Pt/doped ZrO_2. Experimentally this makes it much more difficult to work on the fuel-lean side ($kp_{C_2H_4} \ll k_{ad}p_{O_2}$), where the NEMCA effect is very pronounced, with Pt/β''-Al_2O_3 than with Pt/YSZ. The origin of this difference in the kinetic constant values is not obvious but may be related to the large systematic difference (~0.5 eV) observed[1] in the work functions of Pt/β''-Al_2O_3 vs Pt/YSZ. It was also noticed that during catalyst film preparation the Pt surface gets contaminated by Na, presumably due to Na diffusion during calcination, but that this Na contamination can then be removed electrochemically,[1] as also confirmed by XPS[6,7] and STM.[8]

Figure 9.1 shows a typical galvanostatic and potentiostatic transient. At the start of the experiment the circuit is open and the steady-state (regular) catalytic rate ro is 5.7×10^{-7} mol O/s with a corresponding U^o_{WR} of -430 mV. At t = 0 a galvanostat is used to apply a constant current I = -20 μA between the catalyst and the counter electrode. Sodium cations Na^+ are pumped onto the catalyst surface at a rate I/F of 2.1×10^{-10} mol/s. This causes a 66% decrease in catalytic rate which drops to 2.1×10^{-7} mol O/s. The steady-state change in catalytic rate $\Delta r=-3.6\times10^{-7}$ mol O/s is 1720 times larger than the rate of supply of Na^+. The corresponding enhancement factor Λ is 3440, i.e., the reaction exhibits again electrophobic behaviour as in the case of Pt/YSZ. At the same time the catalyst potential and work function decrease in a complex manner. The catalytic rate transient is complete before the appearance of the second break in the U_{WR} transient at -900 mV, in agreement with the steady-state behaviour described below. The rate relaxation time constant τ is 250 s, in reasonable agreement with:

$$\tau = FN_G\theta_{Na}/I \tag{9.3}$$

where N_G is the catalyst surface area in mol Pt and θ_{Na} can be computed either from Faraday's law or also from the induced Φ change, using literature values for the initial dipole moment P^0_{Na} of Na on Pt.[1] The latter is possible in view of the excellent agreement in the P^0_{Na} values computed from the initial slopes of Φ vs I galvanostatic transient plots, such as Figs. 4.15 and 9.1, with literature P^0_{Na} values as described in detail in Chapter 4. Thus, the dotted line on Fig. 9.1 results from equation (4.25) with $A_C=4.25\times10^{-2}$ m^2, I=-20 μA and the literature value of $P_o=1.75\times10^{-29}$ Cm for the initial dipole moment of Na/Pt(lll).[9]

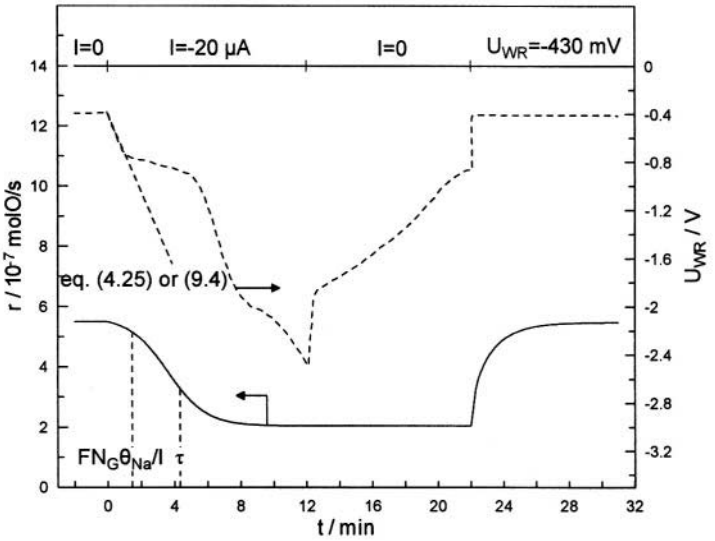

Figure 9.1. Rate and catalyst potential response to application of a negative current (Na supply to the catalyst) during C_2H_4 oxidation on Pt/β″-Al_2O_3, followed by potentiostatic restoration of the initial state[1]; T=291°C, p_{O_2}=5.0 kPa, $p_{C_2H_4}$=2.1×10^{-2} kPa. Reprinted with permission from Academic Press.

As shown on Figure 9.1 when the circuit is opened (I = 0) the catalyst potential starts increasing but the reaction rate stays constant. This is different from the behaviour observed with O^{2-} conducting solid electrolytes and is due to the fact that the spillover oxygen anions can react with the fuel (e.g. C_2H_4, CO), albeit at a slow rate, whereas Na(Pt) can be scavenged from the surface only by electrochemical means.[1] Thus, as shown on Fig. 9.1, when the potentiostat is used to impose the initial catalyst potential, U^{o}_{WR} =-430 mV, then the catalytic rate is restored within 100-150 s to its initial value, since Na(Pt) is now pumped electrochemically as Na^+ back into the β″-Al_2O_3 lattice.

The steady-state effect of work function on catalytic rate is shown on Fig. 9.2. As in the case of using doped-ZrO_2 as the solid electrolyte,[4,5] there is a U_{WR} and corresponding Φ range where the rate increases exponentially with Φ. At higher Φ values the rate levels off because in this region oxygen chemisorption becomes rate limiting and the rate constant k_{ad} is, similarly to the case of YSZ solid electrolyte ion donor, rather insensitive to changing Φ.

Also the rate plateau at low Φ values is strongly reminiscent of the observed behaviour with Pt/YSZ. Thus the behaviour is qualitatively very similar. The inserted θ_{Na} abscissa in Fig. 9.2 is constructed on the basis of Eq. (4.25) or of the following equivalent form of the Helmholz equation:

$$\Delta\Phi = (N_G P^0_{Na}/\varepsilon_0)\theta_{Na} \tag{9.4}$$

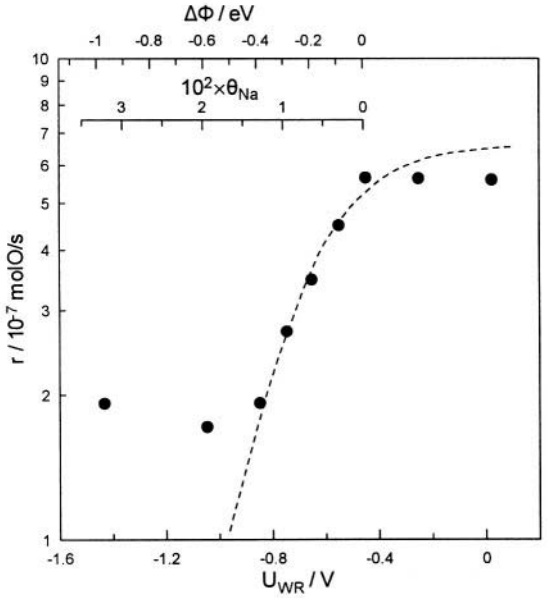

Figure 9.2. Effect of catalyst potential U_{WR}, work function Φ and corresponding Na coverage on the rate of C_2H_4 oxidation on Pt/β″-Al_2O_3.[1] The dashed line is from the kinetic model discussed in ref. 1. p_{O_2}=5.0 kPa, $p_{C_2H_4}$=2.1×10^{-2} kPa, T=291°C, k_{ad} = 12.5 s^{-1}. Reprinted with permission from Academic Press.

and is also in very good agreement with θ_{Na} computed coulometrically via Faraday's law.[1] As shown in Fig. 9.2, a θ_{Na} value of the order of 0.01 suffices to decrease the catalytic rate by a factor of 3.

Figure 9.3 shows the dependence of the Eley-Rideal kinetic constant k on U_{WR} and Φ. For -830 mV<U_{WR}<-430 mV, k is exponentially dependent on Φ according to:

$$\ln(k/k_0)= \alpha e(\Phi-\Phi^*)/k_bT \tag{9.5}$$

with α=0.29. Thus, despite the qualitative similarities in the NEMCA behaviour of C_2H_4 oxidation using Pt/YSZ and Pt/β″-Al_2O_3, there do exist quantitative differences, as α is in the range 0.5 to 1.0 for Pt/YSZ.[4,5]

It is worth emphasizing, however, that in both cases C_2H_4 oxidation exhibits electrophobic behaviour, that the relaxation time constants τ can be estimated from similar formulae (equations (4.32) and (9.3)) and that the enhancement factors Λ can again be estimated from the same formula[1] (equation 4.20).

The fact that very small Na coverages (θ_{Na}=0.015) suffice to induce pronounced (up to 70%) decreases in catalytic rate (i.e. the Na "toxicity"[10,11] is 0.70/0.015 = 47) rules out the possibility of any "geometric" interpretation

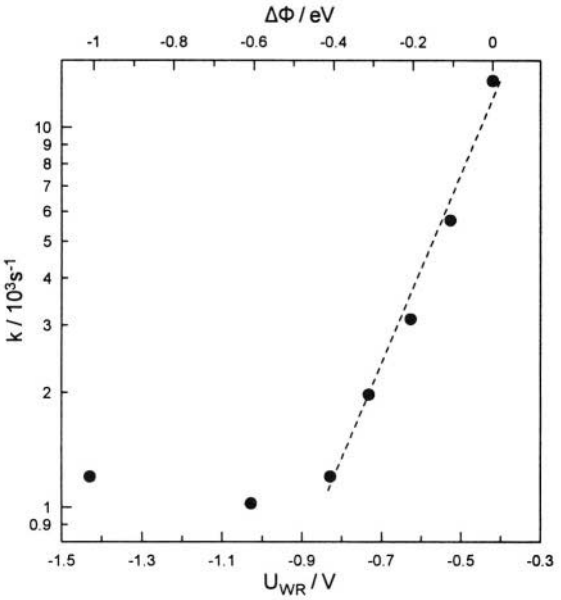

Figure 9.3. Effect of catalyst potential and work function on the kinetic constant k of C_2H_4 oxidation on Pt/β″-Al_2O_3.[1] The dashed line is line from the kinetic model of Ref. 1. p_{O_2}=5.0 kPa, $p_{C_2H_4}$=2.1×10^{-2} kPa, T=291°C, k_{ad} = 12.5 s^{-1}. Reprinted with permission from Academic Press.

of NEMCA. It also provides strong evidence for some "long range" electronic interactions as already confirmed by STM,[8] see Chapter 5. For if the effect of each Na atom were localized to those Pt atoms immediately adjacent to it, then for θ_{Na} = 0.015 one would expect at most a 10% rate decrease, i.e., a factor of 7 smaller than the observed one. Although surface heterogeneity could play a role, the observed behaviour[1] is strongly reminiscent of the infrared spectroscopic (IRS) work of Yates and coworkers,[12] who studied the CO+K/Ni(111) system and found evidence that a single K atom can influence as many as 27 coadsorbed CO molecules.

One can explain the observed exponential decrease in the kinetic constant k with decreasing Φ (Fig. 9.3 and equation 9.5) by the same physical reasoning used to explain the k dependence on Φ with ZrO_2 solid electrolytes: Spillover $Na^{\delta+}$-compensating charge dipoles cause a more or less uniform decrease in Φ and a concomitant increase in the strength of the Pt=O bond, cleavage of which is rate limiting.[1] To the extent that the heat of adsorption of oxygen increases strongly with decreasing Φ (Chapter 2), one can then directly explain the observed exponential dependence of k on Φ.

It is also worth emphasizing the excellent agreement in the initial dipole moment P^0 values for Na/Pt computed in ref. 1 with literature values for Na/Pt(111).[9,13] This agreement shows that Na introduced on the catalyst surface via β″-Al_2O_3 to induce NEMCA is in the same binding state with Na

introduced from the gas phase,[13-17] a point nicely confirmed via the use of XPS by Lambert and coworkers.[6,7,18] The advantage of β''-Al_2O_3 is, as previously discussed, the possibility of in situ monitoring and controlling the dopant coverage.

In a more recent study[19] Harkness and coworkers found that at lower temperatures where the r vs $p_{C_2H_4}$ dependence exhibits a maximum[1,19] the r vs U_{WR} (thus Φ) dependence also exhibits a maximum (volcano behaviour) in excellent agreement with the global promotional rule G3 discussed in Chapter 6.

9.1.2 Ethylene Oxidation on Pt/NASICON

The complete oxidation of C_2H_4 on Pt has also been investigated using NASICON ($Na_3Zr_2Si_2PO_{12}$), which, like β''-Al_2O_3, is a Na^+ conductor.[20]

The behavior of the Pt/NASICON catalyst was investigated[20] at temperatures up to 430°C and gas phase compositions in the range 1-20 kPa O_2 and 0.1-4 kPa C_2H_4. It was found that electrochemical Na^+ supply to the Pt catalyst under near-stoichiometric ethylene to oxygen ratios causes an up to tenfold catalytic rate enhancement for Na coverages of 0.03- 0.08 and that the reaction exhibits volcano behaviour. This was shown in Fig. 4.30, which describes the dependence of the reaction rate on catalyst potential and on sodium coverage. The catalyst surface is Na-free only for potentials above 2.5 V. Moderate Na coverages significantly promote the catalytic rate (Figs. 9.4 and 9.5) while higher coverages cause a sharp decrease in catalytic activity (Fig. 4.30). Before any current or potential application the open circuit

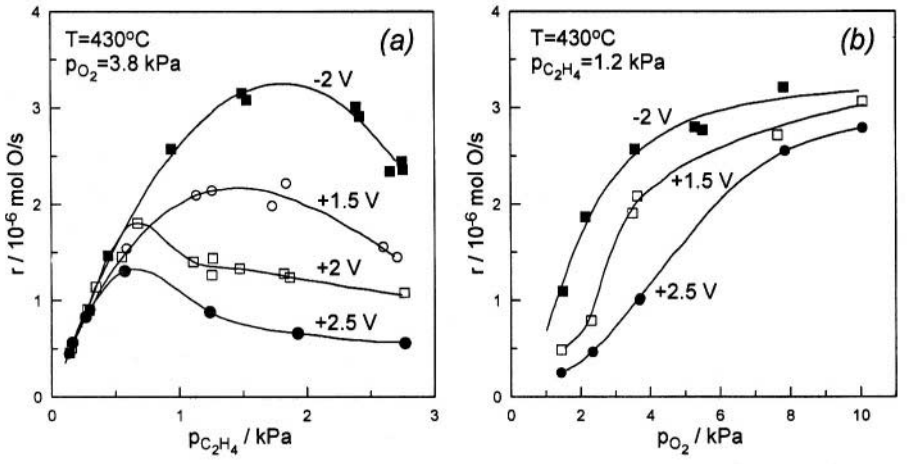

Figure 9.4. Effect of $p_{C_2H_4}$ (a) and p_{O_2} (b) and catalyst potential on the rate of ethylene oxidation on Pt/NASICON.[20] Reproduced by permission of The Electrochemical Society, Inc.

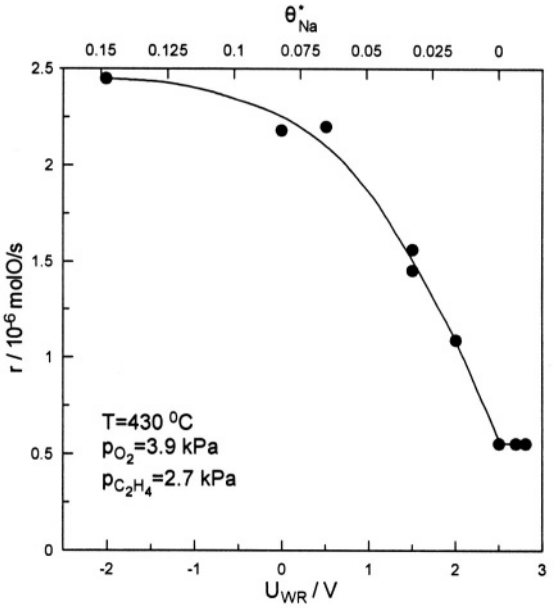

Figure 9.5. Effect of catalyst potential and linearized Na coverage on the rate of ethylene oxidation on Pt/NASICON.[20] Reproduced by permission of The Electrochemical Society, Inc.

potential was between +0.3V (O_2/He mixtures) and -0.5V (reacting mixtures). Since $Na_3Zr_2Si_2PO_{12}$ is a Na^+ conductor it follows that upon negative (positive) potential or current application sodium is transported to (from) the catalyst electrode surface from (to) the solid electrolyte. Similar to electrochemical promotion studies using β''-Al_2O_3 the main charge transfer reaction at the $Na_3Zr_2Si_2PO_{12}$-Pt-gas three phase boundaries is:

$$Na^+(s) + e^- \rightleftharpoons Na(a) \tag{9.1}$$

where $Na^+(s)$ stands for Na^+ in the $Na_3Zr_2Si_2PO_{12}$ solid electrolyte lattice and Na(a) is Na adsorbed on the Pt surface.

The effect shown in Figs. 4.30, 9.4 and 9.5 is quite reversible and the catalyst restores its Na-free activity upon pumping away the Na from the catalyst surface by increasing the catalyst potential. NASICON could be used as an alternative to β''-Al_2O_3 for potential practical applications of electrochemical promotion due to its better thermal stability and resistance to water vapour.

The kinetics depicted in Figures 9.4 in conjunction with Figure 9.5 and 4.30 provide an excellent example of promotional rules L2, and G2 (electrophilic behaviour), as well as rule G3 (volcano type behaviour). As long as the rate is negative order in C_2H_4 and positive order in p_{O_2} (Fig. 9.4)

global electrophilic behaviour is obtained (Fig. 9.5) (Rule G2). The r vs Φ behaviour always traces the r vs $p_{C_2H_4}$ ($=p_D$) behaviour thus volcano type behaviour is observed (Fig. 4.30) at sufficiently low potentials where the r vs $p_{C_2H_4}$ reaction order changes from negative to positive at fixed $p_{C_2H_4}$ (Fig. 9.4).

9.1.3 CO Oxidation on Pt/ β″-Al_2O_3

The reaction was investigated[11] at temperatures 300-430°C. Figures 9.6 and 9.7 as well as Figs. 4.16 and 4.31 show the effect of catalyst potential and corresponding Na coverage θ_{Na}, gaseous composition and temperature on the reaction rate. Figure 9.8 shows the corresponding effect on activation energy. For fuel-rich conditions the reaction exhibits volcano-type behaviour with ρ values up to 9 (Figs. 9.6, 9.7 and 4.16). This is due to enhanced oxygen chemisorption with increasing θ_{Na} followed by poisoning due to very strong oxygen chemisorption and the possible formation of a surface CO-Na-Pt complex. For fuel-lean conditions the reaction is "S-type", i.e., weakly electrophobic (Figs. 9.6, 9.7 and 4.16).

Figure 9.9 shows typical galvanostatic transients. Computed dipole moments of Na/Pt are again in reasonable agreement with the literature value of 1.75×10^{-29} C·m (5.3 Debye)[13]. The promotion index P_{Na} is up to 250 under

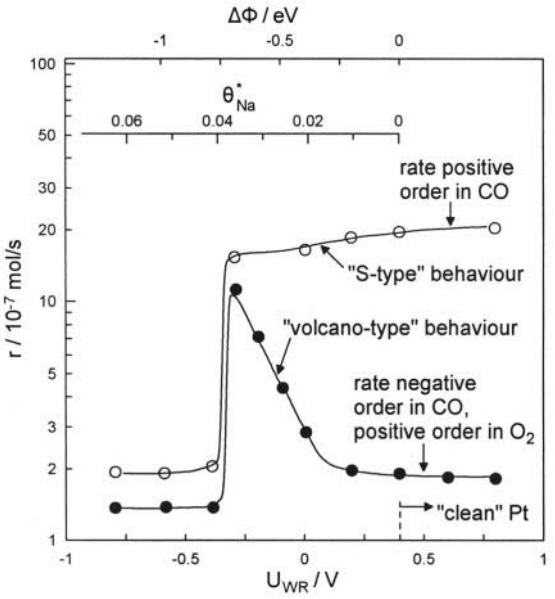

Figure 9.6. Effect of catalyst potential U_{WR} corresponding work-function change $\Delta\Phi$, and linearized Na coverage θ^*_{Na} on the rate of CO oxidation on Pt/β″-Al_2O_3. Conditions: T=350°C , p_{O2}=6 kPa; ●, p_{CO}=5.3 kPa, O, p_{CO}=2.8 kPa. Reprinted with permission from Academic Press.[11]

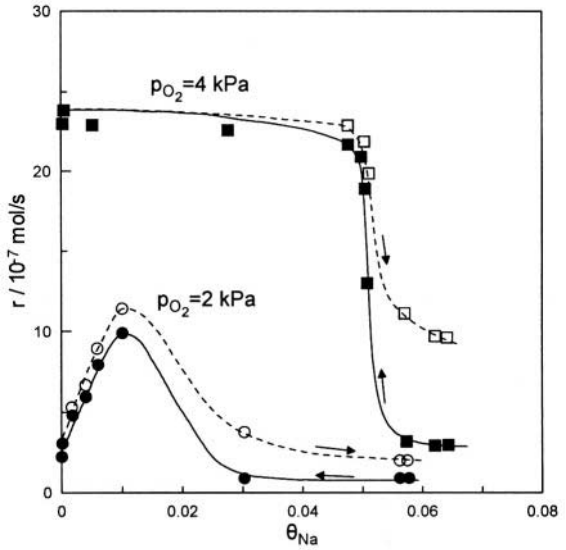

Figure 9.7. Effect of Na coverage θ_{Na} on the rate of CO oxidation on Pt/β″-Al_2O_3 at varying p_{O_2}. Other conditions: p_{CO}=2 kPa, T=350°C. Reprinted with permission from Academic Press.[11]

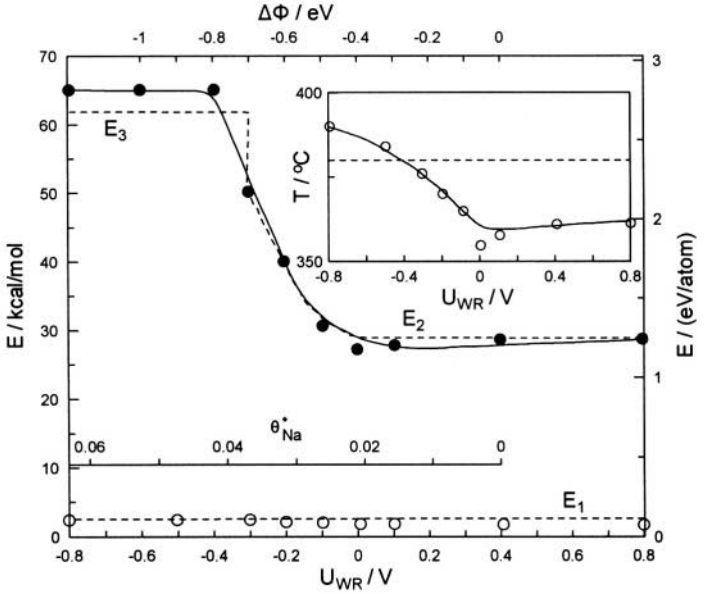

Figure 9.8. Effect of catalyst potential U_{WR} on the apparent activation energy and on the temperature (inset) at which the transition occurs from a high (●) to a low (○) E value. The dashed lines and predicted asymptotic E_1, E_2, E_3 activation energy values are from the kinetic model discussed in ref. 11. Conditions: p_{O_2}=5.8 kPa, p_{CO}=3.5 kPa.[11] Reprinted with permission from Academic Press.

fuel-rich conditions, (Table 4.3). In the region of CO-Na-Pt complex formation P_{Na} is as low as -30 (Fig. 9.6, 4.16 and 4.31). This classical system provides an excellent example of the importance of promotional effects in Catalysis and also facilitates the understanding of NO reduction studies surveyed in this Chapter where removal of surface O by CO, H_2 or hydrocarbons plays an important role in the overall kinetic behaviour.

As already discussed in Chapter 6 (Figure 6.25) the observed complex rate dependence of CO oxidation on p_{CO}, p_{O_2} and U_{WR} (Φ) (Figs. 4.16, 4.31, 9.6 and 9.7) can be described in a semiquantitative fashion by the effective double layer model presented in Chapter 6. The system provides an excellent paradigm of the promotional rules G1, G2 and G3 which are summarized by the general inequalities (6.11) and (6.12) written specifically here for the CO oxidation system:

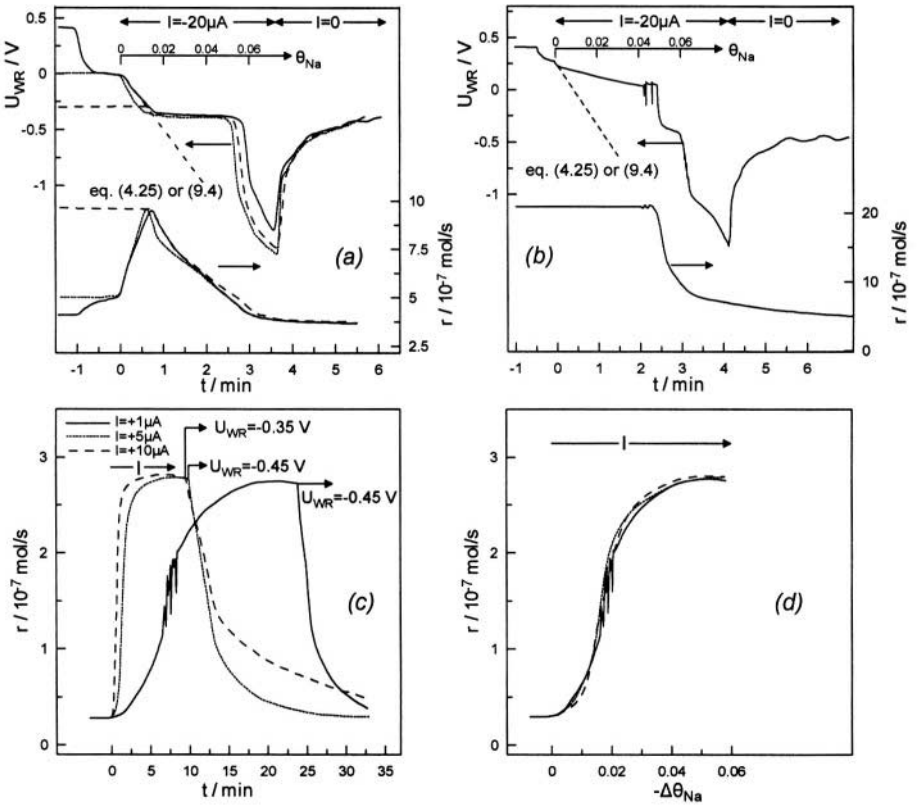

Figure 9.9. Rate and catalyst potential response to application of negative currents (a,b), for the case of "volcano-type" behaviour (a) and "S-type" behaviour (b) of the reaction rate, and to application of positive currents (c,d); see text for discussion. Conditions: (a) p_{CO}=2 kPa, p_{O_2}=2 kPa, T=350°C, catalyst C1; (b) p_{CO}=2 kPa, p_{O_2}=4 kPa, T=350°C, catalyst C1. (c,d): p_{CO} =0.73 kPa, p_{O_2}=0.86 kPa, T=402°C, catalyst C2. Reprinted with permission from Academic Press.[11]

$$\left(\frac{\partial r}{\partial \Phi}\right)_{p_{O_2},p_{CO}} \left(\frac{\partial r}{\partial p_{CO}}\right)_{\Phi,p_{O_2}} > 0 \tag{9.6}$$

$$\left(\frac{\partial r}{\partial \Phi}\right)_{p_{O_2},p_{CO}} \left(\frac{\partial r}{\partial p_{O_2}}\right)_{\Phi,p_{CO}} < 0 \tag{9.7}$$

As already discussed in Chapter 6, these rules are in excellent agreement not only with the electrochemical promotion literature (Figs. 4.16, 4.31, 6.25, 9.6) but also with the classical promotion literature[21] (Fig. 6.11).

9.1.4 Ethylene Epoxidation on Ag/β″-Al_2O_3

The epoxidation of C_2H_4 on Ag/β″-Al_2O_3 was investigated[22] at temperatures 250° to 300°C and high pressure (5 bar) in the presence of $C_2H_4Cl_2$ moderators in order to simulate industrial practice.[22] It was found that technologically important ethylene oxide selectivity values ($S_{C_2H_4O}$≈88%) can

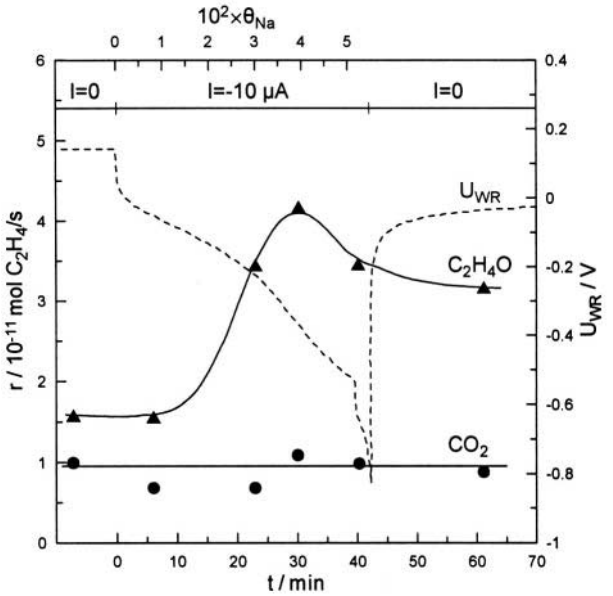

Figure 9.10. Ethylene epoxidation on Ag/β″-Al_2O_3: Transient effect of a negative applied current (Na supply to the catalyst) on the rates of ethylene oxide and CO_2 formation and on catalyst potential (work function) and Na coverage[22]: T=260°C, P=5 atm, p_{O_2}=17.5 kPa, $p_{C_2H_4}$=49 kPa, 0.6 ppm $C_2H_4Cl_2$. Reprinted with permission from Academic Press.

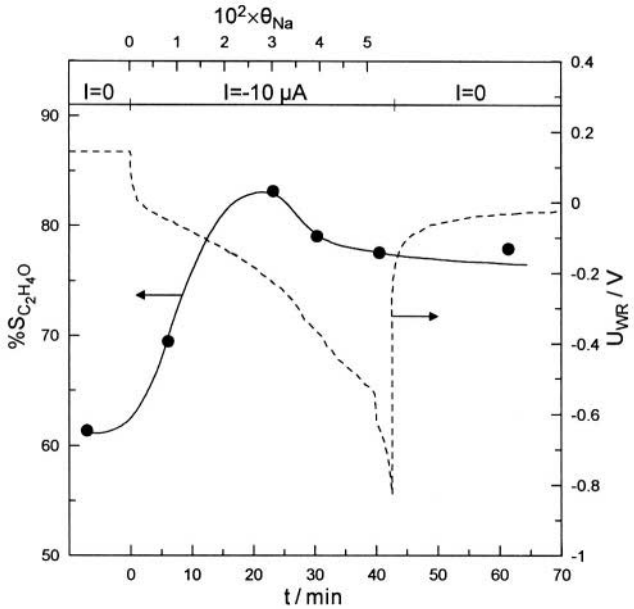

Figure 9.11. Ethylene epoxidation on Ag/β″-Al_2O_3: Transient effect of a negative applied current (Na supply to the catalyst) on catalyst potential, Na coverage and selectivity to ethylene oxide[22]; Conditions as in Fig. 9.10. Reprinted with permission from Academic Press.

be achieved via the combined use of Cl moderators and electrochemical promotion.[22] Figure 9.10 shows a typical galvanostatic experiment.[22] Negative currents, i.e., Na supply to the catalyst, enhances the rate of epoxidation without affecting the rate of CO_2 formation. Consequently the selectivity to ethylene oxide increases substantially (Fig. 9.11).

In Figure 4.42 we have seen already the effect of catalyst potential U_{WR}, corresponding sodium coverage θ^*_{Na} and $C_2H_4Cl_2$ partial pressure on the selectivity to ethylene oxide. For U_{WR} = -0.25 V and $p_{C_2H_4Cl_2}$=1.0 ppm the selectivity to ethylene oxide is 88%, which is one of the highest values reported for this important reaction.[22]

9.1.5 NO Reduction Studies on Pt/β″-Al_2O_3

Recent NEMCA investigations have shown that β″-Al_2O_3, a Na^+ conductor, can be used as an active catalyst support to dramatically enhance the rate and selectivity of several enviromentally important reactions such as NO reduction by CO, H_2 and C_3H_6, all catalyzed by Pt. Sodium supply to the catalyst has been found to enhance not only the catalytic activity, but also product selectivity to nitrogen.

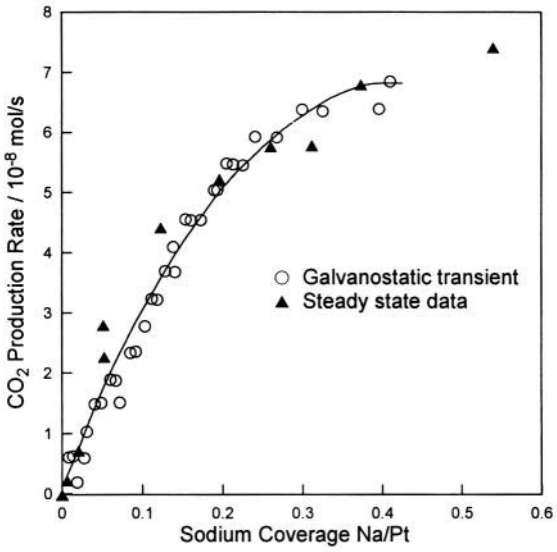

Figure 9.12. Effect of Na coverage on the rate of NO reduction by C_2H_4 on Pt/β″-Al_2O_3. The rate enhancement ratio ρ is nominally infinite; $p_{C_2H_4}$=3 kPa, p_{NO}=0.65 kPa, 480°C.[6] Reprinted with permission from Academic Press.

9.1.5.1 NO Reduction by C_2H_4 on Pt/β″-Al_2O_3

NO reduction by C_2H_4 on Pt/β″-Al_2O_3 was investigated at temperatures 250° and 400°C by Lambert and Harkness[6] both under atmospheric pressure and under high vacuum conditions. The reaction exhibits pronounced electrophilic behaviour (Fig. 9.12) which is due to enhanced NO dissociation in presence of Na on the Pt catalyst surface.[6] The results are very spectacular in that a formally infinite ρ value was obtained[6], i.e. r_0 was immeasurably low on the unpromoted surface (θ_{Na}=0, Fig. 9.12). At higher Na coverages (0.03 to 0.3) the differential promotion index pi_{Na} is up to 500. As also shown in Fig. 9.12 the rate vs θ_{Na} behaviour is identical at steady-state and during galvanostatic transients. This indicates fast speading, via surface diffusion, of the promoting Na species over the entire Pt/gas interface. Similar behaviour is observed with practically all electrochemical promotion studies involving Na on transition metal surfaces.

9.1.5.2 NO Reduction by CO on Pt/β″-Al_2O_3

The reduction of NO by CO on Pt/β″-Al_2O_3 is another system exhibiting spectacular electrochemical promotion behaviour.[7,23,24] Electrochemical supply of Na^+ on the Pt catalyst surface can cause the rates of CO_2 and N_2 formation (r_{CO_2} and r_{N_2}) to increase by 48% and 1300%, respectively, over their values on a clean surface.[23]

An example of the promotional action of sodium supply to the catalyst was given in Fig. 4.40 which shows steady-state (potentiostatic) rate data for

CO_2, N_2 and N_2O production as a function of the catalyst potential, U_{WR}, obtained at 621K for fixed inlet pressures of NO and CO. A sharp increase in reaction rate and product is observed as the catalyst potential is reduced below 0 V, i.e., upon Na supply to the Pt catalyst. The selectivity to N_2, S_{N2}, is enhanced from 17% to 62%. This dramatic enhancement in catalytic performance is due to (a) enhanced NO vs CO chemisorption on Pt with decreasing potential and (b) Na-induced dissociation of chemisorbed NO.

The kinetics depicted in Figures 9.13 and 9.14 are extremely instructive and provide a classical example of global promotional rule G2 (electrophilic behaviour).

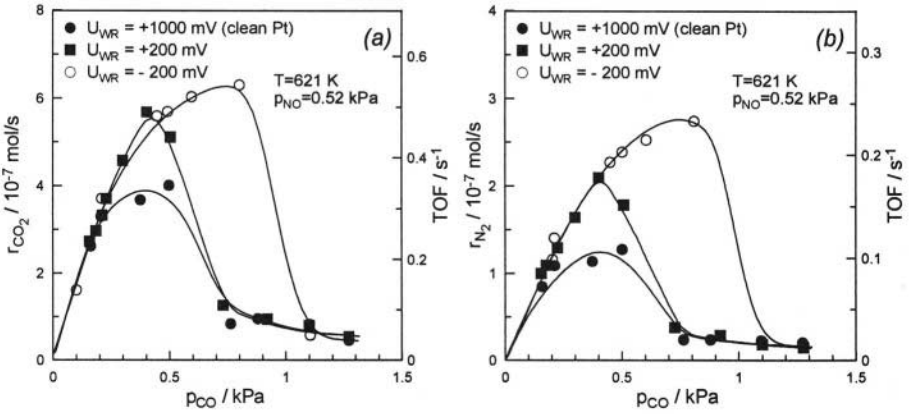

Figure 9.13. Effect of p_{CO} on the rates of CO_2 and N_2 formation at various imposed catalyst potentials on Pt/β″-Al_2O_3.[23] Reprinted with permission from Academic Press.

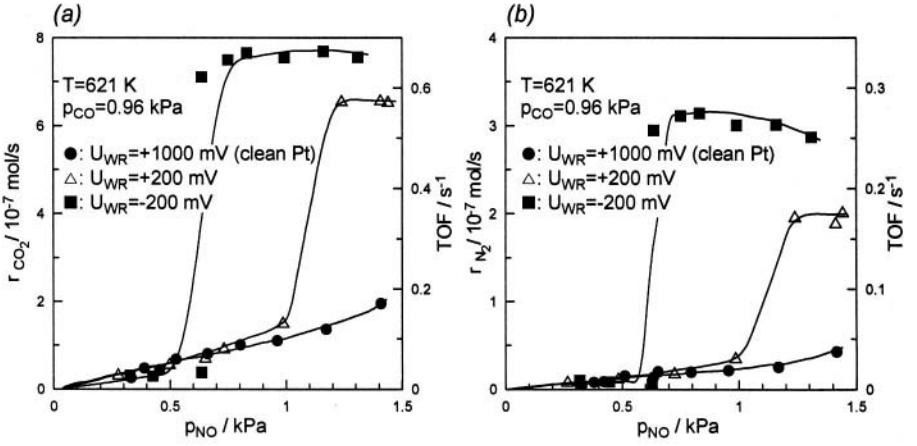

Figure 9.14. Effect of p_{NO} on the rates of CO_2 and N_2 formation at various imposed potentials during NO reduction by CO on Pt/β″-Al_2O_3.[23] Reprinted with permission from Academic Press.

First one should observe that Fig. 4.40, which provides a classical example of electrophilic behaviour, has been obtained with a gaseous composition ($p^0_{CO} = p^0_{NO} = 0.75$ kPa) where the rate is negative order in the electron donor CO (Fig. 9.13) and positive order in the electron acceptor NO (Fig. 9.14). Consequently, in excellent agreement with the global rule G2, the reaction exhibits purely electrophilic behaviour (Fig. 4.40).

Second it is instructive to note the effect of U_{WR} (and thus Φ) on the kinetics (Figs. 9.13 and 9.14) as these figures provide an excellent demonstration of the "fundamental" promotional rules F1 (Eq. 6.18) and F2 (Eq. 6.19) presented in Chapter 6 which for the case of the reaction between CO (=D) and NO (=A) are written as:

$$\left(\frac{\partial\theta_{CO}}{\partial\Phi}\right)_{p_{NO},p_{CO}} \geq 0 \tag{9.8}$$

$$\left(\frac{\partial\theta_{NO}}{\partial\Phi}\right)_{p_{NO},p_{CO}} \leq 0 \tag{9.9}$$

It is clear in Figure 9.13 that increasing U_{WR} (and Φ) causes a pronounced increase in θ_{CO} (Eq. 9.8) as manifest by the pronounced shift of the rate maximum (where $\theta_{CO} \approx \theta_{NO}$) to higher p_{CO} values.

Also in Figure 9.14 it is clear that decreasing U_{WR} (and Φ) causes a pronounced increase in θ_{NO} (Eq. 9.9) as manifest by the shift in reaction order from 1st order at +1 V to near-zero order for –0.2 V.

9.1.5.3 NO Reduction by H_2 on Pt/β″-Al_2O_3

Significant promotional phenomena have been also found[26] in the case of NO reduction by H_2. The enhancement of catalytic activity and selectivity is again due to enhanced NO adsorption and dissociation, caused by the Na supply to the catalyst upon negative current or potential application.

The reaction was studied in the temperature range of 300-430°C.[26] It was found that the increase in the rate of NO reduction to N_2 is typically 10^3-10^5 times larger than the rate of supply of Na and up to 30 times larger than the unpromoted rate. Sodium coverages of 0.06 cause up to 1450% increase in the total rate of NO reduction and enhance the selectivity to nitrogen up to 75% vs 30% on the Na-free surface, as already shown in Figures 4.17 and 4.18.

The system is an excellent example of global rule G2 (electrophilic behaviour) for moderate U_{WR} values (Figs. 4.17, 4.18) and of global rule G3 (volcano behaviour) for very negative U_{WR} values (Fig. 4.17, 4.18).

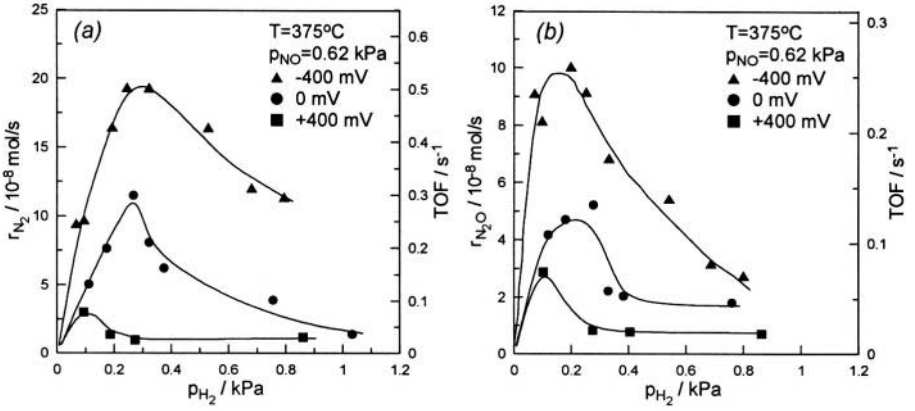

Figure 9.15. Effect of p_{H_2} on the rates of formation of N_2 (a) and N_2O (b) for fixed p_{NO} and various fixed U_{WR} values.[26] Reprinted with permission from Academic Press.

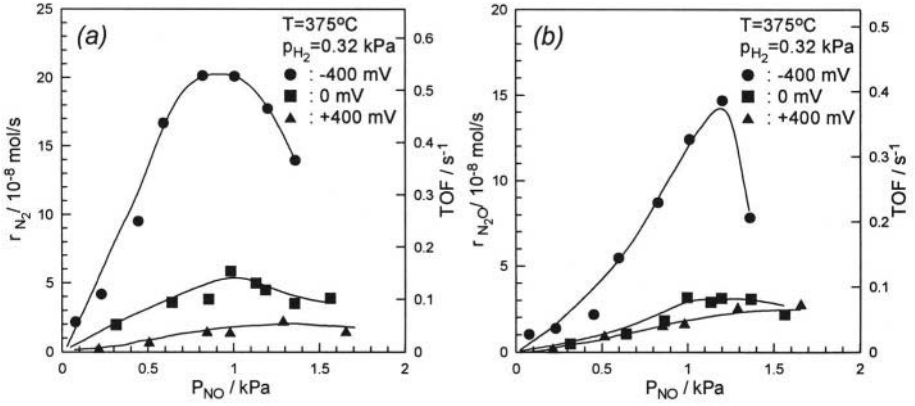

Figure 9.16. Effect of p_{NO} on the rates of formation of N_2 (a) and N_2O (b) for fixed p_{H_2} and various fixed U_{WR} values.[26] Reprinted with permission from Academic Press.

This is manifest in the kinetics depicted in Figures 9.15 and 9.16 which bear interesting similarities and some subtle differences with those of NO reduction by CO discussed in the previous section (Figs. 9.13 and 9.14).

It is clear in Fig. 9.15 that decreasing Φ causes a decrease in the coverage of the electron donor H, as manifest by the shift of the rate maximum to higher p_{H_2} values, according to the fundamental rule F1.

It is also clear from Fig. 9.16 that decreasing U_{WR} and Φ causes a pronounced increase in θ_{NO}, as manifest by the appearance of a rate maximum at sufficiently negative U_{WR} values in excellent agreement with the fundamental rule F2 (Eq. 9.9).

9.1.5.4 NO Reduction by C_3H_6 on Pt/β″-Al_2O_3

The reduction of NO by propene is of great importance in automotive exhaust catalysis.

As expected, the reaction exhibits pronounced electrochemical promotion behaviour[7,25] with a tenfold enhancement in catalytic rate (Fig. 9.17).

Interestingly as shown in Fig. 9.17 the reaction exhibits pronounced volcano-type behaviour with the rate of N_2 production maximized for U_{WR}=-0.3 V.

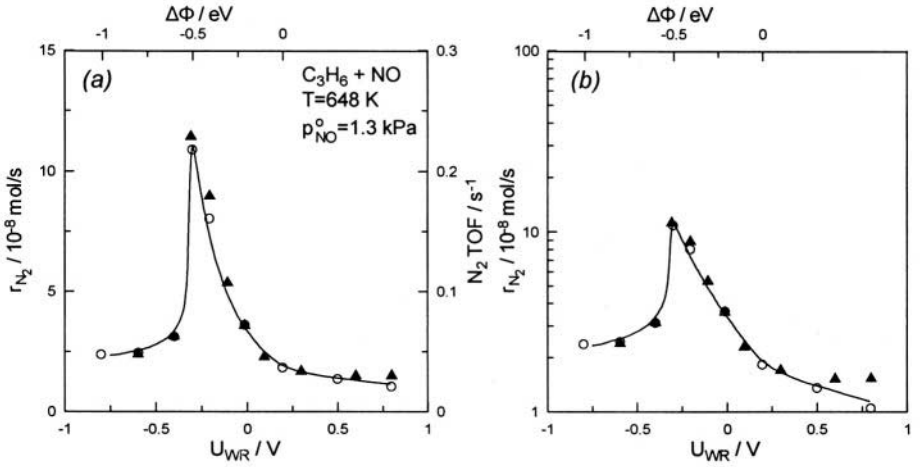

Figure 9.17. Reduction of NO by propene on Pt/β″-Al_2O_3.[7,25] Effect of catalyst potential on the rate of N_2 production. (a) linear rate scale. (b) logarithmic scale. T=375°C, p^o_{NO} =1.27 kPa; $p^o_{propene}$ =1.47 kPa (▲) and 0.60 kPa (○). Reprinted from ref. 7 with permission from the Institute for Ionics.

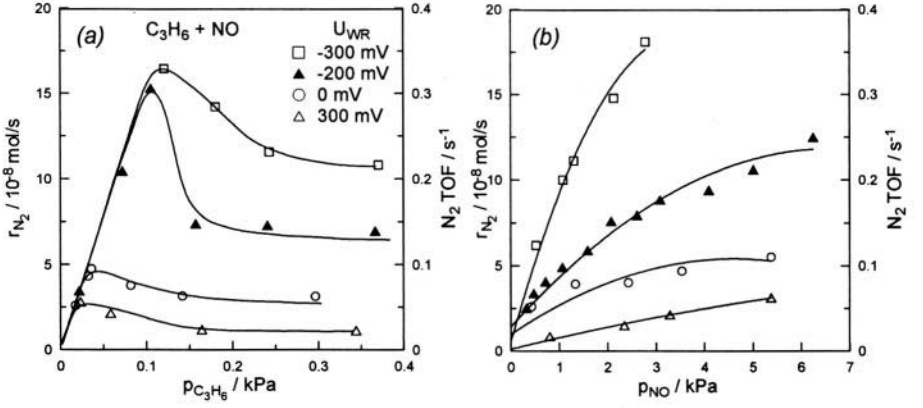

Figure 9.18. Reduction of NO by propene on Pt/β″-Al_2O_3;[7,25] T=648 K; total flowrate 1.3×10^{-4} mol s^{-1} (a) effect of $p_{C_3H_6}$ on N_2 rate at fixed p_{NO} (1.4 kPa) for several values of catalyst potential. (b) effect of p_{NO} on N_2 rate at fixed $p_{C_3H_8}$ (0.27 kPa) for several values of catalyst potential. Reprinted from ref. 7 with permission from the Institute for Ionics.

The appearance of volcano type behaviour is perfectly consistent, via Global Rule G3 (Chapter 6), with the kinetic (Fig. 9.18) which show strong competitive adsorption of propene and NO with propene adsorption being stronger on the Na-free surface ($U_{WR} \geq 0$ V). Negative U_{WR} and $\Delta\Phi$ favors the adsorption of electron acceptor NO vs electron donor C_3H_6 and this is manifest both by the kinetics (Fig. 9.18) and by the observed volcano behaviour (Fig. 9.17). This system is a nice confirmation of Global Rule G3.

Lambert and coworkers,[7,18,25] who were first to study this interesting system, have shown that the nature of the anion (nitrate or carbonate) formed on the catalyst surface in presence of Na^+ plays an important role in the sharpness of the volcano plot obtained upon varying U_{WR}.

9.1.6 Benzene Hydrogenation on Pt/β″-Al_2O_3

Benzene hydrogenation on Pt/β″-Al_2O_3 was investigated at temperatures 100 to 150°C by Cavalca and Haller.[27] The reaction is purely electrophobic, i.e., the rate decreases dramatically with increasing Na coverage (Fig. 9.19). The toxicity index $-PI_{Na^+}$ is up to 50. The effect is due to decreased benzene chemisorption with decreasing U_{WR} and Φ owing to reduced donation of π-electrons to the metal. These results are also quite spectacular, since ρ values approaching zero were obtained,[27] i.e. the rate is totally poisoned with Na coverages of only 0.03 (Fig. 9.19).

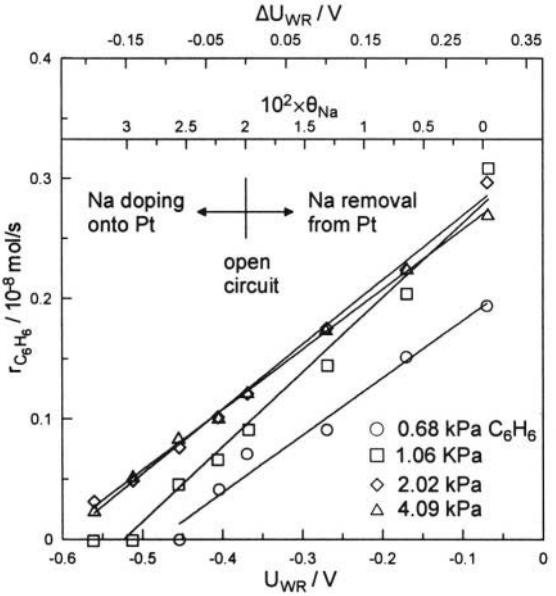

Figure 9.19. Effect of catalyst potential, Na coverage and benzene partial pressure on the rate of benzene hydrogenation on Pt/β″-Al_2O_3;[27,28] T=130°C, p_{H_2}=33.35 kPa, flow rate=81 cm^3(STP)/min.

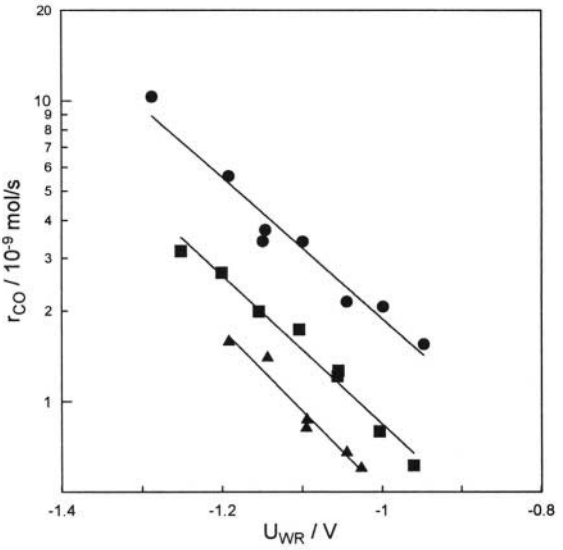

Figure 9.20. Effect of catalyst potential on the rate of CO_2 hydrogenation on Pd/β″-Al_2O_3.[29] p_{H_2} = 67.4 kPa; p_{CO_2}=19.3 kPa; ▲, T=545°C; ■, T=568°C; ●, T=605°C.

As already discussed in Chapter 6, Figure 9.19 provides a nice example of global promotional rule G1: The rate is clearly positive order in the electron donor C_6H_6 (Fig. 9.19) and at the same time is enhanced with increasing Φ (electrophobic behaviour).

9.1.7 CO_2 Hydrogenation on Pd

CO_2 hydrogenation on Pd was investigated[29] under atmospheric pressure and at temperatures 540°C to 605°C. The CO formation rate (reverse water-gas shift reaction) exhibits purely electrophilic behaviour with a rate increase by up to 600% with increasing sodium coverage (Fig. 9.20). This purely electrophilic behaviour is consistent with low reactant coverages and enhanced electron acceptor CO_2 adsorption on the Pd surface with increasing sodium coverage (Rule G2).

9.1.8 Selective C_2H_2 Hydrogenation on Pt/ β″-Al_2O_3 and Pd/β″-Al_2O_3

The hydrogenation of acetylene to ethylene is an industrially important catalytic process commonly catalyzed by promoted Pd catalysts. An industrial catalyst must be highly selective for C_2H_2 vs C_2H_4 hydrogenation in order to avoid formation of C_2H_6 and thus loss of the desired product C_2H_4.There have been two recent studies on the use of electrochemical promotion to enhance the selectivity of Pd[30] and Pt[31] catalysts for the selective hydrogenation of

C_2H_2 to C_2H_4. Both studies are noteworthy in that β''-Al_2O_3 has been used as the solid electrolyte at temperatures as low as 70 – 100°C.

The former study utilized Pd films and gaseous compositions simulating the industrial ones[30] where C_2H_2 must be selectively hydrogenated in a mixture rich in C_2H_4 (Fig. 9.21). Electrochemical supply of Na to the Pd catalyst was found to inhibit both the hydrogenation of C_2H_2 and C_2H_4. The suppression of C_2H_4 hydrogenation, however, was found to be much more pronounced so that the product selectivity to C_2H_4 is significantly enhanced. Parallel kinetic studies utilizing the same feed gaseous composition, space velocity and temperature were carried out using a fully promoted (BASF) industrial Pd based catalyst, As shown in Figure 9.21 the electrochemically promoted Pd film matches and marginally exceeds the performance of the state-of-the art classical catalyst, both in terms of the maximum selectivity (95%) at low C_2H_2 conversion and also in terms of maintaining high (~50%) selectivity at C_2H_4 conversions exceeding 80% under realistic space velocity values. Since most of the electrochemical promotion studies surveyed in this book have been carried out at low (typically less than 10%) reactant conversion (in order to maintain differential reactor conditions and thus ensure isothermality and facilitate the kinetic analysis) this work is important as it for the first time assessed the performance of an electrochemically promoted catalyst under near complete reactant (C_2H_2 and H_2) conversion and showed that the electrochemically promoted catalyst can at least match and marginally exceed the performance of a fully promoted state-of-the-art industrial catalyst.

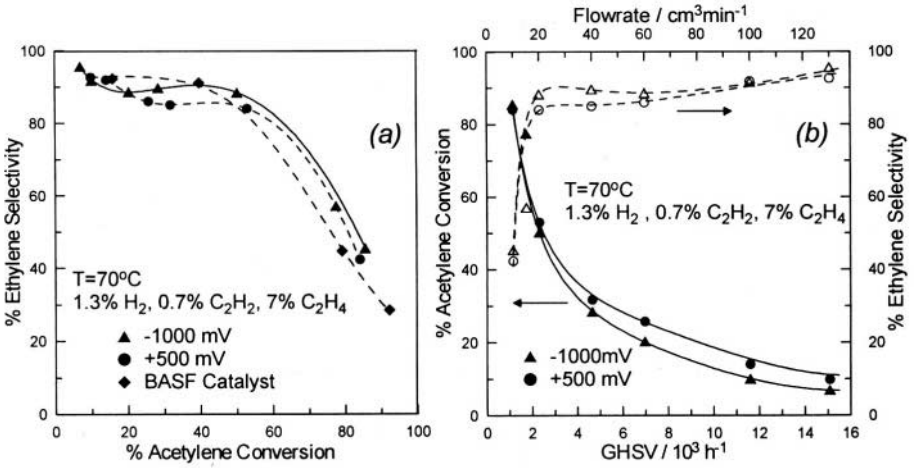

Figure 9.21. (a) Dependence of selectivity on C_2H_2 conversion for various catalyst potentials. The behaviour is compared with this of BASF catalysts (b) Dependence of C_2H_2 conversion (closed symbols, solid lines) and selectivity (open symbols, dashed lines) on flowrate and GHSV for various catalyst potentials. 3-pellet configuration.[30] Reprinted with permission from the Institute for Ionics.

Of equal importance and much more spectacular was the study of Lambert and coworkers[31] utilizing a $Pt/\beta''\text{-}Al_2O_3$ catalyst at temperatures 100 to 300°C (Fig. 9.22). They showed that Na coverages of the order of 0.02 suffice to convert Pt from a totally non-selective catalyst ($S_{C_2H_2}\approx 0$) to a highly selective one ($S_{C_2H_2}=78\%$ at 54% conversion at 160°C), i.e., approaching the performance of a Pd catalyst.

As shown in Fig. 9.22 the behaviour is similar to that obtained on Pd, i.e. purely electrophobic, with a much stronger suppression of C_2H_4 vs C_2H_2 hydrogenation with decreasing potential, thus increasing Na coverage. Similar to the case of C_6H_6 hydrogenation on $Pt/\beta''\text{-}Al_2O_3$, decreasing Φ suppresses the chemisorption of the electron-donor hydrocarbons, i.e. C_2H_2 and C_2H_4 as well as that of H, also an electron-donor. As a result electrophobic behaviour is obtained. The observed enhancement in selectivity seems to indicate Na hinders more strongly C_2H_4 vs C_2H_2 adsorption although the suppression in H chemisorption may also play a role. This is supported by galvanostatic measurements carried out by Lambert and coworkers[31] which show that adsorbed Na interacts strongly with the chemisorbed hydrogen, $H_{(a)}$, relatively weakly with the species formed by acetylene adsorption and very strongly with the adsorbed species formed by acetylene adsorption in the presence of hydrogen.[31]

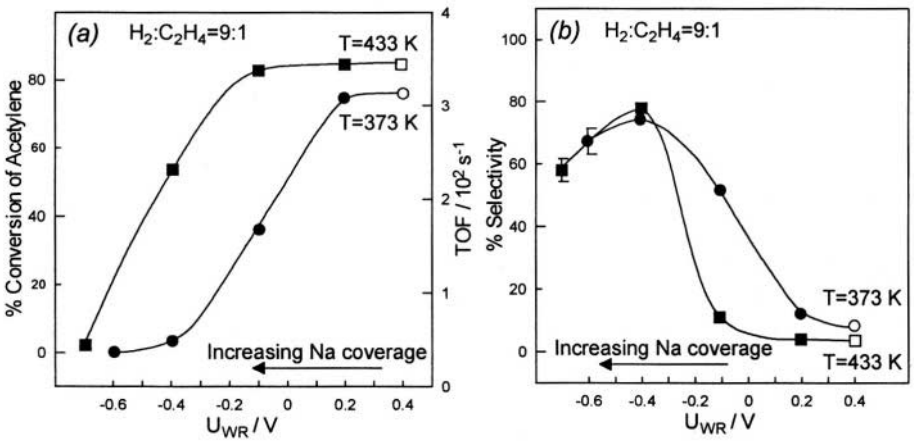

Figure 9.22. Effect of catalyst potential, U_{WR}, on conversion of acetylene (a) and selectivity towards ethene formation (b) with $H_2:C_2H_2=9:1$. Conditions: $p_{H_2}=60$ kPa, $p_{C_2H_2}=7$ kPa. $p_{He}=34$ kPa, total flow rate $F_V=30.3$ cm^3 STP/min. U_{WR} was initially set at +400 mV and was increased in steps until the maximum negative voltage was applied. U_{WR} was then returned to its original value of +400 mV and the open symbols correspond to measurements taken at this point.[31] Reprinted with permission from Academic Press.

9.1.9 NH_3 Decomposition on $Fe/K_2YZr(PO_4)_3$ and on $CaZr_{0.9}In_{0.1}O_{3-\alpha}$

The decomposition of NH_3 has been investigated on Fe films deposited on $K_2YZr(PO_4)_3$, a K^+ conductor,[32] and on $CaZr_{0.9}In_{0.1}O_{3-\alpha}$, a H^+ conductor,[32,33] at temperatures near 500°C. In both cases electrophobic behaviour was observed with ρ values up to 5 and Λ values, for the case of the H^+ conductor, up to 120.[33]

9.1.10 Hydrogen Oxidation on Pt/Glass

Hydrogen oxidation on Pt films deposited on Na^+ and Li^+ glass has been investigated by Zakarina and coworkers[34] at temperatures near 150°C. This interesting work was published only in Russian[34] and thus has not attracted sufficient attention. Faradaic efficiency Λ values as high as 2000, and ρ values in excess of ten were measured. Little is known about the promoting species migrating between the Pt catalyst surface and the glass upon current (μA) application but it is very likely to be alkali (Na^+, Li^+) cations. This system certainly needs further investigation as it may be of significant practical importance.

9.2 THE USE OF H^+ CONDUCTORS

9.2.1 Hydrogen Oxidation on Pt/Nafion

The oxidation of H_2 at room temperature on Pt black electrodes deposited on Nafion 117 was the first electrochemical promotion study utilizing a solid polymer electrolyte.[35]

The experimental setup is shown in Figure 9.23 .The Pt-black catalyst film also served as the working electrode in a Nafion 117 solid polymer electrolyte cell. The Pt-covered side of the Nafion 117 membrane was exposed to the flowing H_2-O_2 mixture and the other side was in contact with a 0.1 M KOH aqueous solution with an immersed Pt counterelectrode. The Pt catalyst-working electrode potential , U_{RHE} ($=U_{WR}$), was measured with respect to a reversible reference H_2 electrode (RHE) via a Luggin capillary in contact with the Pt-free side of the Nafion membrane.

The Pt catalyst-working electrode, shown in Figure 9.24 was deposited on the Nafion 117 membrane using the method described by Takenaka and Torikai,[36] i.e. reduction of H_2PtCl_6 from a 0.01 M solution by a 0.1 M sodium borohydride solution counter-diffusing through the Nafion membrane. The Pt film mass was 12.25 mg and its superficial surface area was 3.14 cm^2. Its true surface area, estimated via stationary cyclic voltammetry from the hydrogen adsorption region, after substracting the double layer charge, was 480 cm^2 corresponding to $N_G=1.2\times10^{-6}$ surface Pt mol.

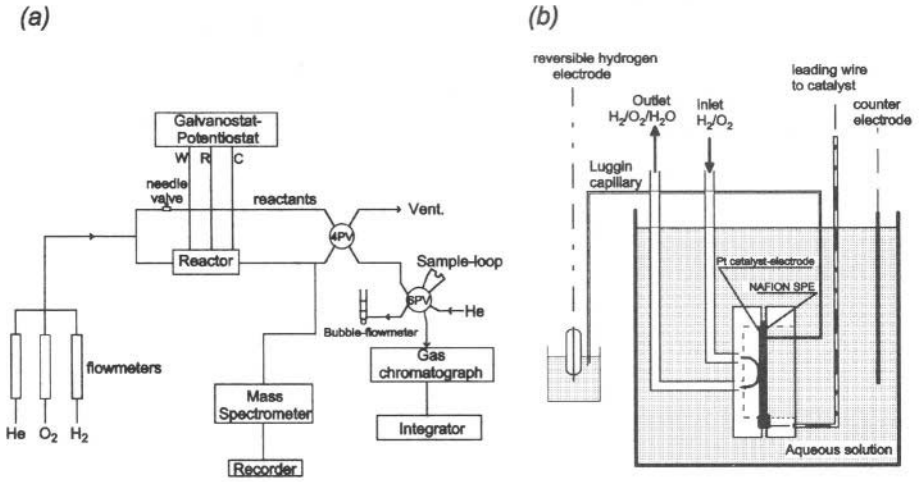

Figure 9.23. Schematic diagram of the apparatus (a, left) and of the electrochemical cell-reactor (b, right) used for H_2 oxidation on Pt/Nafion.[35] Reproduced by permission of The Electrochemical Society, Inc.

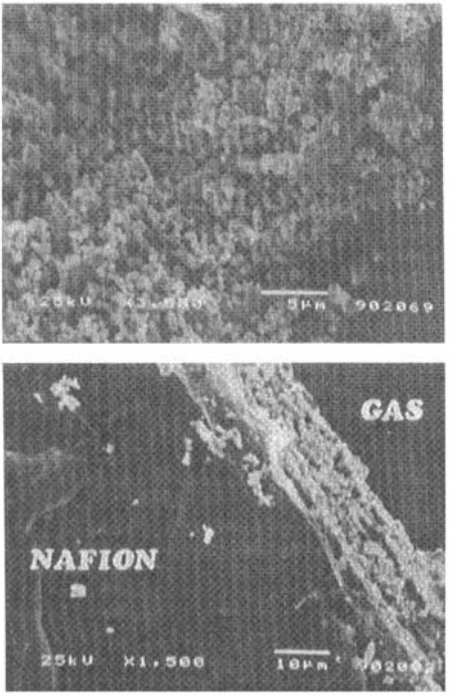

Figure 9.24. SEM of top view (top) and cross section (bottom) of the Pt/Nafion catalyst used for electrochemical promotion of H_2 oxidation.[35] Reproduced by permission of The Electrochemical Society, Inc.

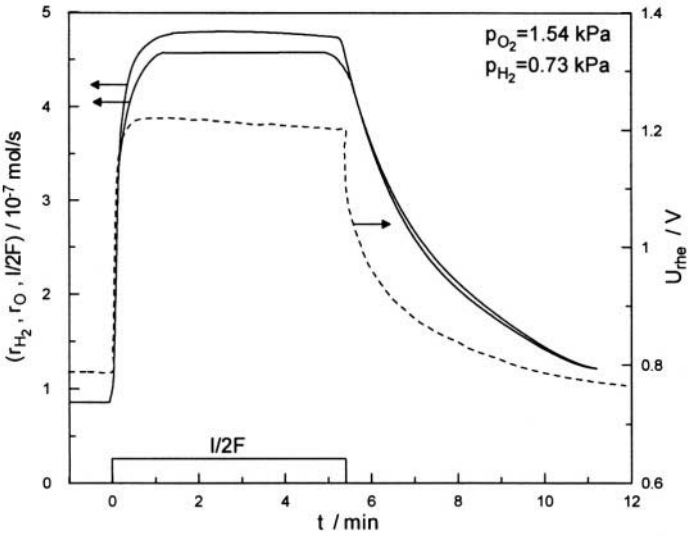

Figure 9.25. Transient effect of applied positive current (I=5 mA) on the rate of consumption of hydrogen (r_{H_2}) and oxygen (r_O); gas molar flow rate $f_m=13\times10^{-5}$ mol/s.[35] Reproduced by permission of The Electrochemical Society, Inc.

9.2.1.1 Galvanostatic Transient

Figure 9.25 shows a typical galvanostatic NEMCA experiment, i.e., it depicts the response of the rates of hydrogen and oxygen consumption and of the catalyst potential upon application of a positive current (I=5 mA). Initially the circuit is open (I=0). Hydrogen and oxygen are consumed on the Pt surface at a steady-state rate $r_c(=r_{H_2}=2r_{O_2}=r_O)$ equal to $0.8\cdot10^{-7}$ mol/s by the catalytic (no net charge transfer) reaction:

$$H_2 + \frac{1}{2}O_2 \xrightarrow{r_c} H_2O \tag{9.10}$$

The open-circuit potential, $U^o_{rhe}(=U^o_{WR})$, is 0.78 V. As shown in subsequent figures, U^o_{rhe} takes values between 0.3 and 0.85 and is an increasing function of the p_{O_2}/p_{H_2} ratio.

At t=0 a constant anodic current I=5mA is applied between the Pt catalyst film and the counter electrode. The catalyst potential, U_{RHE}, reaches a new steady state value U_{RHE}=1.18 V. At the same time the rates of H_2 and O consumption reach, within approximately 60s, their new steady-state values $r_{H_2}=4.75\cdot10^{-7}$ mol/s, $r_O=4.5\cdot10^{-7}$ mol/s. These values are 6 and 5.5 times larger than the open-circuit catalytic rate. The increase in the rate of H_2 consumption ($\Delta r=3.95\cdot10^{-7}$ mol H_2) is 1580 % higher than the rate increase, ($I/2F=2.5\cdot10^{-8}$ mol/s), anticipated from Faraday's Law. This shows clearly that the catalytic activity of the Pt catalyst-electrode has changed substantially. The Faradaic efficiency, Λ, defined from:

$$\Lambda = \Delta r_{H_2}/(I/2F) \tag{9.11}$$

is 15.8 for the galvanostatic experiment of Fig. 9.25.

It is worth noting in Fig. 9.25 that:

$$r_{H_2} - r_O = I/2F \tag{9.12}$$

This equation is always valid at steady state and has been originally derived for the case of NEMCA in alkaline solutions.[37] In the present case of the acidic environment in the Nafion electrolyte the following two electrocatalytic (net charge transfer) reactions take place at the Pt working electrode, presumably at the three-phase-boundaries (tpb) Pt-Nafion-gas:

$$H_2 \xrightarrow{r_{e,1}} 2H^+ + 2e^- \tag{9.13}$$

$$H_2O \overset{r_{e,2}}{\rightleftharpoons} 2H^+ + (1/2)O_2 + 2e^- \tag{9.14}$$

Reaction 9.13 proceeds to the right at a rate $r_{e,1}>0$ as long as $E_{rhe} > 0$ which was always the case in the present work. Reaction 9.14 proceeds to the right ($r_{e,2}>0$) when E_{rhe} exceeds the oxygen reduction potential (1.23 V) and to the left otherwise. It should be noted that in the present case the actual hydrogen and oxygen evolution potential values may deviate significantly from their standard thermodynamic values (0 and 1.23 V respectively) as their actual values depend not only on gaseous composition but also more importantly on the local pH in the membrane at the tpb as manifest also by cyclic voltammetry.[35] In all cases, however, it follows from simple mass and electron balance considerations[35] that:

$$r_{H_2} = r_c + r_{e,1} \tag{9.15}$$

$$r_O = r_c - r_{e,2} \tag{9.16}$$

$$I/2F = r_{e,1} + r_{e,2} \tag{9.17}$$

Combining Eqs. (9.15) to (9.17) one obtains Eq. (9.12) which is in excellent agreement with experiment (Fig. 9.23).

It follows from Eq. 9.14 that when I=0, then $r_{e,2}=-r_{e,1}$. Therefore the open-circuit conditions U^o_{rhe} is a mixed potential bounded between the H_2 and O_2 evolution potentials.

We then apply Equations (9.15) to (9.17) and (9.12) between the final state (I=I) and the initial state (I = 0) of the galvanostatic experiment of Fig. 9.25:

$$\Delta r_{H_2} = \Delta r_c + \Delta r_{e,1} \tag{9.18}$$

$$\Delta r_O = \Delta r_c - \Delta r_{e,2} \tag{9.19}$$

$$I/2F = \Delta r_{e,1} + \Delta r_{e,2} \tag{9.20}$$

$$I/2F = \Delta r_{H_2} - \Delta r_O \tag{9.21}$$

Since both the forward reactions (9.13) and (9.14) are anodic, it follows that a positive I, causing an increase in catalyst potential U_{rhe}, will also cause an increase in both $r_{e,1}$ and $r_{e,2}$, i.e. $\Delta r_{e,1}>0$ and $\Delta r_{e,2}>0$. Consequently, if the rate of the catalytic reaction, r_c, were not changing upon current application ($\Delta r_c=0$) it follows from Eq. (9.19) that:

$$\Delta r_O < 0 \tag{9.22}$$

and from Eq. (9.18) that:

$$\Delta r_{H_2} < I/2F \tag{9.23}$$

On the contrary, as shown in Fig. 9.25, at steady state it is:

$$\Delta r_O = (14.8)\,(I/2F) \tag{9.24}$$

$$\Delta r_{H_2} = (15.8)\,(I/2F) \tag{9.25}$$

This proves conclusively that r_c has changed substantially upon current application. In fact, in view of Eqs. (9.18) and (9.19) one has:

$$(14.8)(I/2F) < \Delta r_c < (15.8)(I/2F) \tag{9.26}$$

or, more generally:

$$\Lambda_O < \Delta r_c /(I/2F) < \Lambda_{H_2} \tag{9.27}$$

where the Faradaic efficiencies Λ_{H_2} and Λ_O are defined, as usually, from:

$$\Lambda_{H_2} = \Delta r_{H_2}/(I/2F); \qquad \Lambda_O = \Delta r_O /(I/2F); \qquad \Lambda_{H_2} - \Lambda_O = 1 \tag{9.28}$$

Consequently, the observed non-faradaic rate enhancement is due to the acceleration of the *catalytic* rate of H_2 oxidation on the Pt catalyst-electrode.

There is an additional important observation to be made in Fig. 9.25 regarding the magnitude of the relaxation time constant, τ, upon current imposition: Electrochemical promotion studies involving both solid electrolytes[4] and aqueous alkaline solutions[37,38] have shown that τ (defined as the time required for the catalytic rate increase to reach 63% of its final steady-state value upon current application) can be estimated from:

$$\tau \approx 2FN_G/I \tag{9.29}$$

where N_G is the catalyst-electrode surface area, expressed in surface mol Pt (N_G=1.2·10^{-6} mol Pt in the present case) and I is the applied current (I=5mA). For the experiment of Fig. 9.25, Eq. (9.29) predicts τ=46 s in good qualitative agreement with the experimental τ value of 20 s. This suggests that the catalytic reaction, but also the non-faradaic catalytic rate enhancement, take place over the entire catalyst-electrode surface area and is not localized at the three phase boundaries Pt-Nafion-gas.

As shown in Fig. 9.25, upon current interruption r_{H_2}, r_O and U_{rhe} return to their open circuit values, showing the reversibility of the effect. It is worth noting that the rate transient parallels, to a large extent, the catalyst potential. This shows the important role of catalyst potential in describing electrochemical promotion.

9.2.1.2 Steady-State Effect of Current

Figure 9.26 shows the steady state effect of applied current I on the induced changes, $\Delta r_{H_2}(=r_{H_2}-r^o_{H_2})$ and $\Delta r_O(=r_O-r^o_O)$, in the rates of consumption of H_2 and O respectively, where the superscript "o" always denotes open-circuit conditions. The dashed lines in Fig. 9.26 are constant Faradaic efficiency, Λ, lines. The maximum measured Λ values are near 40 at low current densities. This value is in excellent qualitative agreement with the following approximate expression which can predict the magnitude of $|\Lambda|$ in NEMCA studies:

$$|\Lambda| \approx 2F\, r^o_O / I_0 \tag{4.20}$$

where $|\Lambda|$ is the predicted absolute value of the Faradaic efficiency Λ, r^o_O is the open-circuit catalytic rate and I_0 is the exchange current of the catalyst-electrolyte interface extracted from current -overpotential Tafel plots (Fig. 9.27) in the presence of the H_2/O_2 mixture. Equation (4.20) has been derived in Chapter 4 and has been found to predict the order of magnitude of $|\Lambda|$ in all previous solid state or aqueous electrochemical promotion studies. This equation suggests that a necessary condition for observing NEMCA ($|\Lambda|>1$) is that the open-circuit catalytic rate r^o_C must be higher than the exchange electrocatalytic rate $I_0/2F$.

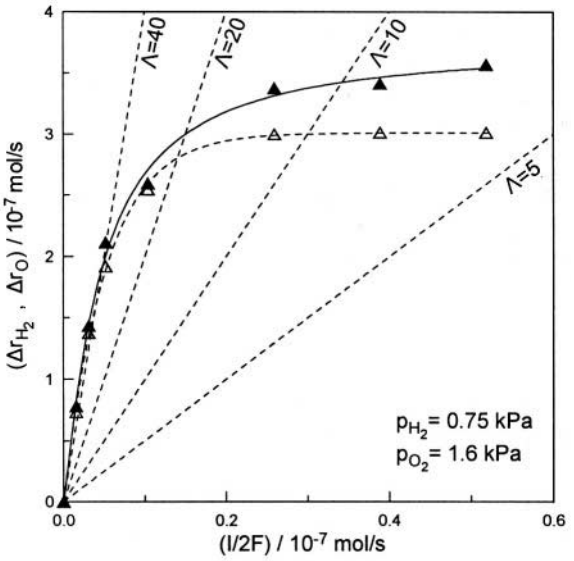

Figure 9.26. Steady-state effect of applied current on the increase in the consumption rates of H_2 (▲) and O_2 (△); $r_C^o = r_{H_2}^o = r_O^o = 0.7\times10^{-7}\,\mathrm{mol/s}$; total molar flowrate f_m=17×10^{-5} mol/s.[35] Reproduced by permission of The Electrochemical Society.

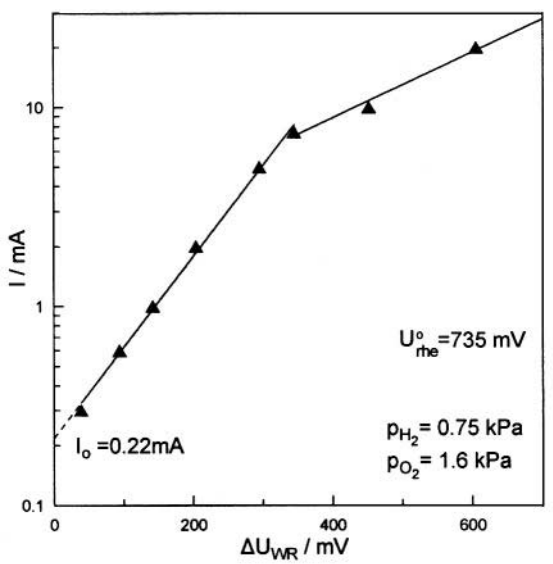

Figure 9.27. Steady-state effect of catalyst overpotential $\Delta U_{WR}(=U_{rhe}- U^o_{rhe})$ on current I. Conditions as in Fig. 9.26.[35] Reproduced by permission of The Electrochemical Society.

As shown in Fig. 9.27 there is a break in the slope of the Tafel plot at $E_{RHE} \approx 1.05$ V with a change in the transfer coefficient from 0.27 to 0.1. As shown below this change is consistent with a change in the surface coverages of adsorbed species as also manifest in the reaction kinetics.

9.2.1.3 Open and Closed Circuit Kinetics

Figure 9.28 shows the dependence of the catalytic rate of oxygen consumption, r_O, on the oxygen partial pressure p_{O_2} at fixed p_{H_2} under open-circuit conditions and for a potentiostatically fixed catalyst potential U_{RHE} ($=U_{WR}$). As also shown in Fig. 9.28, the open-circuit potential U^o_{RHE} increases from 0.33 to 0.8 V as the p_{O_2}/p_{H_2} ratio increases from 0.2 to 3.6.

A very pronounced, 10-fold, increase in catalytic rate is obtained for high p_{O_2}/p_{H_2} values (Fig. 9.28). The rate enhancement ratio ρ_O defined from:

$$\rho_O = \frac{r_O}{r_O^o} \tag{9.30}$$

is thus of the order of 10 for high p_{O_2}/p_{H_2} ratios.

More importantly, as shown in Fig. 9.28, increasing catalyst potential causes a pronounced increase in the p_{O_2} value, $p^*_{O_2}$, which maximizes the

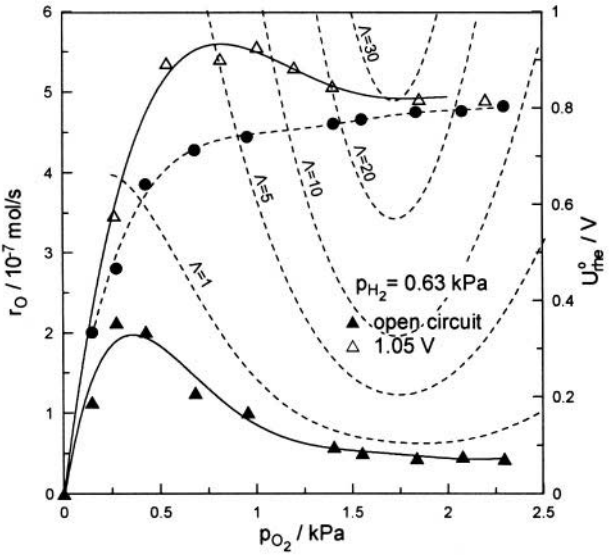

Figure 9.28. Effect of p_{O_2} on the rate of O consumption (▲) and corresponding catalyst potential (●), U^o_{rhe}, under open-circuit conditions and on the rate of O consumption (△) and corresponding Λ_O value under closed-circuit conditions at fixed catalyst potential U_{rhe}=1.05 V; total molar flowrate $f_m=1.7\times10^{-4}$ mol/s.[35] Reproduced by permission of The Electrochemical Society.

catalytic reaction rate. This suggests a weakening in the Pt=O chemisorptive bond with increasing catalyst potential and work function, which is due to the electron acceptor character of adsorbed O.

Figure 9.28 also shows the Faradaic efficiency, $\Lambda_O(=\Delta r_O/(I/2F))$, corresponding to each closed-circuit point; Λ_O reaches values up to 30 for high p_{O_2} values. The constant Λ_O curves shown in Figs. 9.28 and 9.29 are computed from the equation:

$$r_O = r_O^o + \Lambda_O (I/2F) \tag{9.31}$$

where I is the measured current obtained via the constant potential application at each gaseous composition.

Figure 9.29 depicts the effect of H_2 partial pressure, p_{H_2}, on the rate of oxygen consumption, r_O, at a fixed p_{O_2} value for open-circuit operation and for a potentiostatically imposed U_{rhe} value of 0.9 V. Under these conditions the rate enhancement ratio ρ_O takes values up to 20 for intermediate p_{O_2}/p_{H_2} values, i.e. there is a 2000% rate increase. Figure 9.29 also shows the Faradaic efficiency $\Lambda_O(=\Delta r_O/(I/2F))$, corresponding to each closed circuit point. For low p_{H_2} values, Λ_O is up to 300. As also shown in Fig. 9.29 increasing catalyst potential causes not only a very pronounced rate enhancement, but also the onset of the appearance of a rate maximum with respect to p_{H_2}, suggesting a strengthening of the chemisorptive bond of the, electron donor, H with increasing catalyst potential.

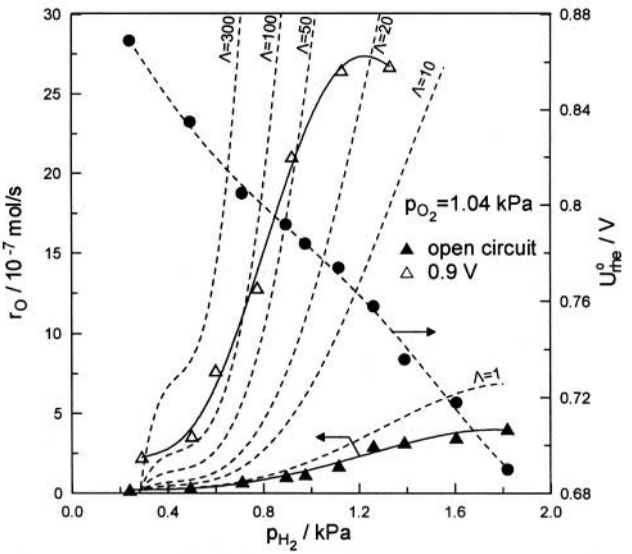

Figure 9.29. Effect of p_{H2} on the rate of O consumption (▲) under open-circuit conditions and corresponding catalyst potential U^o_{rhe}, (●) and on the rate of O consumption (△) and corresponding Λ_O value at a fixed catalyst potential U_{rhe}=0.9 V; f_m=1.7 to $3.5 \cdot 10^{-4}$ mol/s.[35] Reproduced by permission of The Electrochemical Society.

These observations show that, as in NEMCA studies in solid state and aqueous electrochemistry, the observed pronounced catalytic rate modification is primarily due to the change in the binding strength of chemisorbed O and H with changing catalyst potential.

This point is also manifest by the observation of a rate maximum when examining the effect of catalyst potential E_{RHE} on the rates of H_2 and O consumption for fixed gaseous composition (Fig. 9.30). Under open-circuit conditions (U^o_{rhe}=0.74 V) oxygen is more strongly bonded on the surface, the H coverage, θ_H, is low and thus the catalytic rate, which is proportional to $\theta_O \times \theta_H$ according to the Langmuir-Hinshelwood catalytic rate model, is also low. As the potential is increased (Fig. 9.30) the chemisorptive bond of O is weakened and that of H is strengthened with a concomitant decrease in the θ_O/θ_H ratio. At the rate maximum this ratio is near unity. By further increasing U_{rhe} the chemisorptive bond of oxygen becomes very weak, as the oxygen evolution region is approached, and thus θ_O decreases substantially and the catalytic rate decreases (Fig. 9.30).

It is worth noting that the catalytic rate maximum with respect to U_{rhe} (Fig. 9.30) appears to coincide with the break in the Tafel plot (Fig. 9.27). This is consistent with the proposed interpretation of the volcano plot. To the left of the rate maximum the surface is predominantly oxygen covered and to the right predominantly hydrogen covered. This change in relative coverages and thus predominant charge transfer mechanism (Eqs. 9.13 and 9.14) is likely to cause the observed break in the Arrhenius plot. The overall behaviour is in excellent agreement with global promotional rule G3.

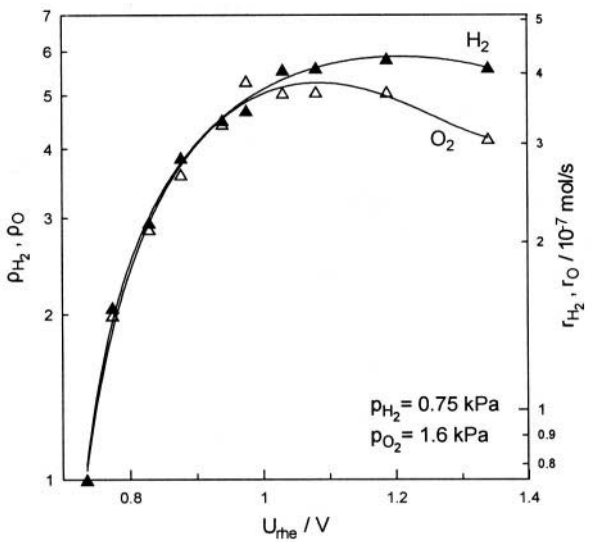

Figure 9.30. Steady-state effect of catalyst potential, U_{rhe}, on the rate enhancement ratios, $\rho_{H2} = r_{H2} / r^o_{H2}$ and $\rho_O = r_O / r^o_O$ and on the corresponding consumption rates of hydrogen and oxygen. Conditions as in Fig. 9.26.[35] Reproduced by permission of The Electrochemical Society.

9.2.2 Isomerization of 1-Butene on Pd-Black/Nafion 117 Cathodes

The isomerization of 1-butene to *cis*- and *trans*- 2-butene on Pd/C/Nafion and Pd-Ru/Nafion electrodes is one of the most remarkable and astonishing electrochemical promotion studies which has appeared in the literature.[39,40] Smotkin and coworkers[39,40] were investigating the electrocatalytic reduction of 1-butene to butane on high surface area Pd/C and Pd-Ru cathodes deposited on Nafion 117 when, to their great surprise, they observed at slightly negative overpotentials (Fig. 9.31) the massive production of 1-butene isomerization, rather than reduction, products, i.e. *cis*- and trans-2-butenes. This is extremely important as it shows that electrochemical promotion can be used also to enhance nonredox catalytic reactions such as isomerization processes.

The electrochemical cell consists of high surface area Pd/C or unsupported Pd-Ru cathodes interfaced to Nafion with a **Pt-black/H_2** counter electrode. The cell configuration, as well as the reactions taking place on the anode and the cathode are the following:

$$H_2 \rightarrow 2H^+ + 2e^- \;\Big|\; Pt \;\Big\|\; \begin{matrix} \text{Nafion} \\ \\ H^+ \rightarrow \end{matrix} \;\Big\|\; \begin{matrix} \text{Pd/C} \\ \text{or} \\ \text{Pd:Ru} \end{matrix} \;\Big|$$

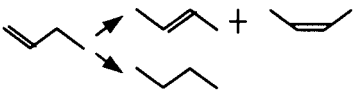

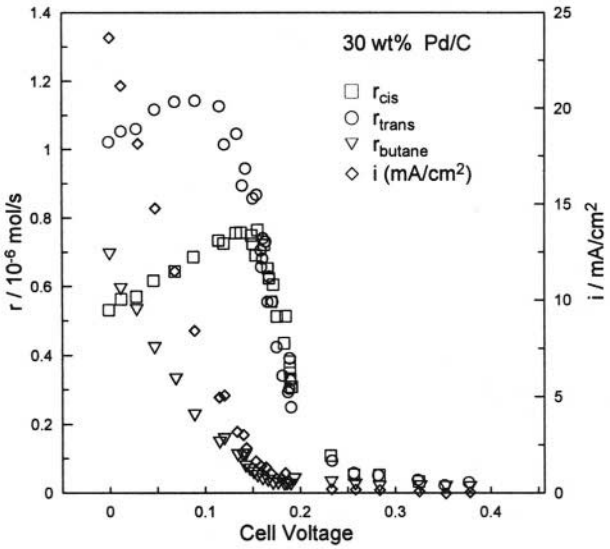

Figure 9.31. Effect of cell potential on the rates of cis- and trans-2-butene and butane formation upon electrochemical reduction of 1-butene on Pd/C/Nafion electrodes at room temperature.[39] Reprinted with permission from the American Chemical Society.

The catalytic-electrocatalytic reactor consists of a membrane electrode assembly, such as Pt-black/Nafion/Pd/C sandwiched between sheets of porous carbon cloth, housed in a fuel cell assembly.

The remarkable NEMCA behavior of the isomerization reaction is shown in Fig. 9.31. At potentials negative with respect to the open circuit potential (~0.38V) the rates of *cis*- and *trans*-2-butene formation start to increase dramatically. At a cell voltage of 0.16 to 0.10V the observed maximum ρ values are 38 and 46, respectively. The absolute Λ values are approximately equal to 28, as computed from the ratio $\Delta r/(I/F)$ (with I/F presenting the rate of proton supply to the catalyst). The system thus exhibits a strong non-faradaic electrophilic behavior.

The addition of a spillover proton to an adsorbed alkene to yield a secondary carbonium ion followed by abstraction of a proton from the C_3 carbon would yield both isomers of 2-butene. The estimated faradaic efficiencies show that each electromigrated proton causes up to 28 molecules of butene to undergo isomerization. This catalytic step is for intermediate potentials much faster than the consumption of the proton by the electrochemical reduction of butene to butane. However, the reduction of butene to butane becomes significant at lower potentials, i.e., less than 0.1V, with a concomitant inhibition of the isomerization process, as manifest in Fig. 9.31 by the appearance of the maxima of the *cis*- and *trans*-butene formation rates.

As shown in Figure 9.31, butane is formed electrocatalytically ($\Lambda_{but} < 1$) since no gaseous H_2 is supplied, thus Λ_{but} is restricted to its electrocatalysis limits ($|\Lambda|<1$) but it is remarkable that even in the negative potential region of electrocatalysis, electrochemically promoted formation of isomerization products continues with large Λ and ρ values (Fig. 9.31).

The discovery of Smotkin and coworkers[39,40] will most likely create a new area of research, important both from the theoretical and from the technological viewpoint.

9.2.3 Ethylene Hydrogenation on $Ni/CsHSO_4$

Ethylene hydrogenation on $Ni/CsHSO_4$ was the first electrochemical promotion study utilizing a H^+ conductor and also the first NEMCA study of a hydrogenation reaction[41] (The first dehydrogenation NEMCA study is discussed in section 10.1). The work was carried out by Politova, Sobyanin and Belyaev at Novosibirsk. The reaction was investigated[41,42] at 150-170°C using Ni as the catalyst supported on $CsHSO_4$, a protonic conductor. The reaction was found to be electrophobic, i.e. proton supply to the Ni catalyst was found to decrease the rate by a factor of 6 (ρ=0.16) and proton removal was found to increase the rate by a factor of 2 (ρ=2). The corresponding Λ

values (=Δr/(-I/F)) are -6 for hydrogen removal and -300 for hydrogen supply. These results are intriguing in that proton supply and removal have the opposite effect from what would be anticipated from mass action kinetic considerations. It is very likely that increasing U_{WR} and Φ, which corresponds to proton removal, enhances the binding of ethylene and hydrogen on the Ni surface, since both are electron donors, and thus enhances the rate of hydrogenation.

9.2.4 Ammonia Synthesis on Fe Supported on a Proton ($CaZr_{0.9}In_{0.1}O_{3-\alpha}$) Conductor

The catalytic synthesis of ammonia from its elements via the Haber-Bosch process is of major industrial importance. The high pressure synthesis is catalyzed by Fe promoted with K_2O, CaO and Al_2O_3.

A recent electrochemical promotion study of NH_3 synthesis[43] utilized a commercial fully promoted Fe-based NH_3 synthesis catalyst (BASF S6 - 10RED) deposited on $CaZr_{0.9}In_{0.1}O_{3-\alpha}$, a proton conductor.

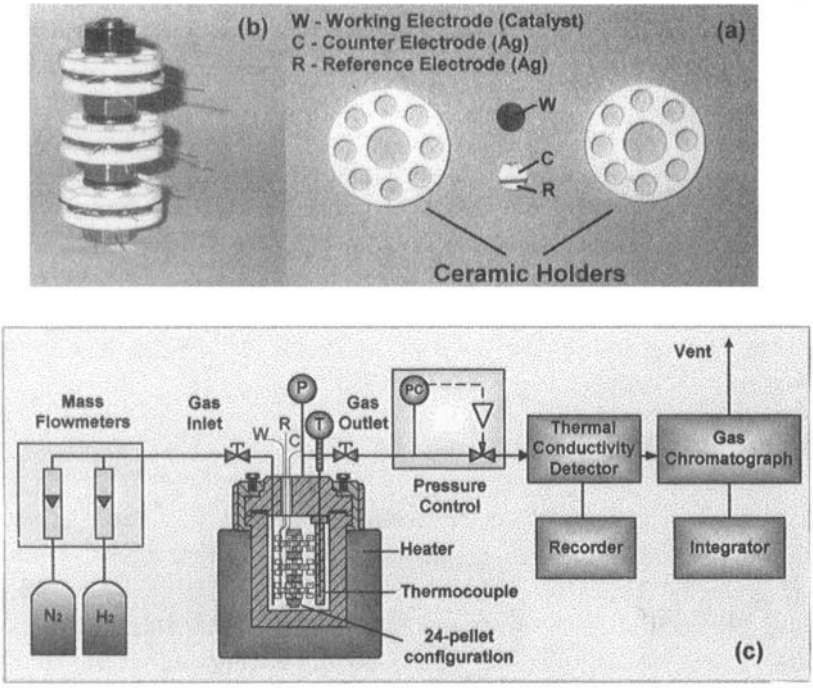

Figure 9.32. Experimental set-up (a) Machinable ceramic holders and two proton conducting pellets showing the location of catalyst, counter and reference electrodes. (b) Twenty four pellet unit. (c) High-pressure reactor, gas feed and analysis unit.[43] Reprinted with permission from the American Chemical Society.

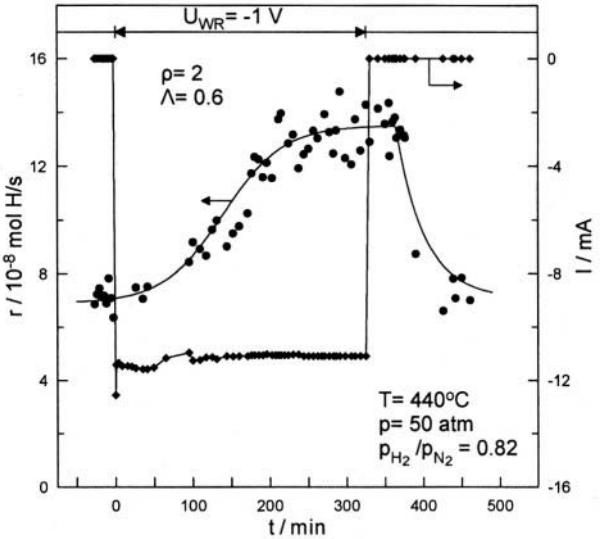

Figure 9.33. Ammonia synthesis rate and current response to a step change in the catalyst potential U_{WR} of the promoted $Fe/CaZr_{0.9}In_{0.1}O_{3-\alpha}$ catalyst.[43] Reprinted with permission from the American Chemical Society.

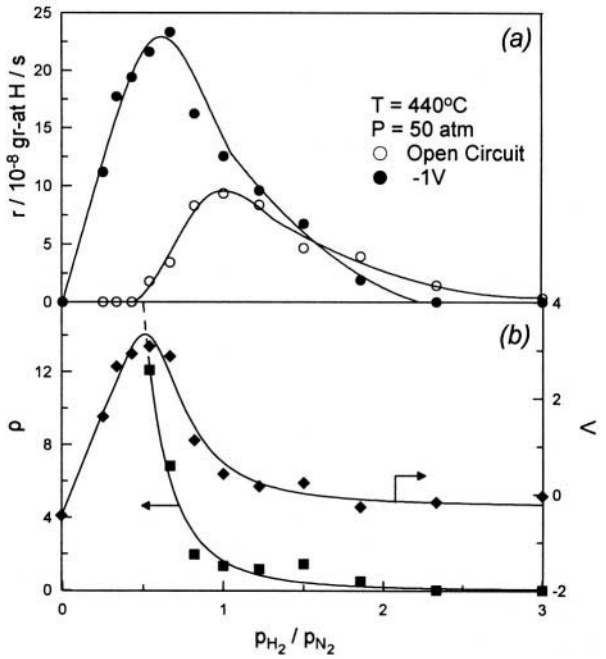

Figure 9.34. (a) Effect of inlet H_2/N_2 ratio on the rate of NH_3 synthesis over promoted $Fe/CaZr_{0.9}In_{0.1}O_{3-\alpha}$ under open-circuit (O) and for U_{WR}=-1.0V (●) (b) Corresponding ρ (r/r_0) (■) and Λ (=$\Delta r_H/(-I/F)$) (◆) values.[43] Reprinted with permission from the American Chemical Society.

This electrochemical promotion study was novel in three respects: a) The catalyst-electrode was a fully promoted industrial catalyst. (b) The study was carried out at high pressure (50 atm). (c) This was the first attempt for the *scale-up* of an electrochemically promoted reactor since 24 $CaZr_{0.9}In_{0.1}O_{3-\alpha}$ cell-pellets, electrically connected in parallel, were placed in the high pressure reactor (Fig. 9.32).[43]

The rate of ammonia production was enhanced by more than 1100% in the nitrogen rich regime (Figs 9.33 and 9.34), upon potential application of -1V between the working electrode and the Ag reference electrode. The extent of the NEMCA effect depends strongly on the kinetic regime of the reaction. Very pronounced non-faradaic behavior is observed in the regime $0.33 \leq H_2/N_2 \leq 0.67$ where ρ values of 12 or more are obtained.

The enhancement in the catalytic activity is due to the electrochemical supply of H^+ to the catalyst which decreases the catalyst work function and thus strengthens the chemisorptive bond of electron acceptor N while at the same time weakening the bonds of electron donor H and NH_3.

9.2.5 Methane Dimerization Using Proton Conductors

The reaction of non-oxidative CH_4 dimerization to ethane and ethylene was investigated by Stoukides and coworkers[44] at 750°C on Ag electrodes in a single-chamber NEMCA reactor arrangement. $SrCe_{0.95}Yb_{0.05}O_3$ was used as the solid electrolyte. This material is known to exhibit both protonic (H^+) and oxide ion (O^{2-}) conductivity, the former dominating at temperatures below 750°C.[44] The reaction is found to be electrophobic with ρ values up to 8. The total selectivity to C_2H_4 and C_2H_6 was near 100%. Thermodynamics place very stringent limits to the maximum equilibrium conversion of this reaction, provided $|\Lambda|>1$. When $|\Lambda|<1$, however, these limitations vanish, as the process is similar to an electrolytic one. No Λ values were reported, unfortunately, in this interesting study[44] which showed that r increases exponentially with U_{WR}. It is likely that the process is electrocatalytic rather than electrochemically promoted.

9.2.6 C_2H_4 Oxidation on $Pt/CaZr_{0.9}In_{0.1}O_{3-\alpha}$

The possibility to induce the NEMCA effect via $CaZr_{0.9}In_{0.1}O_{3-\alpha}$, a proton conductor, was tested for the first time during ethylene oxidation on Pt.[45] $CaZr_{0.9}In_{0.1}O_{3-\alpha}$ is a mechanically robust solid electrolyte material which exhibits mixed proton, oxygen ion and electron hole conduction. Proton conduction dominates at temperatures below 450°C which were used in this investigation.

Negative current application, i.e., proton supply to the catalyst film causes up to 500% reversible enhancement to the rate of C_2H_4 oxidation. The catalytic rate increase is up to 2×10^4 times higher than the rate -I/F, of proton supply to the catalyst.

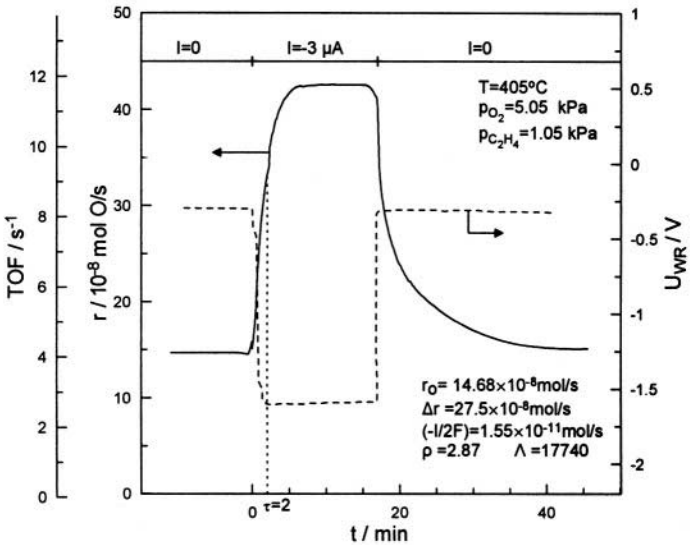

Figure 9.35. Transient effect of applied negative current on the rate and turnover frequency of C_2H_4 oxidation on $Pt/CaZr_{0.9}In_{0.1}O_{3-\alpha}$ (solid curve) and on catalyst potential (dashed curve).[45] Reprinted with permission from the Institute of Ionics.

A typical galvanostatic transient is shown in Fig. 9.35. Negative current application (I=-3μA) between the Pt working electrode and the Au counter electrode causes a reversible 3-fold enhancement in catalytic rate. The effect is strongly nonfaradaic, as the rate increase, **Δr**, is 8880 times larger than the rate, -I/F, of proton transfer to the catalyst and 17740 times larger than the increase in catalytic rate expressed in mol O, -I/2F, anticipated from Faraday's law if all the protons transferred to the catalyst were reacting with oxygen to form H_2O. Protons supplied to the catalyst may react with chemisorbed O(Pt) to form OH:

$$H^+ + O(Pt) + e^- \rightarrow OH(Pt) \tag{9.32}$$

and it is likely that this OH(Pt) species is the electrochemically generated promoting species on the Pt catalyst surface. The observed electrophilic behaviour (Figs. 9.35, 4.29) is consistent with the kinetics which are negative order in C_2H_4[45] and indicate a high coverage of adsorbed C_2H_4. Thus, according to the promotional rule G2 decreasing **Φ** weakens the adsorption of electron donor C_2H_4, enhances the adsorption of electron acceptor O and thus enhances the catalytic rate.

This study is noteworthy because it was the first one showing that a proton conductor can be used for the electrochemical promotion of an oxidation reaction. It underlines that, contrary to chemisorbed H which is a

very reactive species in oxidizing environments such as the ones used in this study,[45] protons are rather stable and, in association with O forming OH (Eq. 9.32), can act as promoters. This is similar to the distinction between O^{2-}, a rather unreactive and effective promoter, and highly reactive normally chemisorbed O, made throughout Chapter 8.

REFERENCES

1. C.G. Vayenas, S. Bebelis, and S. Despotopoulou, Non-Faradaic Electrochemical Modification of Catalytic Activity: 4. The use of β''-Al_2O_3 as the solid electrolyte, *J. Catal.* **128**, 415-435(1991).
2. G.C. Farrington, B. Dunn, and J.C. Thomas, High Conductivity Solid Ionic Conductors, E.T. Takahashi, ed. World Sci. Publ., Singapore (1989).
3. E.C. Subbarao, and H.S. Maiti, Solid electrolytes with oxygen ion conduction, *Solid State Ionics* **11**, 317-338 (1984).
4. S. Bebelis, and C.G. Vayenas, Non-Faradaic Electrochemical Modification of Catalytic Activity: 1. The case of Ethylene Oxidation on Pt, *J. Catal.* **118**, 125-146 (1989).
5. S. Bebelis, M. Makri, A. Buekenhoudt, J. Luyten, S. Brosda, P. Petrolekas, C. Pliangos, and C.G. Vayenas, Electrochemical activation of catalytic reactions using anionic, cationic and mixed conductors, *Solid State Ionics* **129**, 33-46 (2000).
6. I. Harkness, and R.M. Lambert, Electrochemical Promotion of the NO + Ethylene Reaction over Platinum, *J. Catal.* **152**, 211-214 (1995).
7. R.M. Lambert, M. Tikhov, A. Palermo, I.V. Yentekakis, and C.G. Vayenas, Electrochemical Promotion of Environmentally Important Catalytic Reactions, *Ionics* **1**, 366-376(1995).
8. M. Makri, C.G. Vayenas, S. Bebelis, K.H. Besocke, and C. Cavalca, Atomic Resolution Scanning Tunneling Microscopy Imaging of Pt Electrodes Intefaced with β''-Al_2O_3, *Ionics* **2**, 248-253 (1996).
9. J. Hölzl, and F.K.Schulte, Work Function of Metals, in *Solid Surface Physics,* Springer-Verlag, Berlin (1979), pp. 1-150.
10. E. Lamy-Pitara, L. Bencharif, and J. Barbier, Effect of sulphur on the properties of platinum catalysts as characterized by cyclic voltammetry, *Appl. Catal.* **18**, 117-131 (1985).
11. I.V. Yentekakis, G. Moggridge, C.G. Vayenas, and R.M. Lambert, In situ controlled promotion of catalyst surfaces via NEMCA: The effect of Na on the Pt-catalyzed CO oxidation, *J. Catal.* **146**, 292-305 (1994).
12. K.J. Uram, L. Ng, and J.R.Yates Jr., Electrostatic effects between adsorbed species-The K-CO interaction on Ni(111) as studied by infrared reflection - absorption spectroscopy, *Surf. Sci.* **177**, 253-277 (1986).
13. W. Schröder, and J. Hözl, Electronic structure of adsorbed sodium on Pt(III), *Solid State Communications.* **24**, 777-780 (1977).
14. C.A. Papageorgopoulos, and J.M. Chen, Coadsorption of cesium and oxygen on Ni(100). I. Cesium probing of Ni-O bonding, *Surf. Sci.* **52**, 40-52 (1975).
15. B. Delmon, and G.F. Froment, Remote Control of Catalytic Sites by Spillover Species: A Chemical Reaction Engineering Approach, *Catal. Rev.-Sci. Eng* **38**(1), 69-100 (1996).
16. D. Heskett, The interaction range in alkali metal-promoted systems, *Surf. Sci.* **199**, 67-86 (1988).
17. T. Aruga, and Y. Murata, Alkali-metal adsorption on metals, *Progress in Surface* Science **31**, 61-130 (1989).

18. R.M. Lambert, F. Williams, A. Palermo, and M.S. Tikhov, Modelling alkali promotion in heterogeneous catalysis: in situ electrochemical control of catalytic reactions, *Topics in Catalysis* **13**, 91-98 (2000).
19. I.R. Harkness, C. Hardacre, R.M. Lambert, I.V. Yentekakis, and C.G. Vayenas, Ethylene oxidation over Platinum: In situ electrochemical promotion using β''-Al_2O_3 and studies with a Pt(111)/Na model catalyst, *J. Catal.* **160**, 19-26 (1996).
20. P.D. Petrolekas, S. Brosda, and C.G. Vayenas, Electrochemical promotion of Pt catalyst-electrodes deposited on $Na_3Zr_2Si_2PO_{12}$ during Ethylene Oxidation, *J. Electrochem. Soc.* **145**(5), 1469-1477 (1998).
21. I.N. Yakovkin, V.I. Chernyi, and A.G. Naumovetz, Oxidation of CO on Li-precovered Pt, *Surf. Sci.* **442**, 81-89 (1999).
22. C. Karavasilis, S. Bebelis, and C.G. Vayenas, In Situ Controlled Promotion of Catalyst Surfaces via NEMCA: The Effect of Na on the Ag-Catalyzed Ethylene Epoxidation in the Presence of Chlorine Moderators, *J. Catal.* **160**, 205-213 (1996).
23. A. Palermo, R.M. Lambert, I.R. Harkness, I.V. Yentekakis, O. Mar'ina, and C.G. Vayenas, Electrochemical promotion by Na of the Platinum catalyzed reaction between CO and NO, *J. Catal.* **161**, 471-479 (1996).
24. A. Palermo, M.S. Tikhov, N.C. Filkin, R.M. Lambert, I.V. Yentekakis, and C.G. Vayenas, Electrochemical Promotion of NO Reduction by CO and by Propene, *Stud. Surf. Sci. Catal.* **101**, 513-522 (1996).
25. I.V. Yentekakis, A. Palermo, N.C. Filkin, M.S. Tikhov and R.M. Lambert, In situ electrochemical promotion by sodium of the platinum-catalyzed reduction of NO by propene, *J. Phys. Chem. B,* **101**, 3759-3768 (1997).
26. O.A. Mar'ina, I.V. Yentekakis, C.G. Vayenas, A. Palermo, and R.M. Lambert, In situ controlled Promotion of Catalyst Surfaces via NEMCA: The effect of Na on the Pt-catalyzed NO Reduction by H_2, *J. Catal.* **166**, 218-228 (1997).
27. C.A. Cavalca, and G.L. Haller, Solid Electrolytes as Active Catalyst Supports: Electrochemical Modification of Benzene Hydrogenation Activity on Pt/β''(Na)Al_2O_3, *J. Catal.* **177**, 389-395 (1998).
28. C.A. Cavalca, *PhD Thesis,* Yale University (1995).
29. H. Karasali, *PhD Thesis,* Department of Chemical Engineering, University of Patras (1994).
30. A. Giannikos, P. Petrolekas, C. Pliangos, A. Frenzel, C.G. Vayenas, and H. Putter, Electrochemical promotion of Pd for the Hydrogenation of C_2H_2, *Ionics* **4**,161 -169 (1998).
31. S. Tracey, A. Palermo, J.P.H. Vazquez, and R.M. Lambert, In Situ Electrochemical Promotion by Sodium of the Selective Hydrogenation of Acetylene over Platinum, *J. Catal.* **179**, 231-240 (1998).
32. G. Pitselis, P. Petrolekas, and C.G. Vayenas, Electrochemical Promotion of NH_3 decomposition over Fe catalyst films interfaced with K^+ and Na^+ conductors, *Ionics* **3**, 110-117 (1997).
33. S. Balomenou, G. Pitselis, D. Polydoros, A. Giannikos, A. Vradis, A. Frenzel, C. Pliangos, H. Putter, and C.G. Vayenas, Electrochemical Promotion of Pd, Fe and distributed Pt catalyst-electrodes, *Solid State Ionics* **136-137**, 857-862 (2000).
34. I.M. Arinkin, and N.A. Zakarina, Electrochemical control of the rate of gas phase H_2 oxidation on Pt/solid electrolye catalyst, *Electrohimia* **31**(6), 628-630 (1995).
35. D. Tsiplakides, S. Neophytides, O. Enea, M.M. Jaksic, and C.G. Vayenas, Non-faradaic Electrochemical Modification of Catalytic Activity (NEMCA) of Pt Black Electrodes Deposited on Nafion 117 Solid Polymer Electrolyte, *J. Electrochem. Soc.* **144**(6), 2072-2088 (1997).

36. H. Takenaka, and E. Torikai, Japan Pat. 55-38934 (1980).
37. S. Neophytides, D. Tsiplakides, P. Stonehart, M. Jaksic, and C.G. Vayenas, Electrochemical enhancement of a catalytic reaction in aqueous solution, *Nature* **370,** 292-294 (1994).
38. S. Neophytides, D. Tsiplakides, P. Stonehart, M.M. Jaksic, and C.G. Vayenas, Non-Faradaic Electrochemical enhancement of H_2 oxidation in alkaline solutions, *J. Phys. Chem.* **100**, 14803-14814 (1996).
39. L. Ploense, M. Salazar, B. Gurau, and E.S. Smotkin, Proton Spillover Promoted Isomerization of n-Butylenes on Pt-black Cathodes/Nafion 117, *JACS* **119**, 11550-11551 (1997).
40. L. Ploense, M. Salazar, B. Gurau, and E. Smotkin, Spectroscopic study of NEMCA promoted alkene isomerizations at PEM fuel cell Pd-Nafion cathodes, *Solid State Ionics* **136-137**, 713-720 (2000).
41. T.I. Politova, V.A. Sobyanin, and V.D. Belyaev, Ethylene hydrogenation in electrochemical cell with solid proton-conducting electrolyte, *Reaction Kinetics and Catalysis Letters* **41**(2), 321-326 (1990).
42. O.A. Mar'ina, V.A. Sobyanin, and V.D. Belyaev, *Materials Science and Engineering* **B13**, 153-155(1992).
43. C.G. Yiokari, G.E. Pitselis, D.G. Polydoros, A.D. Katsaounis, and C.G. Vayenas, High pressure electrochemical promotion of ammonia synthesis over an industrial iron catalyst, *J. Phys. Chem.* **104**, 10600-10602 (2000).
44. P.H. Chiang, D. Eng, and M. Stoukides, Solid electrolyte aided direct coupling of methane, *J. Catal.* **139**, 683-687(1993).
45. M. Makri, A. Buekenhoudt, J. Luyten, and C.G. Vayenas, Non-Faradaic Electrochemical Modification of the Catalytic Activity of Pt using a $CaZr_{0.9}In_{0.1}O_{3-\alpha}$ Proton Conductor, *Ionics* **2**, 282-288 (1996).

CHAPTER 10

NEMCA WITH AQUEOUS ELECTROLYTES AND INORGANIC MELTS

The discovery of NEMCA in aqueous systems[1-6] is of considerable theoretical and practical importance. Here no ion migration (backspillover) is necessary to account for the observed behaviour which appears again to be due to the effect of changing potential and work function on the binding strength of adsorbates. Here there appears to be only one double-layer of interest, that at the electrode-electrolyte interface, although since gases are produced and/or consumed, the electrode-gas interface may also have a role.

10.1 H_2 EVOLUTION AND ALDEHYDE OXIDATION AT IB METALS IN ALKALINE SOLUTIONS

Heitbaum, Anastasijevic, Baltruschat and coworkers[1,2] were first to report a non-Faradaic enhancement in the rate of H_2 evolution on Cu[1] and Ag[2] electrodes during formaldehyde oxidation. They used differential electrochemical mass spectroscopy[1,2] to measure the rate of H_2 evolution during formaldehyde oxidation on Cu and Ag in weakly alkaline solutions and found Faradaic efficiency Λ values up to 2; Λ was found to increase with decreasing catalyst potential. They attributed their interesting findings to the heterogeneously catalyzed reaction:

$$H_2CO + OH^- \rightarrow HCOO^- + H_2 \qquad (10.1)$$

the rate of which was proposed to be potential-dependent (electrophilic behaviour). The authors concluded that the observed phenomenon is due to the interaction of the electric field of the double layer with the adsorbed H_2CO molecule (water dipole orientation, change in the surface concentration of OH^-) and that the effect is similar to the NEMCA effect of solid state electrochemistry.[1,2]

10.2 HYDROGEN OXIDATION ON Pt IN AQUEOUS ALKALINE SOLUTIONS

The first pronounced demonstration of NEMCA in aqueous electrochemistry was reported[3,4] for the oxidation of H_2 on Pt electrodes in 0.1 M KOH solutions at temperatures 25° to 50° C. The original work was carried out using finely dispersed Pt supported on graphite[3] but identical results were later obtained using Pt black supported on a Teflon frit.[4] In both cases the H_2 - O_2 mixture (p_{O_2} and p_{H_2} were between 0.1 and 2 kPa) was bubbled through a Teflon frit and the rates r_{H_2} (mol H_2/s) and r_O (1/2 mol O_2/s) of H_2 and O_2 consumption were measured via on line gas chromatography and mass spectrometry. The gas flowrates were chosen such that the conversion of H_2 and O_2 was maintained under all conditions below 40%. The absence of diffusional limitations was verified by varying the total gas flowrate between 100 and 600 cm^3 STP/min and observing no significant change in the rates of H_2 and O_2 consumption. No problems with deterioration of catalyst or support were encountered over prolonged periods (~200 h) of operation at potentials below 1.5V with respect to a reference H_2 electrode (rhe) immersed in the same solution. Substitution of the 0.1 M KOH solution with a 0.1 M LiOH solution led to the same results. The Pt counter-electrode was situated in a separate compartment, electrolytically connected via a Flemion membrane, so that the rates of H_2 and O_2 consumption on the working catalyst-electrode could be accurately measured without any interference from the gases produced or consumed at the counter-electrode.

Hydrogen and oxygen are consumed on the Pt surface at a rate, r_c, by the catalytic reaction:

$$H_2 + 1/2O_2 \xrightarrow{r_c} H_2O \tag{10.2}$$

Under open-circuit conditions the catalyst potential $U_{WR} \equiv U_{rhe}$ takes values of the order 0.4-0.85 V, that is -0.35 to +0.1 V on the standard hydrogen electrode scale (she), depending on the hydrogen to oxygen ratio.

When a positive current I is applied between the catalyst-electrode and the Pt counter-electrode, then the catalyst potential U_{rhe} changes to more positive values (Fig. 10.1) and the following electrochemical (net charge-transfer) reactions take place at the Pt catalyst-electrode surface:

$$H_2 + 2OH^- \xrightarrow{r_{e,1}} 2H_2O + 2e^- \tag{10.3}$$

$$2OH^- \xrightarrow{r_{e,2}} (1/2)O_2 + 2H_2O + 2e^- \tag{10.4}$$

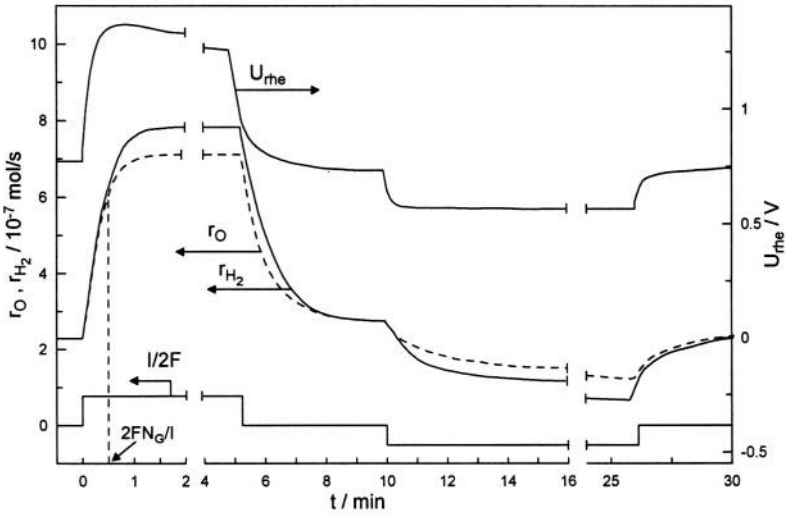

Figure 10.1. NEMCA in aqueous media (0.1 M KOH): Transient effect of applied positive and negative currents (I=15 and -10 mA) on the rates of consumption of hydrogen (r_{H_2}) and oxygen (r_O) on Pt/graphite; p_{H_2}=0.75 kPa, p_{O_2}=1.06 kPa; gas flowrate F_V=280 cm^3/min at STP. Reprinted with permission from Nature, ref. 3, McMillan Magazines Ltd.

where the forward reaction (10.4), that is $r_{e,2}>0$, takes place when U_{rhe} is above the oxygen reduction potential (1.23 V) and the reverse reaction, that is $r_{e,2}<0$, occurs otherwise. It follows from simple mass balance considerations that in general:

$$r_{H_2} = r_c + r_{e,1} \tag{10.5}$$

$$r_O = r_c - r_{e,2} \tag{10.6}$$

$$I/2F = r_{e,1} + r_{e,2} \tag{10.7}$$

and, thus,

$$r_{H_2} - r_O = I/2F \tag{10.8}$$

Consequently if r_c were to remain constant, application of a positive current would increase r_{H_2} by less than I/2F ($\Delta r_{H_2} \leq I/2F$) and would decrease or increase r_O again by less than I/2F ($-I/2F \leq \Delta r_O \leq I/2F$).

Surprisingly, as shown in the galvanostatic transient of Fig. 10.1, Δr_{H_2} is 720% higher than I/2F and Δr_O is 620% higher than I/2F. The increase, Δr_{H_2}, in r_{H_2} is 344% relative to the open-circuit value $r^o_{H_2} = r^o_O = r^o_c$. The Non-Faradaic behaviour ($\Lambda r_{H_2}=\Delta r_{H_2}/(I/2F)=7.2$) is due to the electrochemical activation

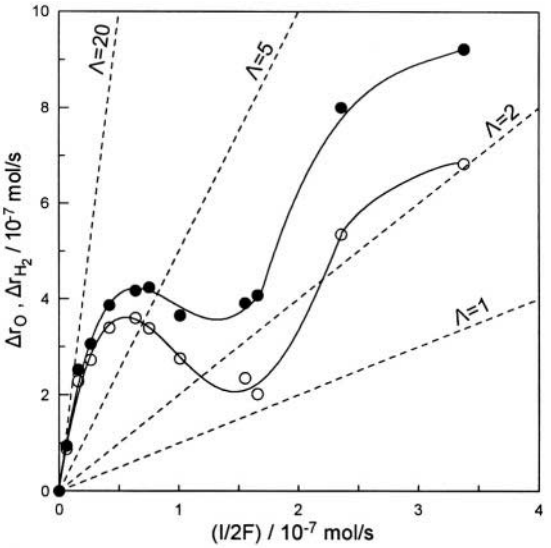

Figure 10.2. NEMCA in H_2 oxidation on Pt/graphite in 0.1 M KOH: Steady-state effect of applied positive (anodic) current (I) on the increase in the rates of hydrogen (●) and oxygen (○) consumption; p_{H_2}=0.8 kPa, p_{O_2}=1.25 kPa; $r^o_{H_2}$ ($=r^o_O=r^o_c$)=2.38×10^{-7} mol/s is the open-circuit catalytic rate; F_V=540 cm^3/min at STP. Reprinted with permission from Nature, McMillan Magazines Ltd.[3]

of the catalytic reaction (10.2), the rate (r_c) of which increases by between 310 and 344%, i.e. between $\Lambda_O(I/2F)$ and $\Lambda_H(I/2F)$. Fig. 10.1 also shows that:

a. The rate relaxation time constant τ upon constant current application is again ~$2FN_G/I$, as in solid-state electrochemical promotion studies.
b. The effect is reversible, i.e., r_{H_2}, r_O and catalyst potential U_{rhe} all return to their open-circuit values upon current interruption.
c. Negative currents also cause a Non-Faradaic decrease in r_{H_2} and r_O.
d. The reaction exhibits electrophobic behaviour, i.e. $\Lambda > 1$ and $\partial r/\partial U > 0$.
e. At steady-state the difference r_{H_2} - r_O always equals I/2F, in accordance with Eq. (10.8).

The steady-state effect of positive current on Δr_{H_2} and Δr_O is shown in Fig. 10.2. The faradaic efficiency Λ exceeds 20 (2000%) fow low currents. Fig. 10.3 shows the corresponding effect of catalyst potential $U_{WR} \equiv U_{rhe}$ on r_{H_2} and r_O, together with the dependence of I on E.

The break in the plot log I vs U_{rhe} coincides with the observed inflection in r_{H_2} and r_O, and corresponds to the onset of Pt oxide formation.[6] As shown in Fig. 10.3 the, predominantly catalytic, rates r_{H_2} and r_O depend exponentially on catalyst potential U_{rhe}, as in studies with solid electrolytes with slopes comparable with the Tafel slopes seen here. This explains why the observed magnitude of the faradaic efficiency Λ (~2-20) is in good agreement with $2F\,r^o_c/I_0$ (r^o_c is the open-circuit catalytic rate and I_0 is the exchange current) which is known to predict the expected magnitude of $|\Lambda|$ in solid-electrolyte studies.

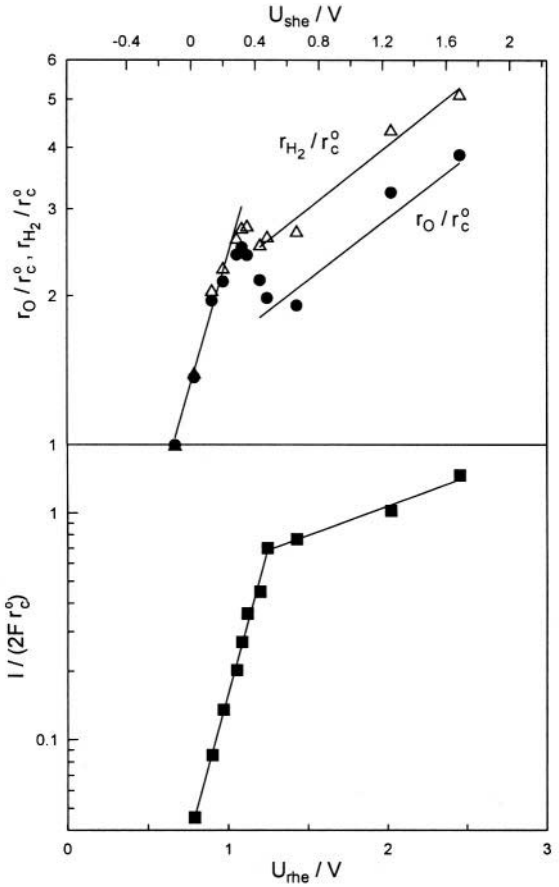

Figure 10.3. Steady-state effect of ohmic-drop-free catalyst potential on current (bottom) and on the rates of hydrogen (△) and oxygen (●) consumption (top) on Pt/graphite; r_{H_2} ($= r_O^o = r_c^o$) $=2.38 \cdot 10^{-7}$ mol/s is the open-circuit catalytic rate; Conditions as in Figure 10.2. Reprinted with permission from Nature, McMillan Magazines Ltd.[3,4]

Figure 10.4 shows the effect of p_{O_2}, p_{H_2} and catalyst potential on the rate of H_2 oxidation. The reaction mechanism is of the Langmuir-Hinshelwood type, as also manifested by the observed rate maxima upon varying p_{O_2} and p_{H_2}. Increasing catalyst potential causes both a pronounced increase in r_{H_2} and a shift of the rate maximum to higher p_{O_2} and lower p_{H_2} values. This shift indicates a weakening in the Pt = O chemisorptive bond and a strengthening in the Pt-H bond, both consistent with the anticipated effect of increased potential and work function on the binding strength of electron acceptor (oxygen) and electron donor (hydrogen) adsorbates. These considerations can also account for the appearance of the local rate maximum with respect to potential on the left of the break in the log I-U_{rhe} curve (Fig. 10.3).

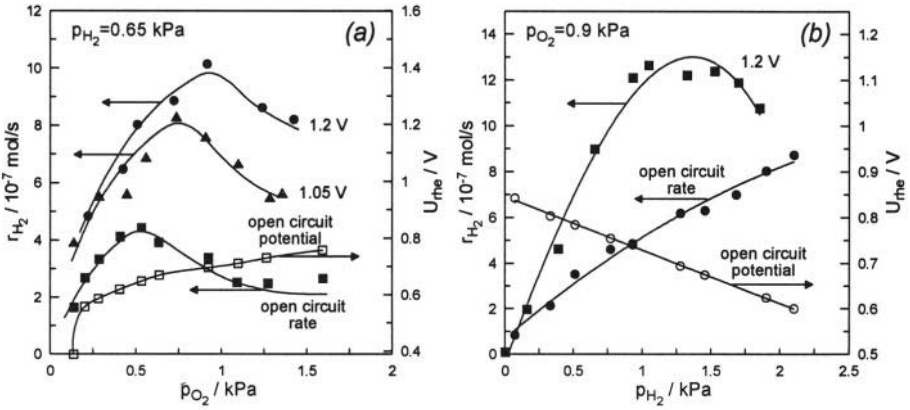

Figure 10.4. Effect of electrode-catalyst potential and oxygen (a) and hydrogen (b) partial pressure on the rate of hydrogen oxidation on Pt/graphite in 0.1 M KOH (a) and 0.1 M LiOH (b); F_V=500 cm^3 STP/min. Reprinted with permission from Nature, McMillan Magazines Ltd.[3]

Thus, similarly to the case of solid-state electrochemistry, the observed Non-Faradaic electrochemical modification of catalytic activity (NEMCA) appears to be due to the effect of changing potential and work function on the binding strength of the adsorbates. Changing catalyst potential affects the electric field in the metal-solution double layer with a concomitant change in the surface concentrations of OH^- and K^+ and in the orientation of H_2O dipoles. These changes will then affect the strength of the Pt=O and Pt-H covalent bonds, both of which have a certain ionic character, via direct electrostatic or through-the-metal interactions.

The NEMCA effect in aqueous electrochemistry may be of considerable technological value, for example in the electrochemical treatment of toxic organics or the production of useful industrial chemicals.

It must be emphasized, however, that since the Faradaic efficiency Λ is on the order of $2Fr_0/I_0$, one anticipates to observe NEMCA behaviour only for those systems where there is a measurable open-circuit catalytic activity r_0. Consequently the low operating temperatures of aqueous electrochemistry may severely limit the number of reactions where Non-Faradaic Λ values can be obtained.

It is also worth noting that the one-to-one correspondence between change in (ohmic drop-free) catalyst potential and work function in solid-state electrochemistry,[7,8] may also be applicable to the work function of liquid-free gas-exposed electrode surfaces in aqueous electrochemistry.[8] Such surfaces, created when gases are consumed or produced on an electrode surface, may also play a role in the observed NEMCA behaviour. The one-to-one correspondence between $e\Delta U_{WR}$ and $\Delta\Phi$ is strongly reminiscent of the similar one-to-one relationship established with emersed electrodes previously polarized in aqueous solutions,[9,10] as already discussed in Chapter 7.

10.3 MALEIC ACID HYDROGENATION ON Pt IN AQUEOUS ACIDIC SOLUTIONS

The hydrogenation of maleic acid ($c_M=10^{-3}$ M) at 26°C on platinized Pt in 0.5 M $HClO_4$ aqueous solution was investigated by Lamy-Pitara, El Mouahid and Barbier[5] in presence of H_2 without and with potential control and also in absence of H_2 via potential control.[5] The results shown in Fig. 10.5 and Table 10.1 show that potential control enhances significantly the rate of hydrogenation with both Λ and ρ approaching "infinity" at $U_{WR}=0.18$ V vs rhe. The reaction, exhibits electrophilic behaviour, i.e. the rate of hydrogenation is enhanced with decreasing (cathodic) catalyst potential.

Table 10.1. Dependence of the ratio of hydrogenation rates obtained by method B (presence of H_2 and external potential control) and by method C (electrocatalytic reduction).[5]

U_{rhe} (mV vs rhe)	$r_{imp}/r_{electrocat}$ (=r/(I/2F))
5	1.3
50	1.5
100	1.9
125	2.1
150	3.2
175	8
180	$\rightarrow\infty$

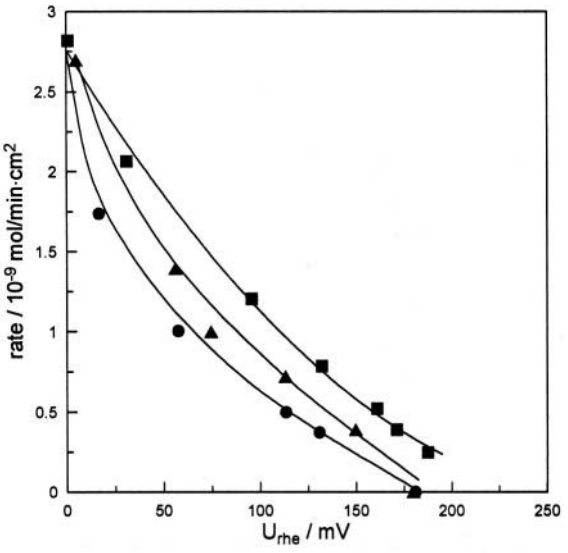

Figure 10.5. Evolution of the intrinsic catalytic activity of platinized platinum for the hydrogenation of maleic acid ($C_m=10^{-3}$ M, 299 K, 0.5 M $HClO_4$), as a function of potential, (▲); spontaneously set potential, (■, ●); imposed potential in absence, (●); and in presence (■); of H_2 (1 atm).[5] Reprinted with permission from Elsevier Science.

Interestingly the electrochemical promotional effect was found only in the case of perchloric acid supporting electrolyte. No promotion effect was found in presence of strongly adsorbed anions (HSO_4^-, Cl^-).

This very interesting work is the first demonstration of NEMCA for a hydrogenation reaction in aqueous solutions. It is also the first demonstration of NEMCA in an acidic solution, as all previous electrochemical promotion studies in aqueous media were restricted to alkaline solutions. This work also underlines the importance of the supporting electrolyte and of the strength of adsorption of the anions in aqueous electrochemical promotion studies.

10.4 PRODUCTION OF AMMONIUM POLYSULFIDE

In a recent patent Anastasijevic and coworkers[11] have described the use of electrochemical promotion to produce ammonium polysulfide, $(NH_4)_2S_x$, is an efficient manner. The novel electrochemically promoted process leads to faradaic efficiency, Λ, values of at least four[11] and $\rho(=r/r_0)$ values of at least eight.[11]

The catalytic (no net charge transfer) reaction which is electrochemically promoted is:

$$O_2 + 2\,S^{2-} + 2H_2O \rightarrow 2S + 4OH^- \qquad (10.9)$$

followed by:

$$(NH_4)_2S + (x-1)S \rightarrow (NH_4)_2\,S_x \qquad (10.10)$$

The ammonium polysulfide, $(NH_4)_2S_x$ (with x=2 to 6) is produced in an electrochemical cell where aqueous ammonium sulfide, $(NH_4)_2S$, solution is supplied as electrolyte. The cell comprises an anode and a gas diffusion carbon cathode over which gaseous O_2 is supplied in contact with the electrolyte.[11] The cell operated continuously at pressures up to 60 bar. The applied potential, U_{WC}, was 0.01 to 5 V. Pronounced electrochemical promotion behaviour was observed at U_{WC} values as low as 0.02 V with a current I=0.5 A.

This new NEMCA process underlines the potential importance of electrochemical promotion in industrial aqueous electrolyte systems.

10.5 SO_2 OXIDATION IN V_2O_5-$K_2S_2O_7$ MELTS

This exciting work carried out by Bjerrum and coworkers[12] in the experimental set up of Fig. 10.6 is truly remarkable for several reasons. The major difference from all electrochemical promotion studies surveyed in this

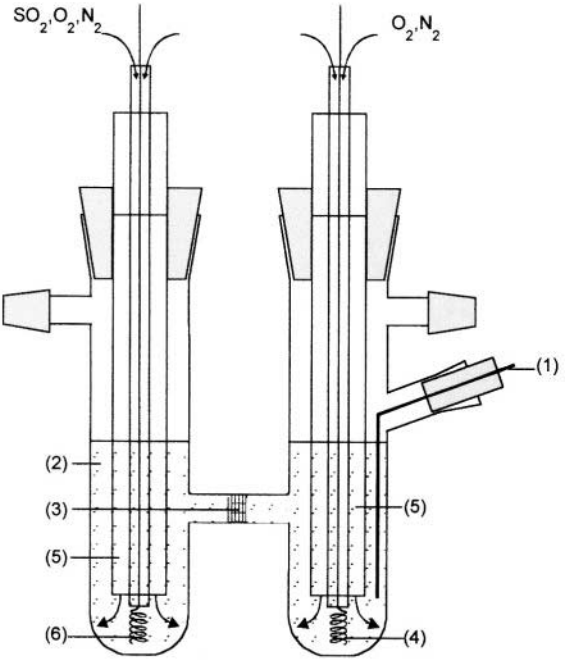

Figure 10.6. Electrochemical cell: (1) reference electrode, (2) molten catalyst, (3) porous Pyrex membrane, (4) counter electrode, (5) gas inlet Pyrex tube, (6) working electrode.[12] Reproduced by permission of the Electrochemical Society.

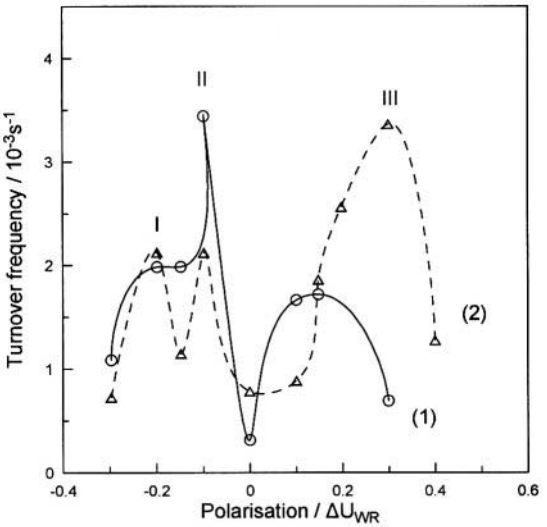

Figure 10.7. Turnover frequency of SO_2 catalytic oxidation [mol SO_2 (conv.)/mol V_2O_5/s] vs working electrode polarization for the molten 10 mol % V_2O_5 – 90 mol% $K_2S_2O_7$ catalyst at (1) 440°C and (2) 460°C.[12] Reproduced by permission of the Electrochemical Society.

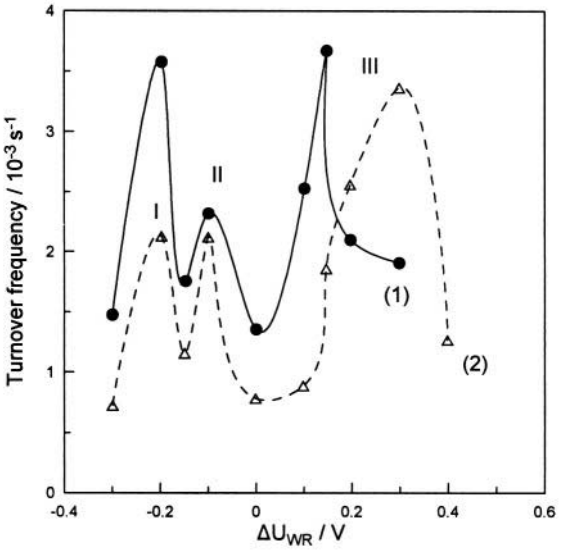

Figure 10.8. Turnover frequency of SO_2 catalytic oxidation [mol SO_2 (conv.)/mol V_2O_5/s] vs. working electrode polarization for the (1) 17 mol % V_2O_5 – 83 mol % $K_2S_2O_7$ catalyst at 460°C and for (2) 10 mol % V_2O_5 – 90 mol% $K_2S_2O_7$ catalyst.[12] Reproduced by permission of the Electrochemical Society.

book, is that here it is the electrolyte (molten salt) and not the electrode which is the active catalyst and it is the electrolyte (or at least part of it) which is being electrochemically promoted.

Figure 10.6 shows the experimental setup. Gold wires were used as working, counter and reference electrodes, inserted into the pyrex tubes which contained the V_2O_5-$K_2S_2O_7$ melt. As shown in Figures 10.7 and 10.8 the dependence of the rate of SO_2 oxidation on catalyst potential is rather complex as the rate exhibits two maxima at negative potentials (-0.1 V and -0.2 V) and one maximum at positive potentials (0.1 to 0.3 V). Approximately speaking, however, one could describe the global behaviour of this reaction as inverted volcano. As shown in Figure 10.9 the apparent faradaic efficiency, Λ, of the process is extremely high and approaches infinite values at negative potentials where very small currents induce pronounced increases in catalytic rate.

Using a similar design the authors also showed (Fig. 10.9, 10.10)[12] that an industrial (VK-58 Haldor-Topsøe) V_2O_5-$K_2S_2O_7$ based catalyst could be electrochemically promoted (ρ=4, $|\Lambda|=10^2$) via polarization at U_{WR}=-0.2 V. This may be of significant practical importance.

Bjerrum and coworkers have assigned the three rate maxima shown in Figs. 10.7 and 10.8 to (starting from the negative potential) (a) destruction of vanadium polymeric chains (b) electric double layer effect at gold working electrode (c) stabilization of V (V) vs V (IV). These explanations are very plausible.

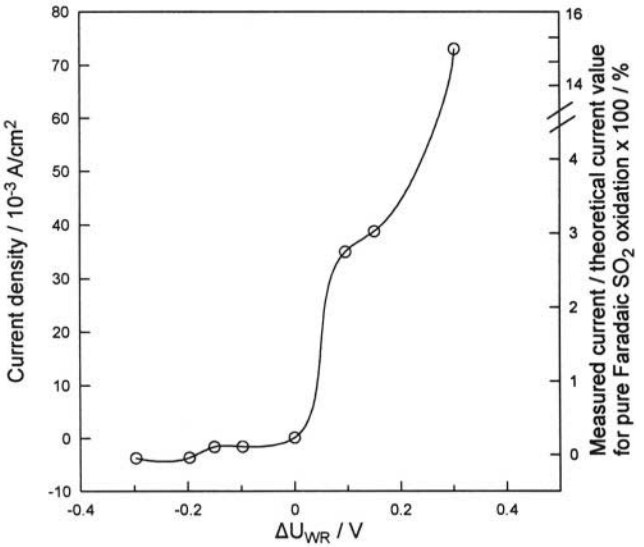

Figure 10.9. Stationary polarization curve obtained with 10 mol % V_2O_5 – 90 mol % $K_2S_2O_7$ catalyst at 440°C.[12] Reproduced by permission of the Electrochemical Society.

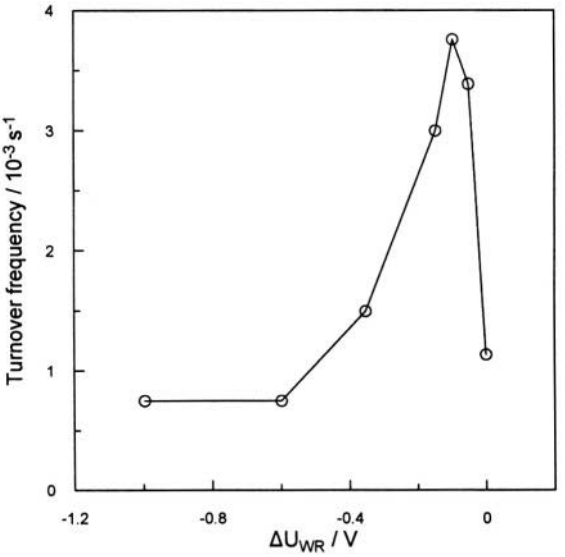

Figure 10.10. Turnover frequency of the SO_2 catalytic oxidation [mol SO_2 (converted)/mol V_2O_5/s] vs. the working electrode polarization for the VK-58 catalyst (Haldor Topsøe A/S) at 400°C.[12] Reproduced by permission of the Electrochemical Society.

Electrochemical promotion of a melt can be further understood in terms of the energy diagram of Figure 7.10: When the working electrode is polarized anodically, it is not only the Fermi level of the electrode which is

decreased, but also the Fermi level of the conductive melt in the vicinity of the working electrode. Thus the Fermi level (and work function) of the melt is a controllable parameter. This view is consistent with the explanation provided by Bjerrum and coworkers[12] for the three rate maxima of this intriguing system.

REFERENCES

1. H. Baltruschat, N.A. Anastasijevic, M. Beltowska-Brzezinska, G. Hambitzer, and J. Heitbaum, Electrochemical detection of organic gases: The development of a formaldehyde sensor, *Ber. Buns. Phys. Chem.* **94**, 996-1000 (1990).
2. N.A. Anastasijevic, H. Baltruschat, and J. Heitbaum, On the hydrogen evolution during the electrochemical oxidation of aldehydes at Ib metals, *Electrochim. Acta* **38**(8), 1067-1072 (1993).
3. S. Neophytides, D. Tsiplakides, P. Stonehart, M. Jaksic, and C.G. Vayenas, Electrochemical enhancement of a catalytic reaction in aqueous solution, *Nature* **370**, 292-294 (1994).
4. S. Neophytides, D. Tsiplakides, P. Stonehart, M.M. Jaksic, and C.G. Vayenas, Non-Faradaic Electrochemical enhancement of H_2 oxidation in alkaline solutions, *J. Phys. Chem.* **100**, 14803-14814 (1996).
5. E. Lamy-Pitara, S.E. Mouahid, and J. Barbier, Effect of anions on catalytic and electrocatalytic hydrogenations and on the electrocatalytic oxidation and evolution of hydrogen on platinum, *Electrochim. Acta* **45**, 4299-4308 (2000).
6. C.G. Vayenas, M.M. Jaksic, S. Bebelis, and S.G. Neophytides, The Electrochemical Activation of Catalysis, in *Modern Aspects of Electrochemistry,* **No. 29**, J.O' M. Bockris, B.E. Conway, and R.E. White, eds., Kluwer Academic/Plenum Publishers, New York (1996), pp. 57-202.
7. C.G. Vayenas, S. Bebelis, and S. Ladas, Dependence of Catalytic Rates on Catalyst Work Function, *Nature* **343**, 625-627 (1990).
8. D. Tsiplakides, and C.G. Vayenas, Electrode work function and absolute potential scale in solid state electrochemistry, *J. Electrochem. Soc.* **148**(5), E189-E202 (2001).
9. E.R. Koetz, H. Neff, and K. Mueller, A UPS, XPS and work function study of emersed silver, platinum and gold electrodes, *J. Electroanal. Chem.* **215**, 331-344 (1986).
10. D.L. Rath, and D.M. Kolb, Continuous work function monitoring for electrode emersion, *Surf. Sci.* **109**, 641-647 (1981).
11. N.A. Anastasijevic, E. Hillrichs, K. Lohrberg, and G. Ungar, US Patent **5,**637,206 (1997).
12. I.M. Petrushina, V.A. Bandur, F. Cappeln, and N.J. Bjerrum, Electrochemical Promotion of Sulfur Dioxide Catalytic Oxidation, *J. Electrochem. Soc.* **147**(8), 3010-3013 (2000).

CHAPTER 11

ELECTROCHEMICAL PROMOTION AND METAL-SUPPORT INTERACTIONS

11.1 METAL-SUPPORT INTERACTIONS

In commercial catalysts the catalytically active phase is usually dispersed on a highly porous and of high (>100 m^2/g) surface area support. This high surface area support, also frequently termed carrier, has pores as small as 10 A and allows for the use of the active phase in a highly dispersed form. The pores are termed macropores when their diameter, d, is larger than 200 Å. When d is smaller than 20 Å the pore is termed micropore. IUPAC recommends the term mesopore when d is between 20 and 200 Å. In most supported commercial catalysts the size of the supported crystallites of the active phase is of the order 10-50 Å (Figure 11.1). This implies that each crystallite consists of few, typically 10 to 1000, atoms. It also implies that a significant portion of the active phase atoms are on the gas-exposed surface of the crystallites and are thus catalytically active. This portion (percentage) is termed catalyst dispersion, D_c, and is defined from:

$$D_c=(\text{number of surface catalyst atoms/total number of catalyst atoms})100 \quad (11.1)$$

Since the catalytically active phase is frequently quite expensive (e.g. noble metals) it is clear that it is in principle advantageous to prepare catalysts with high, approaching 100%, catalyst dispersion D_c. This can be usually accomplished without much difficulty by impregnating the porous carrier with an aqueous solution of a soluble compound (acid or salt) of the active metal followed by drying, calcination and reduction.[1]

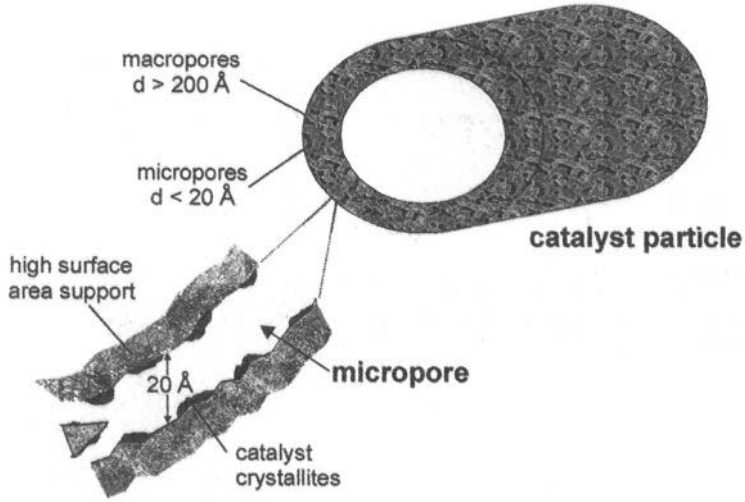

Figure 11.1. Schematic of a commercial supported catalyst pellet and of one of its micropores.

Successful and reproducible preparation of highly dispersed catalysts crucially depends on the state of the carrier surface and on the concentration and pH of the impregnating solution. It is an art and a science for which several good books and reviews exist.[1-5]

In the early days of catalysis the porous high surface area support was usually thought to be inert. It soon became obvious, however, that the catalytic activity, or turnover frequency, of a catalytic reaction on a given active phase is quite often seriously affected both by the crystallite size and by the material of the support.

The former phenomenon is usual referred to as *"particle size effect"* and is pronounced for structure sensitive reactions,[1,2] i.e. catalytic reactions where the rate and/or selectivity is significantly different from one crystallographic plane to another. Structure sensitive reactions (e.g. isomerizations) frequently occur on catalytic sites consisting of an "ensemble" of surface atoms with specific geometry. It is thus reasonable to expect that as the active phase crystallite size decreases, there will be a different distribution of crystallographic planes on the catalyst surface, with the possible disappearance of "ensemble" sites, so that both the catalyst activity and selectivity will be significantly affected. On the other hand *structure insensitive,* also termed *facile*[1,2] reactions (e.g. most hydrogen-nations, some oxidations) are little affected by particle size effects.

The second phenomenon, i.e. the change in catalytic activity or selectivity of the active phase with varying catalyst support, is usually termed *metal-support interaction.* It manifests itself even when the active phase has the same dispersion or average crystallite size on different

supports. Metal-support interactions can influence in a very pronounced way the catalytic and chemisorptive properties of metal and metal oxide catalysts. Typical and spectacular examples are:

(i) the phenomenon of strong metal support interactions (SMSI) discovered by Tauster et al.[6] which attracted worldwide attention for many years.[7]

(ii) the effect of dopant-induced-metal support interactions (DIMSI) studied for years by Verykios and coworkers.[8]

(iii) The relatively recent discovery of the highly active Au/SnO_2 oxidation catalysts by Haruta and coworkers.[9-11]

In all these cases the support has a dramatic effect on the activity and selectivity of the active phase. In classical terminology all these are Schwab effects *"of the second kind"* where an oxide affects the properties of a metal. Schwab effects "of the first kind", where a metal affects the catalytic properties of a catalytic oxide, are less common although in the case of the Au/SnO_2 oxidation catalysts[9,10] it appears that most of the catalytic action takes place at the metal-oxide-gas three phase boundaries.

The nature of metal-support interactions has been the focal point of extensive research and dispute, particularly after the discovery by Tauster et al.[6] of the phenomenon of strong metal-support interactions (SMSI). Although particle-size effects and electronic interactions between the metal particles and the support have been known for years to play a role, the SMSI effect was finally shown to be due to migration of ionic species from the support onto the catalyst particle surface ("decoration").[7] There have been some interesting recent experimental and theoretical advances,[12-19] but a thorough understanding of metal-support interactions is one of the greatest challenges in heterogeneous catalysis.

Although SiO_2 and γ-Al_2O_3 are the most common high surface area industrial catalyst supports (considered in general to give rise to weak metal-support interactions), in recent years there has been an increasing tendency to replace these supports for numerous catalytic applications, mostly oxidations, with TiO_2 or ZrO_2-based porous supports.[20] Little information exists in the open literature as to why this gradual substitution is taking place[17,21] but it is common understanding that these supports, generally believed to lead to stronger metal-support interactions, result in increased activity,[17,21] selectivity and useful lifetime of the metal particles deposited on them.

Two recent publications[22,23] have shown that, at least for the cases of ZrO_2-, TiO_2- and CeO_2- based supports, the mechanism of the metal-support interaction is identical with that of NEMCA when using YSZ. Small metal crystallites on these supports are covered during catalytic reactions with backspillover promoting O^{2-} species which are Λ times less reactive than normally chemisorbed O and which are continuously replenished in the O^{2-} or mixed-conducting support by gaseous O_2 (Fig. 11.2).

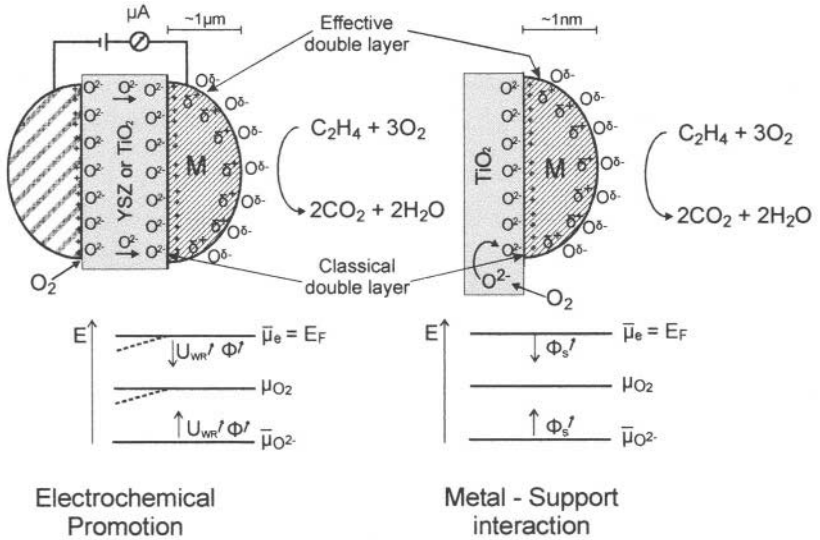

Figure 11.2. Schematic of a metal grain (~μm) in a metal catalyst film deposited on YSZ or TiO_2 under electrochemical promotion conditions (left) and of a metal nanoparticle (~nm) deposited on a porous TiO_2 support (right) showing the locations of the classical double layers formed at the metal/support interface and of the effective double layers formed at the metal/gas interface. The energy diagrams (bottom) indicate schematically the spatial constancy of the Fermi level E_F (or electrochemical potential $\bar{\mu}_e$) of electrons, of the chemical potential of oxygen and of the electrochemical potential of O^{2-}. Note that under electrical bias application (left) $\bar{\mu}_{O^{2-}}$ remains spatially constant but $\bar{\mu}_e$ and μ_{O_2} both bend in the solid electrolyte support (dashed lines). The Fermi level $\bar{\mu}_e$ of the metal can be affected by varying U_{WR} (left) or by varying via doping the Fermi level of the support (right).[22,23]

This implies that Electrochemical Promotion or NEMCA is an electrochemically controlled metal-support interaction. It also implies that metal-support interactions on these supports can be viewed as a self-driven wireless NEMCA system, such as the one explored by Cavalca, Haller and Vayenas for the CH_3OH oxidation system under catalyst-counter electrode short-circuit conditions where gaseous O_2 replenishes O^{2-} in the YSZ support at the vicinity of the counter electrode.[24]

11.2 EXPERIMENTAL CONFIRMATION OF THE MECHANISTIC EQUIVALENCE OF NEMCA AND METAL-SUPPORT INTERACTIONS

Three independent systems were used by Nicole, Tsiplakides, Pliangos, Verykios, Comninellis and Vayenas[22] to show the mechanistic equivalence of NEMCA and metal-support interactions (Fig. 11.3).

Here we discuss the results obtained for the model reaction of C_2H_4 oxidation on IrO_2, Pt and Rh but similar conclusions are reached when using other model reactions such as CO oxidation or NO reduction by CO.[25-27]

The three systems shown in Figure 11.3 were used to compare:

a) The open-circuit and NEMCA induced catalytic activity of IrO_2 (which is a metal-type conducting metal oxide[28]) and of mixed IrO_2-TiO_2 catalysts consisting of micro- and nanoparticles of IrO_2 (active phase) and TiO_2 (inert support) in intimate contact (Fig. 11.3a).[29]
b) The open-circuit and NEMCA induced catalytic activity of Pt films deposited on YSZ[30] and on TiO_2.[31] In this case XPS was also used in vacuum[31,32] to quantify the coverage of the backspillover O^{2-} species on the Pt surface (Fig. 11.3b).
c) The catalytic rate enhancement induced on porous Rh films via electrochemical promotion with YSZ (Fig. 11.3c, left[33]) and that induced on dispersed Rh nanoparticles upon varying the porous, high surface area (~100 m^2/g) catalyst support (TiO_2, SiO_2, γ-Al_2O_3, YSZ and TiO_2 doped with 4 mol% WO_3).[34] In all five cases the Rh metal loading was 0.5 wt%.[34]

In view of the title of this section the reader can anticipate and predict the results of these key experiments[22]:

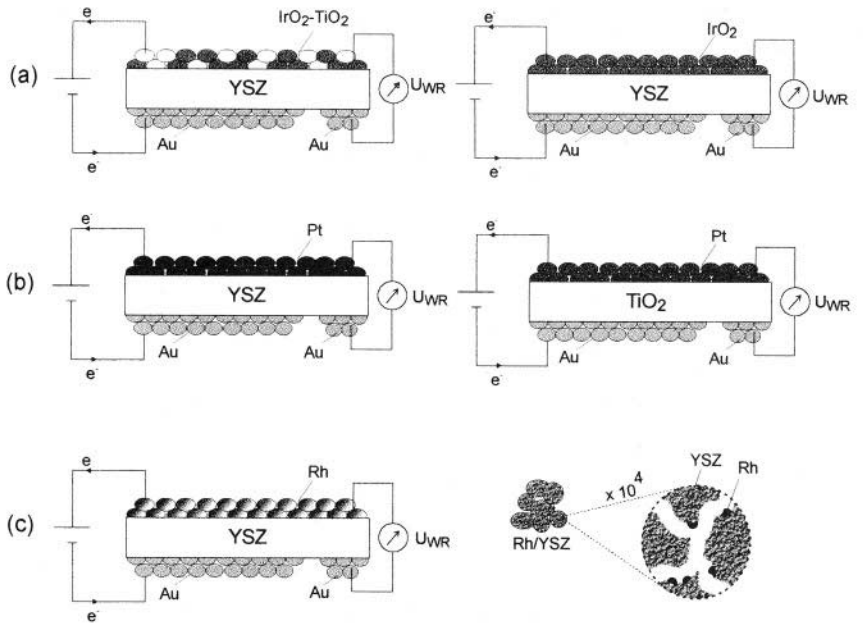

Figure 11.3. Schematic of the experimental setup used (a) to induce electrochemical promotion (via YSZ) on IrO_2 and IrO_2-TiO_2 porous catalyst films (b) to compare the electrochemical promotion induced on Pt via YSZ and via TiO_2 and (c) to compare the electrochemical promotion behaviour induced by varying U_{WR} on a Rh porous catalyst film (left) and on a fully dispersed Rh catalyst supported on porous (80 m^2/g) YSZ support.[22]

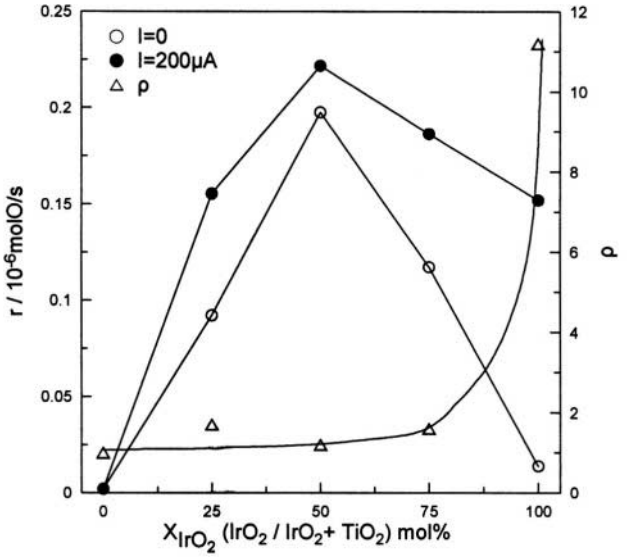

Figure 11.4. Effect of the mole fraction, X_{IrO_2}, of IrO_2 in the IrO_2-TiO_2 catalyst film on the rate of C_2H_4 oxidation under open-circuit conditions (open circles) and under electrochemical promotion conditions (filled circles) via application of I=200 μA; T=380°C, $p_{C_2H_4}$=0.15 kPa, p_{O_2}=20 kPa. Triangles indicate the corresponding electrochemical promotion rate enhancement ratio ρ values.[22,29]

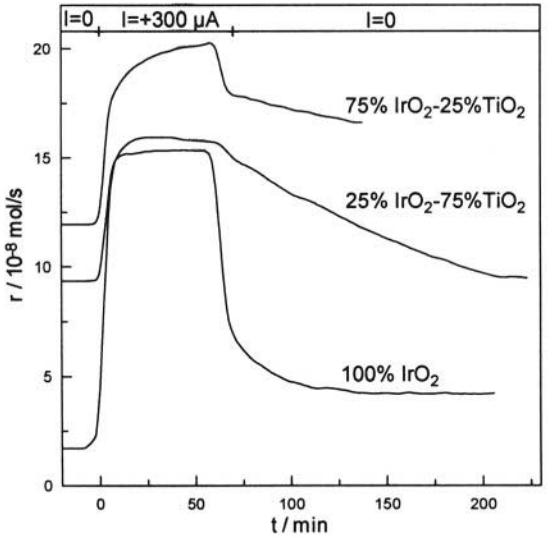

Figure 11.5. Galvanostatic (constant current application) electrochemical promotion (NEMCA) transients during C_2H_4 oxidation on IrO_2-TiO_2 films deposited on YSZ; T=380°C, $p_{C_2H_4}$=0.15 kPa, p_{O_2}=20 kPa.[22,29]

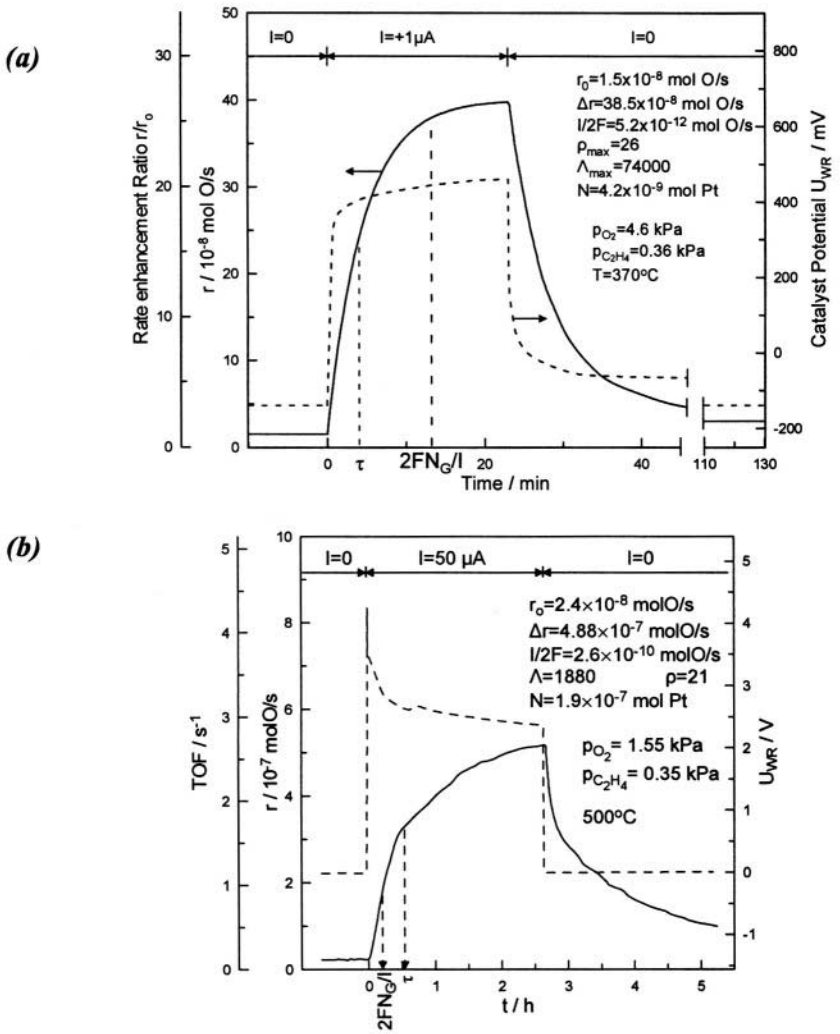

Figure 11.6. Galvanostatic catalytic rate transients showing the equivalence of electrochemical promotion when using YSZ[30] (a) or TiO_2[31] (b) as the Pt metal film support. See text for discussion.[22] Reprinted with permission from Academic Press.

(a) There is similar, roughly 12-fold, maximum rate enhancement induced on the IrO_2 catalyst via NEMCA ($\rho \approx 12$, pure IrO_2, Fig. 11.4) and via metal-support interactions of IrO_2 with TiO_2 ($\rho_{MSI} \approx 13$, $X_{IrO_2} \approx 0.5$, (Fig. 11.4). The parameter ρ_{MSI} is defined from:

$$\rho_{MSI} = r/r_u \tag{11.2}$$

where r_u is the (unpromoted) catalytic rate per unit mass of the active catalyst and r is the same (promoted) catalytic rate, enhanced due to the metal-support interaction.

Moreover, as also shown in Fig. 11.4, there is practically *no electrochemical promotion* ($\rho<1.5$) of the mixed IrO_2-TiO_2 catalyst. It is thus clear that IrO_2 in the IrO_2-TiO_2 catalyst is already at a state equivalent to its electrochemically promoted state.

This ingenious experiment is due to Nicole and Comninellis.[29] Note that pure TiO_2 ($X_{IrO_2}=0$) is always inactive (Fig. 11.4). Note also the galvanostatic NEMCA transients of Figure 11.5. The IrO_2-TiO_2 catalyst can only be marginally affected by electrochemical promotion ($\rho<1.5$) and upon current interruption exhibits quasi-permanent NEMCA behaviour. It thus becomes apparent that TiO_2 is constantly supplying O^{2-} to the IrO_2 surface (Fig. 11.2).

(b) There is similar transient and steady-state electrochemical promotion behaviour of Pt on YSZ and Pt on TiO_2 (Figs. 11.6a and 11.6b) and similar O^{2-} backspillover mechanism of Pt on YSZ and of Pt on TiO_2 as manifest by XPS (Figs. 11.7a and 11.7b).

In particular:

In both cases imposition of a positive current I (with a concomitant rate, I/2F, of supply of O^{2-} to the catalyst for the case of Pt/YSZ and an also concomitant increase in catalyst potential U_{WR}) causes a pronounced, 25 fold in Fig. 11.6a, 22 fold in Fig. 11.6b, increase in catalytic rate ($\rho=26$ and $\rho=23$ respectively).

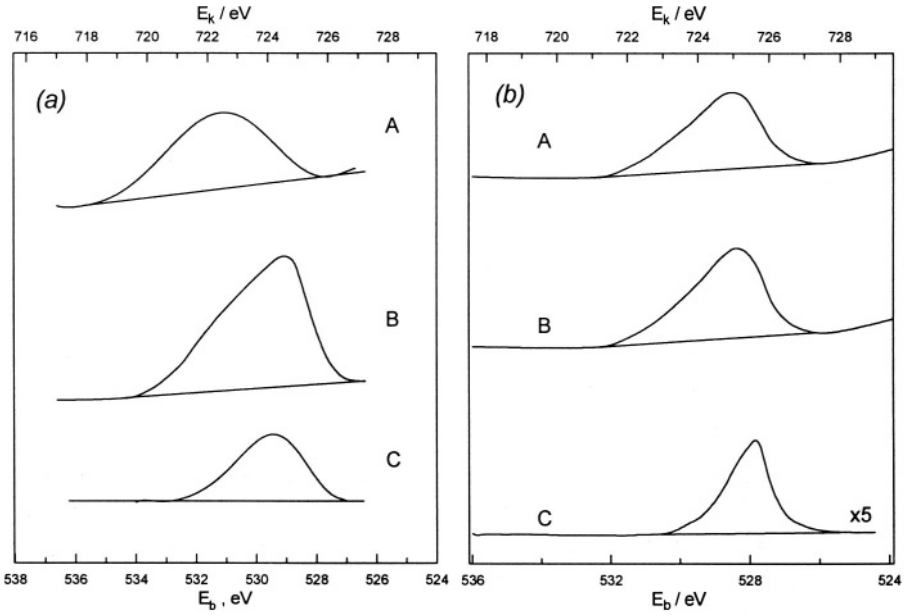

Figure 11.7. XPS confirmation of $O^{\delta-}$ backspillover as the mechanism of electrochemical promotion on Pt films deposited on YSZ (a) and on TiO_2 (b). Adapted from refs.[31,32]. In both cases A is the open-circuit O1s spectrum, B is the O1s spectrum under anodic ($I>0$, $\Delta U_{WR}>0$) polarization and C is the difference spectrum.[22,31,32] Reprinted with permission from the American Chemical Society (a, ref. 32) and from Academic Press (b, 31).

The Faradaic efficiency Λ is $74 \cdot 10^3$ in Fig. 11.6a (YSZ) and $1.88 \cdot 10^3$ in Fig. 11.6b (TiO_2) suggesting that only a fraction f ($\approx$2.5%) of the current I in TiO_2 is anionic (O^{2-}), the rest being electronic, in good agreement with the literature.[31] This is nicely confirmed by comparing the time, τ, required for the rate increase to reach 63% of its steady state value with the parameter $2FN_G/I$ (Fig. 11.6). In the case of YSZ, τ is shorter than $2FN_G/I$ while in the case of TiO_2 τ is longer than $2FN_G/I$, again suggesting that only a fraction of the current I in TiO_2 is ionic. By comparing the ratio $\tau/(2FN_G/I)$ in both cases one may conclude that $f \approx 0.05$, in qualitative agreement with the value estimated from the Faradaic efficiency, Λ, values.

Figure 11.7 confirms that electrochemically induced and controlled O^{2-} backspillover from the support to the metal film surface is the promoting mechanism both in the case of YSZ (Fig. 11.7a) and in TiO_2 (Fig. 11.7b). These figures show the O1s spectrum of the Pt film deposited on YSZ and on TiO_2, first under open-circuit conditions (Fig. 11.7aC, 11.7bA) and then under positive current and potential application (Fig. 11.7aB, 11.7bB). Figures 11.7aC and 11.7bC show the difference spectra. In both cases, XPS clearly shows the presence of the O^{2-} double layer, even under open-circuit conditions (Figs. 11.7aA, 11.7bA) and also clearly confirms the electrochemically controlled backspillover of O^{2-} from the YSZ or TiO_2 support onto the catalyst surface. Note that the binding energy of the backspillover O species is in both cases near 529 eV, which confirms its strongly anionic (probably O^{2-}) state.[31,32]

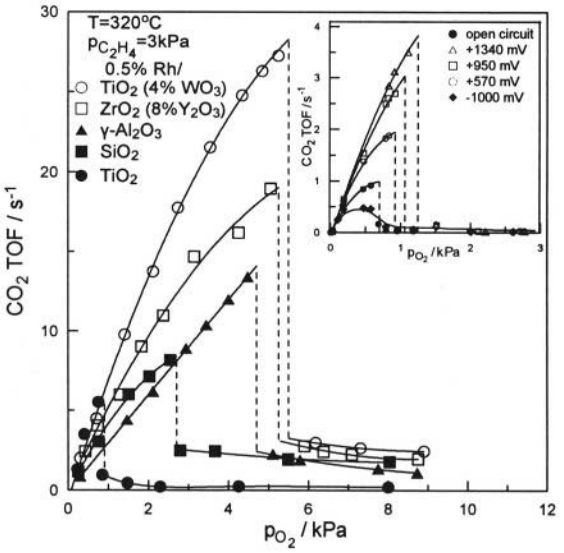

Figure 11.8. Effect of p_{O_2} on the rate (TOF) of C_2H_4 oxidation on Rh supported on five supports of increasing Φ. Catalyst loading 0.5wt%.[22,27] Inset: Electrochemical promotion of a Rh catalyst film deposited on YSZ: Effect of potentiostatically imposed catalyst potential U_{WR} on the rate and TOF dependence on p_{O_2} at fixed $p_{C_2H_4}$.[22,33] Reprinted with permission from Elsevier Science (ref. 27) and Academic Press (ref. 33).

(c) There is similar electrochemical promotion behaviour of Rh films on YSZ and similar metal-support interaction- induced behaviour of *dispersed* Rh on different supports for the model reaction of C_2H_4 oxidation on Pt. (Figs. 11.8 and 11.9). In particular there are very similar ρ values similar ($\rho \approx \rho_{MSI} \approx 120$) upon increasing the potential and work function of the Rh film or upon increasing the work function (or absolute potential) of the support of the dispersed Rh catalyst (Figures 11.8, 11.9 and 11.10).

In more detail:

Figure 11.8 shows the rate dependence on p_{O_2} for the dispersed Rh catalysts deposited on TiO_2, SiO_2, γ-Al_2O_3, YSZ (8mol% Y_2O_3 in ZrO_2) and TiO_2 doped with 4 mol% WO_3. In all five cases the Rh metal loading is 0.5 wt%.[22,23,27]

The inset of Figure 11.8 shows the rate dependence on p_{O_2} (at the same $p_{C_2H_4}$ and T) for the Rh *film* deposited on YSZ at various imposed potentials U_{WR}. The similarity between Figure 11.8 and the inset of Figure 11.8 is striking and underlines the equivalence of metal-support interactions and electrochemical promotion: For low p_{O_2} values the rate is first order in p_{O_2} followed by a sharp decrease at a characteristic p_{O_2} value denoted by $p^*_{O_2}(U^*_{WR})$, which depends on the support (Fig. 11.8) or on the potential (inset of Fig. 11.8). Thereafter the rate becomes very low and negative order

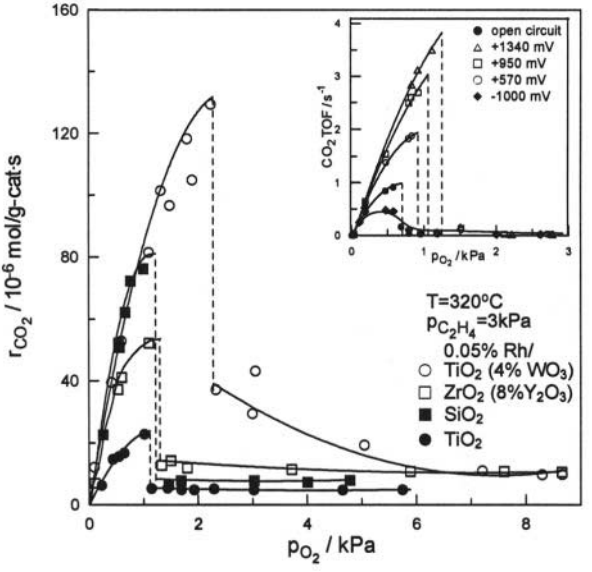

Figure 11.9. Effect of p_{O_2} on the rate of C_2H_4 oxidation on Rh supported on five supports of increasing Φ. Catalyst loading 0.05wt%. Inset: Electrochemical promotion of a Rh catalyst film deposited on YSZ: Effect of potentiostatically imposed catalyst potential U_{WR} on the TOF dependence on p_{O_2} at fixed $p_{C_2H_4}$.[22,33] Inset reprinted with permission from Academic Press.

in p_{O_2}. It has been shown that this sharp rate transition is due to the formation of a catalytically inactive surface Rh oxide.[33] As shown in Figure 11.8 (inset) increasing U_{WR} and thus Φ causes a pronounced increase in $p^*_{O_2}$ and thus a dramatic rate increase at intermediate p_{O_2} values with ρ values up to 100. The same exactly behaviour is obtained (Fig. 11.8) upon varying the dispersed catalyst support in the sequence TiO_2, SiO_2, γ-Al_2O_3, YSZ, $TiO_2(4\%WO_3)$. For intermediate p_{O_2} values the metal-support interaction rate enhancement ratio, ρ_{MSI}, is up to 120 vs $\rho \approx 100$ for the electrochemically promoted system.

This destabilization of surface Rh oxide formation with increasing catalyst potential or work function has been shown to be due to strong lateral repulsive interactions of the backpspillover O^{2-} species and normally chemisorbed oxygen[33] which causes a pronounced, up to 1eV, decrease in the chemisorptive bond strength of normally chemisorbed O.[35,36]

Figure 11.9 is similar to Figure 11.8 except for the Rh catalyst loading on the supports which is now a factor of ten lower, i.e. 0.05 wt%.[22,33]

The behaviour is exactly the same and the sequence of the supports is again the same. As shown below, this requence coincides[22] with the sequence of increasing work function or absolute potential[37] (Chapter 7) of the supports.

By comparing Figure 11.9 and the characteristic $p^*_{O_2}(U^*_{WR})$ rate breaks of the inset of Fig. 11.9 one can assign to each support an equivalent potential U^*_{WR} value (Fig. 11.10). These values are plotted in Figure 11.11 vs the actual work function Φ^o measured via the Kelvin probe technique for the supports at p_{O_2}=1 atm and T=400°C. The measuring principle utilizing a Kelvin probe and the pinning of the Fermi levels of the support and of metal electrodes in contact with it has been discussed already in Chapter 7 in conjunction with the absolute potential scale of solid state electrochemistry.[37]

The good qualitative agreement between eU^*_{WR} variation and Φ^o variation shown in Figure 11.11 for the various supports used, underlines again the common promotional mechanism of electrochemically promoted and metal-support interaction promoted metal catalysts.

The common underlying principle was shown in Figure 11.2. The electrochemical potential of electrons $\bar{\mu}_e$(=E_F, the Fermi level) in the metal catalyst is fixed at that of the Fermi level of the support.[37] This is valid both for electrochemically promoted model catalysts (left) and for seminconducting or ion-conducting-supported metal nanoparticles (right).

On the other hand, the electrochemical potentials of electrons, $\bar{\mu}_e$, oxygen ions, $\bar{\mu}_{O^{2-}}$, and gaseous oxygen, μ_{O_2}, are related via the charge transfer equilibrium at the three-phase-boundaries (tpb) metal-support-gas[38-40]:

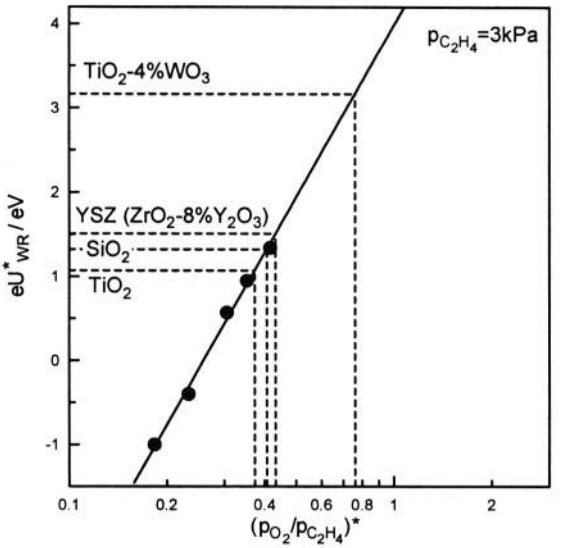

Figure 11.10. Effect of $(p_{O_2}/p_{C_2H_4})^*$ ratio on the potential U^*_{WR} where the rate break occurs during C_2H_4 oxidation on Rh films deposited on YSZ (Figure 11.9 inset, circles) and on the equivalent potential U^*_{WR} where the same rate break occurs on different supports (Figure 11.9).[22]

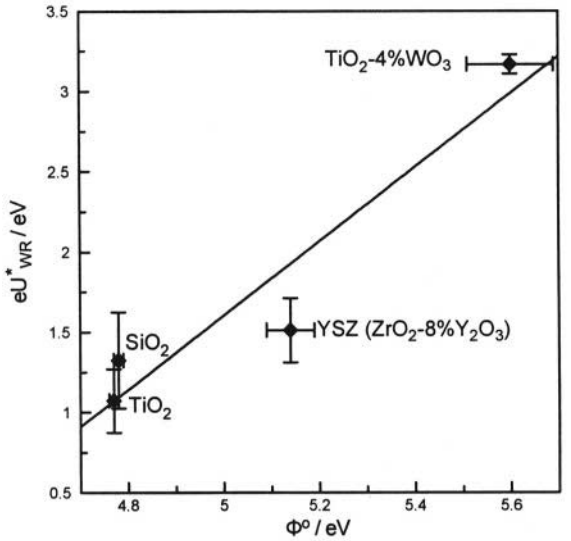

Figure 11.11. Correlation between the equivalent potentials of the supports defined in Figure 11.10 and of the work function or absolute potential[37] of the supports measured via the Kelvin probe technique in p_{O_2} =1 atm at 400°C.[22]

$$O_2(g) + 4e^-(M) \rightleftharpoons 2O^{2-}(S) \tag{11.3}$$

where M stands for the metal catalyst and S stands for the support. This dictates:

$$\bar{\mu}_{O^{2-}(S)} = 2\bar{\mu}_{e(M)} + (1/2)\mu_{O_2(g)} \tag{11.4}$$

However, to the extent that O^{2-} is mobile on the metal surface, one can also consider the equilibrium (11.3) being established also at the catalyst surface (in absence of fast desorption or fast catalytic reactions consuming the backspillover O^{2-} species).[37] In this case one has:

$$\bar{\mu}_{O^{2-}(M)} = 2\bar{\mu}_{e(M)} + (1/2)\mu_{O_2(g)} \tag{11.5}$$

Thus the difference $\bar{\mu}_{O^{2-}(S)} - \bar{\mu}_{O^{2-}(M)}$ is the thermodynamic driving force for O^{2-} backspillover from the support onto the catalyst surface as already discussed in Chapter 3 and as proven by AC Impedance spectroscopy, STM, TPD and XPS as reviewed in Chapter 5. It should be noted in equations (11.4) and (11.5) that the Fermi level of the metal is also the Fermi level of the support.

In electrochemical promotion experiments (Fig. 11.2 left) one can vary $\bar{\mu}_{e(M)} = \bar{\mu}_{e(S)}$ by varying U_{WR} and thus also (Eq. 6.11) Φ. In this way via Eq. (11.5) one can also vary the electrochemical potential and thus coverage of backspillover O^{2-} on the catalyst-electrode surface.

In dispersed metal-support systems (Fig. 11.2 right), one can vary $\bar{\mu}_{e(M)} = \bar{\mu}_{e(S)}$ by varying the support or by doping the support with aliovalent cations. This is known in the literature as dopant-induced metal-support interactions (DIMSI).[8,11,41,42] Thus one can again vary the electrochemical potential and thus the coverage of backspillover O^{2-} on the supported catalyst surface.

This simple model (Fig. 11.2) can account for the observed equivalence between electrochemical promotion and metal-support interaction- induced promotional phenomena. In both cases O^{2-} backspillover to the catalyst surface is the dominant promotional mechanism. A subtle difference may be that in the case of SMSI systems, where Ti has also been shown to migrate on the catalyst surface,[7] the charge on the migrating O^{2-} species may be balanced only partly by the image charge in the metal and partly by the Ti cations on the metal surface. This is possible, at least for some metals, since the stoichiometry between Ti and O in SMSI systems was found to be dependent on the metal.[7] However no evidence for Ti migration on Pt was found in electrochemical promotion studies utilizing TiO_2 as the solid

electrolyte.[31] A detailed mathematical model accounting for diffusion and reaction of the backspillover promoting species is presented in the next section. It should be noted that according to the above equivalence only electrophobic reactions can be promoted by metal-support interactions on YSZ and TiO_2, i.e. only reactions in which the rate increases with potential or work function. This is nicely confirmed by experiment, since C_2H_4 oxidation both on IrO_2 and on Rh is an electrophobic reaction ($\partial r/\partial U_{WR} > 0$) as also shown in Figures 11.4, 11.5, 11.6, 11.8 and 11.9 and also in Chapters 4 and 8. Detailed investigation of C_2H_4 oxidation on different metals and ion conducting supports has shown that it always exhibits electrophobic behaviour under oxygen-rich conditions.[43]

In conclusion the equivalence has been established of electrochemical promotion and metal-support interactions on IrO_2 and Rh catalysts deposited on YSZ, TiO_2 and doped TiO_2 supports. Electrochemical promotion is an electrically controlled metal-support interaction. The corollary is that metal-support interactions on YSZ, TiO_2 and doped TiO_2 supports are similar to "wireless" NEMCA configurations tested already on YSZ pellets (for the electrophobic reaction of CH_3OH oxidation on Pt) by short-circuiting the Pt catalyst and Ag counter electrodes.[24] The carrier continuously supplies promoting $O^{\delta-}$ species to the catalyst surface while spent O^{2-} in the support is continuously replenished by gaseous O_2.

11.3 MATHEMATICAL MODELING: DIMENSIONLESS NUMBERS GOVERNING ELECTROCHEMICAL PROMOTION AND METAL-SUPPORT INTERACTIONS

An important question frequently raised in electrochemical promotion studies is the following: How thick can a porous metal-electrode deposited on a solid electrolyte be in order to maintain the electrochemical promotion (NEMCA) effect? The same type of analysis is applicable regarding the size of nanoparticle catalysts supported on commercial supports such as ZrO_2, TiO_2, YSZ, CeO_2 and doped ZrO_2 or TiO_2. What is the maximum allowable size of supported metal catalyst nanoparticles in order for the above NEMCA-type metal-support interaction mechanism to be fully operative?

Both questions have been recently addressed via a surface diffusion-reaction model developed and solved to describe the effect of electrochemical promotion on porous conductive catalyst films supported on solid electrolyte supports.[23] The model accounts for the migration (backspillover) of promoting anionic, $O^{\delta-}$, species from the solid electrolyte onto the catalyst surface. The

same type of model is then applied[23] to describe the effect of metal-support interactions for the case of finely dispersed metal nanoparticles on ZrO_2 and TiO_2-based porous supports where the same type of $O^{\delta-}$ backspillover mechanism is operative.[24] Two basic dimensionless numbers are obtained which dictate the maximum allowable thickness of electrochemically promoted catalysts, or the maximum crystallite size in dispersed supported metal catalysts, in order to fully utilize the promoting species.

11.3.1 Modeling

11.3.1.1 Physical Considerations and Kinetics

As discussed in Chapter 4 to 10 experiment has shown that electrochemically promoted kinetics very frequently follow the following simple expression:

$$\ln(r/r_o) = \alpha\Delta\Phi/k_bT \tag{11.6}$$

where $\Delta\Phi$ is the change in work function, Φ, of the catalytically active surface induced by the application of a current I and concomitant change, ΔU_{WR}, in the potential of the catalyst- electrode (working electrode, W) relative to a reference (R) electrode. The latter, ΔU_{WR}, is related to $\Delta\Phi$ via an important relationship in solid state electrochemistry:

$$\Delta\Phi = e\Delta U_{WR} \tag{11.7}$$

The parameter α in Equation (11.6) is positive for electrophobic reactions ($\partial r/\partial\Phi>0$, $\Lambda>1$) and negative for electrophilic ones ($\partial r/\partial\Phi<0$, $\Lambda<-1$). As already discussed in Chapters 4 and 6, more complex electrochemical promotion behaviour is frequently encountered, leading to volcano-type or inverted volcano-type behaviour. However, even then equation (11.6) is satisfied over relatively wide (0.2-0.3 eV) $\Delta\Phi$ regions, so we limit the present analysis to this type of promotional kinetics. It should be remembered that Eq. (11.6), originally found as an experimental observation, can be rationalized by rigorous mathematical models which account explicitly for the electrostatic dipole interactions between the adsorbates and the backspillover-formed effective double layer, as discussed in Chapter 6.

The electrochemically induced change in work function $\Delta\Phi$ (eq. (11.6)) is related to the coverage θ_i of the promoting species (e.g. $O^{\delta-}$) on the catalyst surface via the Helmholz equation:

$$\Delta\Phi = \frac{eN_M}{\varepsilon_o} P_i \Delta\theta_i \tag{11.8}$$

where e ($=1.6\cdot10^{-19}$C) is the unit electric charge, $\varepsilon_o=8.85\cdot10^{-12}$ $C^2/J\cdot m$, N_M is the catalyst surface atom density ($atom/m^2$) and P_i is the dipole moment of the backspillover species ($O^{\delta-}$) under consideration. Typically P_i is of the order of 1 D (Debye). The Debye unit, D, equals 1 D$=3.3\cdot10^{-30}$ C·m. In writing the Helmholz equation in the form of Eq. (11.8) we assume that $\Delta\Phi$ is dictated largely by the change in the coverage of the backspillover species ($O^{\delta-}$) and not by any concomitant changes in the coverage of coadsorbed reactants or products (e.g. O). This is reasonable in view of the fact that the ionic backspillover species have significantly higher dipole moment, P_i, values than the more covalently bonded reactants, intermediates and products.

Combining equations (11.6) and (11.8) and noting that:

$$\theta_i = C_i/C_{i,max} \tag{11.9}$$

where C_i is the surface concentration (mol/m^2) of the backspillover species and $C_{i,max}$ is its maximum possible value, one obtains:

$$\ln\rho = \frac{\alpha e N_M P_i}{\varepsilon_o k_b T}\Delta\theta_i \tag{11.10}$$

with $k_b=1.38\cdot10^{-23}$ J/K or equivalently:

$$\ln\rho = \frac{\alpha e N_M P_i}{\varepsilon_o k_b T C_{i,max}}\Delta C_i \tag{11.11}$$

Equation (11.10) can also be written as:

$$\ln\rho=\Pi\Delta\theta_i \tag{11.12}$$

where the dimensionless parameter Π is defined from:

$$\Pi = \frac{\alpha e N_M P_i}{\varepsilon_o k_b T} \tag{11.13}$$

For typical experimental parameter values (α =0.5, $N_M=10^{19}$ $atom/m^2$, P_i=1 D$=3.3\cdot10^{-30}$ C·m, T=673) the dimensionless parameter Π equals 32 which implies, in view of equation (11.12), dramatic rate enhancement ratio ρ values (e.g. ρ =120) even for moderate (~15%) changes in the coverage θ_i of the promoting backspillover species, as experimentally observed.

The promotional kinetics described by equation (11.6) or by its equivalent equation (11.12) imply uniform distribution of the backspillover promoting species on the catalyst surface. This requires fast ion backspillover relative to its desorption or surface reaction.

As already noted the backspillover promoting species $O^{\delta-}$ can eventually desorb as O_2 or may react with an oxidizable reactant (e.g. CO or C_2H_4) albeit at a rate which is Λ times slower than a normally chemisorbed O atom.

It is therefore important to examine under what conditions the above criterion is met (i.e. fast ion backspillover relative to its desorption or consumption) for otherwise the promotional process will be "internally diffusion limited" not due to slow diffusion of the reactants but due to slow diffusion (backspillover) of the promoting species.

11.3.1.2 Mathematical Modeling of Electrochemical Promotion

We consider the porous metal catalyst film shown in Figure 11.12 which is interfaced with an O^{2-} conductor. When a positive current, I, is applied between the catalyst and a counter electrode, oxide ions O^{2-} are supplied from the solid electrolyte to the three phase boundaries (tpb) solid electrolyte-metal-gas at a rate I/2F. Some of these O^{2-} will form O_2 at the tpb and desorb:

$$2O^{2-} \rightarrow O_2(g) + 4e^- \tag{11.14}$$

and some will form backspillover $O^{\delta-}$ species according to the reaction:

$$O^{2-} \rightarrow (O^{\delta-} - \delta^+) + 2e^- \tag{11.15}$$

where $(O^{\delta-} - \delta^+)$ denotes the backspillover $O^{\delta-}$ species in order to emphasize that it is a dipole (i.e. is overall neutral) as it is accompanied by the compensating (screening) charge δ^+ in the metal.

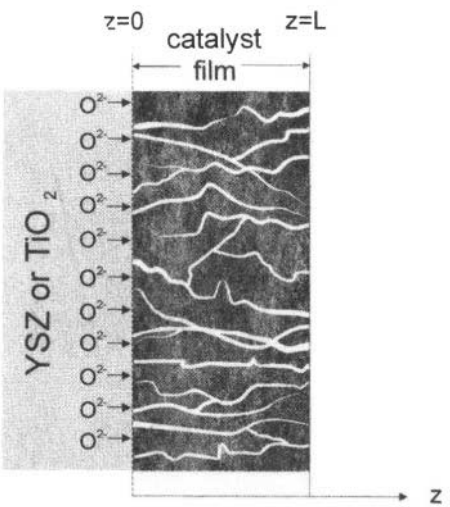

Figure 11.12. Schematic of an electrochemically promoted metal catalyst film supported on a O^{2-} conductor.[23]

We assume that the fraction, f, of O^{2-} arriving at the tpb which follows path (11.15) is proportional to $(1-\theta_i)$ where θ_i is the coverage of $(O^{\delta-} - \delta^+)$ at the tpb (z=0).

We also assume that the rate of consumption of $(O^{\delta-} - \delta^+)$ on the catalyst surface (due to desorption or reaction) is first order in θ_i (or C_i) and denote by D_s the effective surface diffusivity (m^2/s) of the backspillover species on the catalyst surface.

One thus obtains the following differential steady-state mass balance for the surface concentration, C_i, of the promoting species:

$$\frac{d^2C_i}{dz^2} - (k/D_s)C_i = 0 \tag{11.16}$$

where k is the, first order, rate constant for backspillover ion consumption (due to desorption and/or reaction).

One also has the following boundary conditions (Fig. 11.12):

$$z = 0\ ;\ \frac{dC_i}{dz} = -\frac{I}{2FD_s\ell_{tpb}}(1 - C_i/C_{i,max}) \tag{11.17}$$

$$z = L\ ;\ dC_i/dz = 0 \tag{11.18}$$

where ℓ_{tpb} (m) is the three-phase-boundary length.

Recalling that $\theta_i = C_i/C_{i,max}$ and defining $\xi = z/L$, where L is the thickness of the catalyst film, one can write equations (11.16) to (11.18) in the following dimensionless form:

$$\frac{d^2\theta_i}{d\xi^2} - \Phi_P^2\theta_i = 0 \tag{11.19}$$

$$\xi = 0;\ \frac{d\theta_i}{d\xi} = -J\Phi_P^2(1-\theta_i) \tag{11.20}$$

$$\xi = 1;\ d\theta_i/d\xi = 0 \tag{11.21}$$

where the promotional Thiele modulus Φ_P is defined from:

$$\Phi_P = L\sqrt{k/D_s} \tag{11.22}$$

and the dimensionless current J is defined from:

$$J = I/(2FkC_{i,max}L\ell_{tpb}) = I/(2FkC_{i,max}A_c) \tag{11.23}$$

where in the last equality we have expressed the total gas exposed catalyst-electrode surface area, A_c, as $L\,\ell_{tpb}$ by assuming uniform film porosity and local geometry.

Solution of Equation (11.19) with boundary conditions (11.20) and (11.21) gives:

$$\theta_i(\xi)=\frac{\cosh[\Phi_P(1-\xi)]}{\sinh\Phi_P/(\Phi_P J)+\cosh\Phi_P} \tag{11.24}$$

Note that for small Φ_P and large J values $\theta_i(\xi)$ approaches 1 for all J.

The promotional effectiveness factor, η_P, is defined from:

$$\eta_P = \int_0^1 \theta_i(\xi)d\xi \tag{11.25}$$

and expresses the fraction of the total catalyst surface covered by the promotional backspillover species. Substituting equation (11.24) into equation (11.25) and integrating one obtains:

$$1/\eta_P = 1/J+\Phi_P/\tanh\Phi_P \tag{11.26}$$

The dependence of η_P on J and Φ_P is shown in Figure 11.13. As expected, for large J and small Φ_P values η_P approaches unity. This implies maximum promotion of the catalyst surface.

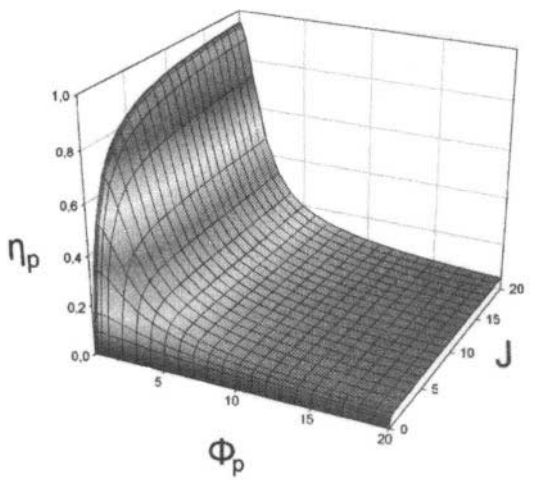

Figure 11.13. Dependence of promotional effectiveness factor, η_p, on Thiele modulus Φ_p and dimensionless current J.[23]

For large (>10) J values equation (11.26) becomes

$$\eta_P \approx \tanh\Phi_P/\Phi_P \tag{11.27}$$

which reduces to:

$$\eta_P \approx 1/\Phi_P \tag{11.28}$$

for large (>10) Φ_P values.

For small J and large Φ_P values one obtains from Equation (11.26):

$$\eta_P = J \tag{11.29}$$

Also in view of equation (11.12) one has:

$$\ln\rho = \int_0^1 \Pi\theta_i(\xi)d\xi \tag{11.30}$$

thus

$$\ln\rho = \Pi\eta_P \tag{11.31}$$

which shows the practical usefulness of the promotional effectiveness factor η_P.

The significance of Equation (11.31), in conjunction with Figure 11.13 and the definitions of Π, Φ_P and J (Table 11.1) is worth emphasizing. In order to obtain a pronounced electrochemical promotion effect, i.e. in order to maximize ρ (=r/r_0), one needs large Π and η_P values. The latter requires large J and small Φ_P values (Fig. 11.13). Small k and L values satisfy both requirements (Table 11.1). This implies that the promoting species must not be too reactive and the catalyst film must be thin.

Table 11.1. **Summary of modelling results. Dimensionless numbers dictating the magnitude of electrochemical promotion and metal support interactions[23]**

$\Pi = \dfrac{\alpha e N_M P_i}{\varepsilon_0 k_b T}$
$J = I/(2FkC_{i,max}L\ell_{tpb}) = I/(2FkC_{i,max}A_c) = (r/A_c)/(\Lambda kC_{i,max})$
$\Phi_p = L\sqrt{k/D_s}$
$\eta_P = 1/(1/J+\Phi_p/\tanh\Phi_p)$
$\rho = \exp(\Pi\eta_P)$

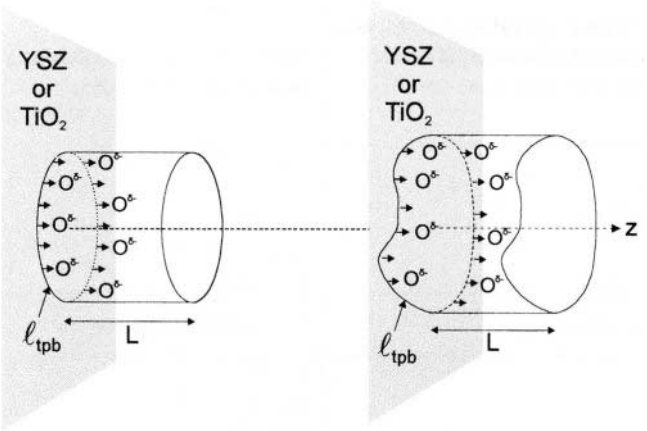

Figure 11.14. Schematic of cylindrical or, more generally, fixed cross-section nanoparticles deposited on an O^{2-} conducting support.[23]

11.3.1.3 Mathematical Modeling of Metal-Support Interactions

The above analysis (Equations 11.16 to 11.31) remains valid when one considers the geometry shown in Figure 11.14 to model a (not necessarily cylindrical) metal crystallite supported on a high surface area support.

The only physical difference is that here the current, I, is not directly measurable and thus the dimensionless current density, J, is not directly computable. This difficulty can, however, be overcome if the ratio of the reactivities, Λ, of normally adsorbed and backspillover oxygen is known (e.g. from electrochemical promotion experiments, where Λ, as already noted, also expresses the Faradaic efficiency). Thus in this case upon combining the definition of Λ with equation (11.23) one obtains the following expression for J:

$$J = \frac{(r/A_c)}{\Lambda k C_{i,max}} \tag{11.32}$$

where r is the measured promoted rate of the catalytic reaction and A_c is the total catalyst surface area.

11.3.2 Numerical Examples

11.3.2.1 Electrochemically Promoted Films

In order to estimate η_P in actual electrochemical promotion experiments we use here typical values[23] of the operating parameters (Table 11.2) to calculate J and Φ. The value of k is estimated on the basis of typical NEMCA galvanostatic transients which show that the lifetime of the promoting $O^{\delta-}$ species on the catalyst surface is typically 10^2 s at temperatures 350°-400°C.

Table 11.2. **Typical operating parameters in electrochemical promotion studies. Electrolyte surface area A_E=1 cm^2, T=400 °C**	*Table 11.3.* **Typical operating parameters in a supported catalyst**
$I = 100\ \mu A$ $k = 10^{-2}\ s^{-1}$ $A_cC_{i,max} = 10^{-7}$ mol $L = 3\ \mu m$ $D_s = 4.\cdot 10^{-11}\ cm^2/s$	$r/A_c = 10^{-6}$ mol/s·cm^2 $\Lambda = 10^2$ $k = 10^{-2}\ s^{-1}$ $C_{i,max} = 10^{-7}$ mol/cm^2 $L = 3$ nm
Computed parameters	**Computed parameters**
$J = 0.5$ $\Phi_p = 4.8$ $\eta_P = 0.15$	$J = 10$ $\Phi_p = 4.8\cdot 10^{-3}$ $\eta_P = 0.91$
Condition for $\Phi < 1$	**Condition for $\Phi < 1$**
$\Phi_p < 1 \Rightarrow L < 0.6\ \mu m$	$\Phi_p < 1 \Rightarrow L < 0.6\ \mu m$

The surface diffusivity D_s is computed (conservatively) from the diffusivity measurements of Lewis and Gomer[44] for O on Pt(111) and Pt(110) near 400°C. They described their data via the equation:

$$D_s = \delta^2\ \nu \exp(\Delta S/R)\exp(-E/RT) \qquad (11.33)$$

with δ=3Å, ΔS=17 cal/mol·K, $\nu=10^{12}\ s^{-1}$, E=34.1 kcal/mol. At 400°C this gives $D_s=4.\cdot 10^{-11}\ cm^2/s$. Thus at 400°C a $O^{\delta-}$ backspillover ion can move approximately 1 μm per s.

The computed J, Φ_p and η_P results (Table 11.2) show the significance of this analysis.[23] It is very likely that many of the published electrochemical promotion data have been obtained under promoter diffusional-controlled conditions, i.e. the actual measured (quite large) ρ values may not correspond to full utilization of the promoting species (η_P=1), so that one could obtain even larger ρ values (=expΠ, eq. (11.31)) if thinner catalyst films are used. This is corroborated by the fact that the highest ρ value for C_2H_4 oxidation on Pt supported on YSZ ($\rho\approx 60$) has been reported so far[30] for a Pt film with surface area corresponding to $4.2\cdot 10^{-9}$ mol Pt[4] (L<0.1 μm), whereas significantly smaller ρ values (~10-20) have been reported[43] for the same reaction on Pt films with surface areas corresponding to 10^{-7} mol Pt (L≈3 μm).[43]

11.3.2.2 Dispersed supported catalysts

In order to estimate η_P in actual fully dispersed Pt, Rh and Pd catalyst deposited on highly porous Y_2O_3-doped-ZrO_2, WO_3-doped-TiO_2, TiO_2 and γ-Al_2O_3 supports used for CO and light hydrocarbon oxidation we use typical operating parameter values (Table 11.3) similar to those used in

Table 11.2 and assume $\Lambda=100$, which is rather conservative value, to compute J via Eq. (11.32) and Φ via Eq. (11.22). The results show $\eta_P \approx 0.91$ which implies that the O^{2-} backspillover mechanism is fully operative under oxidation reaction conditions on nanoparticle metal crystallites supported on ionic or mixed ionic-electronic supports, such as YSZ, TiO_2 and CeO_2. This is quite reasonable in view of the fact that, as already mentioned an adsorbed O atom can migrate 1 μm per s on Pt at 400°C. So unless the oxidation reaction turnover frequency is higher than 10^3 s^{-1}, which is practically never the case, the $O^{\delta-}$ backspillover double layer is present on the supported nanocrystalline catalyst particles.

11.3.3 Summary of Modelling Results

In section 11.3 we saw how a classical reaction engineering approach[45] can been used to model both electrochemical promotion and metal support interactions. The analysis shows that the magnitude of the effect depends on three dimensionless numbers, Π, J and Φ_p (Table 11.3) which dictate the actual value of the promotional effectiveness factor.

11.4 INTERRELATION OF PROMOTION, ELECTROCHEMICAL PROMOTION AND METAL-SUPPORT INTERACTIONS: THE DOUBLE-LAYER MODEL OF CATALYSIS

Promotion, electrochemical promotion and metal-support interactions are three, at a first glance, independent phenomena which can affect catalyst activity and selectivity in a dramatic manner. In Chapter 5 we established the (functional) similarities and (operational) differences of promotion and electrochemical promotion. In this chapter we established again the functional similarities and only operational differences of electrochemical promotion and metal-support interactions on ionic and mixed conducting supports. It is therefore clear that promotion, electrochemical promotion and metal-support interactions on ion-conducting and mixed-conducting supports are three different facets of the same phenomenon. They are all three linked via the phenomenon of spillover-backspillover. And they are all three due to the same underlying cause: The interaction of adsorbed reactants and intermediates with an effective double layer formed by promoting species at the metal/gas interface (Fig. 11.2).

For time scales shorter than that of a catalytic turnover (typically 10^{-2} to 10^2 s) the three phenomena are indistinguishable. Looking at the Na-promoted Pt surface on the cover of this book and imagining that CO oxidation is taking place on that surface, there is no way to distinguish if this is a classically promoted surface where Na has been added from the gas phase,

or an electrochemically promoted one where Na originated from β''-Al_2O_3 interfaced with the Pt crystal, or finally if it is the surface of a larger crystallite deposited on a porous β''-Al_2O_3 carrier where Na has spontaneously migrated on the Pt surface (metal-support interaction). The oxidation of CO will be equally promoted in all three cases.

Similar would be the situation on a Pt surface decorated with O^{2-}, the only difference being the experimental difficulty of introducing O^{2-} with classical promotion and its short lifetime on the catalyst surface, only Λ times longer than the catalytic turnover.

Consequently the proven functional identity of classical promotion, electrochemical promotion and metal-support interactions should not lead the reader to pessimistic conclusions regarding the practical usefulness of electrochemical promotion. Operational differences exist between the three phenomena and it is very difficult to imagine how one can use metal-support interactions with conventional supports to promote an electrophilic reaction or how one can use classical promotion to generate the strongest electronegative promoter, O^{2-}, on a catalyst surface. Furthermore there is no reason to expect that a metal-support-interaction-promoted catalyst is at its "best" electrochemically promoted state. Thus the experimental problem of inducing electrochemical promotion on fully-dispersed catalysts remains an important one, as discussed in the next Chapter.

Having discussed the functional equivalence of classical promotion, electrochemical promotion and metal-support interactions on O^{2-}-conducting and mixed electronic-ionic conducting supports, it is useful to also address and systematize their operational differences. This is attempted in Figure 11.15: The main operational difference is the promoter lifetime, τ_{PR}, on the catalyst surface (Fig. 11.15).

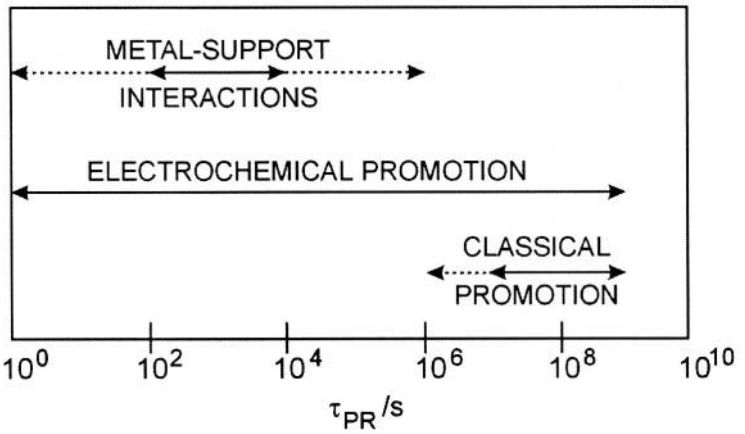

Figure 11.15. Operational range of classical promotion, electrochemical promotion and metal-support interactions in terms of the promoter lifetime on the catalyst surface.

For any practical classical promotion application in a fixed bed catalytic reactor, τ_{PR} must be longer than a year ($\sim 3 \cdot 10^7$ s). But even for lab scale classical promotion experiments t_{PR} values in excess of 10^6 s are required (Fig. 11.15).

On the other hand electrochemical promotion is not subject to any such restrictions regarding t_{PR} (Fig. 11.15). Thus when using O^{2-} conductors or H^+ conductors, t_{PR} is 10^2-10^4 s (Chapters 8 and 9), but when using Na^+ conductors t_{PR} can be well in excess of 10^7 s at low T, but also in the range 10^4-10^6 s for higher T (Chapter 9).

This is an important operational advantage of electrochemical promotion: It permits the use of a wide variety of sacrificial promoters (e.g. O^{2-}, H^+) which have too short life times for classical promotion applications.

REFERENCES

1. M. Boudart, and G. Djega-Mariadassou, *Kinetics of Heterogeneous Catalytic Reactions,* Princeton Univ. Press, Princeton, NJ (1984).
2. L.L. Hegedus, R. Aris, A.T. Bell, M. Boudart, N.Y. Chen, B.C. Gates, W.O. Haag, G.A. Somorjai, and J. Wei, *Catalyst design: Progress and Perspectives,* John Wiley & sons, New York (1987).
3. R.J. Farrauto, and C.H. Bartholomew, *Fundamentals of industrial catalytic processes,* Chapman & Hall, London (1997).
4. C.N. Satterfield, *Heterogeneous Catalysis in Industrial Practice,* McGraw-Hill, Inc. (1991).
5. G. Ertl, H. Knötzinger, and J. Weitcamp, eds., Handbook of Catalysis, VCH Publishers, Weinheim (1997).
6. S.J. Tauster, S.C. Fung, and R.L. Garten, Strong metal-support interactions. Group 8 noble metals supported on TiO_2, *JACS* **100**, 170-175 (1978).
7. G.L. Haller, and D.E. Resasco, Metal-Support Interaction: Group VIII Metals and Reducible Oxides, *Advances in Catalysis* **36**, 173-235 (1989).
8. E.C. Akubuiro, and X.E. Verykios, Effects of dopants on performance of metal crystallites 2. Further characterization of doped supports and catalysts, *J. Catal.* **113**, 106-119 (1988).
9. M. Haruta, A. Ueda, S. Tsubota, and R.M.T. Sanchez, Low-temperature catalytic combustion of methanol and its decomposed derivative over supported gold catalysts, *Catalysis Today* **29**, 443-447 (1996).
10. Y. Iizuka, H. Fujiki, N. Yamauchi, T. Chijiiwa, S. Arai, S. Tsubota, and M. Haruta, Adsorption of CO on gold supported on TiO_2, *Catalysis Today* **36**, 115-123 (1997).
11. S. Tsubota, D.A.H. Cunningham, Y. Bando, and M. Haruta, Preparation of nanometer gold strongly interacted with TiO_2 and the structure sensitivity in low-temperature oxidation of CO, in *Preparation of catalysts VI*, G. Ponchelet, ed. (1995), pp. 227-235.
12. Z. Hong, K.B. Fogash, and J.A. Dumesic, Reaction kinetic behavior of sulfated-zirconia catalysts for butane isomerization, *Catalysis Today* **51**, 269-288 (1999).
13. Y.D. Kim, A.P. Seitsonen, and H. Over, The atomic geometry of oxygen-rich Ru(0001) surfaces: coexistence of (1x1)O and RuO_2(110) domains, *Surf. Sci.* **465**, 1-8 (2000).
14. D.G. Barton, M. Shtein, R.D. Wilson, S.L. Soled, and E. Iglesia, Structure and Electronic Properties of Solid Acids Based on Tungsten Oxide Nanostructures, *J. Phys. Chem.* **103**(4), 630-640 (1999).

15. G. Meitzner, and E. Iglesia, New insights into methanol synthesis catalysts from X-ray absorption spectroscopy, *Catalysis Today* **53**, 433-441 (1999).
16. B.L. Mojet, J.T. Miller, D.E. Ramaker, and D.C. Koningsberger, A new model describing the metal-support interaction in noble metal catalysts, *J. Catal.* **186**, 373-386 (1999).
17. S. Tagliaferri, R.A. Koeppel, and A. Baiker, Influence of rhodium- and ceria-promotion of automotive palladium catalyst on its catalytic behaviour under steady-state and dynamic operation, *Appl. Catal. B* **15**,159-177 (1998).
18. A.Y. Stakheev, and L.M. Kustov, Effects of the support on the morphology and electronic properties of supported metal clusters: modern concepts and progress in 1990s, *Appl. Catal. A* **188**, 3-35 (1999).
19. A. Cimino, D. Gazzoli, and M. Valigi, XPS quantitative analysis and models of supported oxide catalysts, *Journal of Electron Spectroscopy and Related Phenomena* **104**, 1-29 (1999).
20. S. Rossignol, C. Micheaud-Especel, and D. Duprez, Structural and catalytic properties of Zr-Ce-O mixed oxides. Role of the anionic vacancies, *Stud. Surf. Sci. Catal.* **130**, 3327-3332 (2000).
21. R.M. Ferrizz, T. Egami, and J.M. Vohs, Temperature programmed desorption study of the reaction of C_2H_4 and CO on Rh supported on α-Al_2O_3 (0001), YSZ(100) and CeO_2 thin films, *Surf. Sci.* **465**, 127-137 (2000).
22. J. Nicole, D. Tsiplakides, C. Pliangos, X.E. Verykios, C. Comninellis, and C.G. Vayenas, Electrochemical Promotion and Metal-support interactions, *J. Catal.,* in press (2001).
23. C.G. Vayenas, and G. Pitselis, Mathematical Modeling of Electrochemical Promotion and of Metal-Support Interactions, *I&EC Research* **40**(20), 4209-4215 (2001).
24. C. Cavalca, G. Larsen, C.G. Vayenas, and G. Haller, Electrochemical Modification of CH_3OH oxidation selectivity and activity on a Pt single-pellet catalytic reactor, *J. Phys. Chem.* **97**, 6115-6119(1993).
25. I.V. Yentekakis, C.A. Pliangos, V.G. Papadakis, X.E. Verykios, and C.G. Vayenas, Support and NEMCA-induced Promotional Effects on the Activity of Automotive Exhaust Catalysts in A. Frennet and Journal-M. Bastin (eds.) Catalysis and Automotive Pollution Control III, *Stud. Surf. Sci. Catal.* **96**, 375-385 (1995).
26. V.G. Papadakis, C.A. Pliangos, I.V. Yentekakis, X.E. Verykios, and C.G. Vayenas, Development of high performance, Pd-based, three-way catalysts, *Catalysis Today* **29**, 71-75 (1996).
27. C. Pliangos, I.V. Yentekakis, V.G. Papadakis, C.G. Vayenas, and X.E. Verykios, Support-induced promotional effects on the activity of automotive exhaust catalysts 1. The case of oxidation of light hydrocarbons, *Appl. Catal. B* **14**, 161-173 (1997).
28. J. Nicole, and C. Comninellis, Electrochemical promotion of IrO_2 catalyst activity for the gas phase combustion of ethylene, *J. Appl. Electrochem.* **28**, 223-226 (1998).
29. J. Nicole, *PhD Thesis,* EPFL (1999).
30. S. Bebelis, and C.G. Vayenas, Non-Faradaic Electrochemical Modification of Catalytic Activity: 1. The case of Ethylene Oxidation on Pt, *J. Catal.* **118**, 125-146 (1989).
31. C. Pliangos, I.V. Yentekakis, S. Ladas, and C.G. Vayenas, Non-Faradaic Electrochemical Modification of Catalytic Activity: 9. Ethylene oxidation on Pt deposited on TiO_2, *J. Catal.* **159**, 189-203 (1996).
32. S. Ladas, S. Kennou, S. Bebelis, and C.G. Vayenas, Origin of Non-Faradaic Electrochemical Modification of Catalytic Activity, *J. Phys. Chem.* **97**, 8845-8847 (1993).

33. C. Pliangos, I.V. Yentekakis, X.E. Verykios, and C.G. Vayenas, Non-Faradaic Electrochemical Modification of Catalytic Activity: 8. Rh-catalyzed C_2H_4 oxidation, *J. Catal.* **154**, 124-136 (1995).
34. C. Pliangos, *PhD Thesis,* Department of Chemical Engineering, University of Patras (1997).
35. S.G. Neophytides, and C.G. Vayenas, TPD and Cyclic Voltammetric Investigation of the Origin of Electrochemical Promotion in Catalysis, *J. Phys. Chem.* **99**, 17063-17067 (1995).
36. G. Pacchioni, F. Illas, S. Neophytides, and C.G. Vayenas, Quantum-Chemical Study of Electrochemical Promotion in Catalysis, *J. Phys. Chem.* **100**, 16653-16661 (1996).
37. D. Tsiplakides, and C.G. Vayenas, Electrode work function and absolute potential scale in solid state electrochemistry, *J. Electrochem. Soc.* **148**(5), E189-E202 (2001).
38. C.G. Vayenas, and S. Neophytides, Electrochemical Activation of Catalysis: In situ controlled promotion of catalyst surfaces, in *Catalysis-Special periodical Report,* Royal Society of Chemistry, Cambridge (1996), pp. 199-253.
39. C.G. Vayenas, I.V. Yentekakis, S.I. Bebelis, and S.G. Neophytides, In situ Controlled Promotion of Catalyst Surfaces via Solid Electrolytes: The NEMCA effect, *Ber. Buns. Phys. Chem.* **99**(11), 1393-1401 (1995).
40. C.G. Vayenas, and I.V. Yentekakis, Electrochemical Modification of Catalytic Activity, in *Handbook of Catalysis, G.* Ertl, H. Knötzinger, and J. Weitcamp, eds., VCH Publishers, Weinheim (1997), pp. 1310-1338.
41. K.E. Karakitsou, and X.E. Verykios, Effects of altervalent cation doping of TiO_2 on its performance as a photocatalyst for water cleavage, *J. Phys. Chem.* **97**, 1184-1189 (1993).
42. T. Ioannides, and X.E. Verykios, Charge transfer in metal catalysts supported on Doped TiO_2: A Theoretical approach based on metal-semiconductor contact theory, *J. Catal.* **161**, 560-569 (1996).
43. S. Bebelis, M. Makri, A. Buekenhoudt, J. Luyten, S. Brosda, P. Petrolekas, C. Pliangos, and C.G. Vayenas, Electrochemical activation of catalytic reactions using anionic, cationic and mixed conductors, *Solid State Ionics* **129**, 33-46 (2000).
44. R. Lewis, and R. Gomer, Adsorption of Oxygen on Platinum, *Surf. Sci.* **12**, 157-176 (1968).
45. J. Wei, Quo Vadis Reaction Engineering?, *Chem. Eng. Sci.* **47**(9-11), 2983-2984 (1992).

CHAPTER 12

PRACTICAL APPLICATIONS, SUMMARY AND PERSPECTIVES

"The possibility of application of the NEMCA effect in conventional flow reactors and of its extension to oxide catalysts may be of great importance in the future, though both the nature of the migrating, spillover species and their effect on the molecular-scale mechanism require further studies "[1]
B. Grzybowska-Swierkosz and J. Haber, Annual Reports on Chemistry, 1994)

A first and obvious[2] utilization of electrochemical promotion is in the selection and study of the role of promoters for classical supported catalysts. There have been already several demonstrations of this idea.[3-5]

The ultimate direct utilization of electrochemical promotion in commercial reactors (in the chemical industry and in automotive exhaust catalysis) will depend on several technical and economical factors[6] which are intimately related to the following technical considerations and problems:

I. *Material cost minimization:* The main consideration here is the problem of efficient catalyst material utilization which requires the use of thin (e.g. 10 nm thick) catalyst electrodes or dispersed catalysts.[7]

II. *Ease of electrical connection:* Here the main problem is that of efficient electrical current collection, ideally with only two electrical leads entering the reactor and without an excessive number of interconnects, as in fuel cells. This is because the competitor of an electrochemically promoted chemical reactor is not a fuel cell but a classical chemical reactor. The main breakthrough here is the recent discovery of "bipolar" or "wireless" NEMCA,[8-11] i.e. electrochemical promotion induced on catalyst films deposited on a solid electrolyte but not directly connected to an electronic conductor (wire).

III. *Efficient reactor design:* Since the main competitor of an electrochemically promoted chemical reactor is a chemical reactor itself (fixed bed,

monolithic, fluidized bed) it follows that efficient and intelligent reactor designs must be utilized to make an electrochemically promoted reactor commercially attractive.

The first steps in tackling these problems are reviewed in this chapter.

12.1 CLASSICAL PROMOTER SELECTION

This is the first and obvious application of Electrochemical Promotion, which was already proposed in 1992.[2] Electrochemical promotion allows one to quickly and efficiently identify the electrophobic or electrophilic nature of a catalytic reaction and thus (Rules G1 to G4, Chapter 6) to immediately decide if an electronegative or electropositive, respectively, promoter is needed on a conventional catalyst. It also allows one to identify the optimal coverage, θ_P, of the promoting electronegative or electropositive species.

This simple concept has already found some practical applications: The idea to use supported alkali-promoted noble metal catalysts for NO reduction,[3,4] even under mildly oxidizing conditions,[5] came as a direct consequence of electrochemical promotion studies utilizing both YSZ (Chapter 8) and β''-Al_2O_3 (Chapter 9), which showed clearly the electrophilicity of the NO reduction reaction even in presence of coadsorbed O. This dictated the use of a judiciously chosen alkali promoter coverage to enhance both the rate and selectivity under realistic operating conditions on conventional supported catalysts.

Electrochemical promotion has also been used to determine the optimal alkali promoter coverage on Ag epoxidation catalysts as a function of chlorinated hydrocarbon moderator level in the gas phase (Chapter 8).

The fast and efficient screening of various promoters and the selection of optimal promoter dosing via electrochemical promotion is almost certain to find many more applications in the near future.

12.2 MATERIAL COST MINIMIZATION: DISPERSED AND COMMERCIAL CATALYSTS

Most of the electrochemical promotion studies surveyed in this book have been carried out with active catalyst films deposited on solid electrolytes. These films, typically 1 to 10 μm in thickness, consist of catalyst grains (crystallites) typically 0.1 to 1 μm in diameter. Even a diameter of 0.1 μm corresponds to many (~300) atom diameters, assuming an atomic diameter of $3 \cdot 10^{-10}$ m. This means that the active phase dispersion, D_C, as already discussed in Chapter 11, which expresses the fraction of the active phase atoms which are on the surface, and which for spherical particles can be approximated by:

$$D_C \approx 6/(d_p/d_A) \tag{12.1}$$

where d_p is the particle diameter and d_A is the atomic diameter, is small and typically of the order of 10^{-2}-10^{-3} for catalyst particles with diameter 0.1 μm and 1 μm respectively. Such a low dispersion may be acceptable for numerous active catalyst phase materials but can be prohibitive for many noble metal applications.

This problem can in many cases be overcome by dispersing the active phase on an electronically conductive material (Fig. 12.1). There have been already at least three experimental studies,[7,12-15] surveyed here and demonstrating this concept.

A related approach is to interface an industrial promoted catalyst with a solid electrolyte (Fig. 12.2). In this case the bulk of the commercial catalyst must be conductive. This concept has been already demonstrated for the case of NH_3 synthesis on Fe-based promoted commercial catalysts (BASF S6-10 RED)[16] and for the case of SO_2 oxidation on V_2O_5-$K_2S_2O_7$ based catalysts (Haldor-Topsoe VK-58).[17]

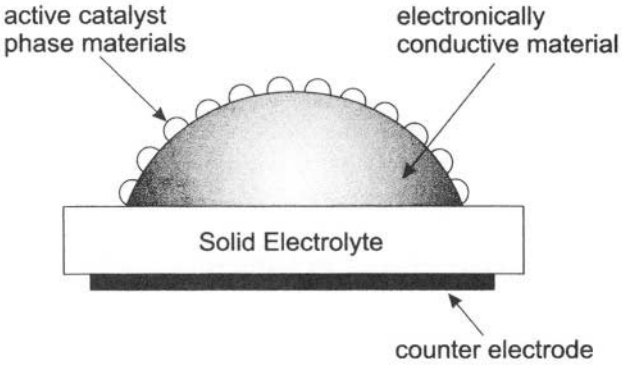

Figure 12.1. Principle of electrochemical promotion of a finely dispersed catalyst deposited on an electronically conductive material.[7,12-15]

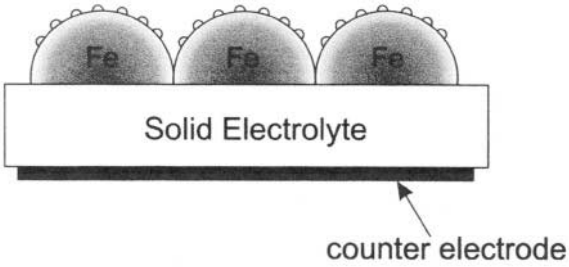

Figure 12.2. Principle of electrochemical promotion of a conductive fully promoted industrial catalyst.[16,17]

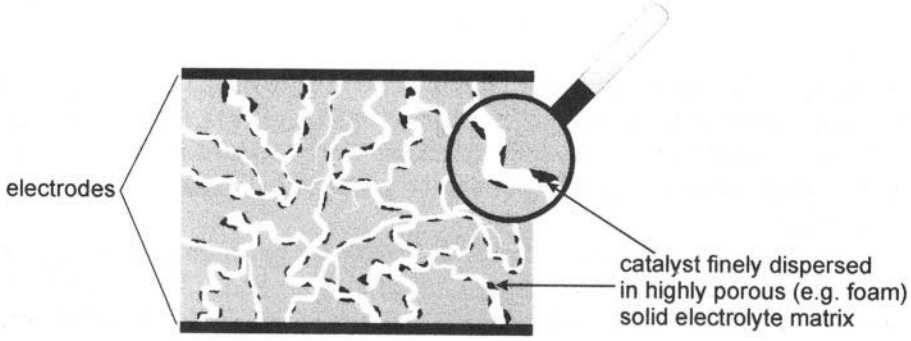

Figure 12.3. Principle of electrochemical promotion of a fully dispersed catalyst.

A third approach, not yet fully demonstrated at the limit of dispersed catalysts, is the induction of electrochemical promotion without an intermediate conductive phase (Fig. 12.3). This approach will be discussed in Section 12.3 in relation to the concept of the bipolar design.

12.2.1 Electrochemical Promotion with Highly Dispersed Catalysts

In these laboratory studies the active catalyst phase (Pt) is highly dispersed on an electronically conductive support (C, Au) in contact with the electrolyte.

12.2.1.1 Ethylene Oxidation on Pt Fully Dispersed on Au Deposited on YSZ

In this study[7] a porous Au film was deposited on YSZ using an Engelhard paste and the methods described in Chapter 4, i.e. calcination at 900°C.

Subsequently the film was impregnated with an aqueous H_2PtCl_6 solution followed by drying, calcination in air at 450°C and reduction with H_2 at 250°C. The resulting finely dispersed Pt catalyst was characterized using H_2 and CO chemisorption. The dispersion of the Pt catalyst was found to be 20-100% in different samples.

Blank kinetic experiments, before Pt deposition, showed that more than 95% of the catalytic rate of C_2H_4 oxidation at 450°C was due to the Pt and not to the Au support electrode.

As shown in Figure 12.4 this finely dispersed Pt catalyst can be electrochemically promoted with ρ values on the order of 3 and Λ values on the order of 10^3. The implication is that oxide ions, O^{2-}, generated or consumed via polarization at the Au/YSZ/gas three-phase-boundaries migrate (backspillover or spillover) on the gas exposed Au electrode surface and reach the finely dispersed Pt catalyst thereby promoting its catalytic activity.

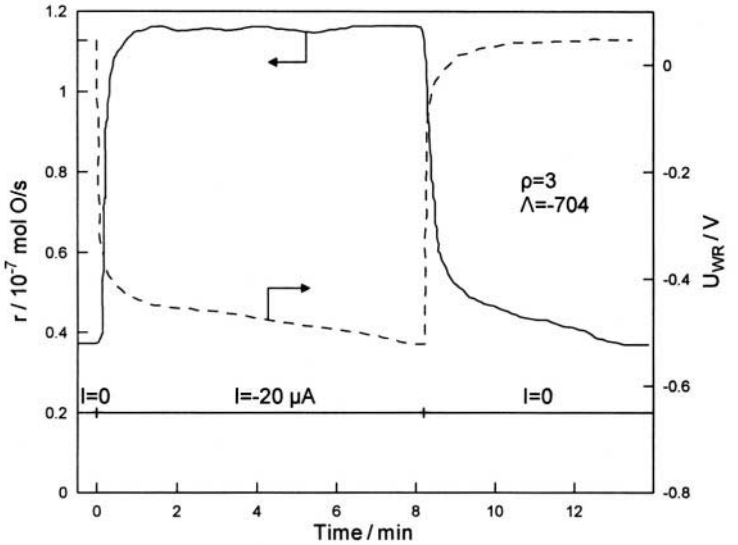

Figure 12.4. Transient effect of an applied negative current (I=-20mA) on the reaction rate r of C_2H_4 oxidation on Pt finely dispersed on Au supported on YSZ (solid curve) and on the catalyst potential U_{WR} (dashed curve). Conditions: catalyst C2, T=421°C, p_{O_2}=14.8 kPa, $p_{C_2H_4}$=0.1 kPa, flow=411 ml/min, open circuit rate: r_o=0.037×10^{-6} mol/s.[7] Reprinted with permission from Academic Press.

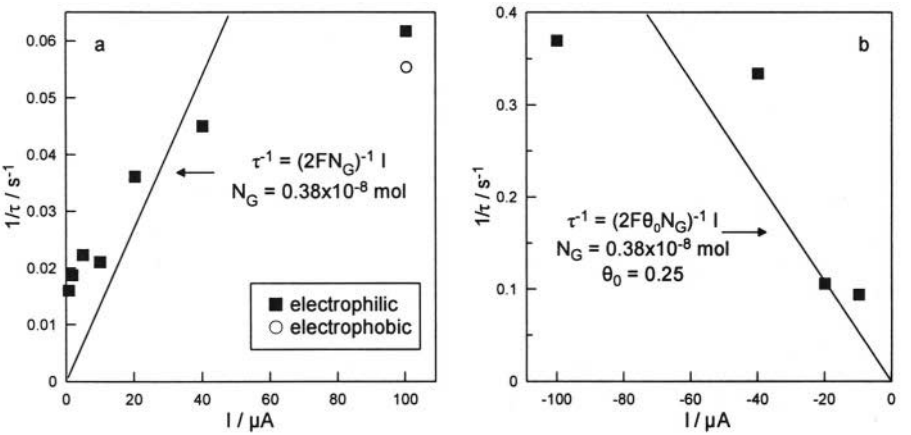

Figure 12.5. Ethylene oxidation on Pt finely dispersed on Au supported on YSZ.[7] Effect of the current I on τ^{-1}, where τ is the time constant measured during a galvanostatic transient experiment with I as the applied current; τ is obtained by fitting either $r/r_0=\exp(-t/\tau)$ or $1-\exp(-t/\tau)$ to the experimental data depending on the sign of the current and whether the reaction is electrophilic or electrophobic. (a) Positive values of I for electrophilic (squares, T=371°C, p_{O_2}=18.0 kPa, $p_{C_2H_4}$=0.6 kPa) and electrophobic behavior (circle, T=421°C, p_{O_2}=14.8 kPa, $p_{C_2H_4}$=0.1 kPa); (b) negative currents, electrophilic behavior (T=421°C, p_{O_2}=14.8 kPa, $p_{C_2H_4}$=0.1 kPa.[7] Reprinted with permission from Academic Press.

As shown in Figure 12.5 the galvanostatic rate time constant τ is of the order of $2FN_G/I$, where N_G is the surface area (in mol) of the *platinum*

catalyst. This implies, as in classical electrochemical promotion experiments (Chapters 4, 5), that steady-state promoted catalytic activity is reached at near-complete coverage of the backspillover promoting ions $O^{\delta-}$.

Although obviously less expensive electron conducting catalyst supports have to be sought for practical applications, this study has clearly established the technical feasibility of inducing NEMCA on finely dispersed noble metal catalysts.

12.2.1.2 H_2 Oxidation on Pt Fully Dispersed on C Electrodes in Aqueous Alkaline Solutions

The electrochemical promotion of H_2 oxidation at room temperature using aqueous alkaline solutions and finely dispersed Pt/graphite electrodes has been already described in section 10.2. Faradaic efficiency, Λ, values up to 20 and ρ values up to 5 were obtained. The dispersion of the Pt catalyst was of the order of 50%.[12,13]

12.2.1.3 1-Butene Isomerization on Pd Fully Dispersed on C Electrodes Deposited on Nafion

The electrochemical promotion of 1-butene isomerization to 2-butene (cis- and trans-) using Nafion as the solid electrolyte and finely dispersed Pd deposited on carbon as the electrode has been described in section 9.2.2.[14,15] Faradaic efficiency, Λ, values up to 28 were obtained in this remarkable study. The Pd dispersion is near complete on the high surface area C support.[14,15]

This study, in conjunction with that discussed in 12.2.1.2, show that when using aqueous electrolytes or Nafion saturated with H_2O, the induction of NEMCA on finely dispersed noble metal catalysts is rather straightforward. The role of the electronically conducting porous C support is only to conduct electrons and to support the finely dispersed catalyst. The promoting species can reach the active catalyst via the electrolyte or via the aqueous film without having to migrate on the surface of the support, as is the case when using ceramic solid electrolytes.

Thus it is fair to say that when using Nafion or aqueous solutions to induce NEMCA, the problem of having a finely dispersed, and thus not expensive, catalyst is already solved.

12.2.2 Electrochemical Promotion of Commercial Catalysts

Two cases of electrochemical promotion of commercial catalysts have been very recently reported in the literature and, not too surprisingly, in both cases the active phase was conductive, electronically or ionically.

12.2.2.1 Electrochemical Promotion of an Industrial NH_3 Synthesis Catalyst

This study has been already discussed in section 9.2.4.[16] A commercial NH_3 synthesis catalyst (BASF S6-10 RED) was milled and deposited via a

slurry on $Ca_{0.9}ZrIn_{0.1}O_{3-\alpha}$ which is a H^+ conducting solid electrolyte.[16] Since the commercial Fe-based catalyst is electronically conducting, as it is not supported on an insulating support (e.g. SiO_2, Al_2O_3), it was found that this catalyst film deposited on the H^+ conductor had sufficient conductivity to also act as an electrode of the solid electrolyte cell.

Faradaic efficiency, Λ, values up to 6 and rate enhancement, ρ, values of at least up to 13 were obtained in this study which was carried out at 50 atm pressure and using a 24-catalyst pellet reactor.[16]

12.2.2.2 Electrochemical Promotion of an Industrial SO_2 Oxidation Catalyst

In parallel to their pioneering electrochemical promotion work using V_2O_5-$K_2S_2O_7$ catalyst melts for SO_2 oxidation surveyed in section 10.3, Bjerrum and coworkers[17] were also able to induce NEMCA on a commercial V_2O_5-$K_2S_2O_7$ based SO_2 oxidation catalyst.[17] Such catalysts are solid at room temperature but their active component (the V_2O_5-$K_2S_2O_7$ melt which is supported usually on porous SiO_2) becomes a liquid above 350°C, thus sufficient electrical conductivity is established across the catalyst pellets to allow for electrochemical promotion experiments. The authors found ρ values up to 4 in this very interesting study.[17]

12.3 BIPOLAR ELECTROCHEMICAL PROMOTION

It has been recently found that direct electrical contact, via a metal wire, to the catalyst-electrode is not necessary to induce the effect of electrochemical promotion.[8-11] It was found that it suffices to apply the potential, or current, between two terminal electrodes which may, or may not, be catalytically active. The concept appears to be very similar with that of the "bipolar" design used now routinely in aqueous electrochemistry.

The implications of this discovery for electrochemical promotion are quite significant since it shows that, at least in principle, the design of an electrochemically promoted reactor can become much simpler than that of a fuel cell.

12.3.1 Electrochemical Promotion of C_2H_4 Oxidation on Pt Using a Bipolar Design

The experimental setup used for the first bipolar or "wireless" NEMCA study is shown in Figure 12.6.[8] An YSZ disc with two terminal Au electrodes and one Pt catalyst film deposited on one side and a reference Au electrode on the other side is placed in a single-chamber reactor. Ethylene oxidation on the Pt catalyst film was chosen as a model reaction.[8]

As shown in Fig. 12.7 application of a potential between the two terminal Au electrodes induces NEMCA on the Pt film which is not connected to any metal wire but is simply in contact with the YSZ solid electrolyte.

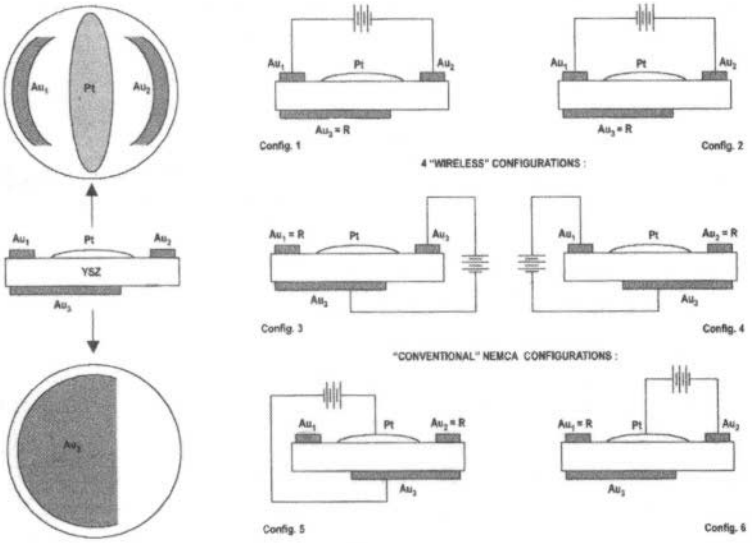

Figure 12.6. Pt catalyst and Au electrode geometry (left); corresponding electrical connection in four "wireless" and two conventional configurations (right). Electrical connections to the reference (R) electrode not shown for simplicity.[8] Reprinted with permission from Academic Press.

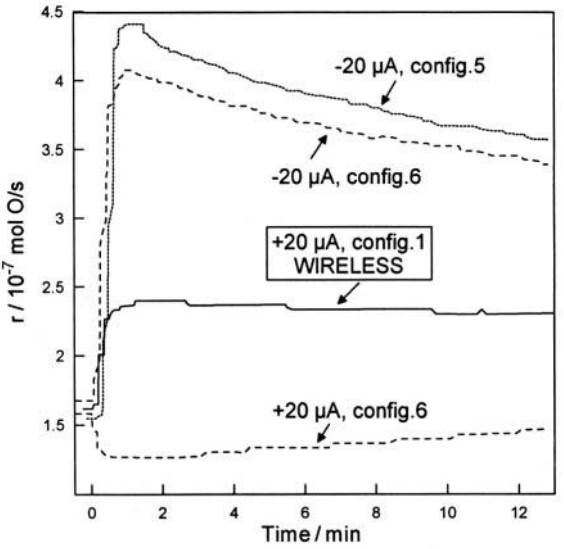

Figure 12.7. Transient effect of an applied current on the rate of ethylene oxidation (expressed in mol O/s) for three different electrode configurations of Fig. 12.6: config. 1, I=+20 μA (solid curve); config. 5, I=-20 μA (dotted curve); and configs. 6, I=+20 and -20 μA (dashed curves). Conditions: T=353°C, $p_{C_2H_4}$=0.65 kPa, p_{O_2}=17.5 kPa, flowrate=200 ml/min.[8] Reprinted with permission from Academic Press.

The observed rate enhancement is roughly half of that obtained in the same setup when the Pt catalyst is connected to a wire and potential is applied between it and one of the Au terminal electrodes.[8]

As in aqueous electrochemistry it appears that application of a potential between the two terminal (Au) electrodes leads to charge separation on the Pt film so that half of it is charged positively and half negatively[8] thus establishing two individual galvanic cells. The Pt film becomes a "bipolar" electrode and half of it is polarized anodically while the other half is polarized cathodically. The fact that ρ is smaller (roughly half) than that obtained upon anodic polarization in a classical electrochemical promotion experiment can be then easily explained.

12.3.2 Electrochemical Promotion of C_2H_4 Oxidation on Pt Using Multi-Stripe and Multi-Dot Bipolar Catalysts

An obvious extension of the bipolar design idea presented in the previous section is the induction of NEMCA using multi-stripe or multi-dot Pt catalysts placed between two terminal Au electrodes, as shown in Figs. 12.8 and 12.9. Both designs have been successfully tested as shown in these figures.[10] Larger terminal voltages are applied here between the two Au electrodes, so that the potential difference in each individual cell formed between the Pt stripes or dots is of the order of 1V.[10]

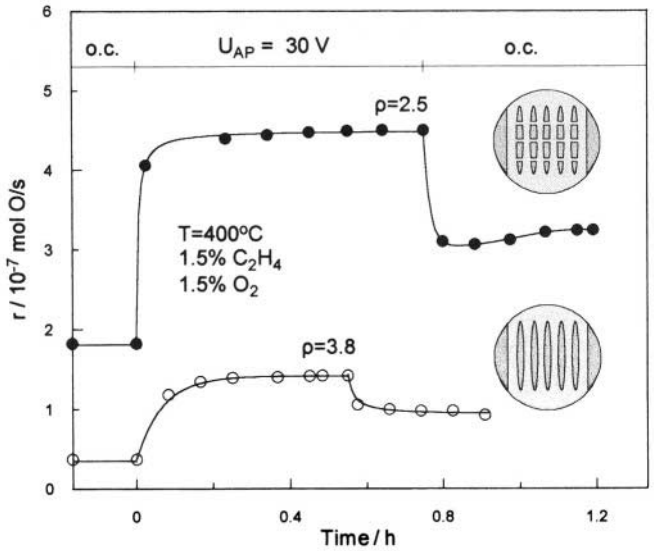

Figure 12.8. Transient effect of an applied potential, U_{AP}, between the two terminal gold electrodes (30 V) on the catalytic rate of ethylene oxidation (expressed in mol O/s) for dotted (filled circles) and multi-striped (open circles) platinum configuration.[10] Reprinted with permission from Elsevier Science.

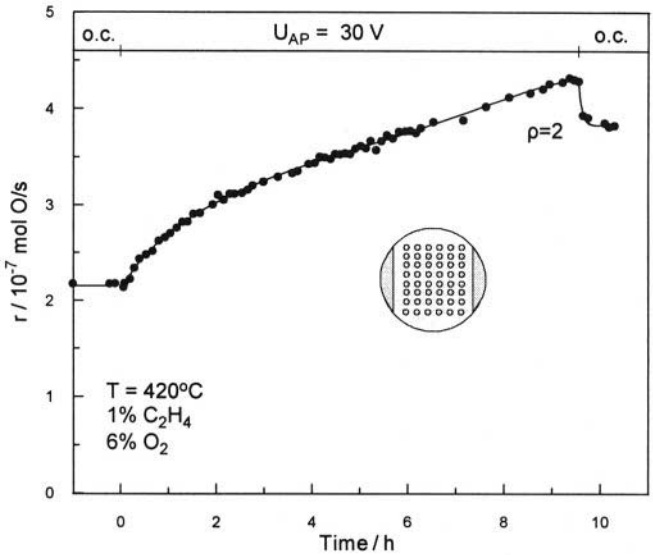

Figure 12.9. Transient effect of an applied potential, U_{AP}, between the two terminal gold electrodes (30 V) on the catalytic rate of ethylene oxidation (expressed in molO/s) for a multi-dotted platinum configuration.[10] Reprinted with permission from Elsevier Science.

A lot of work is currently carried out to extend this idea to fully dispersed two-dimensional (on a YSZ surface) or three-dimensional (in a porous YSZ structure) metal catalysts. The main problems to be overcome is current bypass and internal mass transfer limitations due to the high catalytic activity of such fully dispersed Pt/YSZ catalyst systems.

On the other hand, as already discussed in Chapter 11 in connection to the effect of metal-support interactions, it appears that a fully dispersed noble metal catalyst on porous YSZ is already at a NEMCA or electrochemically-promoted state, i.e. it is covered by an effective double layer of promoting backspillover O^{2-} ions. This can explain both the extreme catalytic activity of ZrO_2- and TiO_2- supported commercial catalysts, as well as the difficulty so far to induce NEMCA on fully dispersed noble metal catalysts deposited on YSZ.

12.3.3 Electrochemical Promotion Using a Bipolar Monolithic Reactor

A brilliant demonstration of the bipolar design concept came recently from the group of Comninellis at EPFL (Fig. 12.10).[9]

A monolith was made from YSZ and the surface of the monolith channels was covered with a RuO_2 catalyst. Two terminal Au electrodes were deposited on the outside surface of the monolith. Potential application between the two terminal Au electrodes was found to induce NEMCA on the RuO_2 catalyst which is not in electrical contact with any metal wire.[9]

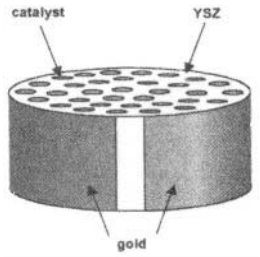

Figure 12.10. Multiple-channel electrochemical cell termed bipolar configuration of second generation.[11] Reprinted with permission from Elsevier Science.

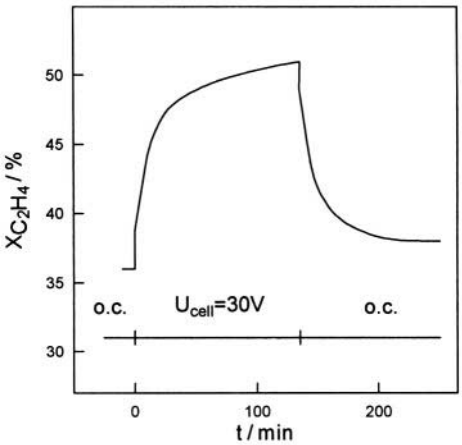

Figure 12.11. Temporal evolution of the ethylene conversion in the multiple-channel RuO_2/YSZ cell during a potentiostatic step of U_{cell}=30 V. OC: open-circuit. Feed composition: C_2H_4:O_2/0.2:12 kPa, F_V=175 cm^3 STP/min, T=360°C.[9] Reprinted with permission from the Electrochemical Society.

The faradaic efficiency Λ values for C_2H_4 oxidation are on the order of 10^3 while C_2H_4 conversion could be enhanced from 35% to 50% (Fig. 12.11).[9]

12.3.4 Electrochemical Promotion of Particulate Matter (Soot) Combustion Using a Ceria-Gadolinia Solid Electrolyte and a Dispersed Perovskite Catalyst

A significant step for the commercialization of bipolar electrochemical promotion units has been made recently by Christensen, Larsen and coworkers at Dinex Filter Technology A/S in Denmark.[18-20] The goal is the development of an efficient catalyst system for the aftertreatment of Diesel exhausts. This is one of the most challenging problems of current catalytic research.

Table 12.1. **Emission standards**

	NO_x g/kWh	CH g/kWh		CO g/kWh		PM g/kWh		Effective
EURO 1	8	1.1		4.5		0.36		1993
EURO 2	7	1.1		4.0		0.15		1996
		ESC	ETC	ESC	ETC	ESC	ETC	
EURO 3	5.0	.66	.78	2.1	5.4	.10	.16	2000
EURO 4	3.5	.46	.55	1.5	4.0	.02	.03	2005
EURO 5	2.0	.25	.25	1.5	1.5	.02	.03	2008
USA EPA	4.0	1.3				0.10		1998

ESC: European Steady Cycle, ETC: European Transient Cycle

Table 12.2. **Needed efficiency**

Given:	EURO2 engine
Wanted:	EURO4 engine
Necessary Conversion Rates	
CH:	Not Critical
CO:	Not Critical
PM:	> 87%
NO_x:	> 50%

Table 12.3. **Parameters for part stream test of reactor on bench engine**

Parameter	Magnitude
Engine Power	18 kW
Reactor Flow	200-250 l/min (20% of total exhaust flow)
Back Pressure	8 m bar
Reactor Volume	1.2l
Reactor Voltage	30 V
Reactor Current	250 mA
Reactor Power	7.5 W
Reactor power consumption (% of engine power)	0.2% (compensated for part flow)

Table 12.4. **Conversion rates for near full scale reactor measured on 1.8 l test engine. Conversion rates in % of raw material**

PM	90
CO	50
CH	50
NO_X	10

The main pollutants in Diesel exhausts are NO_x and particulate matter (PM), mostly soot, with lesser amounts of CO and light hydrocarbons (CH). Table 12.1 shows the corresponding emission standards in Europe and in the USA. These standards are becoming progressively stricter and Table 12.2 shows the needed conversion efficiency of the electrochemically promoted unit in order to meet the EURO4 2005 standards.

The laboratory prototype of the Dinex electrochemically promoted catalyst unit is shown in Figure 12.12 and the assembled unit schematically in Fig. 12.13. It consists (Fig. 12.14) of a tubular bundle porous (ceramic foam) structure made of CeO_2-Gd_2O_3 (CGO) which is an O^{2-} conductor with ionic conductivity significantly higher than YSZ at temperatures below 500°C

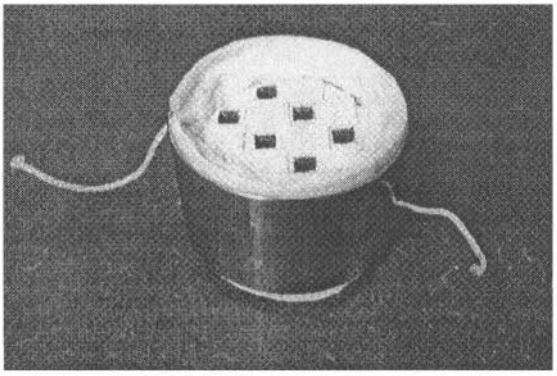

Figure 12.12. Near full scale monolithic Dinex reactor for electrochemically promoted soot combustion.[18-20] Reprinted with permission from the Society of Automotive Engineers.

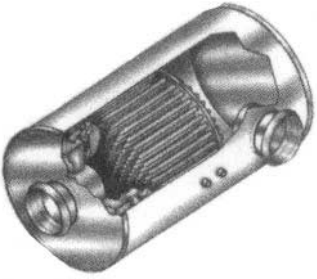

Figure 12.13. Sketch of Dinex electrochemically promoted reactor constructed from single tubes.[18-20] Reprinted with permission from the Society of Automotive Engineers.

(Chapter 3). The active catalyst-electrocatalyst deposited on the CGO structure is based on $LaSrMnO_3$ (LSM), the mixed conducting material used for SOFC cathodes. Electrical potential (~30 V) is applied between two terminal Ag electrodes deposited on the CGO solid electrolyte. The unit was tested on a commercial Diesel engine and the test parameters and results are shown in Tables 12.3 and 12.4 respectively. The reactor performance is excellent regarding soot (particulate matter) combustion but not yet satisfactory regarding NO_x reduction. From the published data of Tables 12.3 and 12.4 and assuming that 80% of the particulate matter mass consists of C atoms one calculates a Faradaic efficiency, Λ, of 66. This is the first demonstration of electrochemical promotion on a pre-commercial unit tested on a real Diesel engine.

The results are very encouraging, and show that, as expected, the power consumption of the electrochemically promoted unit, which is promotional to Λ^{-1}, is negligible in comparison to the Diesel engine power output (Table 12.3). This work demonstrates the great potential of electrochemical promotion for practical applications. The first fifty Dinex units were sold in 2001.

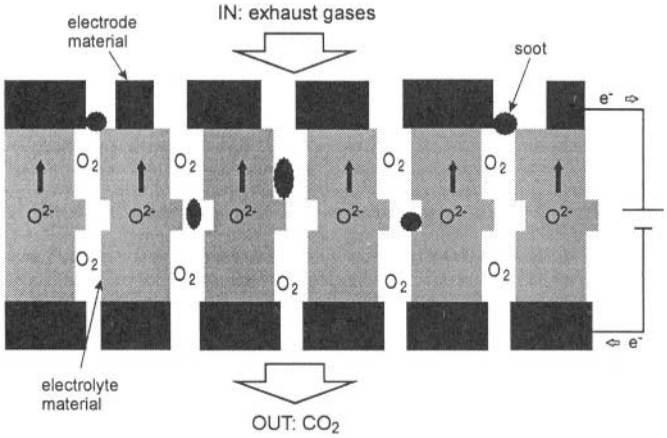

Figure 12.14. Principle of the electrochemically promoted Dinex reactor.[18-20] Reprinted with permission from the Society of Automotive Engineers.

12.4 SUMMARY AND PERSPECTIVES

The electrochemical activation of catalysis, or electrochemical promotion of catalysis (EPOC), or electrochemical promotion, or NEMCA is an exciting phenomenon at the interface of catalysis and electrochemistry.

When first discovered in the eighties as a pronounced apparent violation of Faraday's law it looked like a phenomenon of limited importance, praised however already by several leading electrochemists and surface scientists including Bockris[21] and Pritchard.[22] The subsequent involvement of the groups of Comninellis, Haller, Lambert, Sobyanin, Anastasijevic, Smotkin and others and the continuous discovery of new electrochemically promoted reactions broadened substantially the horizons of electrochemical promotion as it became obvious that the phenomenon was not limited to any particular electrolyte, conductive catalyst or type of reaction.

The ability to alter and control the work function of a catalyst surface via application of a potential, i.e.

$$e\Delta U_{WR} = \Delta\Phi \tag{12.2}$$

caused excitement among both leading surface scientists[1,22] and leading electrochemists,[21,23] although voices of scepticism[24] were also heard. Yet at the end no doubt remained about the validity and sphere of reference of Equation (12.2)[25-27] which is now established as a basic relationship in solid state electrochemistry, and together with:

$$eU_{WR} = \Phi_W - \Phi_R \tag{12.3}$$

allows for the definition of the absolute potential scale in solid state electrochemistry[27] (Chapter 7).

The use of a heavy arsenal of surface science (XPS, UPS, STM, AES, TPD) and electrochemical (cyclic voltammetry, AC Impedance) techniques (Chapter 5) showed that Equations (12.2) and (12.3) simply reflect the formation of an overall neutral backspillover formed *double layer* at the metal/gas interface. It thus became obvious that electrochemical promotion is just *catalysis in presence of a controllable double layer* which affects the bonding strength, E_b, of reactants and intermediates frequently in the simple form:

$$\Delta E_b \approx \alpha_H \Delta\Phi \tag{12.4}$$

and thus also affects catalytic rates, frequently in the simple form:

$$r / r_0 = \exp\left(\frac{\alpha\Delta\Phi}{k_b T}\right) \tag{12.5}$$

where α is positive for electrophobic reactions and negative for electrophilic ones (Chapter 4).

More complex rate vs Φ dependence (volcano or inverted volcano) is also frequently observed and it was recently discovered that the r vs Φ dependence can be predicted on the basis of the open-circuit r vs p_D and r vs p_A dependence, where D and A are the electron donor and electron acceptor reactant respectively (Chapter 6). These surprisingly simple and rigorous promotional rules, applicable both for electrochemical and classical promotion, further confirmed the already established functional equivalence and only operational diffence of electrochemical and classical promotion. It might had taken many more years to find these promotional rules without the ease of varying Φ and the promoter coverage in situ, which electrochemical promotion offers. And it also became apparent that O^{2-}, the most effective electronegative promoter, can only be created efficiently using electrochemical promotion.

At this point one might have concluded that, even without any commercial application, electrochemical promotion had offered something useful to promotion and catalysis by establishing the rules of promotion in addition to providing a useful tool for promoter selection.

Then came the observation that metal electrodes can be electrochemically promoted, but intimate nanocrystalline metal-TiO_2 mixtures cannot, as they are already promoted via O^{2-} spillover (Chapter 11). This important experiment, together with several others, established the mechanistic equivalence of NEMCA with YSZ and metal-support interactions with ZrO_2,

TiO_2 and CeO_2 based supports. The surface of metal crystallites deposited on such supports is decorated with O^{2-} even during catalytic reactions. And this O^{2-} species is Λ (10^2 to 10^5) times less reactive than covalently bonded O. (Chapter 11).

Thus not only *promotion* and *electrochemical promotion* is *catalysis in the presence of a double layer* but apparently the same *applies for supported catalysts undergoing metal-support interactions* (Chapter 11).

Promotion, electrochemical promotion and metal-support interactions are different facets of the same phenomenon, i.e. catalytic reaction in presence of a double layer, which for the case of electrochemical promotion is in situ controllable.

Thus aside from the, very likely, forthcoming technological applications (Chapter 12) electrochemical promotion is a unique and efficient tool for studying the heart of classical catalysis, namely promotion and metal support interactions.

REFERENCES

1. B. Grzybowska-Swierkosz, and J. Haber, *Annual Reports on the Progress of Chemistry*, The Royal Society of Chemistry, Cambridge (1994), p. 395.
2. C.G. Vayenas, S. Bebelis, I.V. Yentekakis, and H.-G. Lintz, Non-Faradaic Electrochemical Modification of Catalytic Activity: A Status Report, in *Monograph published as a Special Issue of Catalysis Today,* Elsevier (1992), pp. 303-442.
3. F.A. Alexandrou, V.G. Papadakis, X.E. Verykios, and C.G. Vayenas. *The promotional effect of Na on the NO reduction by CO on supported Pt, Pd and Rh catalysts* in *Proc. 4th Intnl. Congress on Catalysis and Automotive Pollution Control* **2,** 1-16 (1997).
4. I.V. Yentekakis, R.M. Lambert, M.S. Tikhov, M. Konsolakis, and V. Kiousis, Promotion by sodium in emission control catalysis: A kinetic and spectroscopic study of the Pd-catalyzed reduction on NO by propene, *J. Catal.* **176,** 82-92 (1998).
5. C. Pliangos, C. Raptis, T. Badas, D. Tsiplakides, and C.G. Vayenas, Electrochemical Promotion of a Classically Promoted Rh catalyst for the Reduction of NO, *Electrochim. Acta* **46,** 331-339 (2000).
6. C.G. Vayenas, S. Bebelis, and C. Kyriazis, Solid Electrolytes and Catalysis. Part 2: Non-Faradaic Catalysis, *CHEMTECH* **21,** 500-505 (1991).
7. M. Marwood, and C.G. Vayenas, Electrochemical Promotion of a Dispersed Platinum Catalyst, *J. Catal.* **178,** 429-440(1998).
8. M. Marwood, and C.G. Vayenas, Electrochemical Promotion of Electrochemically isolated Pt catalysts on Stabilized Zirconia, *J. Catal.* **168,** 538-542 (1997).
9. S. Wodiunig, F. Bokeloh, J. Nicole, and C. Comninellis, Electrochemical Promotion of RuO_2 Catalyst Dispersed on an Yttria-Stabilized Zirconia Monolith, *Electrochemical and Solid State Letters* **2**(6), 281-283 (1999).
10. S. Balomenou, G. Pitselis, D. Polydoros, A. Giannikos, A. Vradis, A. Frenzel, C. Pliangos, H. Putter, and C.G. Vayenas, Electrochemical Promotion of Pd, Fe and distributed Pt catalyst-electrodes, *Solid State Ionics* **136-137,** 857-862 (2000).
11. G. Foti, F. Bokeloh, and C. Comninellis, Electrochemical promotion of bipolar electrodes: An estimation of the current bypass, *Electrochim. Acta* **46,** 357-363 (2000).

12. S. Neophytides, D. Tsiplakides, P. Stonehart, M. Jaksic, and C.G. Vayenas, Electrochemical enhancement of a catalytic reaction in aqueous solution, *Nature* **370**, 292-294 (1994).
13. S. Neophytides, D. Tsiplakides, P. Stonehart, M.M. Jaksic, and C.G. Vayenas, Non-Faradaic Electrochemical enhancement of H_2 oxidation in alkaline solutions, *J. Phys. Chem.* **100**, 14803-14814 (1996).
14. L. Ploense, M. Salazar, B. Gurau, and E.S. Smotkin, Proton Spillover Promoted Isomerization of n-Butylenes on Pt-black Cathodes/Nafion 117, *JACS* **119**, 11550-11551 (1997).
15. L. Ploense, M. Salazar, B. Gurau, and E. Smotkin, Spectroscopic study of NEMCA promoted alkene isomerizations at PEM fuel cell Pd-Nafion cathodes, *Solid State Ionics* **136-137**, 713-720 (2000).
16. C.G. Yiokari, G.E. Pitselis, D.G. Polydoros, A.D. Katsaounis, and C.G. Vayenas, High pressure electrochemical promotion of ammonia synthesis over an industrial iron catalyst, J. *Phys. Chem.* **104**, 10600-10602 (2000).
17. I.M. Petrushina, V.A. Bandur, F. Cappeln, and N.J. Bjerrum, Electrochemical Promotion of Sulfur Dioxide Catalytic Oxidation, *J. Electrochem. Soc.* **147(8)**, 3010-3013 (2000).
18. H. Christensen, J. Dinesen, H.H. Engell, L.C. Larsen, K.K. Hansen, and E.M. Skou, Electrochemical Exhaust Gas Purification, *SAE paper 2000-01-0478*, Diesel Exhaust Aftertreatment 2000, (SP 1497) 141-145 (2000).
19. J. Dinesen, S.S. Nissen, and H. Christensen, Electrochemical Diesel Particulate Filter, *SAE paper* **980547**, Diesel Exhaust Aftertreatment (SP-1313) 197-201 (1998).
20. H. Christensen, J. Dinesen, H.H. Engell, and K.K. Hansen, Electrochemical Reactor for Exhaust Gas Purification, *SAE paper* 1999-01-0472, Diesel Exhaust Aftertreatment (SP-1414) 225-229 (1999).
21. J.O.M. Bockris, and Z.S. Minevski, Electrocatalysis: Past, present and future, *Electrochim. Acta* **39**(11/12), 1471-1479 (1994).
22. J. Pritchard, Electrochemical Promotion, *Nature* **343**, 592 (1990).
23. G.-Q. Lu, and A. Wieckowski, Heterogeneous Electrocatalysis: A Core field of Interfacial Science, *Current opinion in Colloid and Interface Science* **5**, 95-100 (2000).
24. R. Parsons, Comment on the paper entitled "On the work function of the gas exposed electrode surfaces in solid state electrochemistry by Professor C.G. Vayenas" *J. Electroanal. Chem.* **486**, 91 (2000).
25. C.G. Vayenas, On the work function of the gas exposed electrode surfaces in solid state electrochemistry, *J. Electroanal. Chem.* **486**, 85-90 (2000).
26. C.G. Vayenas, and D. Tsiplakides, On the work function of the gas-exposed electrode surfaces in solid state electrolyte cells, *Surf. Sci.* **467**, 23-34 (2000).
27. D. Tsiplakides, and C.G. Vayenas, Electrode work function and absolute potential scale in solid state electrochemistry, *J. Electrochem. Soc.* **148**(5), E189-E202 (2001).

APPENDIX A

COMMON QUESTIONS ABOUT ELECTROCHEMICAL PROMOTION

In this Appendix we summarize some of the most common questions asked by physical chemists when they first encounter NEMCA. There are also questions asked after years of exposure in this area. They have been sampled by the authors from more than 100 presentations in International Conferences on Catalysis, Electrochemistry, Solid State Ionics and Surface Science. Some of the questions are easy to answer, some are difficult and there are even some for which there is still no definitive answer. For the sake of the reader who may want to test his understanding up to this point we are first listing the questions separately, then proceed with their answer.

A.1 Questions

1. Is NEMCA a violation of Faraday's laws?

2. What is the difference between electrocatalysis and NEMCA?

3. Is it possible to have $|\Lambda| > 1$ for a reaction with $\Delta G > 0$?

4. Is there a limit for the magnitude of the apparent Faradaic efficiency Λ?

5. Which are the limits of applicability of NEMCA in terms of temperature, reaction type, materials etc.? Why does NEMCA disappear at high temperatures?

6. Does NEMCA work only with poor catalysts?

7. How are ρ and Λ affected upon varying the thickness of the porous catalyst-electrode film?

8. Which are the main traps when studying NEMCA in a laboratory reactor?

During anodic catalyst polarization on an O^{2-} conductor:

9. How does additional oxygen gets adsorbed on a "fully" O-covered Pt surface?

10. Is NEMCA due to Pt oxide formation?

11. Can one get equivalently high O coverages via chemical techniques (high p_{O_2}, use of NO_2, gaseous atomic O)?

12. Is NEMCA (with $\Delta U_{WR} = \pm 1V$) equivalent to the application of the corresponding (via the Nernst equation) huge or extremely low p_{O_2}?

13. What is the origin of NEMCA with cathodic (I<0) polarization?

14. Is the change in catalyst surface work function the origin of NEMCA?

15. Is the gas exposed catalyst-electrode surface always at the point of zero charge (pzc)?

16. Why there exist deviations from $e\Delta U_{WR}=\Delta\Phi$?

17. Does the validity of $e\Delta U_{WR}=\Delta\Phi$ depend on which electrode is grounded?

18. Is work function (Φ), Fermi level E_F or electrochemical potential of electrons $\bar{\mu}$ more relevant for describing NEMCA?

19. What is the origin of permanent NEMCA?

20. What is the effect of gaseous and metal impurities on NEMCA?

21. How do we explain electrophobic ($\partial r/\partial U_{WR}>0$) and electrophilic ($\partial r/\partial U_{WR}<0$) behavior?

22. For a given catalytic reaction does the rate enhancement ratio ρ depend only on U_{WR} or does it also depend on the nature of solid electrolyte (YSZ, β''-Al_2O_3, TiO_2, CeO_2)?

23. Why are NEMCA galvanostatic transients so slow? (compared with electrocatalysis)

24. Can we measure the absolute electrode potential in solid state electrochemistry?

25. Does the concept of absolute electrode potential, defined in chapter 7, allow one to measure the absolute electrical potential difference, $\Delta\varphi$, at a metal/electrolyte interface, one of the famous unresolved problems in electrochemistry?

26. Can we influence the equilibrium conversion of a catalytic reaction via NEMCA?

27. Is NEMCA possible with dispersed catalysts?

28. What is the cost of electricity when carrying out a catalytic reaction under NEMCA conditions?

29. Is NEMCA just a convenient means for introducing promoters in situ on catalyst surfaces?

30. Do we really need the electrolyte to induce NEMCA? Can we just charge the catalyst?

31. Why in a contact potential difference (CPD) experiment the Ψ potentials are nonzero (and the Φ are unaffected) while in a NEMCA setup Ψ vanishes and Φ is affected by U_{WR}?

32. When studying the electrochemical promotion behaviour of catalytic oxidations on metals deposited on YSZ, one always makes the same observation: Positive currents, i.e. O^{2-} supply to the catalyst, cause NEMCA (electrophobic behaviour) only for *high* O_2 to fuel (p_A/p_D) ratios in the gas phase. How can we explain this, at a first glance, counterintuitive but general observation?

33. Do *all* catalytic reactions on conducting catalysts deposited on solid electrolytes exhibit electrochemical promotion (NEMCA) behaviour?

A.2 Answers

1. As noted in Chapter 1 Faraday formulated his 1st law by writing that "the chemical decomposing action of a current is constant for a constant quantity of electricity, not withstanding the greatest variations in its sources, in its intensity, in the size of the electrodes used, in the nature of conductors (or non-conductors) through which it is passed, or in other circumstances".

Although electrochemical promotion ($|\Lambda|>1$) is at first glance a very pronounced violation of Faraday's 1st law, in reality after having established its origin (promoting ion backspillover on the gas exposed electrode surface), the situation is quite interesting and complex: One can still consider that Faraday's 1st law is valid provided one defines as "electrode" not the entire electrode but rather the three-phase-boundaries only or, more generally, that part of the electrode surface where the charge transfer (anodic or cathodic) reaction takes place. This may not always be possible even conceptually, as the same atom(s) on the gas exposed catalyst-electrode surface may function both as a catalyst and as an electrocatalyst. This is also true for the liquid-covered electrode surface in aqueous electrochemistry (Chapter 10). And the problem becomes unsolvable when the promoted catalytic action takes place on the electrolyte surface itself (NEMCA with melts, Chapter 10).

It thus appears safer, rather than trying to introduce such an ambiguous and sometimes impossible definition of an "electrode", simply to replace the "or in other circumstances" in the above expression of the 1st law of Faraday by "provided no catalytic reaction is taking place on the electrode or electrolyte surface". This is not necessary for processes with positive ΔG.

2. Electrocatalysis refers to acceleration of a charge transfer reaction and is thus restricted to Faradaic efficiency, Λ, values between -1 and 1. Electrochemical promotion (NEMCA) refers to electrocatalytically assisted acceleration of a catalytic (no net charge-transfer) reaction, so that the apparent Faradaic efficiency Λ is not limited between -1 and 1.

3. No, this would be a violation of the 2nd Law of Thermodynamics. The value of Λ is restricted between -1 and 1 for reactions with $\Delta G>0$. Thus with reactions with $\Delta G>0$ the original formulation of Faraday's 1st law is always valid.

4. For catalytic reactions with $\Delta G<0$ there is no thermodynamic restriction on the magnitude of $|\Lambda|$. Electrochemical promotion simply makes a catalyst more efficient for bringing the reactive mixture to equilibrium, i.e. minimum G at fixed T and P.

5. The reason is that the backspillover ions desorb to the gas phase directly from the three-phase-boundaries or react directly at the three-phase-boundaries (electrocatalysis, $\Lambda=1$) before they can migrate on the gas-exposed electrode surface and promote the catalytic reaction. The limits of NEMCA are set by the limits of stability of the effective double layer at the metal/gas interface.

6. On the contrary, as shown by equation (4.20):

$$|\Lambda| \approx 2Fr_0/I_0$$

which provides an estimate of the magnitude of $|\Lambda|$ in terms of the open circuit catalytic rate, r_0, and the exchange current, I_0, (Chapter 4), $|\Lambda|$ is larger for active, high r_0, catalysts.

7. The promotional kinetics presented in Chapter 6 assume uniform distribution of the back-spillover promoting species on the catalyst surface. This implies fast ion back-spillover relative to its desorption or reaction. When the thickness of the porous catalyst-electrode is however increased (at fixed three-phase-boundary-length) the point will eventually be reached where ion desorption-reaction (which takes place from the entire gas exposed electrode surface) will become fast relative to ion back-spillover. The rate of promoting ion backspillover migration depends on two parameters: The rate, (I/nF), of their formation at the tpb and their surface diffusivity D_s. When this point is reached severe gradients will develop of the surface ion concentration, C_i, in the direction, z, perpendicular to the solid electrolyte surface (Fig. A.1). The problem is then a classical reaction-diffusion type analysis of the kind frequently performed by chemical engineers to model reaction in porous catalyst pellets. Here however the diffusing-reacting species is not one of the reactants but rather a promoter.

The quantitative solution to the problem is given in section 11.3. The effectiveness factor η_P (≤ 1) which expresses the extent to which the promoting ion is fully utilized ($\eta_P=1$) depends on three dimensionless parameters Π, J and Φ_P; Π is the dimensionless dipole moment of the promoting ion, J is a dimensionless current and Φ_P, a promotional Thiele modulus, is proportional to the film thickness, L.

As it turns out (section 11.3) increasing the thickness, L, of the porous catalyst electrode film is qualitatively similar, in view of Eq. (11.22) with increasing T as they both increase the Thiele modulus Φ_P, thus decrease η_P ($\sim \Phi_P^{-1}$). They both tend to decrease to the coverage of the promoting species on the catalyst surface, thus they both tend to decrease ρ and Λ.

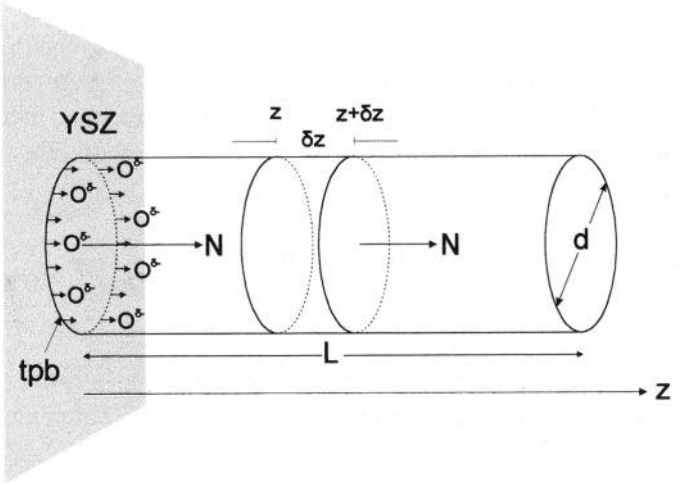

Figure A.1. Schematic presentation of a catalytic cylindrical Pt cluster interfaced with an O^{2-} -conducting solid electrolyte (YSZ) showing the flux, N, of the promoting species.

8. The main experimental traps when studying electrochemical promotion in a laboratory reactor are:

I. Dense (non-porous) catalyst electrode film hindering ion spillover.

II. Very thick (>10 μm) catalyst-electrode film for the reasons described in 7 and in Chapter 11.

III. Complete reactant conversion. Reactant conversion should be kept preferably below 10%. Remedy: Increase the flowrate.

IV. External mass transfer limitations. Symptoms: Rate insensitivity to temperature, rate variation with flowrate. Remedy: Decrease operating temperature, force reactants to directly impinge on the catalyst surface.

V. Operation at very high temperatures or under condition where $2Fr_0/I_0 \approx 1$. Remedy: Lower operating temperature.

VI. Incomplete calcination of the metal catalyst electrode, resulting to coke deposition on the catalyst-electrode surface.

9. The atomic oxygen coverage resulting from gaseous adsorption is very rarely "complete". For example, on Pt θ_O rarely exceeds 0.25 (the 2×2 O structure on Pt(111)). There are always additional sites for chemisorption at very high oxygen chemical potential. Furthermore, the backspillover O^{2-} species may, in general, occupy different surface sites than normally chemisorbed O.

10. XPS has shown that no bulk or surface PtO_2 forms even under severe and prolonged anodic polarization. The back-spillover O^{2-} species is a surface species, not a bulk oxide.

11. This is likely and worth investigating experimentally.

12. This is the case as long as ΔU_{WR} is entirely a concentration polarization and not an activation polarization. As shown in Chapter 6 the use of the simple Nernst-type equation to relate ΔU_{WR} and equivalent surface p_{O_2} (or a_{O_2}) is correct only at constant coverage of adsorbed oxygen, a condition which is extremely difficult to satisfy experimentally. As shown in Chapter 5 and analyzed in Chapter 6, increasing U_{WR} at constant gaseous p_{O_2} and fixed T leads to significant O_2 desorption (due to lateral repulsive interactions with O^{2-}) so that the electrochemical potential of the remaining surface O equals the chemical potential of gaseous O_2.

13. When ion spillover-backspillover is fast, i.e. when $\Delta\Phi = e\Delta U_{WR}$, then even under open-circuit the catalyst electrode surface is partially covered by backspillover O^{2-} ions. Thus it is the removal of such ions via cathodic polarization which causes NEMCA under such conditions.

14. The change in work function is due to the electrochemically controlled ion backspillover, which is at the same time responsible for the rate enhancement, i.e. for NEMCA. Thus work function change and NEMCA are both caused by the same phenomenon and one should not consider one as the cause for the other.

15. No. This happens for only one U_{WR} value for which the electric field strength $\tilde{E}$ vanishes (Fig. 4.48).

16. The reasons are analyzed in detail in Chapter 5. The equation is valid as long as the effective double layer is present at the metal/gas interfaces of the working and reference electrodes. Deviations are basically observed when ion backspillover is not faster than ion desorption or reaction (see also section 11.3).

17. No. A detailed analysis is given in reference Vayenas & Tsiplakides, *Surface Science* **467**, 23 (2000). Of course grounding an electrode (but not more than one!) does not affect electrochemical promotion either.

18. It is clearly the work function Φ. By just charging a metal in vacuum (which affects $\bar{\mu}(= E_F)$) one cannot induce NEMCA, This has been shown by charging one electrode of Pt/YSZ at potentials up to 10^4 V relative to earth (thus decreasing/increasing $\bar{\mu}$ by 10^4 eV) without observing any change in kinetics.

19. It appears to be the electrochemically induced formation or destruction of surface oxides.

20. Not more important than in normal catalytic studies.

21. Electrophobic behaviour ($\partial r/\partial \Phi > 0$) is observed when the catalyst surface is predominantly covered by an electron acceptor adsorbate. In the case of electrophilic behaviour ($\partial r/\partial \Phi < 0$) the surface is predominantly covered by an electron donor adsorbate. For a detailed analysis see Chapter 6.

22. It does depend on the nature of the solid electrolyte. As an example see Table A.1 for the case of C_2H_4 oxidation on Pt deposited on different solid electrolytes.

Then analyze Table A. 1 on the basis of the local and global promotional rules of Chapter 6.

Table A.1. Electrochemical promotion studies of ethylene oxidation on platinum (ref. 43 in Chapter 11)

Solid electrolyte	Promoting species	T,°C	$p_{O_2}/p_{C_2H_4}$	Reaction order	Λ_{max}	ρ_{max}	PI_i	NEMCA behavior
$ZrO_2(Y_2O_3)$	$O^{\delta-}$	295-450	12-16	1st in C_2H_4, 0th in O_2	3×10^5	55	54	electrophobic
β''-Al_2O_3	$Na^{\delta+}$	291	238	1st in C_2H_4, 0th in O_2	-	-		electrophobic
$Na_3Zr_2Si_2PO_{12}$	$Na^{\delta+}$	330-430	1.3-3.8	negative in C_2H_4 positive in O_2	-	10	300	electrophilic
$CaZr_{0.9}In_{0.1}O_{3-\alpha}$	H^- (or OH^-)	380-460	4.8	negative in C_2H_4 positive in O_2	2×10^4	5	-	electrophilic
TiO_2	$O^{\delta-}$ (probably also H^+)	470-540	3.5-12	(i) *oxidizing conditions* positive order in C_2H_4 zero order in O_2	5×10^3	2.5	1.5	electrophobic
			0.2-0.3	(ii) *reducing conditions* almost zero order for both				electrophilic
CeO_2	$O^{\delta-}$	500	1.6-3.7	negative in C_2H_4 positive in O_2 (almost 1st order)	1×10^5	3	2	electrophilic

Table A. 1 provides as an example the case of C_2H_4 oxidation on Pt deposited on various solid electrolytes. Rule G1 (electrophobic behaviour) is obeyed for high $p_{O_2}/p_{C_2H_4}$ ratios while rule G2 (electrophilic behaviour is obeyed for lower $p_{O_2}/p_{C_2H_4}$ ratios.

23. Because the time constant τ is given, approximately, by:

$$\tau \approx 2FN_G/I \tag{4.32}$$

24. Yes, see Chapter 7. It is, simply, the work function of the gas-exposed electrode surface in presence of spillover.

25. No. Because that would imply we know how to split, at least conceptually, the electrochemical potential, $\bar{\mu}$, of electrons (which is the same in the metal and in the electrolyte at their contact) into the chemical potential of electrons, μ, and the electrical potential of electrons, φ, in the metal and in the electrolyte.

26. Of course not.

27. Yes it is. Three examples are discussed in Chapter 12.

28. It is low and of the order Λ^{-1} (a_e/a_c) where a_c is the cost of the product (in mol/$) and a_e is the cost of electricity (in mol e/$)

29. This can be considered to be the case when using alkali ion conductors. But classical promotion by species like O^{2-} or H^+ does not appear to be experimentally feasible, due to the experimental difficulty of introducing them under controlled conditions from the gas phase. Also their short lifetime under reaction conditions essentially limits their usefulness only to situations where they can be continuously replenished on the catalyst surface, i.e. only to electrochemical promotion.

30. The answer is the same as in 18.

31. Because in the former case there is no ion spillover. See Chapter 7.

32. This is a direct consequence of global promotional rule G1: An electronegative promoter (e.g. O^{2-}) will enhance the catalytic rate only when the catalyst surface is predominantly covered by an electron acceptor reactant (e.g. O). If there is little or no O on the surface then O^{2-} will act as a reactant (Faradaic behaviour) and not as a promoter.

33. The answer is in principle yes. We have seen in this book that electrochemical and classical promotion are functionally identical and only

operationally different. Thus, since every catalytic reaction can, in principle and in practice, be classically promoted, the same applies to electrochemical promotion. This does not imply that for a given metal catalyst and catalytic reaction *any* solid electrolyte will do the job. We have seen in this book two necessary and, when taken together, sufficient criteria for obtaining electrochemical promotion ($|\Lambda|>1$):

I. The parameter $2Fr_0/I_0$ ($\approx|\Lambda|$) must be larger than unity (Chapter 4). Catalysis at the metal/gas interface must be faster than electrocatalysis. This is easy to satisfy in solid electrolyte systems and more difficult to satisfy in aqueous electrolyte systems.

II. The promotional effectiveness factor, η_P, (Chapter 11) must be significant, larger than, at least, 0.1. This requires small promotional Thiele modulus, Φ_P, and significant dimensionless current, J, values. This implies thin (low L) catalyst films and slow kinetics of promoter destruction (low k values, Chapter 11).

But all these are problems which can be overcome by appropriate catalyst-electrode design and by appropriate choice of the solid electrolyte and thus of the promoting species.

A few years ago a very competent colleague was very disappointed as he could not induce NEMCA for a certain hydrogenation reaction at $p_{H_2}\approx 1$ bar on Pt/YSZ. Despite the interesting hydrogenation NEMCA behaviour on Pd/YSZ and Rh/YSZ systems described in Chapter 8, such a failure is easy to rationalize: In presence of $p_{H_2}\approx 1$ bar the O^{2-} backspillover double layer on the Pt surface cannot survive. Mathematically (Chapter 11) this implies a very high k value, thus a large Φ_P and small J values, consequently a very small η_P value (Figure 11.13). However the use of a proton conducting or alkali conducting solid electrolyte would certain solve the problem.

APPENDIX B

MATERIALS AND INSTRUMENTATION FOR STARTING ELECTROCHEMICAL PROMOTION EXPERIMENTS

B.1 Catalyst-Electrodes, Solid Electrolytes

Catalyst films used in electrochemical promotion (NEMCA) studies are usually prepared by using commercial metal pastes. Unfluxed pastes should be used, as fluxes may introduce unwanted side reactions or block electrocatalytic and catalytic sites. This action may obscure or even totally inhibit the electrochemical promotion effect.

The usual preparation procedure includes the application of thin coatings of the pastes onto the solid electrolyte surface, followed by drying and calcining. Air should always be fed in the furnace during calcination, in order to assure complete combustion of the organic content of the paste. The calcination temperature program obviously depends on the catalyst to be deposited and on paste composition and plays a key role in obtaining a well-adhered film, which is essential for electrochemical promotion studies. Increasing calcination temperature even by only 20-30°C for a given catalyst paste leads to increased sintering and decreases in both catalyst surface area and length of the metal-solid electrolyte-gas three-phase boundaries (tpb). The latter has a beneficial effect for increasing the polarizability of the metal/solid electrolyte interface and thus observing pronounced nonfaradaic catalytic rate changes. The decrease in catalyst surface may, however, be undesirable in cases where the turnover frequency is very small, resulting in non-measurable catalytic reaction rates for small catalyst surface areas. In general, the optimal calcination temperature for each catalyst and paste has to be found by trial and error. In the case of flat YSZ elements, a proven procedure for enhancing the adherence of catalyst films is to first roughen the YSZ surface by adding a slurry containing fine (1-2 μm) YSZ powder, followed by drying and calcining at 1450-1500°C. Catalyst deposition on

such a roughened surface may, of course, lead to a long tpb line length and to a concomitant decreased polarizability of the catalyst/YSZ interface, but this is definitely preferable to a not well-adhered film.

Catalyst films for electrochemical promotion studies should be thin and porous enough so that the catalytic reaction under study is not subject to internal mass-transfer limitations within the desired operating temperature. Thickness below 10 μm and porosity larger than 30% are usually sufficient to ensure the absence of internal mass-transfer limitations. Several SEM images of such catalyst films have been presented in this book. SEM characterization is very important in assessing the morphological suitability of catalyst films for electrochemical promotion studies and in optimizing the calcination procedure.

Table B.1 summarizes the starting materials (pastes) used in published electrochemical promotion studies, the corresponding supplier and the calcination procedure. The interested reader is referred to the original references for additional details.

Table B.1. Materials and procedures for catalyst-electrode preparation

Catalyst	Starting material	Supplier	Solid Electrolyte	Calcination procedure	Ref.
Pt	A 1121 Pt paste	Engelhard	YSZ	400-450°C (2h), then 800-870°C(20-60 min) or at 900°C for 3h	1-5 6
			β″-Al_2O_3	400°C (1-2h), then 750-830°C (20-30min)	7-10
			CeO_2	900°C (1h)	11
			$Na_3Zr_2Si_2PO_{12}$	900°C (1h) or 650°C (1h)	12
			CaF_2	400°C (2h), then 720°C (20 min)	13
			TiO_2	$\xrightarrow{3°C/min}$ 450°C (1h) $\xrightarrow{2°C/min}$ 830°C (1h)	14
			$CaZr_{0.9}In_{0.1}O_{3-\alpha}$	$\xrightarrow{10°C/min}$ 400°C (2h) $\xrightarrow{5°C/min}$ 900°C (1h)	15
Ag	Silver print 22-201 (Ag suspension in butyl acetate)	GC Electronics	YSZ	Drying at 80°C,400°C (2h), 600-650°C (2h-6h)	16
				200°C (2h), 400°C (2h), 880°C (30 min)	17
				Drying at 60°C, $\xrightarrow{5°C/min}$ 400°C (2h) $\xrightarrow{5°C/min}$ 700°C (2h)	18

			β''-Al_2O_3	400°C (2h), then 550°C (2h)	19
			$SrCe_{0.95}Yb_{0.05}O_{3-\alpha}$	400°C (2h), then 750°C (1h)	20
Rh	A 8826 Rh resinate	Engelhard	YSZ	400°C (2h), then 850°C (6h)	21
				550°C, then reduction at 100°C in 1% H_2 in He	22
Pd	A 1122 Pd paste		YSZ	450°C (6h), then reduction in 2% H_2 in He (60 ml/min) at 60°C for 30 min, further heating in H_2 up to 300°C	23,24
Pd	A 2895 Pd paste		YSZ	450°C (2h), then 800°C (2h)	25
				Drying at 200°C (2h), calcination at 500°C (2h) and then at 900°C (2h)	26
	A 2895 Pd paste		β''-Al_2O_3	450°C (2-3h), then reduction in 1% in He at 25°C for 10-20 min	27
IrO_2	0.1 M $H_2I_5Cl_6$ in isopropanol		YSZ	Drying at 80°C, calcination at 550°C (1h)	28
RuO_2	~0.1 M $RuCl_3$ in isopropanol		YSZ	Drying at 80°C, calcination at 550° (1h)	29
Fe	OL 15/34 Fe paste	Engelhard	$CaZr_{0.9}In_{0.1}O_{3-\alpha}$	450°C (1h), 900°C (1-3h), reduction in 2% H_2 in He at 400°C for 2-3 h	30
			$K_2YZr(PO_4)_3$	450°C (1h), 600°C (1-3h), reduction in 2% H_2 in He at 400°C for 2-3 h	30
Ni	NiO paste	Engelhard	YSZ	450°C (2h), 900°C (1h), heating rate 10°C/min	31
Au	M 8032 Au paste	Demetron	CaF_2	400°C (2h), 720°C (20 min)	13
			β''-Al_2O_3	750-800°C (1h) 800°C (10 min)	8,9,27 19
Au	A1118 Au paste	Engelhard	YSZ	400°C (2h), then 850-900°C (30 min)	25, 29, 30
			β''-Al_2O_3	800°C (1h)	27
			CeO_2	900°C (2h)	11
			$Na_3Zr_2Si_2PO_{12}$	900°C (1h)	12

			$CaZr_{0.9}In_{0.1}O_{3-\alpha}$	900°C (2h)	30
			$K_2YZr(PO_4)_3$	900°C (3h)	30
Au	Au powder (99.9+%) in polyvinyl acetate binder	Aldrich	YSZ	800°C (2h) 900°C (2h) 400°C (2h), then 950°C (2h)	23 24 6
			β''-Al_2O_3	750°C	10
			CeO_2	900°C (2h)	11
Au	Au paste C70219R4	Gwent Electronic Materials Ltd	YSZ	thermal decomposition	32

Addresses of suppliers of catalyst pastes included in Table B.1 are presented below. Other companies (e.g. Johnson-Matthey) may also supply similar products. The suitability of these products for preparing catalyst films for electrochemical promotion studies should be tested on the basis of the requirements already mentioned. A useful approach before proceeding with the study of new systems is to try to reproduce results of electrochemical promotion studies in model systems, such as ethylene oxidation on Pt, which has been thoroughly studied. It has to be pointed out that in general suppliers do not provide calcination procedures or the provided calcination procedures aim to the production of very dense and non-porous films not necessarily suitable for electrochemical promotion studies.

Addresses of suppliers of catalyst pastes included in Table B.1

1. *Engelhard-CLAL UK Ltd*
   Valley Road, Cinderford, Gloucestershire Gl 14 2PB, Uk
   Tel: +44(0)1594822181
   Fax +44(0) 1594822667

2. *Demetron* It is now known as:
   Degussa Metals Catalysts Cerdec AG (dmc²)
   Headoffice
   Postfach 1351
   63403 Hanau
   Tel: +06181 5902, Fax : +06181 592931
   Web site: www.demetron.de

Solid electrolytes

There are no specific requirements for the solid electrolytes (pellets or tubes) used in electrochemical promotion experiments. However they should be stable under the conditions of the experimental study. Also one should know the type of ionic conductivity and the possibility of appearance of mixed ionic-electronic conductivity under the conditions of electrochemical promotion. This is quite essential for the correct interpretation of results. Addresses of suppliers of solid electrolytes included in Table B.1 are presented below:

1. *Didier Werke AG* (YSZ supplier)
   Technische Keramic DICERON
   Didierstrasse 27-31
   W-6200 Wiesbaden 12
   Tel: (0611) 605-0
   Fax (0611) 6052 20

2. *Ionotec Ltd* (β″-alumina suppliers)
   Chesire WA71TQ
   England
   Tel: 0044-1928-579627
   Fax: 0044-1928-579668
   e-mail: ionotec@compuserve.com

3. *TYK Corporation* (H^+ conductors of the type $SrCe_{0.95}Yb_{0.05}O_{3-\alpha}$)
   3-1 Ohbata-Cho
   Tajimi City
   Gifu Pre. 507-8607
   Japan
   Fax: 0081-572-2436-37

4. *Tosoh Europe B. V* (YSZ powder supplier)
   Crown Building-south
   Hullenbergwog 359
   1101 CP Amsterdam Z.O.
   The Netherlands
   Tel +31 20 691 8104, Fax +31 20 691 5458

B.2 Instrumentation

The instrumentation needed for electrochemical promotion studies is not complicated. However, as electrochemical methods are used in order to affect catalytic reactions, one needs access to instrumentation used both in

electrochemical and in catalytic studies. In this respect the typical instrumentation that is used includes the following:

1. *Gas chromatograph,* for the analysis of products and reactants.

The gas chromatograph is better to be equipped both with a thermal conductivity detector (TCD) and with a flame ionization detector (FID). The latter is extremely useful in the analysis of organic substances at low concentrations. Packed columns are normally used, although capillary columns offer certain advantages in the analysis of a variety of products.

Some of the major companies that supply gas chromatographs are:

- *PerkinElmer Analytical Instruments*
  761 Main Avenue, Norwalk,
  Connecticut 06859-0001
  Tel: 203-762-4000, Fax: 203-762-4050,
  E-mail: info@perkin-elmer.com
  Web site: www.instuments.perkinelmer.com

- *Agilent Technologies*
  Corporate address:
  P.O. Box #10395
  Palo Alto, CA 94303
  In the U.S. and Canada call 800-227-9770
  Web site: www.chem.agilent.com

- *Shimadzu Europe Ltd./Shimadzu Deutschland GmbH*
  Marketing and Customer Support Centre
  Albert-Hahn-Straße 6-10
  D - 47269 Duisburg, Germany
  E-Mail: webmaster@shimadzu.de
  Web site: www.sel.shimadzu.com

- *Varian, Inc.*
  3120 Hansen Way
  Palo Alto, CA 94304-1030
  USA
  Phone: +1.650.213.8000
  E-mail: customer.service@varianinc.com
  Web site: www.varianinc.com

2. *Potentiostat-Galvanostat,* for applying fixed values of potential between the catalyst and the reference electrode or fixed value of current between the catalyst and the counter electrode.

Although it is not necessary, the galvanostat-potentiostat is better to incorporate a function generator in order to allow for cyclic voltammetry or other transient electrochemical techniques.

Some of the major companies that supply galvanostats-potentiostats are :

- *Princeton Applied Research (belongs to Perkin Elmer Instruments)*
  801 S. Illinois Ave., Oak Ridge, TN 37831-0895
  Phone: 800-366-2741, 865-482-4411 Ext. 343, Fax: 865-425-1334
  Email: INFO_par@perkinelmer.com
  Web site: www.par-online.com

- *Solartron Analytical*
  Unit B1 Armstrong Mall
  Southwood Business Park
  Farnborough
  Hampshire, GU14 0NR, U.K.
  Tel : +44 (0)1252 556 800 Fax: +44 (0)1252 556 899
  Web site: www.solartronanalytical.com

- *Amel Instruments*
  Via S. Giovanni Battista de la Salle, 4
  20132 Milan - Italy,
  Phone: +39 02 27203060/1-2562173/4-2564918/9 Fax: +39 02 2564832
  E-Mail: amel@amelsrl.com
  web site: amelsrl.com

A gas chromatograph and a potentiostat galvanostat are the minimum basis of a system for electrochemical promotion studies. Although not absolutely necessary, instruments that can continuously monitor the concentration of reactants and products are extremely useful for the identification of steady-state and for recording the transient effect of catalytic rate upon imposition of an electrochemical stimulus. *Infrared analysers or mass spectrometers,* are included in this category. We very strongly encourage the use of on-line infrared analyzers (e.g. for CO_2, CO or NO_x) particularly for newcomers in the field. It is truly exciting and important to be able to *monitor* the catalytic rate.

Some of the major companies that supply infrared analysers or mass spectrometers are:

- *INFICON (Balzers Instruments)* (mass spectrometer supplier)

Postfach 1000
FL 9496 Liechtenstein
Tel: 0041-75-3884111, Fax: 0041-75-3885414
Web site: www.inficon.com

- *VG Gas Analysis Systems* (mass spectrometer supplier)
  Factory One, Ion Path, Road Three
  Winsford Ind Estate
  Winsford Cheshire CW7 2GA
  UK
  Phone : + 44(0)1606 548700, Fax: +44(0)1606 548711
  Web site: www.vggas.com

- *Fischer-Rosemount Gmbh &Co* (IR analysers supplier)
  Geschäftsbereich Analysentechnik
  Industriestrasse 1
  D-63594 Hasselroth
  Germany
  Phone: +49 60 55/884-0, Fax: +49 60 55/884-209

- *Teledyne Analytical Instruments* (IR analysers supplier)
  16830 Chestnut Street
  City of Industry, California 91748-1020, USA
  Tel: (626) 961-9221 or (626) 934-1500, Fax: (626) 961-2538 or (626) 934-1651, Toll Free: (888) 789-8168
  E-Mail: ask_tai@teledyne.com

Finally, the recording of many signals from the output of the analytic and electrochemical instrumentation requires a reliable multi-pen recorder or an equivalent recording system based on a data acquisition card and appropriate software. The recorded signals are normally in the range of a few mV to 10V. The use of reliable temperature controllers and thermocouples is also crucial for the success of the experiments. A lot of suppliers of such equipment can be easily found and will not be reported here.

B.3 Apparatus

A typical apparatus for electrochemical promotion experiments consists of three parts: (a) The gas feed and mixing system (b) the reactor and (c) the analysis and electrochemical measurements system. A detailed schematic of the experimental apparatus is shown in Figure B.1, where the three parts are clearly shown.

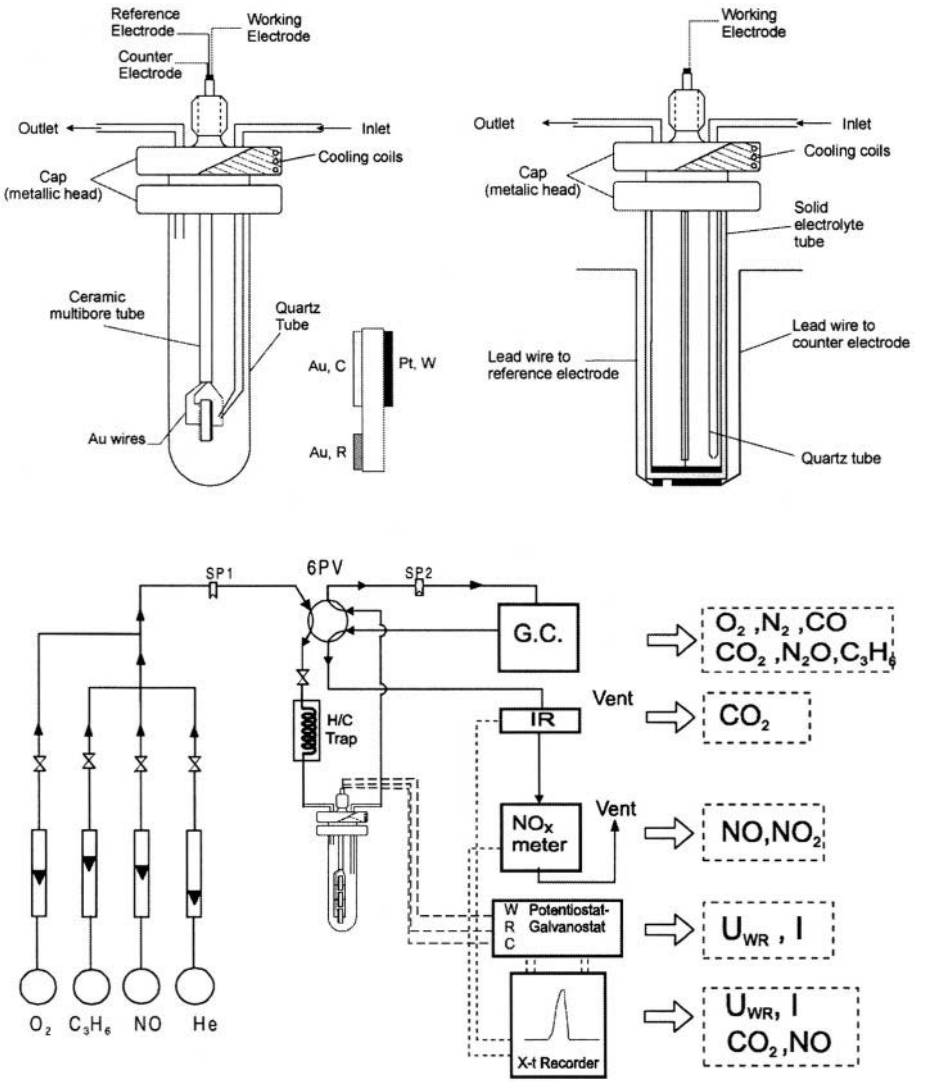

Figure B.1. (Top): Typical reactor designs used in electrochemical promotion studies: single-chamber design (left) and fuel cell type design (right). (Bottom): Typical apparatus for electrochemical promotion studies using a three-pellet single chamber reactor.

The gas feed and mixing system consists mainly of glass flowmeters or electronic mass flowmeters connected to gas bottles. For reactants that are in liquid state at room conditions (e. g. methanol) a saturator is normally used through which helium is sparged and then mixed with the other reactants. In this case all lines connected to the reactor are heated (e.g. at 150°C) to avoid condensation in the lines. In certain cases the gases from the bottles should be pretreated in order to avoid contamination of the catalyst. For example, a

heated (at T>300°C) trap for the decomposition of carbonyls is used in the case of CO feed, as iron carbonyls poison the metal catalysts. Check-valves and on-off valves are used in the gas feed and mixing system for safety reasons and for better control of the system. In most cases the reactant mixture is fed to the reactor through a 6-port valve. This allows for analysis of the reactants or products without interruption of the flow of reactants to the reactor. A 4-port valve can also be used for switching between the analysis of reactants and products. In this case, when selecting the analysis of reactants, the reactor works in a batch mode, which may be undesirable in some cases, e.g. in catalytic systems where the steady state is slowly attained.

Two types of continuous flow solid oxide cell reactors are typically used in electrochemical promotion experiments. The "single chamber" reactor depicted in Fig. B.1 is made of a quartz tube closed at one end. The open end of the tube is mounted on a stainless steel cap, which has provisions for the introduction of reactants and removal of products as well as for the insertion of a thermocouple and connecting wires to the electrodes of the cell. A solid electrolyte disk, with three porous electrodes deposited on it, is appropriately clamped inside the reactor. Au wires are normally used to connect the catalyst-working electrode as well as the two Au auxiliary electrodes with the external circuit. These wires are mechanically pressed onto the corresponding electrodes, using an appropriate ceramic holder. A thermocouple, inserted in a closed-end quartz tube is used to measure the temperature of the solid electrolyte pellet.

The second type of reactor is the "fuel cell type" reactor (Fig. B.1), which is similar to conventional fuel cells. It consists of a closed-end solid electrolyte tube appropriately mounted on a stainless steel cap, similar to the one in the single pellet reactor. The tube usually sits on an appropriately machined (Macor) base which facilitates wire attachment to the counter and reference electrode and allows for ambient air circulation over these electrodes. The porous electrodes are deposited on both sides of the bottom of the solid electrolyte tube, the working electrode in the inner side, exposed to the reaction mixture, and the counter and reference electrodes on the outer side, exposed to ambient air. The auxiliary electrodes in this case are usually porous Pt or Ag films, as there is no need to be inert. Ag electrodes offer the advantage of low polarisability of the auxiliary electrode/solid electrolyte interface. However, Pt auxiliary electrodes are comparatively more stable and can be used at higher temperatures, thus they are normally the preferred choice. It has to be emphasized that the reference electrodes in electrochemical promotion studies (as in many cases in solid state electrochemistry) do not correspond necessarily to inherently non-polarizable interfaces. However they can be used as reference electrodes as long as the current passing through them during the measurements is negligible. The main advantage of the "single-chamber" type reactor is its

simplicity and the ability to use cheaper solid electrolyte elements (disks instead of tubes). However in this case the open circuit potential measurements and their dependence on gas phase composition and temperature do not offer the precise information that can be acquired from similar measurements in the "fuel cell type " reactor, where the gas phase electrode is exposed to a reference gas phase mixture (e.g. ambient air).

As already mentioned, the analysis system consists typically of on line gas chromatography and, if available, by mass spectrometry and/or IR spectroscopy. The products from the reactor or, alternatively, the reactants (selection is made by switching a 4-port or 6-port valve) are directed to the gas chromatograph via a 6-port valve. This valve allows for sampling of certain gas volume and subsequent injection into one of the columns of the gas chromatograph. The selection between the two columns of the gas chromatograph is made via a 4-port valve. A cheaper alternative to the use of the 6-port sampling valve and the use of the 4- or 6- port valve for selection between the analysis of reactants and products is the use of a gas syringe of certain volume (e.g. 2ml) and the provision for sampling ports (e.g. a tee fitting with the sampling port capped with a septum) in the lines of reactants and products. As discussed below, this solution is not applicable in the case of condensables reactants or products.

The mass spectrometer sampling capillary or the dispersive infra-red analyzers used for continuous analysis and monitoring of the gas phase composition are situated between the reactor and the sampling valve, as close to the reactor as possible, in order to avoid any delay in the recording of changes in the composition of reactants or products. This delay should be taken into account when plotting simultaneously the time dependence of catalyst potential or current and gas phase concentration of the reactants or products.

B.4 Procedures

Before starting an electrochemical promotion experiment, one should check carefully that the catalytic reaction under study is not subject to external or internal mass transfer limitations within the desired operating temperature range, which can obscure or even completely hide the electrochemical promotion effect.

Checking the absence of external mass transfer limitations is a rather easy procedure. One has simply to vary the total volumetric flowrate while keeping constant the partial pressures of the reactants. In the absence of external mass transfer limitations the rate of consumption of reactants does not change with varying flowrate. As kinetic rate constants increase exponentially with increasing temperature while the dependence of mass transfer coefficient on temperature is weak ($\sim T^{3/2}$ in the worst case), absence

of external mass transfer limitations at the highest temperature of the experiments implies a similar situation at lower temperatures.

Checking the absence of internal mass transfer limitations is a more difficult task. A procedure that can be applied in the case of catalyst electrode films is the measurement of the open circuit potential of the catalyst relative to a reference electrode under fixed gas phase atmosphere (e.g. oxygen in helium) and for different thickness of the catalyst film. Changing of the catalyst potential above a certain thickness of the catalyst film implies the onset of the appearance of internal mass transfer limitations. Such checking procedures applied in previous electrochemical promotion studies allow one to safely assume that porous catalyst films (porosity above 20-30%) with thickness not exceeding ~10μm are not expected to exhibit internal mass transfer limitations. The absence of internal mass transfer limitations can also be checked by application of the Weisz-Prater criterion (see, for example ref. 33), provided that one has reliable values for the diffusion coefficient within the catalyst film.

Besides mass transfer limitations, it is very important in electrochemical promotion experiments to compute the maximum mass-balance allowable rate enhancement. This is intimately related to the conversion of the limiting reactant under open circuit conditions, as the conversion of the latter cannot exceed 100%. In this respect keeping the open circuit conversion as low as possible (normally by using a small amount of catalyst) allows the system to exhibit a pronounced rate enhancement ratio.

Concerning the enhancement factor or faradaic efficiency value Λ, it is quite useful to estimate, before starting the electrochemical promotion experiments, the expected value of faradaic efficiency for the specific system using Eq. (4.20). Knowledge of this value is helpful both in the evaluation of results but also in the design of the experiment, as one could change for example the calcination procedure of the catalyst to achieve lower exchange current density values and, thus, higher Λ values.

Last but not least, one should check the inertness of the auxiliary electrodes in single-pellet arrangements, both under open and closed circuit conditions and, also, via the closure of the carbon balance, the appearance of coke deposition. This is especially important in systems with a variety of products (e.g. selective oxidations), where the exact value of selectivity towards specific products is of key interest. This in turn points out the importance of the use of a good analytical system and of its careful calibration.

A typical electrochemical promotion experiment includes kinetic measurements under open and closed circuit conditions as well as study of the effect of catalyst potential or work function on catalytic rate and selectivity under steady state and transient conditions. In kinetic measurements one should change the partial pressure of each reactant while

keeping the partial pressures of other reactants constant. This can be easily achieved by using diluted mixtures of reactants in an inert gas, such as helium. Operating the reactor under differential conditions (conversion below approximately 5%) renders the analysis of kinetic results quite easy, even if the reactor does not exhibit exactly the behavior of a continuous stirred tank reactor. In the case of condensable reactants or products the corresponding lines should be heated at an appropriate temperature. In this case the use of multi port valves for sampling and injection of the samples in the gas chromatograph columns is preferred, compared to the use of a gas syringe. However one should keep the lines between the sampling point and the injection point as short as possible and use low diameter tube (e.g. 1/8″O.D.) in order to avoid axial dispersion and poor analysis due to concomitant increase of the width of the peaks and possible overlapping. When continuously monitoring the concentration of the reactants or products in the reacting mixture using e.g. a mass spectrometer, one should also take into account the delay in recording corresponding concentration changes due to the distance between the sampling point and the analysis chamber. The elimination of dead volumes in the flow system is also important, especially in isothermal titration experiments for the determination of catalyst surface area. As a summary, before starting an electrochemical promotion experiment, one should have a good command of the techniques to be used and a thorough knowledge of the experimental set up.

REFERENCES

1. S. Bebelis, and C.G. Vayenas, Non-Faradaic Electrochemical Modification of Catalytic Activity: 1. The case of Ethylene Oxidation on Pt, *J. Catal.* **118,** 125-146 (1989).
2. C.G. Vayenas, and S. Neophytides, Non-Faradaic Electrochemical Modification of Catalytic Activity: 3. The Case of Methanol Oxidation on Pt, *J. Catal.* **127,** 645-664 (1991).
3. J. Yi, A. Kaloyannis, and C.G. Vayenas, High Temperature cyclic voltammetry of Pt electrodes in solid electrolyte cells, *Electrochim. Acta* **38**(17), 2533-2539 (1993).
4. M. Marwood, and C.G. Vayenas, Electrochemical Promotion of Electrochemically isolated Pt catalysts on Stabilized Zirconia, *J. Catal.* **168,** 538-542 (1997).
5. A. Kaloyannis, and C.G. Vayenas, Non-Faradaic Electrochemical Modification of Catalytic Activity. 11. Ethane Oxidation on Pt, *J. Catal.* **171,** 148-159 (1997).
6. A. Kaloyannis, and C.G. Vayenas, Non-Faradaic electrochemical modification of catalytic activity. 12: Propylene oxidation on Pt, *J. Catal.* **182,** 37-47 (1998).
7. C.G. Vayenas, S. Bebelis, and S. Despotopoulou, Non-Faradaic Electrochemical Modification of Catalytic Activity: 4. The use of β''-Al_2O_3 as the solid electrolyte, *J. Catal.* **128,** 415-435 (1991).
8. I.V. Yentekakis, G. Moggridge, C.G. Vayenas, and R.M. Lambert, In situ controlled promotion of catalyst surfaces via NEMCA: The effect of Na on the Pt-catalyzed CO oxidation, *J. Catal.* **146,** 292-305 (1994).

9. O.A. Mar'ina, I.V. Yentekakis, C.G. Vayenas, A. Palermo, and R.M. Lambert, In situ controlled Promotion of Catalyst Surfaces via NEMCA: The effect of Na on the Pt-catalyzed NO Reduction by H_2, *J. Catal.* **166,** 218-228 (1997).
10. A. Palermo, R.M. Lambert, I.R. Harkness, I.V. Yentekakis, O. Mar'ina, and C.G. Vayenas, Electrochemical promotion by Na of the Platinum catalyzed reaction between CO and NO, *J. Catal.* **161,** 471-479 (1996).
11. P.D. Petrolekas, S. Balomenou, and C.G. Vayenas, Electrochemical promotion of Ethylene Oxidation on Pt Catalyst Films deposited on CeO_2, *J. Electrochem. Soc.* **145**(4), 1202-1206 (1998).
12. P.D. Petrolekas, S. Brosda, and C.G. Vayenas, Electrochemical promotion of Pt catalyst-electrodes deposited on $Na_3Zr_2Si_2PO_{12}$ during Ethylene Oxidation, *J. Electrochem. Soc.* **145**(5), 1469-1477 (1998).
13. I.V. Yentekakis, and C.G. Vayenas, In situ controlled promotion of Pt for CO oxidation via NEMCA using CaF_2 as the solid electrolyte, *J. Catal.* **149,** 238-242 (1994).
14. C. Pliangos, I.V. Yentekakis, S. Ladas, and C.G. Vayenas, Non-Faradaic Electrochemical Modification of Catalytic Activity: 9. Ethylene oxidation on Pt deposited on TiO_2, *J. Catal.* **159,** 189-203 (1996).
15. M. Makri, A. Buekenhoudt, J. Luyten, and C.G. Vayenas, Non-Faradaic Electrochemical Modification of the Catalytic Activity of Pt using a $CaZr_{0.9}In_{0.1}O_{3-\alpha}$ Proton Conductor, *Ionics* **2,** 282-288 (1996).
16. S. Bebelis, and C.G. Vayenas, Non-Faradaic Electrochemical Modification of Catalytic Activity: 6. The epoxidation of Ethylene on Ag/ZrO_2(8mol%) Y_2O_3, *J. Catal.* **138,** 588-610(1992).
17. P. Tsiakaras, and C.G. Vayenas, Oxidative Coupling of CH_4 on Ag catalyst-electrodes deposited on ZrO_2(8mol% Y_2O_3), *J. Catal.* **144,** 333-347 (1993).
18. C. Karavasilis, S. Bebelis, and C.G. Vayenas, Non-Faradaic Electrochemical Modification of Catalytic Activity: 10. Ethylene epoxidation on Ag deposited on stabilized ZrO_2 in presence of chlorine moderators, *J. Catal.* **160,** 190-204 (1996).
19. C. Karavasilis, S. Bebelis, and C.G. Vayenas, In Situ Controlled Promotion of Catalyst Surfaces via NEMCA: The Effect of Na on the Ag-Catalyzed Ethylene Epoxidation in the Presence of Chlorine Moderators, *J. Catal.* **160,** 205-213 (1996).
20. P.H. Chiang, D. Eng, H. Alqahtany, and M. Stoukides, Nonoxidative methane coupling with the aid of solid electrolytes, *Ionics* **53-56,** 135-141 (1992).
21. C. Pliangos, I.V. Yentekakis, X.E. Verykios, and C.G. Vayenas, Non-Faradaic Electrochemical Modification of Catalytic Activity: 8. Rh-catalyzed C_2H_4 oxidation, J. *Catal.* **154,** 124-136 (1995).
22. C. Pliangos, C. Raptis, T. Badas, D. Tsiplakides, and C.G. Vayenas, Electrochemical Promotion of a Classically Promoted Rh catalyst for the Reduction of NO, *Electrochim. Acta* **46,** 331-339 (2000).
23. M. Marwood, A. Kaloyannis, and C.G. Vayenas, Electrochemical Promotion of the NO reduction by C_2H_4 on Pt/YSZ and by CO on Pd/YSZ, *Ionics* **2,** 302-311 (1996).
24. M. Marwood, and C.G. Vayenas, Electrochemical Promotion of the Catalytic Reduction of NO by CO on Palladium, *J. Catal.* **170,** 275-284 (1997).
25. A. Giannikos, A.D. Frantzis, C. Pliangos, S. Bebelis, and C.G. Vayenas, Electrochemical Promotion of CH_4 oxidation on Pd, *Ionics* **4,** 53-60 (1998).
26. C. Athanasiou, G. Marnellos, P. Tsiakaras, and M. Stoukides, *Ionics* **2,** 353 (1996).
27. A. Giannikos, P. Petrolekas, C. Pliangos, A. Frenzel, C.G. Vayenas, and H. Putter, Electrochemical promotion of Pd for the Hydrogenation of C_2H_2, *Ionics* **4,** 161-169 (1998).

28. J. Nicole, and C. Comninellis, Electrochemical promotion of IrO_2 catalyst activity for the gas phase combustion of ethylene, *J. Appl. Electrochem.* **28,** 223-226 (1998).
29. S. Wodiunig, and C. Comninellis, Electrochemical Promotion of RuO_2 Catalysts for the Gas Phase Combustion of C_2H_4, *Journal of the European Ceramic Society* **19,** 931-934 (1999).
30. G. Pitselis, P. Petrolekas, and C.G. Vayenas, Electrochemical Promotion of NH_3 decomposition on Fe using H^+, Na^+ and K^+ conductors, *Ionics* **3,** 110-117 (1997).
31. I.V. Yentekakis, Y. Jiang, S. Neophytides, S. Bebelis, and C.G. Vayenas, Catalysis, Electrocatalysis and Electrochemical Promotion of the Steam Reforming of Methane over Ni Film and Ni-YSZ cermet Anodes, *Ionics* **1,** 491-498 (1995).
32. G. Foti, O. Lavanchy, and C. Comninellis, Electrochemical promotion of Rh catalyst in gas-phase reduction of NO by propylene, *J. Appl. Electrochem.* **30,** 1223-1228 (2000).
33. G.F. Froment, and K.B. Bischoff, *Chemical Reactor Analysis and Design,* John Wiley & Sons, New York (1979).

APPENDIX C

MAIN RESEARCH GROUPS

The seventeen research groups listed below have made already (2000) significant contributions to the rapidly growing Electrochemical Promotion (NEMCA) literature. They are listed and discussed here, both in order to pay tribute to their valuable contributions, but also in order to facilitate contact with them of other research groups interested in entering the field of Electrochemical Promotion.

The groups are listed in alphabetical order of the senior researcher, but the other key researcher names are also mentioned.

1. **N. Anastasijevic:** The name of Dr. Anastasijevic is associated both to the first NEMCA study in liquids (Chapter 10), together with Baltruschat and Heitbaum, but also with the development at LURGI of a new NEMCA-based process for the production of ammonium polysulfide (Chapter 10). Chronologically he was the first aqueous electrochemist who realized the importance and potential of NEMCA.

Dr. N. Anastasijevic
LURGI AG
Lurgi Allee 5
Postfach 11-12-31
D-6000 Frankfurt am Main
Germany

E-mail: anastasijevic@yahoo.de,
nikola.anastasijevic@lurgi.de

2. **N.J. Bjerrum:** The group of Professor Bjerrum was the first to demonstrate NEMCA with a molten salt catalyst (Chapter 10) and also with a commercial V_2O_5-based SO_2 oxidation catalyst (Chapter 12). Both discoveries are of significant practical importance.

Professor Niels J. Bjerrum
Materials Science Group, Department of Chemistry
Technical University of Denmark
DK-2800 Lungby
Denmark

Phone: +454525 2307
Fax: +4545883136
e-mail: njb@kemi.dtu.dk

3. **Ch. Comninellis:** The importance of the outstanding contributions of the group of Professor Comninellis at EPFL (Drs. G. Foti, M. Marwood, J. Nicole, S. Wodiunig, E. Varkaraki, Mr. I. Bolzonella) to the electrochemical promotion literature can hardly be overemphasized.

The group was first to demonstrate NEMCA on metal oxides (IrO_2, RuO_2) and with their NEMCA studies on IrO_2-TiO_2/YSZ contributed significantly to establishing the similarity between electrochemical promotion and classical metal-support interactions.

They first reported and studied "permanent NEMCA" and via cyclic voltammetry established the dependence of metal/solid electrolyte capacitance on porous metal film mass, which confirms the O^{2-} backspillover promoting mechanism.

They also dramatically advanced the bipolar design concept, first explored by Marwood and Vayenas to induce NEMCA in monolithic YSZ structures, a key step for the practical utilization of NEMCA.

Professor Christos Comninellis
EPFL
Chemistry Department
Institute of Chemical Engineering
CH-1015 Lausanne
Switzerland

Tel.:+41-21-693 3674
Fax:+41-21-693 3680
E-mail:Christos.Comninellis@epfl.ch

4. **C. Christensen, L. Larsen:** The small group of Dr. C. Christensen and L. Larsen at DINEX, Denmark has already reported significant advances in utilizing NEMCA in automotive exhaust catalysis of commercial Diesel engines for soot combustion. Although faradaic efficiency, Λ, values are not given explicitly in their publications (Chapter 12) their published data show Λ values of at least 60 in their very promising perovskite/CGO soot combustion prototype system (Chapter 12)

Dr. Henrik Christensen
Project Leader
DINEX A/S
Fynsveij 39
DK-5500 Middelfart
Denmark

Tel: +45-63412523
Fax:+45-53412525
E-mail: hc@dinex.dk

Dr. Lars Chr. Larsen
Development Manager
DINEX A/S
Fynsveij 39
DK-5500 Middelfart
Denmark

Tel: +45-63412527
Fax:+45-53412525
E-mail: lcl@dinex.dk

5. **W. Göpel:** The UPS and work function measurements (Chapter 5) published by the group of the late Professor Göpel (together with Prof. Wiemhöfer and Drs. Zipprich and Vöhrer) was the first confirmation of the work-function-potential equivalence reported by the Patras group, and together with their UPS spectra, provided strong confirmation of the O^{2-} backspillover electrochemical promotion mechanism.

In general the group of the late Professor Göpel pioneered the use of surface science techniques in solid state electrochemistry.

6. **G. Haller:** The group of Professor Haller and his students C. Cavalca and S. Kim at Yale has made pioneering contributions by demostrating NEMCA for benzene hydrogenation on $Pt/\beta''\text{-}Al_2O_3$, a key system from the fundamental catalysis viewpoint (Chapter 9), and also by first utilizing self-driven (no external electrical supply) NEMCA catalyst pellets, together with C. Vayenas (Chapter 8), in one of the first demonstrations of the single-chamber NEMCA design. Professor Haller has also significantly contributed to making electrochemical promotion understood by the catalytic community.

Professor Gary Haller
Yale University
Department of Chemical Engineering
Jonathan Eduards College
68 High Street, PO Box 208220
CT 06520-8220 New Haven, Connecticut - U.S.A.

Tel.:+1-203432 0356
Fax: +1 203 432 0761
E-mail: gary.haller@yale.edu

7. **R. Imbihl, J. Janek:** The groups of Professors Imbihl and Janek have made important contributions in the use of PEEM, work function measurement and XPS (Chapter 5) to establish the O^{2-} backspillover mechanism of electrochemical promotion under UHV conditions.

Professor Ronald Imbihl
University of Hannover
Institute for Physical Chemistry
Callinstrasse 3-3a
D-30167 Hannover
Germany

Tel.+49-511-762-2349
Fax.+49-511-762-4009
E-mail: imbihl@mbox.pci.uni-hannover.de

Professor Jürgen Janek
Institute of Physical Chemistry
Justus-Liebig-University Gießen
Heinrich-Buff-Ring 58
D-35392 Gießen
Germany

Tel. +49 (0)641 99-34501
Fax. +49 (0)641 99-34509
E-mail: juergen.janek@phys.chemie.uni-giessen.de

8. R. Lambert: The importance of the outstanding contributions of Professor Lambert's group and his coworkers M. Tikhov, A. Palermo and others to the electrochemical promotion literature utilizing Na^+ conductors can hardly be overemphasized. Lambert and coworkers elegantly proved via XPS the Na spillover-backspillover nature of electrochemical promotion with β''-Al_2O_3. His group studied with great success various metal/ β''-Al_2O_3 systems for the reduction of NO_x, collaborated for years with the Patras group in elucidating the origin of NEMCA and used electrochemical promotion principles to develop highly active classically promoted supported catalysts. Lambert contributed more than anyone else not only in enhancing the understanding of the surface chemistry of electrochemical promotion with Na^+ conductors, but also in dissipating this knowledge to the surface science community.

Professor Richard Lambert
Department of Chemistry
University of Cambridge
Lensfield Road
CB2 1EW Cambridge
U.K.

Tel.: +44 1223 336467
Fax: +44 1223 336362
E-mail: rmll@cam.ac.uk

9. E. Lamy-Pitara and J. Barbier: The group of Professor Barbier and Dr. Lamy-Pitara was first to demonstrate NEMCA in an aqueous phase catalytic hydrogenation reaction (Chapter 10). This work is of very significant theoretical and potentially practical importance.

Profeesor J. Barbier
Laboratoire de Catalyse en Chimie Organique (LACCO)
UMR 6503
Université de Poitiers 40
Avenue du Recteur Pineau 86022 Poitiers Cedex
France

Dr. E. Lamy-Pitara
Laboratoire de Catalyse en Chimie Organique (LACCO)
UMR 6503
Université de Poitiers 40
Avenue du Recteur Pineau 86022 Poitiers Cedex
France

10. W.Y. Lee: The group of Professor Lee in Korea has made interesting NEMCA studies of methanol oxidation on Ag/YSZ (Chapter 8).

Professor Wha Young Lee
Department of Chemical Engineering
Seoul National University
Shinlim-dong, Kwanak-ku, Seul, 151-742
Korea

11. I. Metcalfe: The group of Professor Metcalfe has combined kinetic and work function measurements to investigate the electrochemical promotion of CO oxidation on Pt/YSZ and, more recently, had made important modeling advances for the fundamental description of electrochemical promotion at the molecular level.

Professor Ian S. Metcalfe
The Kenneth Denbigh Chemical Engineering Building
University of Edinburgh
King's Buildings, Mayfield Road
Edinburgh EH9 3JL
United Kingdom

Phone: +44 (0) 1316-508553
Fax: +44-131-650-6551
e-mail: ian@chemeng.ed.ac.uk

12. G. Pacchioni: Professor Pacchioni, together with Professor Illas, both well-known theoretical chemists, were first to perform rigorous quantum mechanical cluster calculations simulating electrochemical promotion (Chapter 5). Their results are of great significance and are in excellent agreement with experiment.

Professor Gianfranco Pacchioni
Dipartimento di Scienza dei Materiali
Università di Milano-Bicocca
Instituto Nazionale per la Fisica della Materia
via Cozzi, 53-20125, Milano
Italy

Phone: + 39 - 02 6448 5137
Fax: + 39 - 02 6448 5400
e-mail: Gianfranco.Pacchioni@mater.unimib.it

Professor Fransesco Illas
Departament de Quimica Fisica
Facultat de Quimica
Universitat de Barcelona
Marti i Franques 1
E-08028 Barcelona
Spain

Phone: + 34 93 402 1229
Fax: + 34 93 402 1231
e-mail: f.illas@qf.ub.es

13. E. Smotkin: The group of Professor Smotkin at Illinois (IIT) was first to demonstrate NEMCA for an isomerization reaction (1-butene to cis-and trans-2-butene) over a Pd/Nafion catalyst at room temperature. This important and spectacular discovery underlines the great potential of Nafion for inducing NEMCA at low temperatures for numerous important organic synthesis reactions.

Professor Eugene Smotkin
IIT
10 West 33rd St.
Department of Chemical and
Environmental Engineering
IL 60616 Chicago, Illinois
U.S.A.

Tel.: +1-312-567-3453
Fax: +1-312-567-8882
E-mail: esmotkin@charlie.cns.iit.edu

14. V. Sobyanin, V. Belyaev: The group of Professors Sobyanin and Belyaev at Novosibirsk, together with their students Drs. Politova, Galvita and Mar'ina, was the second group which reported NEMCA (Chapters 1 and 8). They have made numerous exciting NEMCA studies utilizing YSZ and were first to use a proton conductor ($CsHSO_4$) to induce electrochemical promotion of ethane dehydrogenation. Their numerous contributions include a chain-type mechanism for NEMCA with YSZ, where the chain length, Λ, dictates the apparent faradaic efficiency. This interesting kinetic idea bears several conceptual similarities with currently established ion-backspillover mechanism of NEMCA.

Professor Vladimir Sobyanin
Boreskov Institute of Catalysis
Prospekt Akademika Lavrentieva 5
Novosibirsk, RU-630090
Russia

Fax: +7(383)2-34-30-56
e-mail: sobyanin@sirius.catalysis.nsk.su

Professor Vladimir Belyaev
Boreskov Institute of Catalysis
Prospekt Akademika Lavrentieva 5
Novosibirsk, RU-630090
Russia

Fax: +7(383)2-34-30-56
e-mail: belyaev@catalysis.nsk.su

15. M. Stoukides: The name of M. Stoukides is associated with the first electrochemical promotion studies and publications in 1981 (Chapter 1) when he as a graduate student of C. Vayenas at MIT was investigating ethylene epoxidation on Ag/YSZ. In recent years the group of Professor M. Stoukides in Thessaloniki has made interesting electrochemical promotion studies of H_2S decomposition and C_2H_4 and NH_3 synthesis at elevated temperatures near the border of electrochemical promotion and electrocatalysis.

Professor Michael Stoukides
University of Thessaloniki
Dept. of Chemical Engineering
GR-54006 Thessaloniki
GREECE

Phone: +3031 996165
Fax: +3031 996165

E-mail: stoukidi@alexandros.cperi.forth.gr

16. P. Tsiakaras: The group of Prof. P. Tsiakaras at the University of Thessaly has very recently made interesting electrochemical promotion studies of ethanol oxidation on Pt/YSZ.

Professor Panagiotis Tsiakaras
University of Thessaly
Department of Mechanical & Industrial Engineering
Pedion Areos
GR-383 34 Volos
Greece

Phone: +30421 74065
Fax: +30421 74065
E-mail: tsiak@uth.gr

17. C. Vayenas: The group of C. Vayenas first at MIT (coworkers M. Stoukides, J. Michaels, R. Farr, D. Ortman, M. Manton) and then at U. Patras (coworkers Prof. M. Jaksic, Prof. S. Bebelis, Dr. S. Neophytides, Prof. I. Yentekakis, Prof. P. Tsiakaras, Dr. C. Pliangos, Dr. M. Makri, Dr. C. Karavasilis, Dr. E. Karasali, Dr. O. Mar'ina, Dr. P. Petrolekas, Dr. M. Marwood, Dr. S. Brosda, Dr. D. Tsiplakides, Dr. C. Yiokari, Ms. S. Balomenou, Mr. C. Raptis, Mr. T. Bathas and others) was first to report a non-Faradaic catalytic rate enhancement in 1981 and to demonstrate the generality of the phenomenon in 1988 when the group first proposed the acronym NEMCA. The group has published more than one hundred publications both on the phenomenology and on the fundamentals of electrochemical promotion. Through the invaluable help of Professor M. Jaksic the group also published some of the first aqueous electrolyte NEMCA papers. Through the precious collaboration of Dr. K. Besocke the group obtained the first STM confirmation of the ion backspillover mechanism of electrochemical promotion.

Professor C.G. Vayenas
Department of Chemical Engineering
1, Caratheodory St.
University of Patras
GR-26500 Patras - GREECE

Phone: +3061-997576
Fax: +3061-997269
E-mail: cat@chemeng.upatras.gr

In completing this list of groups active in the area of electrochemical promotion it would be a great omission if the names were not mentioned and acknowledged of some prominent scientists who, although not directly involved in NEMCA publications, have nevertheless made outstanding contributions to explaining the principles of Electrochemical Promotion to a wide electrochemical, catalytic and surface science audience. These include:

1. Professor J.O' M. Bockris who grasped from the very beginning the importance of electrochemical promotion and explained it in a truly lucid manner in his excellent monographs and books.
2. Professor W. Vielstich who has praised the importance of NEMCA in his very fine recent Electrochemistry book and added his own unpublished aqueous electrolyte results to underline the significance of this new area.
3. Professor J. Pritchard who, as a reviewer of the first NEMCA Nature paper in 1990, immediately grasped the importance of the field and wrote a deep and thorough editorial in Nature where he first proposed the term "Electrochemical Promotion".
4. Professor J. Haber who wrote a lucid article describing Electrochemical Promotion in his Annual Chemistry Report of the Royal Society in 1994.

5. Dr. F. Kalhammer of EPRI in the USA who, as an outstanding former PhD student of the late Professor G.M. Schwab, has understood Electrochemical Promotion as deeply as anyone else, and has done a tremendous job through his truly outstanding technical writing to disseminate NEMCA research and to inform scientific funding agencies and industry about the potential applications of electrochemical promotion.

Index